DOE/MC/26042-5152
UC-103

PFBC HGCU Test Facility
Technical Progress Report

Third Quarter, CY 1995

DISCLAIMER

Prepared by:

American Electric Power Service Corporation
Columbus, Ohio 43215

Prepared for:

The United States Department of Energy
Under DOE Instrument No. DE-FC21-89MC26042

October, 1995

DISCLAIMER

I. INTRODUCTION

This is the twenty-fourth and final Technical Progress Report submitted to the Department of Energy (DOE) in connection with the cooperative agreement between the DOE and Ohio Power Company for the Tidd PFBC Hot Gas Clean Up Test Facility. This report covers the work completed during the Third Quarter of CY 1995.

II. WORK ACCOMPLISHED DURING THE REPORTING PERIOD

All activity this quarter was directed toward the completion of the program final report. A draft copy of the final report was forwarded to DOE during this quarter, and DOE submitted their comments on the report to AEPSC. DOE requested that Westinghouse write an appendix to the report covering the performance of the fail-safe regenerator devices during Tidd operation, and Westinghouse subsequently prepared the appendix. Additional DOE comments were incorporated into the report, and it will be issued in camera-ready form by the end of October, 1995, which is the program end date.

Appendix 1 presents the results of filter candle posttest examination by Westinghouse performed on selected filter candles following final shutdown of the system.

III. MANPOWER REPORT AND COST DATA

As of September 30, 1995, the AEPSC Engineering, Design and Project Support cumulative work-hours were 73,942.9 or 107% of the total 69,097 revised work-hours projected for the project. Figure 1 compares the actual work-hours expended versus the current estimate. For the reporting

APPENDIX 1

ADVANCED PARTICLE FILTER

Technical Progress Report No. 20 and 21

April through September 1995

Prepared by

Westinghouse Science and Technology Center

Pittsburgh, Pennsylvania

For

American Electric Power Service Corporation

Columbus, Ohio

AEPSC Contract No. C8014

TIDD ADVANCED PARTICLE FILTER

SUMMARY

The final APF test run number 34 was completed on March 30, 1995. This last quarterly report summarizes inspections of the filter's internal ceramic components and laboratory characterizations of various ceramic materials exposed during this run.

REPORT HIGHLIGHTS

Appendix A provides a summary of the observations that were made during the April 26, 1995 borescope inspection of the Westinghouse Advanced Particulate Filter (W-APF) system internals at the American Electric Power (AEP) Demonstration Plant in Brilliant, Ohio. Although ash bridging was not observed within the W-APF, several of the DuPont PRD-66 filter elements were observed to have failed in array B/T.

At the conclusion of Test Segment #5, the W-APF internals were removed from the pressure vessel and place in a maintenance structure for further inspection, ash sampling, and final candle disassembly. Appendix B describes the appearance of the internals during the May 11, 1995 lift, and provides comments on the description of the ash cake layer and general appearance of the various filter elements after 1110 hours of pressurized fluidized-bed combustion (PFBC) operation.

As part of the filter material surveillance program, the residual bulk material strength, filter elongation, and permeability were determined for select filter elements. The results of these efforts are summarized in Appendix C.

Tenaciously bonded ash resulted along the candle filter holder mounts in all three top arrays. As a result, removal of the filters from the top arrays was extremely difficult in comparison to removal of the filter elements from alternate arrays. Appendix D explores the composition, morphology, and particle size of the ash/sorbent that deposited along the filter holder mounts, as well as deposit formations which resulted at alternate locations within the W-APF.

Three additional Appendices are provided which selectively explore the morphological changes within the various filter materials, as well as the interaction with ash/sorbent fines. These include: Appendix E; Characterization of the Ash Deposit and Surveillance Schumacher Dia

Schumalith F40 Candle Filters; Appendix F, Description of the DuPont PRD-66 Candle Filters at the Conclusion of Test Segment #5; and Appendix G, Characterization of the Oxide-Based Filament Wound DuPont PRD-66 Filter Matrix.

APPENDIX A

W-APF BORESCOPE INSPECTION

M. A. Alvin
April 26, 1995

A summary of the observations which were made during conduct of the April 26, 1995 borescope inspection of the Westinghouse Advanced Particulate Filter internals follows:

- Absence of ash bridging between adjacent candle filters, dust shed, and/or plenum pipes in all nine arrays.
- Absence of ash in the W-APF ash hopper.
- An ash cake layer was evident along the filter elements. Possibly thinner cake remained along the alumina/mullite, while a somewhat thicker layer remained along the clay bonded SiC filter elements.
- Schumacher Dia Schumalith F40 surveillance candles appeared to be intact, achieving 5855 hours of operation.
- Coors alumina/mullite and Pall Vitropore 442T surveillance candles appeared to be intact, achieving 2815 hours of operation.
- All ten 3M CVI-SiC candles appeared to be intact.
- All newly installed Pall Vitropore 442T candles (Test Segment 5) appeared to be intact (~150 filter elements).
- With the exception of one filter, all newly installed Coors alumina/mullite candles (Test Segment 5) appeared to be intact (~96 out of ~97 filter elements). Failure occurred along an outer ring candle in plenum A/M. Fracture was at approximately the mid-section of the filter body.
- Two DuPont PRD-66 candles were seen to be intact in plenum B/T. Three PRD-66 filters were seen to have failed at approximately the mid-section of each filter body. Several adjacent PRD-66 filters were seen to have failed near the flange. Further inspection will be needed to determine whether the candles installed around the outer ring of plenum B/T, adjacent to the shroud, remained intact (~5-10 elements). Complete inspection of this array could not be conducted due to restricted access of the top nozzle port.

APPENDIX B

WESTINGHOUSE ADVANCED PARTICULATE FILTRATION SYSTEM AFTER COMPLETION OF TEST SEGMENT #5

M. A. Alvin
June 23, 1995

GENERAL DESCRIPTION

On May 11, 1995, the Westinghouse Advanced Particulate Filtration (W-APF) system was removed from the pressure vessel and positioned into its maintenance structure. Prior to the lift, a fine layer of dust was evident along the top of the pressure vessel's tubesheet (Figure 1). Dust was also evident along the ID surface of the B/T pulse pipe which corresponded to the array which contained the failed DuPont PRD-66 candle filters (i.e., borescope inspection on April 26, 1995). During the lift on May 11, 1995, it became readily apparent that ash bridging had virtually been eliminated within the W-APF system after 1110 hours of test operation in Test Segment #5 (i.e., January 13, 1995 through March 30, 1995; Table 1).

As shown in Figures 2 and 3, two candles were broken in Cluster A. These included failure below the flange of an alumina/mullite candle filter located in position A/T-20, and a mid-body failure at ~1000 mm below the flange of an alumina/mullite candle filter positioned in A/M-20. Candle A/T-20 was positioned directly above candle A/M-20, both of which were off-tangent to the shroud. Since a segment of an alumina/mullite candle filter end cap had been found in the ash hopper discharge after 775 hours of test operation, and candle pieces had not been found in the bottom of the W-APF filter vessel either before or after the lift, both Coors alumina/mullite candle filters were expected to have failed during test operation in Test Segment #5.

Ninety-one Pall Vitropore 442T candles had been initially installed in Cluster C (Figure 4; Table 2). After 1110 hours of operation at Tidd, all of the Pall Vitropore 442T candles remained intact.

Twenty-two DuPont PRD-66 candle filters had been installed in the B/T array. After 232 hours of test operation, segments of the PRD-66 candles had been found in the ash hopper discharge. Similarly after 775 hours of test operation, additional segments of the DuPont PRD-66 filters were again found in the ash hopper discharge. Post-test inspection of the W-APF indicated that only two of the original PRD-66 candles remained intact (i.e., B/T-6 and B/T-8), while three had suffered fracture at approximately three-quarters below the flange (i.e., B/T-10, B/T-11, and B/T-12), and sixteen had failed directly below the flange (Figure 5).

Ten 3M CVI-SiC composite candles had been installed in positions C/T-16, C/T-17, C/T-18, C/T-19, C/T-20, B/B-3, B/B-4, B/B-5, B/B-6, and B/B-7. These elements remained intact after 1110 hours of pressurized fluidized-bed combustion (PFBC) operation at the American Electric Power (AEP) Demonstration Plant in Test Segment #5.

//

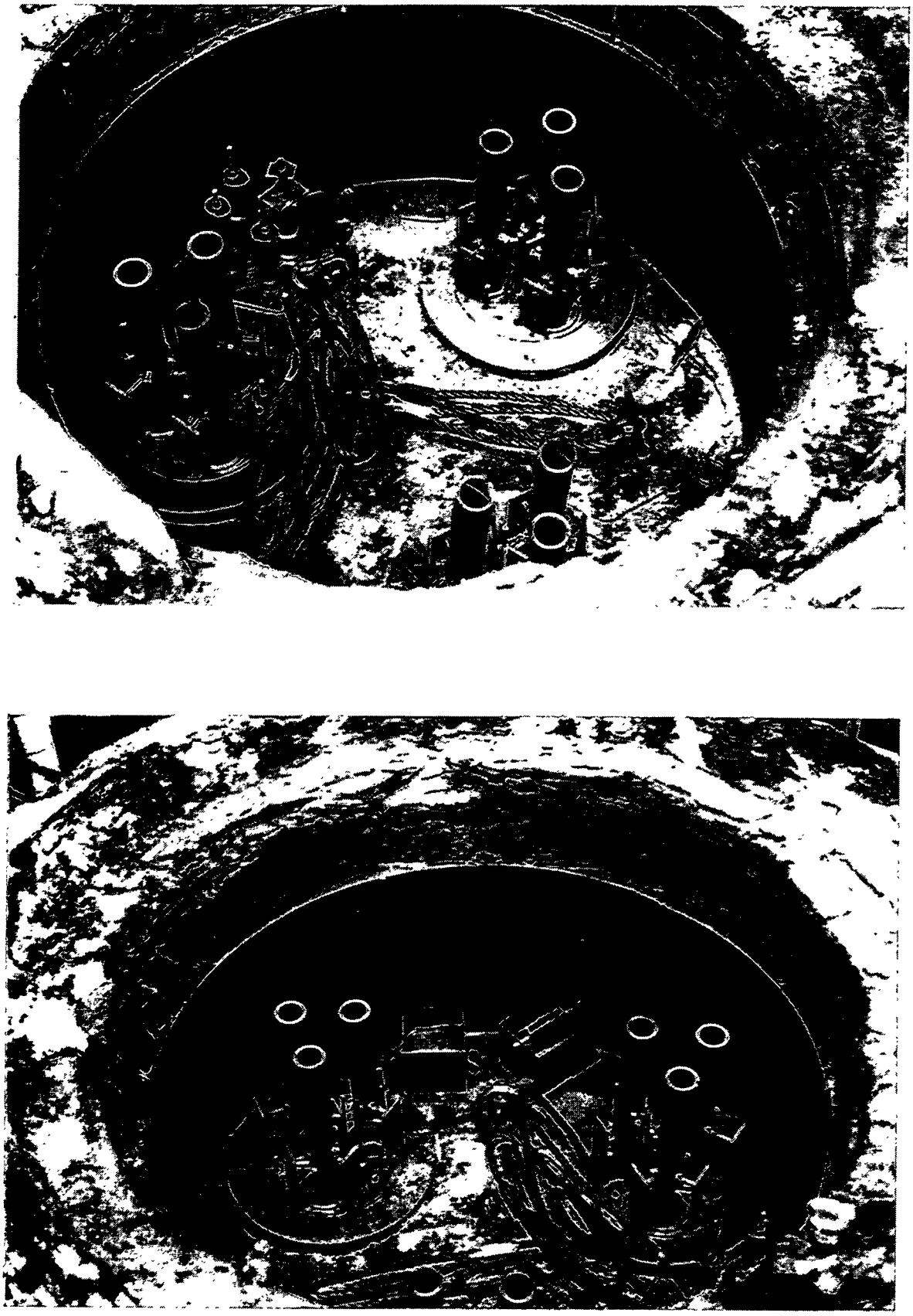

Figure 1 – W-APF Tubesheet After Test Segment #5

TABLE 1
WESTINGHOUSE PFBC HOT GAS FILTER TESTING AT AEP

PFBC Test Segment	1 10/92 - 12/92	2 7/93 - 9/93	3 1/94 - 4/94	4 7/94 - 10/94	5 1/95 - 3/95
Operating Time, Hrs	464	1295	1279	1705	1110
Operating Temperature, °C	730 - 790	620 - 790	650 - 780	660 - 760	760 - 845
Filter Elements	384	384	384	288	288
Schumacher F40	384	384	384	258	5
Schumacher FT20	—	—	—	8	—
Pall Vitropore 442T	—	—	—	8	153
Coors Alumina/Mullite	—	—	—	8	98
3M CVI-SiC Composite	—	—	—	3	10
DuPont PRD-66	—	—	—	3	22

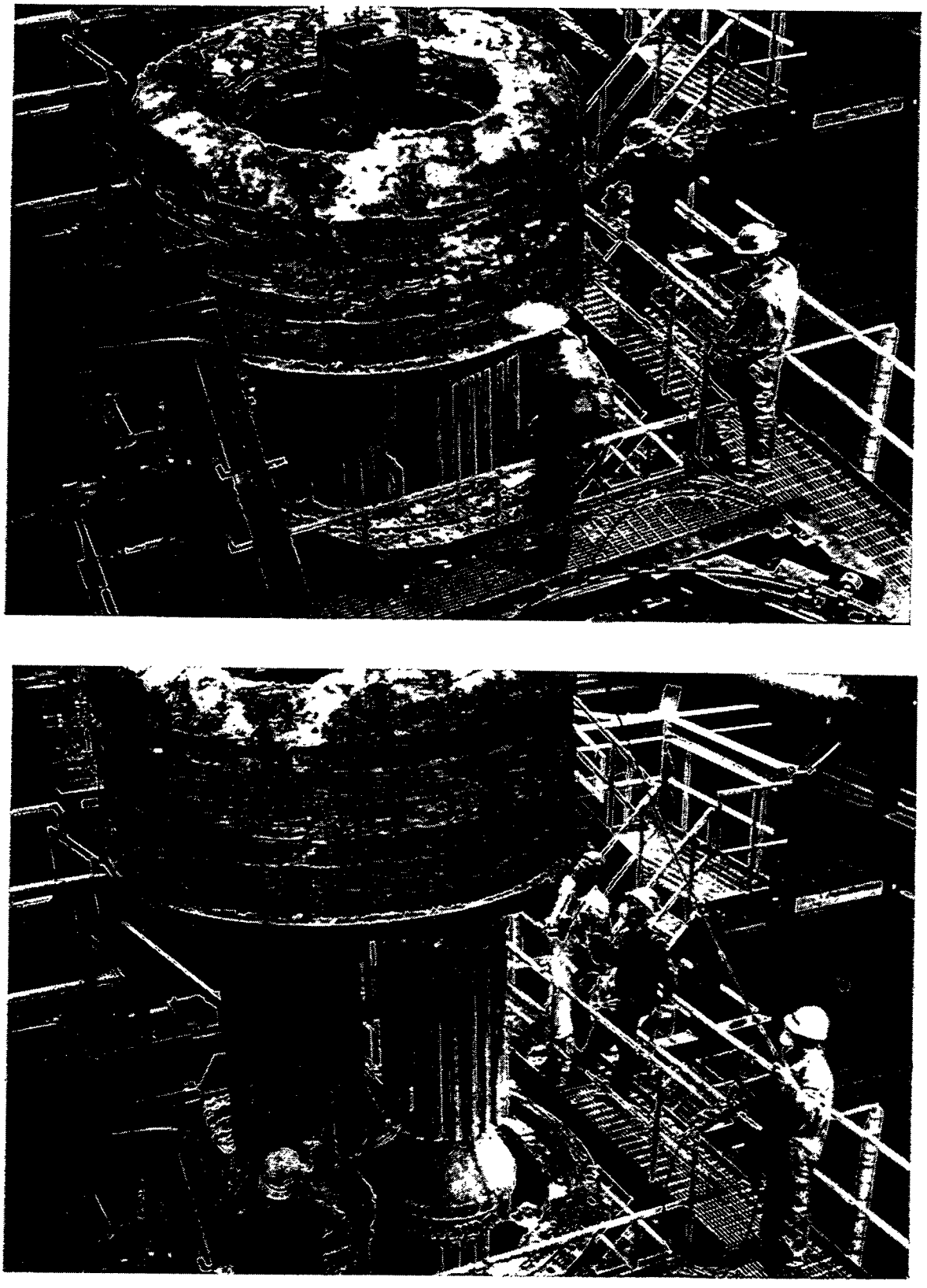

Figure 2 – Top Candle Filter Arrays In The W-APF After Conduct Of Test Segment #5

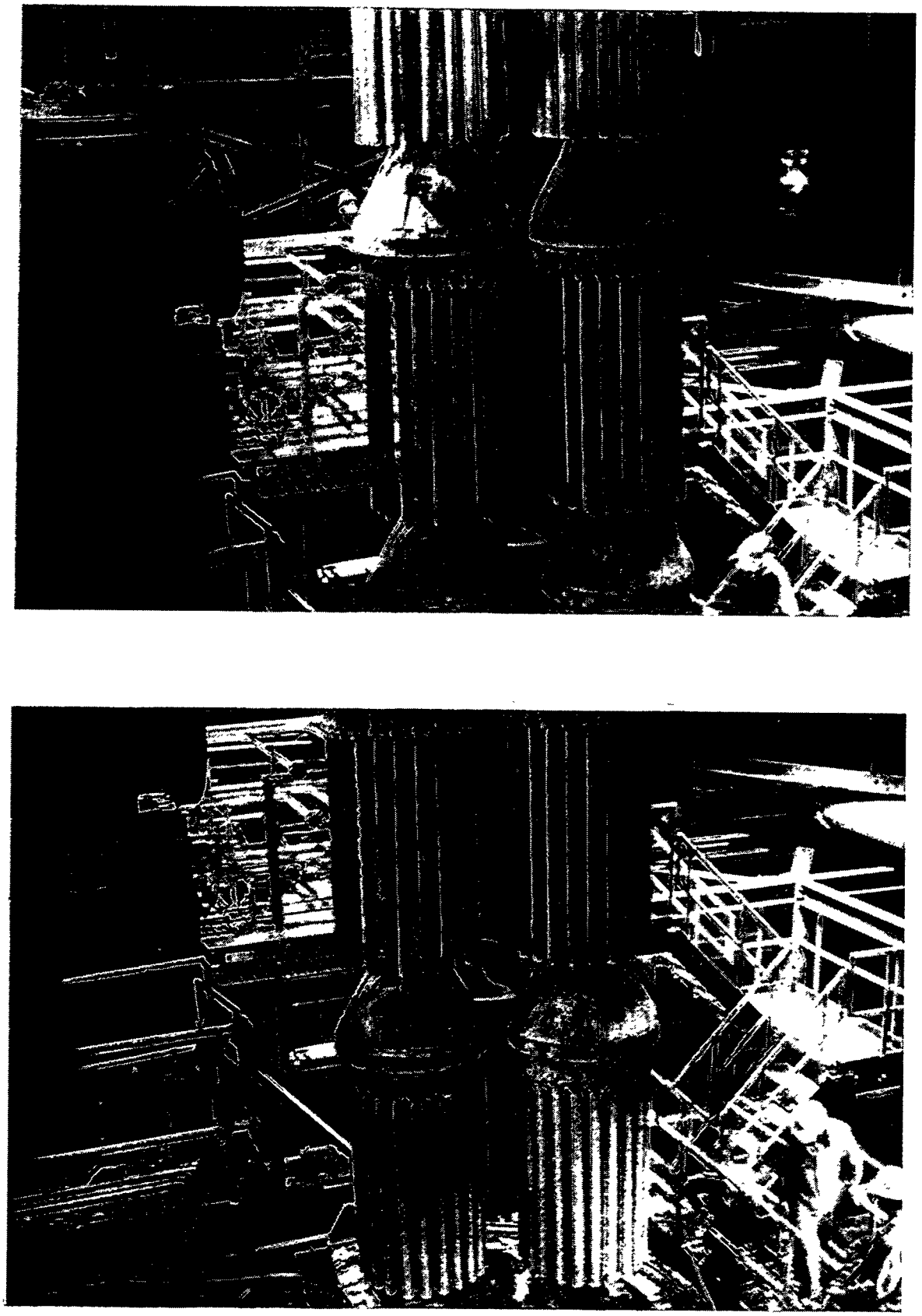

Figure 3 – Middle And Bottom Arrays In The W-APF After Conduct Of Test Segment #5

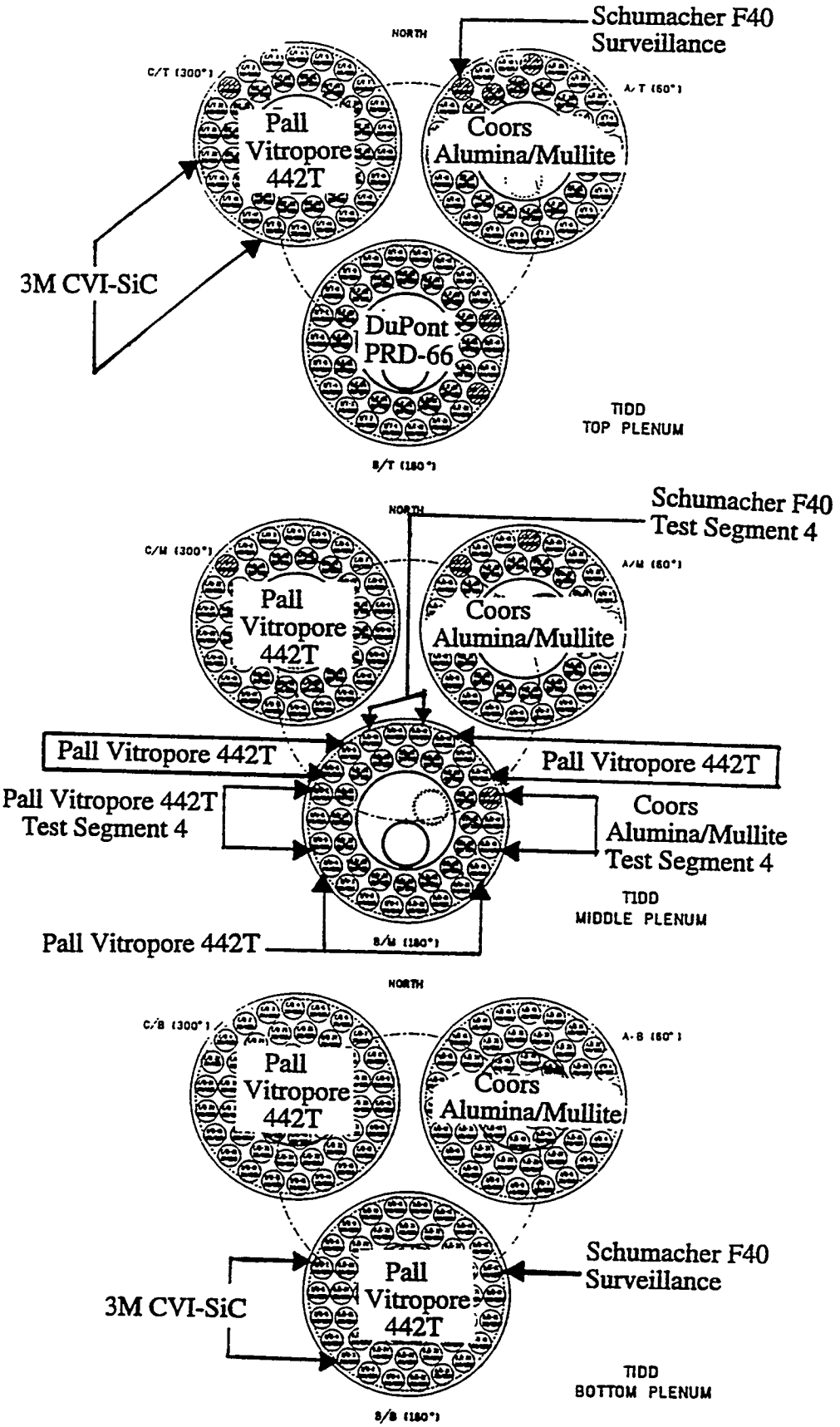

Figure 4 — Filter Locations During Operation Of The W-APF System In Test Segment #5

TABLE 2
CANDLE FILTERS USED IN THE W-APF IN TEST SEGMENT #5

Plenum Location	Filters
A/T	21 Coors Alumina/Mullite P-100A-1 1 Schumacher F40 (Surveillance)
A/M	22 Coors Alumina/Mullite P-100A-1
A/B	52 Coors Alumina/Mullite P-100A-1
B/T	22 DuPont PRD-66
B/M	3 Coors Alumina/Mullite (Test Segment 4) 3 Pall Vitropore 442T (Test Segment 4) 3 Schumacher F40 (Test Segments 3 and 4) 13 Pall Vitropore 442T
B/B	1 Schumacher F40 (Surveillance) 5 3M CVI-SiC Composite 46 Pall Vitropore 442T
C/T	5 3M CVI-SiC Composite 17 Pall Vitropore 442T
C/M	22 Pall Vitropore 442T
C/B	52 Pall Vitropore 442T

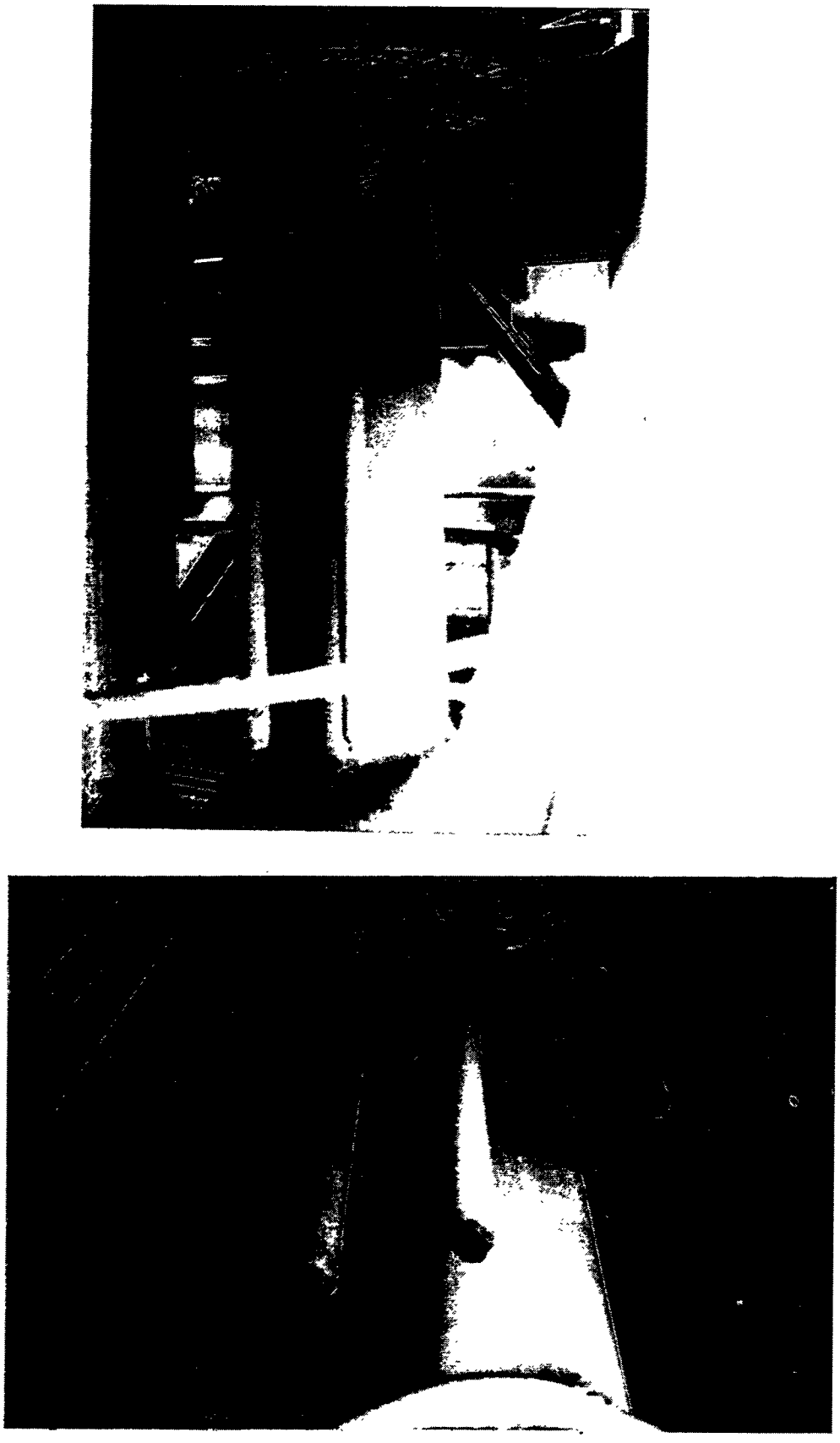

Figure 5 – W-APF B/T Array Containing The Remaining DuPont PRD-66 Candle Filters After Operation In Test Segment #5

Two Schumacher Dia Schumalith F40 surveillance candles had been installed in positions A/T-16 and B/B-16. Both filters remained intact, surviving 5855 hours of field operation. In addition three Schumacher Dia Schumalith F40 filters had been positioned in B/M-10, B/M-11, and B/M-12. These had been previously operated in Test Segments 3 and 4 at AEP, acquiring 2984 hours of field operation prior to initiating Test Segment #5. As a result of successful operation in Test Segment #5, all three Schumacher Dia Schumalith F40 candle filters acquired 4094 hours of PFBC life.

Three Coors alumina/mullite filters which had been operated in Test Segment #4 were installed in positions B/M-16, B/M-17, and B/M-18, and successfully acquired 2815 hours of PFBC operation. Similarly, three Pall Vitropore 442T filters which had been operated in Test Segment #4 were installed in positions B/M-5, B/M-6, and B/M-7, and successfully acquired 2815 hours of PFBC operation.

Although the Coors alumina/mullite, Schumacher Dia Schumalith F40, and 3M CVI-SiC composite filters visually appeared to remain intact, several of the filter elements were found to have ash tightly packed inside the bottom of the candles, causing hairline fractures to occur (Figure 6). As a result, one of the Coors alumina/mullite and one of the Schumacher Dia Schumalith F40 surveillance candles failed during disassembly from the array (Figures 7 and 8). Ash had similarly been tightly packed into the bottom of a 3M CVI-SiC composite filter, and as shown in Figure 9, the bottom of the candle had ruptured. Due to the graceful failure nature of the fiber composite matrix (i.e., fiber reinforced, fracture toughened material), the 3M CVI-SiC composite candle end cap remained attached to the body. During removal of the Pall Vitropore 442T and/or remaining DuPont PRD-66 candles, preliminary information indicated that failure of the Pall and DuPont end caps had not occurred as a result of ash fill.

As shown in Figure 10, the thermal expansion of the ID filled ash is approximately twice that of the Coors alumina/mullite and/or Schumacher Dia Schumalith F40 filter matrix. The thermal of expansion for the 3M CVI-SiC composite and DuPont PRD-66 filter matrix as identified by SRI, is similar to that shown in Figure 10 for the Coors and Schumacher materials.(1) What has been considered to result was that during failure of the DuPont PRD-66 filter elements in array A/T, fines were back pulsed into the ID of the remaining intact filter elements. During repetitive plant startups (i.e., 10 cooldown/heatup cycles during Test Segment #5), the ash in the candle ID expanded during heatup, causing a load to be applied to the ID wall of the filter element. During cooldown, hydration of the ash also increased the volume and density of the ID bore ash, again causing expansion and an additional load was applied to the ID surface of the filter elements. Ultimately, hairline cracks resulted along the end caps of several filter elements. Although hairline cracks were evident along the filter end caps at termination of Test Segment #5, the candles remained intact in the array after the lift had been conducted. Similarly, the fractured candle filter surfaces were virtually clean, free of dust tracks penetrating across the 10-15 mm walls. This indicated that fines were not carried through the filter wall during process operation, and that perhaps failure resulted during the final hours of field testing.

Since elongation of the clay bonded silicon carbide candles is known to have occurred during operation in Test Segment #4 and Test Segment #5 at AEP, the final length of these filters is expected to be somewhat different than their documented, as-manufactured filter lengths. Since Westinghouse had chosen not to clean and/or identify the resulting length of each filter element, the

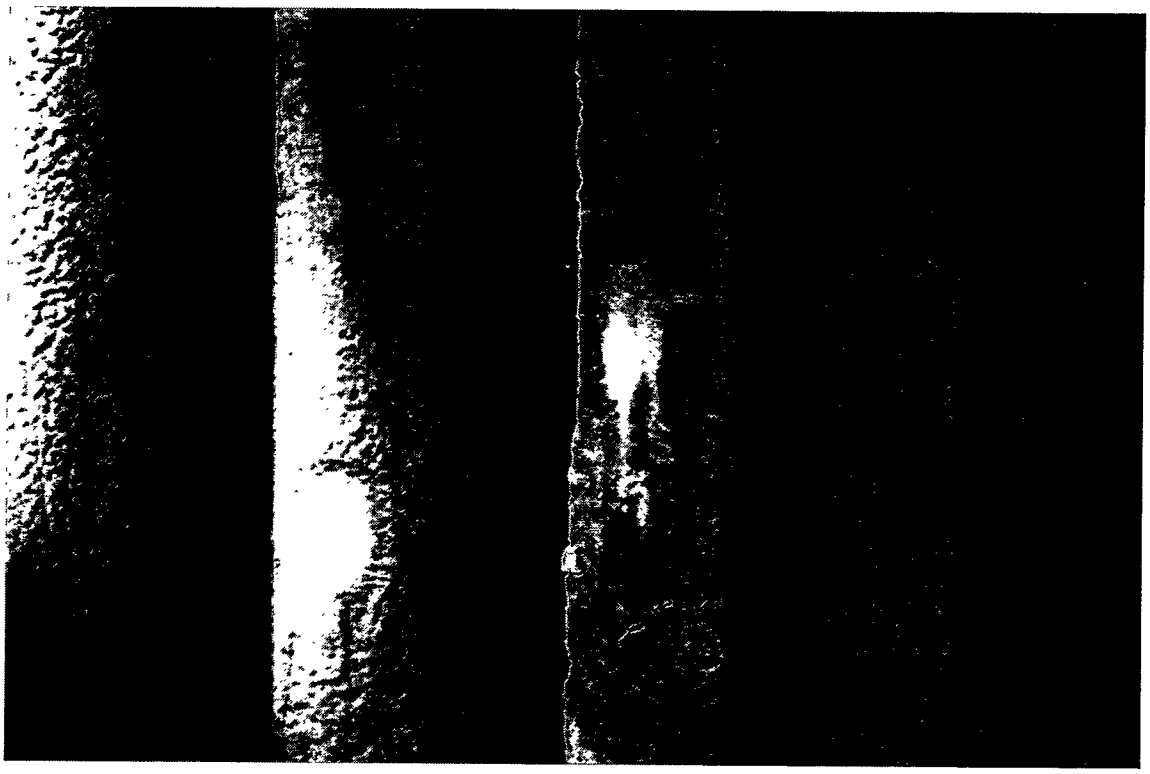

Figure 6 – Hairline Cracks Along The Bottom End Caps Of Several Ash Filled Filter Elements After Operation In Test Segment #5

Figure 7a – Ash Filled ID Bore Of A Coors Alumina/Mullite Candle Filter

Figure 7b – Ash Filled ID Bore Of A Coors Alumina/Mullite Candle Filter

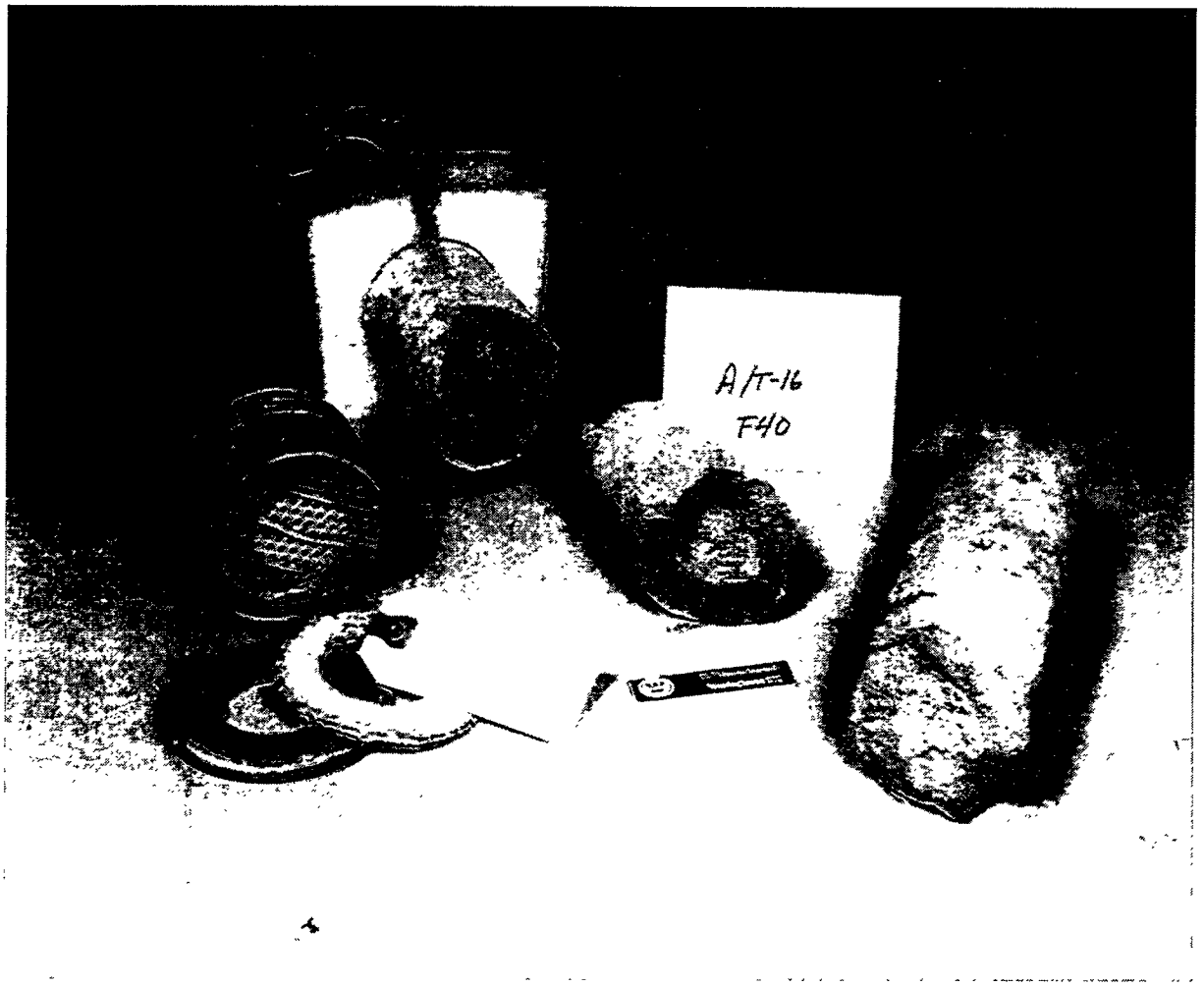

Figure 8 – Ash Filled ID Bore Of A Schumacher Dia Schumalith F40 Candle Filter

Figure 9a – Ash Filled ID Bore Of A 3M CVI-SiC Composite Candle Filter

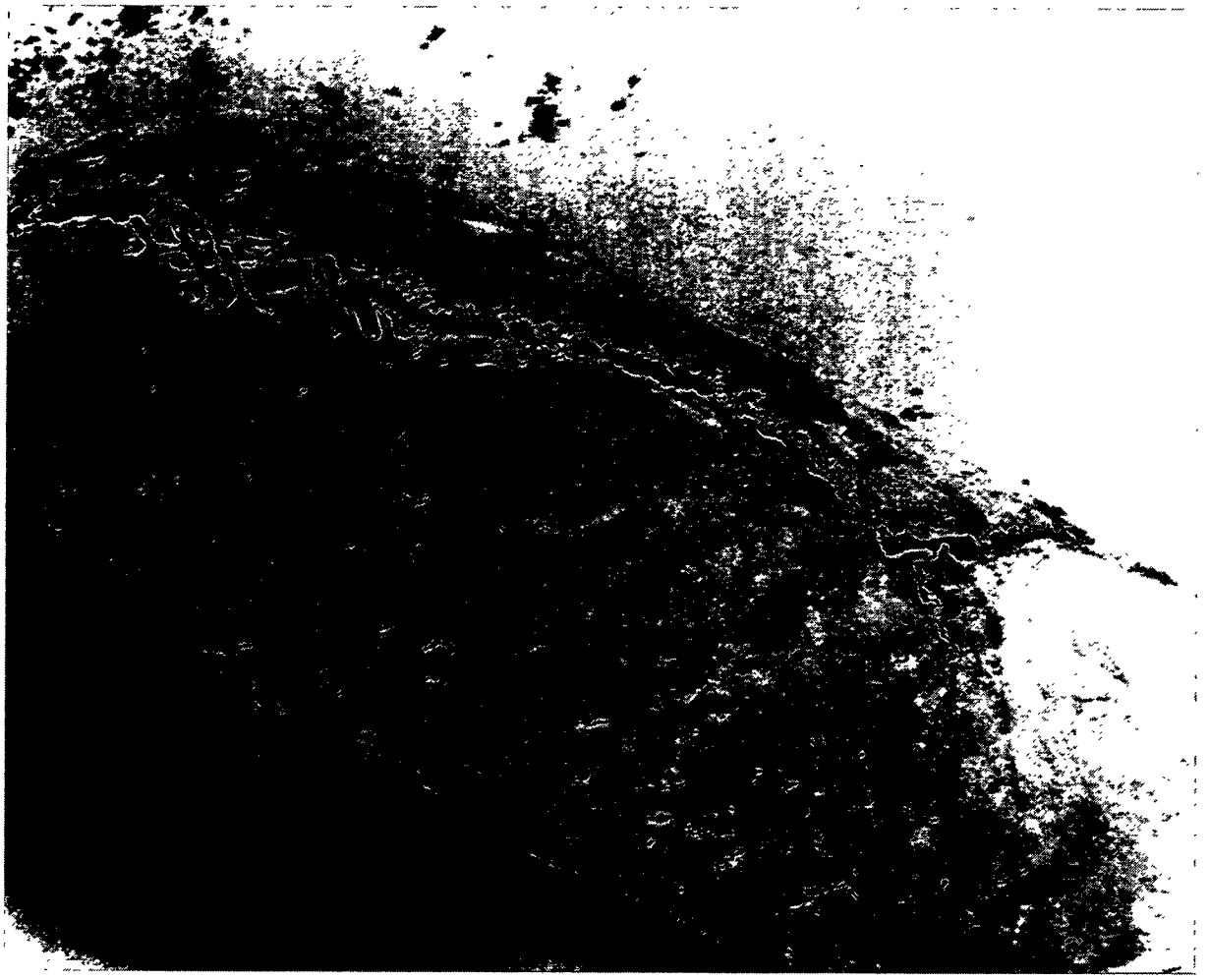

Figure 9b – Ruptured Ash Filled 3M CVI-SiC Composite Filter End Cap

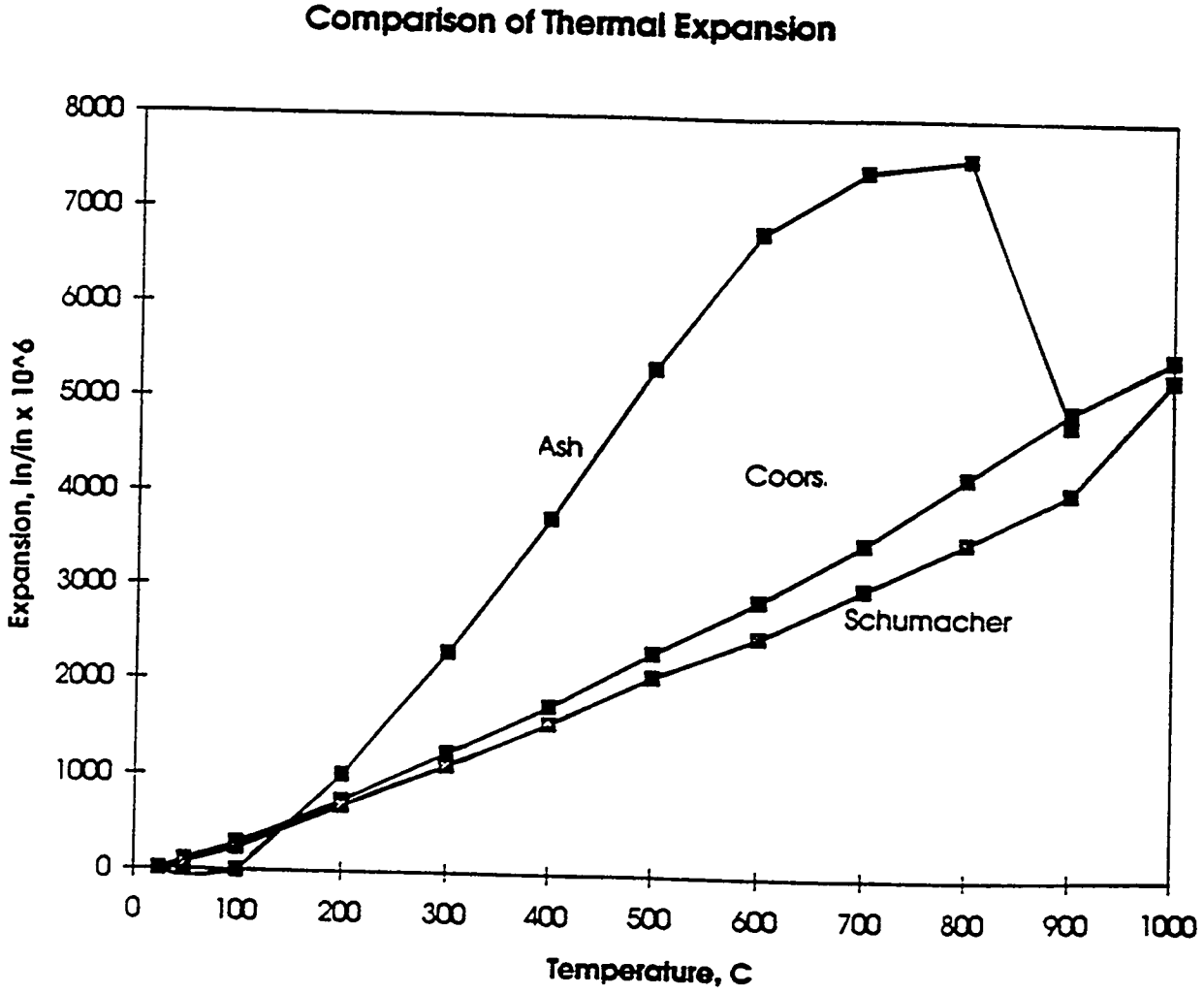

Figure 10 – Comparison Of The Thermal Expansion Of The Ash In The Candle ID Bore And Various Porous Ceramic Candle Filter Matrices

ash depth in each filter element was estimated (i.e., an average candle filter element length for each filter element type was assumed, minus respective initial wall and/or end cap thickness). As shown in Figure 11 and Table 3, ash primarily filled the top and middle candle arrays.

In the following sections, descriptions of the various W-APF arrays, as well as outer ash cake characteristics are presented.

DESCRIPTION OF THE FILTER ARRAYS

As shown in Figure 12, ash had been deposited along the outer surface of the filters in the top arrays, but had not bridged between the elements and/or plenum pipe and dust sheds after 1110 hours of operation in Test Segment #5 at AEP. A heavier ash cake deposit was, however, found along the bottom of the Schumacher Dia Schumalith F40 surveillance filter element that was positioned in location A/T-16, in comparison to the alumina/mullite candles that had been installed in Cluster A/T (i.e., bottom photo in Figure 12; top photo in Figure 13). A relatively thin dust cake layer uniformly deposited along the outer surfaces of the Coors alumina/mullite Cluster A/T's filters. In contrast, a heavier deposit remained along the Pall Vitropore 442T filter elements in Cluster C/T, and frequently a heavier dust cake deposit was found along the bottom of the Pall Vitropore 442T candle filters (i.e., initiation of the elephant foot formation; bottom photo of Figure 14). Heavier deposits of hard encrusted ash were found along all of the top array filter holder mounts (Figure 14).

Moving to the A/M array, a thin ash cake deposit was readily evident along the Coors alumina/mullite filter elements (Figure 15). Ash "flow streamers" were visibly evident along the dust cake surface. The top photograph of Figure 15a shows the mid-body fracture of the alumina/mullite candle filter which had been positioned in location A/M-16. As opposed to the 6-8 inch longitudinal fractures which resulted in the alumina/mullite filter matrix after operation in Ahlstrom's 900°C pressurized circulating fluidized-bed combustion (PCFBC) test facility in Karhula, Finland, failure of the Coors alumina/mullite filter at AEP spanned only 2-3 inches of the filter body after 1110 hours of lower temperature operation.

Figure 16 illustrates the heavier dust cake deposit that resulted along the Pall Vitropore 442T candles in the C/M array. Nodules were readily evident, as well as the thicker ash cake deposit which resulted along the end cap of the Pall filter elements (i.e., initiation of the elephant foot formation). Frequently spalling of the heavier dust cake deposit was observed along the bottom end cap of the Pall Vitropore 442T filter elements (i.e., top photo in Figure 16b).

Figures 17 and 18 provide a comparison of the residual dust cake that deposited and remained along the Coors alumina/mullite (top photographs) and Pall Vitropore 442T (bottom photographs) candles in the bottom filter arrays. Heavier deposits of ash were evident in these arrays in comparison to the deposits which formed along the top and middle arrays. The relatively heavy nodular ash formation that remained along the bottom of the Pall Vitropore 442T candles is shown in Figure 18. In the bottom photograph of Figure 18, the ash nodules are seen to be "buried' beneath a final ash deposit which covered the Pall Vitropore 442T filters.

As shown in Figure 19, a relatively uniform ash coating covered the ten 3M CVI-SiC candles that were positioned in the C/T and B/B arrays. Figure 20 provides an additional

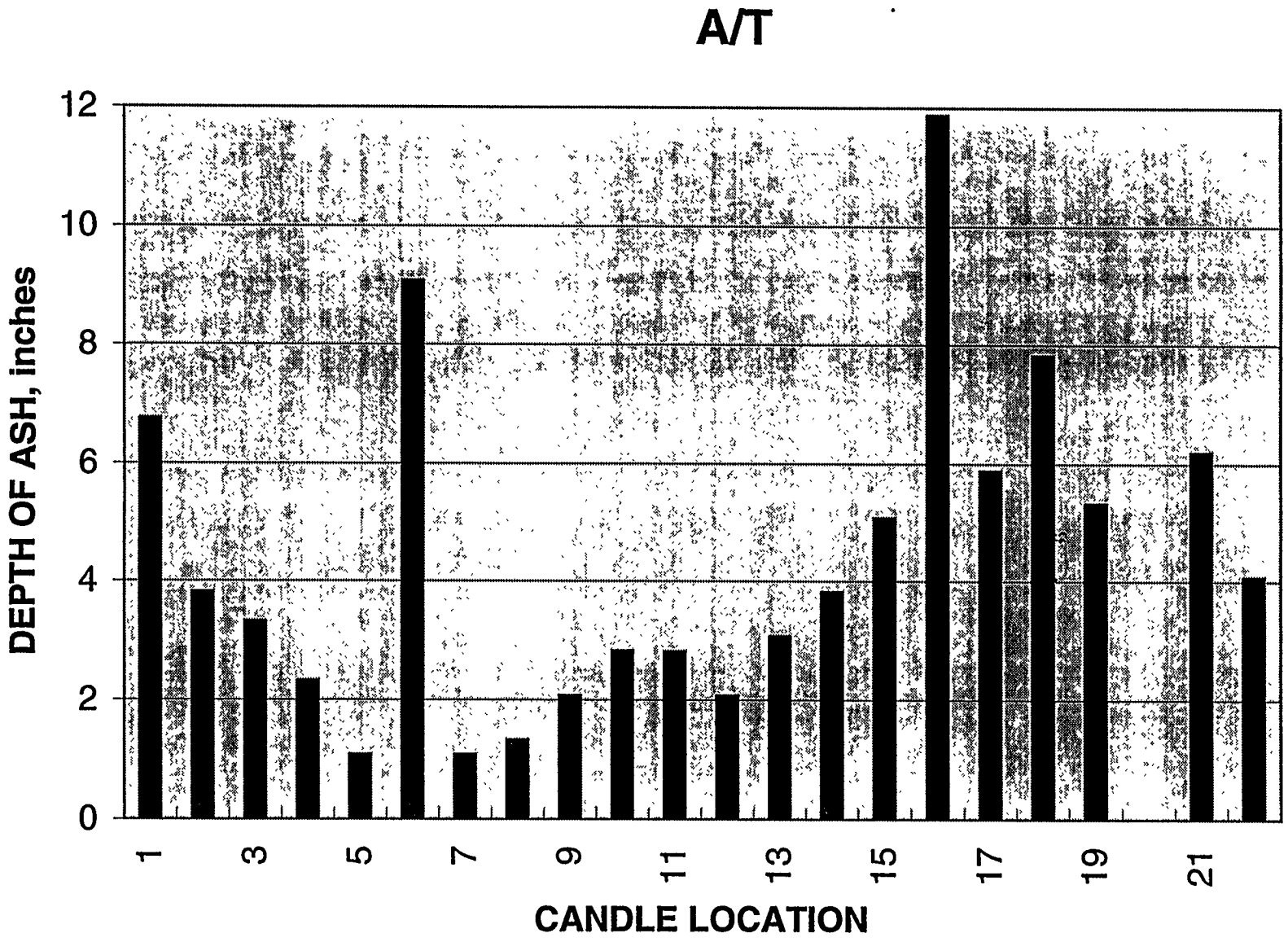

Figure 11a – Depth Of Ash In The A/T Schumacher Dia Schumalith F40 Surveillance Filter And Coors Alumina/Mullite Candle Filters (Test Segment #5)

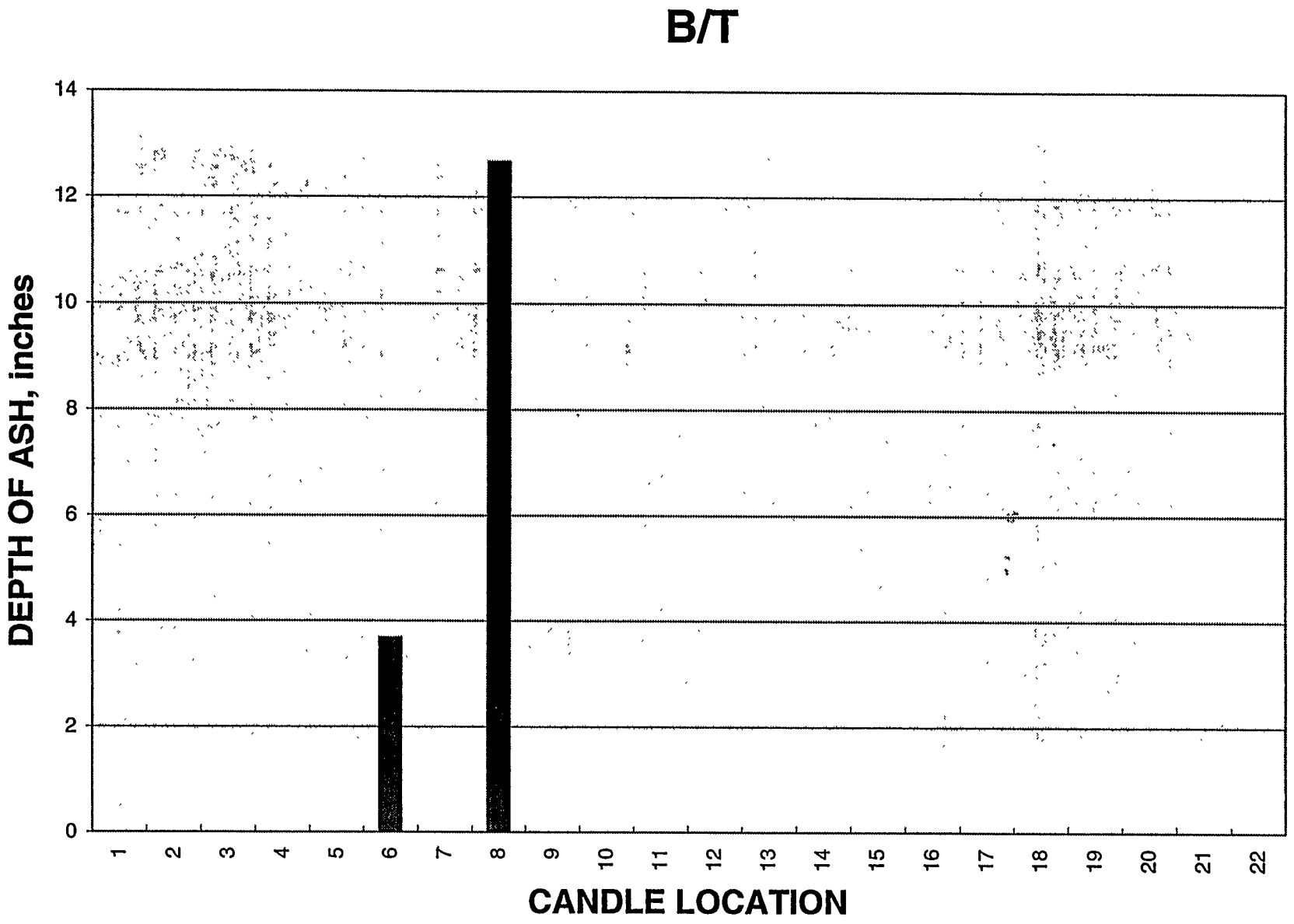

Figure 11b – Depth Of Ash In The Remaining B/T DuPont PRD-66 Candle Filters (Test Segment #5)

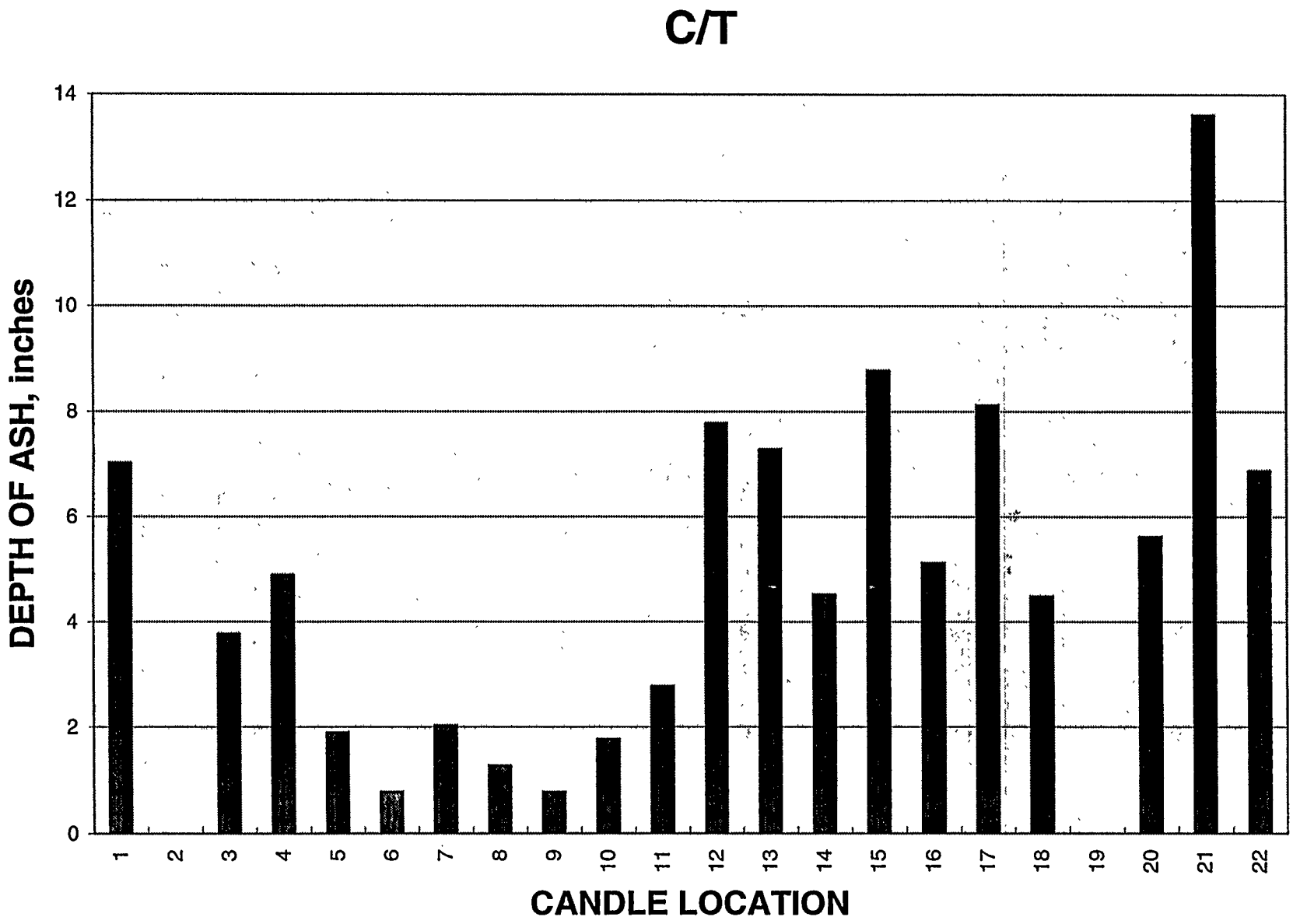

Figure 11c – Depth Of Ash In The C/T Pall Vitropore 442T and 3M CVI-SiC Composite Filters (Test Segment #5)

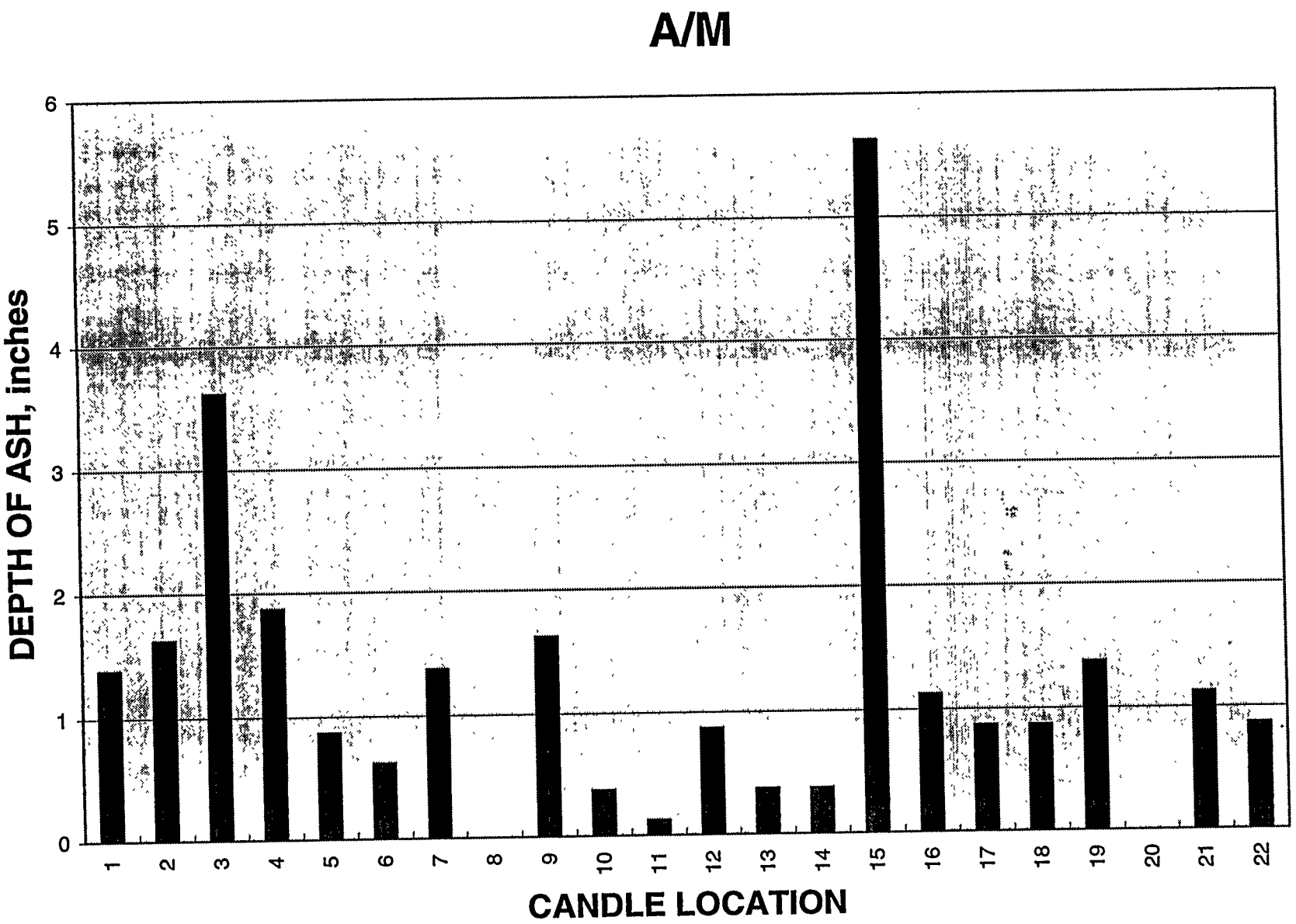

Figure 11d – Depth Of Ash In The A/M Coors Alumina/Mullite Filters (Test Segment #5)

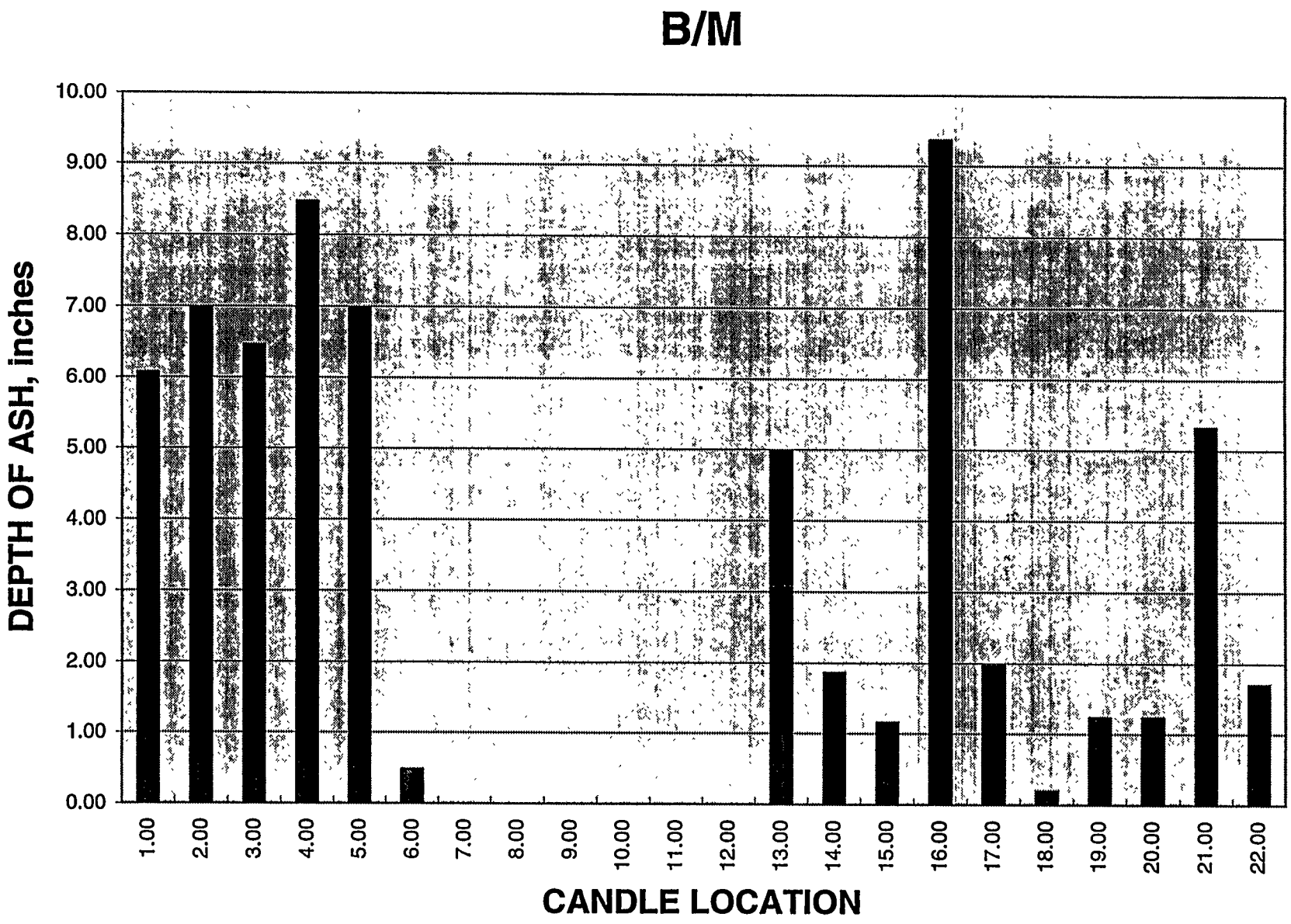

Figure 11e – Depth Of Ash In The Coors Alumina/Mullite, Schumacher Dia Schumalith F40, And Pall Vitropore 442T Candle Filters In Array B/M (Test Segment #5)

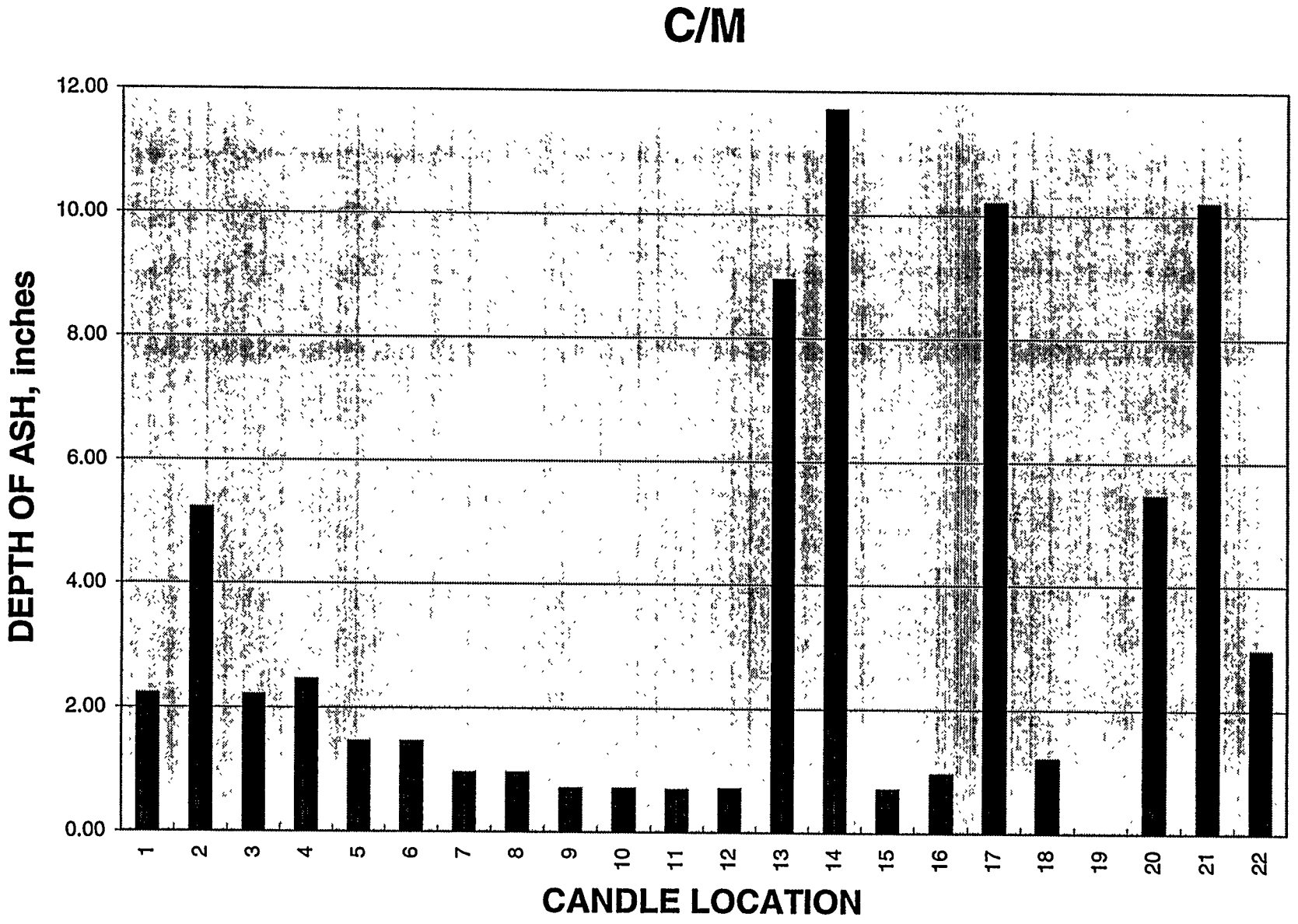

Figure 11f – Depth Of Ash In The C/M Pall Vitropore 442T Filters (Test Segment #5)

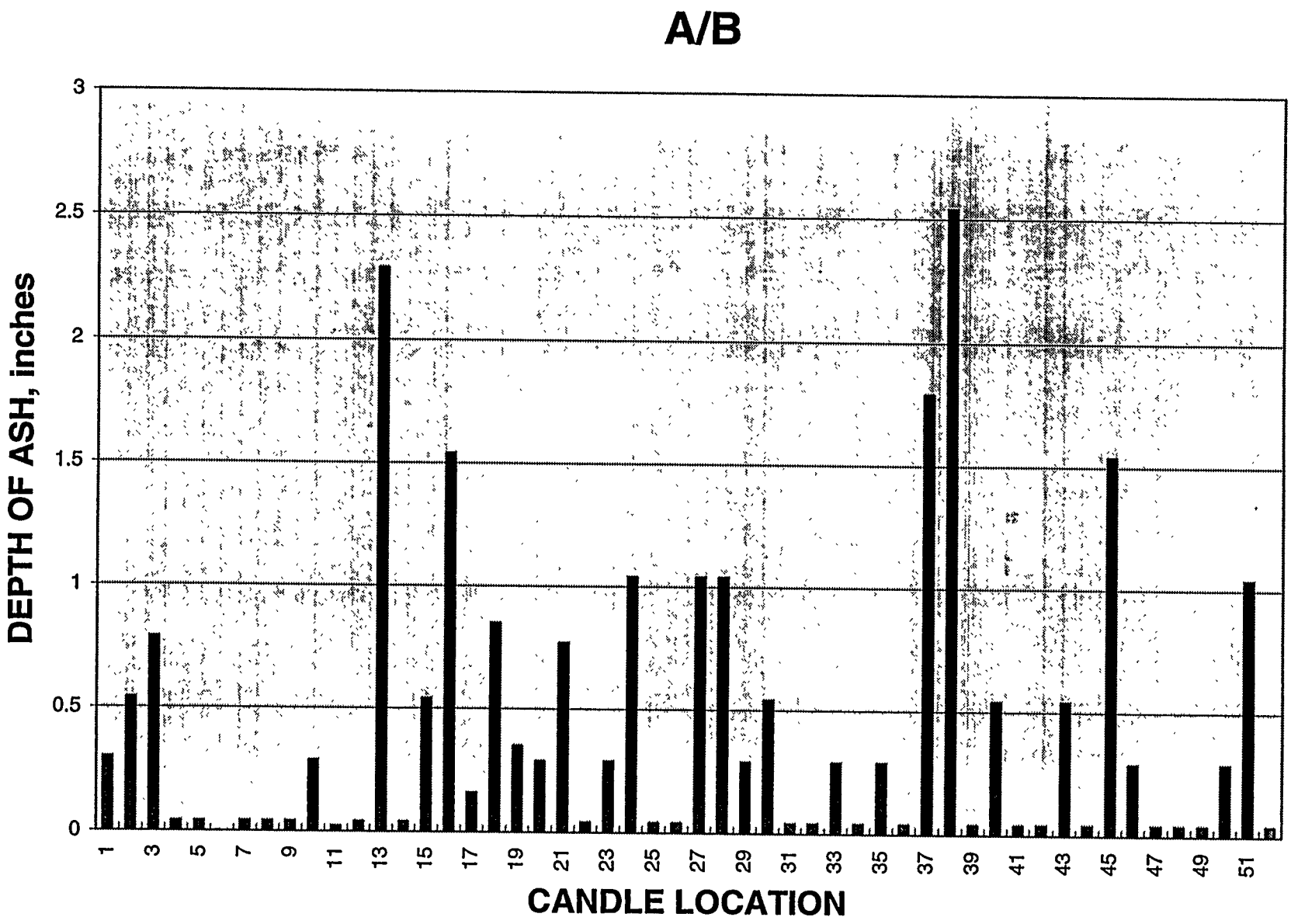

Figure 11g – Depth Of Ash In The A/B Coors Alumina/Mullite Filters (Test Segment #5)

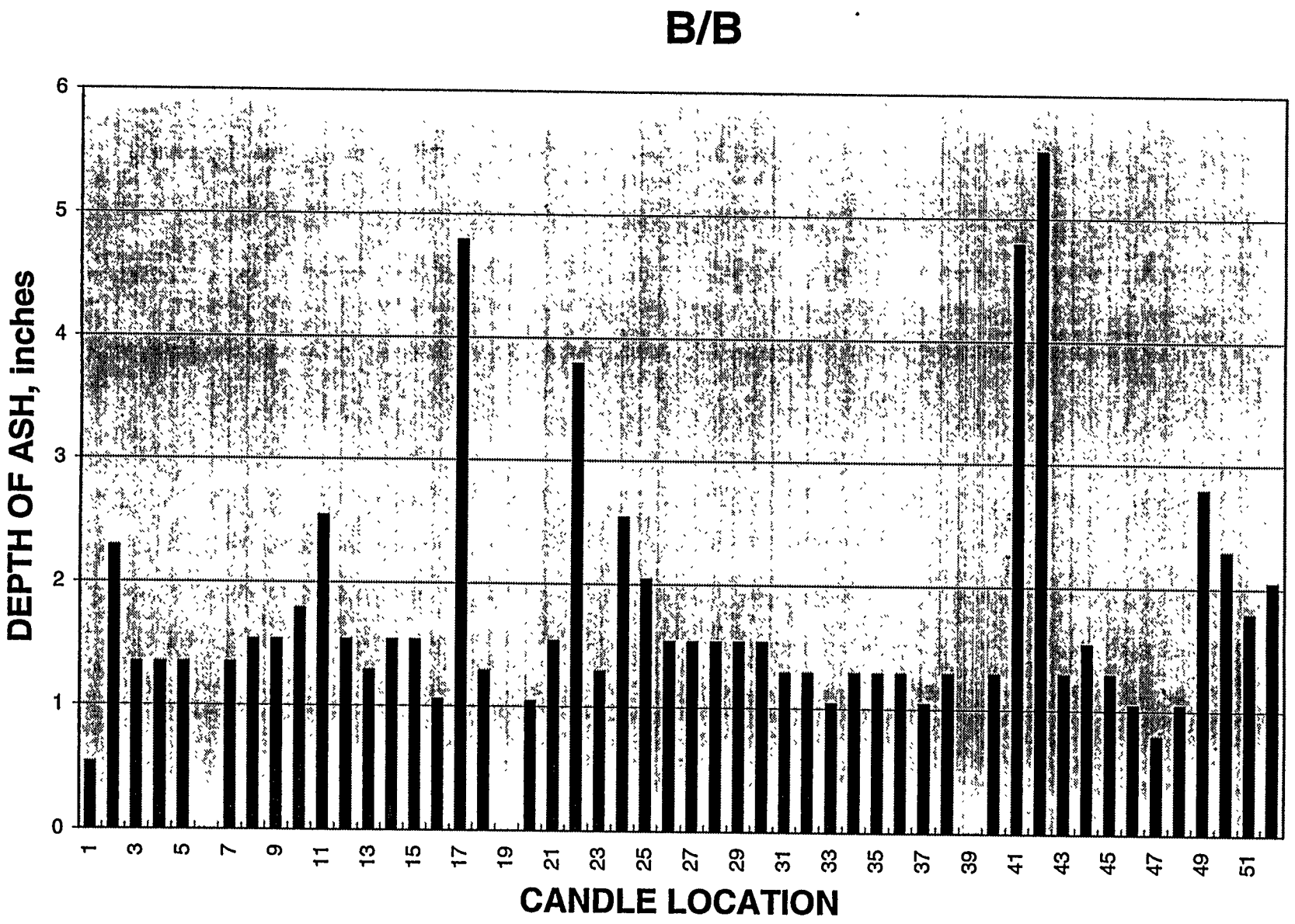

Figure 11h – Depth Of Ash In The B/B Schumacher Dia Schumalith F40 Surveillance Filter and Pall Vitropore 442T And 3M CVI-SiC Composite Filters (Test Segment #5)

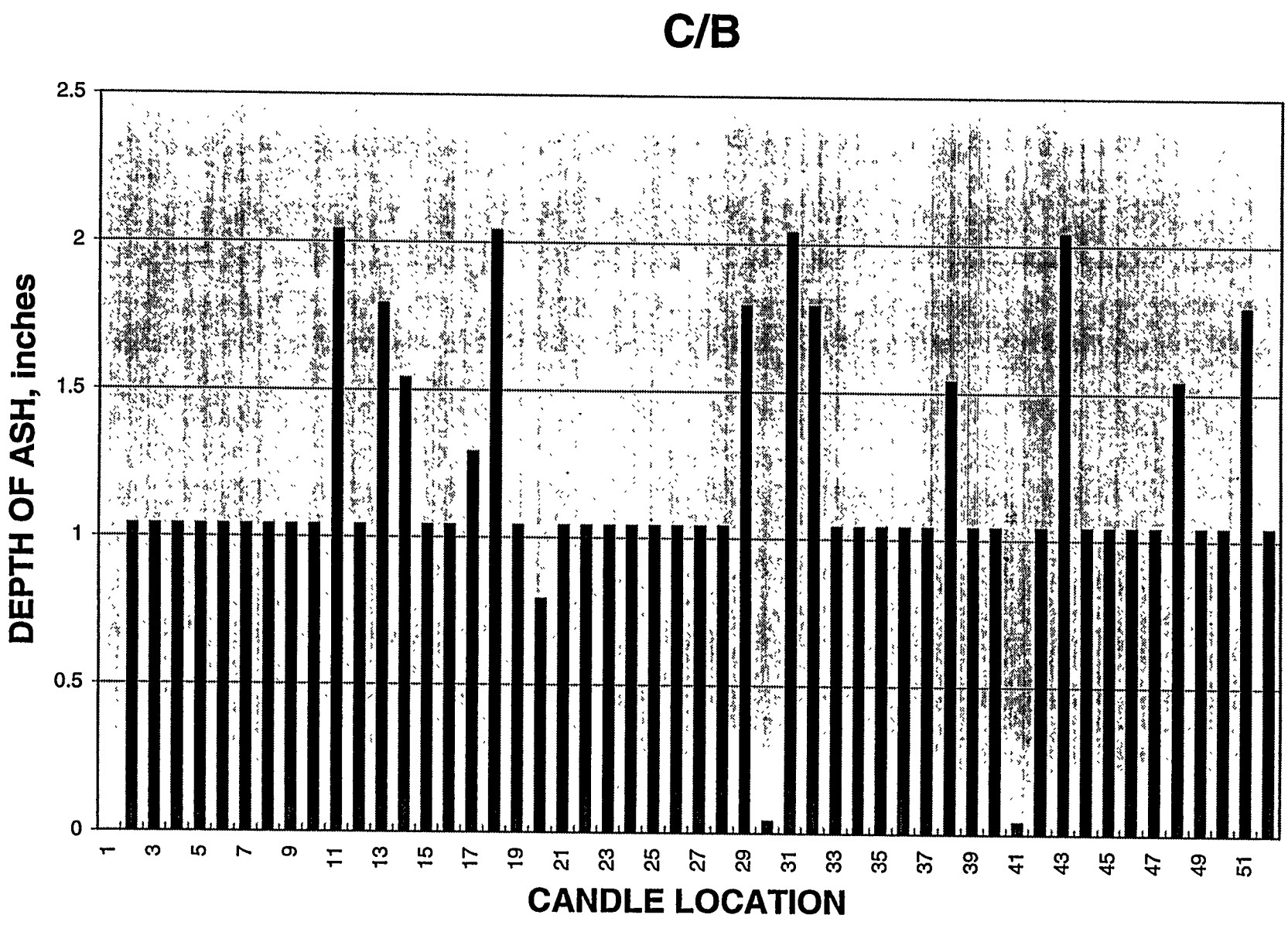

Figure 11i –Depth Of Ash In The C/B Pall Vitropore 442T Filters (Test Segment #5)

TABLE 3
CANDLE FILTER LENGTHS AND ASH DEPTHS
-- TOP ARRAYS --
-- W-APF AEP TEST SEGMENT #5, MAY 1995 --

Filter Array	Final Length (inch)	Ash Depth (inch)	Filter Array	Final Length (inch)	Ash Depth (inch)	Filter Array	Final Length (inch)	Ash Depth (inch)
A/T-1	59.57	52.32	B/T-1		NA	C/T-1	59.25	51.26
A/T-2		55.25	B/T-2		NA	C/T-2		
A-T-3		55.75	B/T-3		NA	C/T-3		54.5
A/T-4		56.75	B/T-4		NA	C/T-4		53.38
A/T-5		58	B/T-5		NA	C/T-5		56.38
A/T-6		50	B/T-6	59.13	54.49	C/T-6		57.5
A/T-7		58	B/T-7		NA	C/T-7		56.25
A/T-8		57.75	B/T-8	59.17	45.51	C/T-8		57
A/T-9		57	B/T-9		NA	C/T-9		57.5
A/T-10		56.25	B/T-10		NA	C/T-10		56.5
A/T-11	59.21	56.26	B/T-11		NA	C/T-11	59.25	55.51
A/T-12		57	B/T-12		NA	C/T-12		50.5
A/T-13		56	B/T-13		NA	C/T-13		51
A/T-14		55.25	B/T-14		NA	C/T-14		53.75
A/T-15		54	B/T-15		NA	C/T-15		49.5
A/T-16	59.88	47.2	B/T-16		NA	C/T-16 (3M)		55
A/T-17	59.17	53.19	B/T-17		NA	C/T-17 (3M)		52
A/T-18		51.25	B/T-18		NA	C/T-18 (3M)	60.31	55.63
A/T-19		53.75	B/T-19		NA	C/T-19 (3M)		--
A/T-20			B/T-20		NA	C/T-20 (3M)		54.5
A/T-21		52.88	B/T-21		NA	C/T-21		46.5
A/T-22		55	B/T-22		NA	C/T-22		53.25

NA: Filter Failed.
A/T: 10 mm (0.39 inch) Alumina/Mullite End Cap.
B/T: 25 mm (0.98 inch) DuPont End Cap.
C/T: 25 mm (0.98 inch) Pall Vitropore 442T End Cap; 5 mm (0.2 inch) 3M CVI-SiC Composite End Cap.

TABLE 3 (Cont'd)
CANDLE FILTER LENGTHS AND ASH DEPTHS
-- MIDDLE ARRAYS --
-- W-APF AEP TEST SEGMENT #5, MAY 1995 --

Filter Array	Final Length (inch)	Ash Depth (inch)	Filter Array	Final Length (inch)	Ash Depth (inch)	Filter Array	Final Length (inch)	Ash Depth (inch)
A/M-1	59.76	57.99	B/M-1 (P)	59.25	52.40	C/M-1	59.21	55.98
A/M-2		57.75	B/M-2 (P)	59.29	51.50	C/M-2	59.17	52.99
A/M-3		55.75	B/M-3 (P)	59.21	52.01	C/M-3		56
A/M-4		57.5	B/M-4 (P)	59.21	50.00	C/M-4		55.75
A/M-5		58.5	B/M-5 (P)	59.96	51.50	C/M-5		56.75
A/M-6		58.75	B/M-6 (P)	59.80	57.99	C/M-6		56.75
A/M-7		58	B/M-7 (P)	59.88		C/M-7		57.25
A/M-8			B/M-8 (P)	59.25		C/M-8		57.25
A/M-9		57.75	B/M-9 (P)	59.17		C/M-9		57.5
A/M-10		59	B/M-10 (S)	59.80		C/M-10		57.5
A/M-11	59.76	59.25	B/M-11 (S)	59.76		C/M-11	59.17	57.52
A/M-12		58.5	B/M-12 (S)	59.72		C/M-12		57.5
A/M-13		59	B/M-13 (P)	59.25	53.50	C/M-13		49.25
A/M-14		59	B/M-14 (P)	59.21	56.61	C/M-14		46.5
A/M-15		53.75	B/M-15 (P)	59.25	57.32	C/M-15		57.5
A/M-16		58.25	B/M-16 (C)	59.09	49.37	C/M-16		57.25
A/M-17		58.5	B/M-17 (C)	59.13	56.77	C/M-17		48
A/M-18		58.5	B/M-18 (C)	59.13	58.54	C/M-18		57
A/M-19		58	B/M-19 (P)	59.13	57.24	C/M-19		
A/M-20			B/M-20 (P)	59.17	57.24	C/M-20		52.75
A/M-21		58.25	B/M-21 (P)	59.29	53.15	C/M-21		48
A/M-22		58.5	B/M-22 (P)	59.17	56.77	C/M-22		55.25

A/M: 10 mm (0.39 inch) Alumina/Mullite End Cap.
B/M: Combination Of Coors (C); Vitropore 442T (P); Schumacher F40 (S) From Various Test Segments.
C/M: 25 mm (0.98 inch) Pall Vitropore 442T End Cap.

TABLE 3 (Cont'd)
CANDLE FILTER LENGTHS AND ASH DEPTHS
-- BOTTOM ARRAYS --
-- W-APF AEP TEST SEGMENT #5, MAY 1995 --

Filter Array	Final Length (inch)	Ash Depth (inch)	Filter Array	Final Length (inch)	Ash Depth (inch)	Filter Array	Final Length (inch)	Ash Depth (inch)
A/B-1	59.21	58.74	B/B-1	59.17	58.5	C/B-1		
A/B-2		58.5	B/B-2		56.75	C/B-2		58
A/B-3		58.25	B/B-3 (3M)		59	C/B-3		58
A/B-4		59	B/B-4 (3M)		59	C/B-4		58
A/B-5		59	B/B-5 (3M)		59	C/B-5		58
A/B-6		59.25	B/B-6 (3M)	60.55		C/B-6		58
A/B-7		59	B/B-7 (3M)		59	C/B-7		58
A/B-8		59	B/B-8		57.5	C/B-8		58
A/B-9		59	B/B-9		57.5	C/B-9		58
A/B-10		58.75	B/B-10		57.25	C/B-10		58
A/B-11	59.84	59.02	B/B-11		56.5	C/B-11	59.25	57
A/B-12		59	B/B-12		57.5	C/B-12		58
A/B-13		56.75	B/B-13		57.75	C/B-13		57.25
A/B-14		59	B/B-14		57.5	C/B-14		57.5
A/B-15		58.5	B/B-15		57.5	C/B-15		58
A/B-16		57.5	B/B-16	59.92	57.99	C/B-16		58
A/B-17		58.88	B/B-17		54.25	C/B-17		57.75
A/B-18		58.19	B/B-18		57.75	C/B-18		57
A/B-19		58.69	B/B-19			C/B-19		58
A/B-20		58.75	B/B-20		58	C/B-20		58.25
A/B-21	59.25	58.27	B/B-21		57.5	C/B-21		58
A/B-22		59	B/B-22		55.25	C/B-22		58
A/B-23		58.75	B/B-23		57.75	C/B-23		58
A/B-24		58	B/B-24		56.5	C/B-24		58
A/B-25		59	B/B-25		57	C/B-25		58
A/B-26		59	B/B-26		57.5	C/B-26		58
A/B-27		58	B/B-27		57.5	C/B-27		58
A/B-28		58	B/B-28		57.5	C/B-28		58
A/B-29		58.75	B/B-29		57.5	C/B-29		57.25
A/B-30		58.5	B/B-30		57.5	C/B-30		59

TABLE 3 (Cont'd)
CANDLE FILTER LENGTHS AND ASH DEPTHS
-- BOTTOM ARRAYS --
-- W-APF AEP TEST SEGMENT #5, MAY 1995 --

Filter Array	Final Length (inch)	Ash Depth (inch)	Filter Array	Final Length (inch)	Ash Depth (inch)	Filter Array	Final Length (inch)	Ash Depth (inch)
A/B-31		59	B/B-31		57.75	C/B-31		57
A/B-32		59	B/B-32		57.75	C/B-32		57.25
A/B-33		58.75	B/B-33		58	C/B-33		58
A/B-34		59	B/B-34		57.75	C/B-34		58
A/B-35		58.75	B/B-35		57.75	C/B-35		58
A/B-36		59	B/B-36		57.75	C/B-36		58
A/B-37		57.25	B/B-37		58	C/B-37		58
A/B-38		56.5	B/B-38		57.75	C/B-38		57.5
A.B-39		59	B/B-39			C/B-39		58
A/B-40		58.5	B/B-40		57.75	C/B-40		58
A/B-41		59	B/B-41		54.25	C/B-41		59
A/B-42		59	B/B-42		53.5	C/B-42		58
A.B-43		58.5	B/B-43		57.75	C/B-43		57
A/B-44		59	B/B-44		57.5	C/B-44		58
A/B-45		57.5	B/B-45		57.75	C/B-45		58
A/B-46		58.75	B/B-46		58	C/B-46		58
A/B-47		59	B/B-47		58.25	C/B-47		58
A/B-48		59	B/B-48		58	C/B-48		57.5
A/B-49		59	B/B-49		56.25	C/B-49		58
A/B-50		58.75	B/B-50		56.75	C/B-50		58
A/B-51		58	B/B-51		57.25	C/B-51		57.25
A/B-52		59	B/B-52		57	C/B-52		58

A/B: 10 mm (0.39 inch) Alumina/Mullite End Cap.
B/B: 25 mm (0.98 inch) Pall Vitropore 442T End Cap; 5 mm (0.20 inch) 3M CVI-SiC Composite End Cap.
C/B: 25 mm (0.98 inch) Pall Vitropore 442T End Cap.

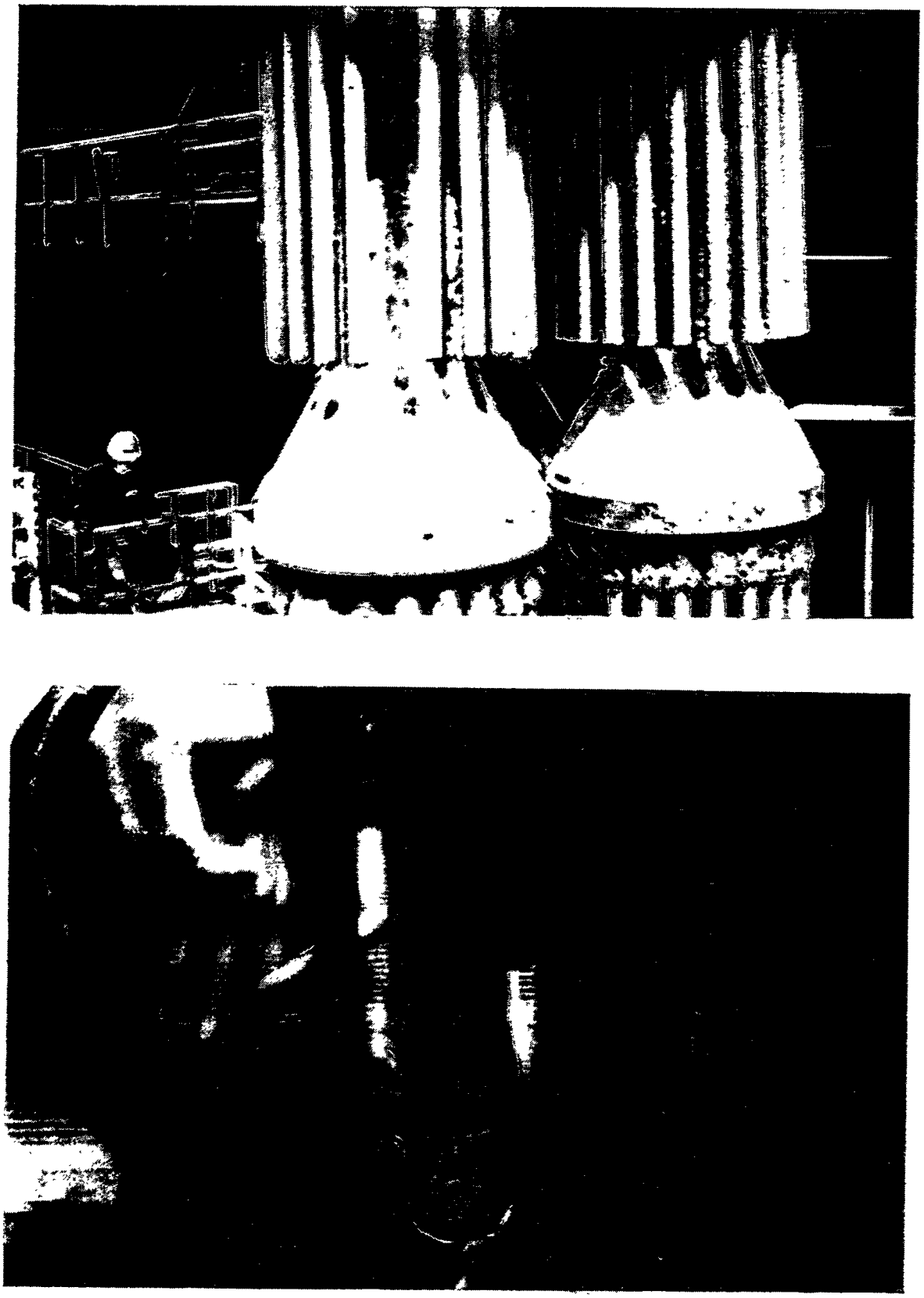

Figure 12 — W-APF Top Filter Arrays

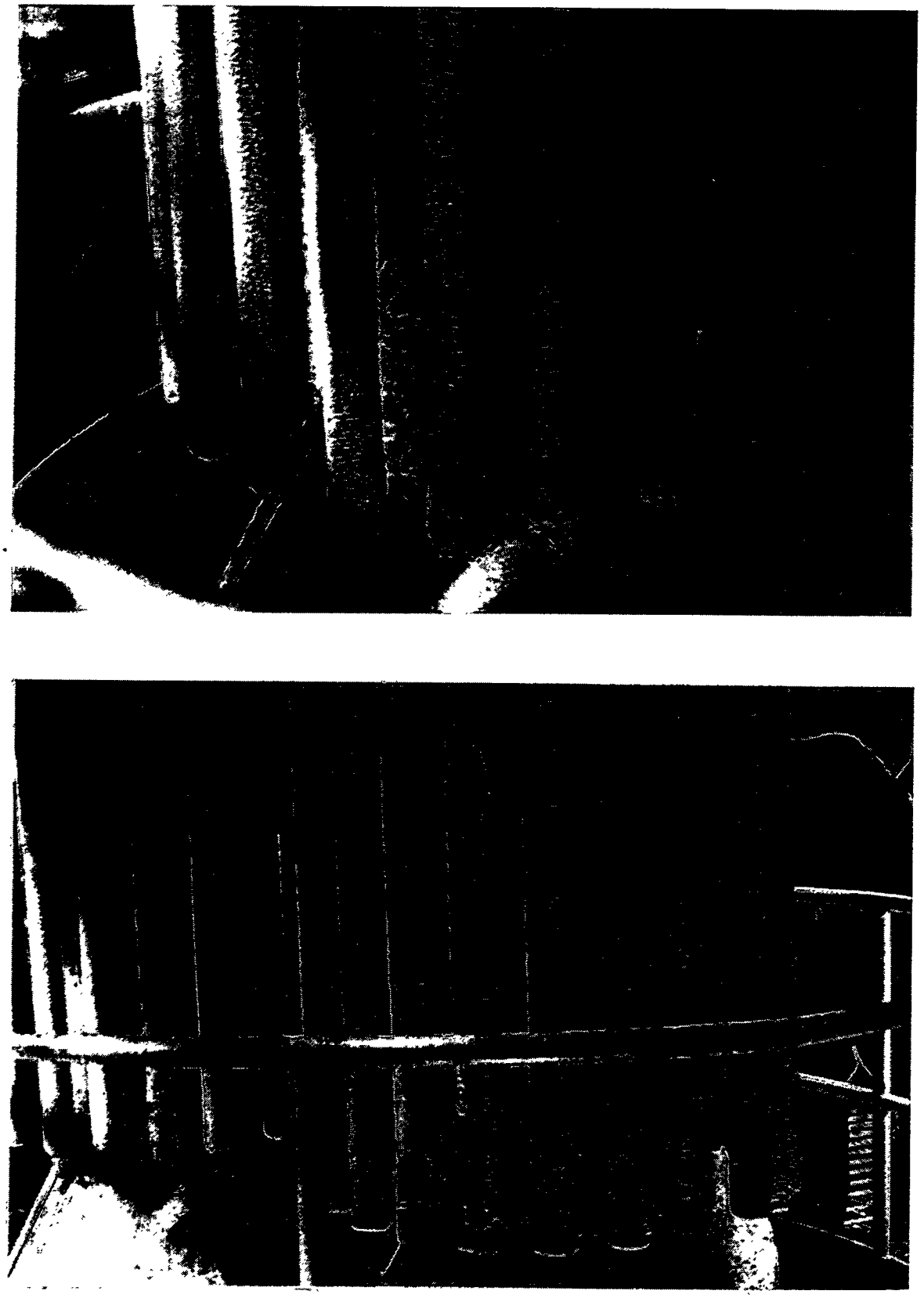

Figure 13 – Thin Dust Cake Formation Along The A/T Coors Alumina/Mullite Candle Filters. Thicker Dust Cake Formation Along the C/T Pall Vitropore 442T Candle Filters.

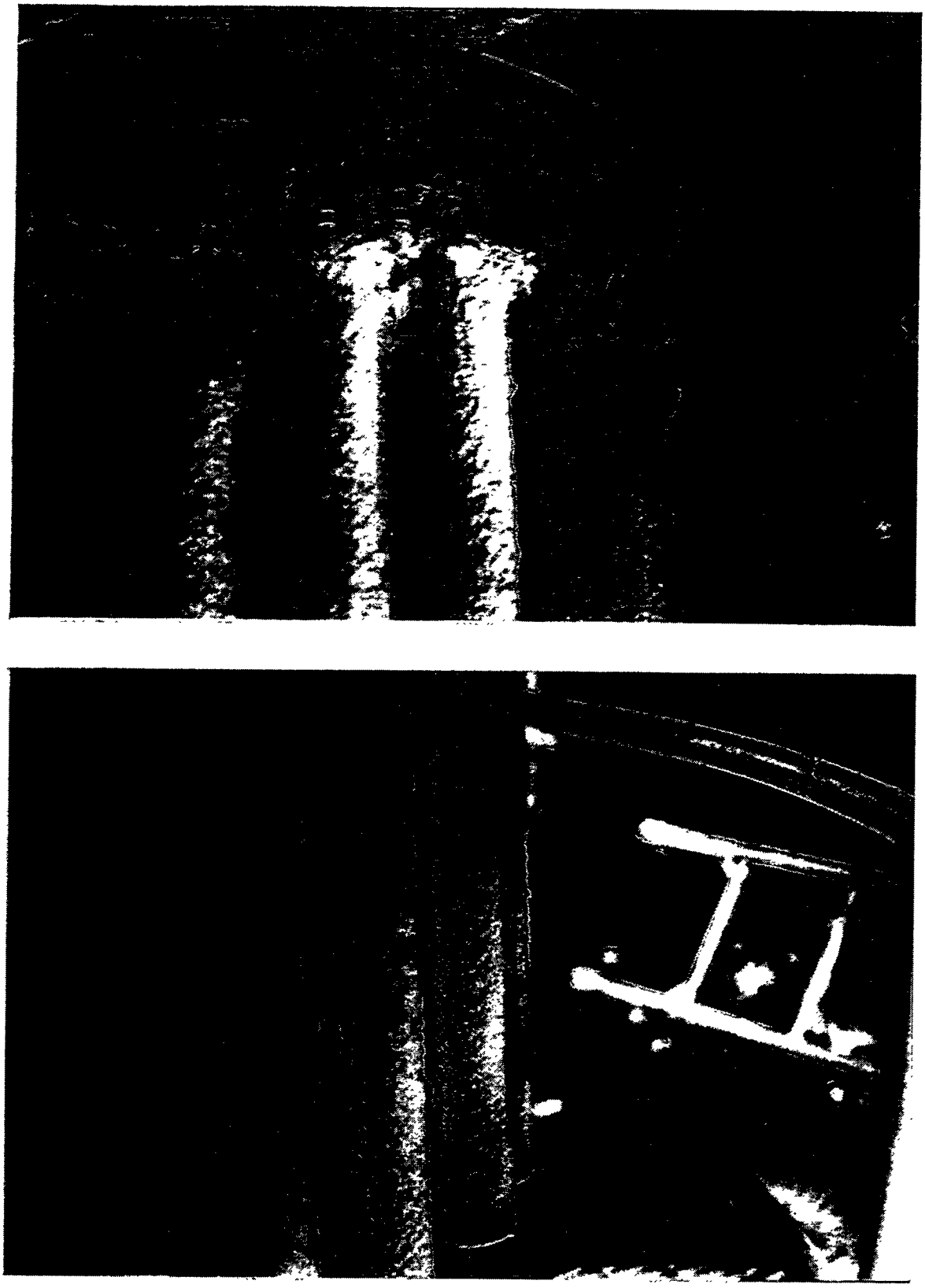

Figure 14 – Heavy Ash Cake Deposits Found Along The Top Array Filter Holder Mounts (Top Photo). Heavy Ash Cake Deposits Along The C/T Pall Vitropore 442T Filter Elements (Bottom Photo).

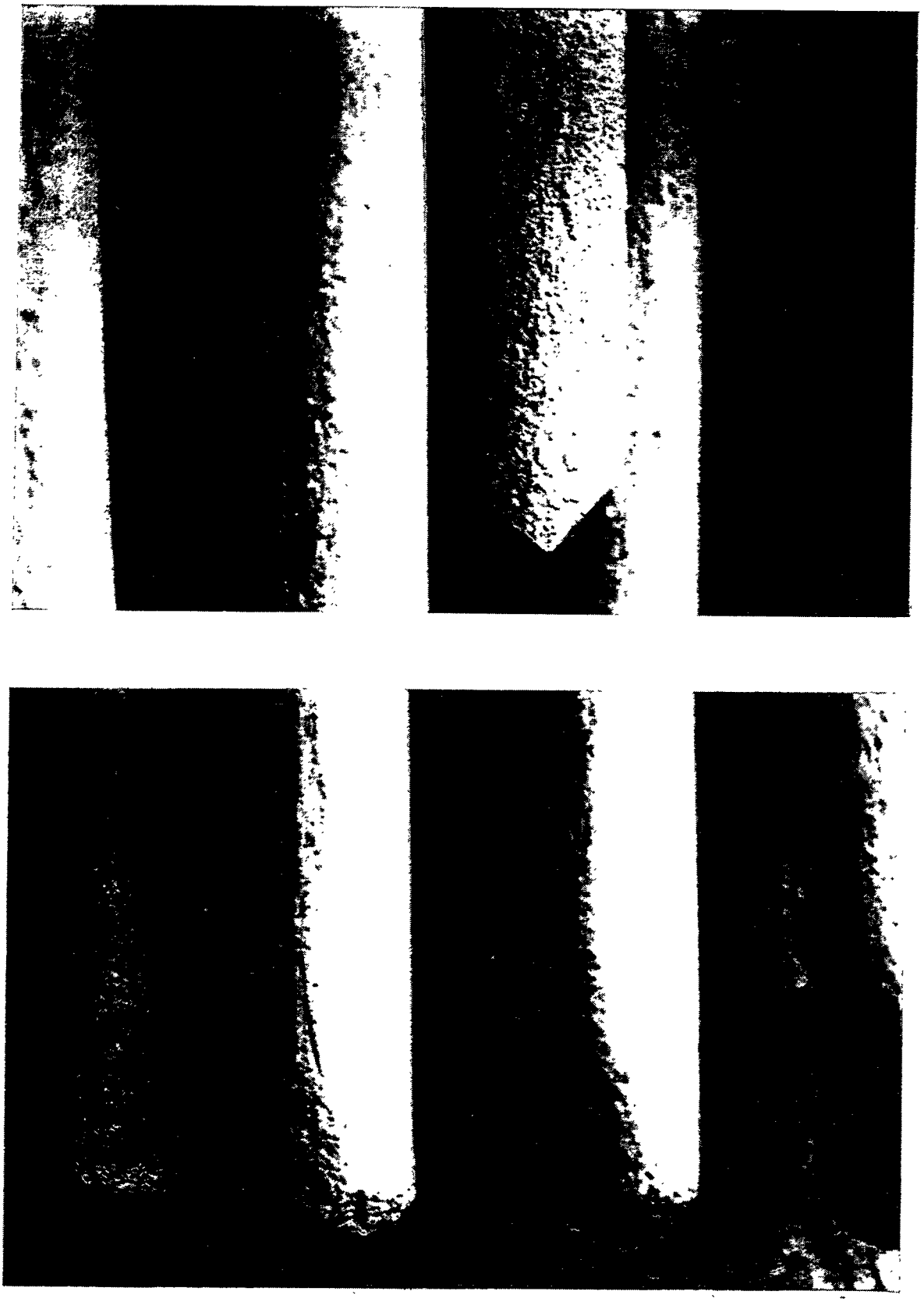

Figure 15a – Fractured Coors Alumina/Mullite Candle Filter (Test Segment #5)

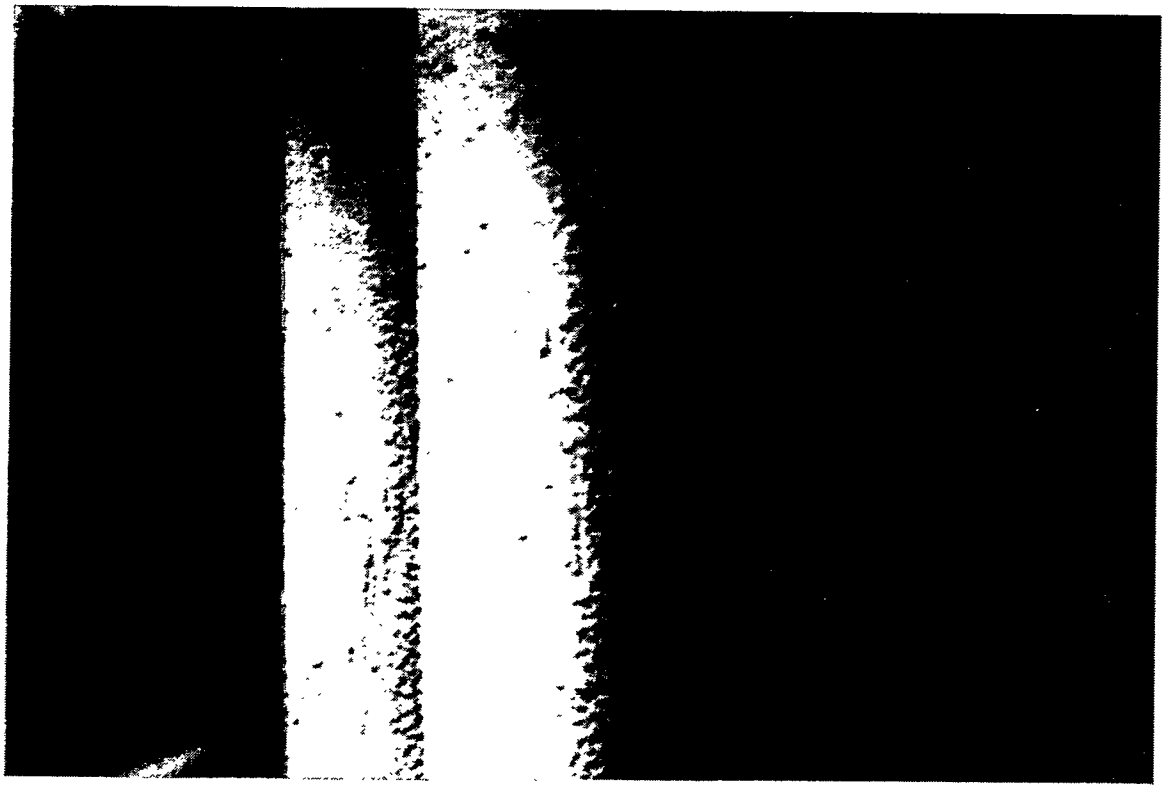

Figure 15b – Ash Cake Formations Along The Coors Alumina/Mullite Candle Filters In The A/M Array (Test Segment #5)

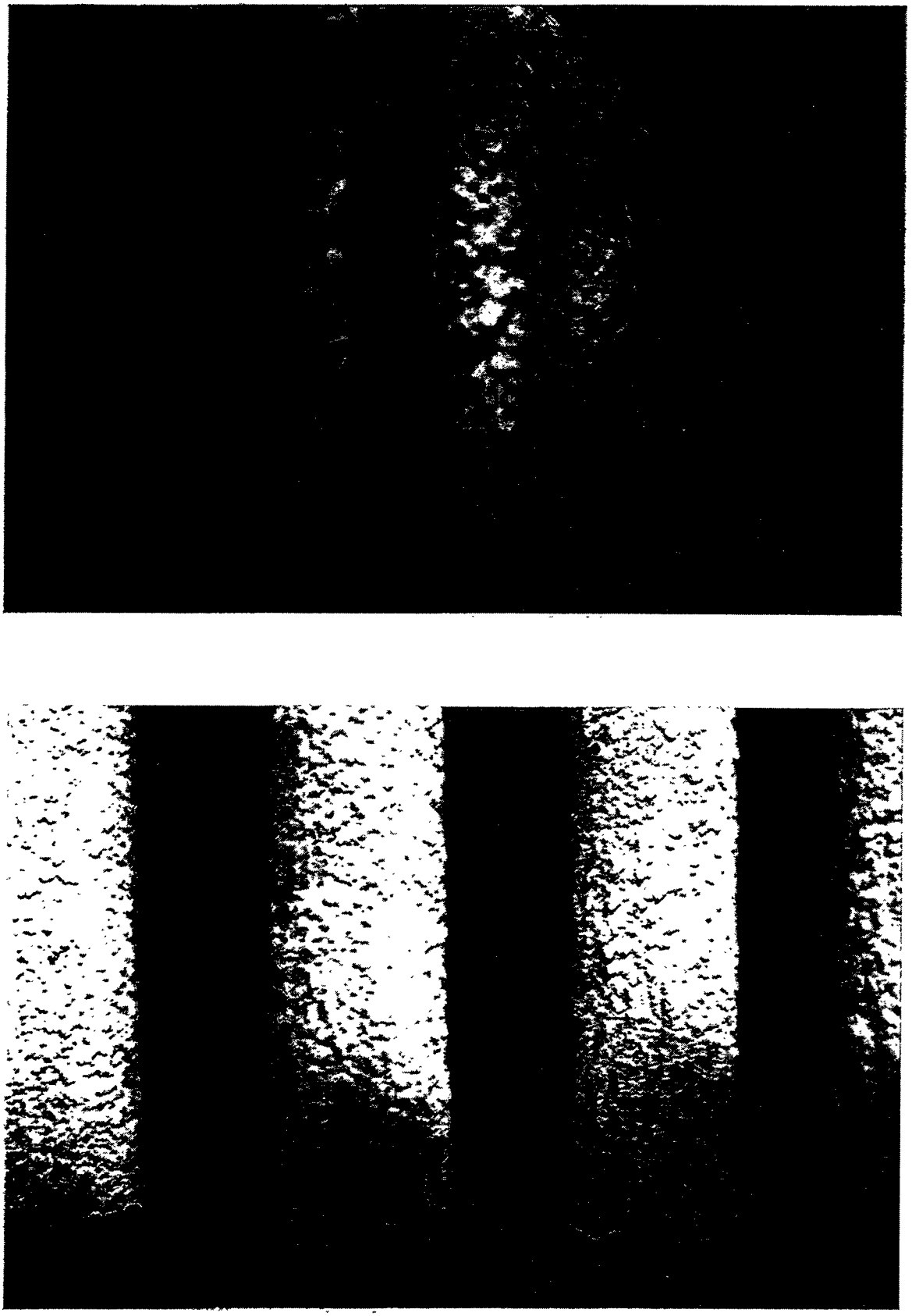

Figure 16a – Dust Cake Formations Along The Pall Vitropore 442T Candle Filters In The C/M Array (Test Segment #5)

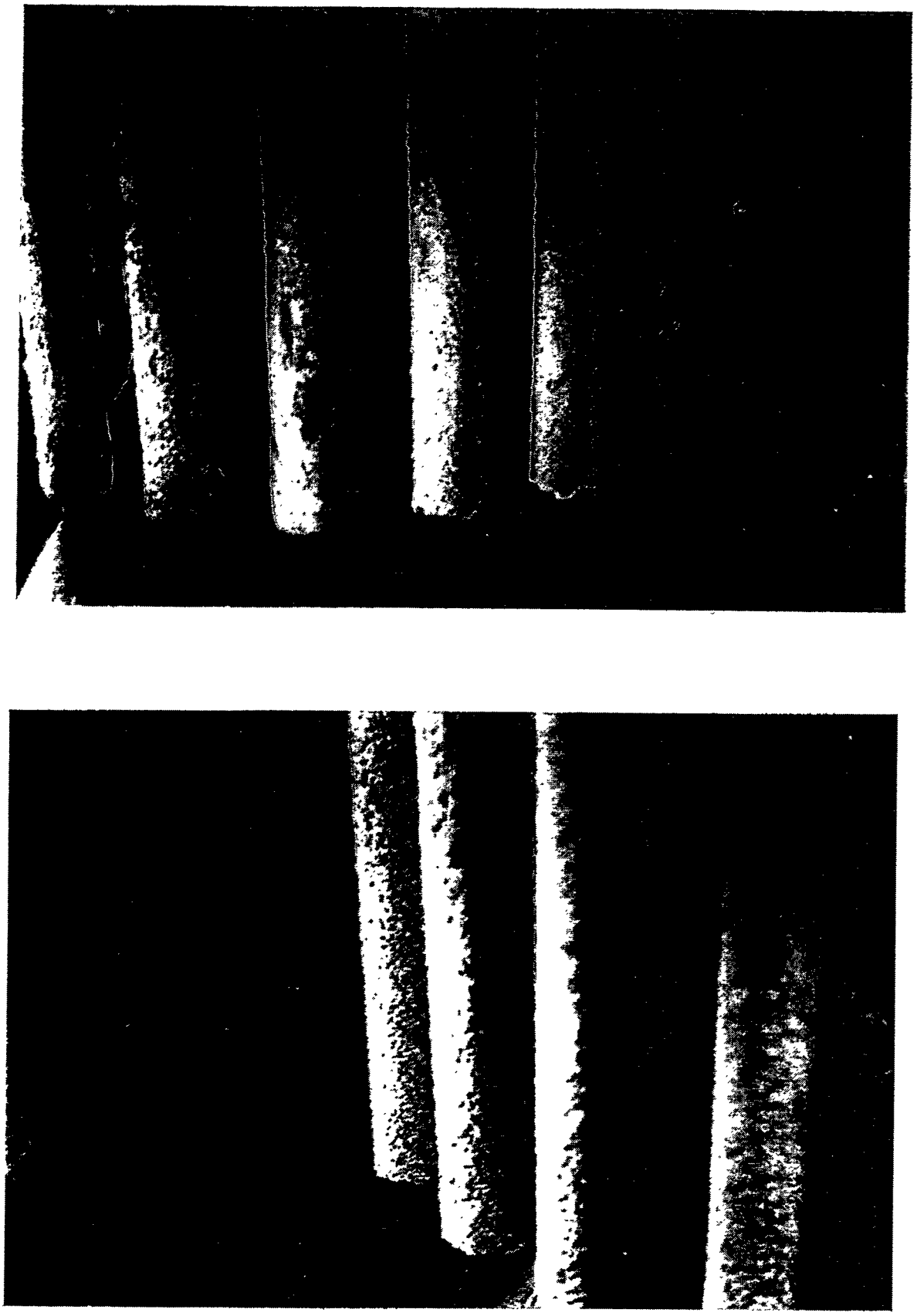

Figure 16b – Dust Cake Formations Along The Pall Vitropore 442T Candle Filters In The C/M Array (Test Segment #5)

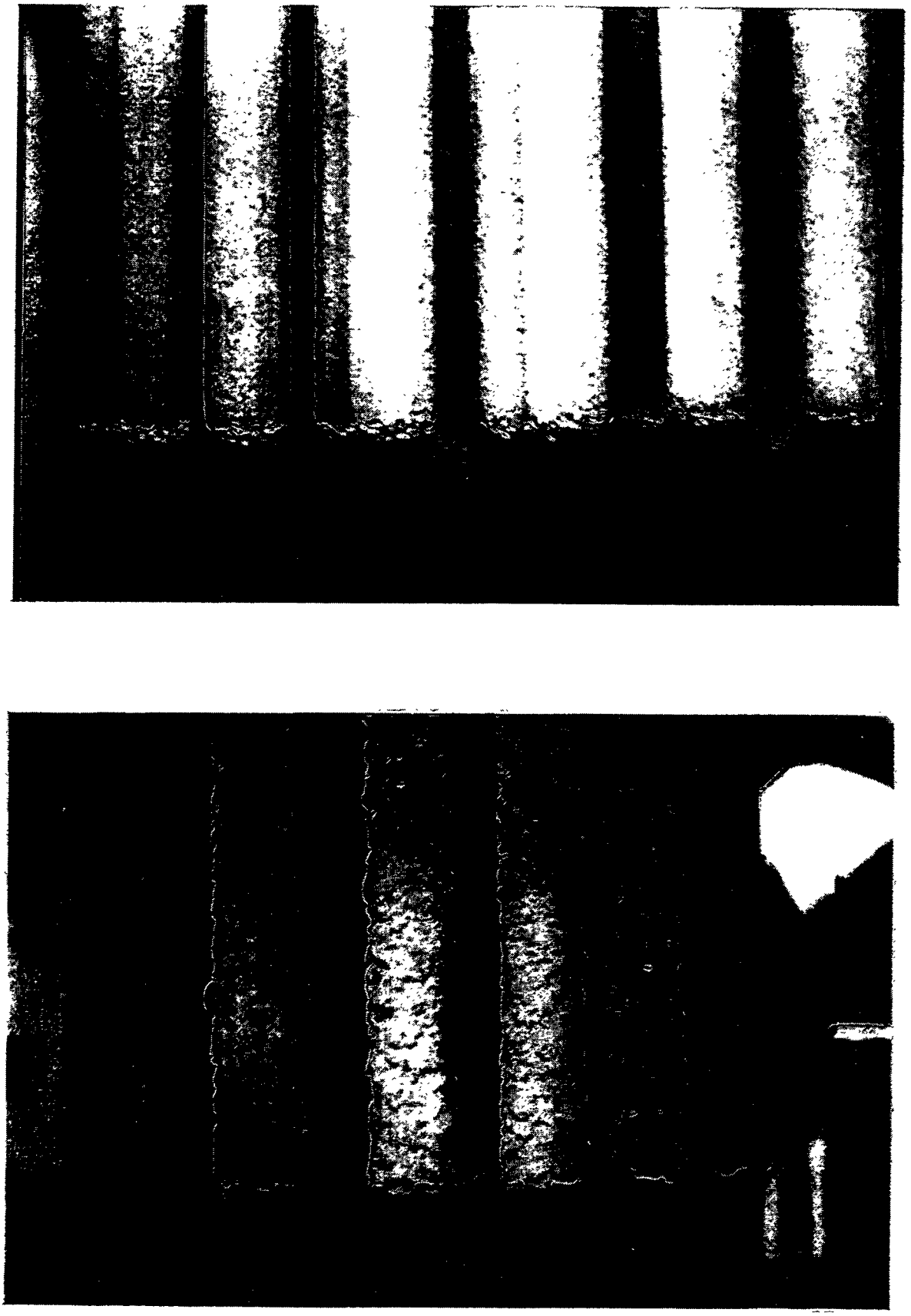

Figure 17 — Comparison Of The Ash Cake Formations along The Coors Alumina/Mullite And Pall Vitropore 442T Candles In The Bottom Filter Arrays At AEP (Test Segment #5)

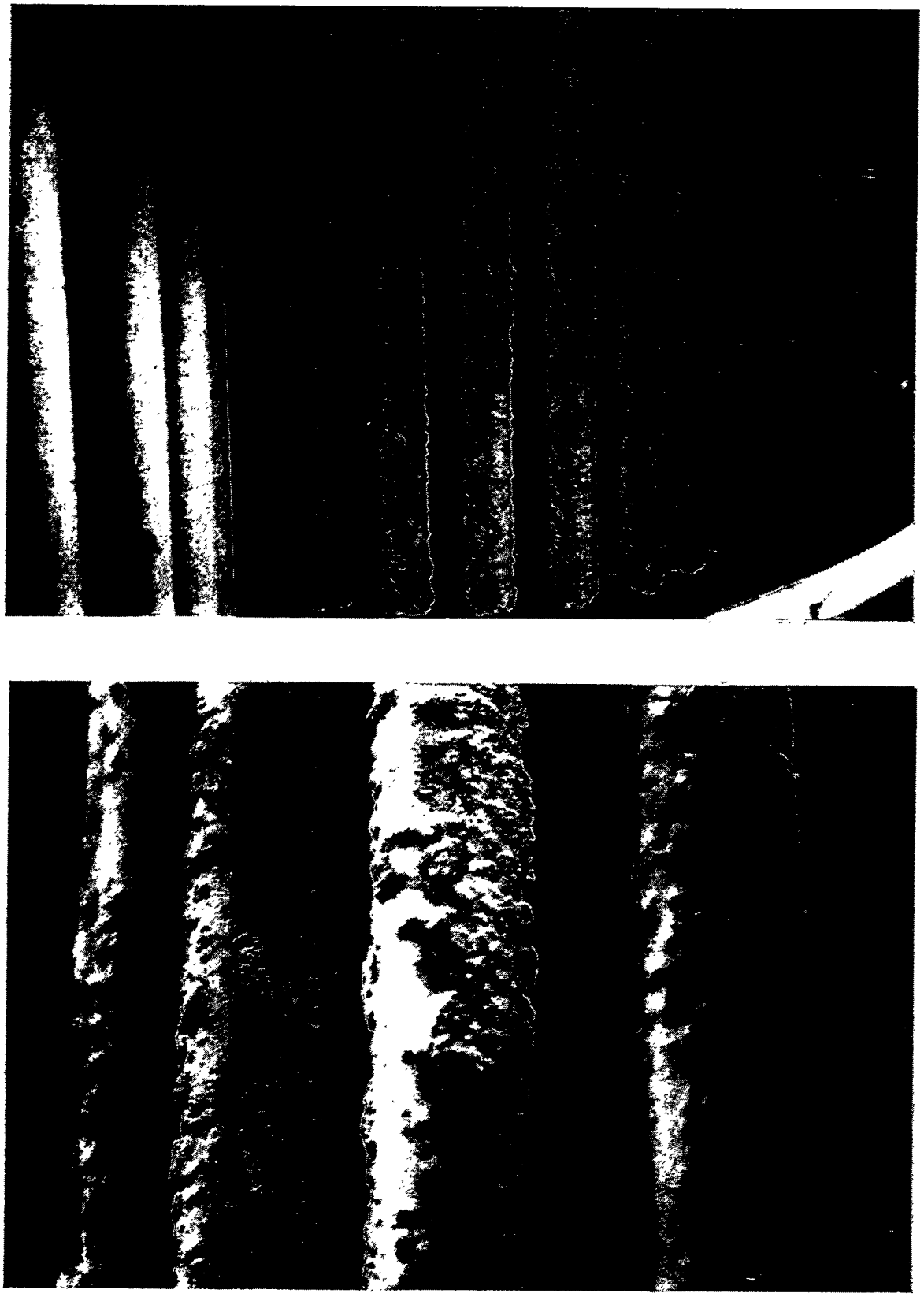

Figure 18 – Comparison Of The Ash Cake Formations Aong The Coors Alumina/Mullite And Pall Vitropore 442T Candles In The Bottom Filter Arrays At AEP (Test Segment #5)

RM-34728

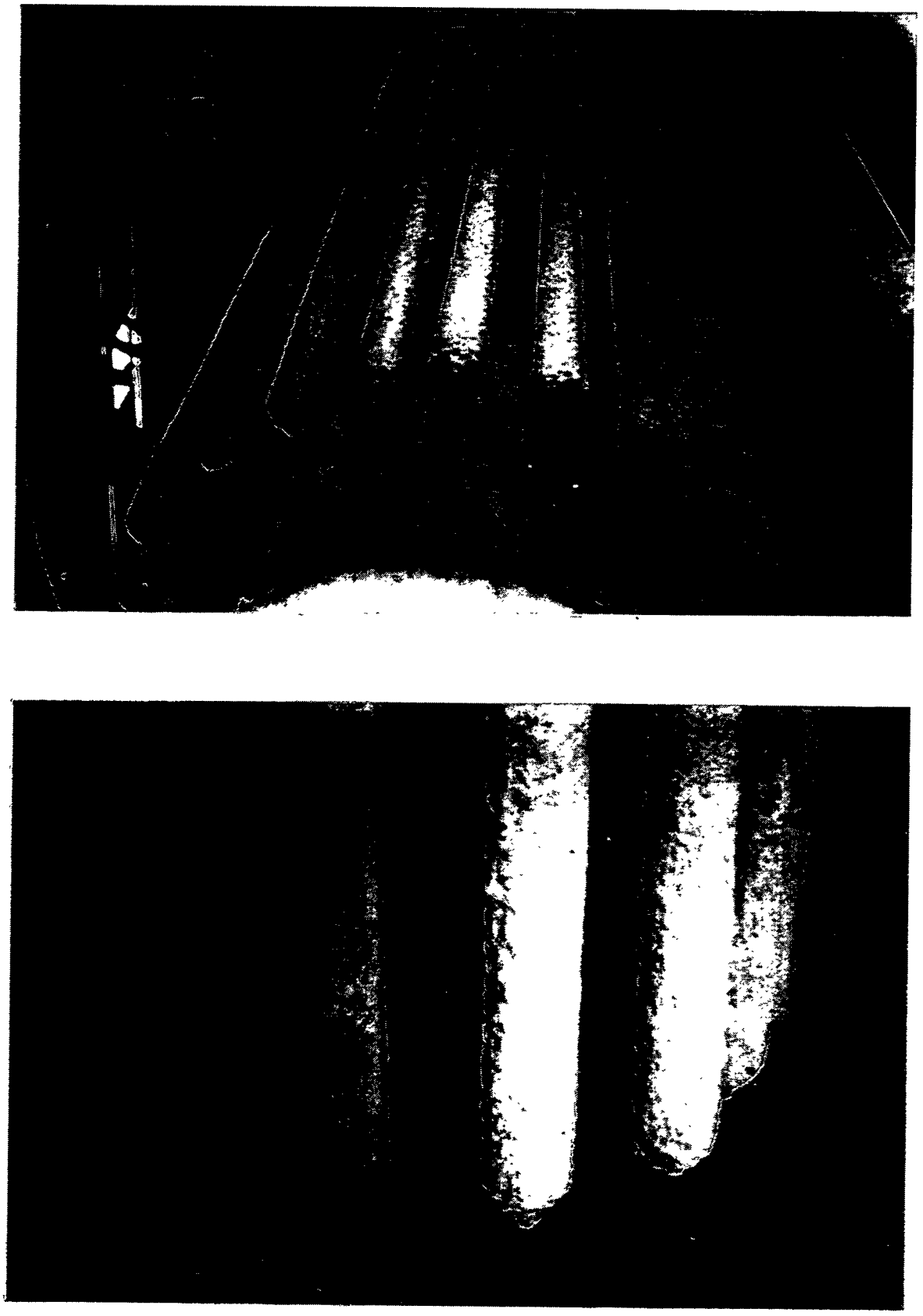

Figure 19 – Relatively Uniform ash Cake Deposit Formation Along The 3M CVI-SiC Composite Candle Filters In The C/T and B/B Arrays (Test Segment #5)

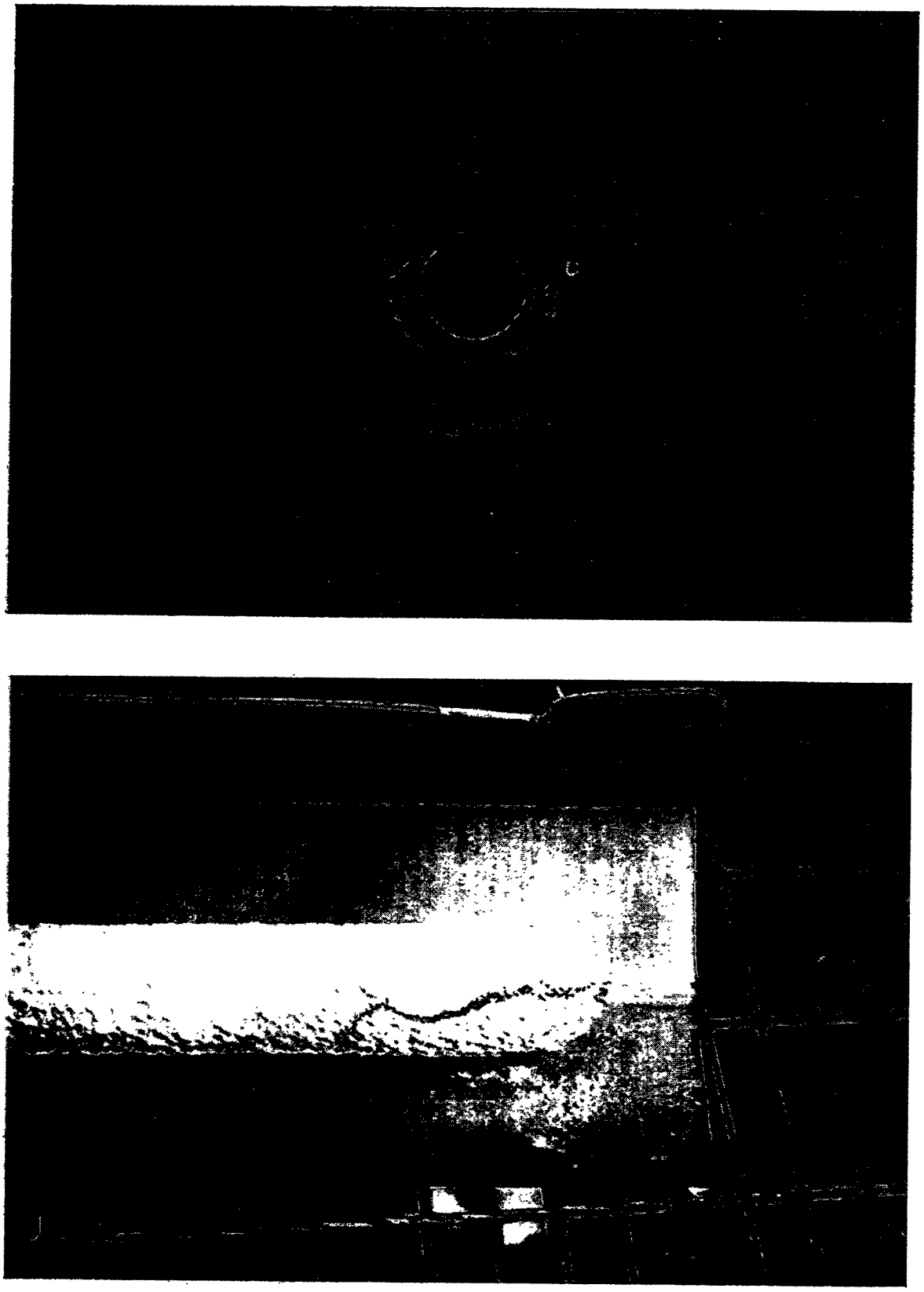

Figure 20 – Graceful Failure Of The Ash Filled ID Bore Of The 3M CVI-SiC Composite Filters. Virtually Ash-Free Top Gasket And Fail-safe/Regenerator Device Above The Failed 3M CVI-SiC Composite Filter

RM-34730

photograph of the ash filled 3M CVI-SiC composite filter that ruptured along the end cap, but which remained as an intact candle during testing in Test Segment #5. As shown in the top photograph of Figure 19, the top gasket and fail-safe/regenerator are virtually clean, even though ash filled the bottom of the 3M CVI-SiC composite filter.

Figure 21 provides one final photograph which illustrates the relatively ash-free W-APF arrays at the conclusions of testing in Test Segment #5.

ASH CAKE FORMATION AND CANDLE SURFACE DESCRIPTION

A relatively thick ash cake layer remained along the surface of the Schumacher Dia Schumalith F40 surveillance candle filter which had been positioned in location A/T-16 after 1110 hours of operation in Test Segment #5 (Figure 22). Similarly, a thick ash cake formed along the outer surface of the Pall Vitropore 442T filter elements (Figure 23). Initiation of the elephant foot formation was also evident along the bottom of the Pall Vitropore 442T candles (i.e., bottom photograph in Figure 23). Both the top gasket and fail-safe/regenerator unit which were positioned above the Pall Vitropore 442T candle filter which had been located in position C/T-1 were relatively clean after 1110 hours of operation in Test Segment #5.

A thinner ash cake formation resulted along the alumina/mullite candle filters that were positioned in locations A/T-1 and A/T-17 (Figure 24). A thicker ash cake formation, however, resulted along the bottom end cap of the alumina/mullite candle filter that was located in position A/T-1 (Figure 25).

Since the alumina/mullite candle that was positioned in A/T-20 had suffered failure at the base of its flange, the fail-safe/regenerator device that was positioned above the failed filter showed evidence of dust collection and/or plugging along its surface (Figure 26). The top gasket and the top surface of candle filter A/T were relatively clean, indicating the absence of a leak path in this area. In contrast, the top of the adjacent metal ring which contacted the fail-safe/regenerator was encrusted with ash fines, possibly indicating a leak path between the top ring and fail-safe/regenerator due back pulsing of fines and/or the normal PFBC gas/fines forward flow after plugging of the fail-safe unit.

Figure 27 illustrates the ash cake formations that remained along the surface of the 3M CVI-SiC composite candle that was positioned in location C/T-18. Thick ash nodules were not evident along the outer surface of the 3M filter as those which were observed along the surface of the Pall Vitropore 442T candle filters. The "sesame seed" pin-holes which resulted along the surface of the ash cake deposit during Test Segment #4, were not evident along the relatively thick ash cake deposit that formed along the 3M filters during operation in Test Segment #5.

Ash was readily observed along the outer gasketed flange surface of the 1100 hour PFBC-exposed 3M CVI-SiC composite candle that had been positioned in C/T-18. Ash was also found along the top of the flange and along the metal insert which was used to stabilize the 3M CVI-SiC composite candle filter in the Westinghouse filter mount (Figure 28). Dust accumulation was generally observed between the metal insert and the primary or internal gasket seal. The ash cake that formed along the outer surface of the flange was considered to have resulted from a gas path leak between the Westinghouse holder mount and the 3M filter flange.

Figure 21 – Ash Free W-APF System At The Conclusion Of Test Segment #5

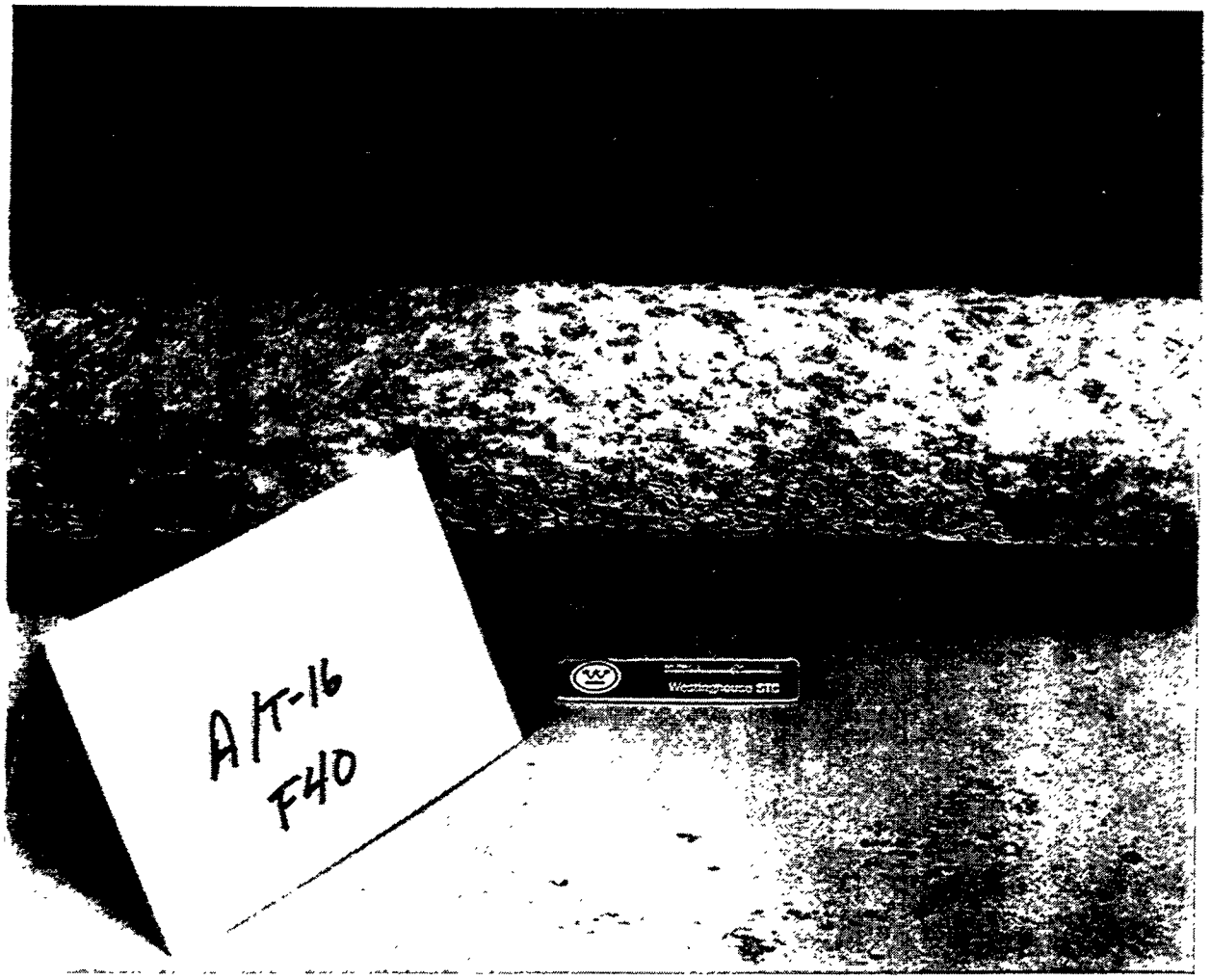

Figure 22 – Ash Cake Formation Along The Schumacher Dia Schumalith F40 Surveillance Candle In Position A/T-16

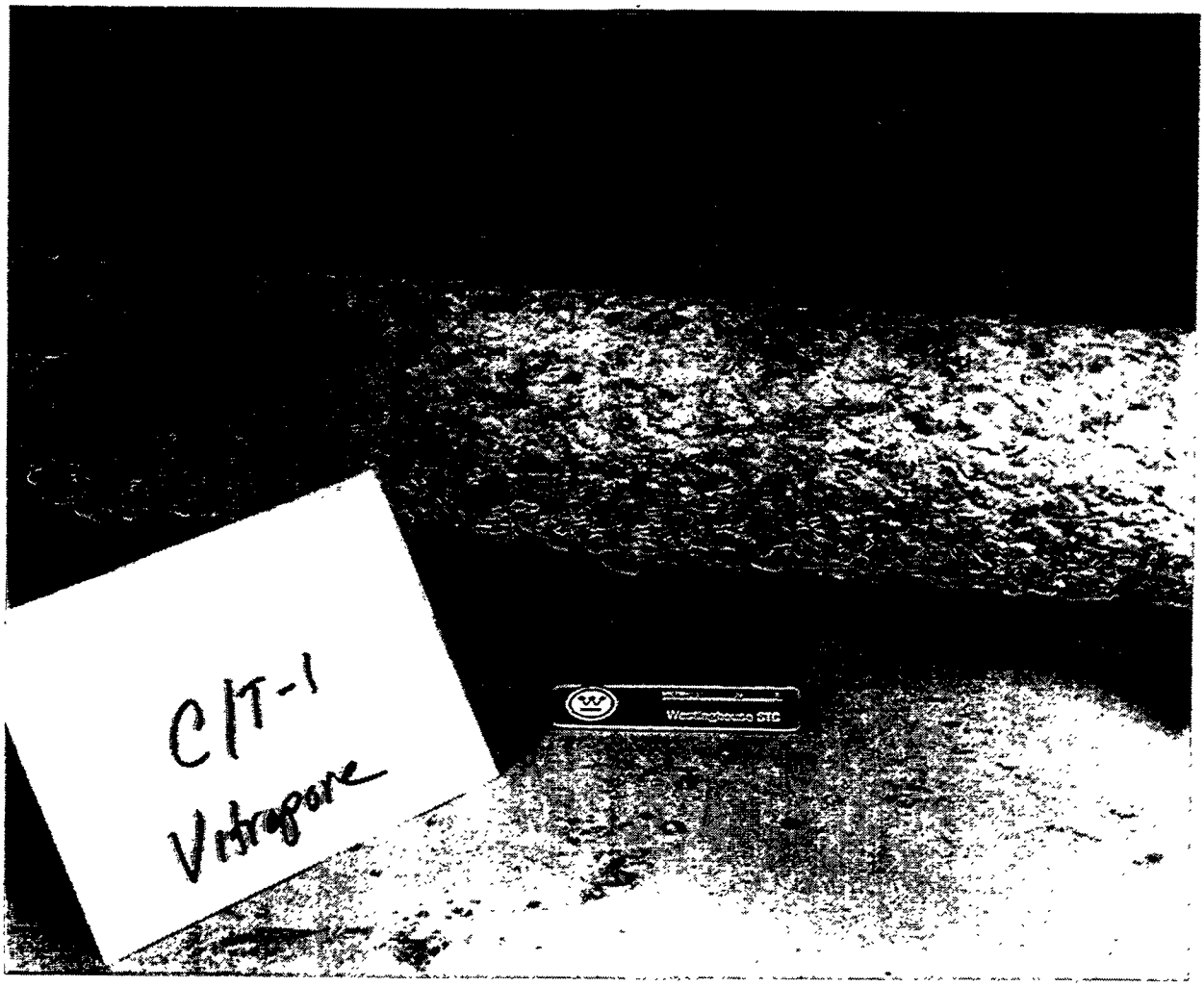

Figure 23a – Ash Cake Formation Along The Pall Vitropore 442T Candle In Position C/T-1

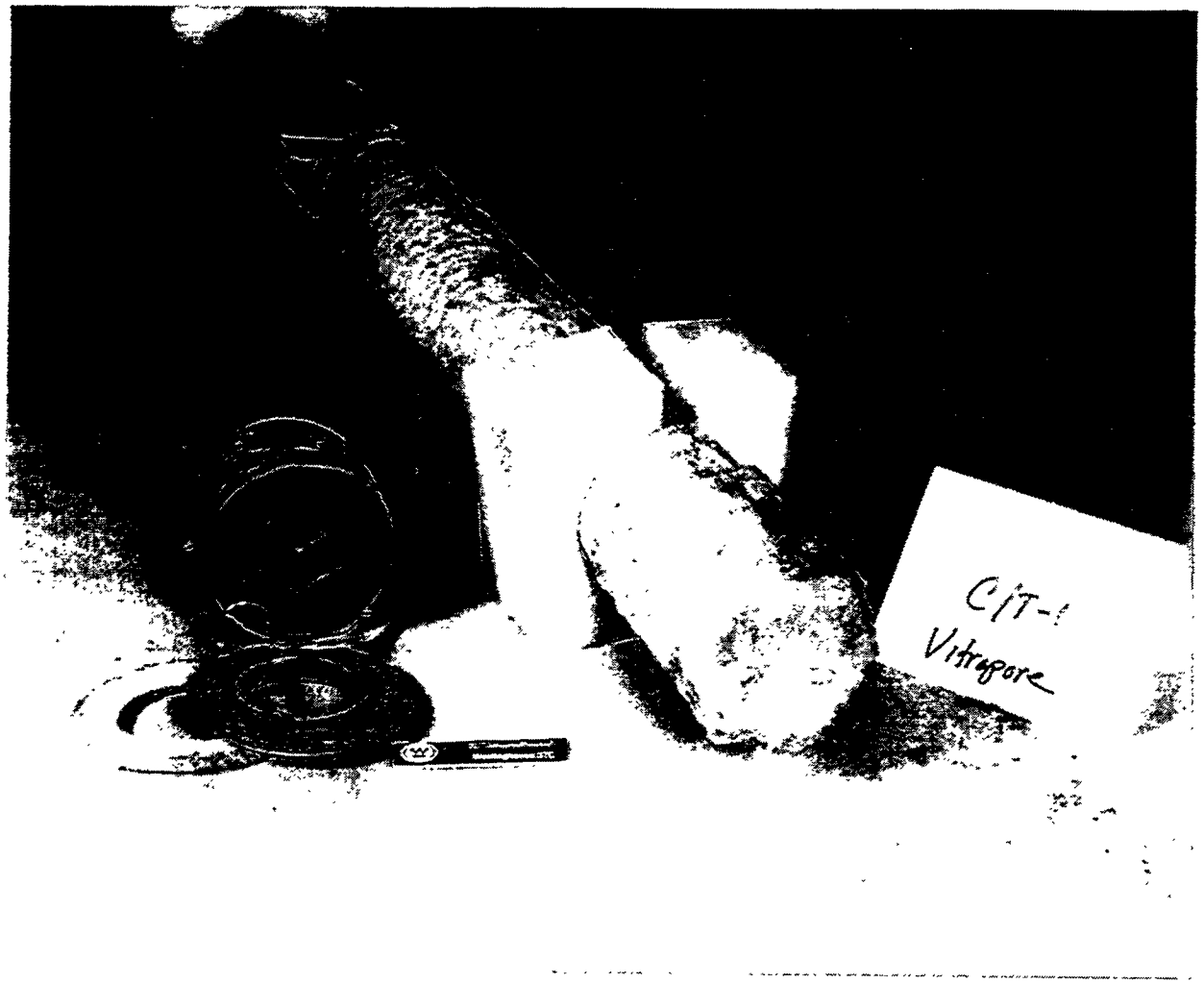

Figure 23b – Thick Ash Cake Deposit Along The Bottom End Cap Of The Pall Vitropore 442T Candle Filter That Had Been Located In Position C/T-1 During Test Segment #5

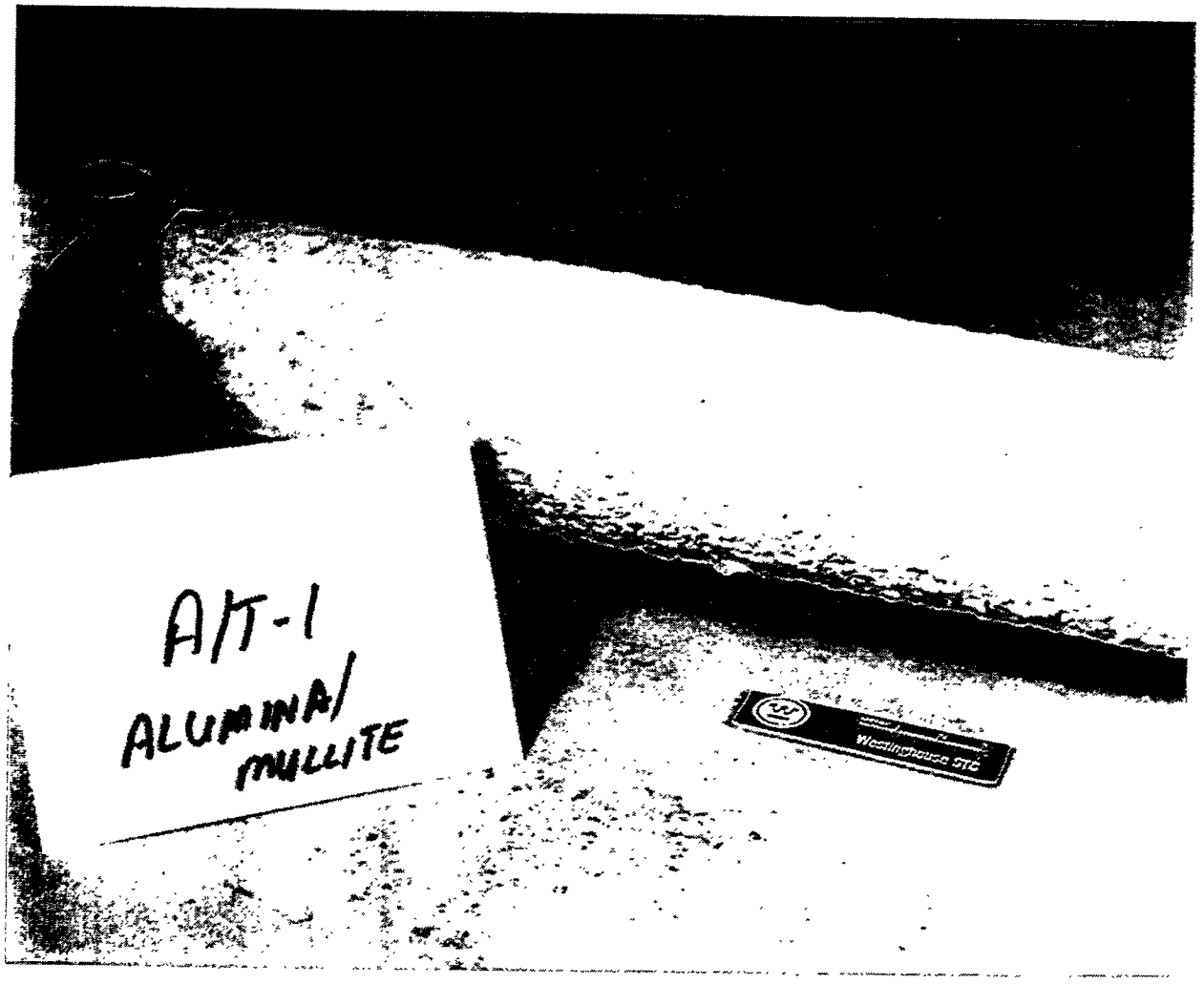

Figure 24a – Ash Cake Formation Along The Coors Alumina/Mullite Filter In Position A/T-1

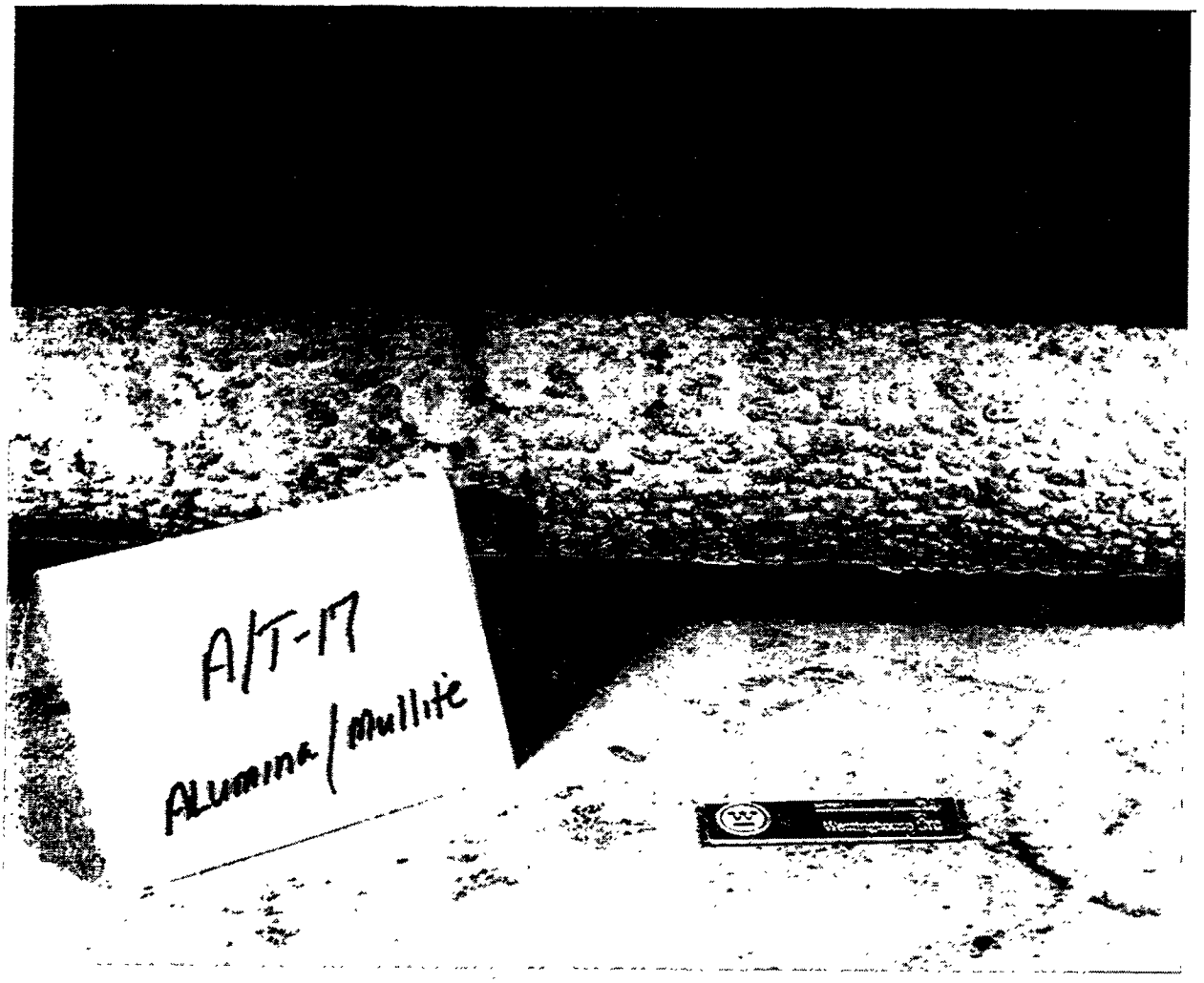

Figure 24b – Ash Cake Formation Along The Coors Alumina/Mullite Filter In Position A/T-17

Figure 25 – Ash Cake Formation Along The End Cap Of The Coors Alumina/Mullite Candle Filter In Position A/T-1

Figure 26a — Top Gasket, Metal Ring, And Fail-Safe/Regenerator Device Positioned Above The Coors Alumina/Mullite Candle Filter In Position A/T-20

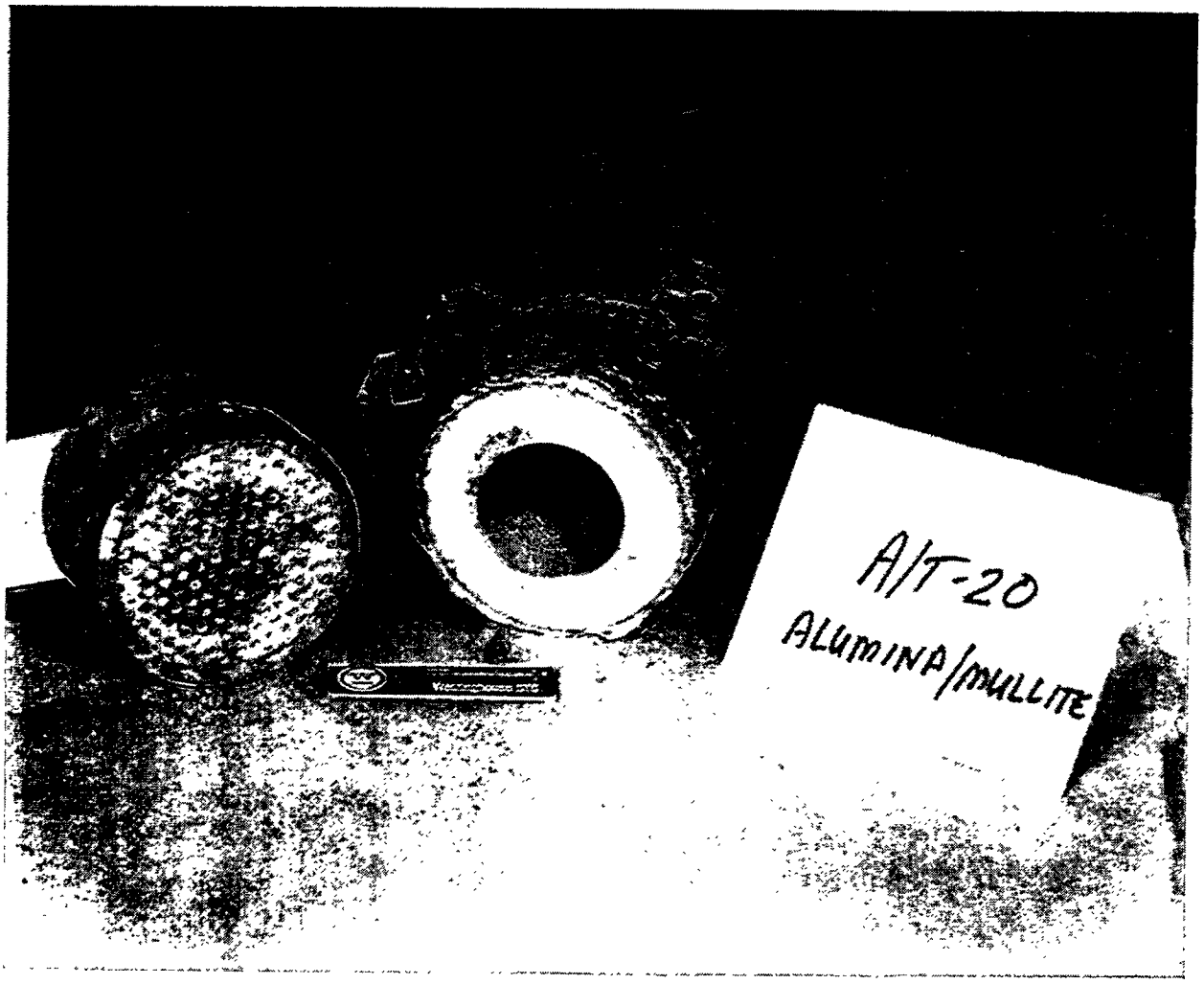

Figure 26b – Fail-Safe/Regenerator Above The Failed Coors Alumina/Mullite Candle Filter Located In A/T-20

Figure 27 – Ash Cake Formation Along The 3M CVI-SiC Composite Candle Filter in Position C/T-18

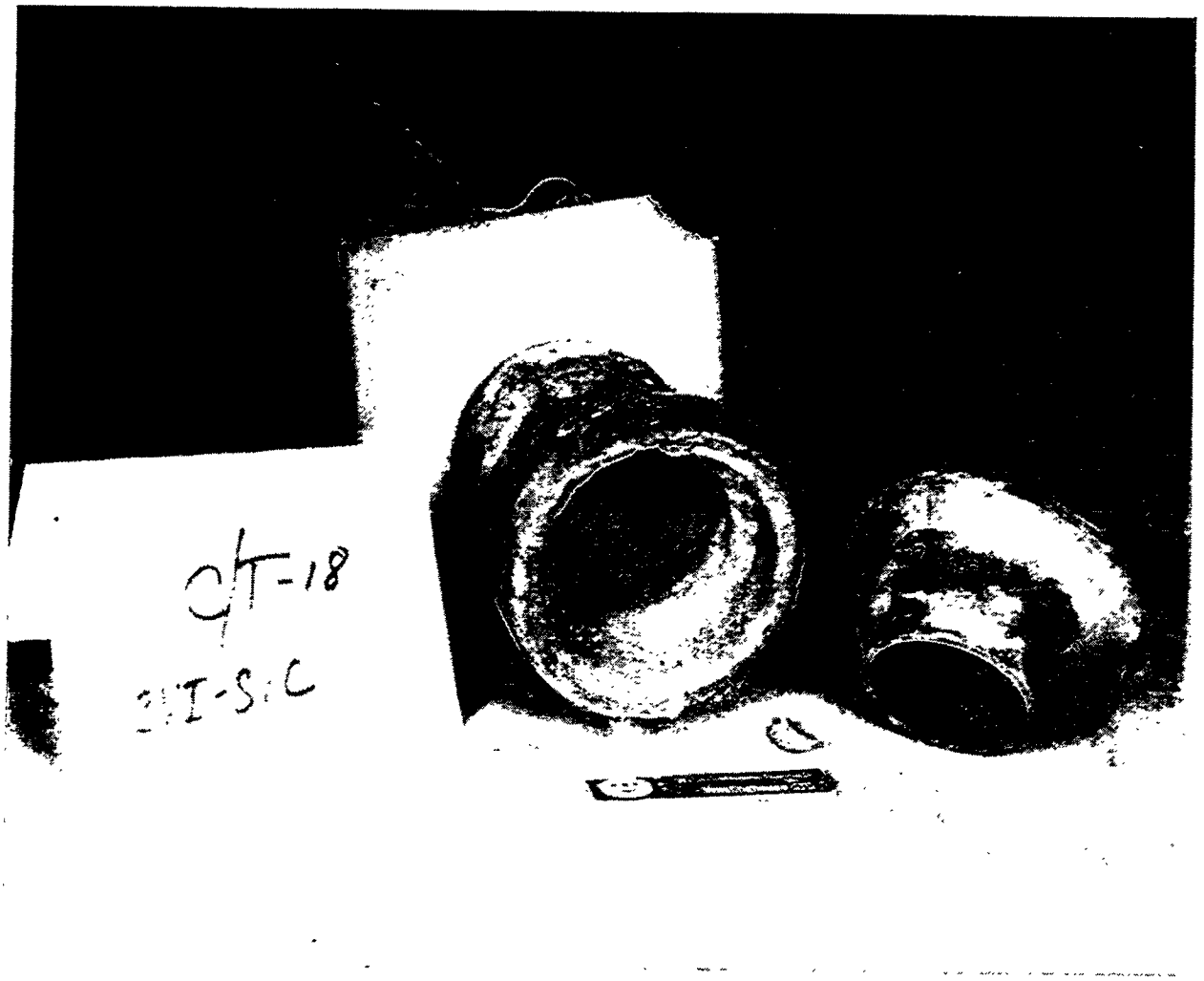

Figure 28 – Ash Cake Formation Along The Outer And Inner Surfaces Of The 3M CVI-SiC Composite Flange (Position C/T-18; Test Segment #5)

Figure 29 illustrates the fractured DuPont PRD-66 filter element which had been located in position B/T-2. Failure of the element resulted at approximately the mid-body, forming a "step-like" fracture through the filament wound or layered 6-7 mm PRD-66 filter matrix. During removal of the DuPont PRD-66 filter from position B/T-2, failure also occurred along the flange which had been tightly held in the filter mount. A heavy deposit of ash was evident along the bottom nut of the filter holder mount (Figure 29b). A dark red stain was prominent along a section of the filter body below the gasket sleeve. In several areas, sections of the membrane, as well as subsurface filament wound layers were removed, forming ~1-2 inch "divot-like" areas along the outer surface of the filter element. The DuPont PRD-66 filter element which had been positioned in B/T-2 also contained ash along its ID surface, as well as within its matrix.

An intact DuPont PRD-66 filter element was removed from location B/T-6. A thin 1-2 mm ash cake layer remained along the outer surface of the filter element (Figure 30). Ash was seen to be heavily caked along the inside wall of the filter holder mount, while the top gasket seal that contacted the DuPont PRD-66 filter flange was relatively clean (Figure 30a). Dust was evident within the fail-safe/regenerator device that was positioned above the DuPont PRD-66 candle filter located in position B/T-6.

"Divot-like" formations were also evident along the outer surface of the PRD-66 filter that was positioned in B/T-6. The series of photographs shown in Figure 30 were taken down the length of the filter body, beginning at the flange and moving towards the end cap. The darkened red stain was not as prominent along the B/T-6 PRD-66 filter element as it had been along the B/T-2 PRD-66 filter element. The "divot-like" formation typically tracked as two lines down the length of the filter body. The "divot-like" formation resulted along the surface of the filter element that was off-tangent to the plenum.

Figure 31 illustrates the failed DuPont PRD-66 filter element that had been located in position B/T-11. Again failure of the filter element's flange resulted during disassembly and removal from the filter holder. The red ash stain was once again evident in isolated areas along the surface of the B/T-11 filter element. Divots were also evident, again tracking in line formations. Divots resulted along both the red stained areas of the filter element, as well as along the as-manufactured white sections of the DuPont PRD-66 filter matrix. The fractured surface of the PRD-66 filter typically followed the filament winding pattern (i.e.,, diagonal diamond weave), with slight layering through the filament wound structure (Figures 31g and 31h). The red stain was also evident along the ID surface of the candle, near the fractured surface.

Figure 32 illustrates the failed DuPont PRD-66 filter element that was located in position B/T-12. Again the red stain was evident along the filter body. Divots were also present along both the red stained and as-manufactured white filter body. Again the divots resulted in line formations. The fractured surface followed the diamond diagonal weave, as well as the filament wound layering.

Figure 33 illustrates the thick ash deposit that had been formed at the base of the flange along the outer surface of the DuPont PRD-66 candle which had been located in position B/T-5. This candle failed during operation at AEP in Test Segment #5. The thick ash deposit was below the external mat-filled, middle gasket that was positioned at the base of the filter's flange.

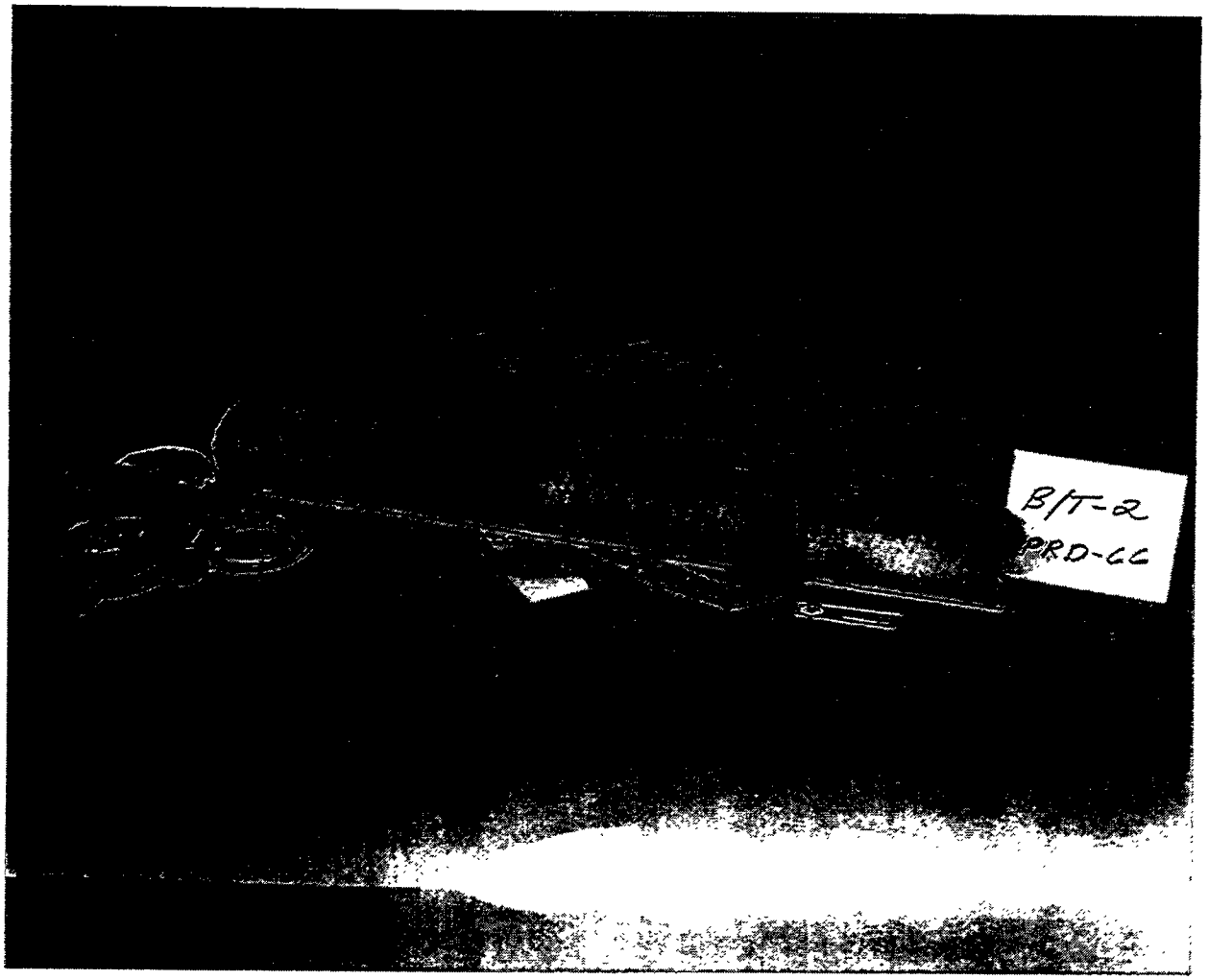

Figure 29a – Failed DuPont PRD-66 Candle Filter (Position B/T-2; Test Segment #5)

Figure 29b – Failed DuPont PRD-66 Candle Filter (Position B/T-2; Test Segment #5)

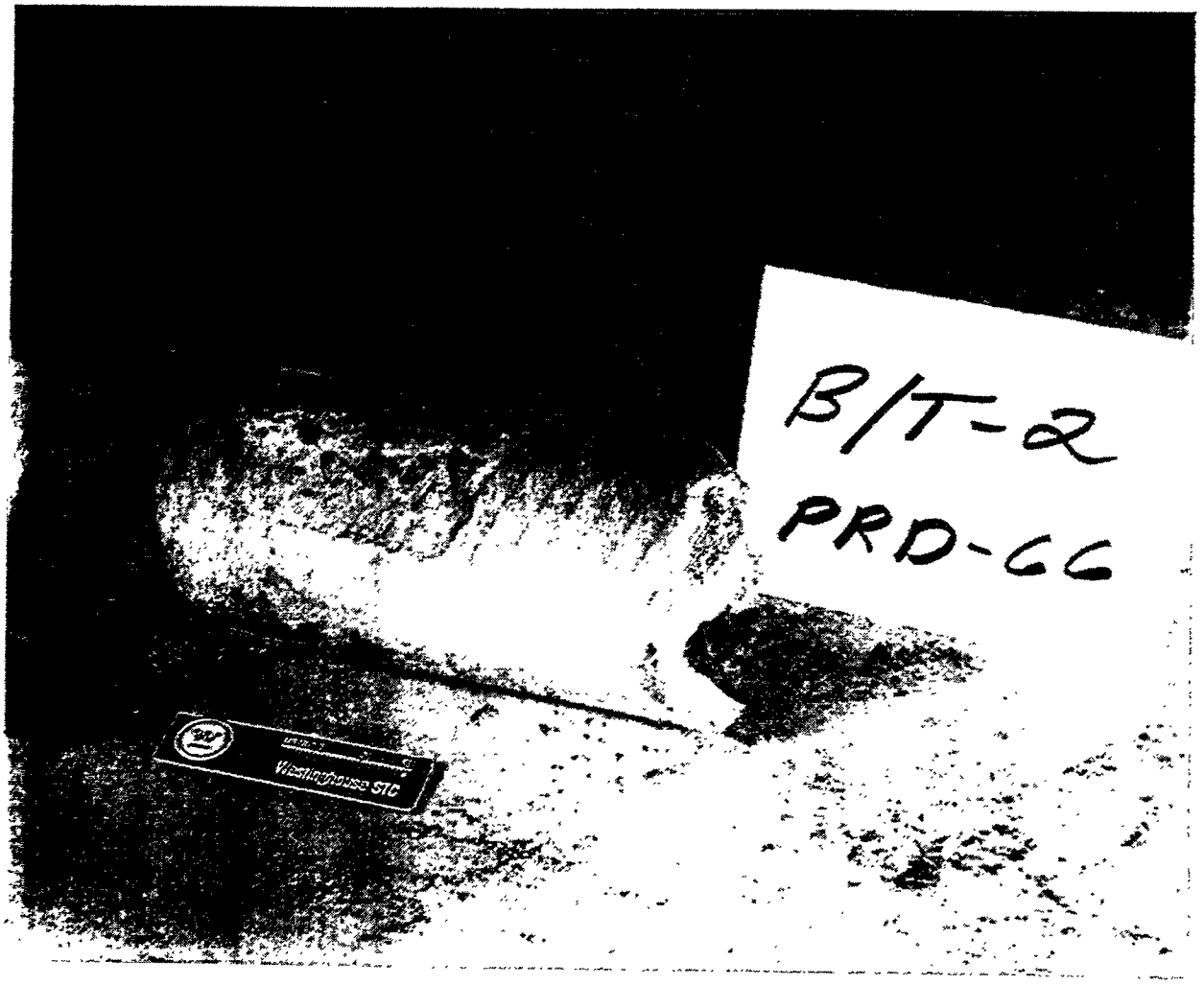

Figure 29c – Failed DuPont PRD-66 Candle Filter (Position B/T-2; Test Segment #5)

Figure 30a – Intact DuPont PRD-66 Candle Filter (Position B/T-6; Test Segment #5)

Figure 30b – Intact DuPont PRD-66 Candle Filter (Position B/T-6; Test Segment #5)

Figure 30c – Intact DuPont PRD-66 Candle Filter (Position B/T-6; Test Segment #5)

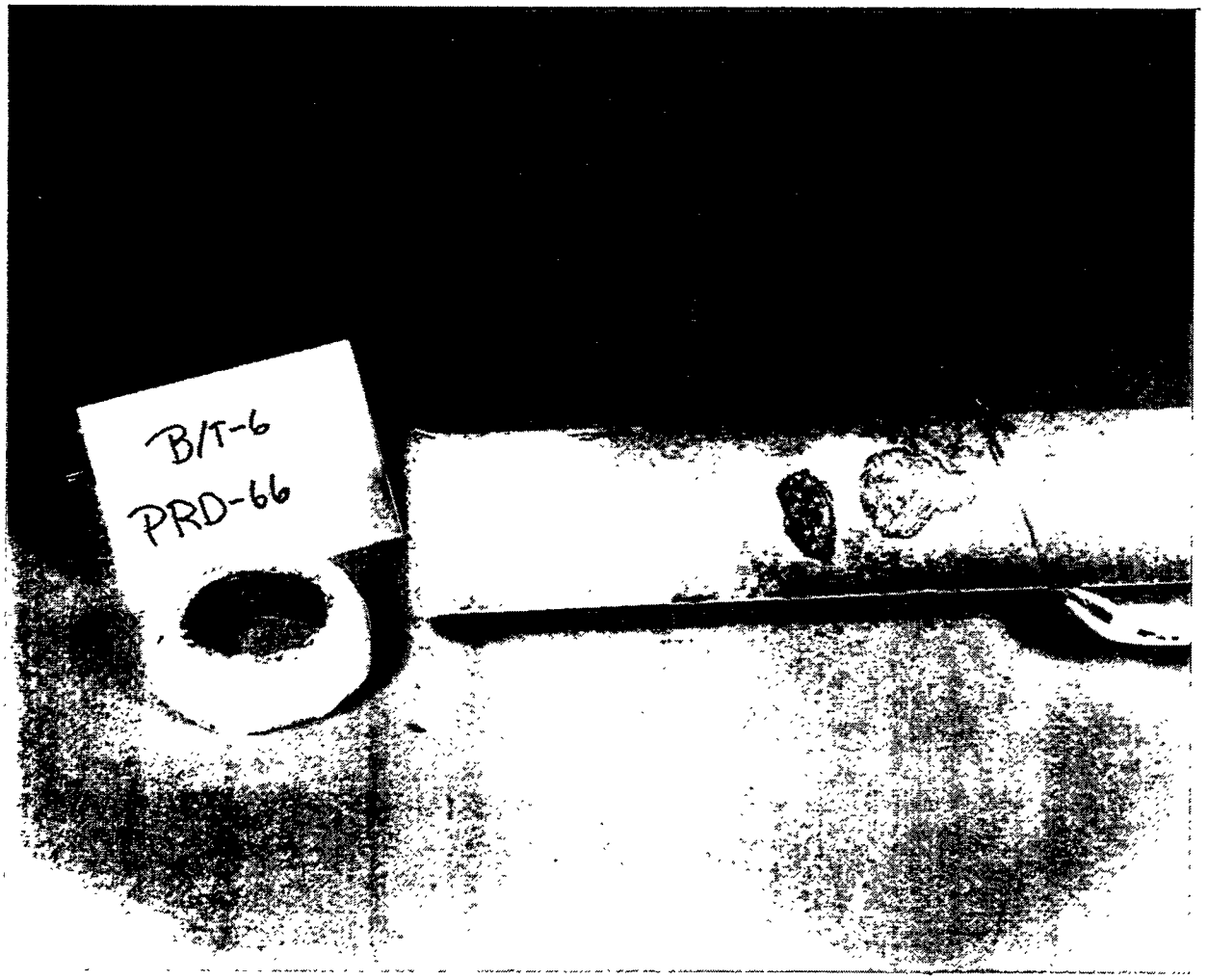

Figure 30d – Intact DuPont PRD-66 Candle Filter (Position B/T-6; Test Segment #5)

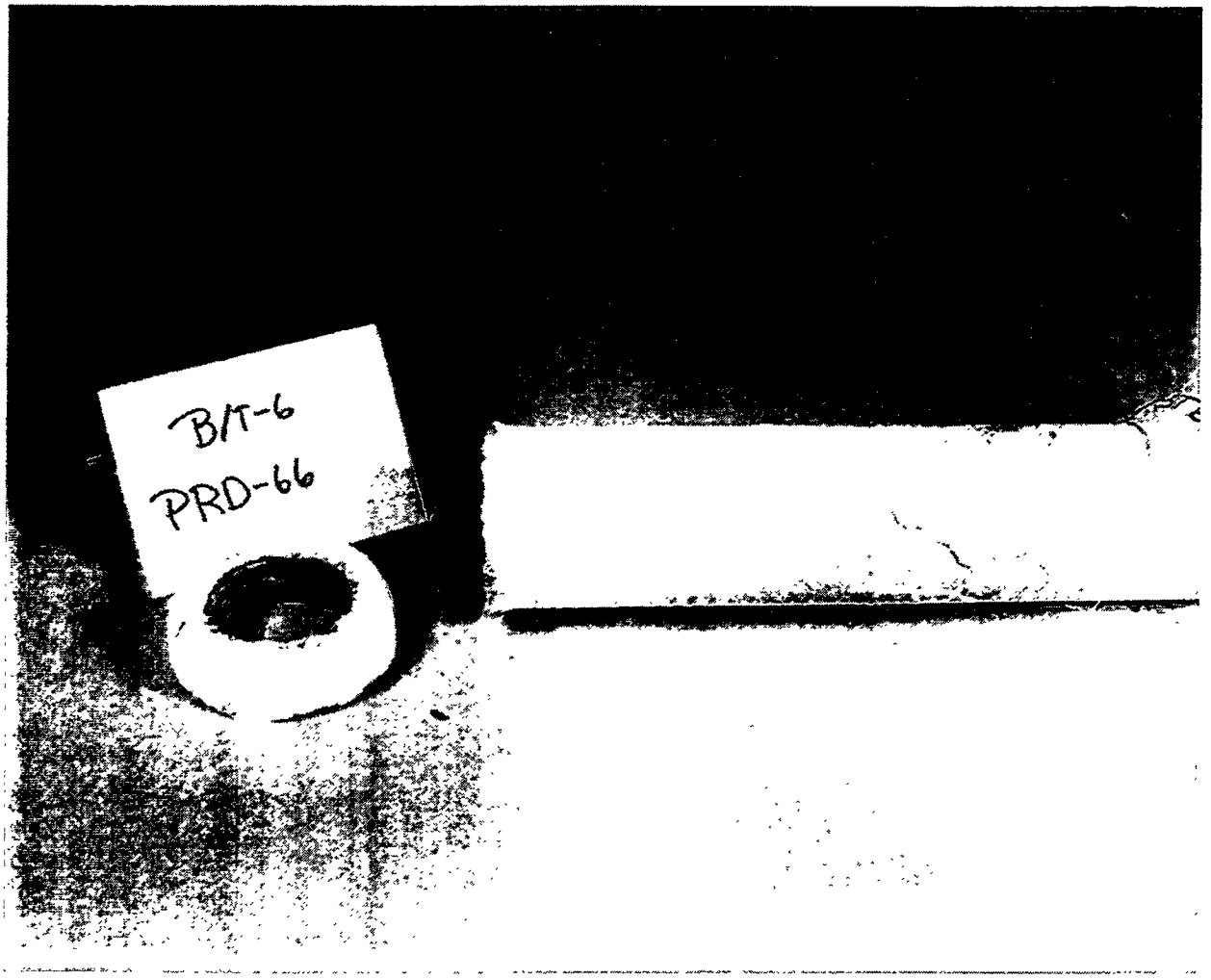

Figure 30e – Intact DuPont PRD-66 Candle Filter (Position B/T-6; Test Segment #5)

Figure 30f — Intact DuPont PRD-66 Candle Filter (Position B/T-6; Test Segment #5)

Figure 30g – Intact DuPont PRD-66 Candle Filter (Position B/T-6; Test Segment #5)

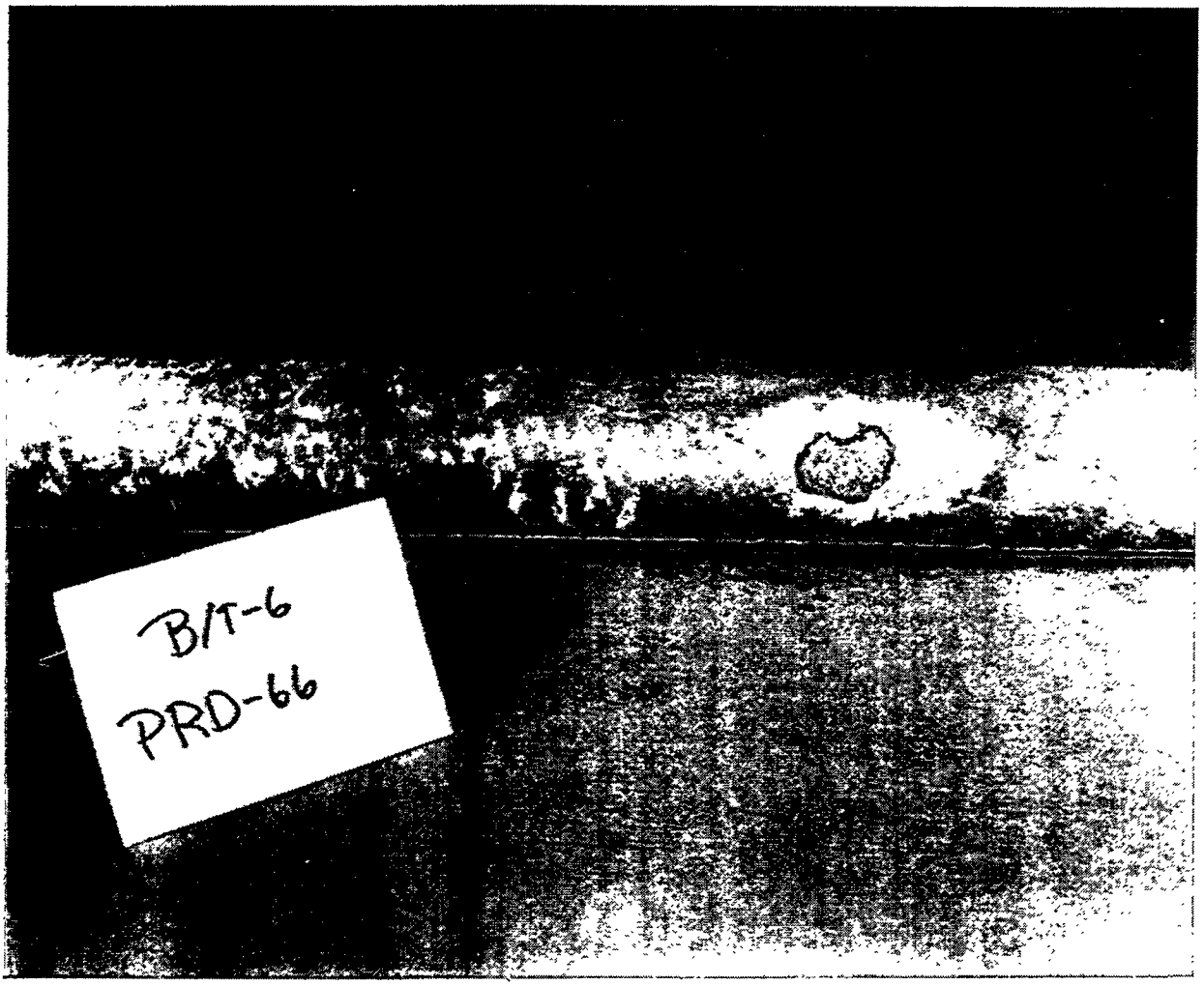

Figure 30h – Intact DuPont PRD-66 Candle Filter (Position B/T-6; Test Segment #5)

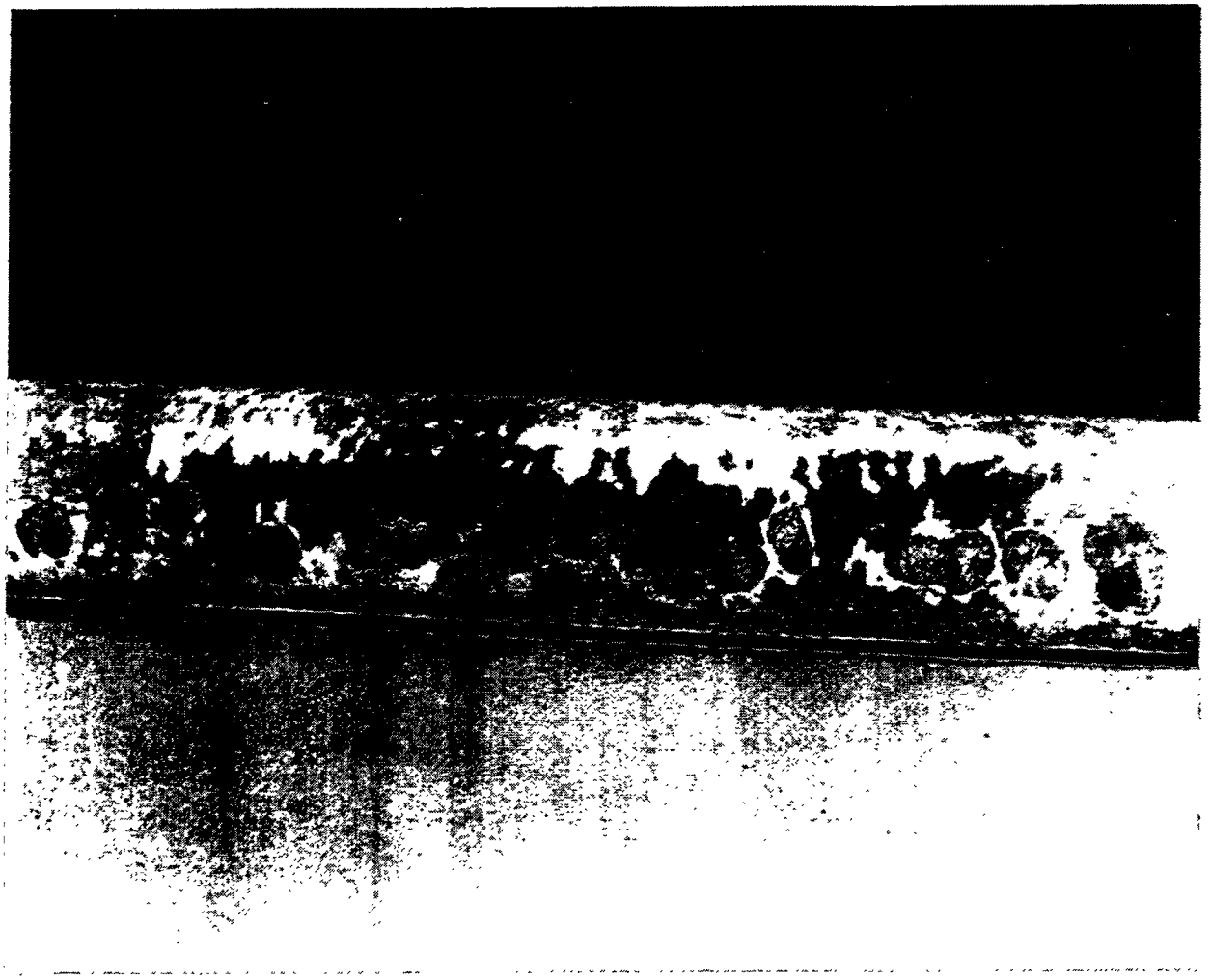

Figure 30i –Intact DuPont PRD-66 Candle Filter (Position B/T-6; Test Segment #5)

Figure 31a – Failed DuPont PRD-66 Candle Filter (Position B/T-11; Test Segment #5)

Figure 31b – Failed DuPont PRD-66 Candle Filter (Position B/T-11; Test Segment #5)

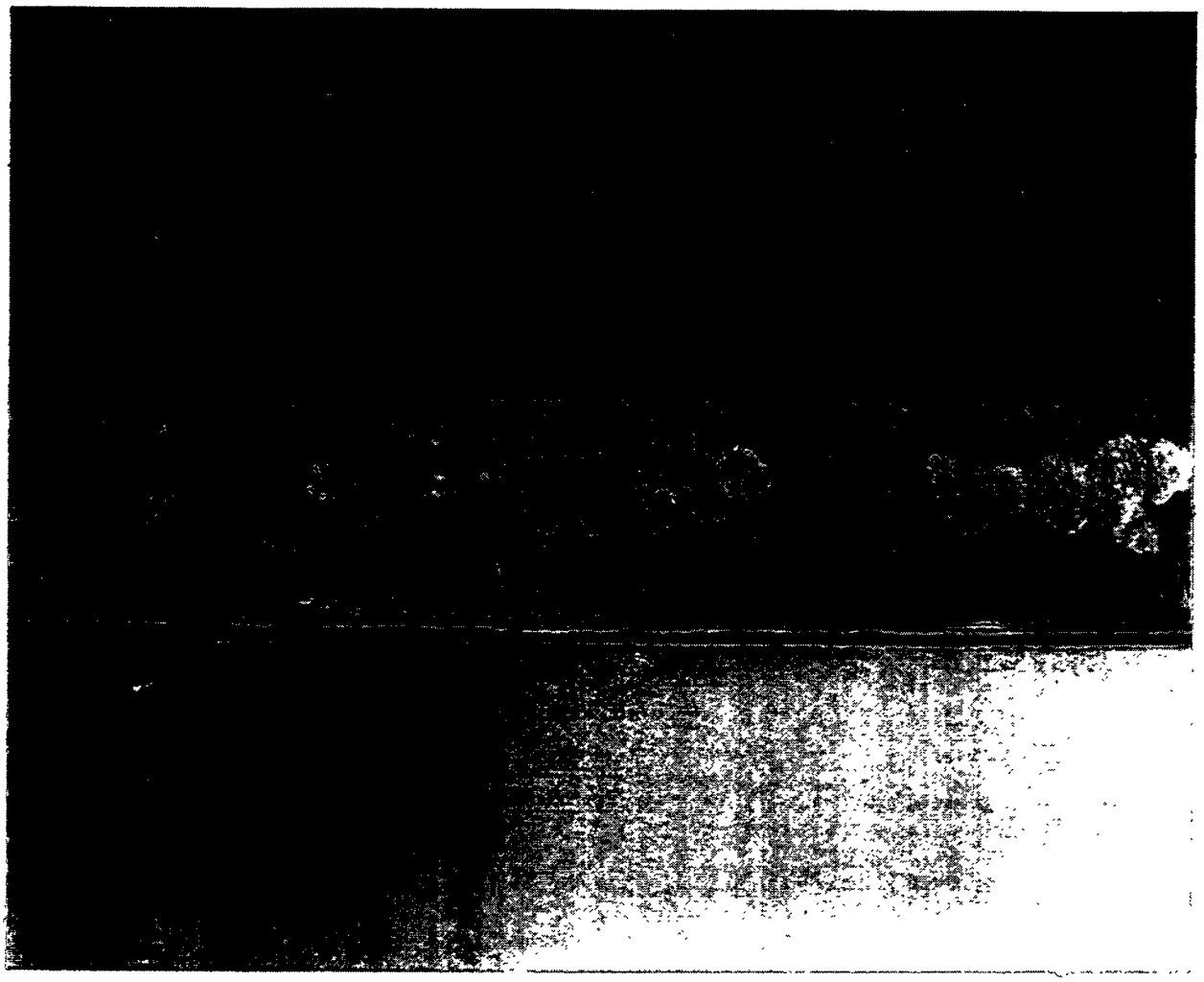

Figure 31c – Failed DuPont PRD-66 Candle Filter (Position B/T-11; Test Segment #5)

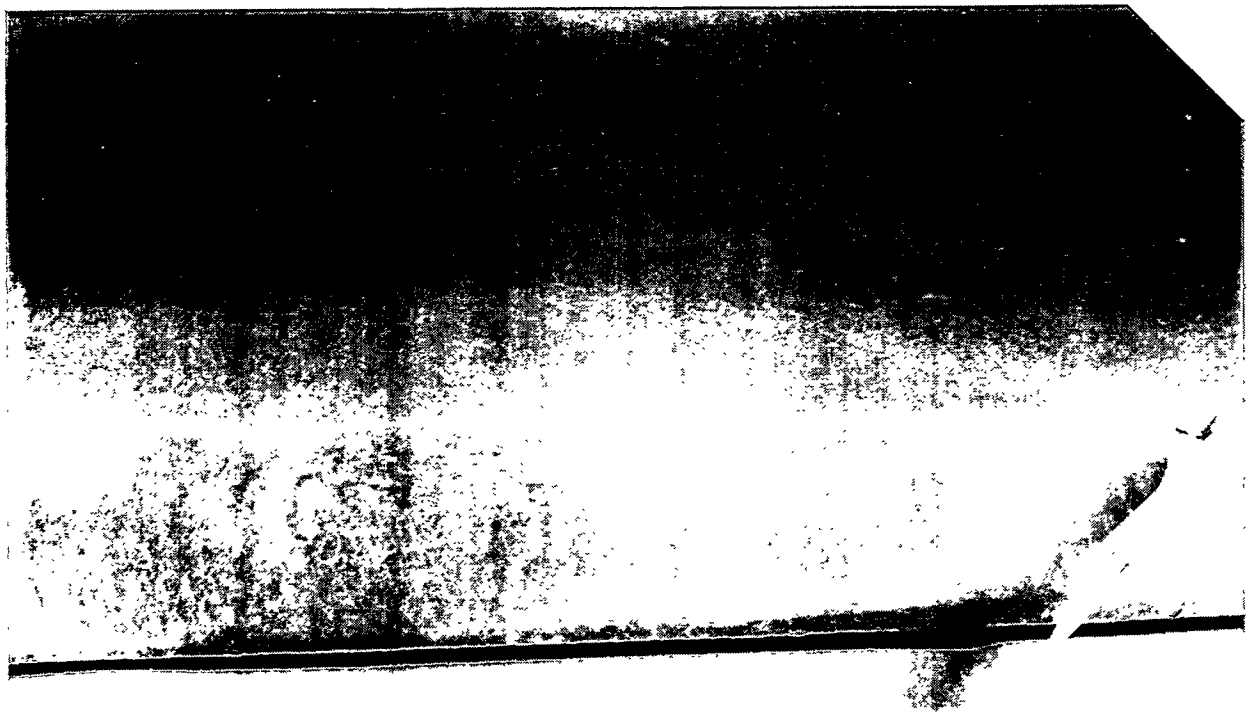

Figure 31d – Failed DuPont PRD-66 Candle Filter (Position B/T-11; Test Segment #5)

Figure 31e – Failed DuPont PRD-66 Candle Filter (Position B/T-11; Test Segment #5)

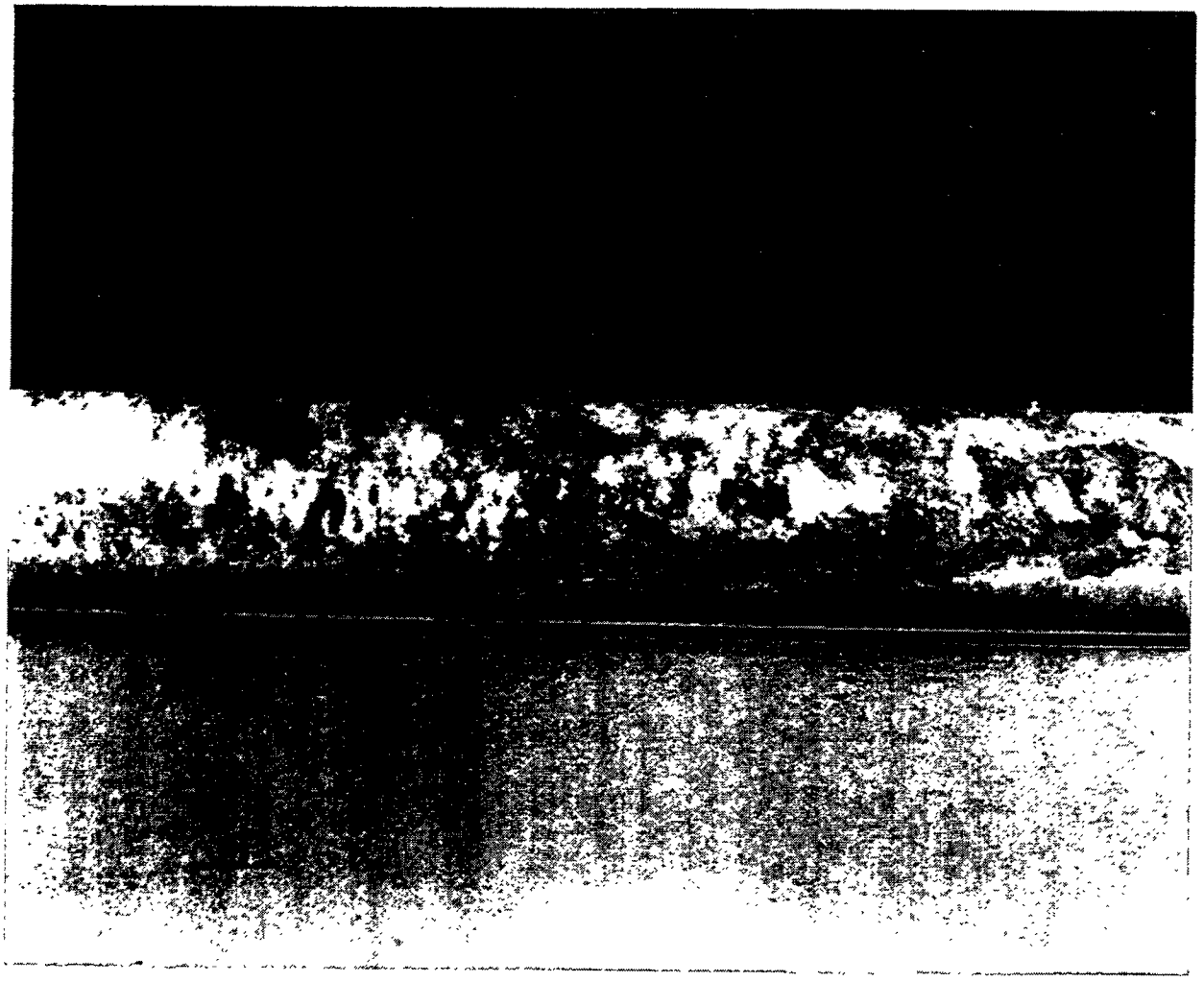

Figure 31f — Failed DuPont PRD-66 Candle Filter (Position B/T-11; Test Segment #5)

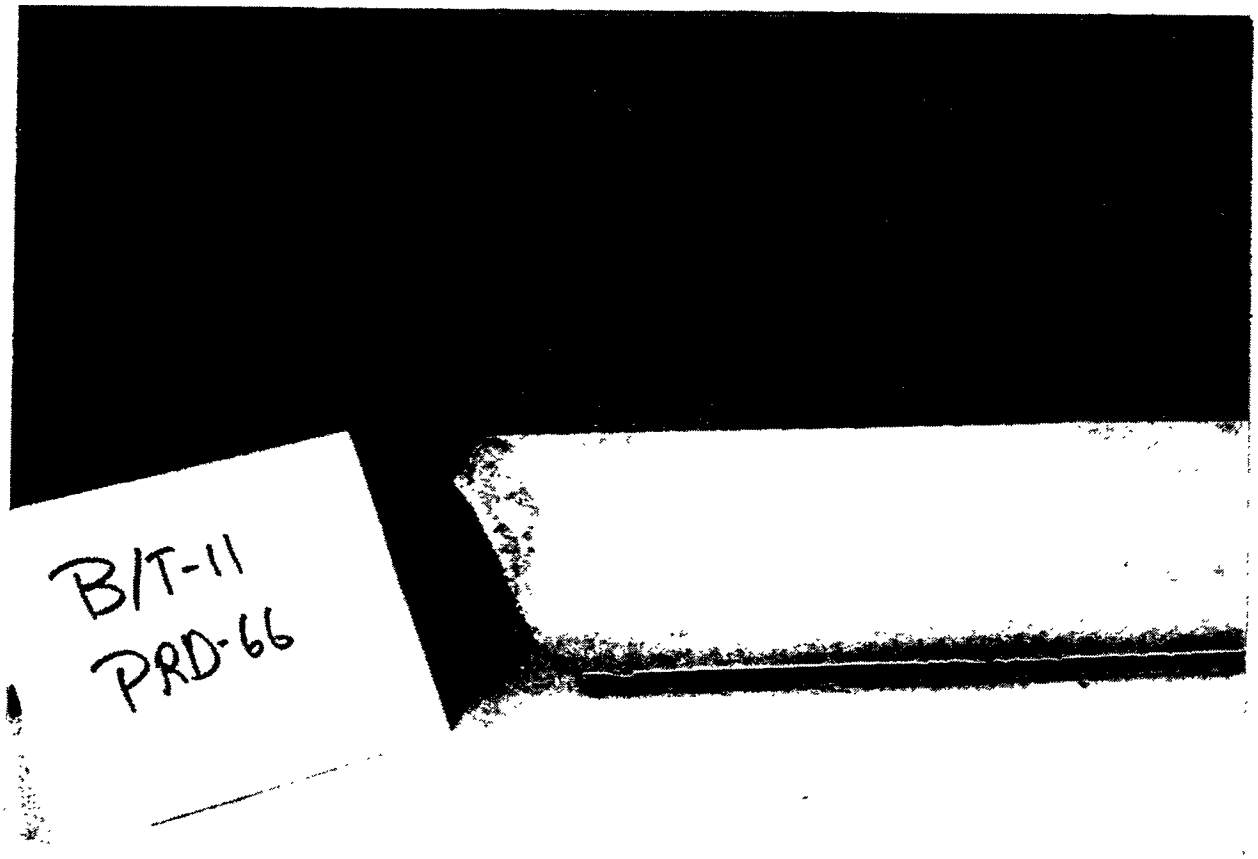

Figure 31g – Failed DuPont PRD-66 Candle Filter (Position B/T-11; Test Segment #5)

Figure 31h – Failed DuPont PRD-66 Candle Filter (Position B/T-11; Test Segment #5)

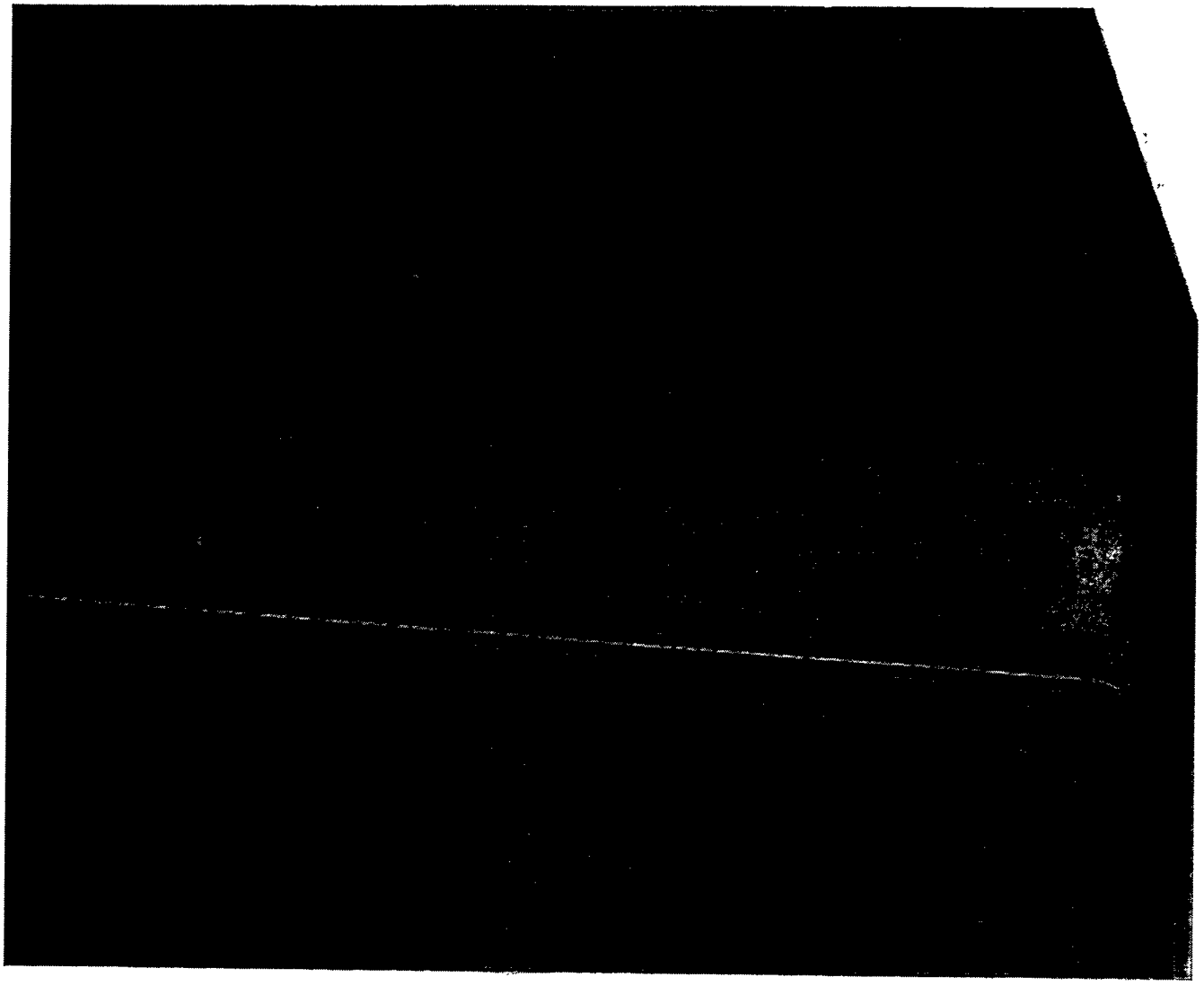

Figure 32a – Failed DuPont PRD-66 Candle Filter (Position B/T-12; Test Segment #5)

Figure 32b – Failed DuPont PRD-66 Candle Filter (Position B/T-12; Test Segment #5)

Figure 32c – Failed DuPont PRD-66 Candle Filter (Position B/T-12; Test Segment #5)

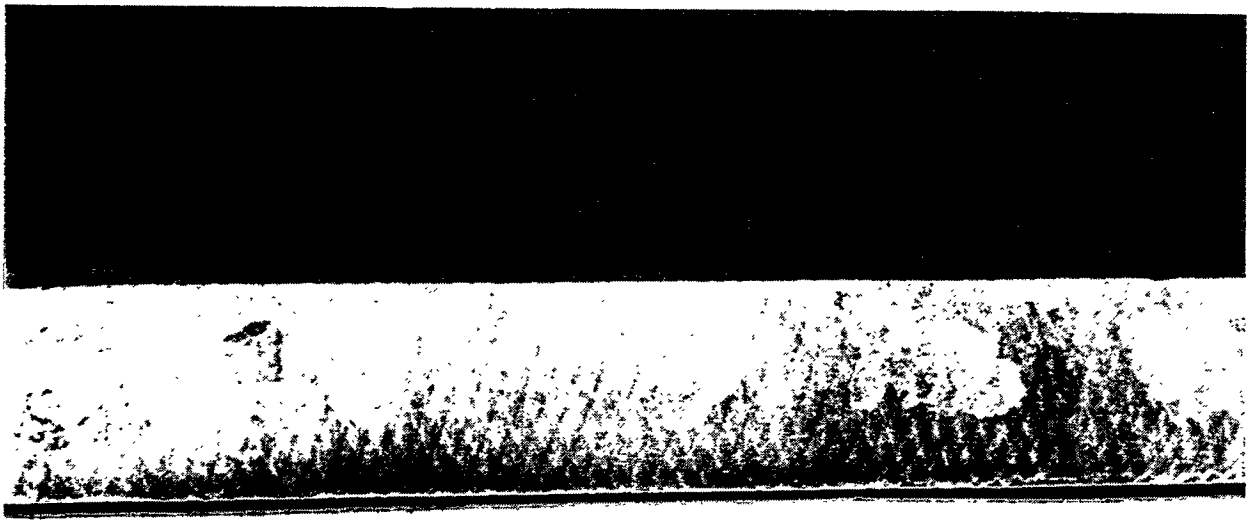

Figure 32d – Failed DuPont PRD-66 Candle Filter (Position B/T-12; Test Segment #5)

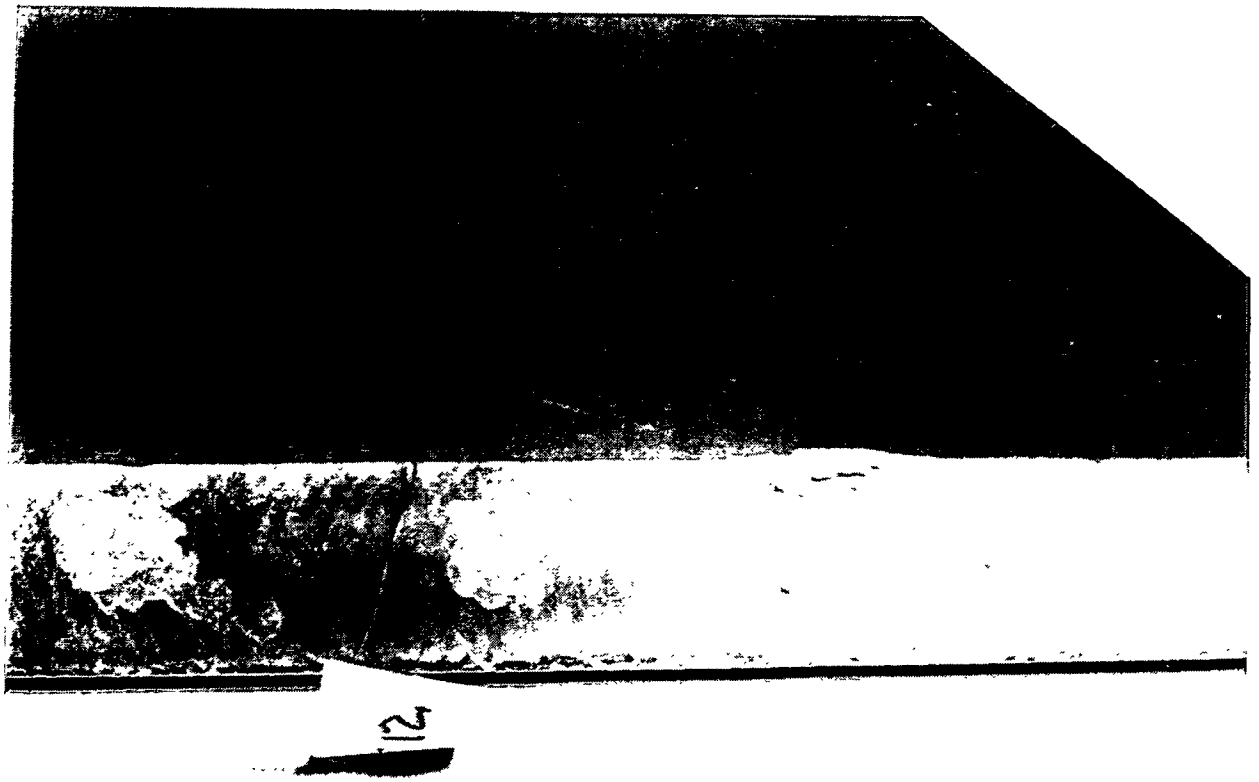

Figure 32e – Failed DuPont PRD-66 Candle Filter (Position B/T-12; Test Segment #5)

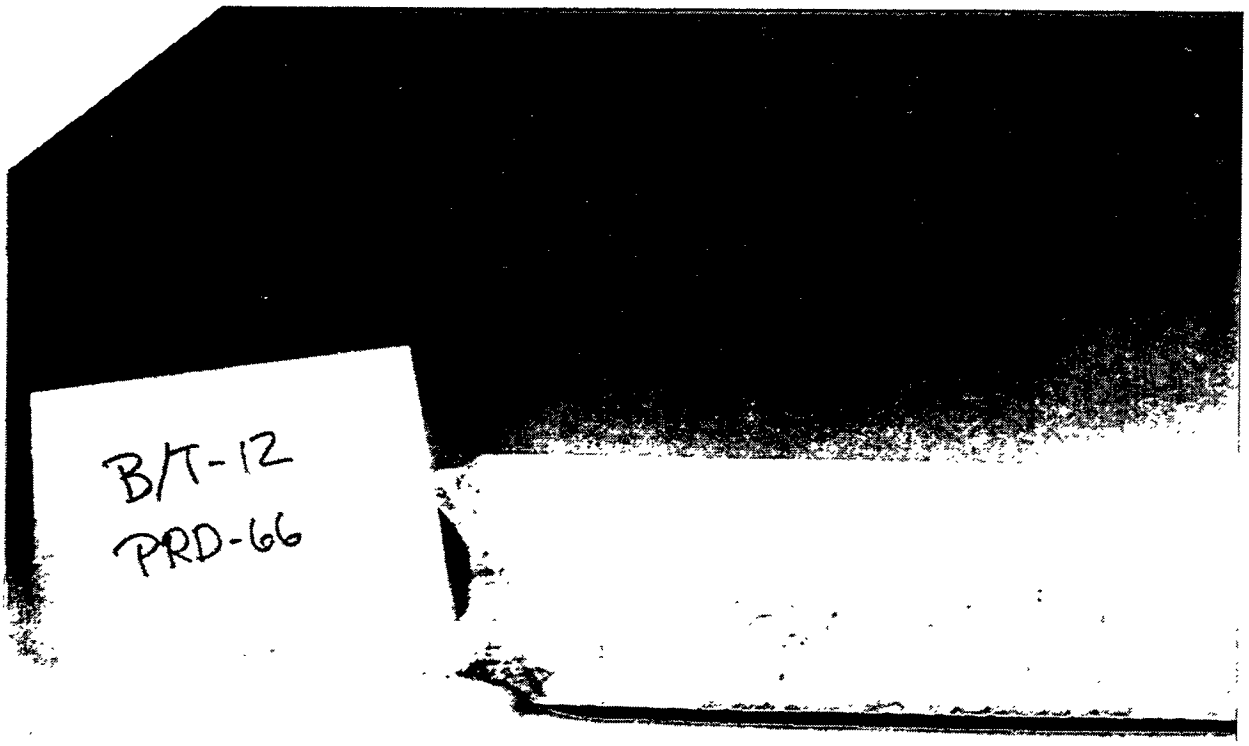

Figure 32f – Failed DuPont PRD-66 Candle Filter (Position B/T-12; Test Segment #5)

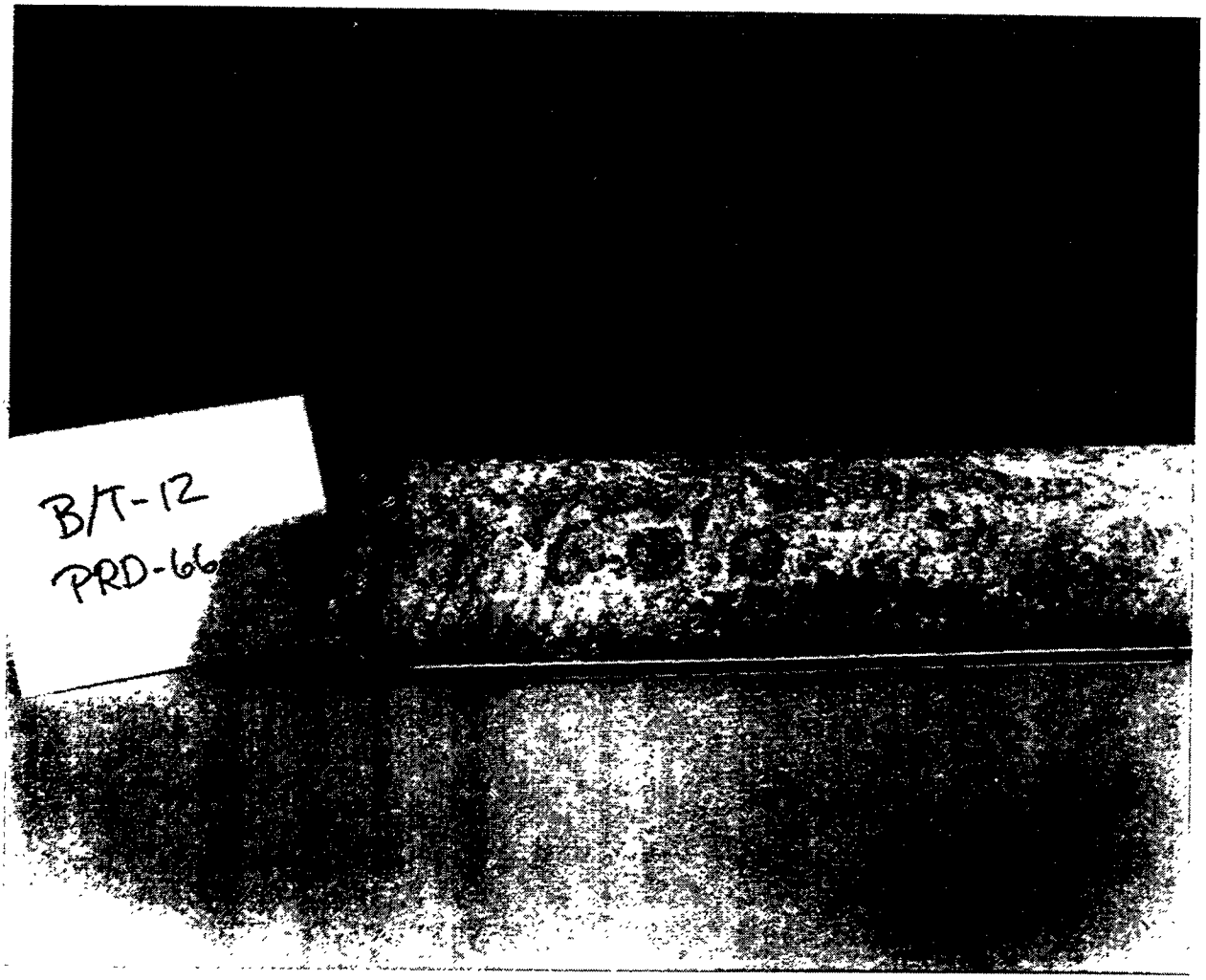

Figure 32g – Failed DuPont PRD-66 Candle Filter (Position B/T-12; Test Segment #5)

Figure 33 – Bottom Holder Nut From A Failed DuPont PRD-66 Candle Filter That Was Located In Position B/T-5 (Test Segment #5)

Frequently during inspection of the failed DuPont PRD-66 filters, the red stain followed a contour that may have suggested condensation and/or gas/ash flow lines along the length of the filter element. These flow lines were typically observed along one side of the filter element, generally off-center from the candle/plenum tangent point. The red stain was also evident along the dust sheds, directly below the PRD-66 candle end caps (Figure 34). Tracking of ash as it falls from the filter elements is expected to have resulted along the dust shed. Perhaps the gas flow path in the top arrays, and/or pulse cleaning gas as it was emitted from an adjacent failed candle filter may be responsible for the red stain that resulted along the PRD-66 candle filters. The red stain along the top array PRD-66 dust sheds was commonly found along the alternate top and middle array sheds. Figure 34 also illustrates the thicker ash cake formation that resulted along the bottom of the PRD-66 candle filters. Shedding and/or spalling of the ash cake layers was evident.

One final comment before closing this section is that the red stain that was commonly found along the DuPont PRD-66 candle filters was not observed along the alternate filter elements (i.e., not even on the white Coors alumina/mullite filter surface). What is expected to have occurred is that ash fines (i.e., red in color from the iron content in the ash) were carried to and became embedded below the membrane and within the bulk filter structure of the DuPont PRD-66 matrix.

REFERENCES

1. J. D. Spain, "Properties of Ceramic Candle Filters," Advanced Coal-Fired Power Systems '95, DOE/METC Contractor's Review Meeting, Morgantown, WV, June 27-29, 1995.

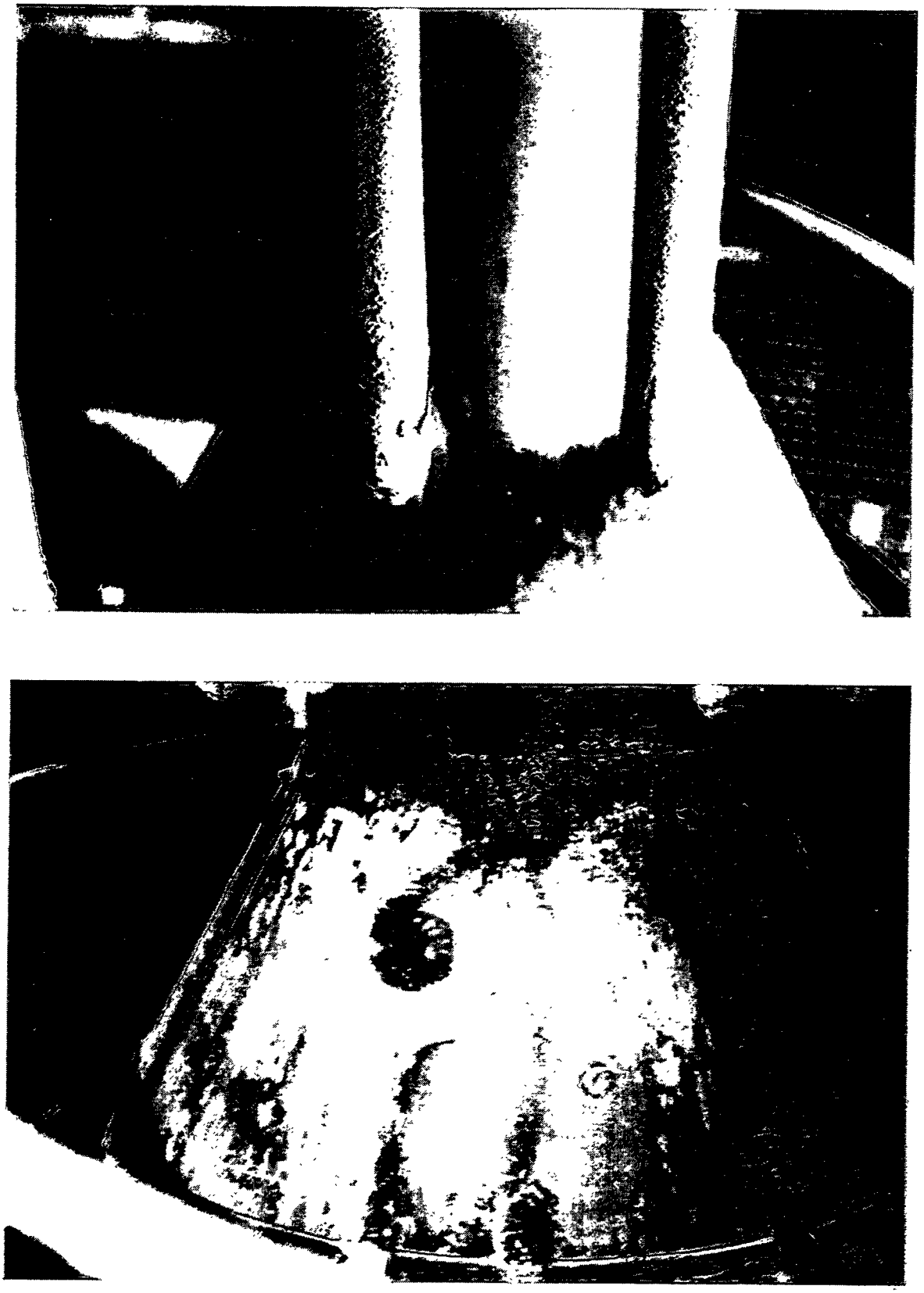

Figure 34 – Red Ash Stain Along The Top And Middle Dust Sheds

APPENDIX C

FILTER ASSESSMENT AND MATERIALS CHARACTERIZATION

M. A. Alvin
July 14, 1995

INTRODUCTION

This Appendix provides a summary of the hot gas filter materials development effort that was conducted by Westinghouse during operation of our Advanced Particulate Filtration (W-APF) system at the American Electric Power (AEP) Demonstration Plant in Brilliant, Ohio. The operating conditions during the entire 5855 hour test program, and the post-test status of the various filter arrays are reviewed.

A discussion is also presented which details the visual inspection of the candle filters after removal of the W-APF internals from the pressure vessel in May 1995. The residual material strengths of the first generation monolithic and advanced, second generation filter elements are also presented.

HOT GAS FILTER TESTING AT AEP

The operating conditions during conduct of the five Test Segments at AEP are provided in Table 1. Initially clay bonded silicon carbide Schumacher Dia Schumalith F40 candle filters which were manufactured in 1991 were utilized to remove particulates released during pressurized fluidized-bed combustion of coal. Bridging frequently resulted in the W-APF causing failure of the clay bonded silicon carbide candle filters. In Test Segments #4 and #5, second generation, advanced filter elements (i.e., Coors alumina/mullite; 3M CVI-SiC composite; and DuPont PRD-66 filters) were installed within the W-APF, and were operated with the primary cyclone either partially detuned or completely removed from service (Table 2). A summary of the test runs for the five Test Segments is provided in Table 3.

Initially 384 Schumacher Dia Schumalith F40 candle filters were installed in the W-APF. After Test Segment #1, all bottom array candles were removed and replaced with newly fabricated Schumacher Dia Schumalith F40 candle filters which had been manufactured in 1992. Due to the extensive bridging that resulted in Test Segment #2, all 384 candle filters were removed from the system, and replaced with newly fabricated Schumacher Dia Schumalith F40 candles that were manufactured in 1992. After Test Segment #3, the top and middle arrays were recandled with newly manufactured and/or aged Schumacher Dia Schumalith F40 filters, and thirty alternate first and/or second generation filters were installed in array B/M and C/M. During conduct of Test Segment #4, all inner row candles had been removed (i.e., blanked off) from the top and middle arrays, and a false bottom was installed on A/M in an attempt to prevent ash accumulation around the filter holder mount. After conduct of Test Segment #4, all 288 filters were removed from the various arrays, and were replaced primarily with Pall Vitropore 442T clay bonded silicon carbide, and Coors alumina/mullite filters. In addition 3M CVI-SiC composite and DuPont PRD-66 filters

TABLE 1
SUMMARY OF THE W-PFBC HOT GAS TESTING AT AEP

Test Segment	1 10/92-12/92	2 7/93-9/93	3 1/94-4/94	4 7/94-10/94	5 1/95-3/95
Number Of Candles	384	384	384	288	288
Primary Cyclone	In-Service	In-Service	Detuned	Detuned	Inactive
Operating Hours	464.4	1295	1278.8	1705.8	1110.4
Operating Temperature, °C	730-790	620-790	650-780	660-760	760-845
Nominal Face Velocity, cm/s	2.4-3.3	2.3-3.3	2.3-3.3	3.0-4.4	4.5
Inlet Dust Loading, ppmw	600	600	3200	3200	18000
Ash Mass Mean, µm	1-3	1-3	5-7	5-7	27

TABLE 2
SUMMARY OF THE CANDLE FILTERS INSTALLED IN THE W-APF AT AEP

PFBC Test Segment	1 10-92-12/92	2 7/93-9/93	3 1/94-4/94	4 7/94-10/94	5 1/95-3/95
Operating Time, Hrs.	464	1295	1279	1705	1110
Operating Temperature, °C	730-790	620-790	650-780	660-760	760-845
Number of Filter Elements					
Schumacher F40	384	384	384	258	5
Schumacher FT20	---	---	---	8	---
Pall Vitropore 442T	---	---	---	8	153
Coors Alumina/Mullite	---	---	---	8	98
3M CVI-SiC Composite	---	---	---	3	10
DuPont PRD-66	---	---	---	3	22

TABLE 3
SUMMARY OF THE TIDD HGCU TESTING

RUN NO.	COAL FIRE DATE	COAL FIRE TIME	UNIT TRIP DATE	UNIT TRIP TIME	COAL FIRE HOURS	NOTES
0	05/21/92	20:26	05/23/92	07:41	35.2	Bypass mode. Coal fire hours not included in totals. Unit trip due to XJ-4 failure.
1	10/28/92	18:10	11/01/92	23:32	101.4	Unit trip due to HGCU ash lockhopper pluggage.
2	11/17/92	09:33	11/17/92	10:50	1.3	Unit trip due to plugged primary cyclones.
3	11/21/92	18:41	11/24/92	22:50	76.2	Unit trip due to coal paste problems.
4	11/25/92	12:11	12/07/92	09:56	285.7	Warm startup. Unit trip due to XJ-7 failure. 21 candles found broken during outage.
TOTAL FOR RUNS 1 - 4					**464.5**	
5	06/30/93	17:28	07/03/93	05:04	59.6	Shutdown to change GT telemetry instrumentation.
6	07/05/93	00:35	07/05/93	17:17	16.7	Completed GT testing.
7	07/18/93	18:20	08/05/93	12:22	426.0	Shutdown due to ash buildup on APF liner.
8	08/09/93	10:18	08/09/93	11:37	1.3	GT trip due to bearing vibration.
9	08/10/93	22:29	08/14/93	05:27	79.0	Warm startup. Shutdown due to low O2 resulting from high coal paste excursion.
10	08/19/93	17:48	08/24/93	13:28	115.7	Manual combustor trip due to unstable bed conditions after switching to limestone.
11	08/29/93	23:31	09/23/93	20:12	596.7	Combustor trip due to leak in sorbent transport pipe. 62 candles found broken during outage.
TOTAL FOR RUNS 5 - 11					**1295.0**	
12	01/10/94	06:41	01/11/94	01:36	18.9	Manual combustor trip due to plugged primary cyclone.
13	01/15/94	23:42	01/29/94	20:31	332.8	Manual combustor trip due to boiler tube leak.
14	02/17/94	14:58	02/18/94	14:14	23.3	Manual combustor trip due to leak in HGCU gas sample connection.
15	02/19/94	06:12	02/25/94	13:09	150.9	Manual combustor trip due to loss of sorbent air compr.
16	03/03/94	10:22	03/09/94	11:30	145.1	Manual combustor trip due to loss of two paste pumps.
17	03/16/94	14:48	03/23/94	10:50	164.0	GT trip due to low lube oil pressure.
18	03/31/94	09:04	04/18/94	20:43	443.7	Manual combustor trip due to internal sorbent injection pipe leak. 28 candles found broken during outage.
TOTAL FOR RUNS 12 - 18					**1278.8**	
19	07/16/94	01:56	07/16/94	04:27	2.5	Manual combustor trip due to loss of three paste pumps.
20	07/16/94	12:59	07/16/94	13:55	0.9	Manual combustor trip due to plugged primary cyclones.
21	07/20/94	19:18	07/27/94	12:08	160.8	Shutdown due to GT vibration.
22	07/28/94	09:59	08/25/94	17:47	679.8	Manual combustor trip due to bad signal relay from the ST generator. 12 candles found broken during outage.
23	09/03/94	01:01	09/10/94	04:07	171.1	Manual combustor trip due to sorbent pipe leak. Operated part-time with P11 cyclone totally spoiled.
24	09/22/94	17:02	10/21/94	11:39	690.6	Planned outage. 30 total candles found broken during outage.
TOTAL FOR RUNS 19 - 24					**1705.8**	
25	01/13/95	13:24	01/13/95	17:47	4.4	Manual combustor trip due to plugged primary cyclone.
26	01/18/95	15:53	01/19/95	08:39	16.8	GT trip due to low control fluid pressure.
27	01/20/95	17:35	01/21/95	00:44	7.1	Manual combustor trip due to unstable bed conditions.
28	01/27/95	00:58	02/02/95	02:05	145.1	Manual comb. trip due to hot spot on HGCU pipe flange.
29	02/09/95	00:30	02/09/95	15:09	14.7	Combustor trip due to high SSH outlet temperature.
30	02/10/95	04:05	02/10/95	18:34	14.5	Hot restart. Manual combustor trip due to gasket leak on HGCU surge hopper.
31	02/11/95	09:26	02/12/95	17:51	32.4	Hot restart. Manual combustor trip due to plugged HGCU Alternate Ash Removal Line.
32	02/13/95	11:40	02/16/95	12:43	73.0	Hot Restart. Combustor trip due to plugged paste nozzles.
33	02/18/95	19:29	03/08/95	14:40	427.2	Manual combustor trip due to loss of two paste pumps.
34	03/14/95	17:15	03/30/95	08:27	375.2	Planned Final Shutdown.
TOTAL FOR RUNS 25 - 34					**1110.4**	
TOTAL FOR RUNS 1 - 34					**5854.5**	

were installed within the top and bottom filter arrays. As in Test Segment #4, the inner row candles in the top and middle arrays were removed during conduct of Test Segment #5.

CANDLE FILTER INSPECTION

A description of the ash cake deposit which resulted along the outer surface of the various candle filters is provided in an alternate Appendix. Measurements of the ash cake thickness at various location along the filter body were made for 19 candles which had been operated in Test Segment #5. As shown in Table 4, the thickness of the residual cake layer appeared to increase at the bottom of the filter elements. As also shown in Table 4, ash accumulation within the ID bore of the filter elements occurred (i.e., end cap area) as a result of pulse cleaning the filter array with 18 failed candle filters. Fracture of the ceramic filter matrix resulted near the end cap area of an alumina/mullite and a clay bonded silicon carbide candle filter which had been filled ~6-8 inches with ash.

Although bridging had not occurred within the various arrays in Test Segment #5, the ash/sorbent cake formed a layer which had a significantly high gas flow resistance (i.e., initial gas flow resistance of a Schumacher Dia Schumalith F40 filter is 4 in-wg/fpm).

MATERIAL STRENGTH CHARACTERIZATION

Operation of the W-APF system at the AEP PFBC Tidd Demonstration Plant in Brilliant, Ohio, was conducted in five test campaigns. Schumacher Dia Schumalith F40 clay bonded silicon carbide candle filters were exposed to process operating temperatures ranging between 620 and 790°C for periods of 464.5, 1295, 1279, and 1705.8 hours in Test Segments #1 through #4, and between 760 and 845°C for 1110 hours in Test Segment #5 (Table 1). In Test Segment #4, eight Schumacher Dia Schumalith FT20, eight Coors alumina/mullite, eight Pall Vitropore 442T candles were included in the 288 candle filter system, while 98 Coors alumina/mullite, and 153 Pall Vitropore 442T candles were installed in the W-APF in Test Segment #5. During conduct of Test Segments #4 and #5 at AEP, several advanced, second generation filter elements were also installed within various arrays. The following sections present a discussion of the currently available Test Segment #4 and #5 material characterization analyses for the first generation monolithic and advanced second generation porous ceramic candle filters.[1,2]

Schumacher Dia Schumalith F40

Schumacher Dia Schumalith F40 surveillance candles successfully achieved 5855 hours of operation in the W-APF system at Tidd. The residual bulk strength of the Schumacher Dia Schumalith F40 matrix was determined via room temperature and process temperature C-ring compressive and tensile testing using 15 mm samples that were cut with a diamond wheel from the PFBC-exposed filter elements. As shown in Figure 1 and Table 5, the bulk strength of the Schumacher Dia Schumalith F40 matrix decreased during the initial 1000-2000 hours of PFBC operation. With continued operation, however, the bulk strength of the Schumacher Dia Schumalith F40 matrix remained constant. The residual or "conditioned" strength was considered to result from the complete or nearly complete crystallization of the binder phase that encapsulated the silicon carbide grains, as well as the bond posts or ligament surfaces.

TABLE 4
W-APF CANDLE FILTER INSPECTION/EVALUATION

Filter Location	Filter ID No.	Test Segment	Δ Length, mm	Ash Depth, mm	Ash Layer Thickness, mm (Candle OD) Top	Middle	Bottom	Flow Resistance, in-wg @ 10 ft/min
Schumacher Dia Schumalith F40 - 5855 Hours								
B/B-16	S492/322B	1-5	7	49	1-4	1-2	2-3	
A/T-16	S228/318B	1-5	5	322	2-3	1-2	2-3	
Pall Vitropore 442T - 2815 Hours								
B/M-5	R3-300	4-5	27	222	0-2	1-2	3-4	29.9*
B/M-6	R4-301	4-5	17	46	1-2	1-4	1-3	70
B/M-7	R2-302	4-5	19					
Pall Vitropore 442T - 1110 Hours								
B/B-1	R1-375	5	1	17	1-2	2-4	3-4	21.4
B/M-1	R3-306	5	0	174	0-2	1-2	4-6	67.2
B/M-13	R4-296	5	1	146	1-2	2	3-4	67.2
B/M-14	R4-344	5	2	66	1-2	1-2	2-4	48.1
B/M-15	R1-315	5	2	49	1-3	1-2	1-2	77.6
B/M-19	R2-286	5	(3) **	48	1-3	1-2	3	24.6
B/M-2	R2-341	5	4	198	1	1	1	89.4
B/M-3	R5-316	5	0	183	0-1	2	3-6	95.6
B/M-4	R4-341	5	2	234	1-2	2-3	5-6	93.6
B/M-8	R3-298	5	0					
B/M-9	R5-345	5	0					
B/M-20	R1-342	5	1	49	1	1-2	1	29.9
B/M-22	R1-341	5	4	156	2	1-2	3-4	79
C/B-11	R2-370	5	3	57	2-3	2-4	2-4	
C/M-1	R4-402	5	0	82	1	1-2	1-2	
C/M-2	R3-386	5	1	157	0-2	1	3-4	65.1
C/T-11	R3-396	5	3	95	1	2-3	3-4	

* Broken At Flange During Post-Test Inspection.
** ( ) Indicate Negative Values.

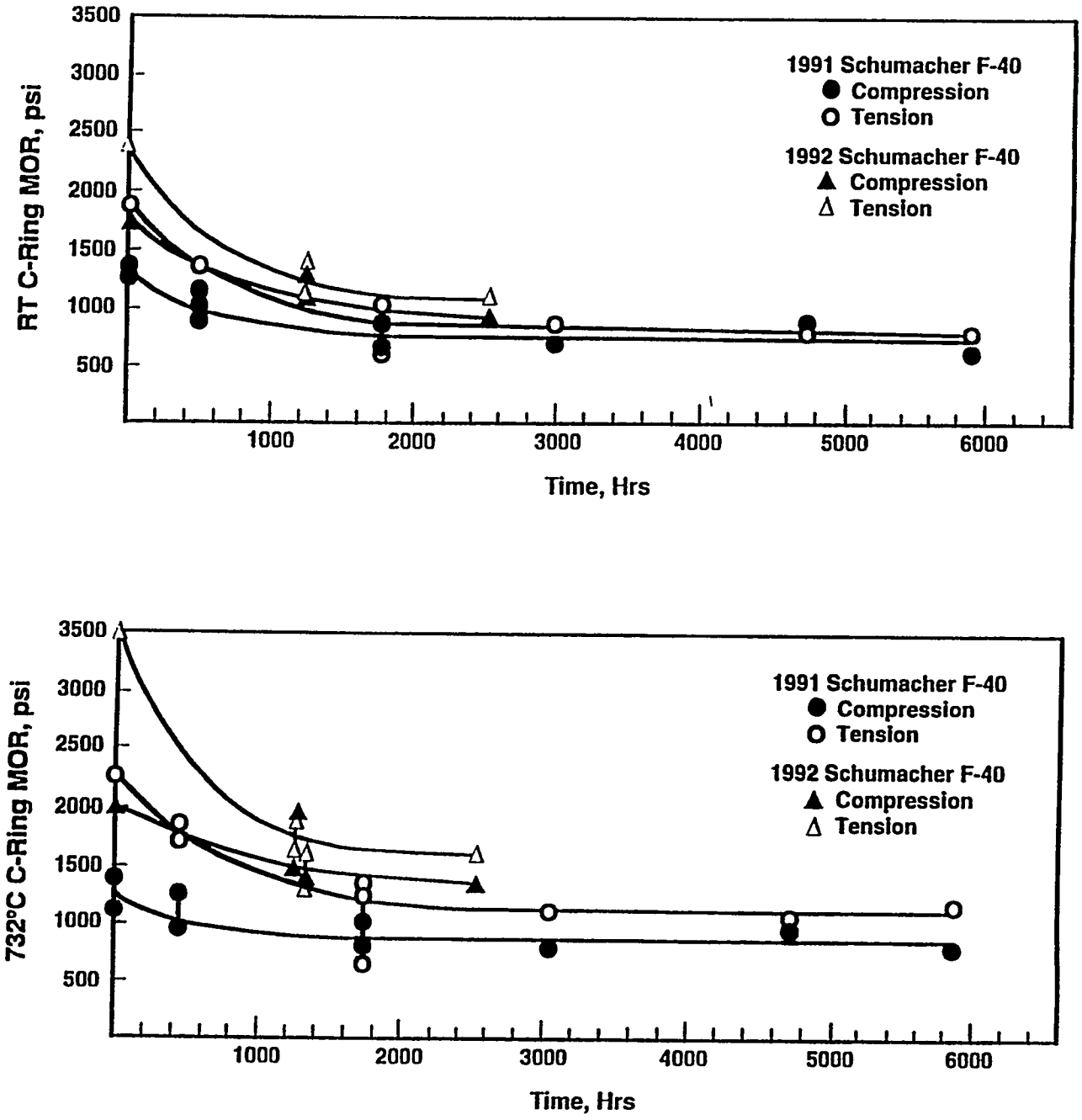

Figure 1 — Residual Strength of the Schumacher Dia Schumalith F40 Candle Filters During Operation in the W-APF at AEP

TABLE 5
CANDLE FILTER BULK MATRIX STRENGTH

Filter Matrix	Candle Filter Location	Test Segment No.	Operating Time, Hrs	C-Ring Testing: Room Temperature Strength, psi Compression	C-Ring Testing: Room Temperature Strength, psi Tension	C-Ring Testing: High Temperature (732°C) Strength, psi Compression	C-Ring Testing: High Temperature (732°C) Strength, psi Tension
Schumacher Dia Schumalith F40 - 1991 Production Lot							
S153/317B	---	---	---	1300±213	1907±111	1416±127	2328±228
S504/322B	B/T-1	1	464	1120±123		1226±116	
S436/321B	B/M-1	1	464	1096±116		1172±134	
S193/318B	B/B-1	1	464	1147±119		1245±108	
S065/314B	A/B-6	1	464	940± 60		1056±131	
S106/317B	B/B-45	1	464	1180±98		1230±127	
S324/319B	B/B-9	1	464	1083±148	1438±108	1137±101	1778±246
S109/317B	B/B-41	1	464	1140±120	1424±162	1132±112	1873±174
S215/378B	B/M-22	1,2	1760	908±72	1117±91	1064±72	1418±122
S447/322B	A/T-22	1,2	1760	794±50	709±71	1028±94	973±121
S455/322B	B/T-22	1,2	1760	793±58	711±89	989±77	885±54
S523/322B	C/T-22	1,2	1760	793±39	1016±134	968±96	1252±241
S418/321B	B/T-16	1,2,3	3038	720±57	944±172	890±65	1284±199
S422/322B	B/B-16	1,2,3,4	4734	870±145	816±112	1031±105	1139±160
S228/318B	A/T-16	1,2,3,4,5	5855	592±56	763±87	777±57	1208±99
						891±52 (a)	966±47 (a)
Schumacher Dia Schumalith FT20							
S199/315E	---	---	----	2296±261	2268±167	3034±148	2708±360
S039/312E	C/M-15	4	1705	2283±184	2370±238	3041±238	3102±272
Pall Vitropore 442T							
R2-325	---	---	---	2857±186	2574±177	3430±221	3029±149
R5-325	B/M-20	4	1705	2311±231	2034±139	2453±187	2138±180
R2-360	C/T-1	5	1110	2569±132	2277±156	2721±138	2201±212
						2454±214 (a)	2115±238 (a)
Coors Alumina/Mullite							
DC-013	---	---	---	2575±182	2721±415	3107±276	3353±231
DC-003	B/M-16	4	1705	2475±189	2903±289	2738±161	3291±246
DC-056	A/T-17	5	1110	2079±140	2392±130	2368±93	2636±238
						2512±107 (a)	2717±167 (a)
DC-068	A/T-1	5	1110	1958±68	2544±214	1800±135	2542±196
						2079±85 (a)	2659±109 (a)
DC-002	B/M-17	4,5	2815	2097±119	2063±178	2200±141	2146±362
						2360±116(a)	2287±251(a)

(a) High Temperature Strength Testing Conducted at 843°C

TABLE 5 (cont'd)

CANDLE FILTER BULK MATRIX STRENGTH

				C-Ring Testing					
		Test	Operating	Room Temperature		High Temperature (732°C)		High Temperature (843°C)	
Filter	Filter	Segment	Time,	Strength, psi		Strength, psi		Strength, psi	
ID No.	Location	No.	Hrs	Compression	Tension	Compression	Tension	Compression	Tension
D-99	---	---	---	1219±162	1265±188	1277±178	1304±327	NA	NA
D-132	B/M-7	4	1705	1830±238	1725±320	1884±142	1642±401	NA	NA
D-237	B/M-8	5	1110	1533±202	1380±188	1897±256	1356±104	1872±230	1460±197

				Diametral O-Ring Testing					
	Candle	Test	Operating	Room Temperature		High Temperature (732°C)		High Temperature (843°C)	
	Filter	Segment	Time,	Strength, psi		Strength, psi		Strength, psi	
Filter ID No.	Location	No.	Hrs		Triaxial		Triaxial		Triaxial
				Composite	Briad	Composite	Braid	Composite	Braid
43-1-2	---	---	---	1341±254	14026±2012	1060±219	11012±1795	NA	NA
43-1-6	B/M-15	4	1705	1696±195	18220±1356	1429±159	15599±2246	NA	NA
45-18-02	C/T-18	5	1110	2333±415	18975±3117	2225±361	18001±3745	1850±299	16173±2245

NA: Not Available.

In order to ascertain whether the Schumacher Dia Schumalith F40 filter matrix experienced creep during operation in the PFBC environment, the overall length of the surveillance filter elements were measured during outages, and compared to their initial, as-manufactured lengths. After 5855 hours of operation in the W-APF at AEP, the 1.5 m elements were observed to have elongated by 5-7 mm. Cracks were not evident along the external surface of the filter elements (i.e., particularly below the flange).

During operation of the W-APF in the initial test segments, failure of the Schumacher Dia Schumalith F40 filter elements had previously occurred at the base of the flange, primarily during cool-down after ash bridging extensively deposited fines between adjacent filter elements, and/or the plenum support pipe and dust sheds. Failure of the Schumacher Dia Schumalith F40 filter matrix also resulted when a densified plug of fines was embedded within the ID bore of the filter element. The difference between the thermal coefficient of expansion of the ash, ceramic, and/or metal structure was considered to be responsible when failure of the Schumacher Dia Schumalith F40 clay bonded silicon carbide filters occurred at AEP.

Schumacher Dia Schumalith FT20

Eight improved, high temperature, creep resistant Schumacher Dia Schumalith FT20 clay bonded silicon carbide candles were installed and operated in the W-APF system in Test Segment #4 at AEP. The initial bulk strength of the Schumacher Dia Schumalith FT20 matrix was stronger than the 1991 Schumacher Dia Schumalith F40 filter production lot which had been used throughout the entire test program. The as-manufactured bulk strength of the Schumacher Dia Schumalith FT20 matrix was, however, comparable to the 1992 Schumacher Dia Schumalith F40 filter production lot.

As shown in Table 5, the residual bulk strength of the Schumacher Dia Schumalith FT20 matrix after 1705 hours of successful operation in the W-APF at AEP was comparable to that of the initial bulk strength of the filter matrix. Scanning electron microscopy/energy dispersive x-ray analyses (SEM/EDAX) are currently being performed to discern whether changes within the morphology of the binder phase that encapsulates the silicon carbide grains have occurred.

Pall Vitropore 442T

During operation at AEP in Test Segment #4, eight Pall Vitropore 442T filter elements were installed and operated in the W-APF system. All eight filter elements were successfully operated for a period of 1705 hours. As shown in Table 5, a loss of bulk material strength resulted in the Pall Vitropore 442T filter matrix (i.e., 19% room temperature and 29% process temperature compressive strength; 21% room temperature and 29% process temperature tensile strength).

Three of the Test Segment #4 Pall Vitropore 442T filter elements were reinstalled in the W-APF, and were successfully operated for a period of 1110 hours in Test Segment #5. Post-test inspection indicated that the Pall Vitropore 442T filters elongated by 17-20 mm after 2815 hours of operation at AEP. Cracks were not evident along the elongated Pall Vitropore 442T candle filter body (i.e., particularly below the flange).

During operation in Test Segment #5, 150 newly manufactured Pall Vitropore 442T candle filter elements were installed in the W-APF system. All candles remained intact after 1110 hours of operation. Post-test characterization of seventeen elements indicated that the filters elongated by 0-4 mm. Since the filter elements were identically manufactured for both test segments at AEP, the limited elongation of the clay bonded silicon carbide filter matrix after 1110 hours of operation in the 760-845°C, PFBC environment in test Segment #5 vs 17-20 mm elongation after 1705 hours of operation in the 660-760°C, PFBC environment implies the lag time that is required to initiate high temperature creep within the binder containing Pall Vitropore 442T filter matrix.

Alumina/Mullite

Eight Coors alumina/mullite filters were installed in the W-APF system during conduct of Test Segment #4 at AEP. All Coors alumina/mullite filter elements remained intact after 1705 hours of operation in the 660-760°C PFBC gas environment. The residual bulk strength of the 1705 hour PFBC-exposed Coors alumina/mullite filter matrix was comparable to that of the as-manufactured filter matrix (Table 5).

Three of the Test Segment #4 Coors alumina/mullite filters were installed in the W-APF system prior to initiating Test Segment #5. Post-test inspection indicated that all three of the Coors alumina/mullite filters remained intact, achieving 2815 hours of successful operation. Materials characterization of the 2815 hour, PFBC-exposed, Coors alumina/mullite filter matrix is currently being conducted.

In addition 95 newly manufactured Coors alumina/mullite filters were installed in the W-APF system during conduct of Test Segment #5 at AEP. After 1110 hours of PFBC operation at temperatures of 760-845°C, two of the 95 filters had failed, while the remaining 93 Coors alumina/mullite filters remained intact. One of the Coors alumina/mullite filters failed directly below the flange, while the second filters fractured at approximately 1000 mm below the flange. The circumferential fracture of the mid-body failed Coors alumina/mullite filter was similar to the fracture patterns generated during HTHP thermal transient testing at Westinghouse vs the longitudinal fractures experienced in the matrix during operation in the Ahlstrom PCFBC test facility in Karhula, Finland. The difference between the nearly circumferential vs longitudinal fracture may reflect the response of the matrix to the lower operating temperatures and/or the redesigned end cap and uniform wall thickness that was utilized to produce candle filters for use at AEP and at Westinghouse.

Characterization of the residual bulk strength of the 1110 hour, PFBC-exposed, Coors alumina/mullite filter elements indicated that the Coors alumina/mullite matrix tends to lose strength during operation in the 760-845°C, oxidizing environment (i.e., 22% room temperature and 33% process temperature compressive strength; 9% room temperature and 23% process temperature tensile strength). These data perhaps imply a sensitivity of the Coors alumina/mullite matrix to process operating temperature which may either induce or accelerate phase changes, or enhance crack propagation properties along the ID surface and/or through the 10 mm filter wall.

A further reduction to residual bulk strength along the ID surface and/or through the filter wall was exhibited within the Coors alumina/mullite filter matrix after 2815 hours of operation in the PFBC environment (Test Segment #4 and #5).

As shown in Figure 2, extensive mullitization resulted along the pore cavity wall of the Coors alumina/mullite filter matrix as both operating time and process temperature increased. As determined by qualitative x-ray diffraction analysis, minor dissociation of mullite that was present in the as-manufactured Coors filter matrix was initiated early during process operation. Simultaneously a reduction and/or depletion of the as-manufactured anorthite and glass phases resulted, leading to the production of trace and minor concentrations of alumina, cordierite and cristobalite within the bulk matrix. Retention of the bulk matrix strength with time will largely depend on the rate of cristobalite and cordierite grain growth, which could ultimately lead to the formation of microcracks and loss of material strength. Since phase conversion appears to have stabilized within the first 1100 hours of operation, additional microcrack formation and/or loss of bulk material strength would be attributed to thermal fatigue (i.e., increased pulse intensity or duration) and/or thermal shock of the Coors alumina/mullite filter matrix during high temperature PFBC process operation.

Post-test inspection of the W-APF arrays indicated that one of the Coors alumina/mullite filters had a hairline crack at ~8 inches from the end cap of the filter element. After removal of the element from its filter holder, ash was evident within the ID bore of the candle. Although the hairline crack was visibly evident, tracking of fines across the 10 mm candle filter wall was not apparent. Fracture of the Coors alumina/mullite matrix was considered to have occurred when a densified plug of fines was embedded within the ID bore of the filter element. The difference in thermal coefficient of expansion of the ash and the porous ceramic filter was considered to be responsible for crack initiation within the alumina/mullite filter body.

Comment

Although the Coors alumina/mullite filter matrix experienced a loss of bulk strength in Test Segment #5, and the Pall Vitropore 442T filter elements experienced elongation in Test Segment #4, and lost strength in Test Segments #4 and #5, virtually no change in bulk strength was evident for the improved, high temperature, creep resistant Schumacher Dia Schumalith FT20 filter matrix after 1705 hours of operation at AEP. What has clearly been demonstrated was that the Schumacher Dia Schumalith F40 matrix experienced numerous phase changes and a loss of bulk material strength, but attained a "conditioned" strength of 600-1200 psi which was acceptable for extended operation in the PFBC environment.

3M CVI-SiC Composite Filters

Three 3M CVI-SiC composite filters had been initially installed in a middle array in the W-APF in July 1994, and after 1015 hours of operation, two of the elements failed at the base of their flange. The third 3M filter element, which remained intact and achieved 1705 hours of PFBC test operation prior to termination of Test Segment #4 at AEP, was recovered for materials characterization.

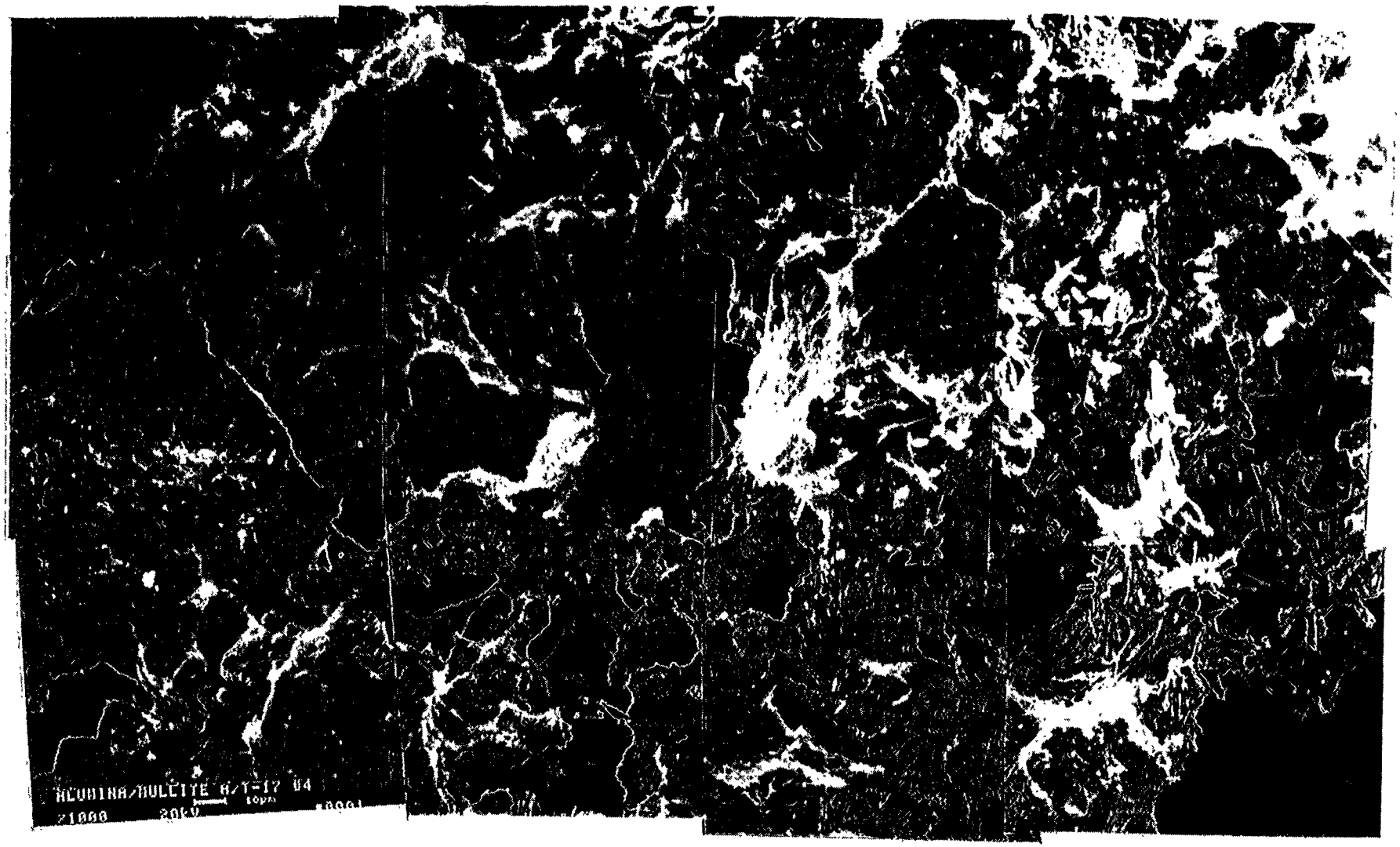

Figure 2a. - Crystallization of the Coors Alumina/Mullite Filter Matrix after 1100 Hrs of PFBC Operation in Test Segment #4

107

Figure 2b - Crystallization of the Coors Alumina/Mullite Filter Matrix after 2815 Hrs of PFBC Operation in Test Segments #4 and #5

Post-test, room temperature, gas flow resistance measurements of the intact PFBC-exposed 3M filter indicted that the pressure drop across the element was ~220 in-wg at a gas face velocity of 10 ft/min. The room temperature pressure drop across the ash coated 3M filter was relatively high in comparison to alternate filter elements which were exposed to similar PFBC test conditions (i.e., Coors alumina/mullite: 50 in-wg at 10 ft/min). The high pressure drop across the 3M PFBC-exposed candle filter was attributed to the adherence of the dust cake layer along and within the confinement layer, as well as through the filtration mat, and triaxial support braid.

Characterization of the 3M CVI-SiC matrix via scanning electron microscopy/energy dispersive x-ray analysis indicated that minor changes in the morphology of the filter matrix had occurred after 1705 hours of operation in the 660-760°C, W-APF system at AEP. Due to deposition of the thin <1 μm interface coating, it was frequently difficult to discern whether the interface coating had remained intact. A gap or separation was considered to exist between the CVI-SiC coating and the underlying Nextel™ 312 fibers in several areas of the PFBC-exposed 3M composite filter matrix. In the high temperature PFBC environment, oxidation of the interface coating is expected to occur.

Post-test diametral compressive strength testing indicated that the strength of the PFBC-exposed 3M CVI-SiC composite matrix was greater than that of the as-manufactured filter matrix (Table 6). Crystallization of the amorphous phase which is initially expected to be present in the as-manufactured Nextel™ 312 fibers, may be responsible for strengthening of the filter matrix. Alternately, due to accumulation of fines within the PFBC-exposed matrix, "wedging" of fines in between the SiC coated fibers may require a higher load to be applied to the matrix prior to failure, thus generating what appeared to be a strengthened composite matrix. During diametral compressive strength testing, the relatively low load bearing, 732°C (i.e., nominal operating temperature), PFBC-exposed, 3M CVI-SiC matrix generally retained the graceful fiber "pull-out" characteristics of the fracture toughened, as-manufactured matrix.

Testing was reinitiated at AEP in January 1995 during which time ten newly manufactured, 3M CVI-SIC composite filters were installed in the W-APF system. After 1110 hours of filter operation at temperatures ranging between 760 and 845°C, testing was terminated. Post-test inspection of the filter cluster indicated that all ten of the 3M CVI-SiC composite filter elements were intact. Further inspection of the 3M candles indicated that ash had been carried into the ID bore of the elements due to a breach within an alternate filter array. As a result, ash fines became tightly packed in the bottom of the filter elements. After cool-down of the W-APF, cracks were evident along the internally ash plugged section of at least one filter element. Along an alternate 3M filter element, a 25.4 mm diameter hole was evident along the outer confinement layer. The location of the removed confinement layer was ~75 mm below the flange.

Assuming that the strength of the as-manufactured 3M filters which were used for testing at Tidd in Test Segment #5 was equivalent to the strength of the as-manufactured filter elements which were used in Test Segment #4, strength characterization of the 1110 hour, Tidd-exposed, 3M CVI-SiC composite filter elements indicated that the ash-filled matrix once again appeared to increase. The shape of the load vs deflection curves generated during high temperature C-ring strength testing are being evaluated to determine the residual fracture toughness of the 3M CVI-SiC composite filter matrix after 1110 hours of exposure in the elevated temperature PFBC environment.

TABLE 6
RESIDUAL STRENGTH OF THE 3M CVI-SiC COMPOSITE FILTER MATRIX
AFTER EXPOSURE IN THE W-APF

Filter ID No.	Candle Filter Location	Test Segment No.	Operating Time, Hrs	Diametral O-Ring Testing					
				Room Temperature Strength, psi		High Temperature (732°C) Strength, psi		High Temperature (843°C) Strength, psi	
				Composite	Triaxial Briad	Composite	Triaxial Braid	Composite	Triaxial Braid
43-1-2	—	—	—	1341±254	14026±2012	1060±219	11012±1795	NA	NA
43-1-6	B/M-15	4	1705	1696±195	18220±1356	1429±159	15599±2246	NA	NA
45-18-02	C/T-18	5	1110	2333±415	18975±3117	2225±361	18001±3745	1850±299	16173±2245

NA: Not Available.

DuPont PRD-66 Filament Wound Filters

During operation of the W-APF system in Test Segment #4, three DuPont PRD-66 filter elements were installed in a middle array. After 1705 hours of operation, all three filters remained intact. During C-ring preparation of the Tidd-exposed PRD-66 filter element, magnesium sulfate recrystallized along the outer surface of the filter, as a result of leaching of the ash that was contained within the filter ID bore and wall during wet cutting with a diamond wheel. Post-test strength characterization of the PRD-66 matrix indicated that the bulk strength of the ash filled matrix tended to increase after 1705 hours of operation at AEP in Test Segment #4 (Table 7).

Twenty-two DuPont PRD-66 candle filters were installed in a top array for operation in Test Segment #5. After ~232 hours of operation, sections of the PRD-66 matrix were identified in the ash hopper discharge, implying that failure had occurred. Testing continued, and after ~775 hours of operation, additional sections of the PRD-66 filter matrix were evident in the ash hopper discharge.

Testing was terminated after 1110 hours of operation in Test Segment #5. Post-test inspection of the W-APF internals indicated that ash bridging had been eliminated as the result of completely detuning the primary cyclone. Only two of the DuPont PRD-66 filter elements remained intact, four had suffered either mid-body fracture or failure at a location that was ~3/4 below the flange, and sixteen filters had fractured at the base of the flange. The outer surface of the intact and fractured filters was generally "ash free", particularly along the portion of the body that was adjacent to the plenum pipe, and to approximately mid-way down the length of the filter element. Alternately 1-2 mm of ash was deposited along the outer surface of the PRD-66 candles, near the bottom end cap. "Divot-like" formations resulted in lines which ran parallel down both sides of the remaining intact and fractured filter elements. Localized "divoting" was also observed underneath the outer protected gasket sleeve, as well as in alternate, isolated areas along the filter body. Currently the mechanisms leading to "divoting", flange fracture, and mid-body failure of the DuPont PRD-66 filter elements in Test Segment #5 are under investigation. Since the PRD-66 filter array had suffered failure after ~232 hours of operation, ash filled the inside bore of the remaining PRD-66 candles (i.e., 120 mm and 350 mm) during pulse cycling. Unlike the 3M CVI-SiC matrix, failure of the ash-filled PRD-66 end cap region was not observed.

Assuming that the strength of the PRD-66 elements used in Test Segment #5 was equivalent to the strength of the PRD-66 elements used in Test Segment #4, post-test strength characterization of the 1110 hour Tidd-exposed PRD-66 filter matrix indicated that an increase in strength appeared to have occurred along the ash-filled OD surface, while virtually no change in strength was detected along the ID or pulse cycled surface of the filament wound matrix.

CONCLUSIONS

- Generally successful performance of all filter materials resulted at PFBC operating temperatures of 700-800°C.

- Conditioning of the Schumacher Dia Schumalith F40 filter matrix occurred (i.e., bulk strength stabilization; phase changes) during extended operation in the PFBC environment.

TABLE 7
RESIDUAL STRENGTH OF THE DuPONT PRD-66 FILTER MATRIX
AFTER EXPOSURE IN THE W-APF AT AEP

Filter ID No.	Filter Location	Test Segment No.	Operating Time, Hrs	C-Ring Testing: Room Temperature Strength, psi		High Temperature (732°C) Strength, psi		High Temperature (843°C) Strength, psi	
				Compression	Tension	Compression	Tension	Compression	Tension
D-99	—	—	—	1219±162	1265±188	1277±178	1304±327	NA	NA
D-132	B/M-7	4	1705	1830±238	1725±320	1884±142	1642±401	NA	NA
D-237	B/M-8	5	1110	1533±202	1380±188	1897±256	1356±104	1872±230	1460±197

- High temperature creep of the nonoxide-based, binder containing monolithic materials has been addressed by the various candle filter suppliers through the production of improved high temperature binder, creep resistant filter materials.

- Advanced second generation filter materials have been introduced and operated in the PFBC environments.

REFERENCES

1. M. A. Alvin, T. E. Lippert, E. S. Diaz, and E. E. Smeltzer, "Thermal and Chemical Stability of Ceramic Candle Filters," Paper presented at the DOE/METC Advanced Coal-Fired Power Systems '95 Review Meeting, Morgantown, WV, June 27-29, 1995.

2. M. A. Alvin, T. E. Lippert, E. S. Diaz, and E. E. Smeltzer, "Filter Component Assessment," Paper presented at the DOE/METC Advanced Coal-Fired Power Systems '95 Review Meeting, Morgantown, WV, June 27-29, 1995.

APPENDIX D

CHARACTERIZATION OF TIDD ASH DEPOSITS IN THE W-APF

— TEST SEGMENT #5 —

M. A. Alvin
July 6, 1995

Ash samples were recovered from various locations in the Westinghouse Advanced Particulate Filtration (W-APF) vessel at AEP in May 1995 after completion of Test Segment #5. Table 1 provides a brief description of these materials.

Several distinctive features were evident in the Test Segment #5 ash sample materials. These included:

- A typically thin, lighter color, outer layer of ash covered a thick red ash cake deposit. Previously Westinghouse learned that final deposition of fines within the filter vessel resulted from carryover of primary cyclone ash during plant shutdown.

- Generally the ash which surrounded the top filter holders was an extremely hard, dense material, in comparison to ash which deposited along/within the middle and bottom array holders.

- Generally a thinner coating of ash remained along the surface of the Coors alumina/mullite and DuPont PRD-66 candle filters in comparison to the thicker ash deposits which formed along the Pall Vitropore 442T and Schumacher Dia Schumalith F40 candle filters.

- A heavier deposit of ash was evident along the Pall Vitropore 442T candles in the bottom arrays in comparison to the thinner ash deposit which remained along the top and middle array Pall Vitropore 442T filter elements.

- The thicker ash deposit which formed along the end caps of the Pall Vitropore 442T candles in the bottom arrays resembled the initiation of the elephant foot cake formation.

- A thin layer of ash remained along the various plenum pipes, and was easily removed. After removal, the ash generally retained the contour of the plenum pipe.

- A very densely packed, extremely hard, ash plug formed in the bottom ID bore of various filter elements.

In this report, we will describe:

- The morphology and elemental composition of the ash which deposited along/within the filter holder mounts. Similar information will be presented for the ash deposit which formed within the ID bore of the candle filters.

TABLE 1
ASH SAMPLES REMOVED FROM THE W-APF
-- TEST SEGMENT #5 --

1. Ash from the top of the Coors alumina/mullite candle near the filter holder of the middle array. The cake formation at the top of the candle appeared to be thinner than at the bottom of the filter element.

2. Ash from the top of a DuPont PRD-66 candle filter in the B/T array. The cake formation along the top of the filter appeared to be thinner than along the bottom of the filter element. The surface of the ash cake was white in color, while the remainder of the cake was characteristically red in color.

3. Ash from the top of the Coors alumina/mullite candle filter in the A/B array.

4. Ash near the top of the Pall Vitropore 442T candle filter in the C/B array.

5. Ash from the top of the Pall Vitropore 442T candle filter in the C/T array. A white outer coating of ash was evident.

6. Ash from the bottom of a Coors alumina/mullite candle filter in the B/M array. A thin layer of cake resulted which had a white outer surface color.

7. Ash from a middle array filter holder mount. The cake was very friable, similar to that deposited along the bottom array filter holder mounts.

8. Ash from the bottom of a Coors alumina/mullite candle filter in the A/B array. The deposit was a relatively thin layer of ash.

9. Ash from the bottom of a Pall Vitropore 442T candle filter in the C/B array. The thick deposit resembled the initiation of the elephant foot formation. The cake in this location was somewhat hardened. The cake contained a thin, white or tan outer surface layer which coated a thicker red ash/sorbent deposit.

10. Ash removed from the C/T filter holder mount. The deposit was very hard and had to be chiseled out. Once removed, the sample retained the contour of the filter holder, and contained several striated layers.

11. Thick deposit of cake removed from the elephant foot which formed along the Pall Vitropore 442T candle filter in the C/T array. The typically reddish ash cake deposit was evident below a thin, outer, white or tan ash layer. The deposit was thick and cohesive.

12. Ash which deposited along the 3M CVI-SiC composite filters.

13. Ash from the Pall Vitropore 442T candles near the flange.

14. ~5 mm ash flake adjacent to the divot which formed along the surface of the DuPont PRD-66 filter element.

TABLE 1 (cont'd)
ASH SAMPLES REMOVED FROM THE W-APF
-- TEST SEGMENT #5 --

15. Light tan ash deposit which formed above the darker "red stain" residue along the A/T dust shed.

16. "Red stain" from the A/T and C/T dust sheds.

17. Ash from a middle array plenum pipe. This deposit was easily removed.

18. Ash from the middle array sheds

19. Ash from the A/T and C/T plenum pipes. This deposit was easily removed.

20. White ash deposit which formed at the base of the plenum pipe and shed in the middle array. The material was very friable.

21. Ash from the B/M plenum pipe. The deposit was removed as flakes which retained the contour of the plenum pipe. The outer surface of the deposit was white in color, while a darker ash formation was evident below the outer coating.

22. Ash from the ID bore plug of the 5855 hour Schumacher Dia Schumalith F40 surveillance candle filter. Very hard, densely packed ash.

23. Ash from the ID bore of the Coors alumina/mullite candle filter that was located in position A/T-17. Very hard, densely packed ash.

- The phases or compounds which were identified for fourteen ash materials that were recovered from various locations within the filter cluster.

- The thermal expansion of the ID bore ash in comparison to the thermal expansion of the porous ceramic filter materials.

- The density and strength of ash which collected within the ID bore of the various candle filters. Similarly, the density and strength of bridged ash material that was removed from various filter arrays in Test Segment #3 (i.e., in-service of the primary cyclone), and Test Segment #4 (i.e., partially detuned cyclone) will be presented.

TOP FILTER HOLDER MOUNT ASH

During the lift on May 11, 1995, it was readily apparent that ash bridging had virtually been eliminated within the W-APF system after 1110 hours of test operation in Test Segment #5 (i.e., January 13, 1995 through March 30, 1995; Figure 1). Ash, however, continued to deposit along/within the various filter holder mounts. A very hard, densely packed deposit of ash fines collected along/within the top array holder mounts. This ash was extremely difficult to remove. In contrast, the ash cake which collected along/within the middle and bottom array filter holder mounts was significantly easier to remove.

The scanning electron micrographs (SEMs) shown in Figure 2 illustrate the morphology of the hard ash deposit which collected along/within the filter holder mounts of the C/T array. Five distinct layers of ash were evident along the outer surface of the ~12 mm (~0.5 inch) thick ash deposit (Figure 2a). The outermost layer (i.e., Layer 1), was white in color and was ~0.75 mm thick. Layer 2 was also white in color and was ~0.5 mm thick. Layer 3 was tan and was ~0.75 mm thick, while Layer #4 was pink in color and was ~1-2 mm thick. Layer 5 was red in color, and was considered to be representative of the majority of the ash which collected along the outer surface of the filter elements. The layered ash formations which resulted along/within the filter holder mounts were considered to reflect carryover and/or deposition of fines during the various startup and shutdown periods in Test Segment #5.

Energy dispersive x-ray analysis (EDAX) of Area 1 shown in Photo 1, Figure 2a, identified the presence of 9.23% Mg, 8.06% S, 2.89% Ca, 2.15% Si, 0.72% Al, 0.48% Fe, 0.28% Cr, 0.26% K, and 75.94% O (i.e., atomic percent basis; possible carbon content not considered). The elemental composition implies the presence of a highly sulfated magnesium complex with minor contributions of calcium (i.e., possibly as a sulfate), ash (i.e., silicon, aluminum, and possibly iron), and metal debris (i.e., chromium and possibly iron). As shown in Figure 2b, a molten or sintered phase was present within Layer 1 of the filter holder deposit (i.e., outermost layer from the metal filter holder surface).[a] EDAX analysis of the "melt-like" or sintered phase indicated the presence of 13.76% Mg, 9.66% S, 0.47% Ca, 0.30% Si, and 75.80% O (i.e., $MgSO_4$; Photo 3, Figure 2a). Interdispersed within the magnesium sulfate melt

[a] Bulk diffusion at the Tamman temperature of 853°F for $MgSO_4$ is considered to be responsible for the "melt-like" or sintered phase formation in the filter holder ash deposit. The melting and Tamman temperatures for the various sorbent constituents follows: $MgSO_4$ — 2165°F and 853°F; $CaSO_4$ —2642°F and 1091°F; $CaCO_3$ — 2442°F and 991°F; CaO — 4658°F and 2160°F; MgO — 5072°F and 2310°F.

Figure 1 – W-APF System At The Conclusion Of Test Segment #5

Figure 2a – Ash Deposit Along The C/T Filter Holder Mount

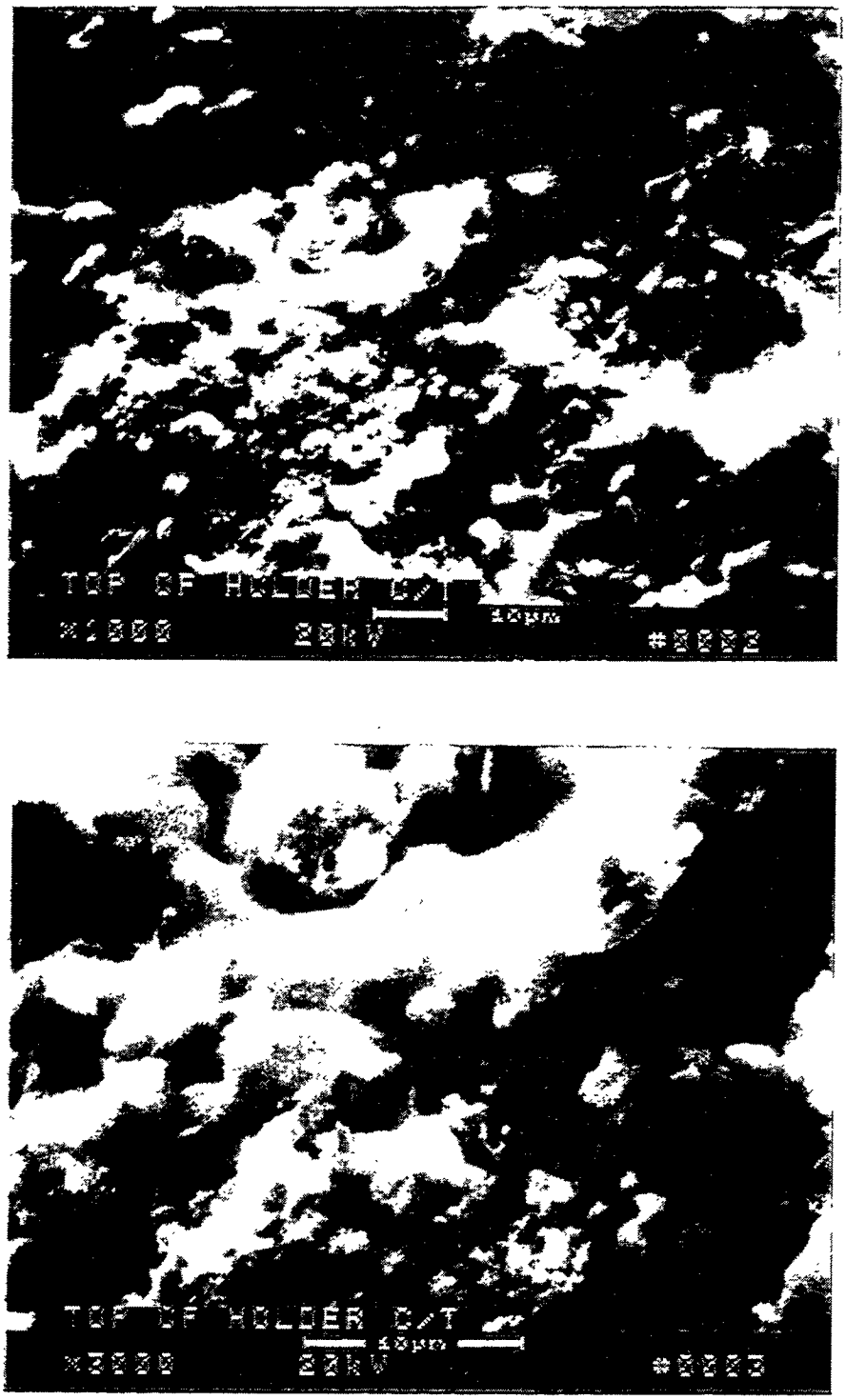

Figure 2b — "Melt-Like" Magnesium Sulfate Phase Formed Within The C/T Filter Holder Mount Ash Deposit (Layer 1)

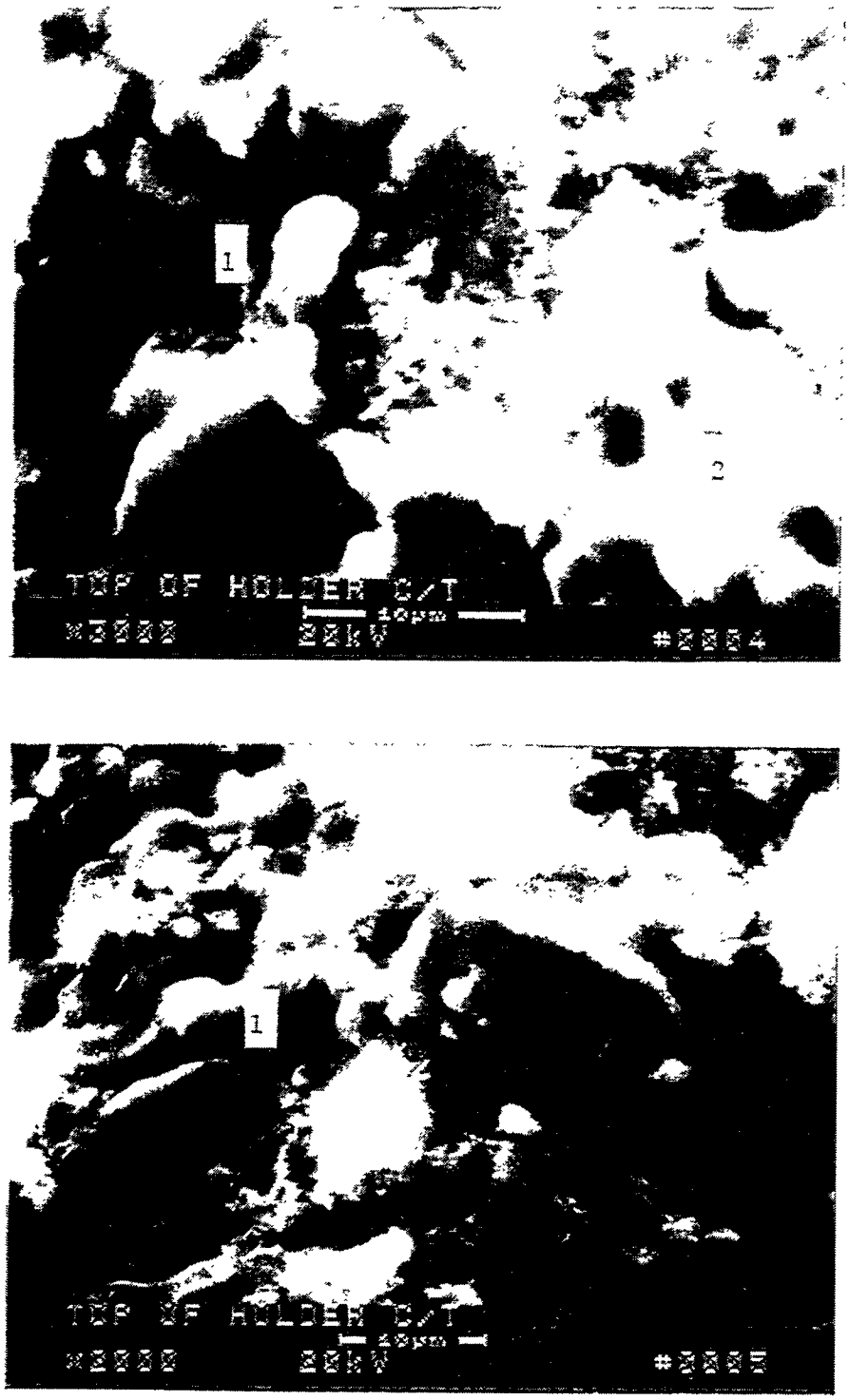

Figure 2c – Morphology Of The Ash Deposit Which Collected Along The C/T Filter Holder Mount (Layer 1)

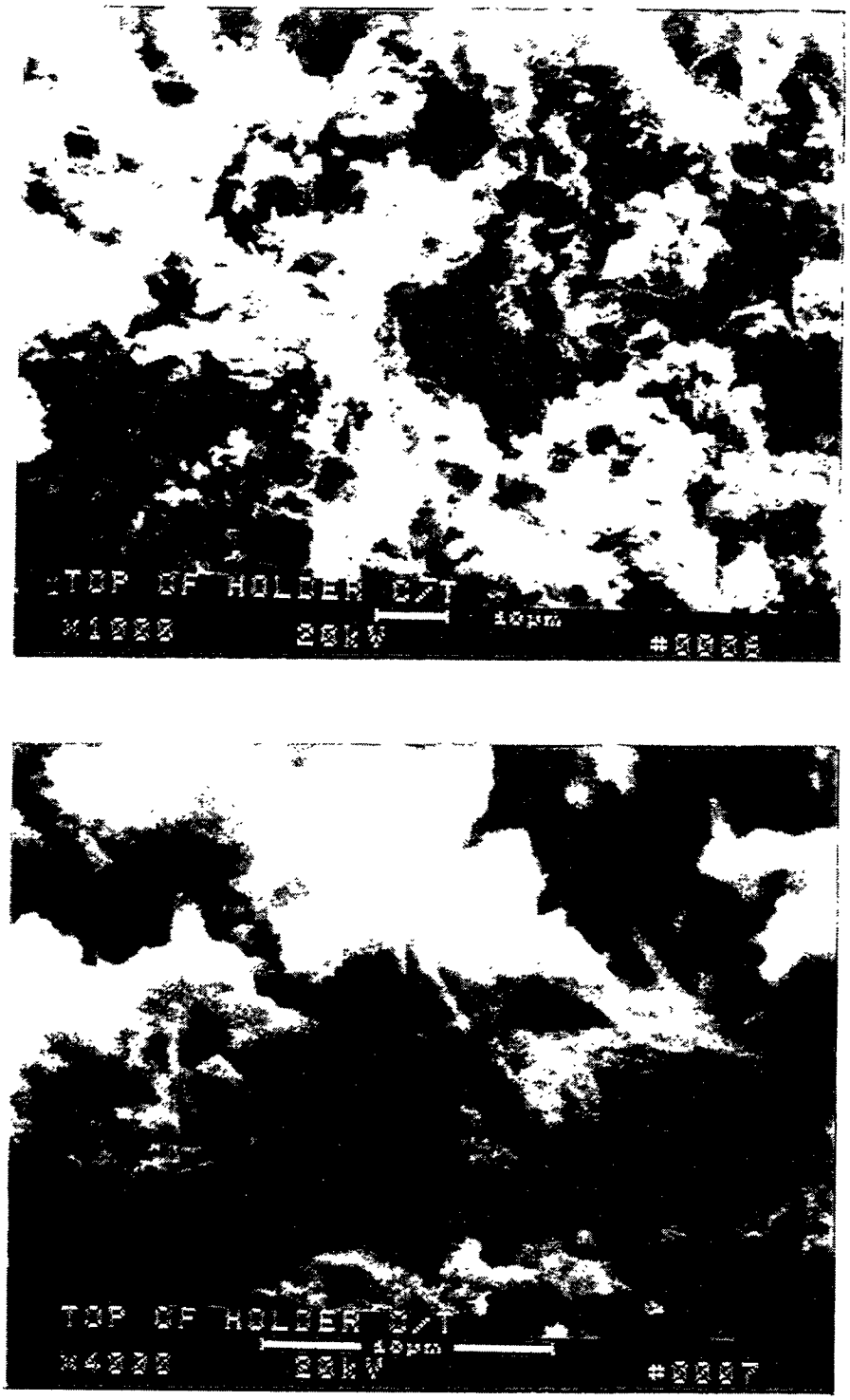

Figure 2d – Crystalline Growth Phase Within The Ash Collected Along The C/T Filter Holder Mount (Layer 2)

Figure 2e – Morphology Of The Fines Collected In Layer 2 Of The C/T Filter Holder Mount. Crystal Growth Is Evident.

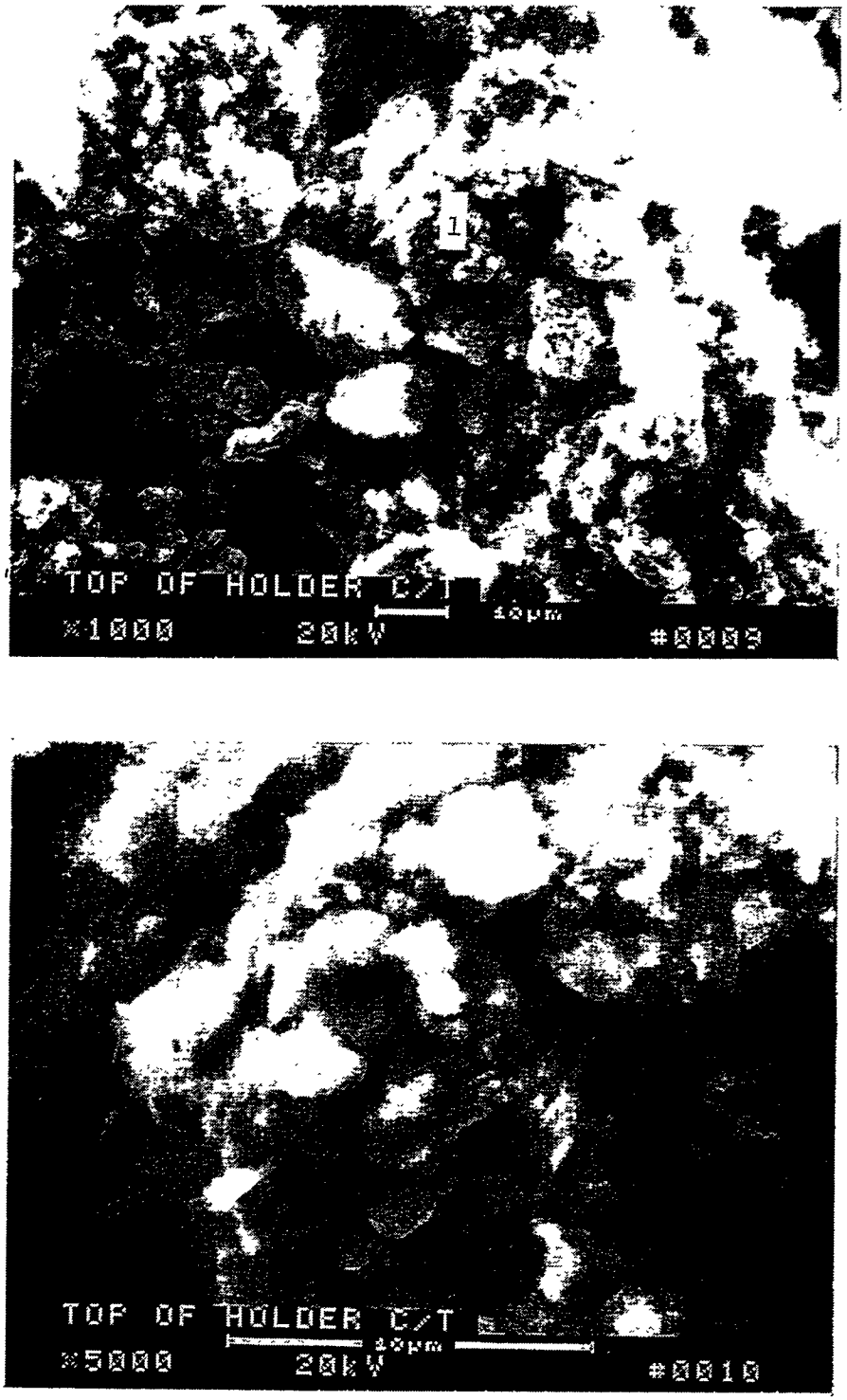

Figure 2f – Morphology Of The Ash Deposit Which Collected Along The C/T Filter Holder Mount (Layer 2)

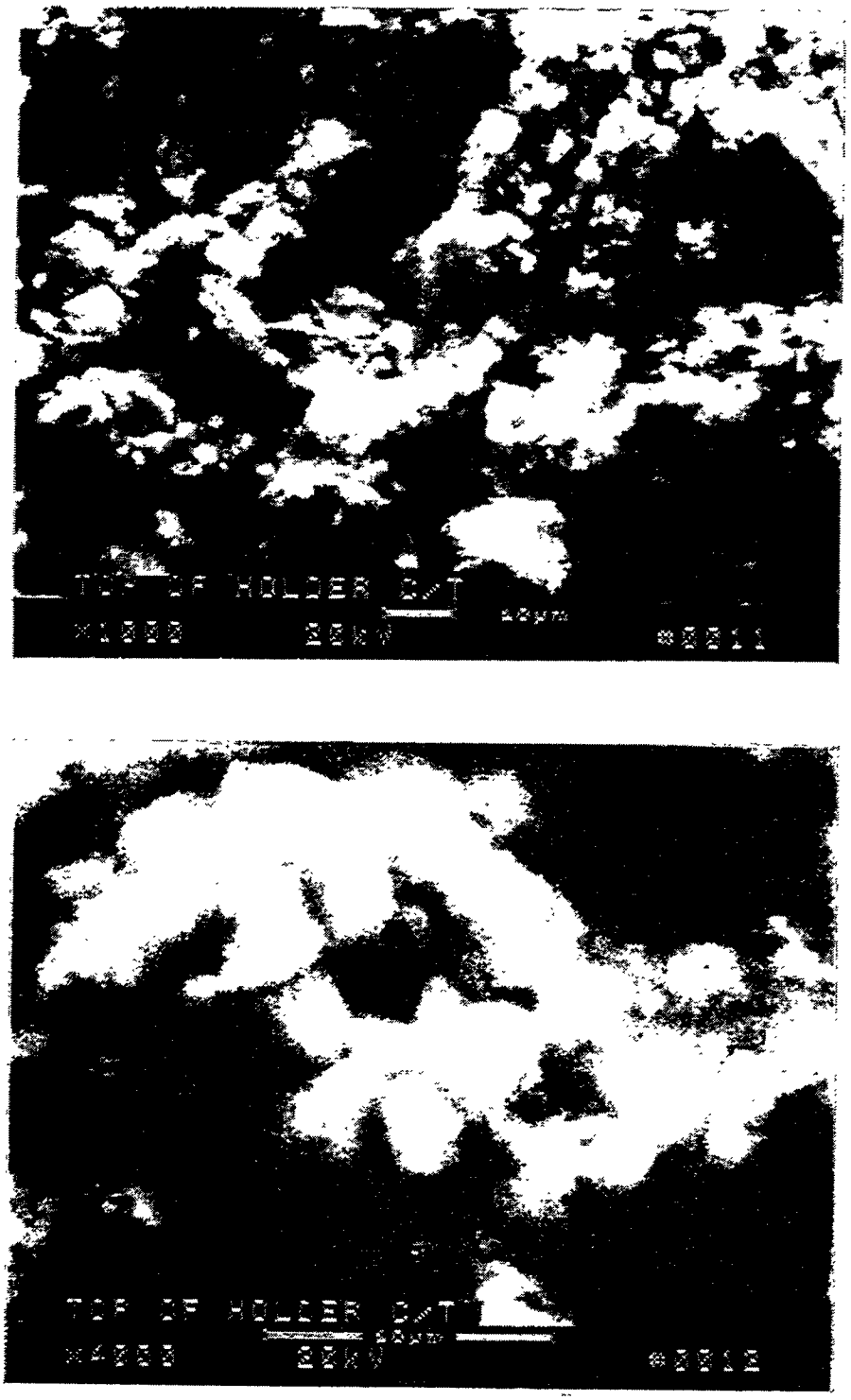

Figure 2g – Morphology Of The Ash Deposit Which Formed Along The C/T Filter Holder Mount (Layer 3)

Figure 2h – Morphology Of The Ash Deposit Which Collected Along The C/T Filter Holder Mount (Layer 3)

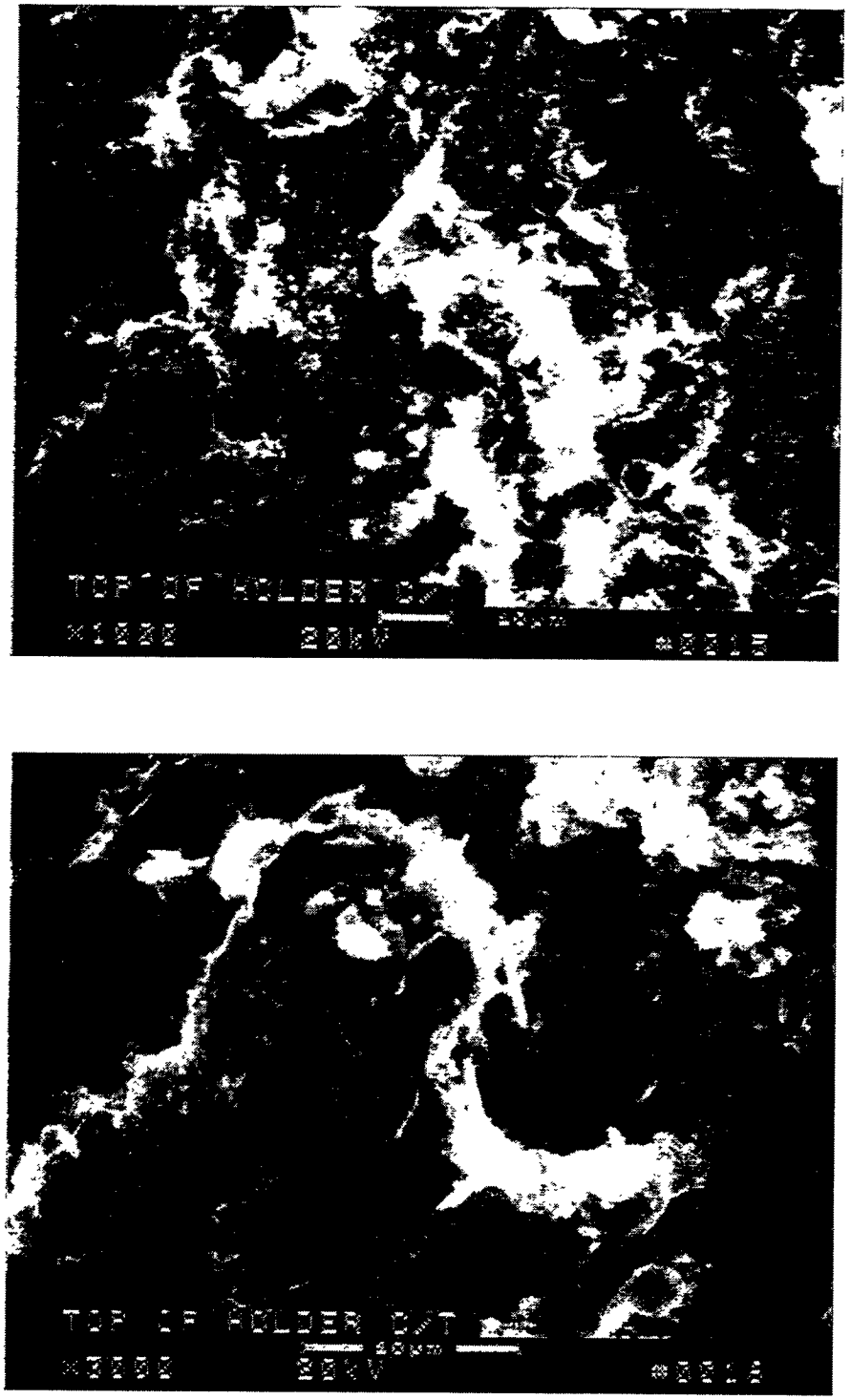

Figure 2i – Morphology Of The Ash Deposit Which Formed Along The C/T Filter Holder Mount (Layer 3)

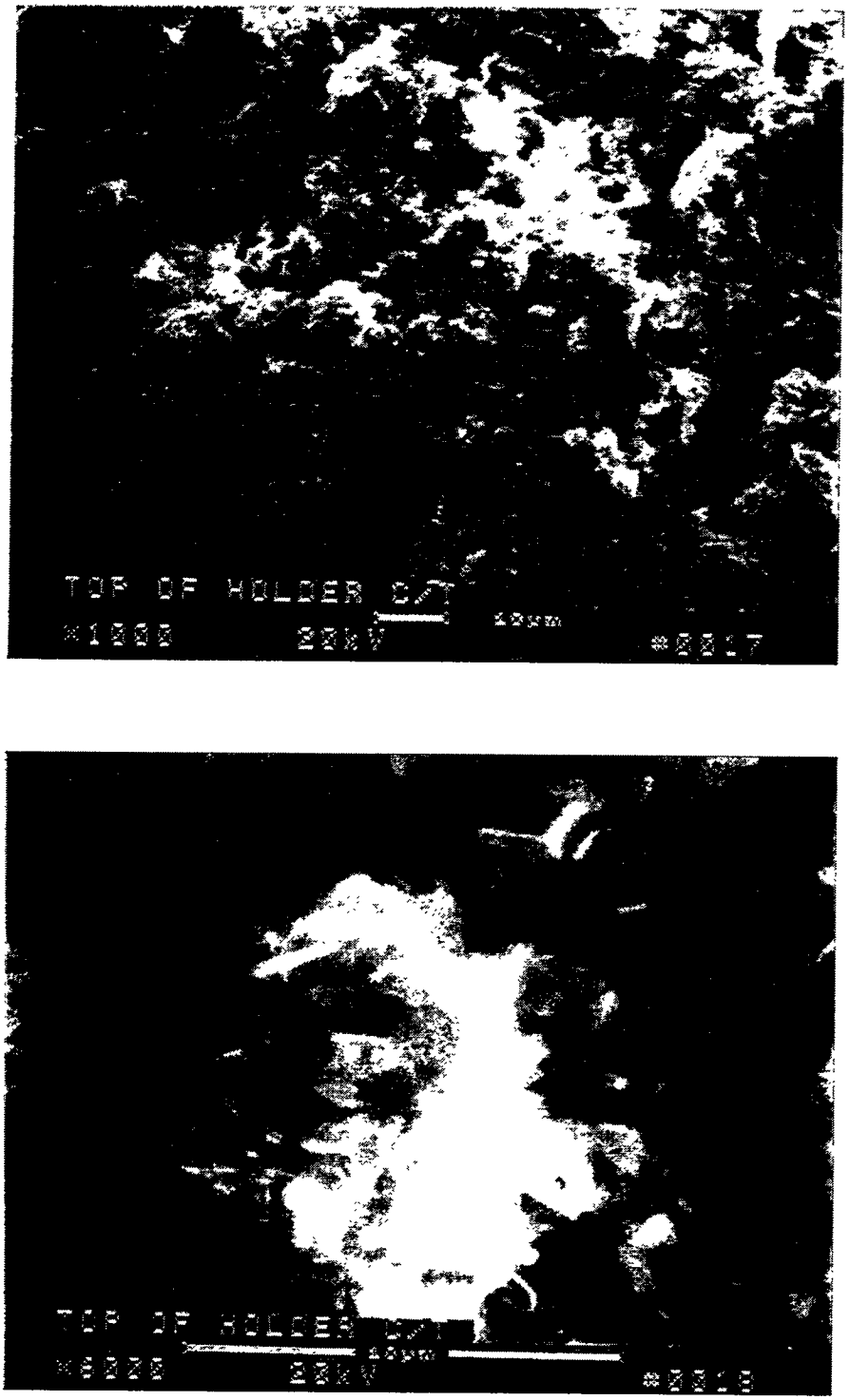

Figure 2j — Morphology Of The Ash Deposit Which Formed Along The C/T Filter Holder Mount (Layer 4)

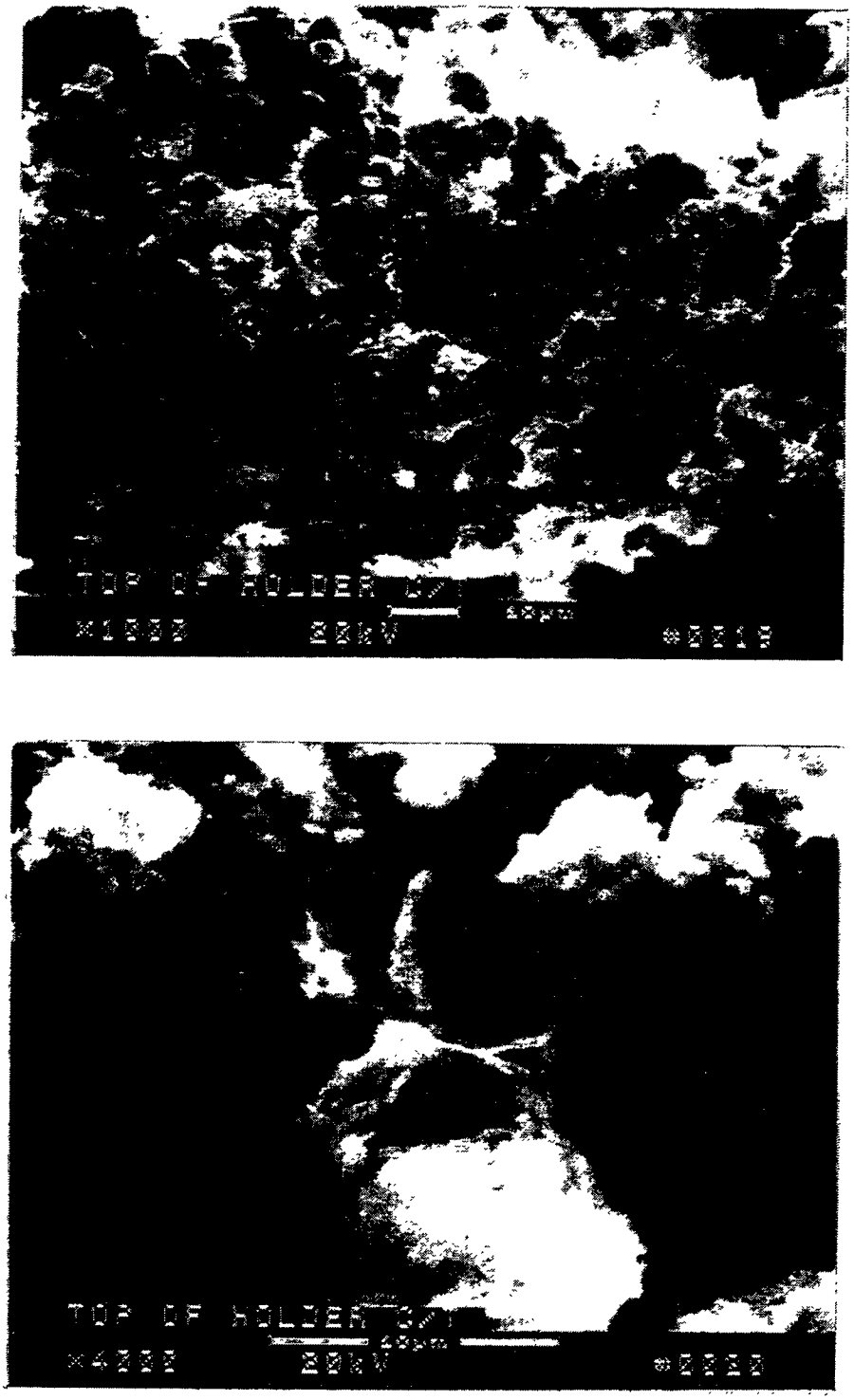

Figure 2k – Morphology Of The Ash Formation That Collected Along The C/T Filter Holder Mount At ~2 mm From The Layer 4/Layer 5 Interface

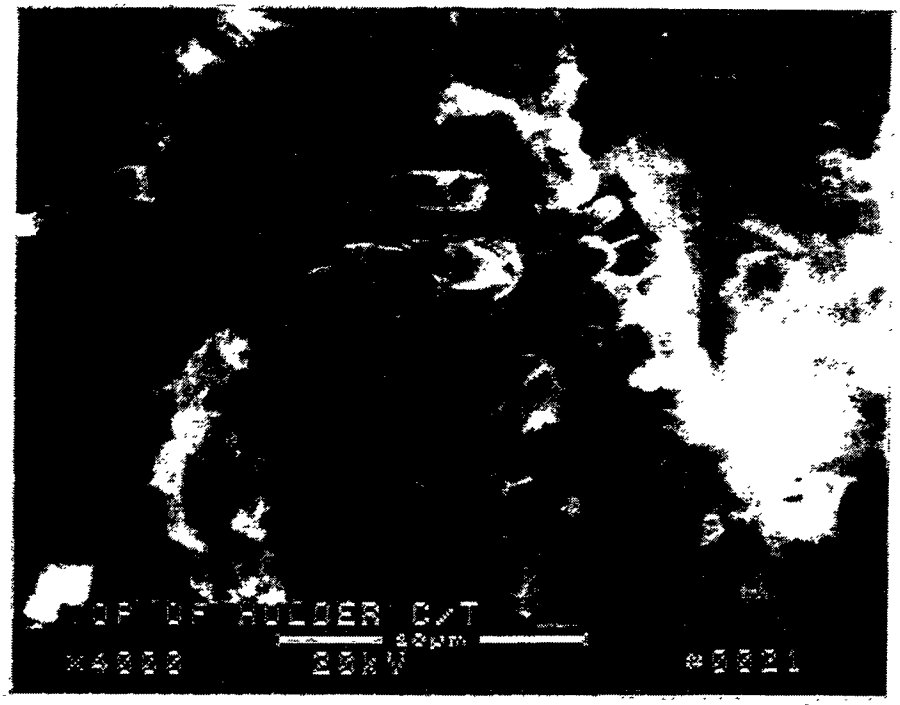

Figure 21 # Crystal Growth Within The Ash Formation That Collected Along The C/T Filter Holder Mount At ~2 mm From The Layer 4/Layer 5 Interface

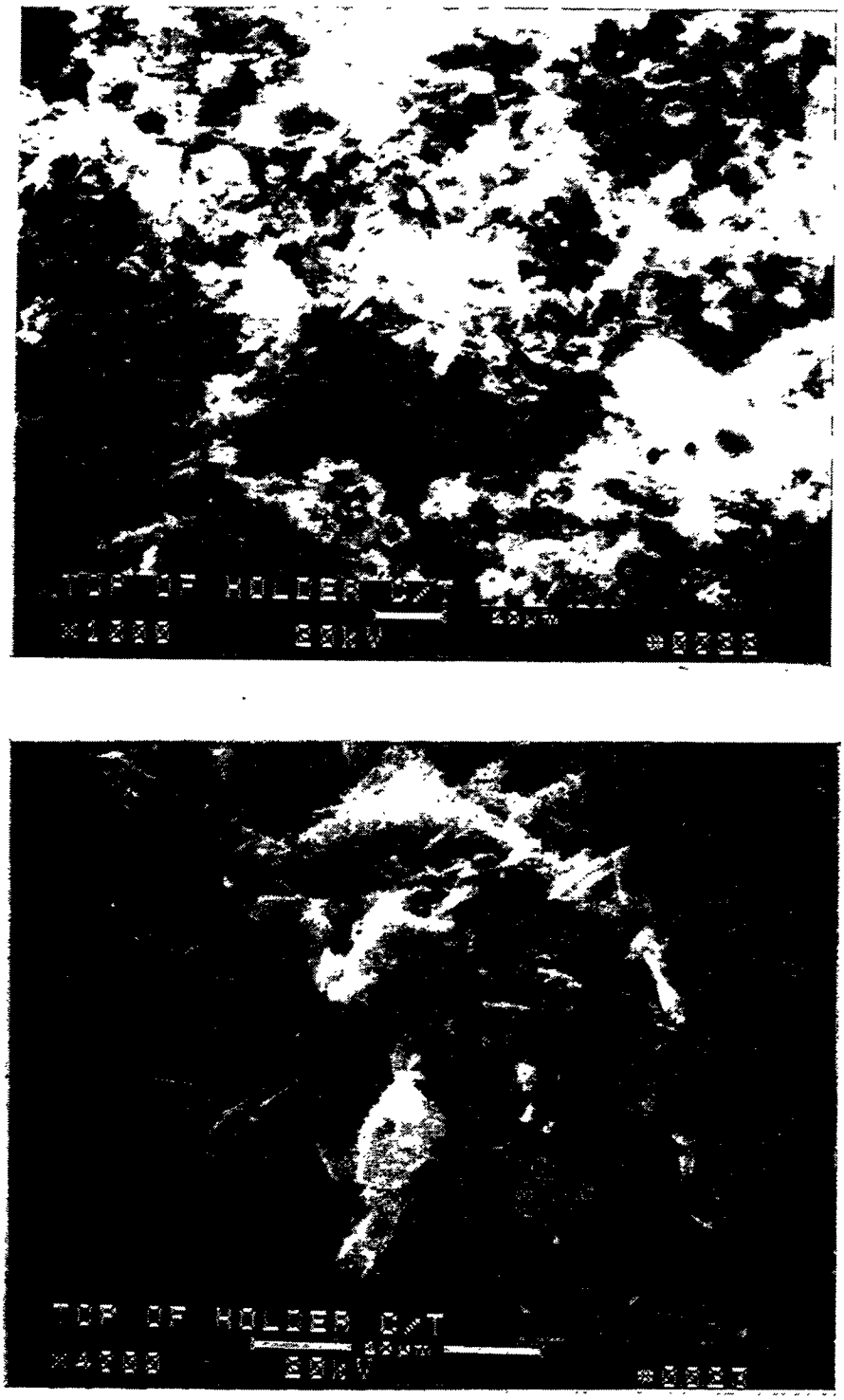

Figure 2m –Extensive Crystal Growth Within The Ash Formation That Collected Along The C/T Filter Holder Mount At ~4 mm From The Layer 4/Layer 5 Interface

Figure 2n – Crystal Growth Within The Ash Formation That Collected At An Alternate Location Along The Filter Holder Mount At ~4 mm From The Layer 4/Layer 5 Interface

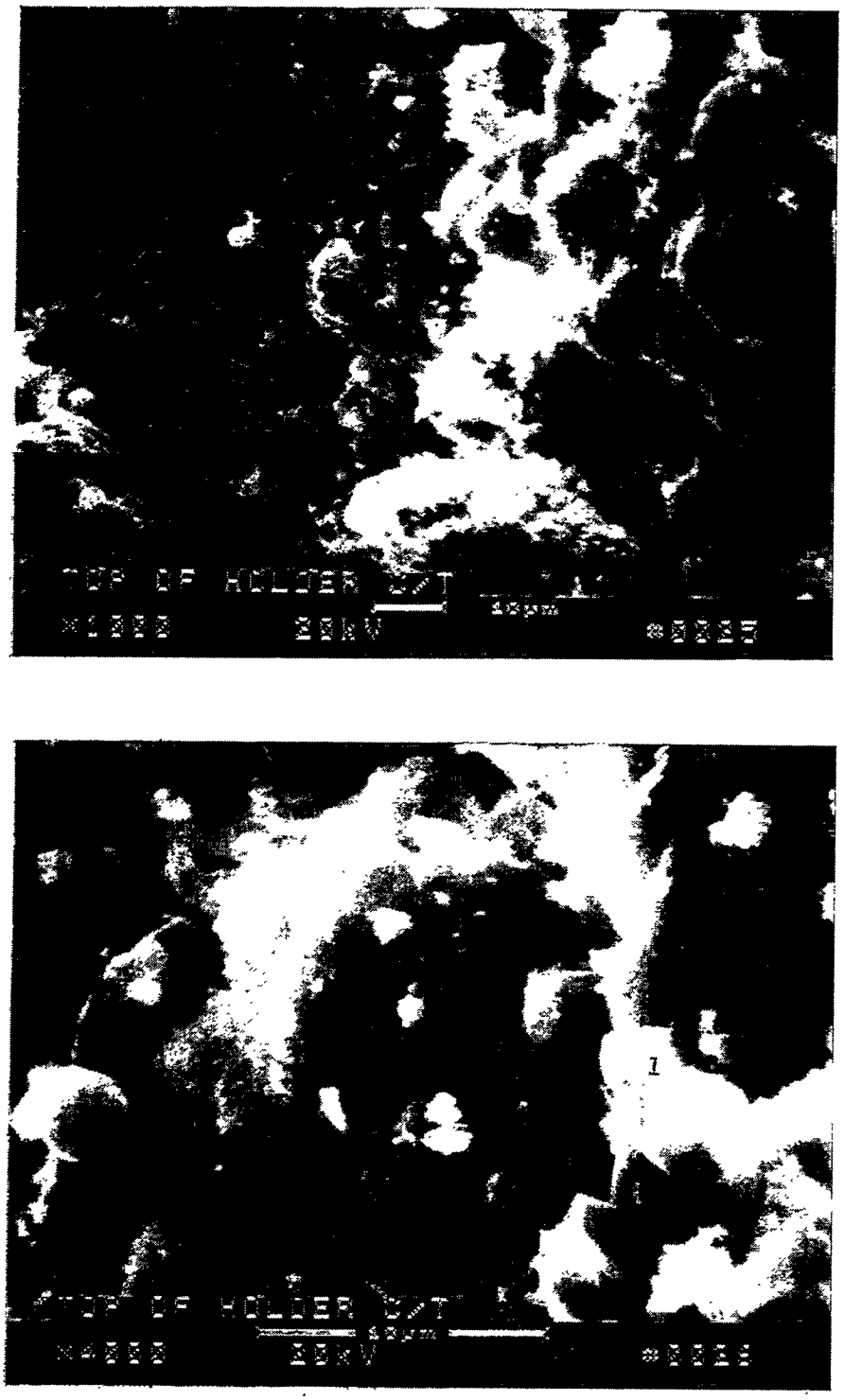

Figure 2o – Magnesium Sulfate-Enriched Melt Which Formed Within The Ash Deposit At ~2 mm From The Metal Filter Holder Mount Surface

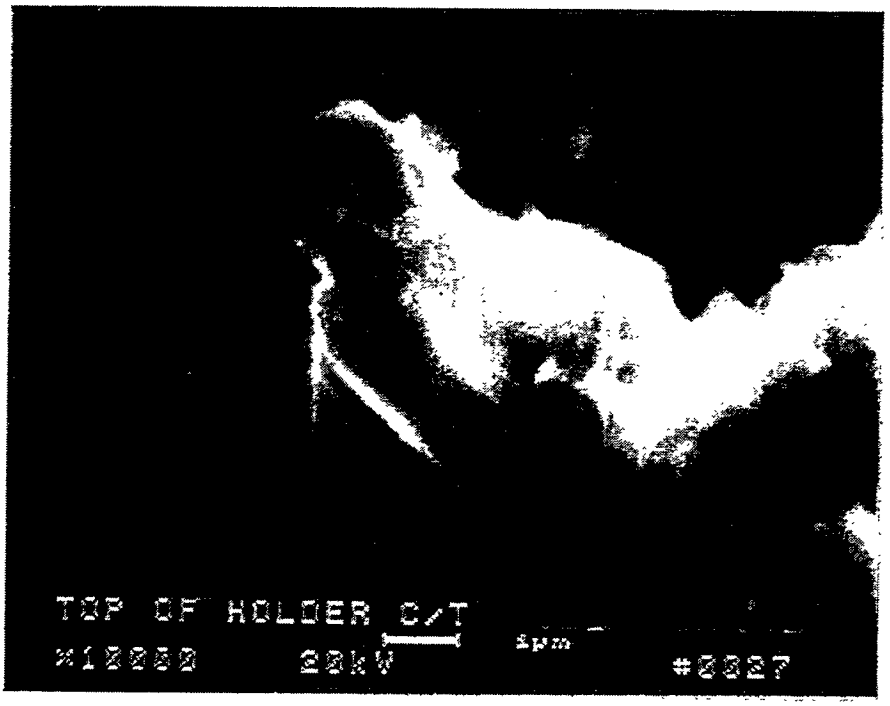

Figure 2p – Hexagonal Magnesium Silicate Crystal Growth Within The Fines That Deposited At ~2 mm From The Metal Filter Holder Mount Surface

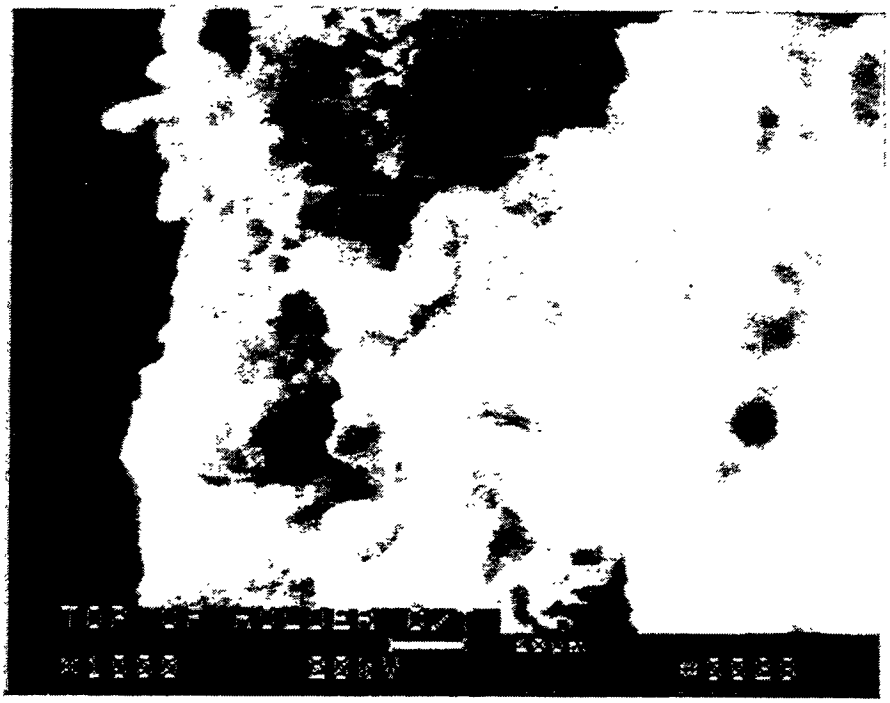

Figure 2q – "Melt-Like" Phase Which Formed Within The Ash Deposit Near The C/T Filter Holder Mount

were fines which contained 9.59% Mg, 8.10% K, 5.56% Si, 3.03% S, 1.52% Ca, 0.16% Al, and 72.24% O.

At an alternate location in Layer 1, EDAX analyses of the fines shown in Area 1, Photo 4, Figure 2c, indicated the presence of a sulfur-enriched calcium-magnesium complex (i.e., 10.13% S, 7.24% Ca, 3.46% Mg, 0.96% Si, 0.12% Al, 0.11% K, and 77.99% O), as well as the magnesium sulfate melt (i.e., Area 2, Photo 4, Figure 2c; Area 1, Photo 5, Figure 2c).

In contrast to the densely packed layers of fines collected in Layer 1, a somewhat more open porosity ash structure was evident in the fines collected in Layer 2. "Crystalline-like" growth features were evident in Layer 2, extending intermittently into the voids which were formed within the ash deposit (Photo 7, Figure 2d).

Sorbent and ash fines were identified to be present in the ash deposit shown in Photo 8, Figure 2e. Unlike the fines deposited in Layer 1, the fines shown in Photo 8, Figure 2e (i.e., Layer 2) contained 8.67% Si, 7.37% Mg, 7.19% S, 5.80% Ca, 0.70% Cl, 0.53% Al, 0.36% K, and 69.37% O.

Figure 2f illustrates the morphology of the ash collected at an alternate location in Layer 2. Agglomerates were evident in the ash matrix which contained numerous sintered (i.e., point contact) or fused micron and submicron fines, as well as crystalline phase growth. EDAX analyses of the fines shown in Photo 10, Figure 2f, indicated the presence of generally a higher calcium vs magnesium sulfated complex; a low concentration of chlorine and chromium, but a relatively high concentration of iron (i.e., 7.64% S, 7.30% Fe, 6.27% Ca, 3.11% Al, 2.84% Mg, 1.97% Si, 0.36% Cr, 0.29% Cl, 0.12% K, and 70.10% O.

Densely packed agglomerated fines were evident in Layer 3 (Figure 2g). As in Layer 2, crystalline phase growth was evident along the surface of fines in Layer 3 (Photo 14, Figure 2h). Area scan analyses of the fines shown in Photo 14, Figure 2h, indicated the presence of 9.54% S, 7.65% Ca, 4.25% Mg, 2.18% Si, 1.04% Al, and 75.34% O. The agglomerated and/or fused fines which were collected at an alternate location in Layer 3 are shown in Figure 2i.

Crystallization similarly resulted along the surface of the agglomerated fines that were present in Layer 4 (Figure 2j). EDAX analyses of the agglomerated and/or sintered fines shown in Photo 18, Figure 2j, indicated the presence of 9.84% S, 8.30% Ca, 4.83% Mg, 4.46% Si, 0.95% Al, 0.44% Fe, and 71.18% O.

Layer 5 consisted of ~8 mm of ash/sorbent fines. SEM and/or SEM/EDAX analyses were conducted at consecutive 2 mm intervals moving toward the surface of the ash that was in contact with the metal filter holder. A "web-like" structure was evident between adjacent sintered or agglomerated fines (Figure 2k). Dendritic or "whisker-like" crystalline phases were also present within the ash/sorbent fines collected in Layer 5 (Photo 20, Figure 2k; Photo 21, Figure 2l).

Extensive crystallization was evident at 4 mm below the Layer 4/Layer 5 interface (Figures 2m and 2n). As identified by EDAX, the dendritic structure shown in Photo 23, Figure 2m, contained 8.67% Mg, 6.23% S, 6.22% Si, 5.22% Ca, 2.07% Fe, 1.70% Al, 0.26% K, and 69.64% O.

At 6 mm from the Layer 4/Layer 5 interface a rather extensive "melt-like" formation was once again evident (Figure 2o). As along the outermost surface of the metal filter holder mount deposit, the melt principally contained a magnesium sulfate-enriched matrix (i.e., 12.50% Mg, 7.55% S, 1.04% Si, 0.89% Al, 0.79% Ca, 0.22% Fe, 0.10% K, and 76.91% O), and hexagonal magnesium silicate crystalline phase growth (i.e., 17.11% Mg, 9.56% Si, 1.32% S, 0.94% Al, 0.34% Fe, 0.25% Ca, 0.12% K, and 70.36% O). The hexagonal crystals shown in Photo 26, Figure 2o, are shown at higher magnification in Photo 27, Figure 2p.

The "melt-like" material which was initially deposited along the metal filter holder mount was identified by EDAX to be enriched with a magnesium sulfate complex which contained calcium, aluminum, silicon, iron, and oxygen (Figure 2q).

CANDLE ID BORE ASH DEPOSIT

As a result of failure of twenty DuPont PRD-66 and two Coors alumina/mullite candle filters during operation of the W-APF in Test Segment #5 at AEP, fines were released into the plenum and off gases, and were subsequently pulsed back into the ID bores of the remaining intact candle filters. Failure of the DuPont PRD-66 filter elements was initially observed after 232 hours of test operation in Test Segment #5, which permitted fines collection within the candle IDs for 878 hours (i.e., 1110 hours of total test operation). During this time, ash became tightly compacted at the bottom of the filter elements, and depending on location, filled the candles to depths of <1-~14 inches. During conduct of Test Segment #5, the W-APF experienced 10 heatup/cooldown cycles. As a result, during heatup of the vessel to operating temperatures of 760-845°C, the ash expanded, applying a force along the ID wall of the filter element. Similarly, during cooldown, the ash hydrated, again causing a volume increase, further applying a load to the ID wall of the filter elements. Through repetitive cycling, and continued ash filling, several of the candles experienced crack formation at ~6-8 inches above the filter element end cap (i.e., ash fill level; Figure 3). Although crack formations were evident above the end caps of several filter elements, catastrophic failure of these candles did not result during in-service operation.

SEM/EDAX analyses were performed on the ID bore ash. As shown in Figure 4a, the ash is very densely packed. Carbon was utilized to prepare the sample, in order to permit semi-quantitative compositional identification (i.e., if gold were used, the sulfur content of the material would be masked). This resulted in poor resolution of the fines that were present in the sample, which suggested sintering of adjacent fines. EDAX analyses of the area shown in Photo 3, Figure 4b, indicated the presence of 5.76% S, 5.41% Mg, 4.63% Si, 3.26% Al, 3.11% Ca, 1.36% Fe, 0.37% K, and 76.09% O. Ash shown in Photo 4, Figure 4b, was identified to contain 6.61% S, 6.41% Mg, 2.96% Si, 2.51% Ca, 1.94% Al, 0.72% Fe, 0.25% K, and 78.58% O, while ash shown in Photo 5, Figure 4c, was identified to contain 6.34% Mg, 5.84% S, 3.80% Si, 2.24% Ca, 1.94% Al, 0.52% Fe, 0.26% K, and 79.06% O.

A second sample of the densely packed fines was prepared for additional SEM analyses. A gold coating was applied to the outer surface of the material in order to provide higher resolution micrographs of the deposit matrix. Although the relatively irregularly shaped ~10-30 μm fines were tightly packed (Figure 4d), sintering may have only resulted at point contact between the adjacent fines.

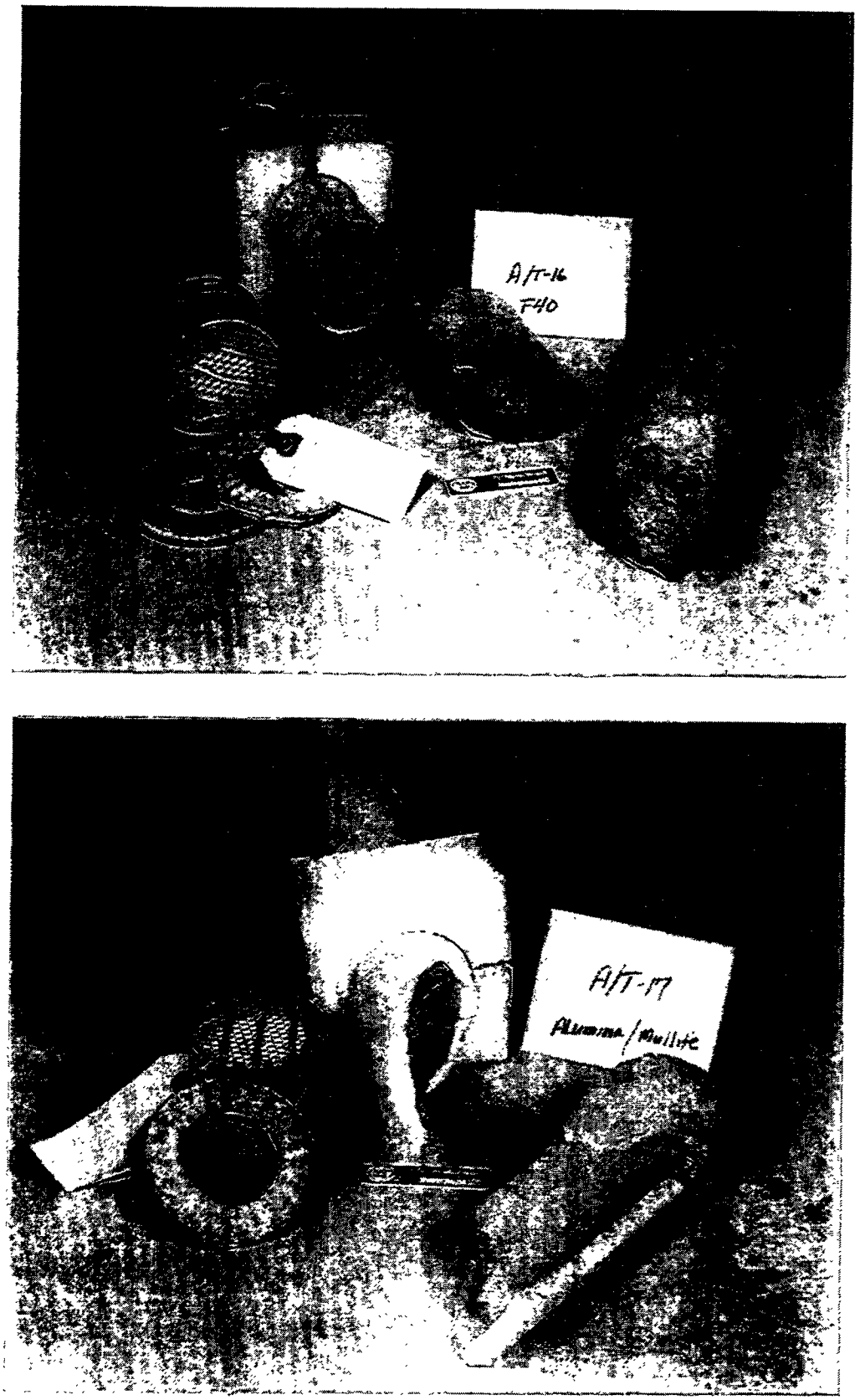

Figure 3 — Tightly Packed Ash Within The ID Bore Of The Porous Ceramic Candles (Test Segment #5)

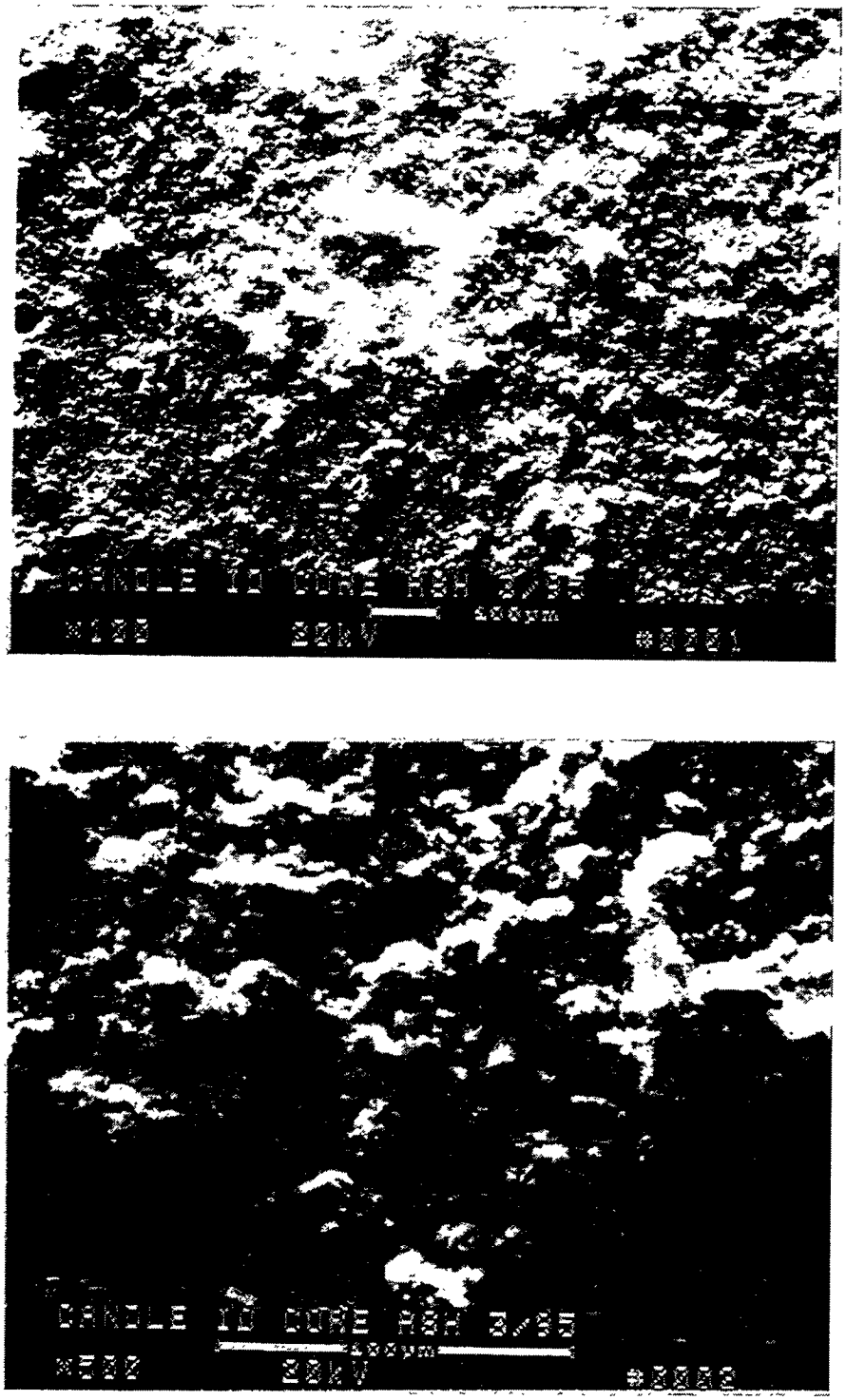

Figure 4a – Morphology Of The Densely Packed Ash In The ID Bore Of The Porous Ceramic Candles (Test Segment #5)

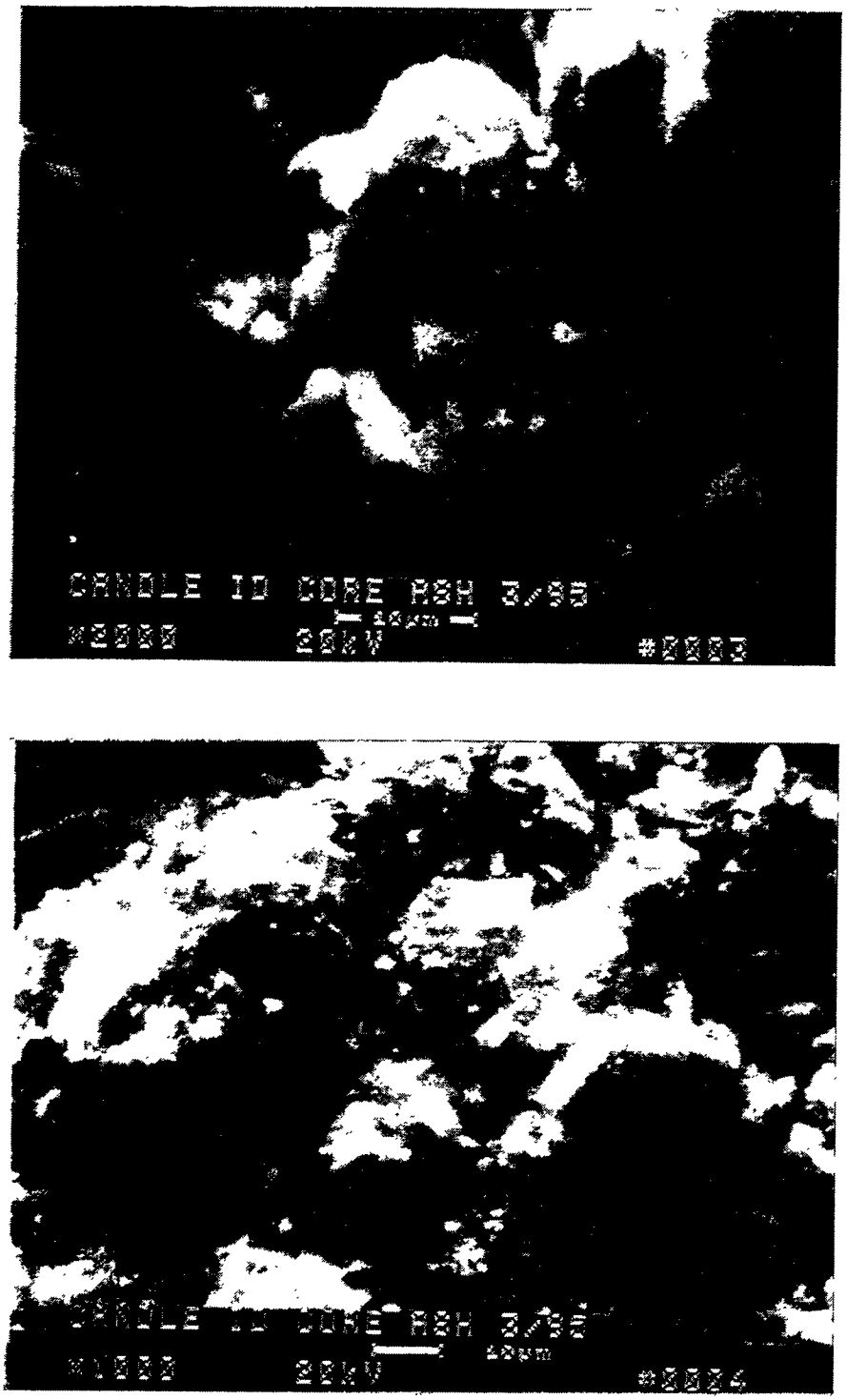

Figure 4b – Higher Magnification Of The Candle ID Bore Ash

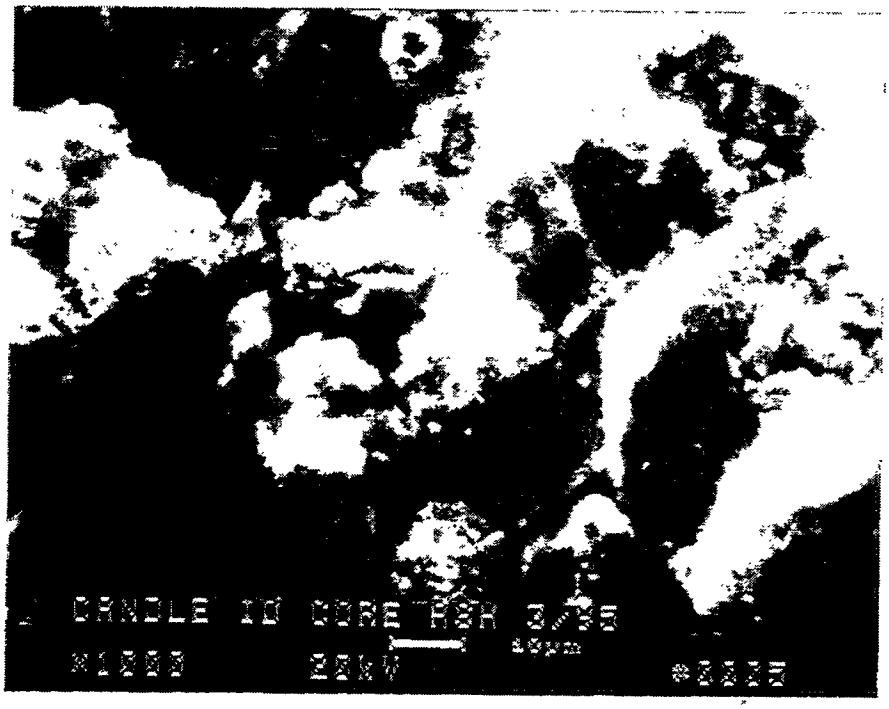

Figure 4c – Morphology Of ID Bore Ash At An Alternate Location Within The Removed Deposit

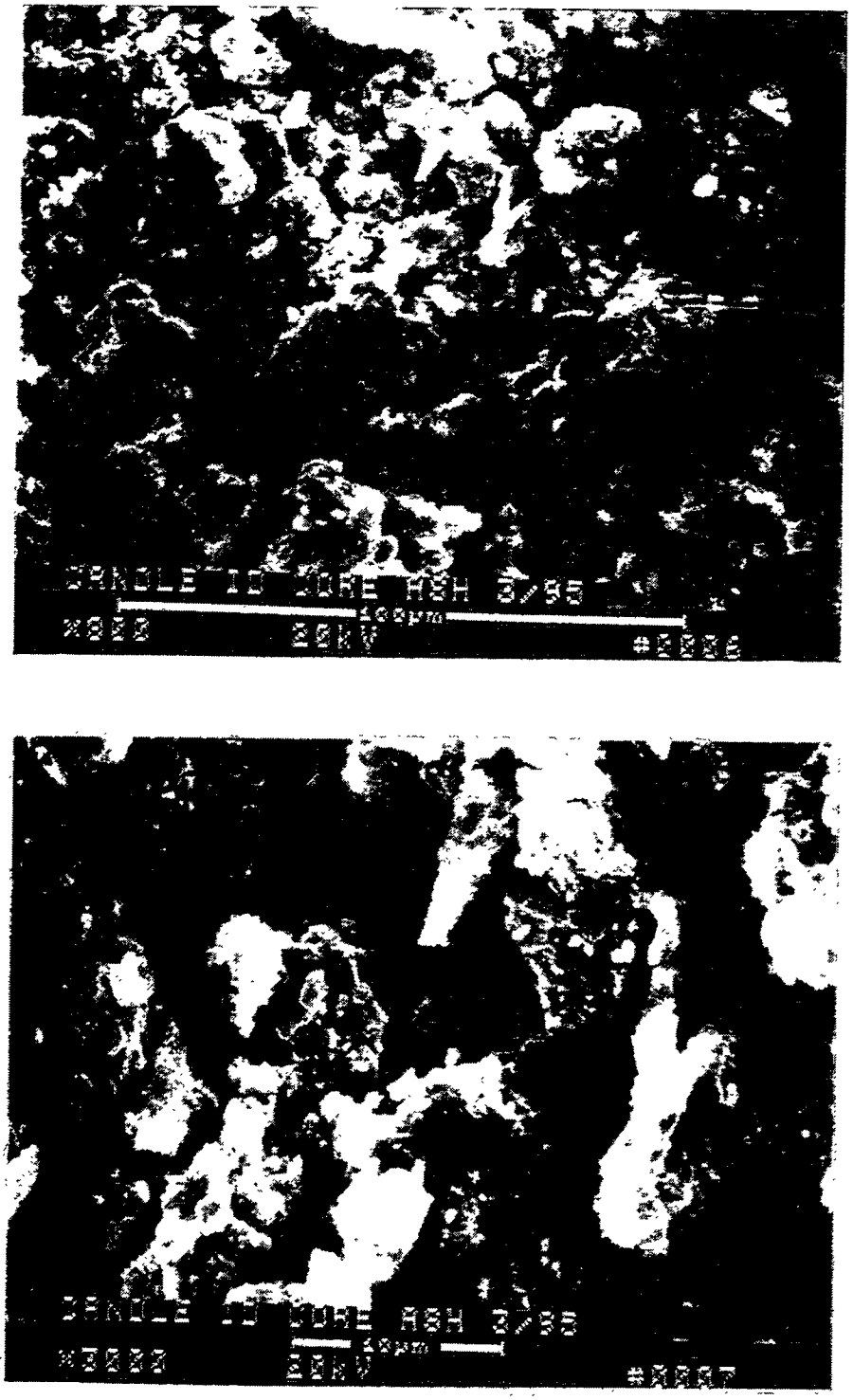

Figure 4d – Morphology Of The Densely Packed Ash In The ID Bore Of The Porous Ceramic Candles (Gold Coated)

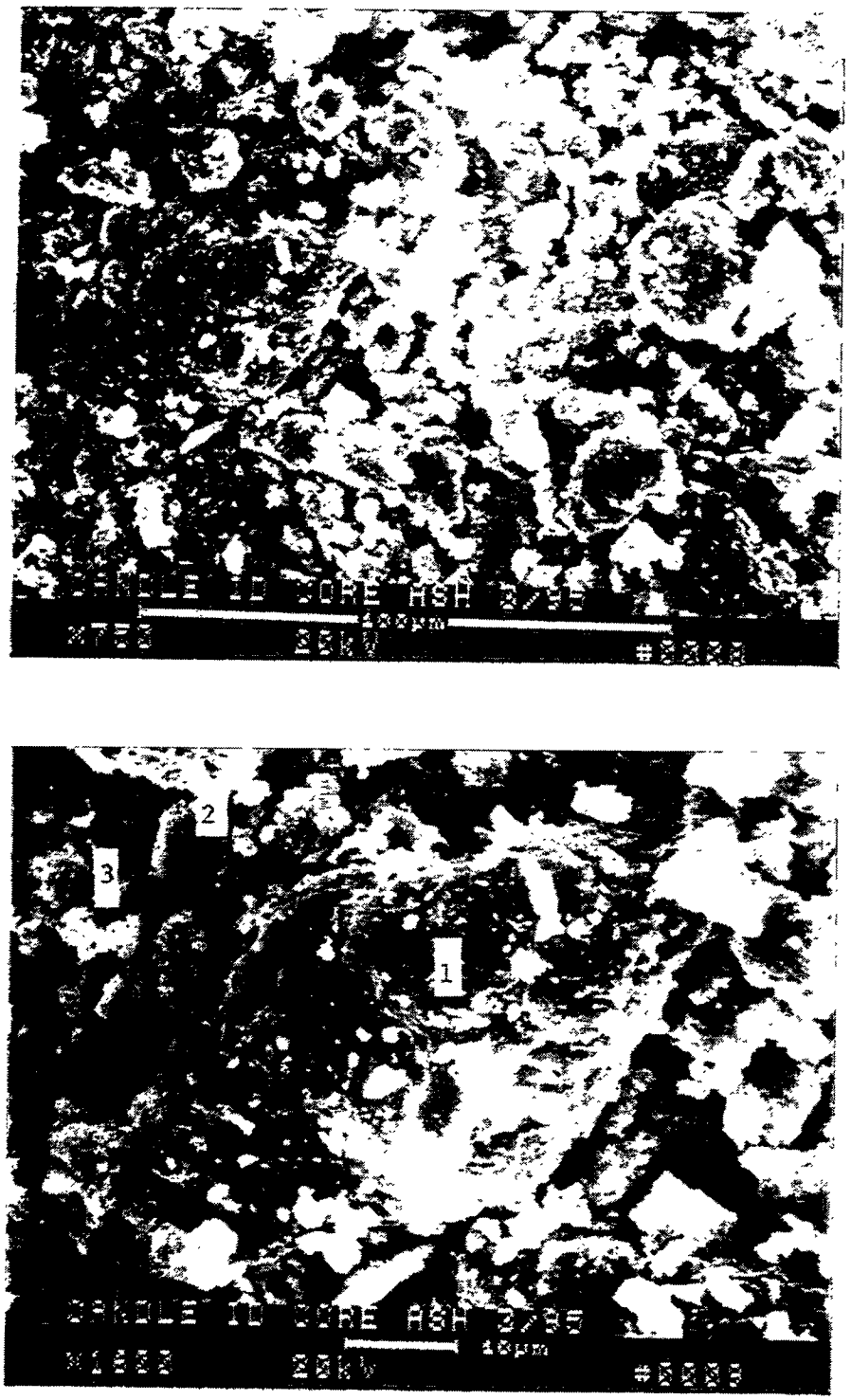

Figure 4e – Morphology Of The Densely Packed Ash At An Alternate Location Within The Porous Ceramic Candle Filter ID Bore (Gold Coated)

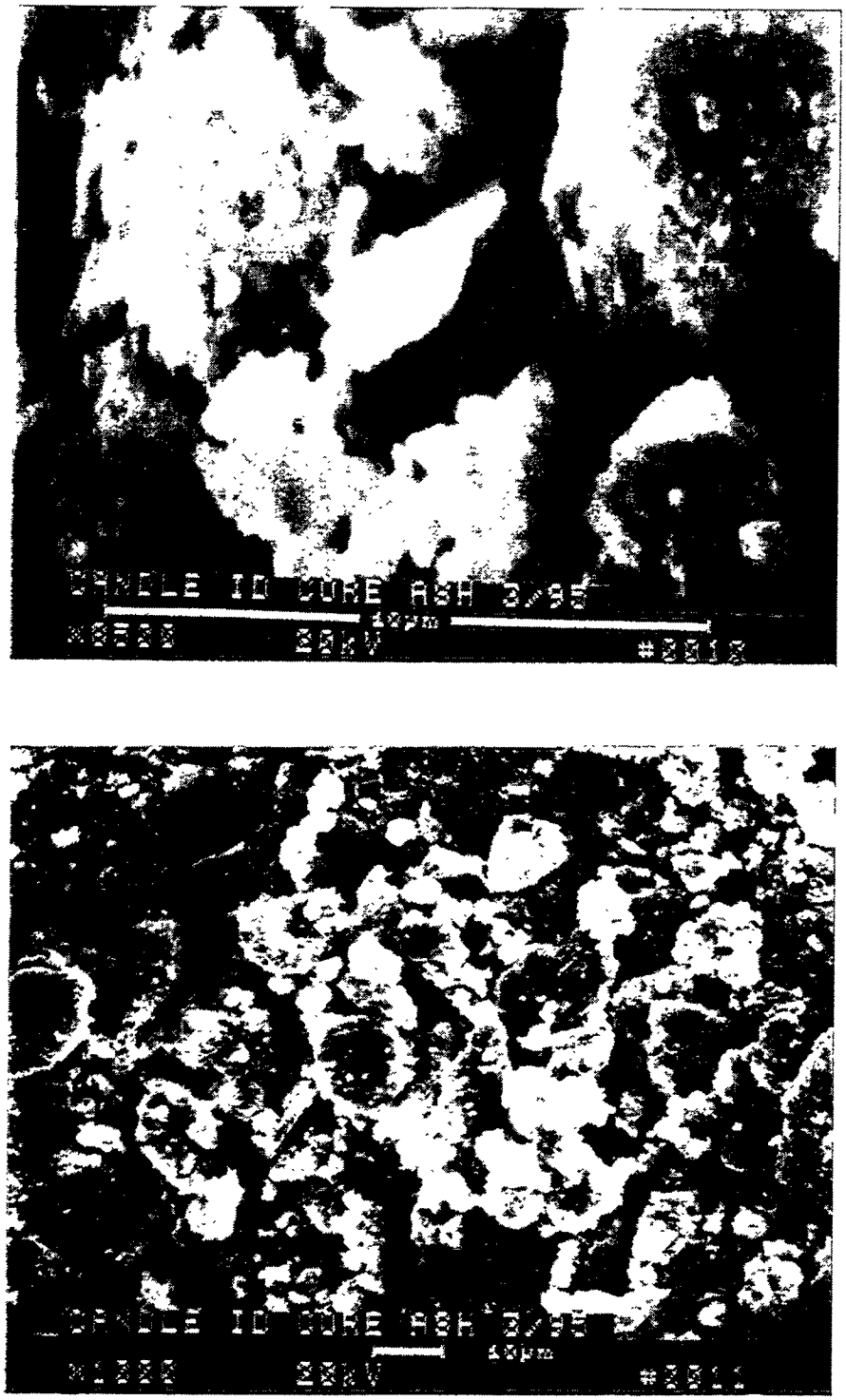

Figure 4f — Morphology Of The Densely Packed Ash At An Alternate Location Within The Porous Ceramic Candle Filter ID Bore (Gold Coated)

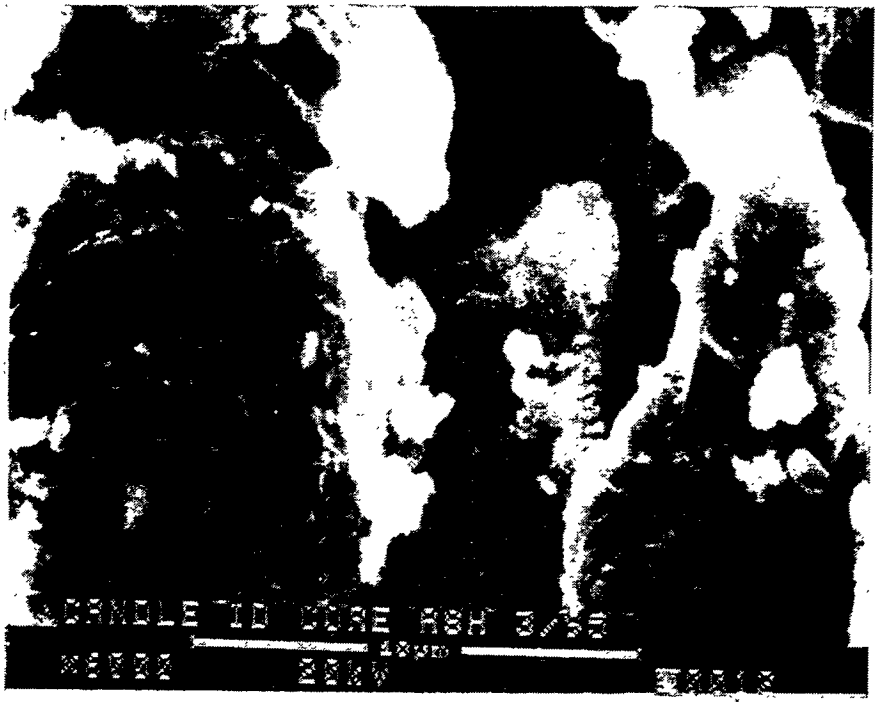

Figure 4g – Higher Magnification Of The Densely Packed Candle Filter ID Bore Ash (Gold Coated)

Figure 4e illustrates the morphology of the densely packed fines at an alternate location along the ID bore ash sample. The ~40-50 μm particle shown in Area 1, Photo 9, Figure 4e, was identified to be magnesium-calcium-sulfur-enriched, while the <5 μm particle shown in Area 2 was silicon and aluminum-enriched. The finer agglomerates shown in Area 3, Photo 9, Figure 4e, were identified to be enriched with iron, but also contained calcium, sulfur, aluminum, and silicon. Areas 2 and 3, Photo 9, Figure 4e, are shown at higher magnification in Photo 10, Figure 4f. Additional micrographs of the densely packed ID bore fines are provided in Photo 11, Figure 4f, and Photo 12, Figure 4g.

As ash collected within the candle ID bore, fines compacted forming a very dense plug. Near the top of the plug, the fines were initially loosely packed, and the pulse jet track was evident within the plug formation. The friable, more loosely packed fines were also subjected to SEM/EDAX analyses.

As shown in Figure 5a, the ash was rather densely packed. Area 1, Photo 1, Figure 5a, was identified by EDAX analysis to contain 23.93% Fe, 6.82% Cr, 2.12% Ni, 1.39% Mg, 1.21% Al, 1.03% Si, 0.53% S, 0.36% Ca, 0.11% K, and 62.51% O. The presence of iron, chromium, and nickel within the ash fines represented metal debris (i.e., oxidation; scaling, etc.) from either the steel pulse pipes, filter holders, etc., that were located above the candle filter. EDAX analyses of the fines shown in Area 2, Photo 1, Figure 5a, indicated the presence of 6.17% Mg, 5.40% S, 4.73% Si, 3.54% Ca, 2.01 Al, 1.74% Fe, 0.29% Cr, 0.28% K, and 75.84% O, while Area 3, Photo 1, Figure 5a, was identified to contain 22.02% Cr, 15.92% Fe, 0.42% Si, 0.42% S, 0.30% Mg, 0.30% Al, 0.19% Ca, 0.11% K, and 60.31% O.

The 300-400 μm particle shown in Area 1, Photo 2, Figure 5a, is shown at higher magnification in Photo 3, Figure 5b. EDAX analysis of this particle also identified the presence of iron, chromium, and nickel (i.e., stainless steel or a low manganese-containing alloy).

The relatively uniformly sized ash particles shown in Photo 4, Figure 5b, were identified by EDAX analysis to contain aluminum, silicon, magnesium, calcium, and oxygen. Since gold was used to coat this sample, sulfur was expected to be present. One unique feature in the 20-30 μm fines was the crack formations that resulted along the surface of the particles (Area 1, Photo 4, Figure 5b).

Figures 5c, 5d, and 5e illustrate the submicron fines which formed the agglomerated ash structures within the ID bore deposit. The spherical fines shown in Photo 8, Figure 5d, was identified by EDAX to contain aluminum and silicon, while the agglomerate shown in Photo 9, Figure 5e was identified to contain calcium, sulfur (i.e., very high concentration above the gold detection peak), silicon, aluminum, magnesium, and iron.

X-RAY DIFFRACTION ANALYSES

Various ash samples were subjected to x-ray diffraction (XRD) analysis. As shown in Table 2, these included:

- Material removed from the top, middle, and bottom array filter holder mounts (Samples 1, 2, and 3).

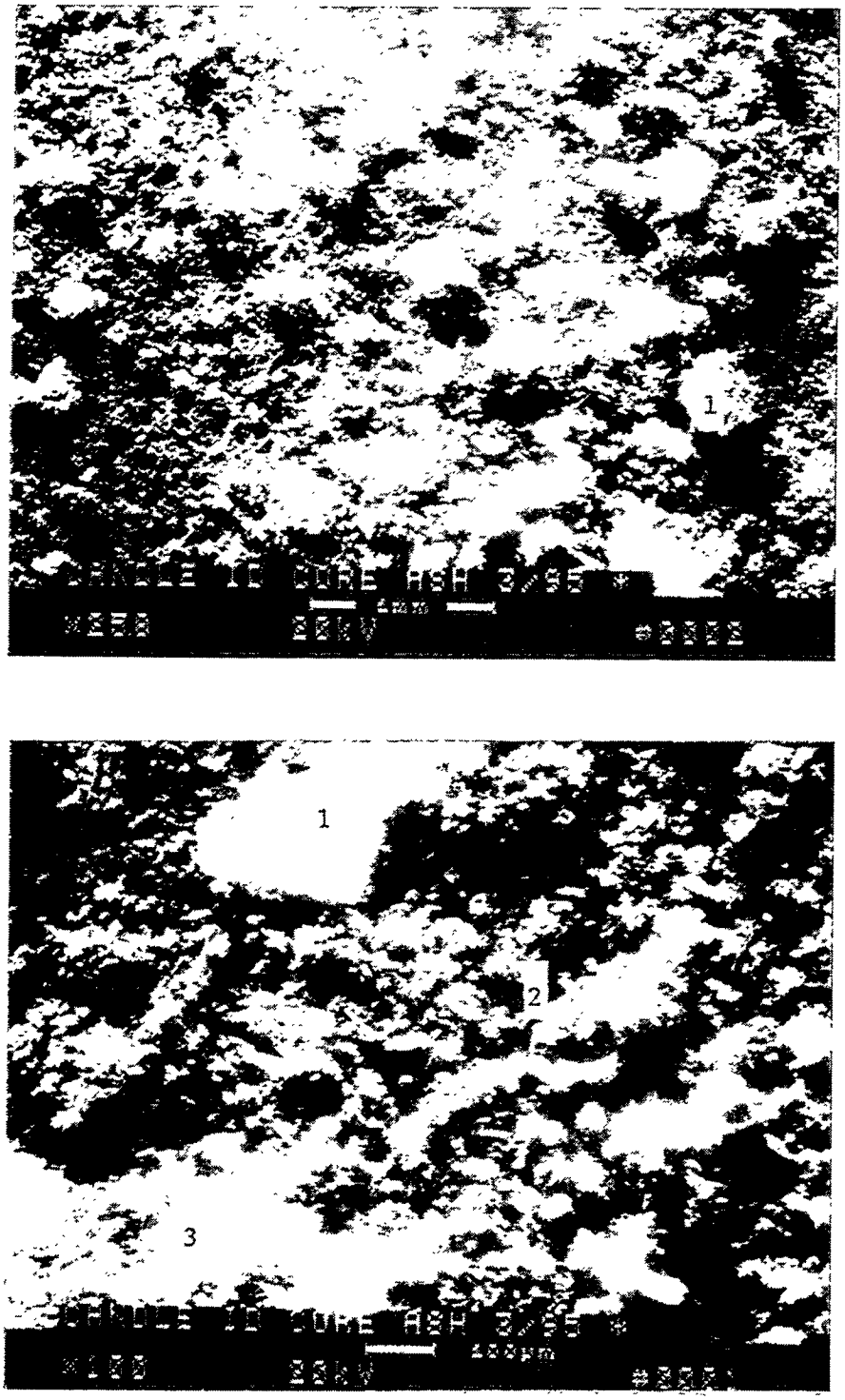

Figure 5a – Morphology Of The Loosely Packed Ash In The Candle ID Bore

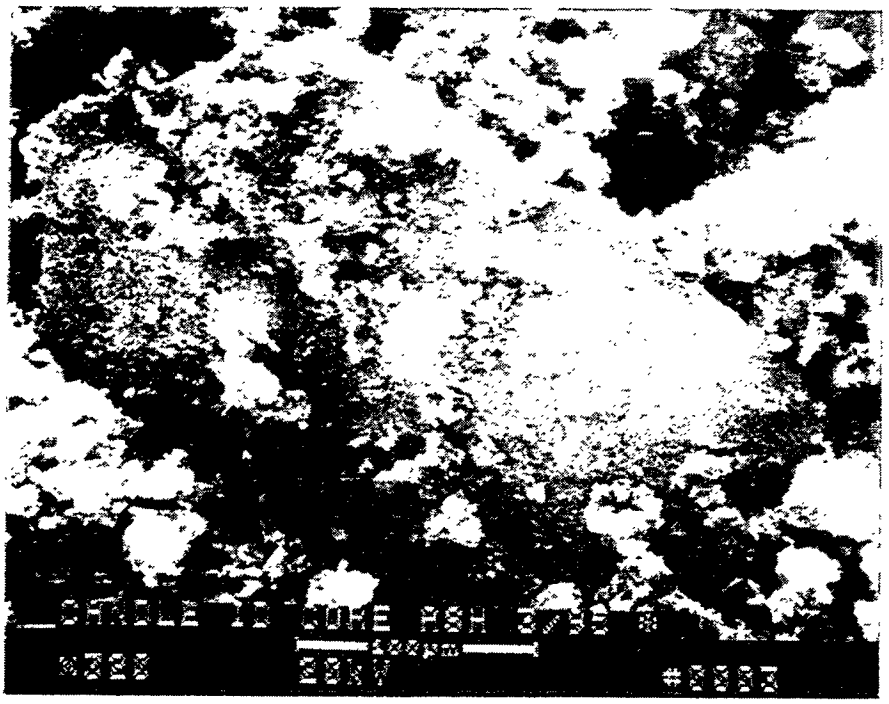

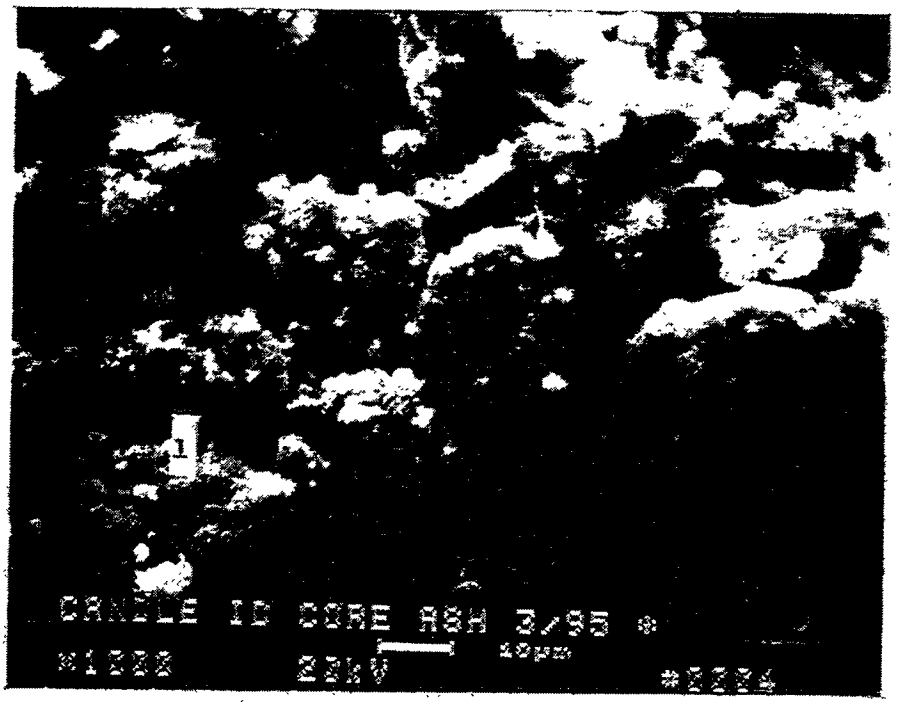

Figure 5b – Higher Magnification Micrographs Of The Loosely Packed Ash In The Candle ID Bore

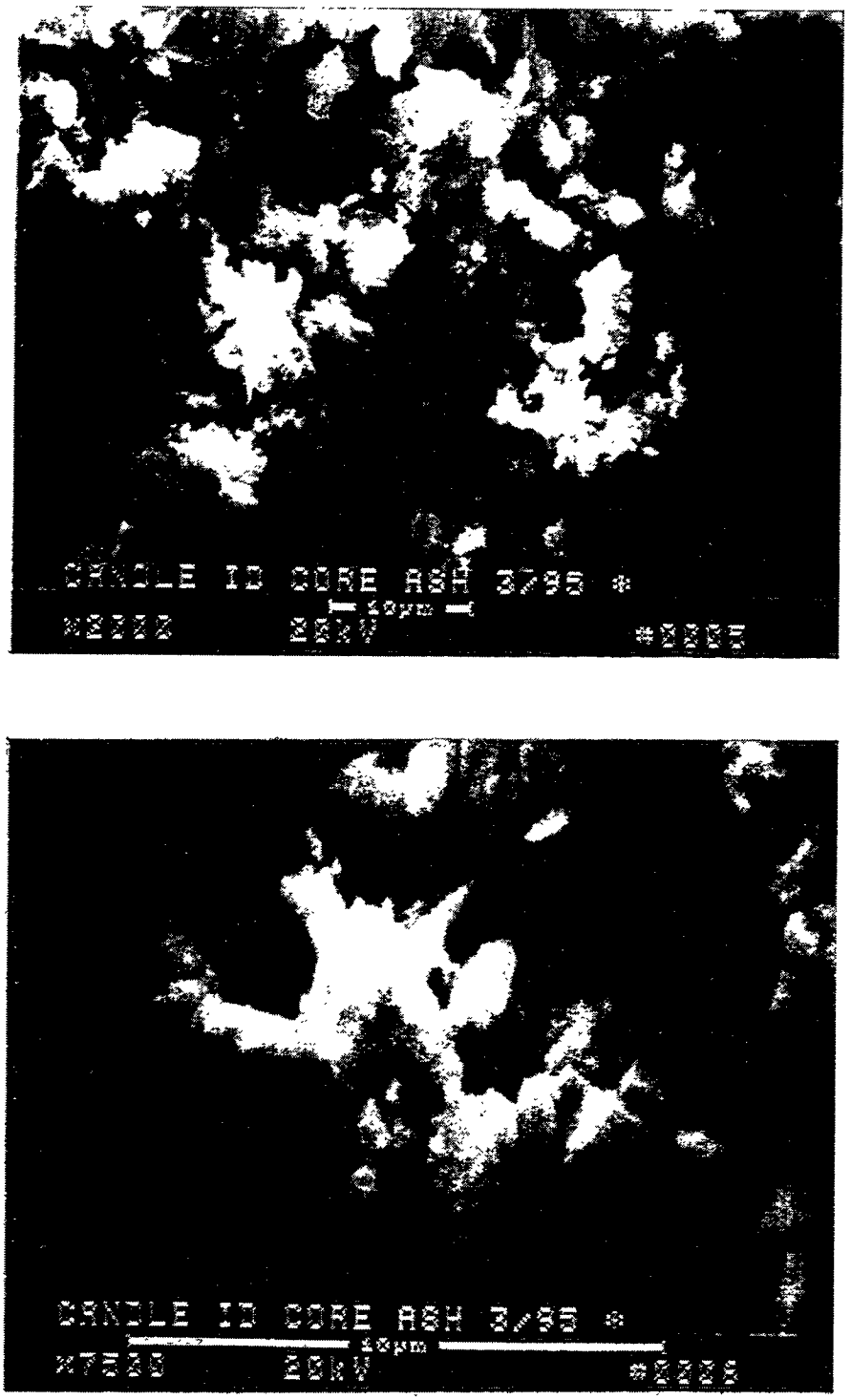

Figure 5c – High Magnification Micrographs Of The Agglomerated Ash In The Candle ID Bore

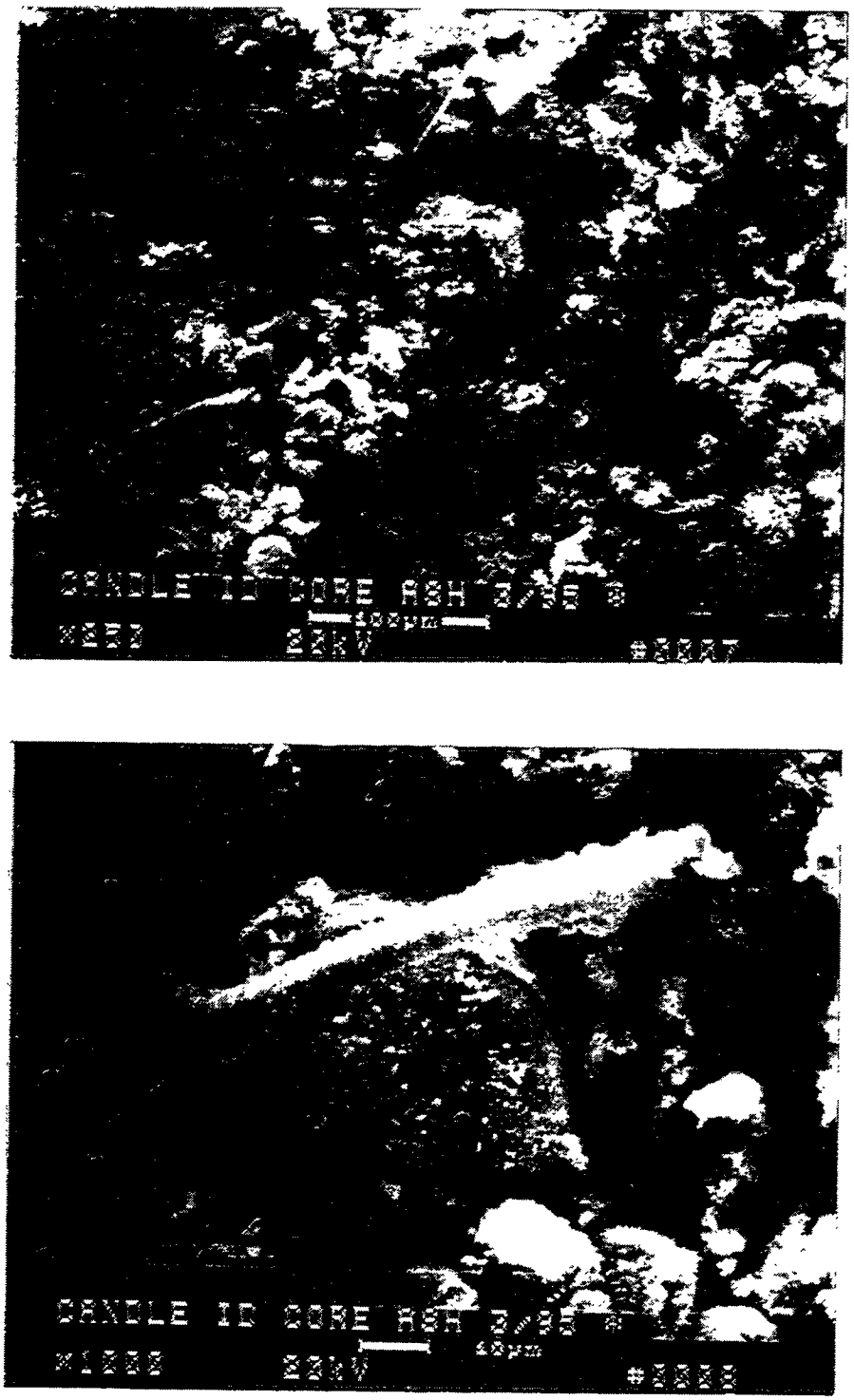

Figure 5d – Morphology Of The Loosely Packed Ash At An Alternate Location In The Candle ID Bore

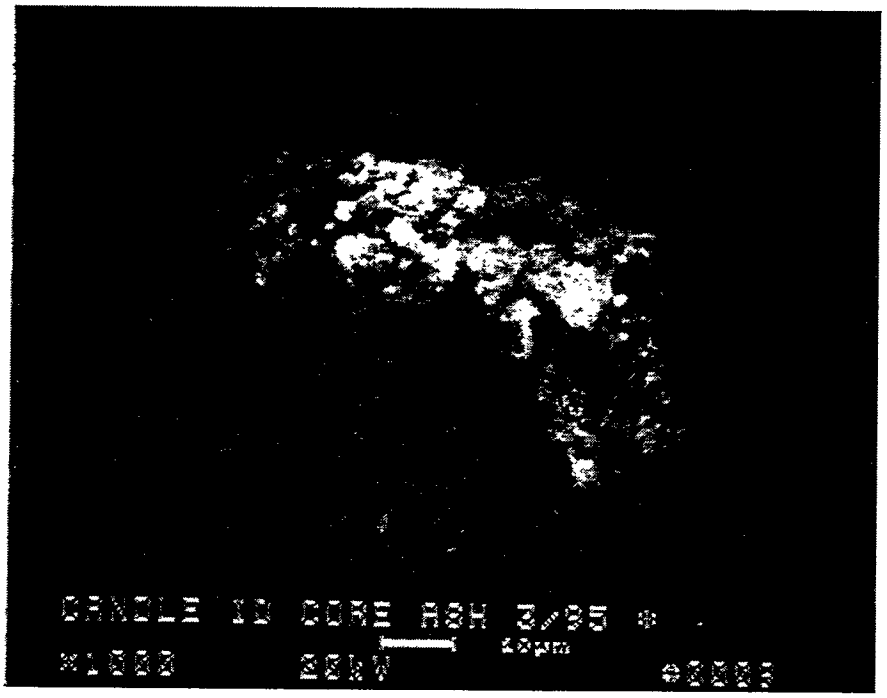

Figure 5e – Agglomerated Ash Fines In The Loosely Packed Ash That Filled The Candle ID Bore

TABLE 2
SEMI-QUANTITATIVE XRD ANALYSES OF THE AS SAMPLES
REMOVED FROM THE W-APF IN MAY 1995

(semi-quantitative values given in wt.%; JCPDS numbers given in brackets)

Sample No.	XRD File #	Calcium Sulfate *Anhydrite* $CaSO_4$ [37-1496]	Iron Oxide *Hematite* Fe_2O_3 [33-664]	Magnesium Sulfate Hydrate *Hexahydrite* $MgSO_4 \cdot 6H_2O$ [24-719]	Carbon C [26-1080]	Magnesium Oxide *Periclase* MgO [43-1022] (a)	Calcium Carbonate *Calcite* $CaCO_3$ [5-586]	Calcium Magnesium Silicate *Monticellite* $CaMgSiO_4$ [35-590]	Calcium Sulfate $CaSO_4$ [37-184] (b)	Magnesium Sulfate Hydrate *Epsomite* $MgSO_4 \cdot 7H_2O$ [36-419]	Magnesium Sulfate Hydrate $MgSO_4 \cdot 3H_2O$ [26-1228] (b)	Magnesium Calcium Carbonate $Mg_3Ca(CO_3)_4$ [14-409] (b)	Unknown(s) (wt.%)	Total No. of Lines Identified/ No. of Unknown Lines	Intensity of Largest Unknown Line
1	10995	88	4	4	---	---	---	---	---	---	---	---	---	---	---
2	11095	72	4	---	11	9	---	---	---	---	---	---	4	35/2	4
3	11195	20	---	---	---	29	27	11	8	---	---	---	4(c)	27/4	6
4	11295	75	7	---	11	---	---	---	---	2	---	---	5(c)	37/5	17
5	11395	65	4	5	16	---	3	---	---	4	---	---	5	40/8	7
6	11495	63	6	3	17	possible trace	---	---	---	7	---	---	3	37/3	5
7	11595	61	6	11	8	---	---	---	6	4	---	---	4	29/2	7
8	11695	47	4	6	18	7	9	---	---	6	---	---	4	44/5	7
9	11795	73	7	12	---	---	2	---	---	---	4	possible trace	3	41/3	9
10	11895	48	3	3	17	11	11	---	---	5	---	possible trace	2	43/1	3
11	11995	45	4	4	18	9	12	---	---	5	---	---	3	39/4	6
12	12095	61	5	7	6	4	5	---	---	7	---	---	5	33/2	7
13	12195	64	7	12	---	---	7	---	---	10	---	---	---	30/3	9
14	12295	40	3	7	---	---	10	9	---	31	---	---	---	16/0	---
														54/0	---

D-39 152

Sample Descriptions

1. Top of C/T Holder-Hard Chunk
2. Top Holder of Middle Array-Powdery, Tan
3. Top Holder, Bottom Array-Compressed Chunk, Light Tan
4. Plug Schumacher (Reddish)
5. Plug Coors (Top) (Tan)
6. Base of Shed-Middle Array
7. Plenum Falkes-Mid-(Contour Retained) Medium Tan
8. Vitropore Top-Tannish Powdery
9. Vitropore Bottom-Red Compressed Chunks
10. Coors Bottom-Light Tan
11. Coors Top-Little Redder, Light Tan
12. Mid Stripe (Little Powder) Tan
13. Top Stripe (Little Deposit)
14. PRD Flake

Notes:

a. Difficult to positively identify the presence of MgO (Periclase) because its XRD pattern overlaps peaks associated with both $CaSO_4$ and Fe_2O_3.
b. Overall match is not particularly good.
c. Possible match with 4 wt.% unknown is Magnesium Calcium Carbonate, Huntite, $Mg_3Ca(CO_3)_4$, JCPDS 14-409. Note that overall match is not very good.
d. Possible match with 2 wt.% unknown is Magnesium Sulfate Hydrate, Kieserite, $MgSO_4 \cdot H_2O$, JCPDS 33-882. Note that overall match is not very good.

- The dense ash plug which formed within the ID bore of the Schumacher Dia Schumalith F40 and Coors alumina/mullite candle filters (Samples 4 and 5).
- Ash which collected at the base of the shed/plenum pipe (Sample 6).
- Ash which adhered to the plenum pipe (Sample 7).
- Ash removed along the length of the Pall Vitropore 442T and Coors alumina/mullite candle filters (Samples 8, 9, 10, and 11).
- The "red stain" deposit which formed along the top and middle array dust sheds (Samples 12 and 13).
- An ash "flake" which was easily remove from the surface of the DuPont PRD-66 filter element (Sample 14).

During operation in Test Segment #5 at AEP, either selective deposition of ash occurred within the filter arrays, particularly along the filter holder mounts, or a temperature gradient within the vessel promoted bulk diffusion and/or reactions to occur within the deposited fines. The tenaciously bonded, densely packed cake which formed along the top array filter holder mounts, primarily contained 88 wt% anhydrite (i.e., $CaSO_4$), 4 wt% hematite (i.e., Fe_2O_3), and 4 wt% magnesium sulfate hydrate (i.e., hexahydrite).

Moving to the middle array, the anhydrite content in the filter holder mount cake decreased to 72 wt%, hematite was present at concentrations of 4 wt%, and carbon and either magnesium oxide or $CaSO_4/Fe_2O_3$ were selectively deposited. Along the bottom array filter holder mount, anhydrite was present at 20 wt%, periclase (MgO) and/or $CaSO_4/Fe_2O_3$ were present at 29 wt%, calcium carbonate was determined to be present at 27 wt%, monticellite (i.e., calcium magnesium silicate) was detected at concentrations of 11 wt%, and $CaSO_4$ was identified to be present at 8 wt%.

Deposition and/or reactions which lead to the formation of selective phases of the sorbent material most likely resulted from the temperature gradient which resulted within the W-APF vessel during operation in Test Segment #5.

Within the densely packed candle ID bore fines in the A/T array, anhydrite, hematite, carbon, calcium carbonate, epsomite (i.e., magnesium sulfate hydrate), and infrequently magnesium sulfate hydrate (i.e., hexahydrite) were detected.

A rather dramatic difference in the ash composition which deposited at the top and bottom of the Pall Vitropore 442T candle filters was evident. The thick deposit which formed along the end cap of the Pall Vitropore 442T filter which resembled initiation of the elephant foot formation, contained a relatively high concentration of calcium sulfate and magnesium sulfate hydrate (i.e., hexahyrite). The thinner ash cake layer that formed along the top of the Vitropore 442T candle filter contained carbon, periclase, calcium carbonate, and epsomite.

Subtle phase differences resulted in the dust cake that was removed from the top and bottom areas of the Coors alumina/mullite candle filters. The relatively smooth surface finish of the Coors alumina/mullite candle filter, as well as the uniform body/end cap wall thickness of this element may limit ash adherence during extended field operation. Retention of the ash fines along a

candle filter surface (i.e., along the Pall Vitropore 442T filter, particularly along the bottom end caps), may promote continued reaction with the pressurized fluidized-bed combustion (PFBC) gas phase environment, resulting in a highly sulfated, tenaciously bonded, sintered or "melt-like" dust cake layer.

The red stain that was evident along the dust sheds at the conclusion of Test Segment #5 at AEP, typically contained anhydrite and hydrated magnesium sulfate.

The ash flakes which lifted but remained attached to the surface of the DuPont PRD-66 filter element contained the magnesium sulfate hydrate complex. This was considered to be the phase responsible for the formation of the tenaciously bonded ash/sorbent deposit which collected along the top holder mounts.

The presence of the hydrated magnesium sulfate complexes that were identified by XRD analyses for the various ash samples most likely resulted from continued sorption of moisture by the material after removal from the W-APF vessel. The hydroscopic nature of the ash was supported by the fact that during the 2-3 week time period between removal from the W-APF and sample characterization, the weight of the dust cake material nearly doubled while the sample remained exposed to room temperature air.

THERMAL EXPANSION OF THE ASH AND POROUS CERAMIC FILTER MATERIALS

The thermal expansion of the ash which filled the ID bore of the candle filters in Test Segment #5 was determined in an attempt to identify the mechanism of end cap candle filter failure. As shown in Figure 6, the thermal expansion of the ID filled ash is approximately twice that of the Coors alumina/mullite and/or Schumacher Dia Schumalith F40 filter matrix. What has been considered to have occurred was that during failure of the DuPont PRD-66 filter elements in array A/T, fines were back pulsed into the ID of the remaining intact filter elements. During repetitive plant startups (i.e., 10 cooldown/heatup cycles during Test Segment #5), the ash in the candle ID expanded during heatup, causing a load to be applied to the ID wall of the filter element. During cooldown, hydration of the ash also increased the volume and density of the ID bore ash, again causing expansion and an additional load to be applied to the ID surface of the filter elements.

Ultimately, hairline cracks resulted along the end caps of several filter elements. Although hairline cracks were evident along the filter end caps at termination of Test Segment #5, the candles remained intact in the array after the lift had been conducted. Similarly, the fractured candle filter surfaces were virtually clean, free of dust tracks penetrating across the 10-15 mm walls. This indicated that fines were not carried through the filter wall during process operation, and that perhaps failure resulted during the final hours of field testing.

ASH STRENGTH AND DENSITY

The densely packed ID bore ash was removed as a solid plug from the test Segment #5 candle filter elements. The density of the ID bore ash as shown in Table 3 was determined to be 1.19 ± 0.1 g/cm^3. When subjected to strength testing, the axial strength of the ash plug was determined to be 309.4 psi, while the transaxial strength of the ash plug ranged from 160.7 to 212.9 psi.

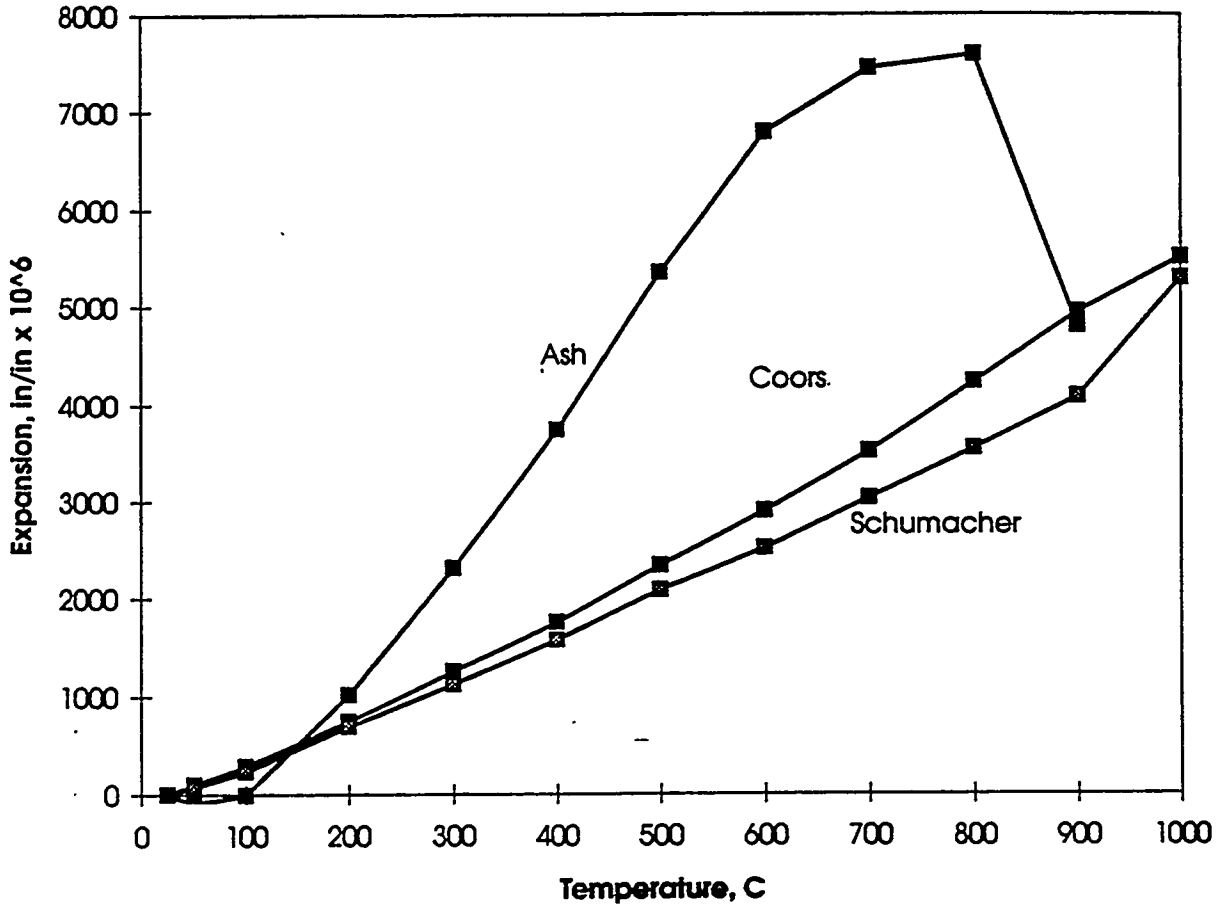

Figure 6 – Thermal Expansion OF The ID Bore Ash And Porous Ceramic Candle Filter Elements

TABLE 3
DENSITY AND STRENGTH OF THE ID BORE ASH

A/T-17: Coors Alumina/Mullite Candle
A/T-16: Schumacher Dia Schumalith F40 Candle

Sample		Length inch	Width inch	Thick inch	weight gr	Density gr/cm^3	Peak loac lbs	Stress psi
AT-17	2 trans	0.75	0.83	0.75	9.2	1.20	132.5	212.9
AT-16	3 trans	0.70	0.64	0.62	4.75	1.04	72	160.7

Sample		Length inch	Diameter inch	weight gr	Density gr/cm^3	Peak loac lbs	Stress psi
AT-17	1 axial	0.58	1.62	22	1.12		
AT-17	2 axial	2.50	1.62	108.9	1.29		
AT-16	4 axial	1.46	1.17	32.6	1.27		
AT-16	1 axial	0.66	1.16	14.2	1.24	530	309.4

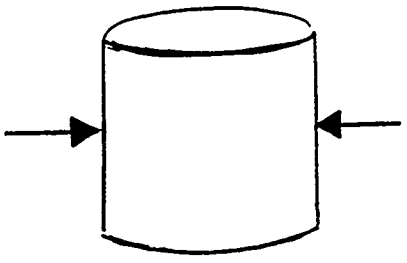

Transaxial

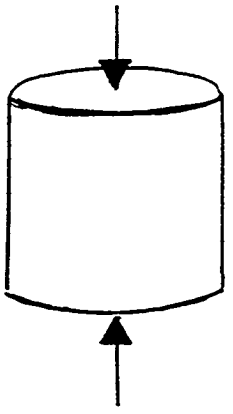

Axial

Ash bridges which originally formed within the filter arrays were eliminated in Test Segment #5 after completely eliminating carryover from the primary cyclone. As shown in Table 4, the density of eight ash/sorbent samples which had been removed from various locations within the W-APF ranged from 0.44-0.85 g/cm^3. Sample of ash/sorbent removed from the top and bottom holders were high density cake formations, while ash/sorbent which deposited along the Coors candles were lower density materials.

Very little differences in the density of the ash which collected at the top vs the bottom of the Pall Vitropore 442T candles resulted even though a thicker deposit formed along the bottom of the Pall Vitropore 442T filter elements.

Ash bridges which formed during Test Segment #4 when the primary cyclone was partially detuned were identified to have a density of 0.59±0.1 g/cm^3, and a peak load strength which ranged between 1.0 and 8.0 psi (Table 5). When the primary cyclone was fully activated in Test Segment #3, the density of the ash bridges which formed between adjacent filter elements and/or the plenum pipes and dust sheds was 0.54±0.04 gm/cm^3, while the strength of the bridged material ranged between 16.9 and 53.9 psi.

TABLE 4
DENSITY OF ASH AT VARIOUS LOCATIONS WITHIN THE W-APF
-- TEST SEGMENT #5 --

DENSITIES OF ASH FROM VARIOUS SOURCES					
Sample	High	Wt	Density		
	inch	Gr	Gr/cm^3		
A	0.158	23.45	0.78		
B	0.191	21	0.44		
C	0.182	22.6	0.60		
D	0.5	35	0.61		
E	0.478	33.6	0.59		
F	0.15	23.7	0.85		
G	0.255	28.3	0.78		
H	0.405	32	0.64		

A: Ash from the top of the Coors alumina/mullite candle filter in the A/B array.
B: Ash from the Coors alumina/mullite candle filter in the middle array.
C: Ash from the top of the Pall Vitropore 442T candle filter in the C/T array.
D: Ash from the end cap of a C/B Pall Vitropore 442T candle filter (i.e., elephant foot formation).
E: Bottom elephant foot formation along a B/M candle filter.
F: Ash from the C/T filter holder mount. Very hard ash deposit which was chiseled off in order to remove it from the holder.
G: Ash from the C/B filter holder mount.
H. Ash at the base of the plenum pipe/dust shed.

TABLE 5
DENSITY AND STRENGTH OF ASH BRIDGES FORMED WITHIN THE W-APF
-- Tidd May 5, 1994 - Test Segment #3 --
-- Tidd October 1994 - Test Segment #4 --

COMPRESSION STRENGTH OF ASH
From solid ash formations

Sample	Length inch	Width inch	Thick inch	weight gr	Density gr/cm^3	Peak load lbs	Stress psi
Tidd May 5							
1	1.18	0.82	0.82	6.782	0.52	23.5	24.3
2	1.1	1.093	1.05	9.3114	0.45	33.3	27.7
3	0.9	0.8	1.07	6.717	0.53	13.7	19.0
4	1.05	0.8	1.04	8.179	0.57	33.9	40.4
5	1.04	1	0.9	8.5718	0.56	17.6	16.9
6	1.06	0.85	1.1	9.385	0.58	48.6	53.9
					0.54		30.4
Tidd Oct							
1	1.73	0.9	0.85	12.8966	0.59	1.6	1.0
2	1.18	0.8	1	10.6105	0.69	1.8	1.9
3	1.02	0.78	1.05	6.881	0.50	6.4	8.0
							3.7

APPENDIX E
CHARACTERIZATION OF THE ASH DEPOSIT AND SURVEILLANCE SCHUMACHER DIA SCHUMALITH F40 CANDLE FILTER

M. A. Alvin
July 9, 1995

INTRODUCTION

Schumacher Dia Schumalith F40 surveillance candles successfully achieved 5855 hours of operation in the W-APF system at Tidd. The residual bulk strength of the Schumacher Dia Schumalith F40 matrix was determined via room temperature and process temperature C-ring compressive and tensile testing using 15 mm samples that were cut with a diamond wheel from the PFBC-exposed filter elements. As shown in Figure 1, the bulk strength of the Schumacher Dia Schumalith F40 matrix decreased during the initial 1000-2000 hours of PFBC operation. With continued operation, however, the bulk strength of the Schumacher Dia Schumalith F40 matrix remained constant. The residual or "conditioned" strength was considered to result from the complete or nearly complete crystallization of the binder phase that encapsulated the silicon carbide grains, as well as the bond posts or ligament surfaces.(1)

In order to ascertain whether the Schumacher Dia Schumalith F40 filter matrix experienced creep during operation in the PFBC environment, the overall length of the surveillance filter elements were measured during outages, and compared to their initial, as-manufactured lengths. After 5855 hours of operation in the W-APF at AEP, the 1.5 m elements were observed to have elongated by 5-7 mm. Cracks were not evident along the external surface of the filter elements (i.e., particularly below the flange).

During operation of the W-APF in the initial test segments, failure of the Schumacher Dia Schumalith F40 filter elements had previously occurred at the base of the flange, primarily during cool-down after ash bridging extensively deposited fines between adjacent filter elements, and/or the plenum support pipe and dust sheds. Failure of the Schumacher Dia Schumalith F40 filter matrix also resulted during cool-down when a densified plug of fines was embedded within the ID bore of the filter element. The difference between the thermal coefficient of expansion of the ash, ceramic, and/or metal structure was considered to be responsible when failure of the Schumacher Dia Schumalith F40 clay bonded silicon carbide filters occurred at AEP.

ASH DEPOSIT CHARACTERIZATION

The surveillance Schumacher Dia Schumalith F40 candle filter S228/318B was reinstalled in position A/T-16 prior to initiating Test Segment #5. This candle had been successfully operated

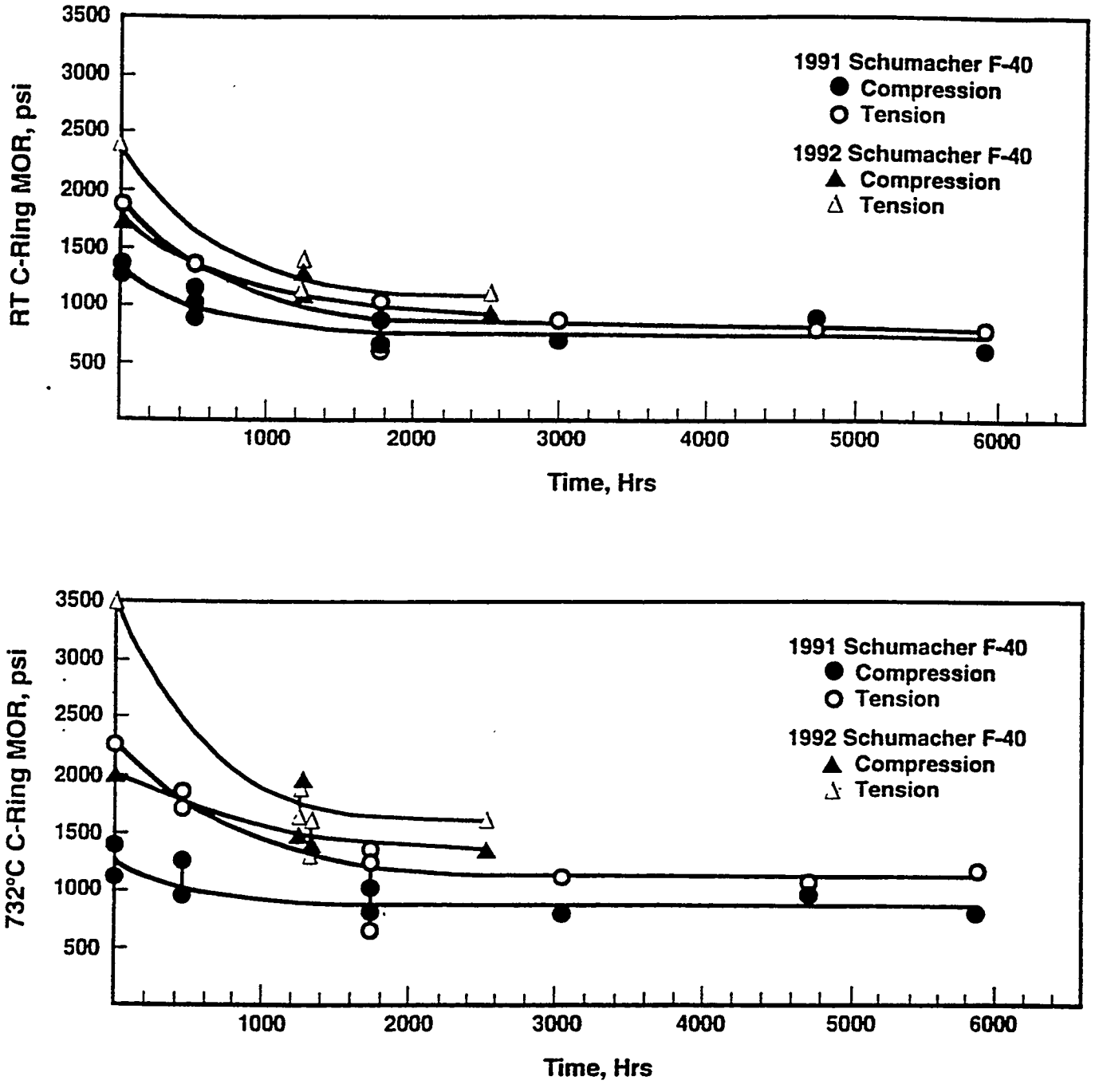

Figure 1 — Residual Strength of the Schumacher Dia Schumalith F40 Candle Filters During Operation in the W-APF at AEP

in the W-APF since testing began in Test Segment #1 in October 1992, and acquired 5855 hours of field operation at the completion of testing at AEP in May 1995. A portion of the ash cake layer which formed along the outer surface of the filter element in Test Segment #5 was carefully removed as an intact ~6 mm ash/sorbent nodule, and was cross-sectioned and subjected to scanning electron microscopy/energy dispersive x-ray analyses (SEM/EDAX). Characteristically, the outer surface of the ash nodule was white in color, followed by a pink layer, and subsequently a red layer of material.

Nine areas were initially selected for characterization through the cross-sectioned, ~6 mm ash nodule. In addition, both inner and outer surfaces of the ash nodule were also characterized. Carbon was utilized during sample preparation so as to permit detection of sulfur within the ash matrix. As shown in Figure 2a, the ash nodule appeared to contain densely packed fines throughout its entire thickness.

As shown by the EDAX analyses in Table 1, the ash nodule was principally silicon-enriched (i.e., 10.39-12.83 atomic percent), with an ~1:1 atomic percent ratio of calcium and magnesium to sulfur (i.e., complete or nearly completely sulfated sorbent), minor contributions of aluminum, and low concentrations of iron, potassium, sodium, and titanium. Only minor variations in the elemental concentrations were observed through the cross-sectioned ash nodule. For the most part, the ash nodule appeared to be compositionally homogeneous.

A series of SEMs is provided in Figures 2b through 2s which illustrate the morphology of the ash fines through the cross-sectioned, ~6 mm ash nodule. The sample used for this exercise was coated with gold in order to produce high resolution micrographs.

Figures 2b and 2c indicate that although the ash fines were densely packed, porosity remained within the ash which deposited near the surface of the Schumacher Dia Schumalith F40 candle filter. The ash in this area consisted of an interconnected network of agglomerated submicron and micron (i.e., ~3-5 μm) fines. The submicron and micron fines characteristically had rounded surface features.

Similar agglomerated features were evident in the fines that deposited at ~50 μm above the candle filter surface. Figure 2d shows the significantly open structure (i.e., high porosity) of the resulting deposit.

The agglomerated and sintered features of the ash were evident in the fines that deposited at ~100 μm and ~150 μm above the surface of the filter element (Figure 2e). This was readily evident in the ash which deposited at ~200 μm and ~250 μm above the filter surface (Figure 2f). Relatively large (i.e., ~5-7 μm) fines with smooth, featureless (i.e., amorphous or sintered characteristics) surfaces were present among the interconnected, agglomerated, submicron and micron fines which deposited at ~300 μm and ~350 μm above the surface of the filter element (Figure 2g).

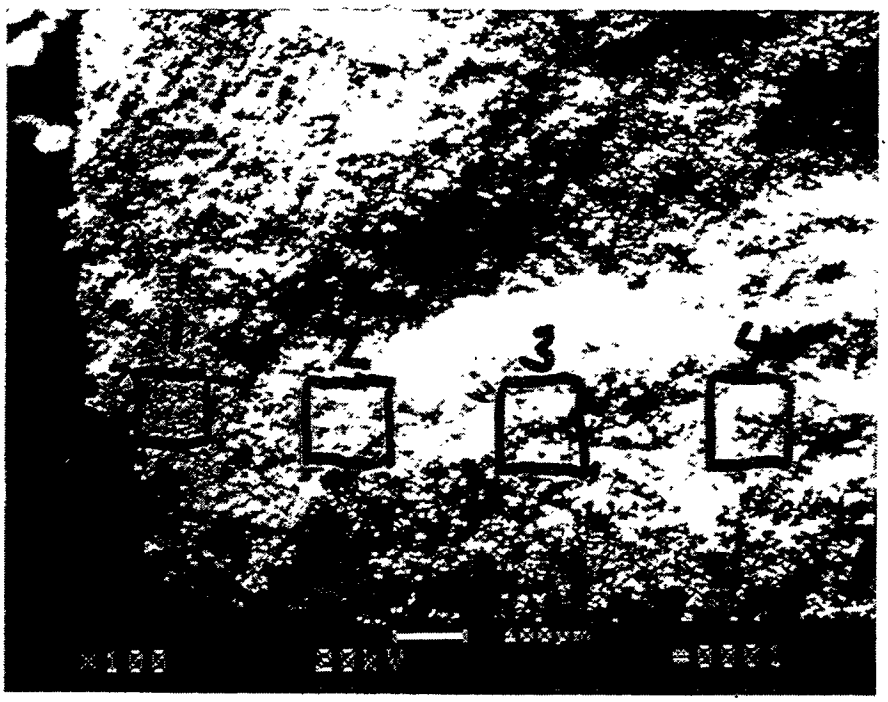

Figure 2a – Ash Nodule Deposited Along The Surface Of the Schumacher Dia Schumalith F40 Candle Filter After 5855 Hours Of Operation In The PFBC Environment At AEP

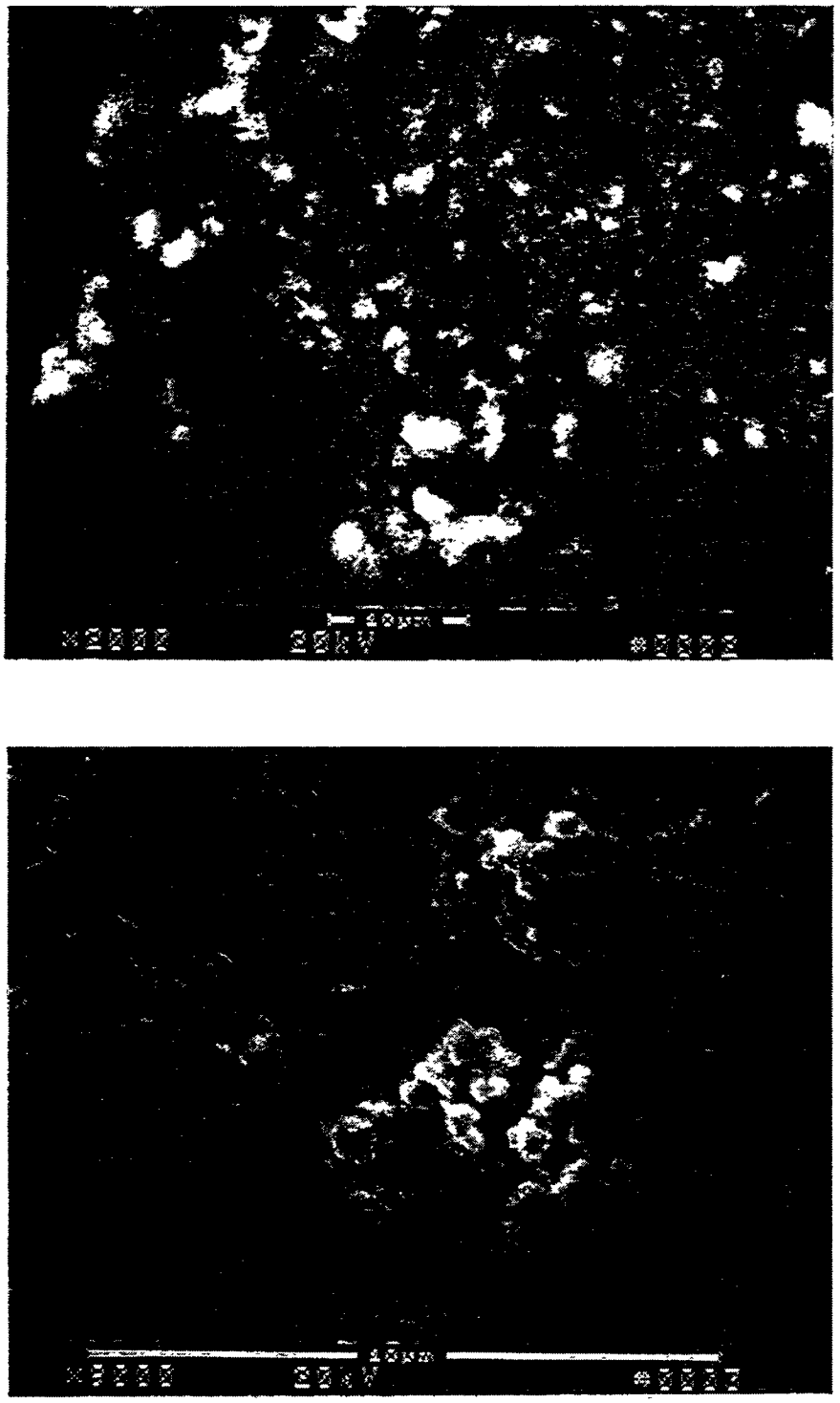

Figure 2b – Morphology Of The Cross-Sectioned Ash Deposit Near The Candle Filter Surface

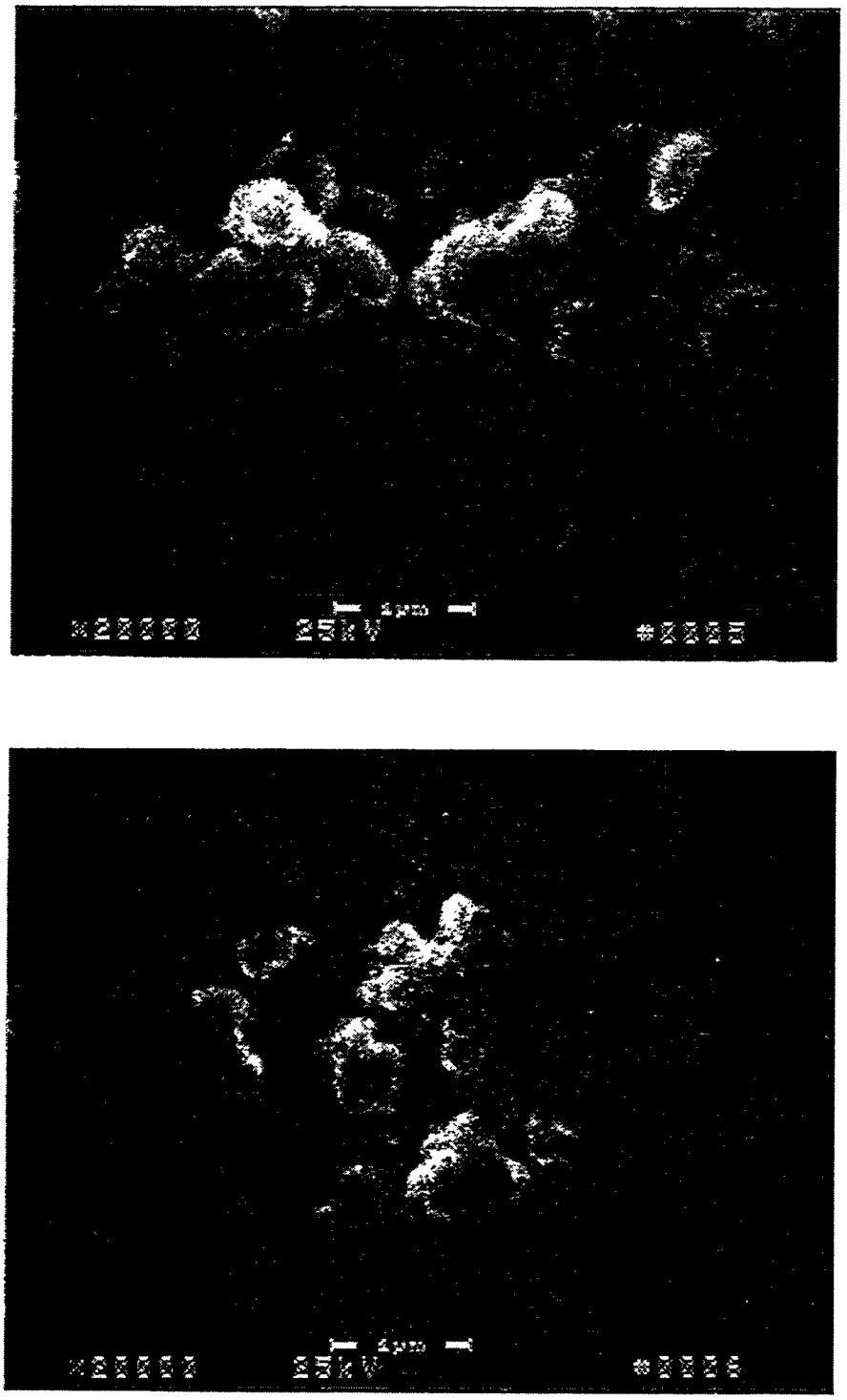

Figure 2c — Higher Magnification Micrographs Illustrating The Morphology Of The Cross-Sectioned Ash Deposit Near The Candle Filter Surface

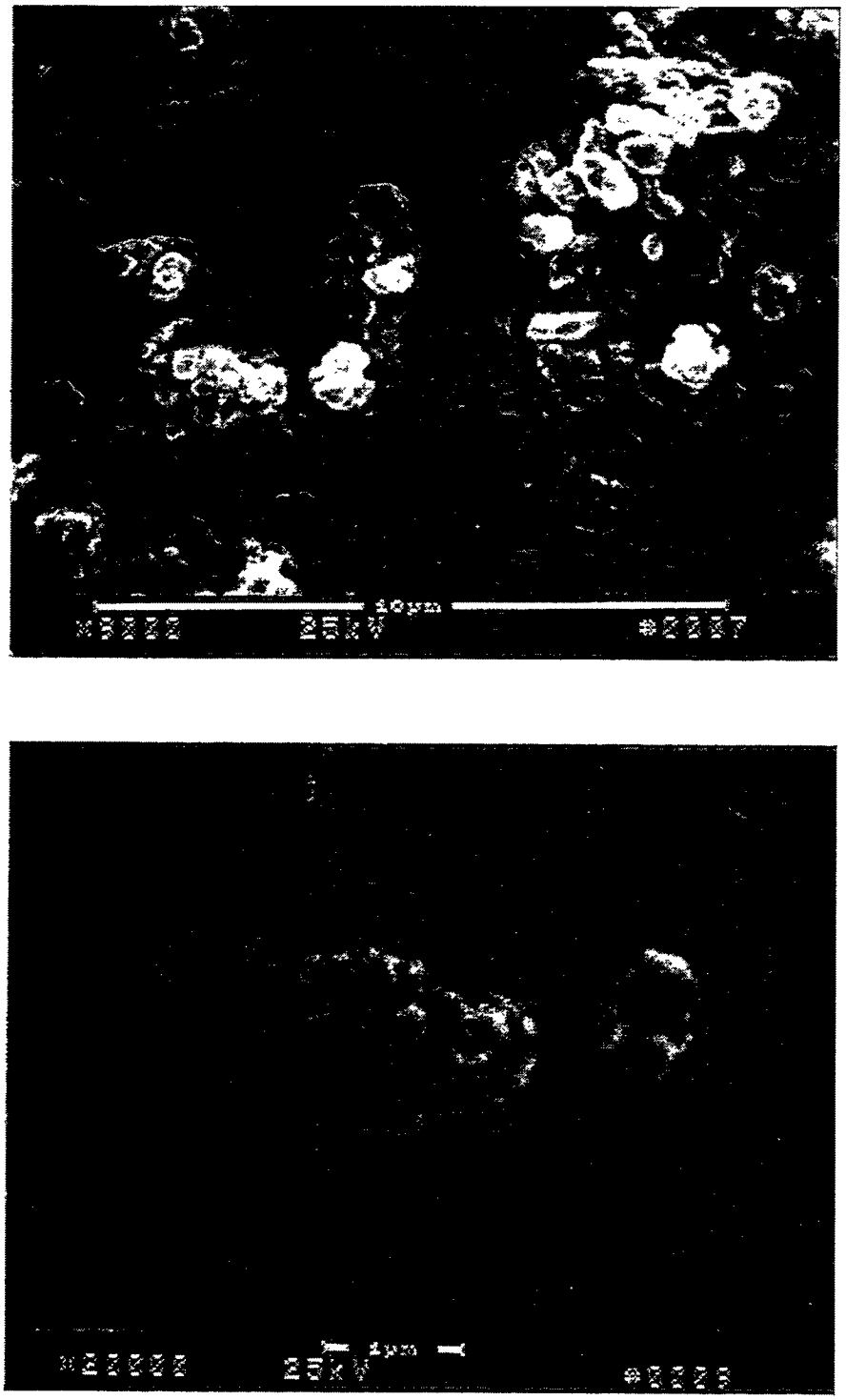

Figure 2d – Morphology Of The Cross-Sectioned Ash Deposit At ~50 μm Above The Surface Of The Candle Filter

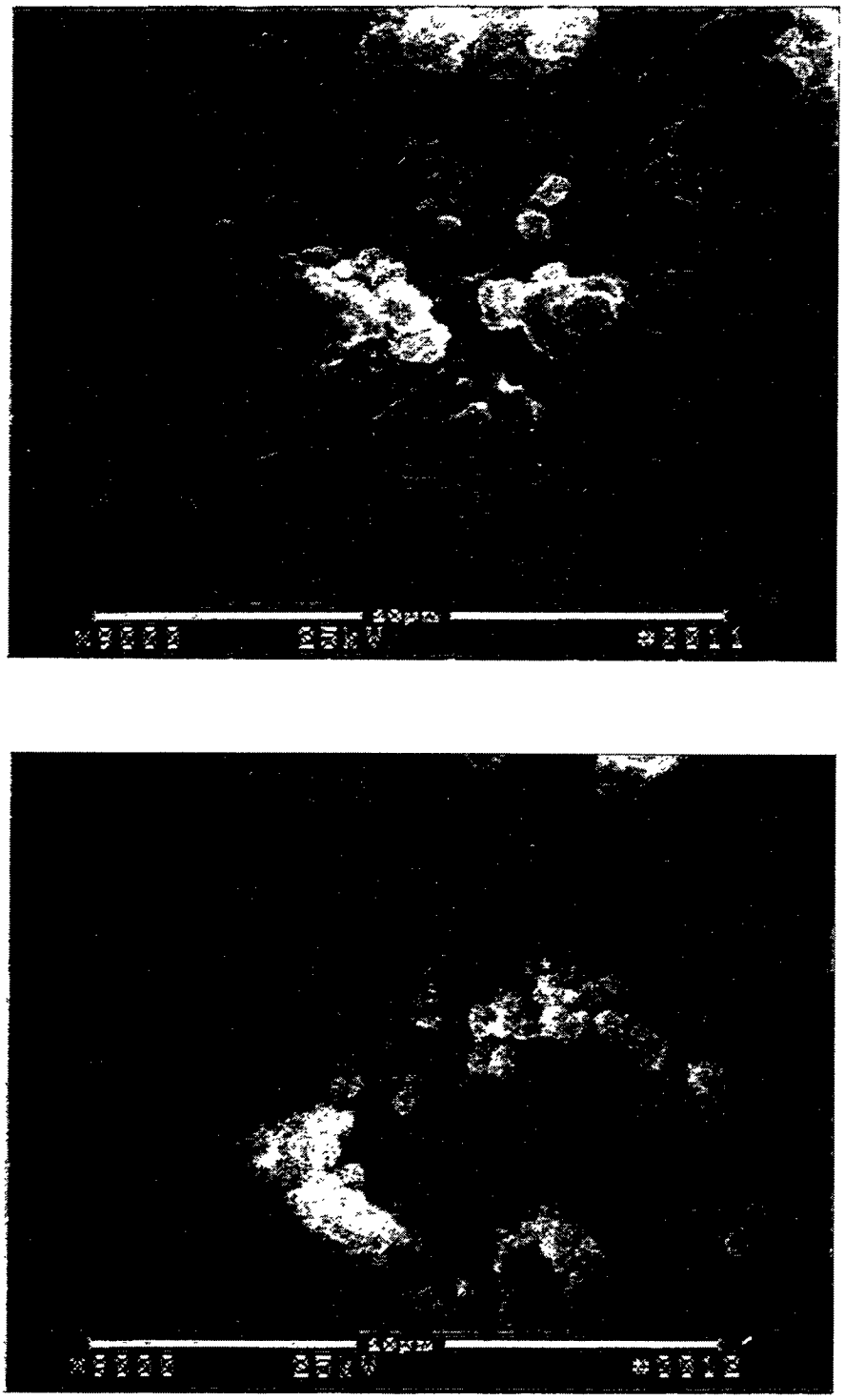

Figure 2e — Morphology Of The Cross-Sectioned Ash Deposit At ~100 μm (Top Micrograph) And ~150 μm Above The Surface Of The Candle Filter (Bottom Micrograph)

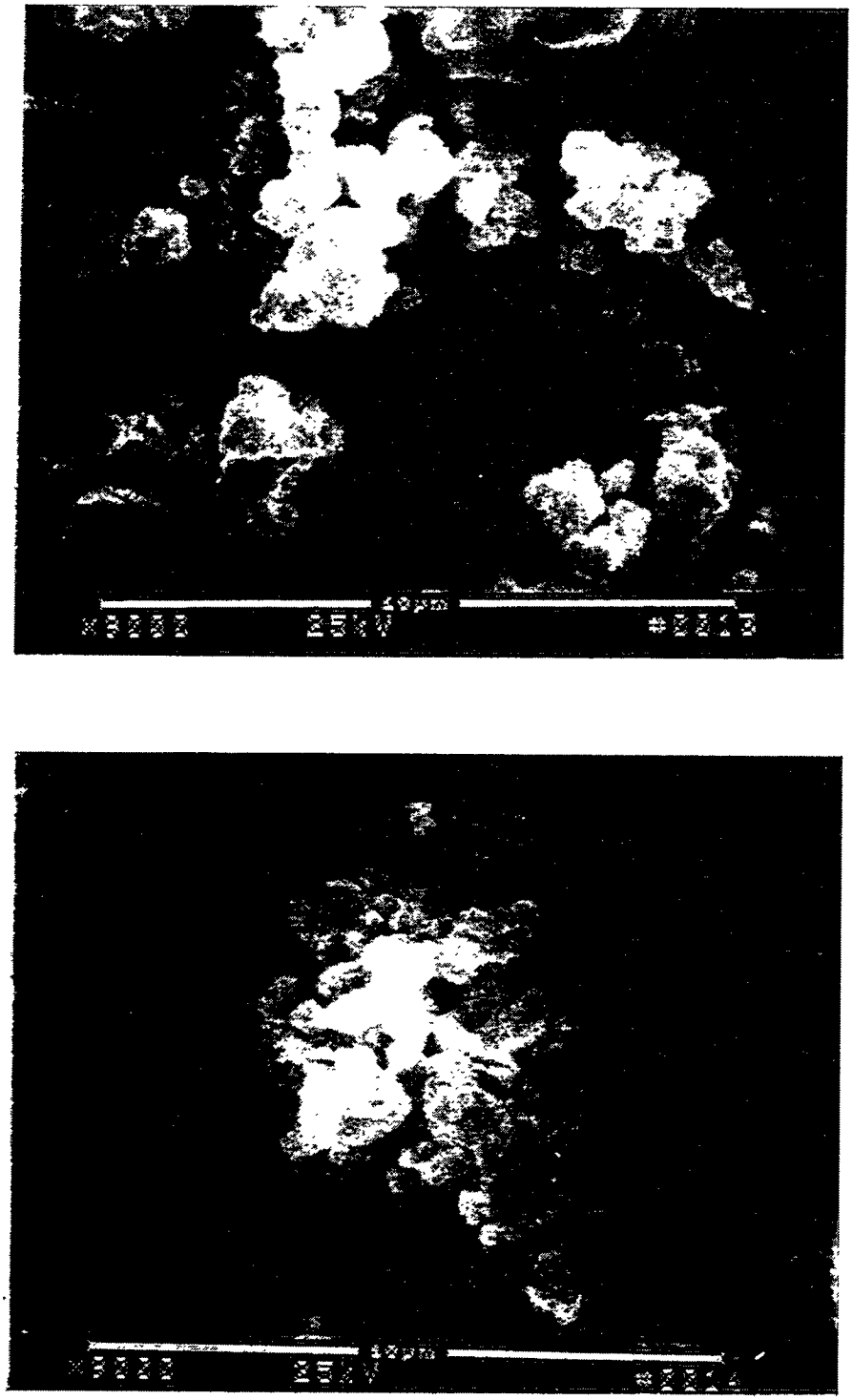

Figure 2f — Morphology Of The Cross-Sectioned Ash Deposit At ~200 μm (Top Micrograph) And ~250 μm Above The Surface Of The Candle Filter (Bottom Micrograph)

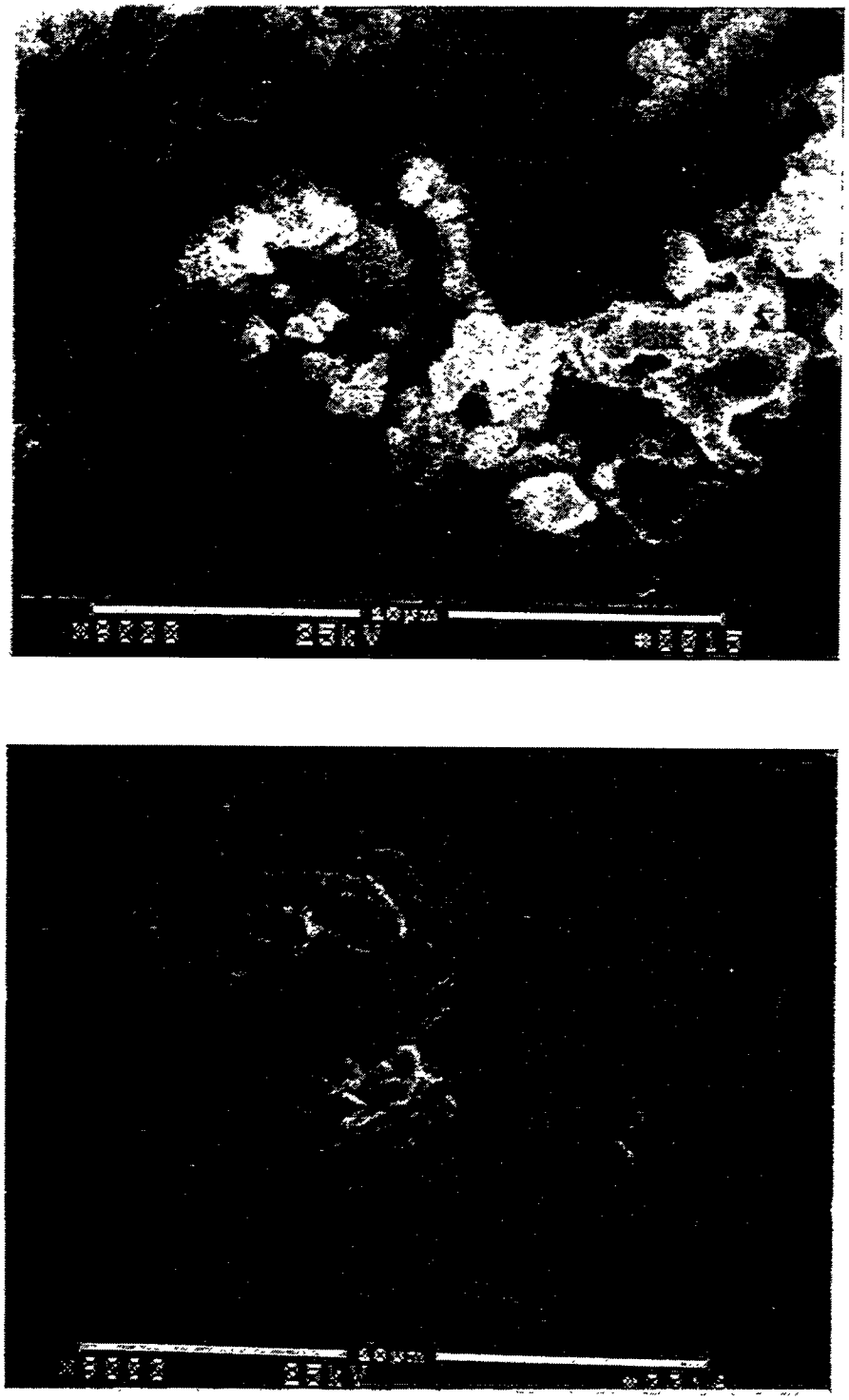

Figure 2g – Morphology Of The Cross-Sectioned Ash Deposit At ~300 μm (Top Micrograph) And ~350 μm Above The Surface Of The Candle Filter (Bottom Micrograph)

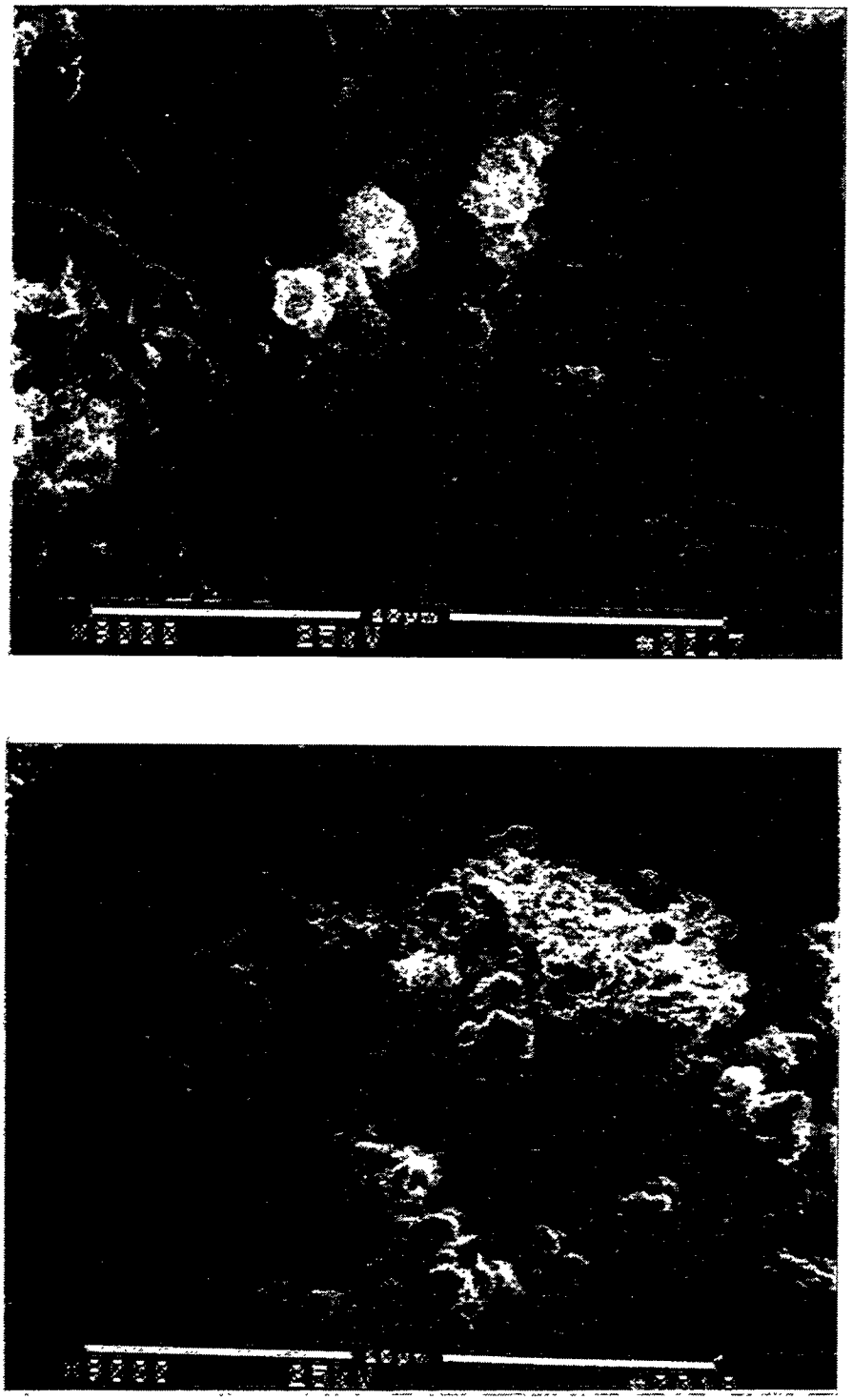

Figure 2h – Morphology Of The Cross-Sectioned Ash Deposit At ~400 μm (Top Micrograph) And ~450 μm Above The Surface Of The Candle Filter (Bottom Micrograph)

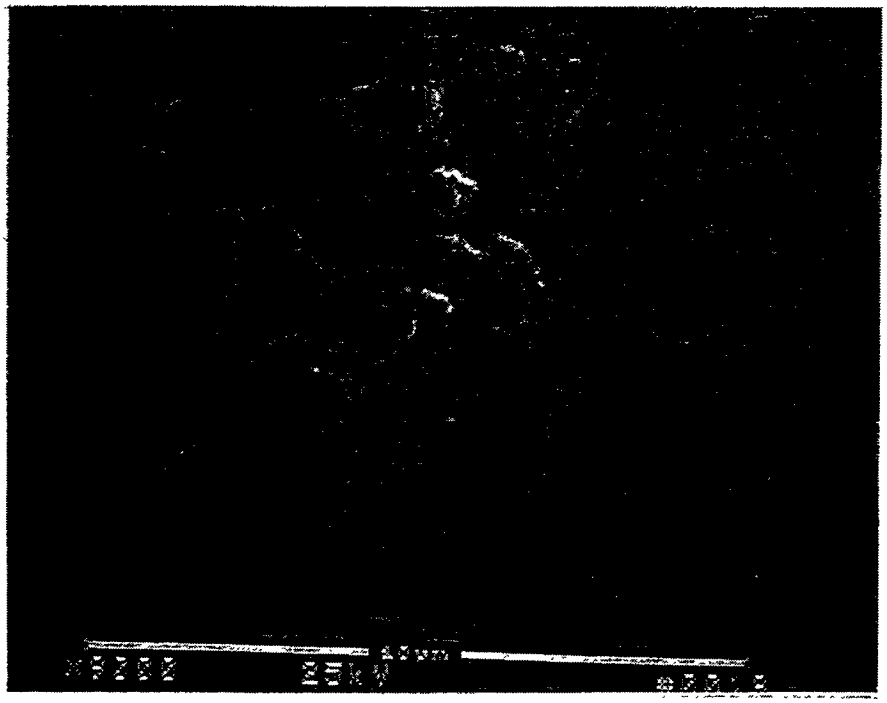

Figure 2i – Morphology Of The Cross-Sectioned Ash Deposit At ~500 μm Above The Suface Of The Candle Filter

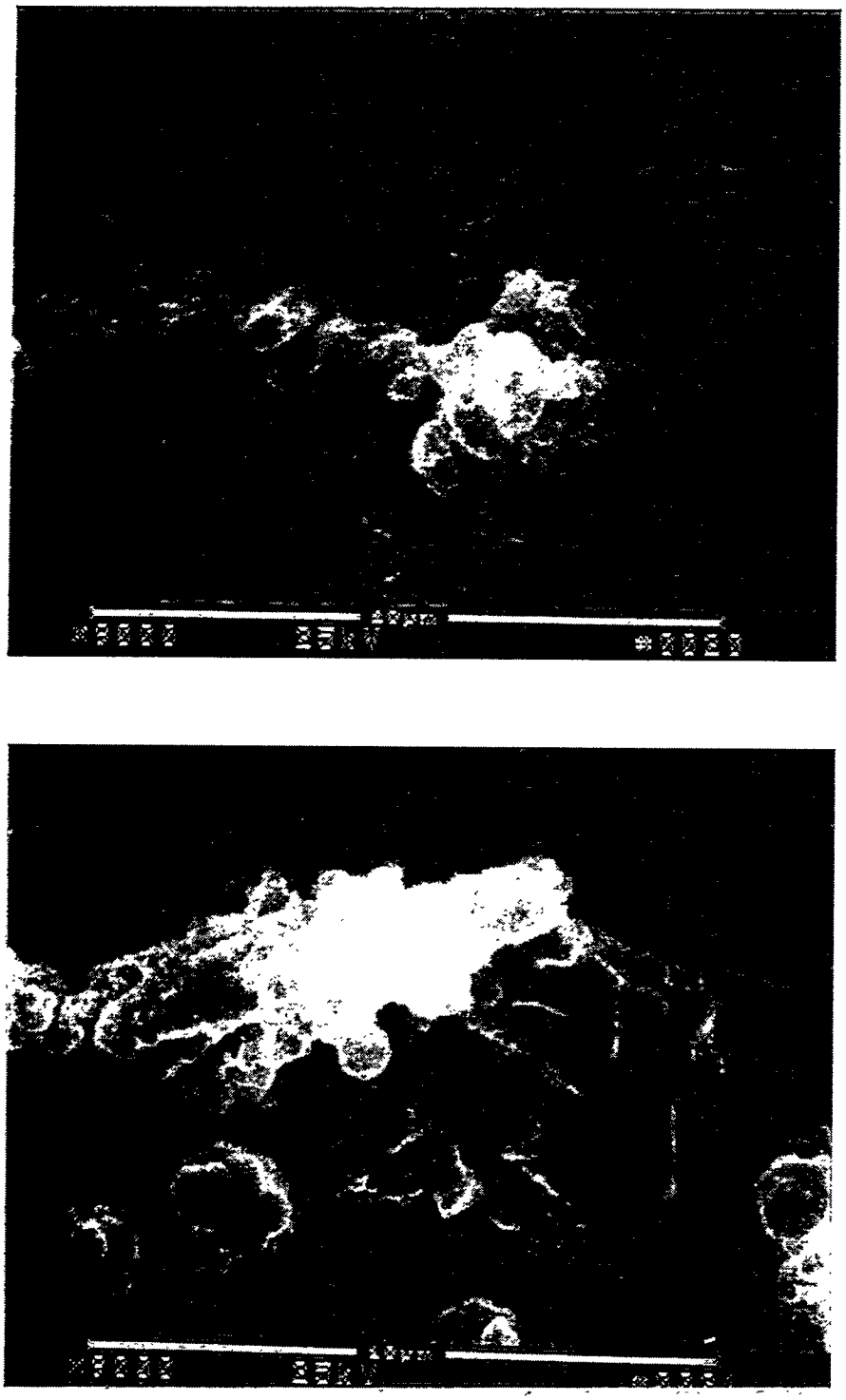

Figure 2j — Morphology Of The Cross-Sectioned Ash Deposit At ~600 μm (Top Micrograph) And ~800 μm Above The Surface Of The Candle Filter (Bottom Micrograph)

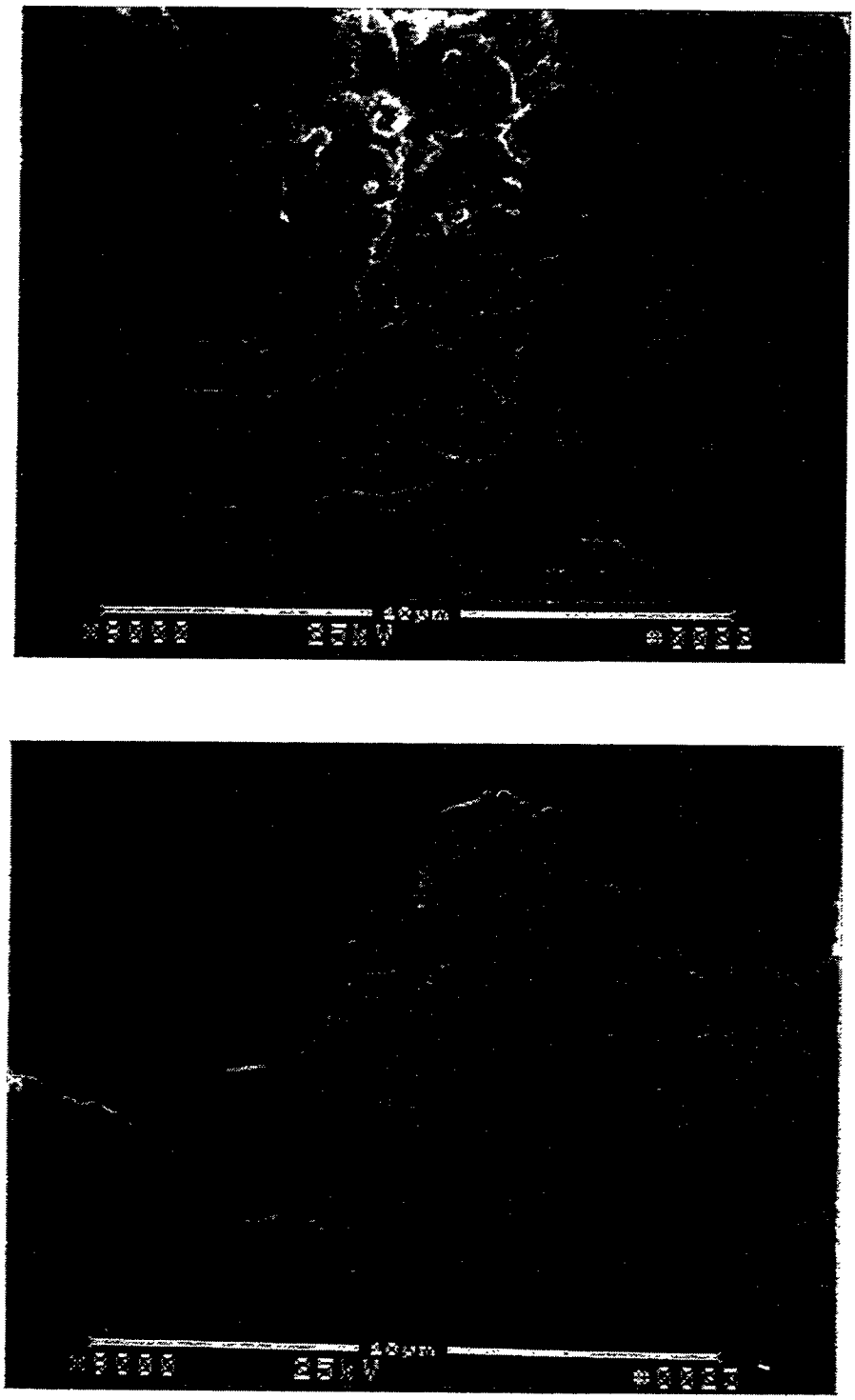

Figure 2k – Morphology Of The Cross-Sectioned Ash Deposit At ~1 mm (Top Micrograph) And ~2 mm Above The Surface Of The Candle Filter (Bottom Micrograph)

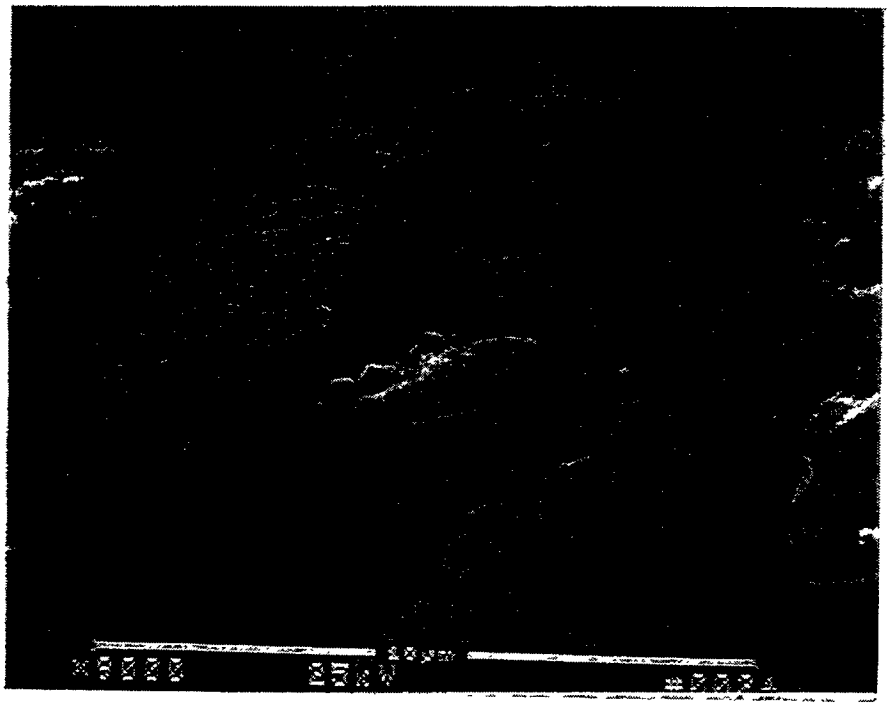

Figure 2l — Morphology Of The Cross-Sectioned Ash Deposit At ~3 mm Above The Surface Of The Candle Filter

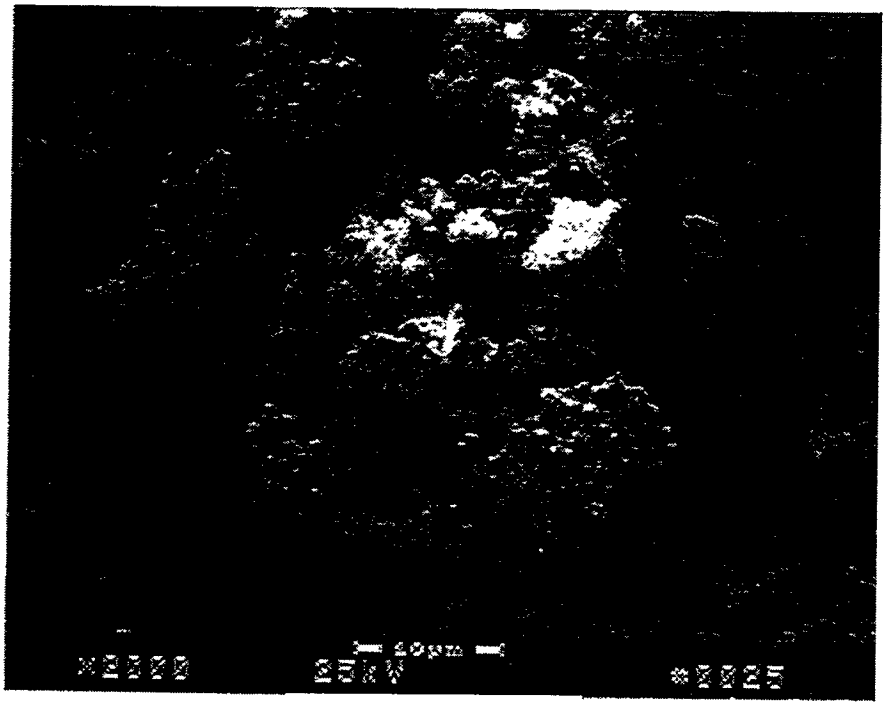

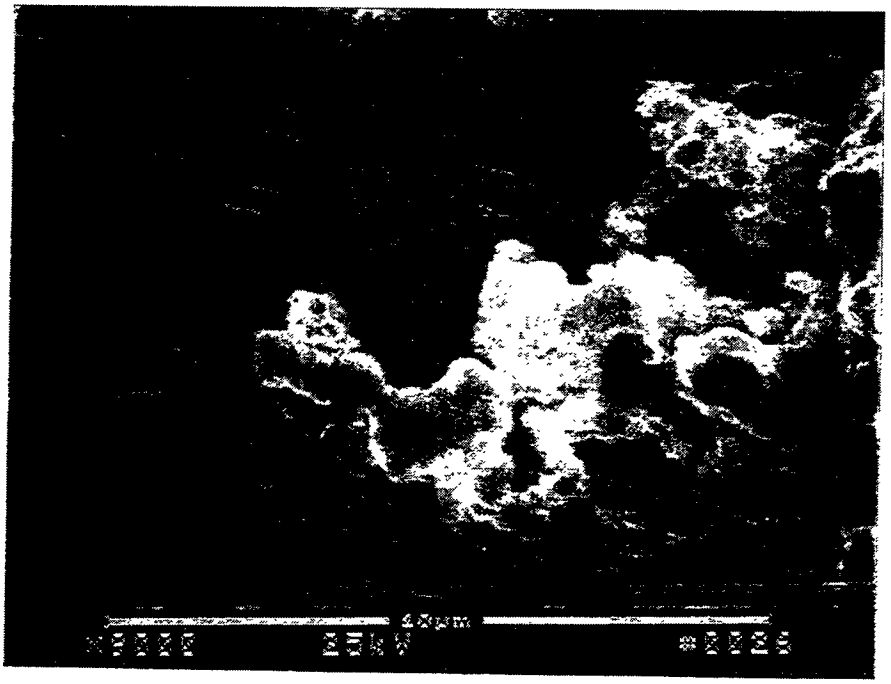

Figure 2m –Morphology Of The Cross-Sectioned Ash Deposit At ~4 mm Above The Surface Of The Candle Filter

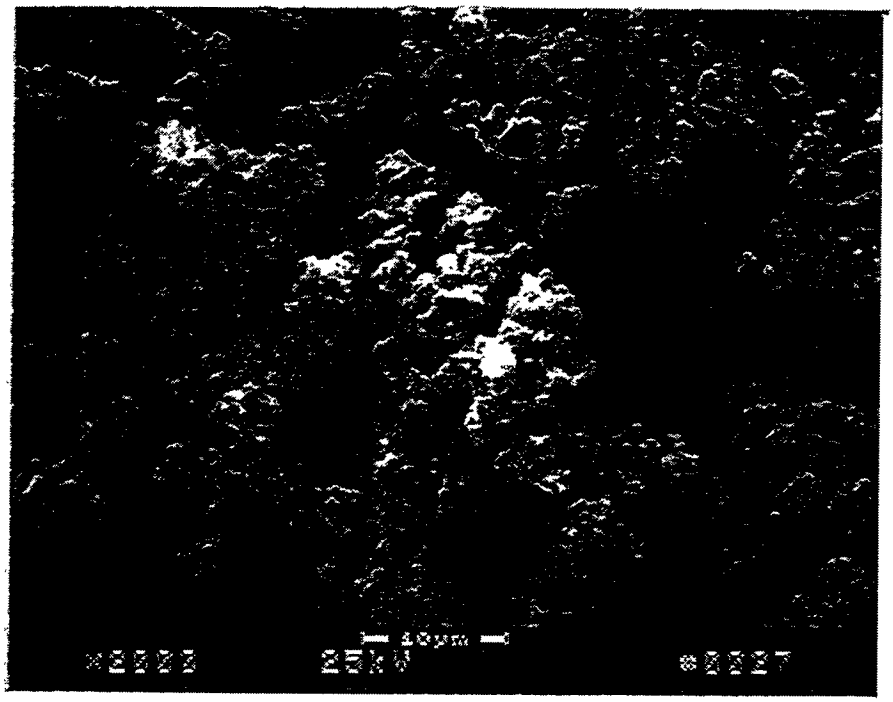

Figure 2n – Morphology Of The Cross-Sectioned Ash Deposit At ~4.5 mm Above The Surface Of The Candle Filter

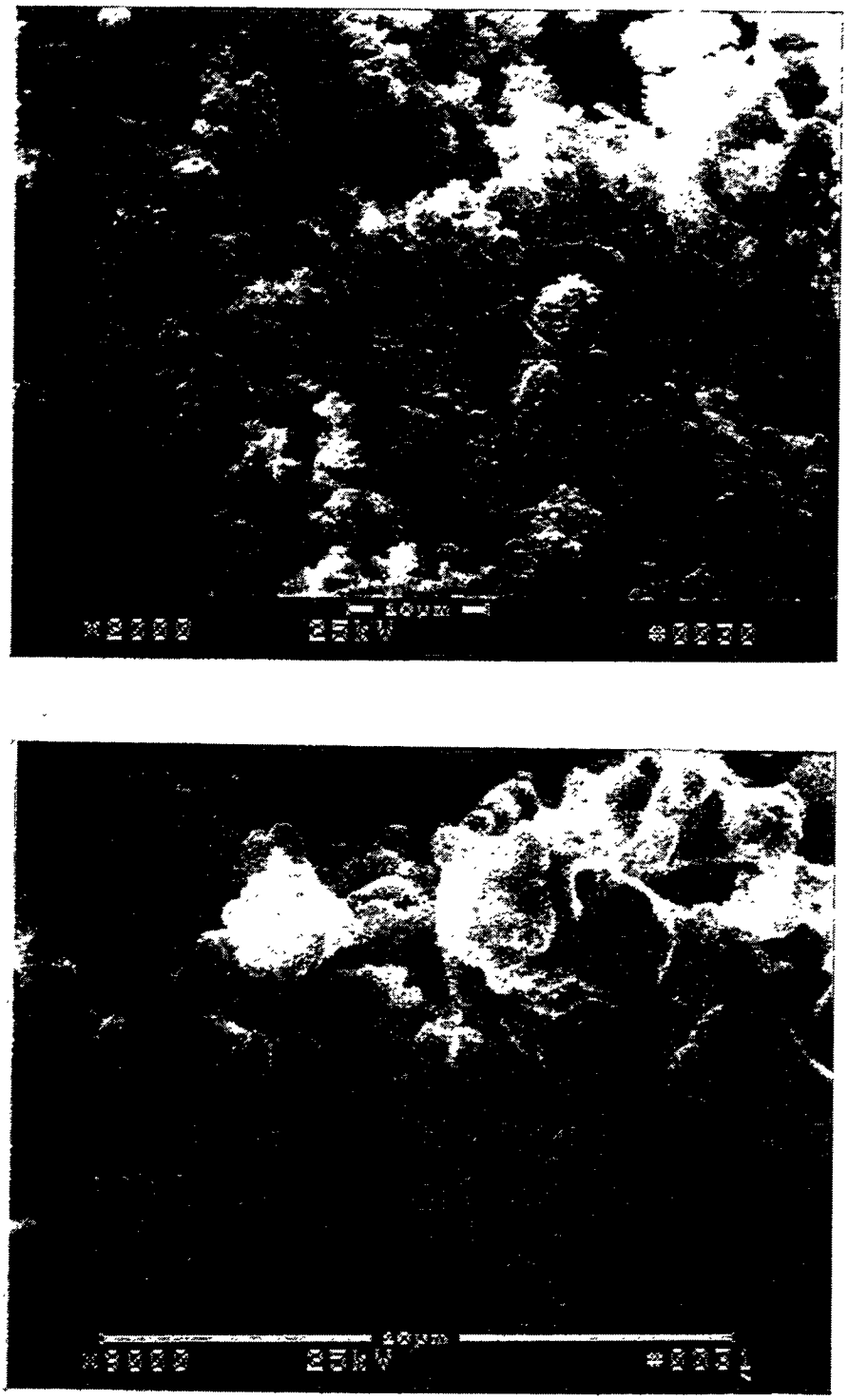

Figure 2o – Morphology Of The Outer Surface Of The Candle Filter Ash Deposit

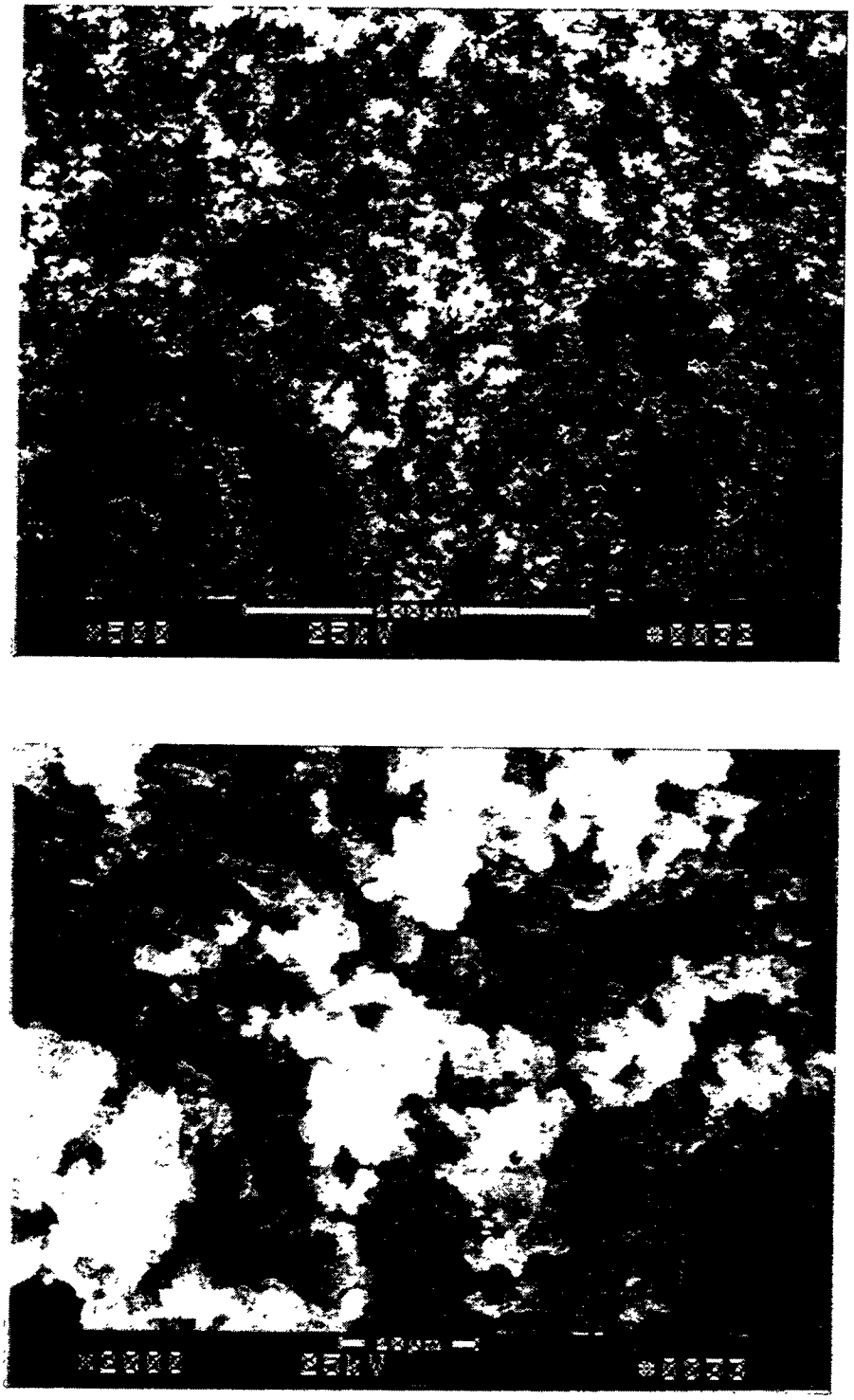

Figure 2p – Morphology Of The Outer Surface Of The Candle Filter Ash Deposit

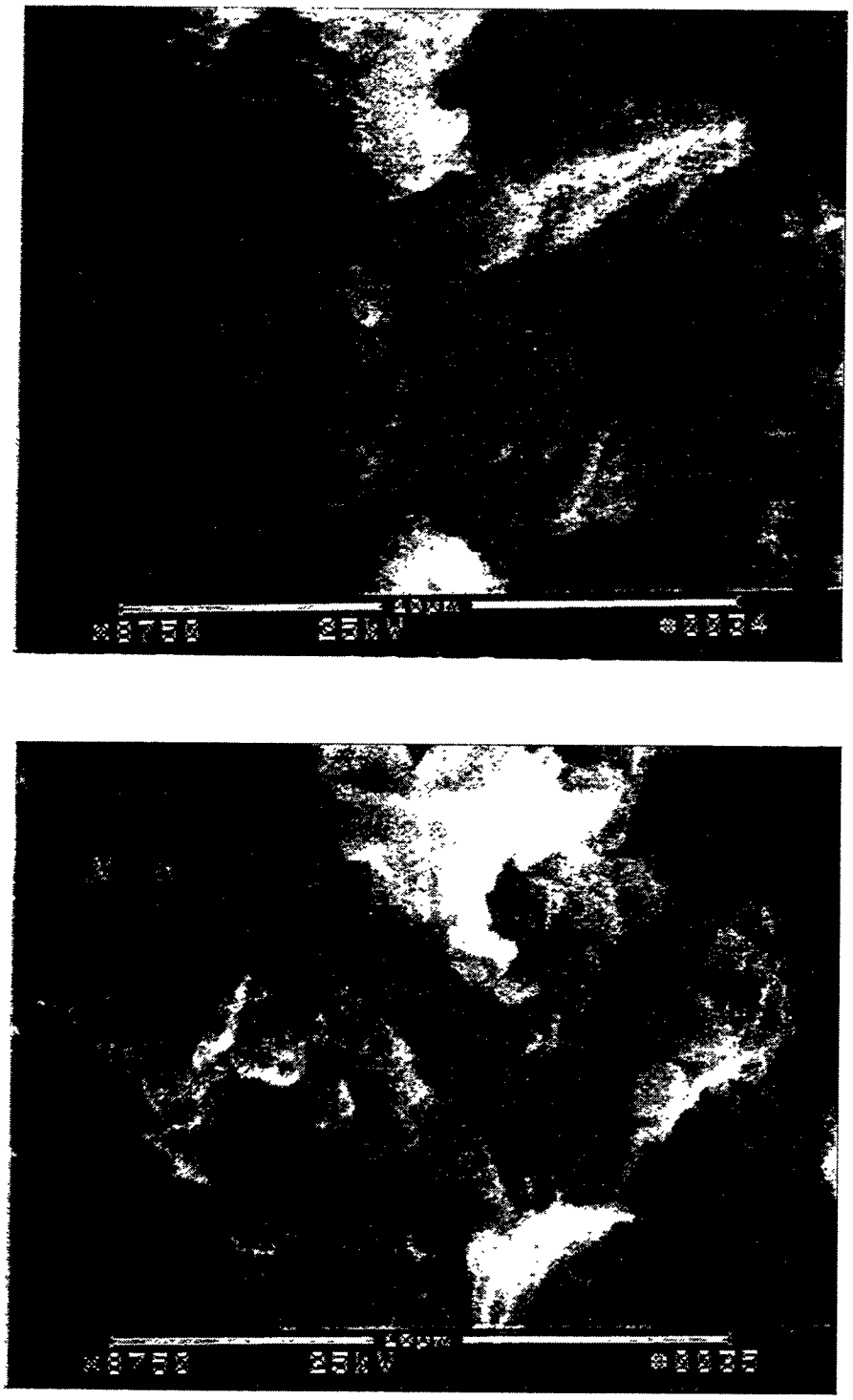

Figure 2q – Higher Magnification Micrographs Illustrating The Morphology Of The Outer Surface Of The Candle Filter Ash Deposit

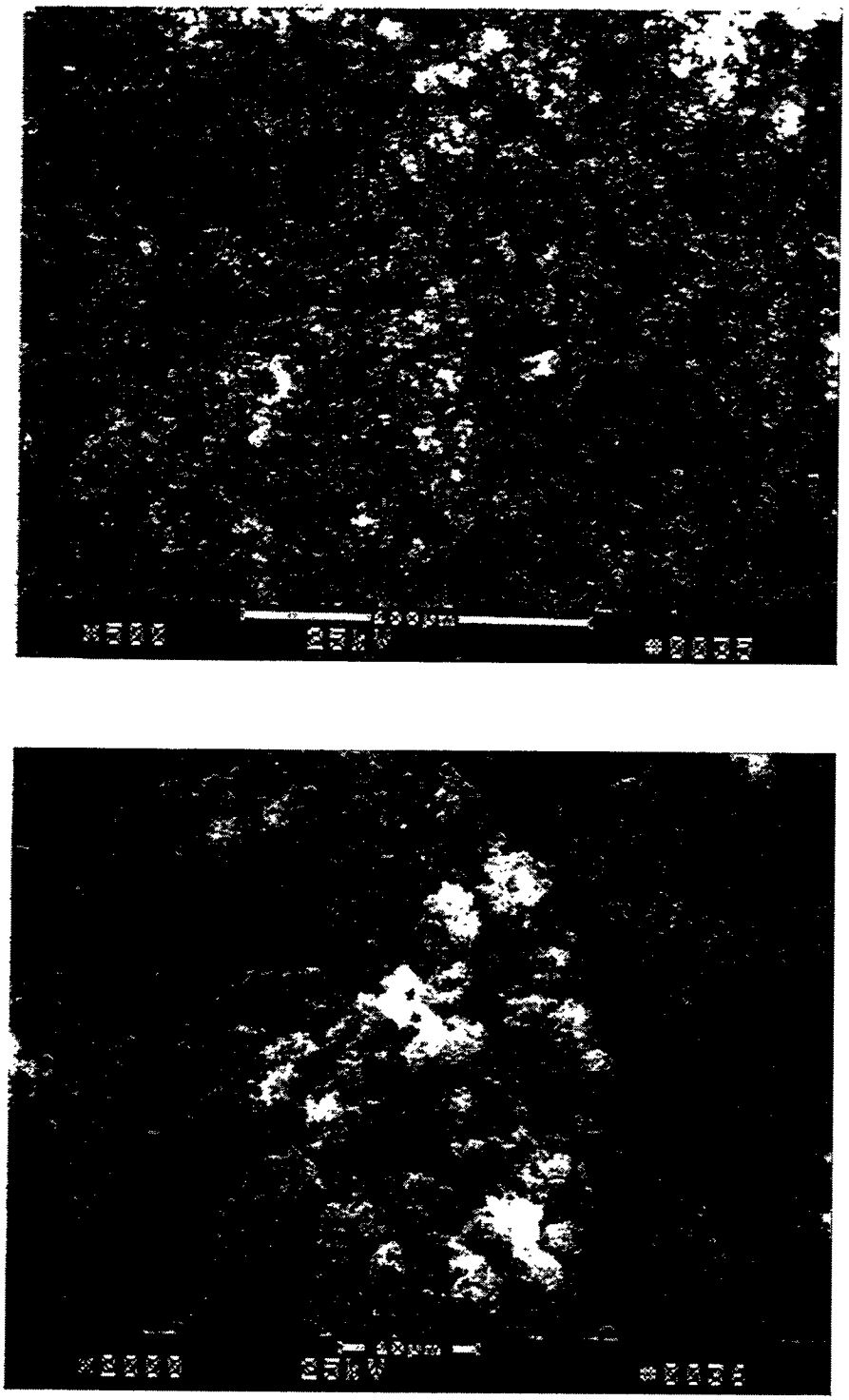

Figure 2r — Morphology Of The Inner Surface Of The Candle Filter Ash Deposit

Figure 2s — Higher Magnification Micrograph Illustrating The Morphology Of The Inner Surface Of The Candle Filter Ash Deposit

TABLE 1
ELEMENTAL COMPOSITION OF THE ASH NODULE WHICH FORMED ALONG THE OUTER SURFACE OF THE SCHUMACHER DIA SCHUMALITH F40 CANDLE FILTER

EDAX Analysis, Atomic Percent
Location Relative To The ID Surface

Element	ID	100 µm	300 µm	500-600 µm	700-800 µm	2 mm	3 mm	4 mm	5 mm	6 mm	OD
O	78.77	78.77	78.6	78.87	78.52	78.6	78.76	78.01	77.97	76.57	79.79
Na	0	0	0.19	0.16	0.21	0.21	0.18	0.01	0.1	0.19	0
Mg	1.47	4.95	2.26	2.4	1.98	2.26	1.95	1.83	1.98	2	2
Al	1.78	1.3	1.69	1.57	1.68	1.56	1.69	1.77	1.81	1.67	1.56
Si	12.07	8.25	11.36	10.39	11.27	10.43	11.35	12.42	11.82	12.83	10.25
S	2.83	3.26	3.15	3.75	3.74	3.79	3.4	3.42	3.57	3.38	3.61
K	0.36	0.22	0.31	0.29	0.35	0.47	0.32	0.3	0.33	0.45	0.32
Ca	1.4	2.67	1.72	1.82	1.63	1.96	1.63	1.61	1.66	1.87	1.83
Ti	0.12	0.05	0.1	0.07	0.11	0.11	0.11	0.04	0.08	0.03	0.06
Fe	1.22	0.53	0.64	0.69	0.5	0.6	0.61	0.59	0.68	1.01	0.57

At ~400 μm, ~450 μm, and ~500 μm above the surface of the filter, numerous submicron and micron fines were evident within the highly porous, interconnected, agglomerated ash network. As previously described, the fines characteristically had rounded surface features (Figures 2h and 2i).

At ~600 μm and ~800 μm above the surface of the filter element, extensive formations of the relatively large (i.e., 3-7 μm), amorphous or sintered fines were evident. Frequently these particles appeared to serve as substrates for "collection" and adherence of the submicron and micron agglomerated, interconnected network of ash fines (Figure 2j).

Moving to 1 mm and 2 mm above the surface of the filter, larger, amorphous or sintered fines were frequently detected. Limited collection of the submicron and micron agglomerated ash fines was evident in this area of the deposit (Figure 2k).

At 3 mm from the filter surface, flat, "plate-like", larger ash/sorbent fines were evident within the deposit (i.e., 1 μm thick x 5-10 μm long; Figure 2l). Once again the sintered, micron and submicron, agglomerated network of fines was present in the deposit which formed at ~4 mm and ~4.5 mm above the surface of the filter element (Figure 2m and 2n).

Figures 2o, 2p, and 2q illustrate the morphology of the fines which resulted along the outer surface of the ash nodule, This material was considered to be the final material that deposited and remained along the surface of the deposit at the conclusion of Test Segment #5. The ash/sorbent fines which resulted along the outer surface of the deposit formed a relatively open, highly porous structure, containing the sintered, agglomerated network of submicron and micron fines.

Additional micrographs are provided in Figure 2r and 2s which illustrate the morphology of the ash/sorbent material which collected directly along the surface of the candle filter. When the fines shown in Figure 2r and 2s are compared with the fines shown in Figures 2o, 2p, and 2q, very little difference in the morphology of the fines is evident (i.e., ID or early deposition vs OD or later deposition, respectively). We cannot state with complete confidence that the material deposited directly along the candle filter surface resulted during initiation of testing in Test Segment #5.[b] Pulse cleaning of the filter may have released a significant portion of the ash matrix in the continually growing nodule. What can be stated is that although slight variation in the morphology of the fines was evident within the ~6 mm ash nodule, the deposit clearly appeared to be uniform and homogeneous within the various cross-sectioned locations that were characterized. This supports the EDAX analyses presented in Table 1.

---

[b] The surveillance candle was wash after each test segment, prior to reinstallation into the W-APF array. In this manner, ash was removed from the surface of the candle filter. Fines which remained embedded within the membrane from previous test segments, may not have been completely removed during the cleaning of the filter element.

FILTER MATRIX CHARACTERIZATION

A section of the porous ceramic filter matrix was removed from the 5855 hour PFBC-exposed Schumacher Dia Schumalith F40 candle filter (i.e., S228/321B, A/T-16), The ash cake deposit was removed from the filter surface, and the sample was prepared for SEM/EDAX characterization via the application of a carbon coating.

A shown in Figure 3a, the fibrous aluminosilicate outer membrane of the candle filter appeared to remain intact after 5855 hours of PFBC operation. Residual fines were present along the fibrous membrane surface. Figure 3b provides higher magnification SEMs which illustrate the affinity of the submicron and micron agglomerated fines to adhere to the aluminosilicate membrane fibers. Fines were embedded between the membrane fibers, along the outer surface of the filter element (Figure 3c). EDAX analysis of the fiber shown in Photo 4, Figure 3b, indicated the presence of 67.67% O, 27.76% Al, and 4.57% Si (i.e., atomic percent basis). The fines shown in Photo 6, Figure 3c, were identified by EDAX to contain 57.77% O, 16.89% C, 14.15% Mg, 8.68% Si, 1.27% Al, 0.42% Fe, 0.41% S, 0.32% Ca, and 0.10% K.[c]

Extensive interconnectivity was evident in the submicron and micron agglomerated network of fines which collected along the outer surface of the filter element. The high interconnectivity and relatively open porous nature of the collected ash was readily evident at alternate locations along the surface of the candle filter (Figure 3d). EDAX analysis of the fines shown in Photo 8, Figure 3d, identified the presence of 53.49% O, 20.49% C, 9.12% Mg, 9.02% Si, 4.11% Al, 1.26% S, 1.24% Ca, 0.93% Fe, and 0.33% K.

Below the fibrous outer membrane, the highly open, porous nature of the clay bonded silicon carbide Schumacher Dia Schumalith F40 filter matrix was evident after 5855 hours of PFBC operation at AEP (Figure 3e). Fines were infrequently observed to adhere to the surface of the silicon carbide grains at localized areas below the membrane surface. What was readily evident was that the binder phase of the 5855 hour PFBC-exposed filter matrix contained extensive crack formations after sample preparation. Often sections of the binder were removed from the underlying or support grain.

Although the integrity of the ligament or bond posts within the 5855 hour PFBC-exposed Schumacher Dia Schumalith F40 candle filter were retained, complete crystallization of the binder which coated the silicon carbide grains was evident (Figure 3f). Below the binder coating, the surface of the silicon carbide grains showed evidence of hole formations and/or pitting (Figure 3g). EDAX analysis of Area 1, Photo 12, Figure 3g, identified the presence of silicon, oxygen, and

---

[c] Minor contribution of carbon may be expected from the sample preparation, however, the majority of the 16.89% C was expected to result directly from the ash/sorbent composition.

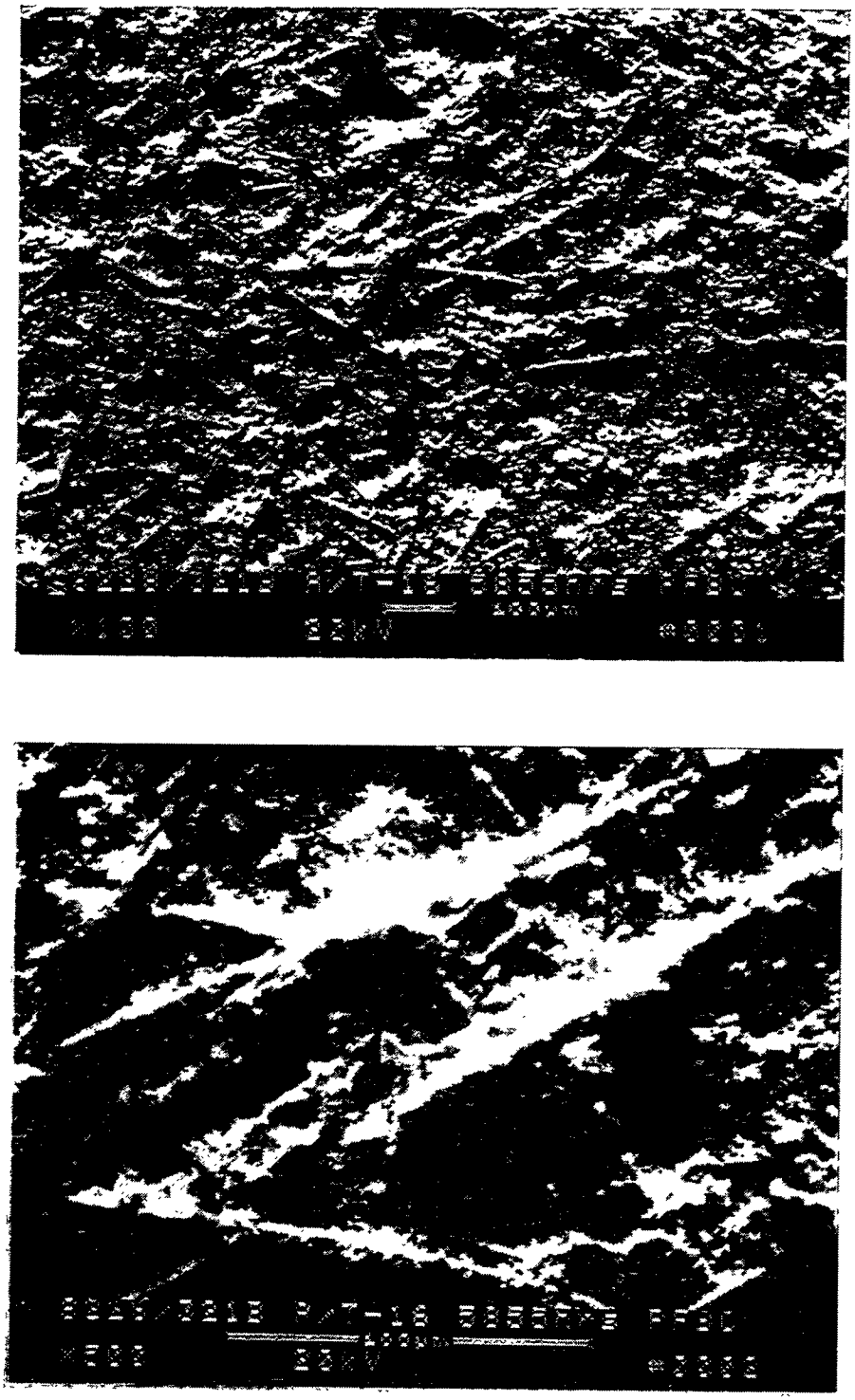

Figure 3a – Outer Surface Of The Schumacher Dia Schumalith F40 Candle Filter After 5855 Hours Of Exposure In The PFBC Environment At AEP

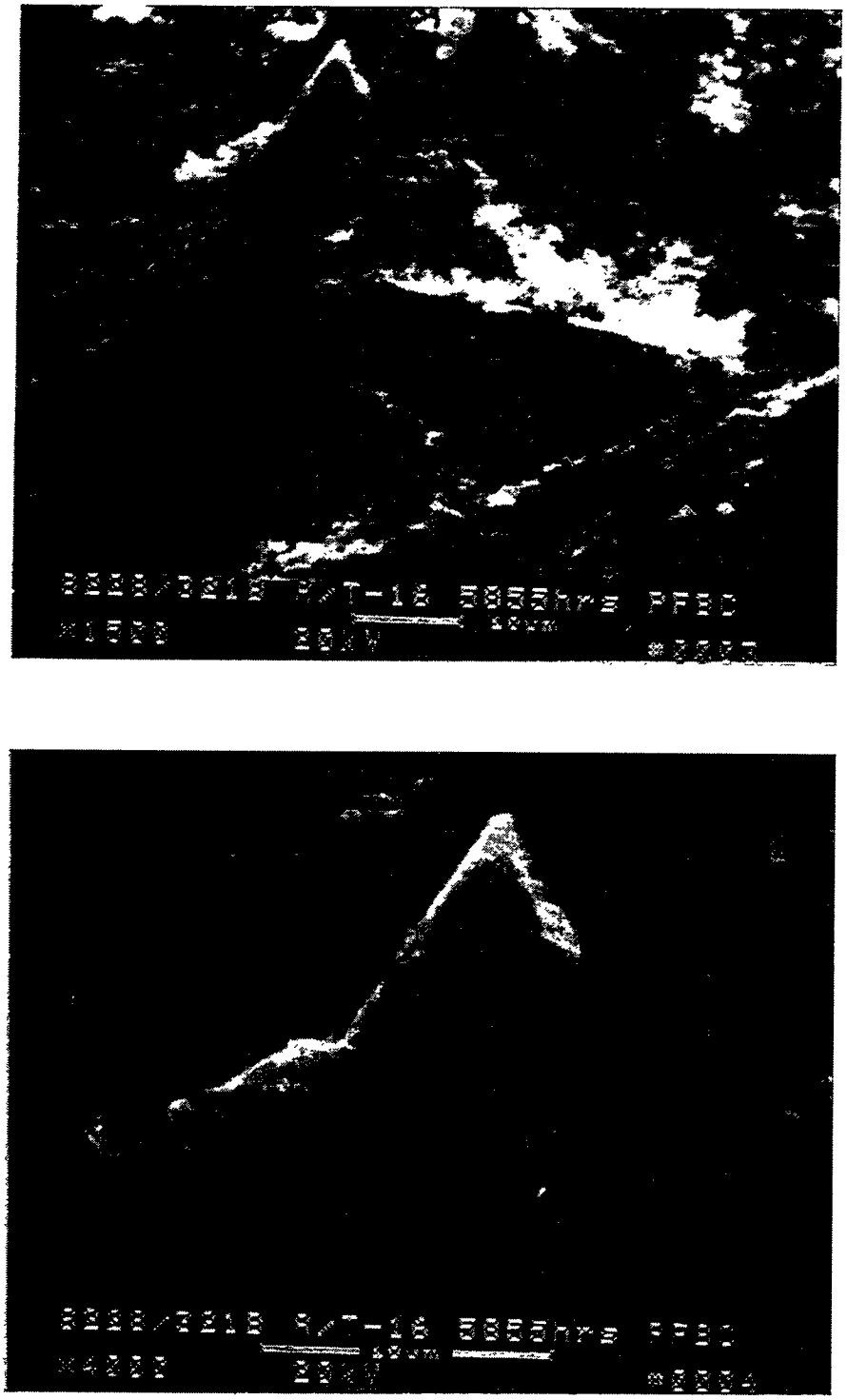

Figure 3b – Higher Magnification Micrographs Illustrating The Morphology Of The Fibrous Outer Membrane Of The 5855 Hour PFBC-Exposed Schumacher Dia Schumalith F40 Candle Filter

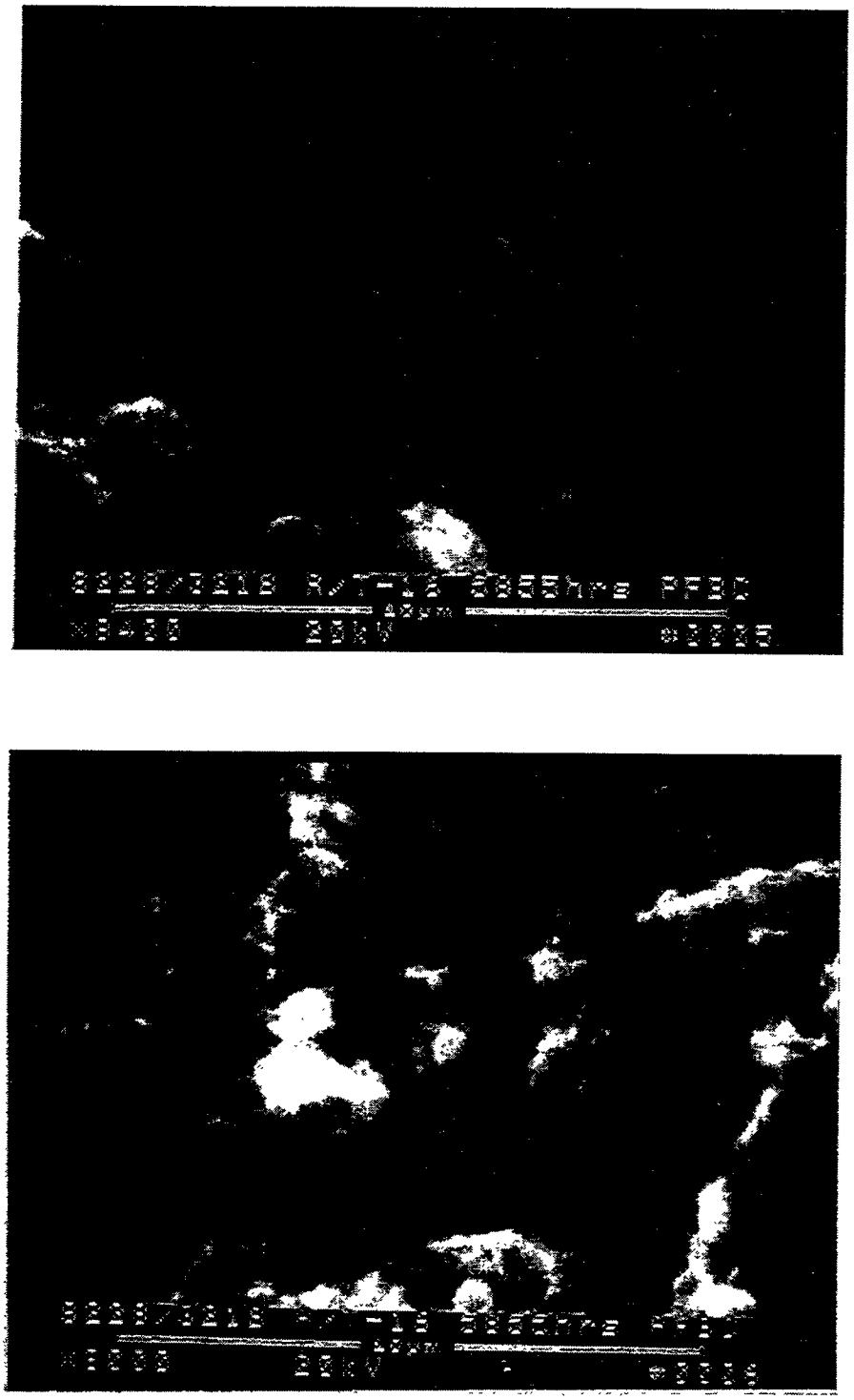

Figure 3c – Morphology Of The Ash Fines That Remained Along The Membrane Surface Of The 5855 Hour PFBC-Exposed Schumacher Dia Schumalith F40 Candle Filter

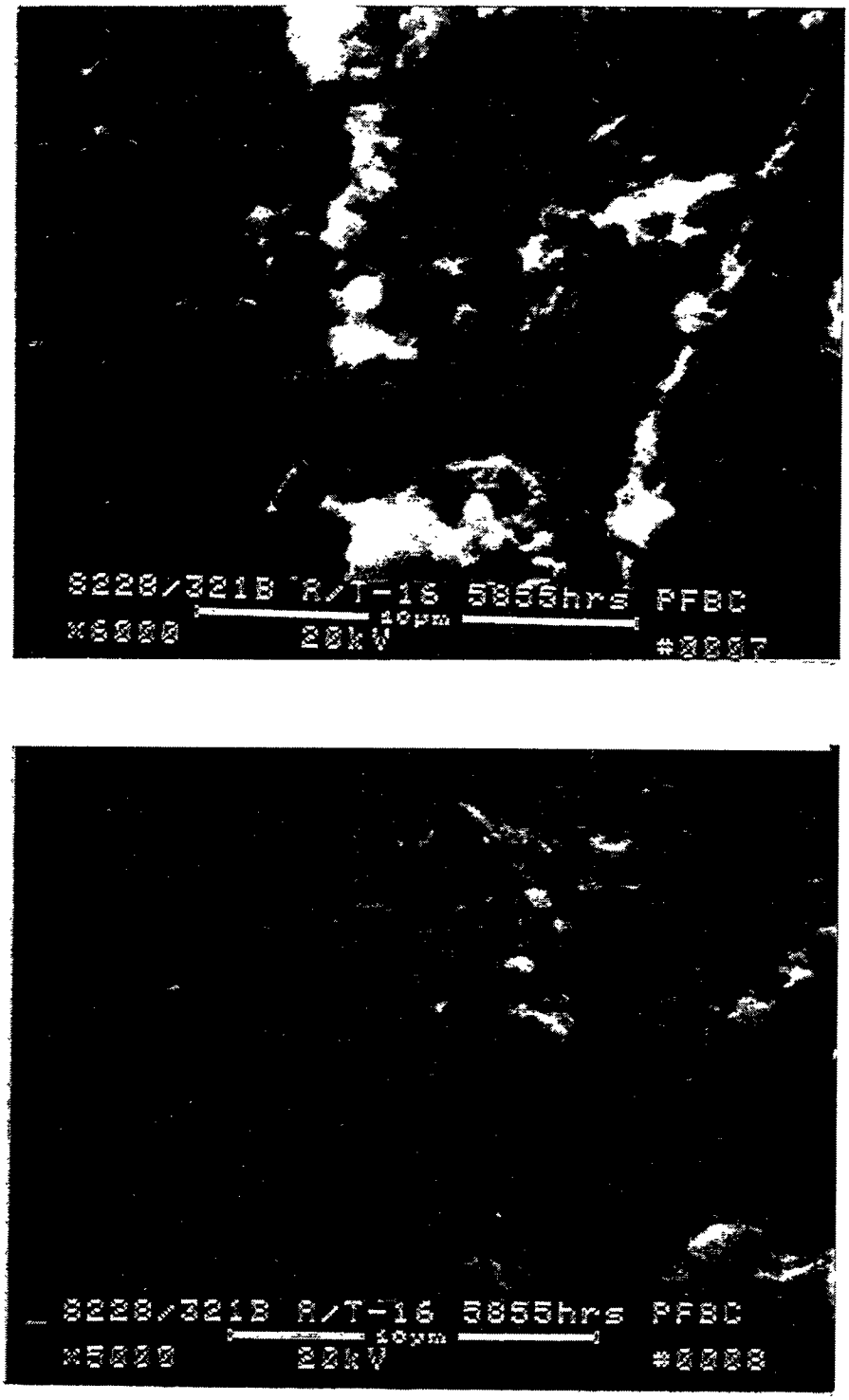

Figure 3d – Morphology Of The Ash Fines That Remained Along The Membrane Surface Of The 5855 Hour PFBC-Exposed Schumacher Dia Schumalith F40 Candle Filter

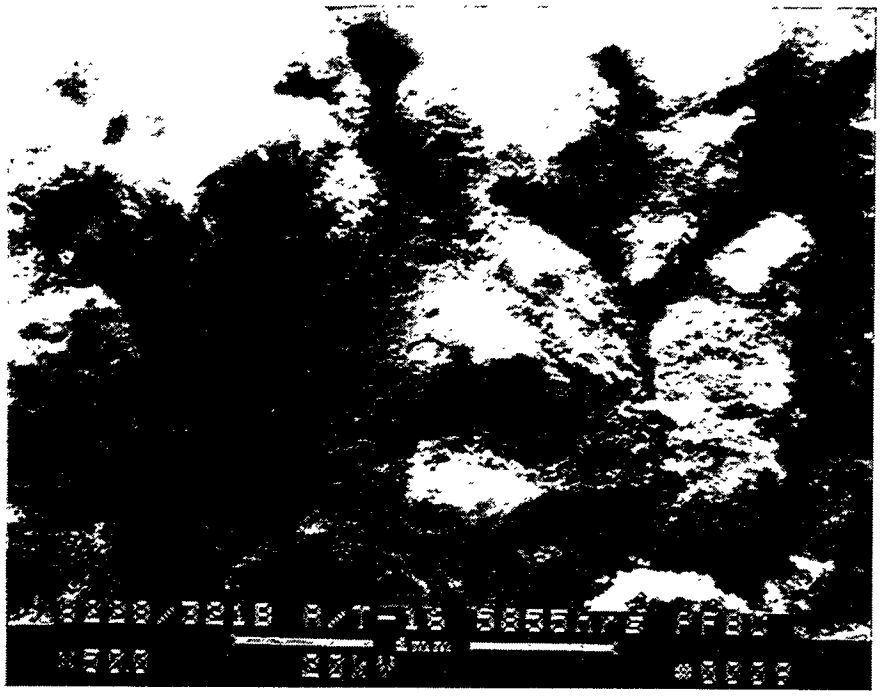

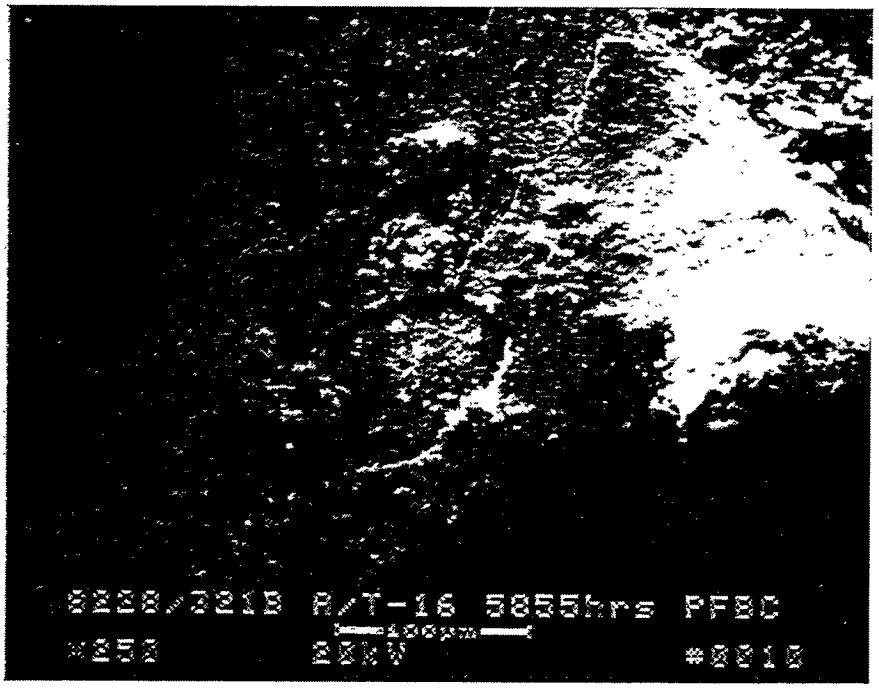

Figure 3e – Morphology Of The Binder Coated Silicon Carbide Grains Below The Fibrous Membrane Layer Of The Schumacher Dia Schumalith F40 Candle Filter That Experienced 5855 Hours Of Operation In The PFBC Environment At AEP

(a)

(b)

(c)

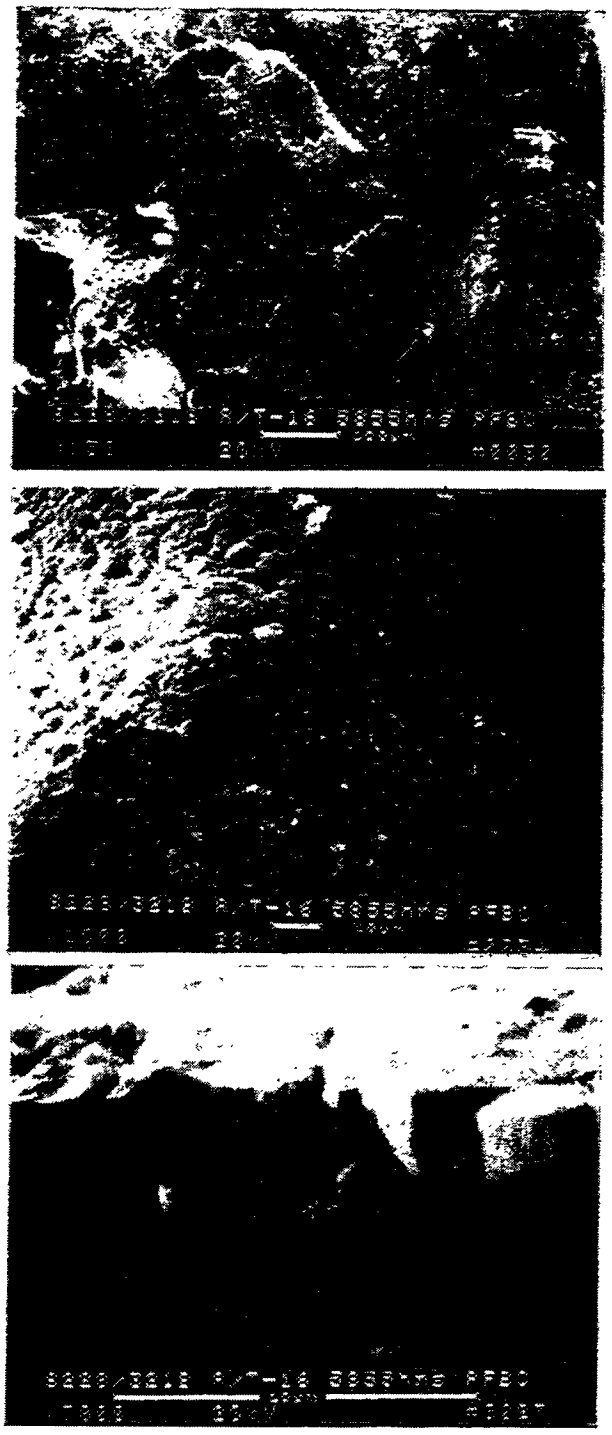

Figure 3f — Micrographs Illustrating Crystallization Of The Binder Phase In The Schumacher Dia Schumalith F40 Filter Matrix After 5855 Hours Of Operation In The W-APF At AEP. (a) Support Matrix; (b) Binder Coated Grains; (c) Cross-Sectioned Binder Phase

Figure 3g – Micrographs Illustrating The Crystallized Binder And Mottled Silicon Carbide Grain Surface Of The Schumacher Dia Schumalith F40 Candle Filter After 5855 Hours Of PFBC Operation At AEP

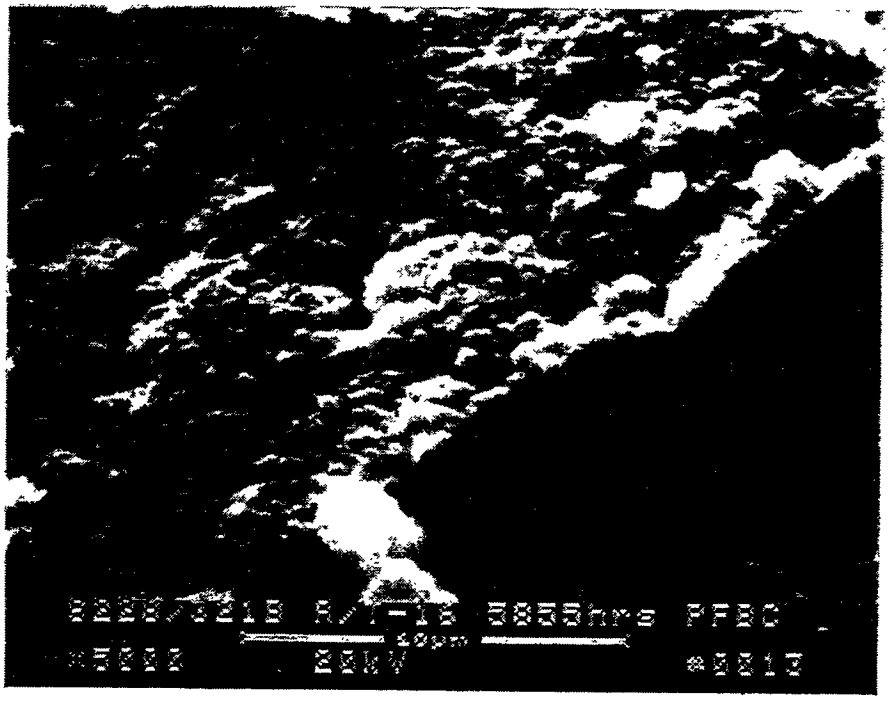

Figure 3h – Crystallized Binder Coating Of The 58955 Hours PFBC-Exposed Schumacher Dia Schumalith F40 Candle Filter Matrix

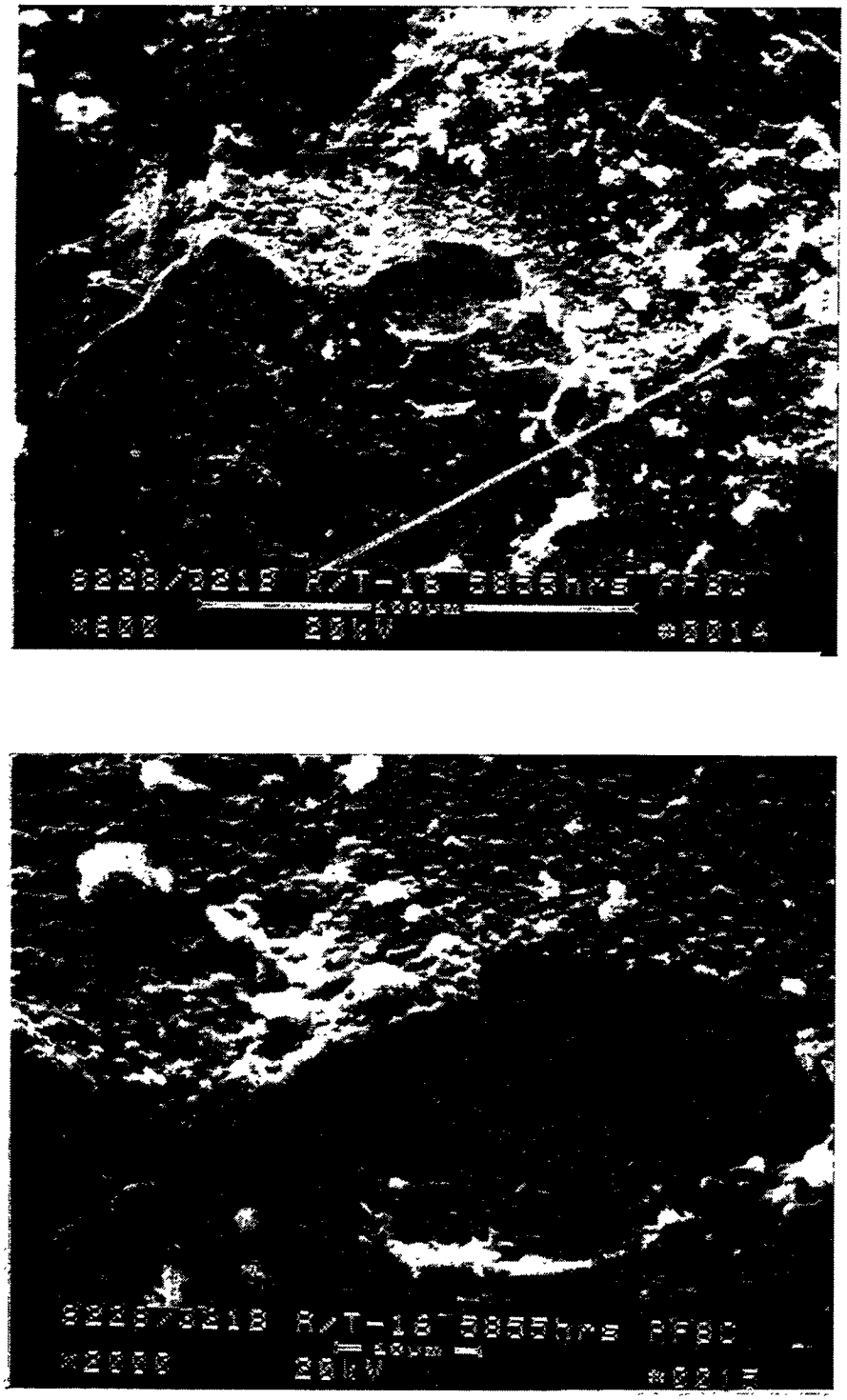

Figure 3i — Crystallized Binder And Exposed Silicon Carbide Grain Surface

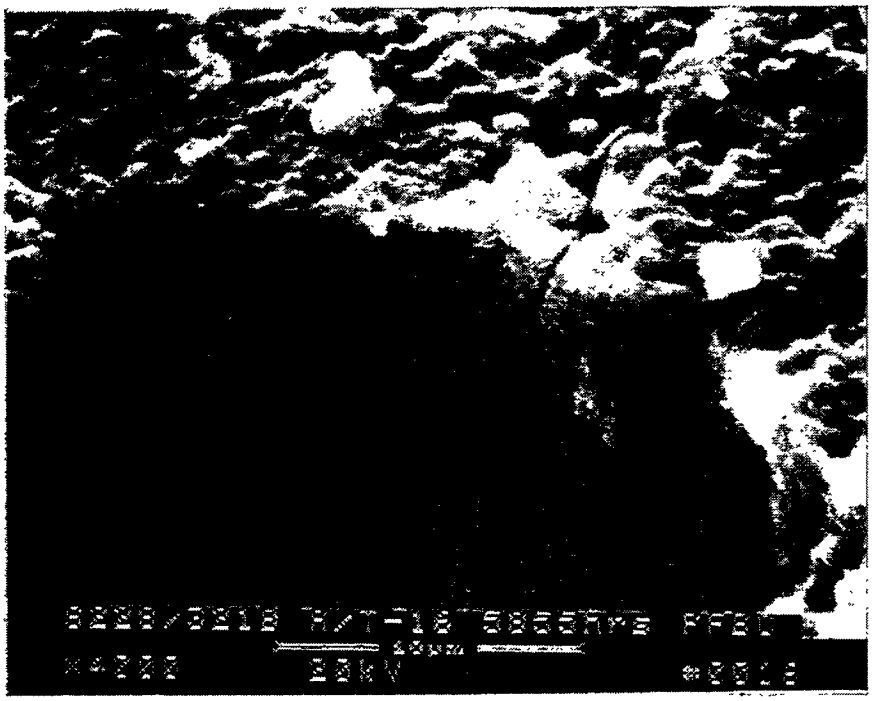

Figure 3j— Higher Magnification Micrograph Illustrating The Schumacher Dia Schumalith F40 Binder/Grain Interface After 5855 Hours Of PFBC Operation At AEP

carbon along the surface of the "pitted" silicon carbide grain (i.e., absence of aluminum from the binder). Alternately the ~5 μm crystallized binder phase coating which encapsulated the silicon carbide grain was identified by EDAX to contain silicon, aluminum, and oxygen (Photo 13, Figure 3h).

Additional micrographs are shown in Figures 3i and 3j, which illustrate the crystallized nature of the residual binder coating which remained along the surface of the silicon carbide grains in the 5855 hour PFBC-exposed Schumacher Dia Schumalith F40 filter matrix. Secondary reactions at the binder/grain interface may have occurred (i.e., oxidation of the surface of the silicon carbide grain, promoting the formation of SiO_x or SiO_2, which adhered to, and/or reacted with the crystallized binder coating). The micrograph shown in Photo 16, Figure 3j, illustrates the crack formations which readily occurred during sample preparation not only through/along the binder coating, but also at the "reacted" grain/binder interface.

A section of the filter matrix which was cut with a wet diamond grinding wheel was further subjected to SEM/EDAX analyses. As shown in Figure 4, fines were present within the matrix, penetrating to depths of ~5-7 mm from the ID surface into the 15 mm Schumacher Dia Schumalith F40 filter wall.

Figure 5a provides a series of SEMs which detail the microstructure of the 5855 hour PFBC-exposed Schumacher Dia Schumalith F40 filter matrix. After drying, carbon was used to coat the sample. Frequently dendritic formations were evident along the surface of the silicon carbide grains that were located near the OD surface of the filter element (Figures 5a and 5b). The dendrites appeared to grow from a central area, and extend outwardly, attaching themselves to ash/sorbent fines and/or the silicon carbide grains. EDAX analyses of the crystalline dendritic formation shown in Photo 5, Figure 5c, indicated the presence of 79.39% O, 10.55% S, 7.77% Ca, 0.73% Na, 0.51% Si, 0.48% Mg, 0.29% Al, and 0.28% K (i.e., atomic percent basis; primarily $CaSO_4$-enriched).

At the point of attachment, the dendritic matrix was identified by EDAX analysis to contain 80.16% O, 8.21% S, 5.74% Ca, 2.17% Si, 2.02% Al, 0.51% Na, 0.50% Fe, 0.45% Mg, and 0.24% K (Area 1, Photo 6, Figure 5d). The mottled surface near the calcium sulfate-enriched dendritic formation (Photo 7, Figure 5d) was identified by EDAX to contain 78.60% O, 12.55% Si, 3.93% Al, 2.00% Mg, 1.56% S, 0.58% Fe, 0.28% Na, 0.20% Ca, 0.19% K, and 0.10% Ti.

When viewed directly along the OD surface of the 5855 hour PFBC-exposed Schumacher Dia Schumalith F40 filter element, the topography of the matrix clearly showed the presence of the silicon carbide grains and the calcium sulfate-enriched dendritic formations (Figure 5e). Porosity, as well as the as-manufactured aluminosilicate fibrous membrane were not readily apparent in this area of the filter matrix. Figure 5f provides a higher magnification montage of the OD surface illustrating the residual binder coating along the silicon carbide grains, as well as the calcium

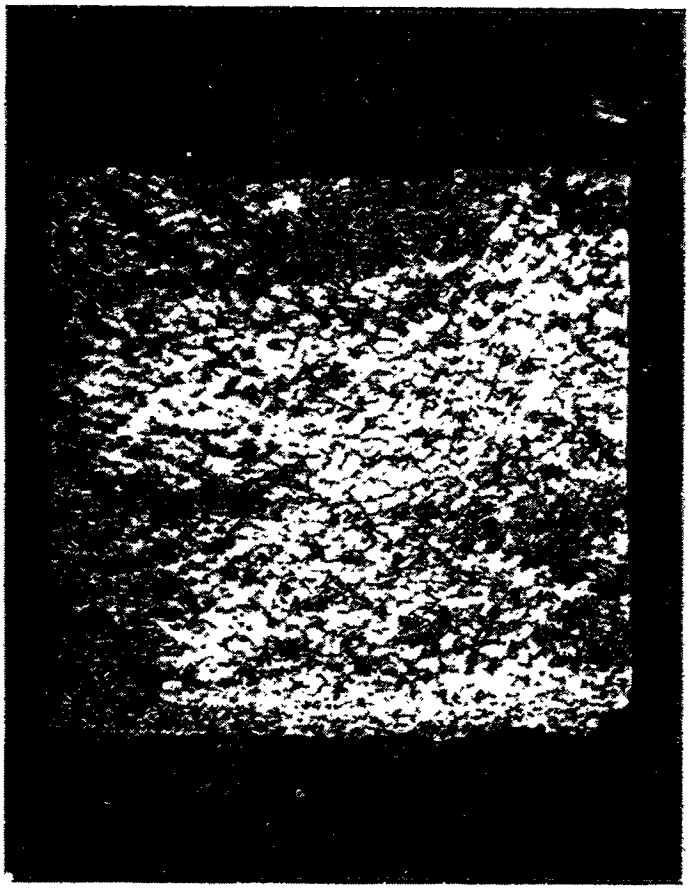

ID OD

Figure 4 – Cross-Sectioned Wall Of The 5855 Hour PFBC-Exposed Schumacher Dia Schumalith F40 Filter Matrix

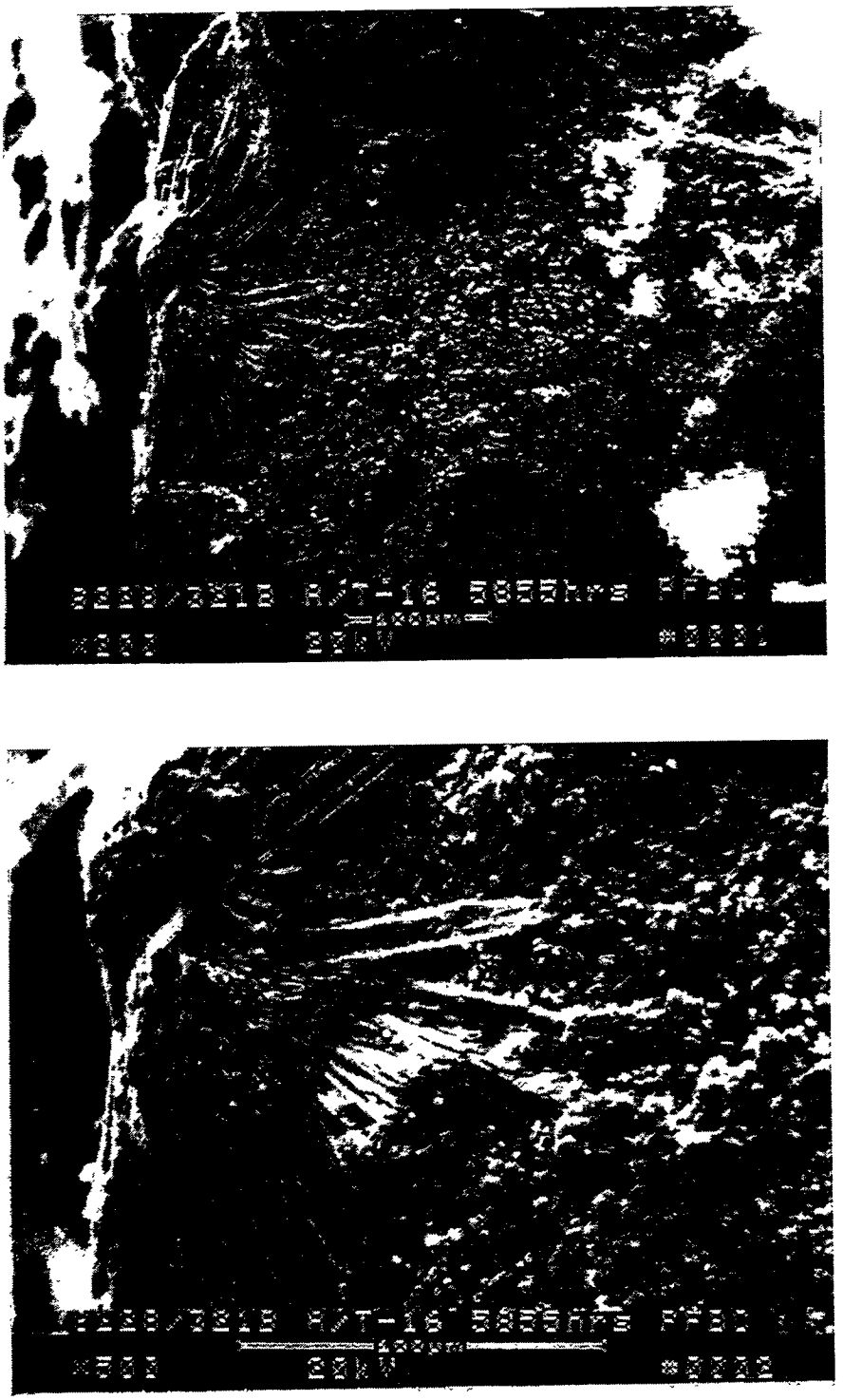

Figure 5a — Calcium Sulfate-Enriched Dendritic Formations That Resulted Along The 5855 Hour PFBC-Exposed Schumacher Dia Schumalith F40 Filter Matrix After Wet Cutting

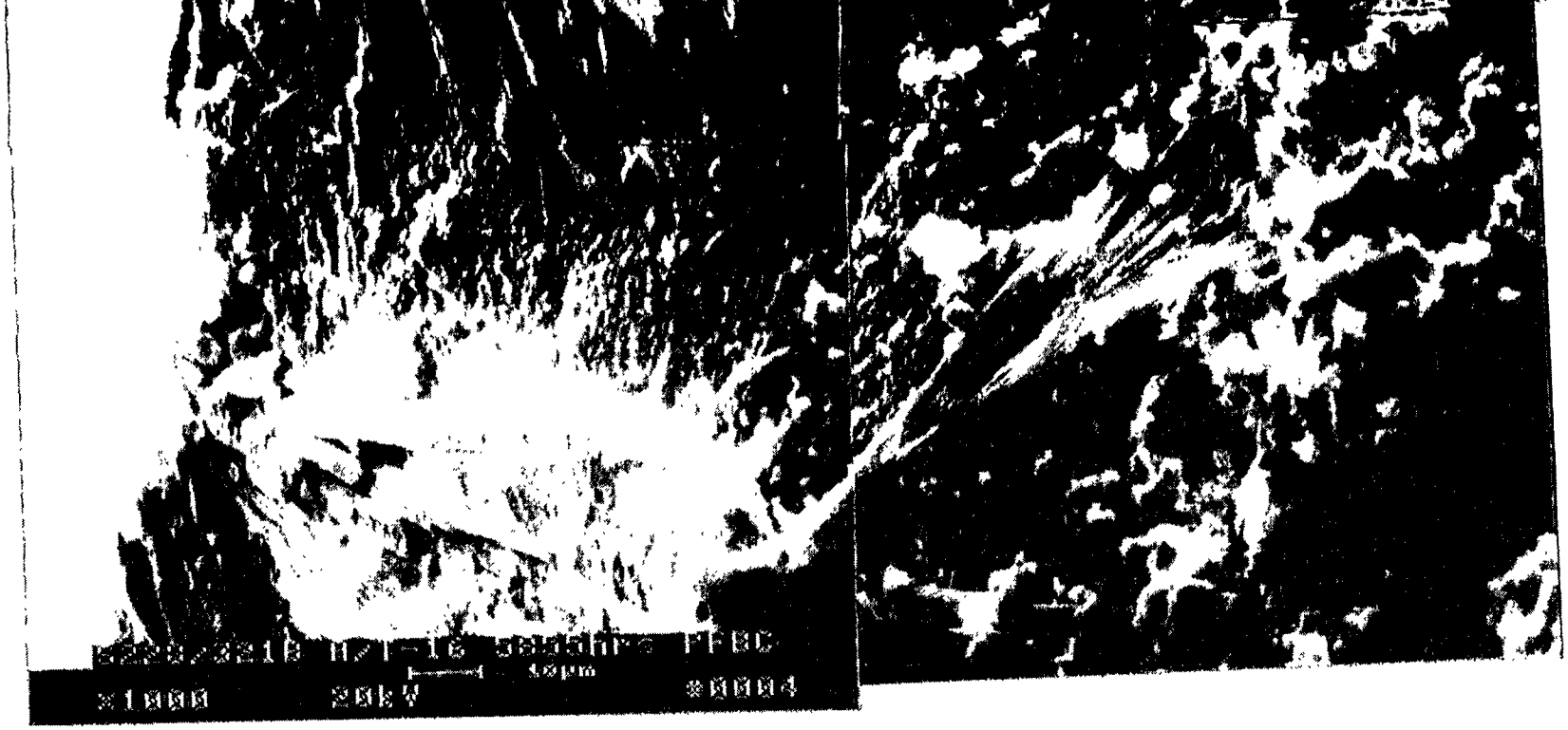

Figure 5b – Higher Magnification Montage Of The Calcium Sulfate-Enriched Dendritic Formations

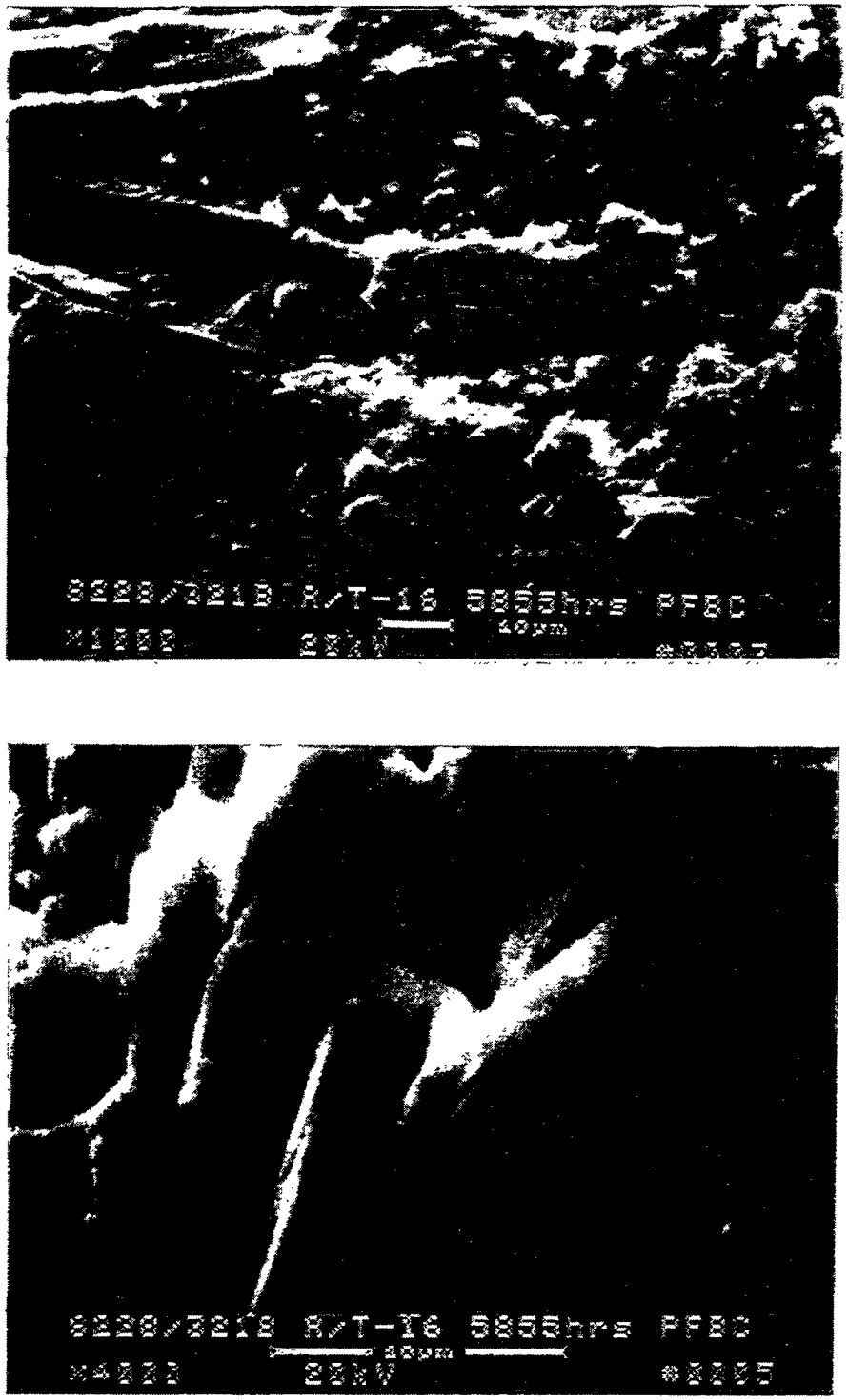

Figure 5c – Micrographs Illustrating The Attachment Of Dendritic Formations Along The Surface Of The 5855 Hour PFBC-Exposed Schumacher Dia Schumalith F40 Filter Matrix (Top Micrograph), As Well As Crystalline Formation At The Center Of The Dendrite (Bottom Micrograph)

RM-34850

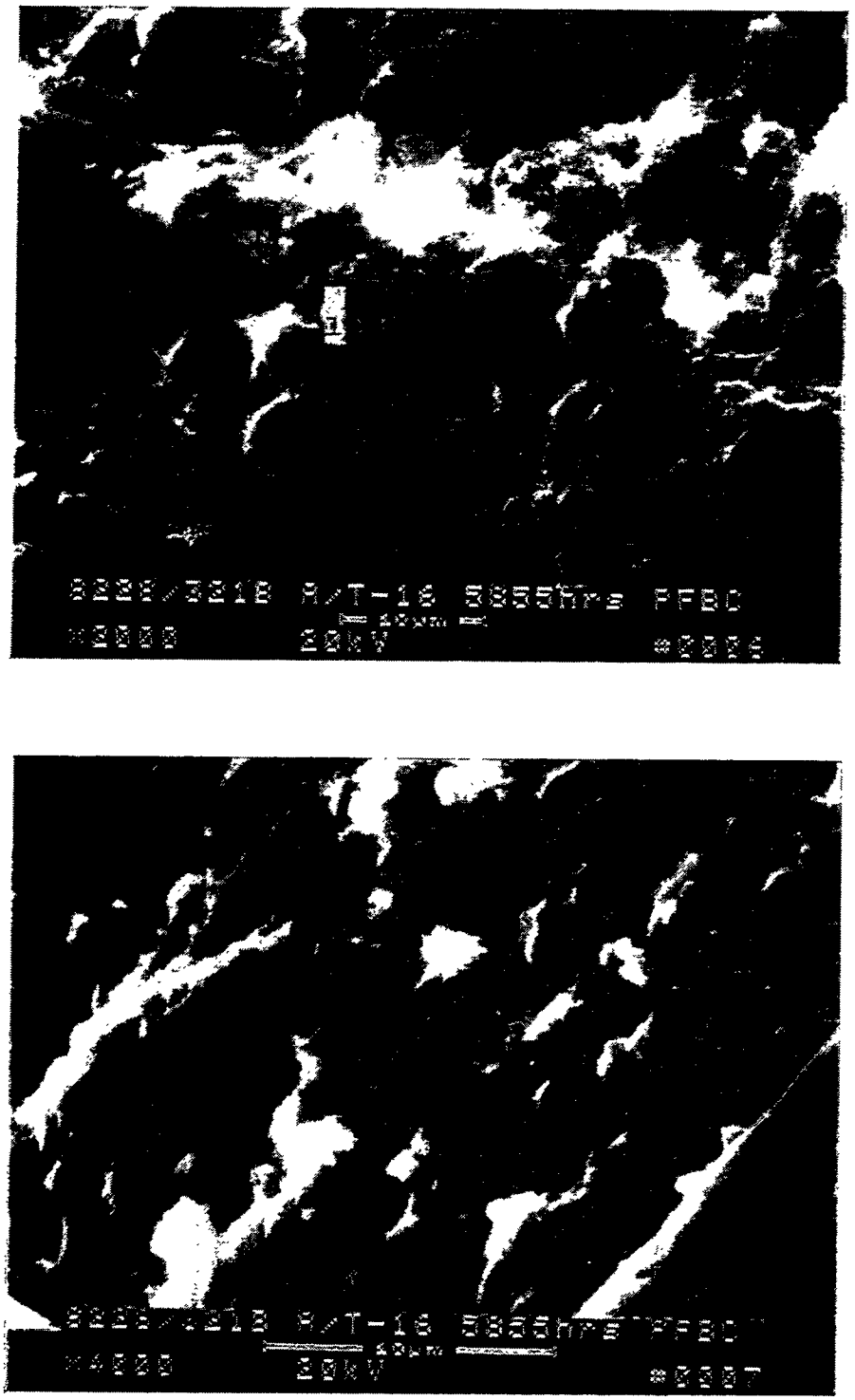

Figure 5d – Additional Micrographs Illustrating The Morphology Of The Dendritic Phase Formation (Top Micrograph), And Silicon Carbide Grain Surface (Bottom Micrograph)

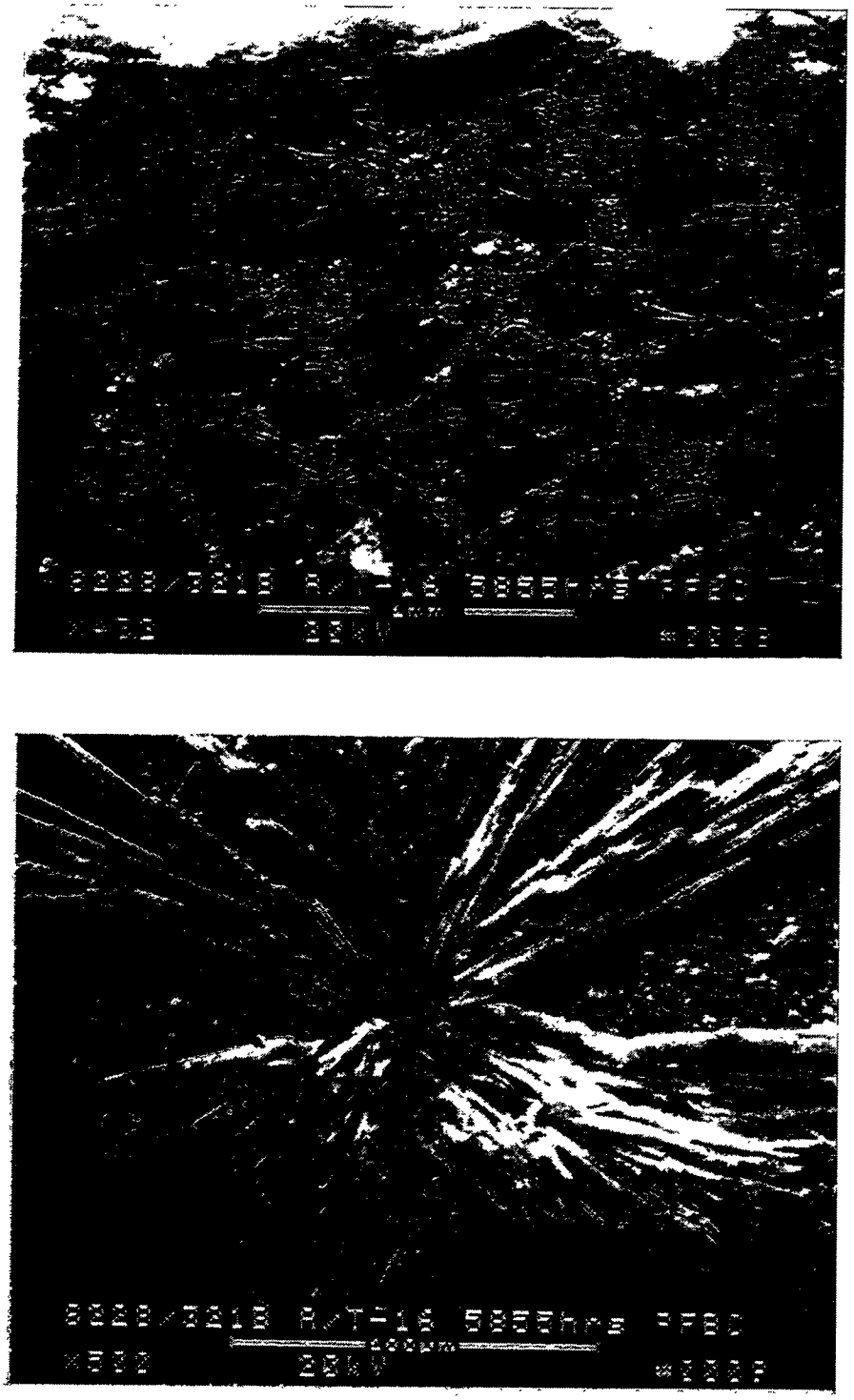

Figure 5e – Silicon Carbide Grains And Dendritic Formations

2

Figure 5f — High Magnification Montage Illustrating The Calcium Sulfate Dendritic Formations Along The Silicon Carbide Binder Coated Grains In The 5855 Hour PFBC-Exposed Schumacher Dia Schumalith F40 Filter Matrix

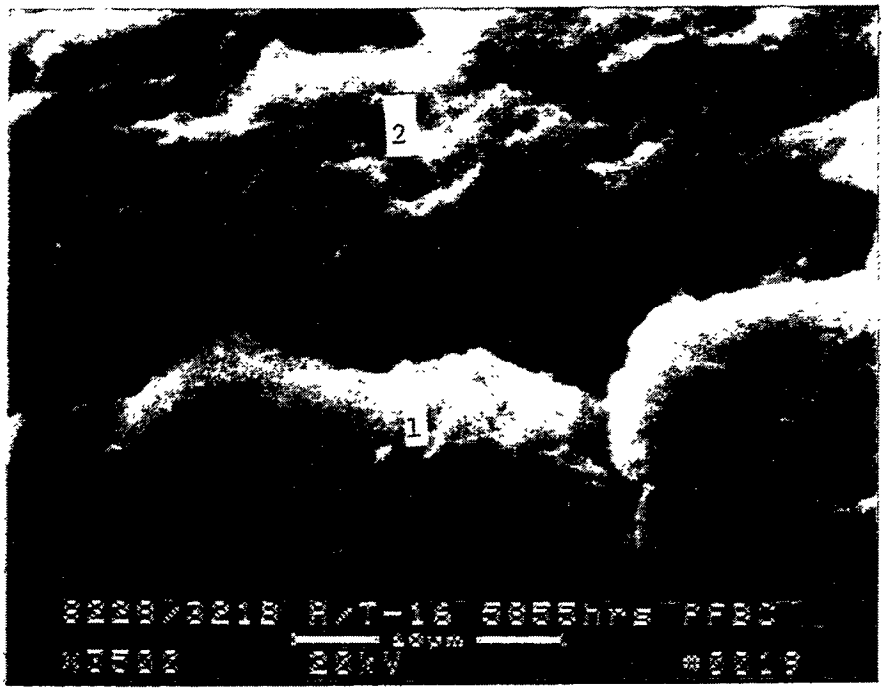

Figure 5g – Higher Magnification Micrographs (
Grains In The 5855 Hour PFBC-Exp
Filter Matrix

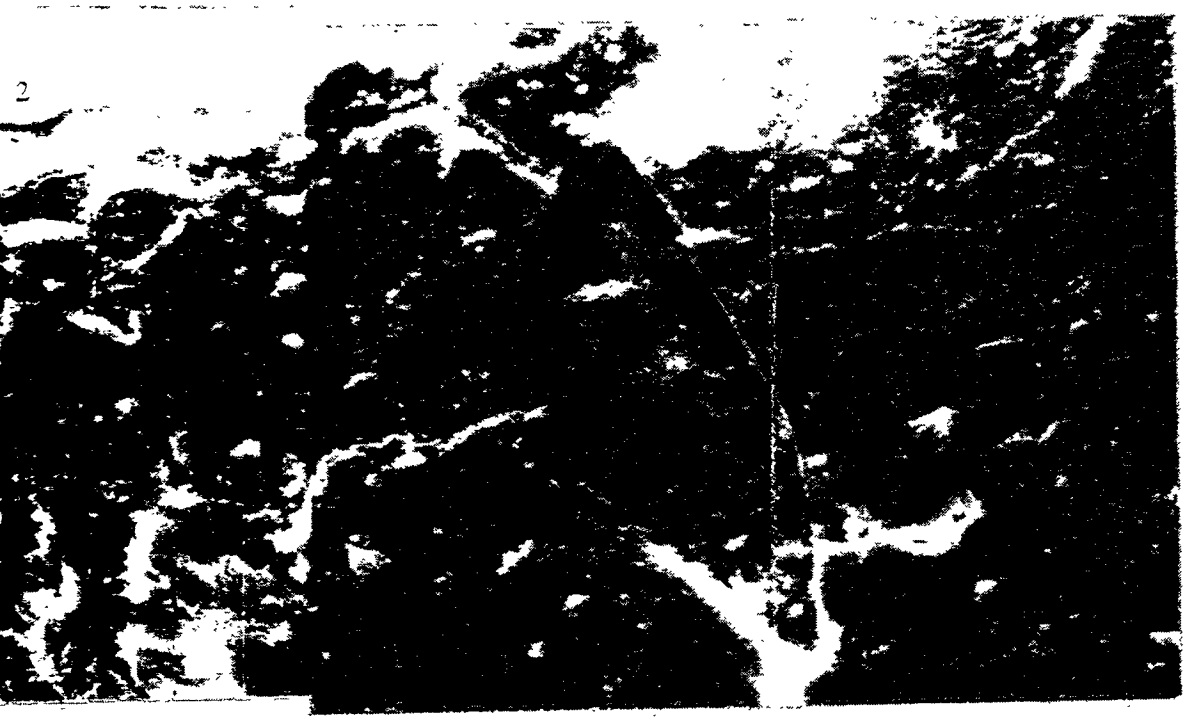

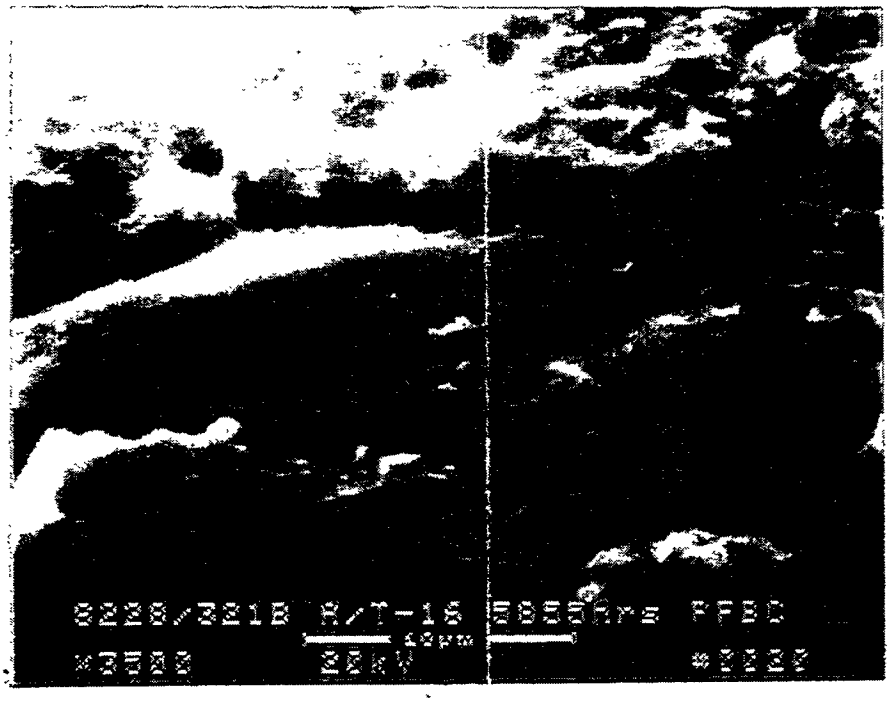

The Binder Coated Silicon Carbide
ed Schumacher Dia Schumalith F40

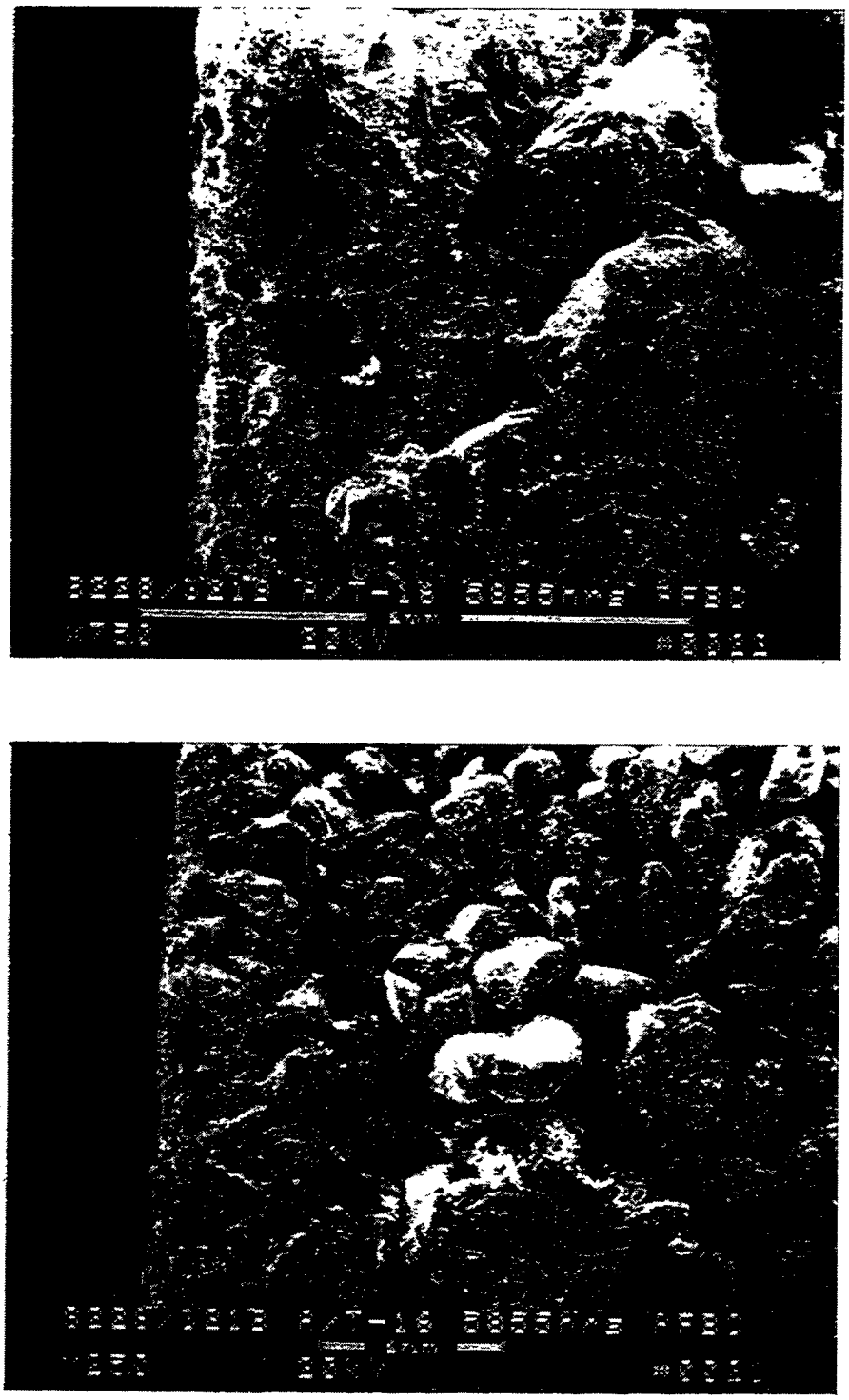

Figure 5h – Morphology Of The Cross-Sectioned 5855 Hour PFBC-Exposed Schumacher Dia Schumalith F40 Filter Matrix

Figure 5i — Extensive Crystallization Of The E
5855 Hour PFBC-Exposed Schum

ler Phase Which Formed Along The
er Dia Schumalith F40 Filter Matrix

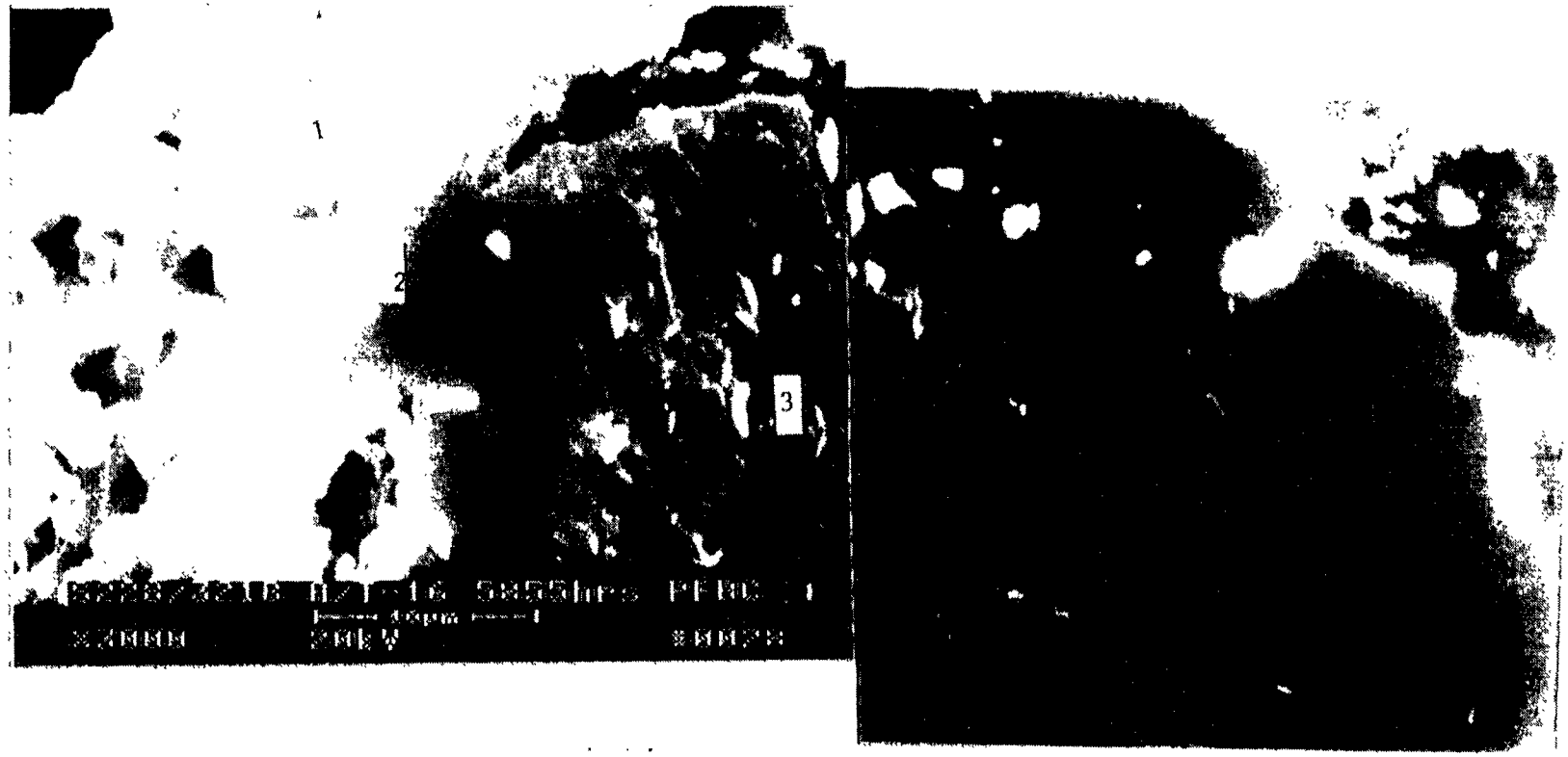

Figure 5j — Higher Magnification Montage Illustrating Separation Of The Crystallized Binder From The Silicon Carbide Grain

206

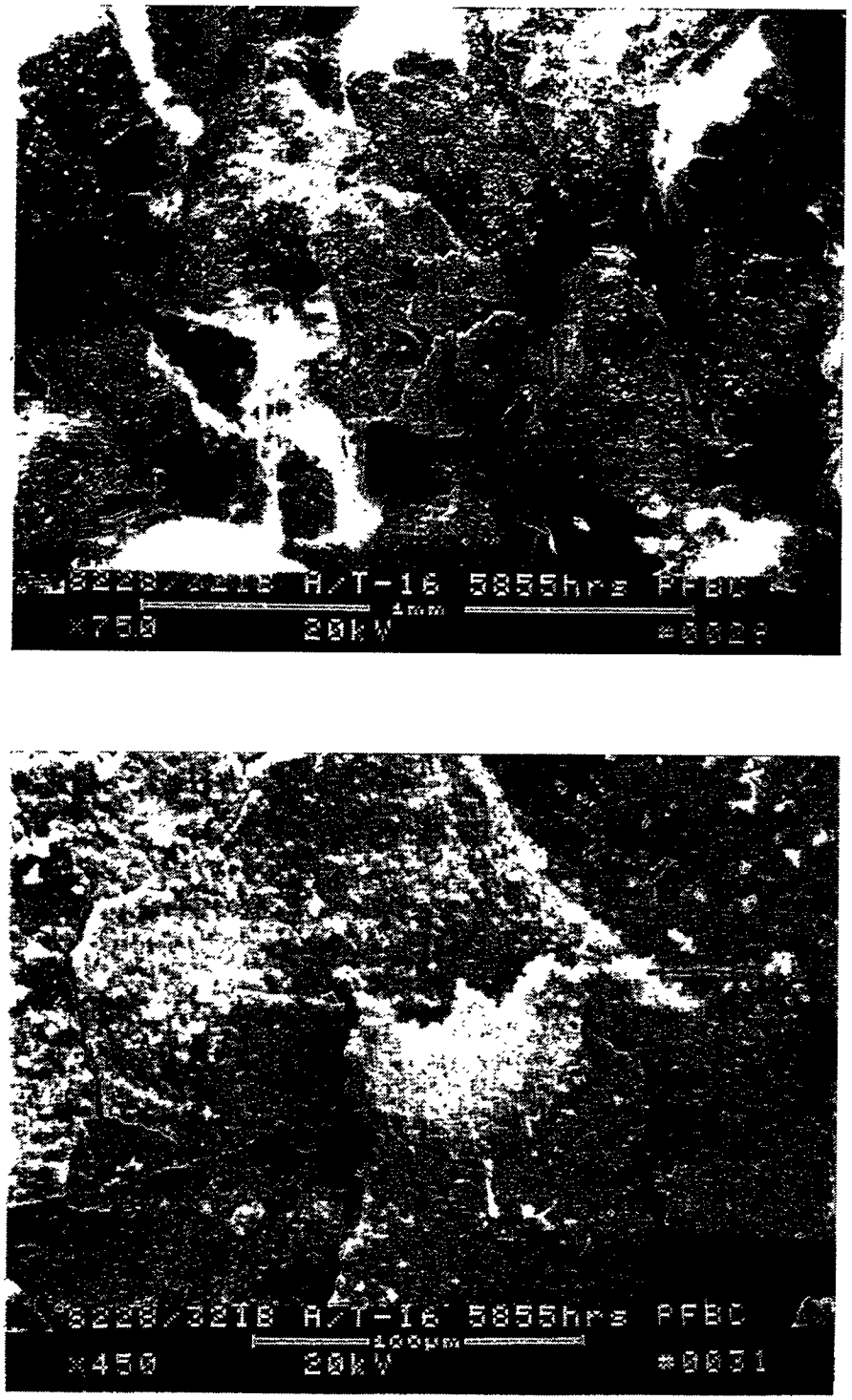

Figure 5k – Crystallization Of The Binder Phase Along Silicon Carbide Grains That Were 4-5 Grains Below The Outer Membrane Surface

Figure 51 – Morphology Of The Outer Surface Of The Crystallized Binder Phase

Figure 5m –Morphology Of The Crystallized Clay Binder At ~15 Grains Below The OD Membrane Surface

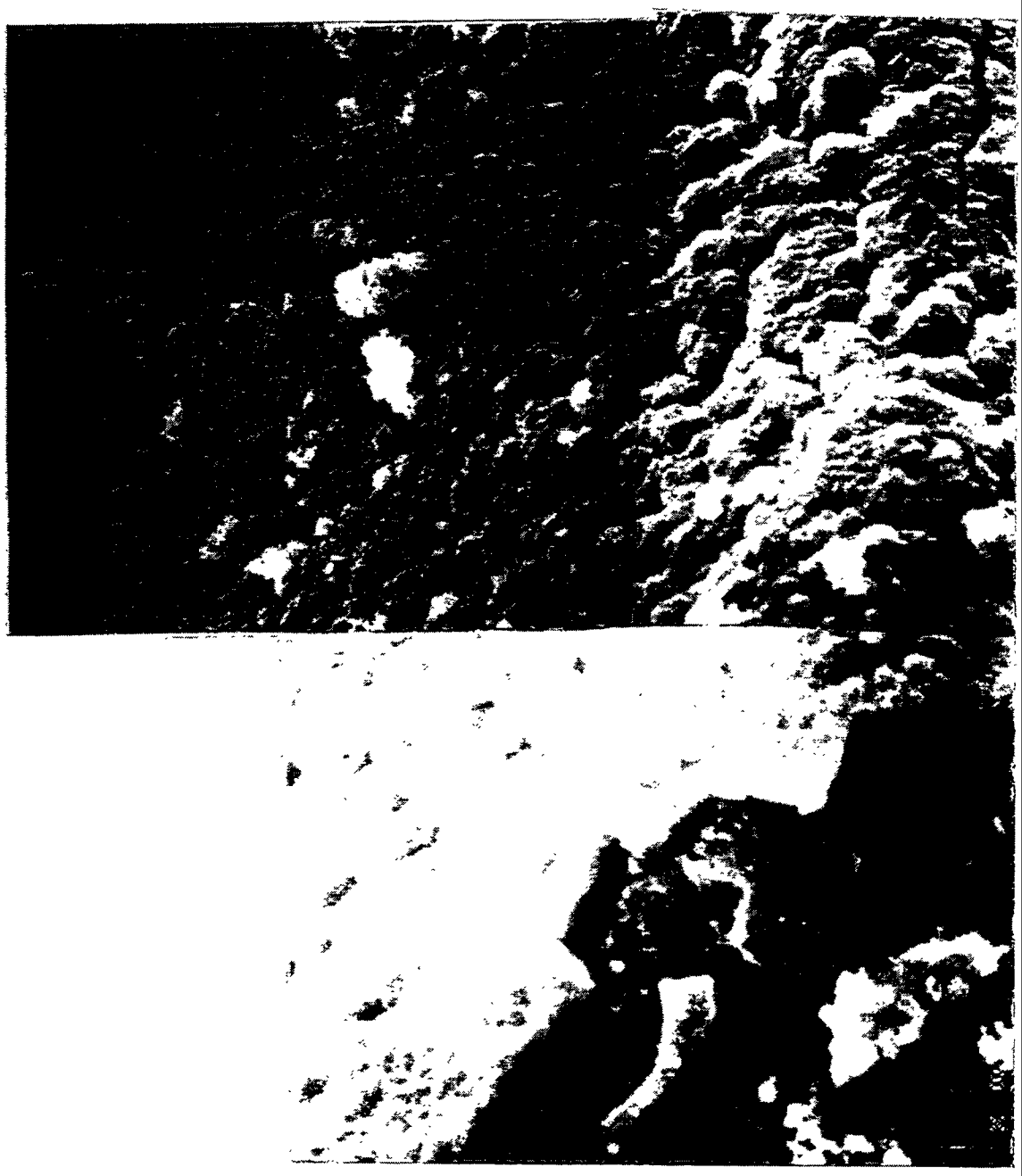

Figure 5n – High Magnification Montage Illustrating Tl
Crystallized Binder Phase From The Surfac
Exposed Silicon Carbide Grain

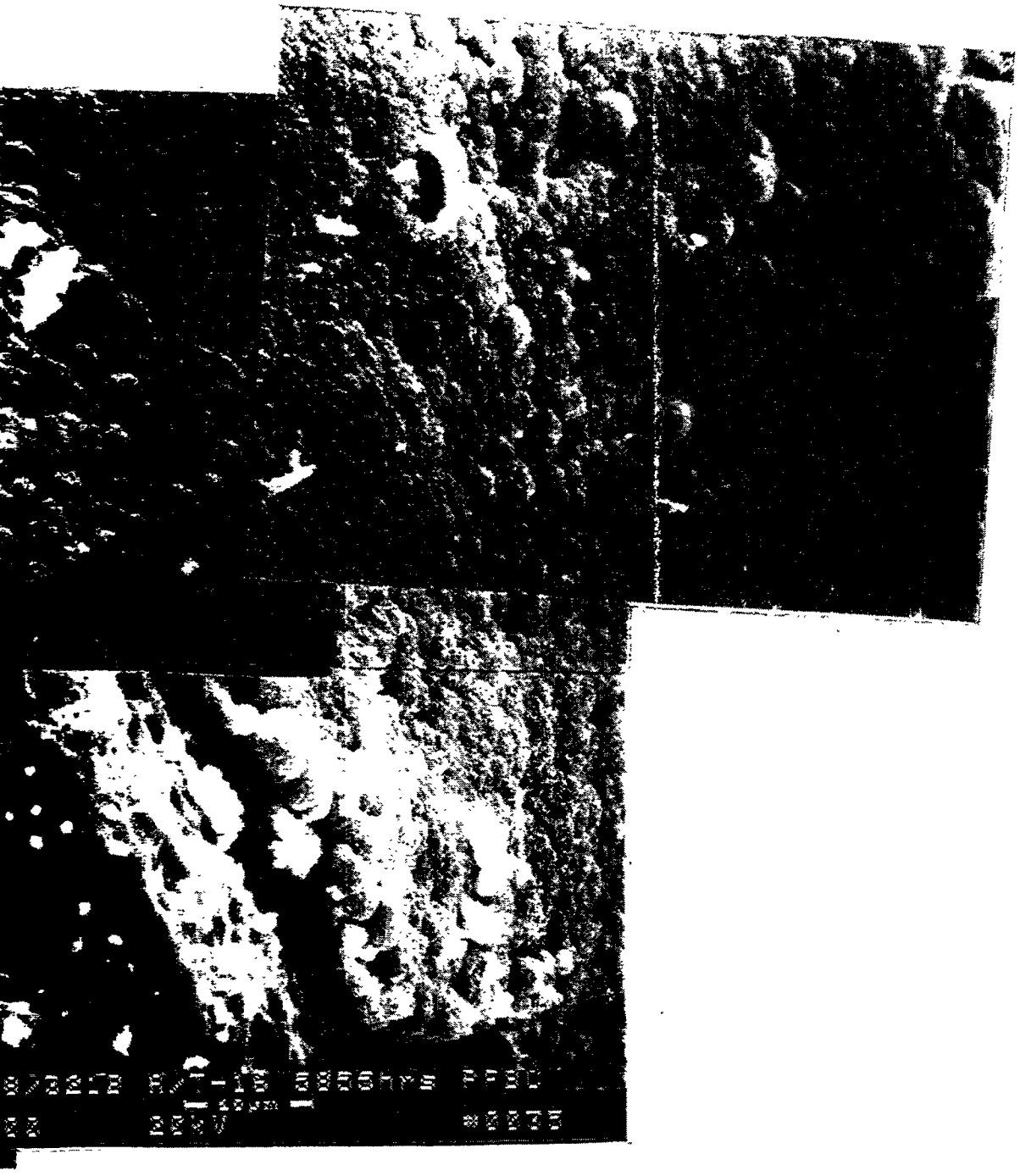

Detachment Of The
Of the 5855 Hour PFBC-

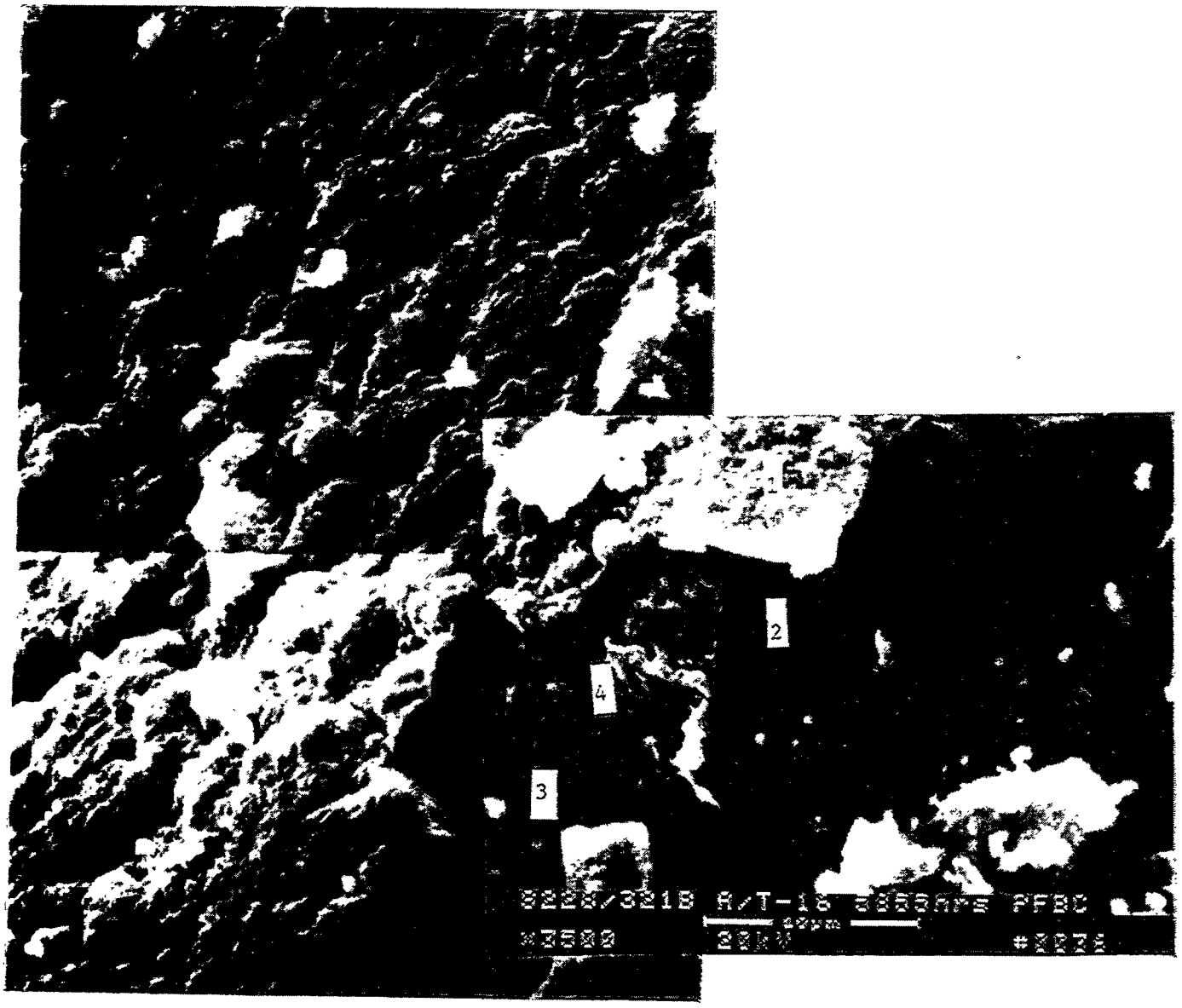

Figure 5o – Higher Magnification Montage Illustrating The Morphology Of The Detached Crystallized Binder Phase And The Underlying Mottled Surface Of The Silicon Carbide Grain

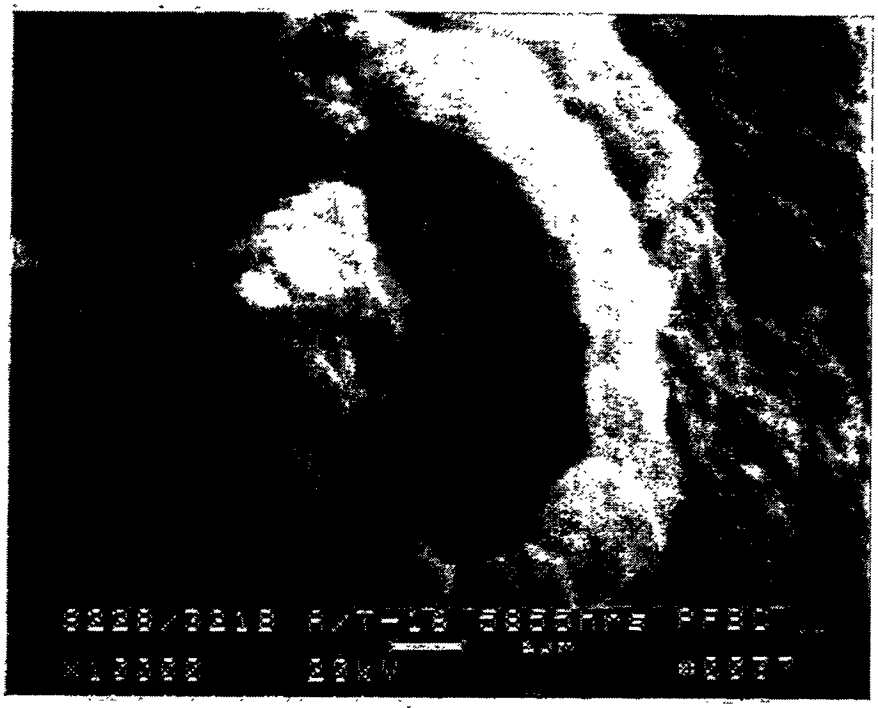

Figure 5p – Hole Formation Along The Crystallized Binder Surface

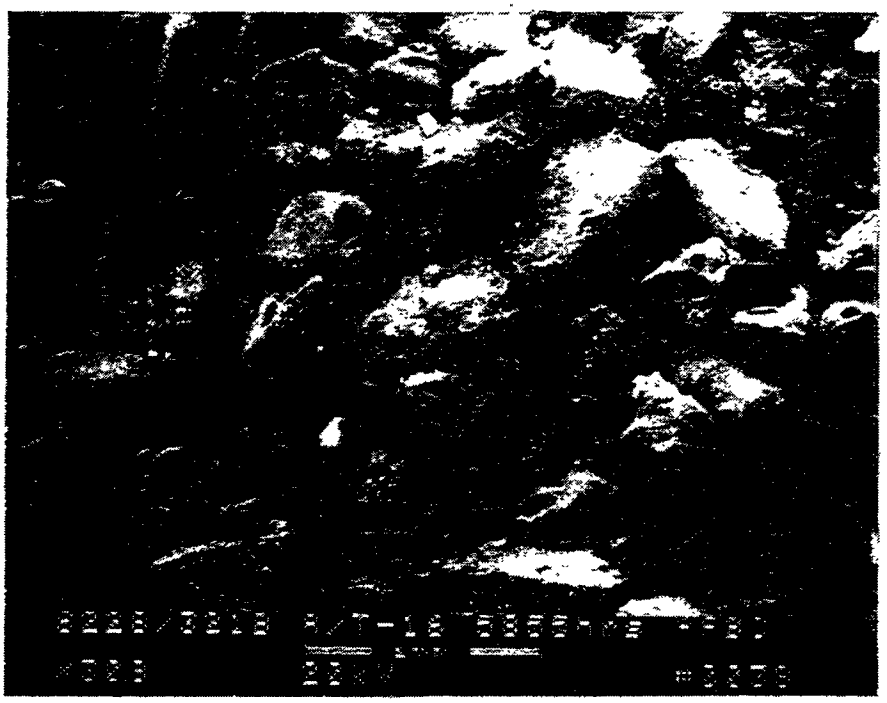

Figure 5q - 5855 Hour PFBC-Exposed Schumacher Dia Schumalith F40 Filter Matrix

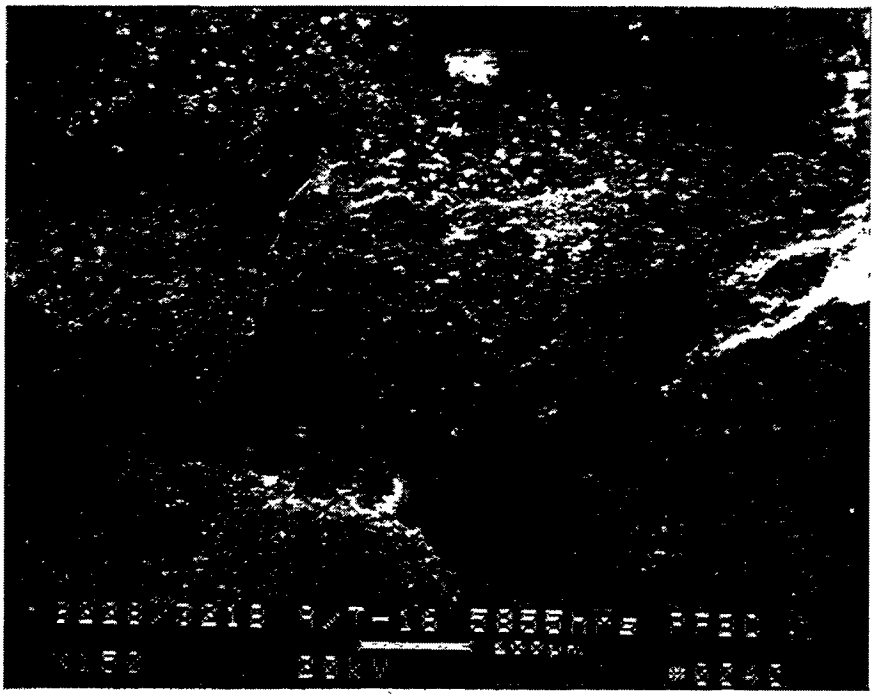

Figure 5r - Morphology At The Mid-Section Of The 5855 Hour PFBC-Exposed Schumacher Dia Schumalith F40 Filter Wall

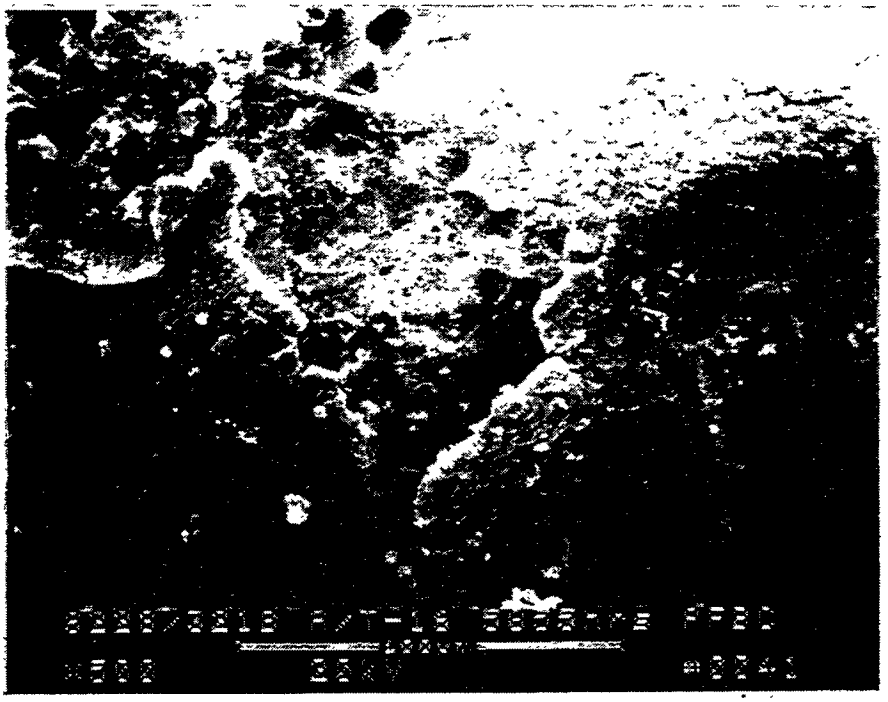

Figure 5s — Crystallized Binder Along The Silicon Carbide Grains At The Mid-Section Of The Schumacher Dia Schumalith F40 Filter Wall

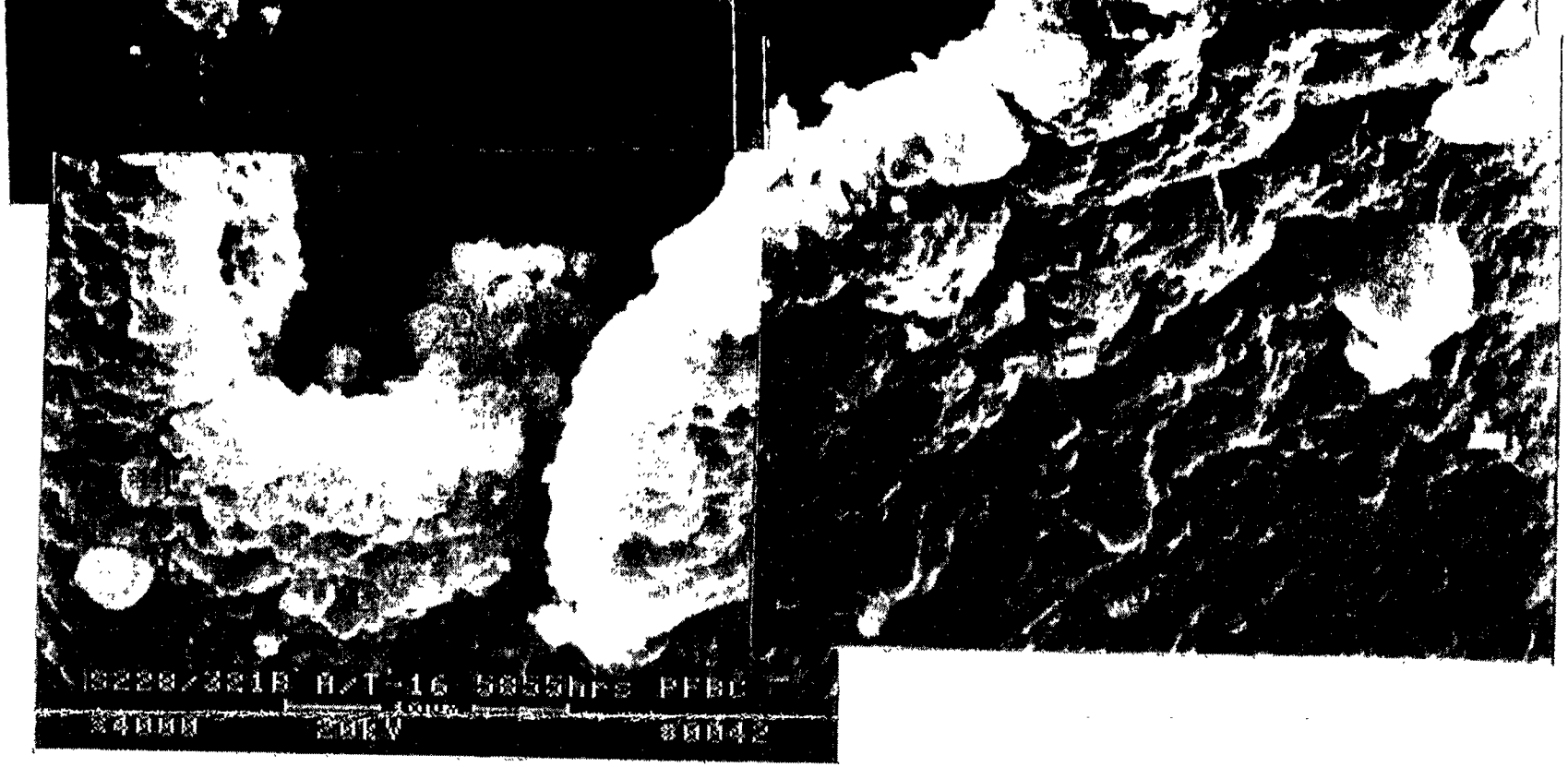

Figure 5t — Higher Magnification Montage Illustrating The Detachment Of The Crystallized Binder Phase From The Mottled Silicon Carbide Grain Surface

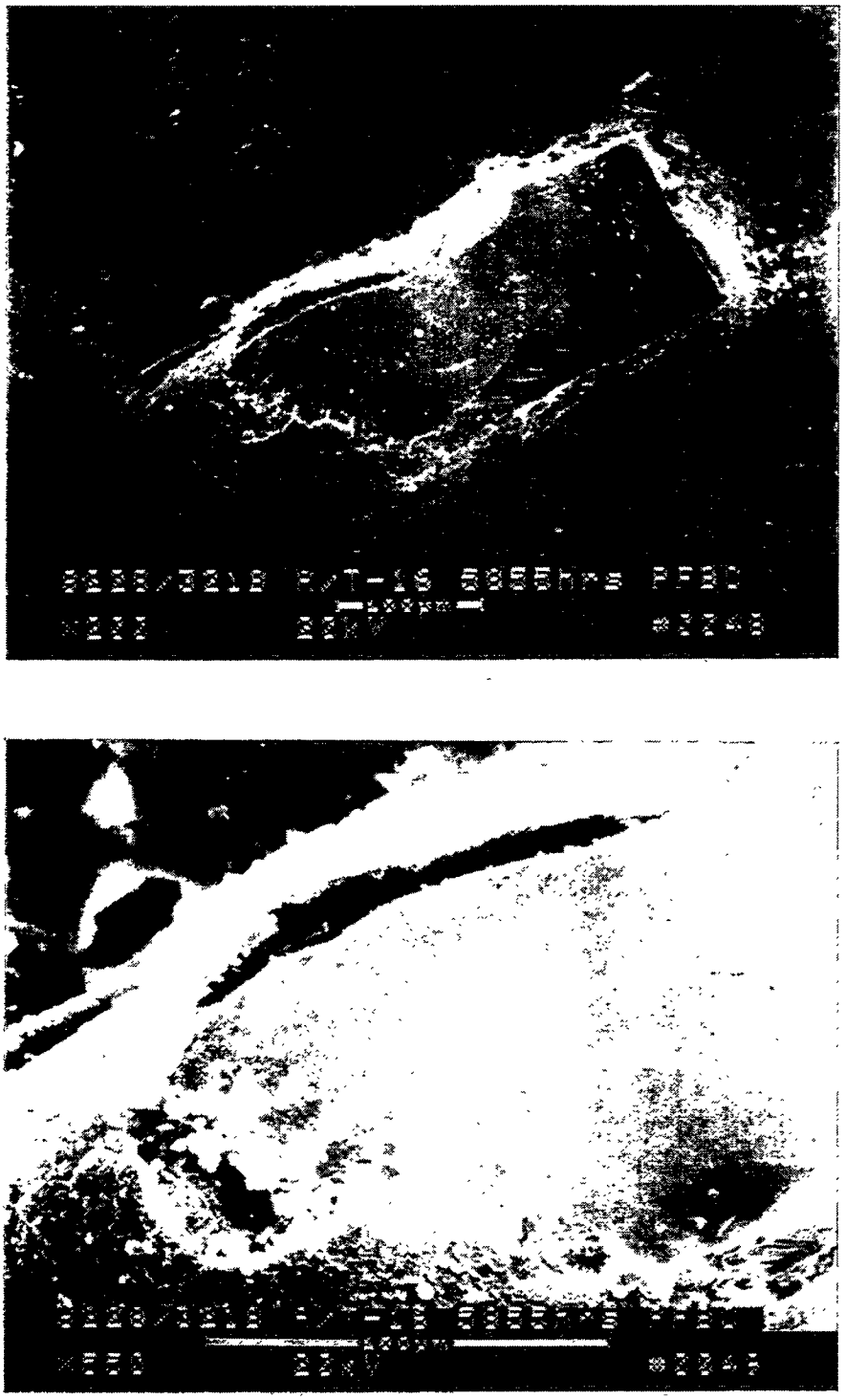

Figure 5u – Morphology Of The Crystallized Binder At An Alternate Location Within The Schumacher Dia Schumalith F40 Filter Matrix

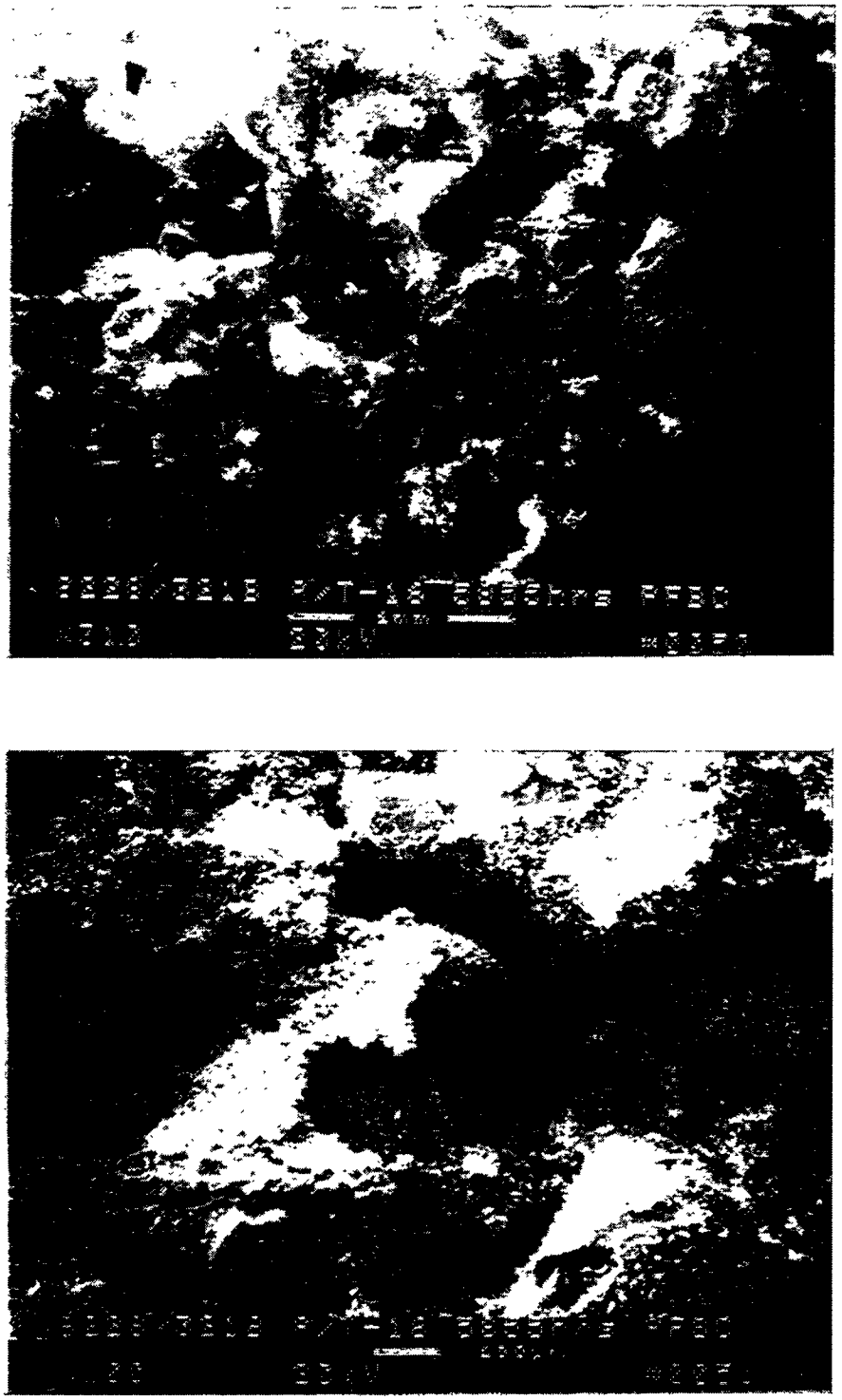

Figure 5v – Morphology Of The 5855 Hour PFBC-Exposed Schumacher Dia Schumalith F40 Filter Matrix (ID Wall)

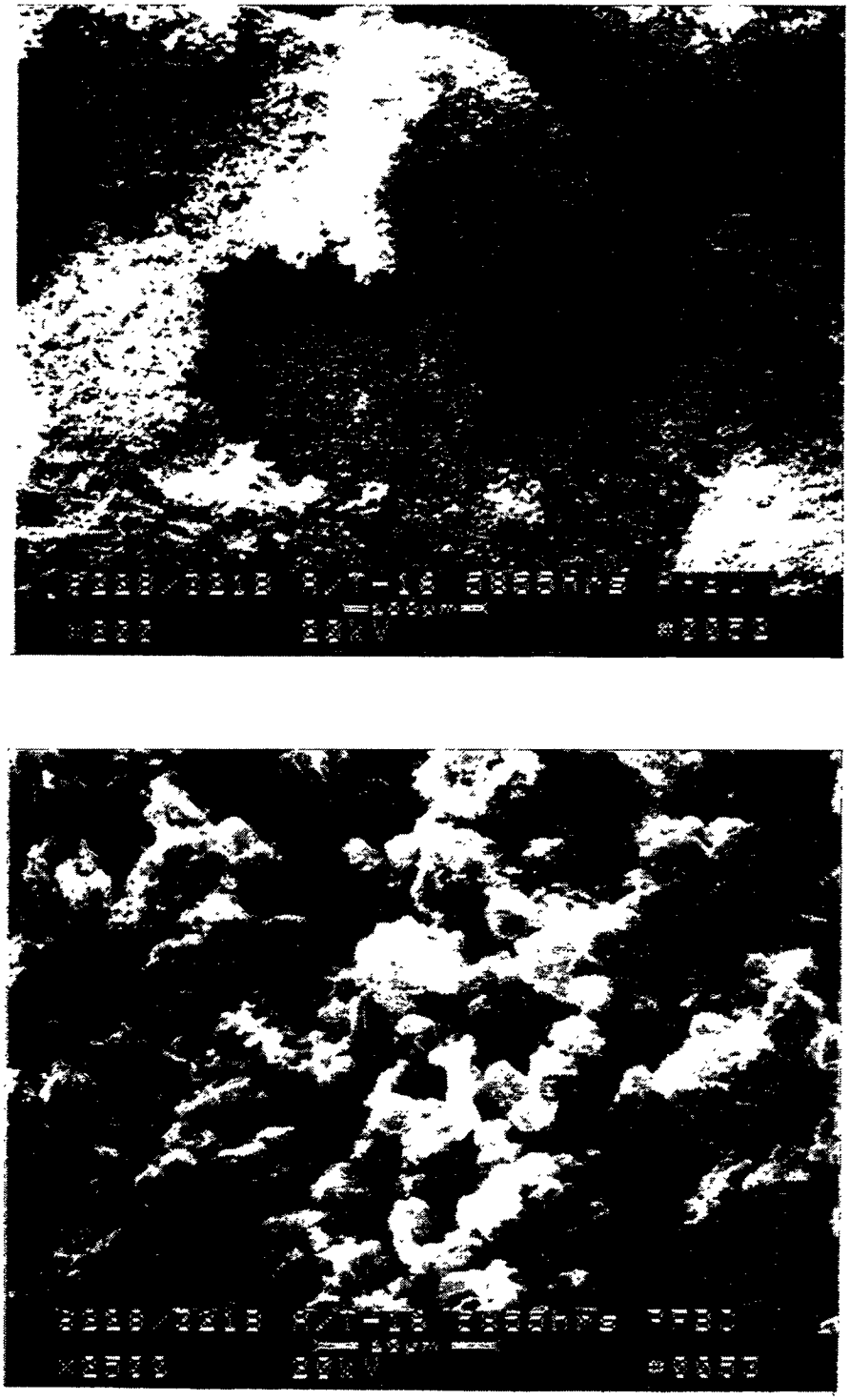

Figure 5w –Fines Penetration Into The ID Surface Of The 5855 Hour PFBC-Exposed Schumacher Dia Schumalith F40 Filter

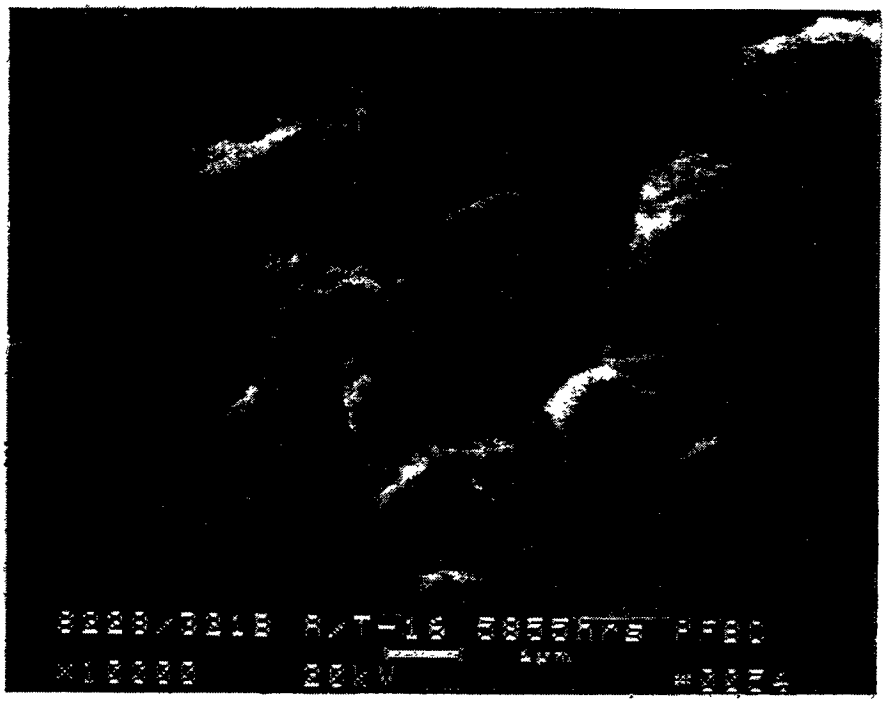

Figure 5x – Sintered Fines Entrapped Within The ID Wall Of The 5855 Hour PFBC-Exposed Schumacher Dia Schumalith F40 Filter Matrix

sulfate-enriched dendritic formations. The surface of the silicon carbide grain was frequently featureless in this area of the matrix, and was identified by EDAX analyses to contain 77.84% O, 14.27% Si, 2.78% Al, 2.39% Mg, 1.64% S, 0.32% Fe, 0.29% K, 0.20% Na, 0.19% Ca, and 0.08% Ti (Area 1, Photo 14, Figure 5f). In contrast, the "mud crack" features which resulted along the silicon carbide grains as shown in Area 2, Photo 14, Figure 5f, were identified by EDAX to contain 73.26% O, 20.71% Si, 1.93% Mg, 1.53% S, 1.23% Al, 0.53% Na, 0.32% K, 0.26% Fe, and 0.25% Ca.

As shown in Photo 18, Figure 5g, the mottled, crystallized binder phase coated the silicon carbide grains of the 5855 hour PFBC-exposed Schumacher Dia Schumalith F40 filter matrix. Area 1, Photo 18, Figure 5g is shown at higher magnification in Photo 19, Figure 5g. EDAX analysis of this area identified the presence of 77.00% O, 18.84% Si, 1.94% Al, 0.63% Mg, 0.54% S, 0.38% Na, 0.25% Fe, 0.22% K, and 0.20% Ca (i.e., binder-enriched area). In contrast, however, the pitted matrix shown in Area 2, Photo 19, Figure 5g primarily consisted of silicon, carbon, and oxygen (i.e., oxidation of the silicon carbide grain).

Area 2, Photo 18, Figure 5g is shown at higher magnification in Photo 20, Figure 5g. The majority of the binder phase appeared to be lifted from the underlying, pitted, silicon carbide grain, while sections of the binder appeared to remain attached to the "reacted" grain surface.

The sample of the Schumacher Dia Schumalith F40 filter matrix was subsequently coated with gold in order to provide additional high resolution micrographs. As shown in Figure 5h, the cross-sectioned wall retained its highly porous, as-manufactured, open structure below the fibrous OD membrane surface. At higher magnification (Photo 25, Figure 5i), the binder coating which encapsulated the silicon carbide grains crystallized, and was readily detached from the underlying support grain. Numerous cracks were evident along the crystallized binder coating. The surface of the underlying grain in many areas appeared to be mottled or pitted, unlike the smooth, as-manufactured silicon carbide grain surface.

Figure 5j shows the binder attached to the outer surface of a silicon carbide grain. The ~5 μm crystallized binder appeared to have lifted and become detached from the silicon carbide grain. The exposed silicon carbide grain was considered to originally be below the binder ligament or bond post which had been cleaved from the surface of the grain during sample preparation. EDAX analysis of Area 1, Photo 28, Figure 5j indicated the presence of 60.56% O, 33.29% Si, 3.53% Al, 1.44% K, 0.64% Ca, and 0.54% Fe (i.e., surface of the crystallized binder coating). Moving through the cross-sectioned binder wall (Area 2, Photo 28, Figure 5j), the composition of the matrix as identified by EDAX analyses indicated the presence of 49.47% O, 39.81% Si, 5.85% K, 4.66% Al, and 0.22% Fe. EDAX analysis of Area 3, Photo 28, Figure 5j identified the presence of 71.97% Si and 28.03% O (i.e., oxidation of the silicon carbide grain).

At 4-5 grains below the OD membrane, extensive spalling of the crystallized binder which coated the silicon carbide grains was evident (Figure 5k). The morphology of the outer surface of the crystallized binder is shown in Figure 5l.

Similar crystallization of the binder phase, as well as spalling or cracking of the binder along the silicon carbide grain occurred at ~15 grains below the OD surface membrane (Figure 5m). The high magnification montage shown in Photo 35, Figure 5n illustrates several features of the 5855 hour PFBC-exposed Schumacher Dia Schumalith F40 filter matrix. These include:

- Extensive crystallization of the binder coating
- Extensive crack formation and spalling of the binder coating
- Surface pitting of the silicon carbide grain.

The morphology along the pitted surface of the silicon carbide grain is shown at higher magnification in Figure 5o. EDAX analysis of Area 1, Photo 36, Figure 5o indicated the presence of silicon and oxygen, while Areas 2 and 3, and the pitted matrix in Area 4 were identified to be part of the silicon carbide grain. An isolated "hole-like" formation occurred along the crystallized binder coating (Figure 5p).

Figures 5q - 5s illustrate the morphology of the 5855 hour PFBC-exposed Schumacher Dia Schumalith F40 filter matrix at ~7.5 mm from either the OD or ID surface of the filter wall. Once again crystallization of the binder was readily evident, as well as the retained open porosity of the matrix. Spalling and crack formations in the binder phase, and pitting along the surface of the silicon carbide grain were evident (Figure 5t).

Figure 5u illustrates the morphology of additional silicon carbide grains at an alternate location along the mid-section of the filter body. Crystallization of the binder phase occurred, as well as spalling and lifting of the binder from the support grain.

Figures 5v, 5w, and 5x illustrate the morphology of the 5855 hour PFBC-exposed Schumacher Dia Schumalith F40 filter matrix along the ID wall of the filter element. Fines filled the porous ceramic filter ID wall. The morphology of the fines which were collected within the filter wall is clearly shown in Photo 53, Figure 5w, and Photo 54, Figure 5x. The rounded or sintered features of the ash/sorbent deposited fines were readily evident. The composition of the fines shown in Figure 5w was identified by EDAX to include 58.73% O, 21.07% Si, 9.22% Al, 6.00% Fe, 3.62% Ca, 1.37% K, with sulfur expected to also be present (i.e., masked by gold coating).

CONCLUSIONS

- The residual strength of the Schumacher Dia Schumalith F40 matrix initially experienced a loss of bulk strength, prior to conditioning to a residual strength of ~1000 psi at PFBC process operating temperatures.

- Crystallization of the binder phase was considered to be largely responsible for the resulting conditioned strength of the PFBC-exposed Schumacher Dia Schumalith F40 candle filter matrix.

- Oxidation and/or reactions along the silicon carbide grain surface (i.e., directly below the crystallized binder phase) are suspected to have been initiated after operation of the Schumacher Dia Schumalith F40 filter matrix in the PFBC environment.

REFERENCE

1. M. A. Alvin, T. E. Lippert, E. S. Diaz, and E. E. Smeltzer, "Thermal and Chemical Stability of Ceramic Candle Filters," Advanced Coal-Fired Power Systems '95 Review Meeting, Morgantown, WV, June 27-29, 1995.

APPENDIX F

DESCRIPTION OF THE DuPONT PRD-66 CANDLE FILTERS AT THE CONCLUSION OF TEST SEGMENT #5

M. A. Alvin
May 30, 1995

GENERAL DESCRIPTION

The filter identification numbers and positions of the twenty-two PRD-66 candles that were installed within the Westinghouse Advanced Particulate Filtration (W-APF) B/T array prior to January 1995 are shown in Figure 1. During the 1110 hours of pressurized fluidized-bed combustion (PFBC) operation in Test Segment #5 (i.e., January 13, 1995 - March 30, 1995), all inner ring candles were blanked off in this array which permitted filtration to occur only through the outer ring of the DuPont PRD-66 filter elements.

Post-test inspection of the W-APF on May 11, 1995 indicated that only two full length PRD-66 candle filters remained in the B/T array after 1110 hours of test operation. These were located in position B/T-6 (D-252) and B/T-8 (D-237). In addition, four filters were observed to have failed at either ~750 mm below the flange (i.e., mid-body fracture of D-247 in B/T-2), or ~1125 mm below the flange (i.e., three-quarter body fracture of D-253 in B/T-10; D-231 in B/T-11; and D-255 in B/T-12). The remaining DuPont PRD-66 filter elements fractured at the base of the flange, within the densified area of the filter body (i.e., at ~1/4-1/2 inch below the densified internal insert; Figure 2). All DuPont PRD-66 filter elements were observed to be tightly held within the holder mount design after 1110 hours of test operation in Test Segment #5.

A dark red stain was frequently evident along the outer surface of the PRD-66 filter body (i.e., below the flange section of the fractured, as well as intact elements; Figure 3). When the candles were viewed at a location that was tangent to the B/T plenum, the red stain was typically present along one side of the filter body (Figure 4). The position of the red stain was considered to have resulted from the impact of fines along the candle surface from either pulse cycling of an adjacent failed filter element, or from the gas/particle flow path that resulted during high temperature process operation. Efforts will be directed to confirm whether fines were present along the outer surface of the PRD-66 filter elements, as well as within the bulk filter matrix beneath the thin filament wound membrane.

Frequently divots were observed along the sides of the full length or fractured candle filters (Figure 5). The divots were positioned as long stripes down the length of the remaining filter elements. Remnants of the "divot-like" formations were present at the fractured surfaces of the PRD-66 filter elements (Figure 6). This implied that perhaps once the divot had formed, and that the wall had thinned substantially and consequently weakened, failure of the element occurred.

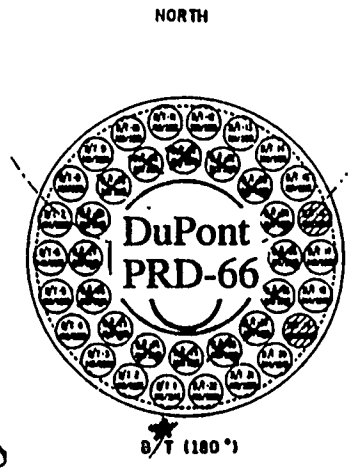

Location	ID No.	Characteristics	Location	ID No.	Characteristics
B/T-1	D-258	Flange Failure	B/T-12	D-255	3/4 Length Failure
B/T-2	D-247	Mid-Body Fracture	B/T-13	D-221	Flange Failure
B/T-3	D-226	Flange Failure	B/T-14	D-235	Flange Failure
B/T-4	D-248	Flange Failure	B/T-15	D-224	Flange Failure
B/T-5	D-251	Flange Failure	B/T-16	D-227	Flange Failure
B/T-6	D-252	Intact	B/T-17	D-232	Flange Failure
B/T-7	D-240	Flange Failure	B/T-18	D-222	Flange Failure
B/T-8	D-237	Intact	B/T-19	D-223	Flange Failure
B/T-9	D-220	Flange Failure	B/T-20	D-260	Flange Failure
B/T-10	D-253	3/4 Length Failure	B/T-21	D-257	Flange Failure
B/T-11	D-231	3/4 Length Failure	B/T-22	D-261	Flange Failure

Figure 1 – DuPont PRD-66 Filter Element Identification Numbers And Locations Within The W-APF During Operation In Test Segment #5

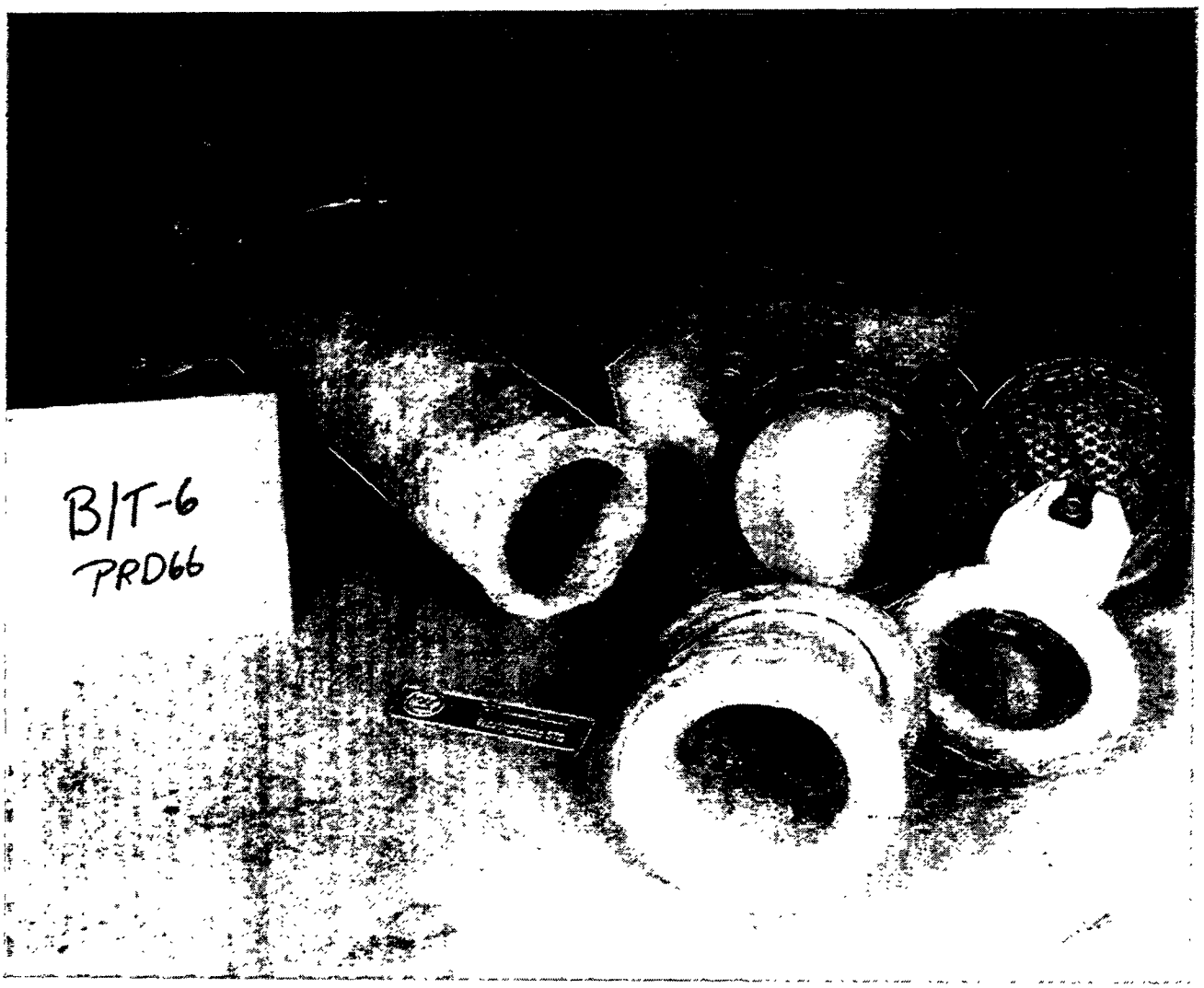

Figure 2 — Flange Failure Of The DuPont PRD-66 Filter Elements In Test Segment #5

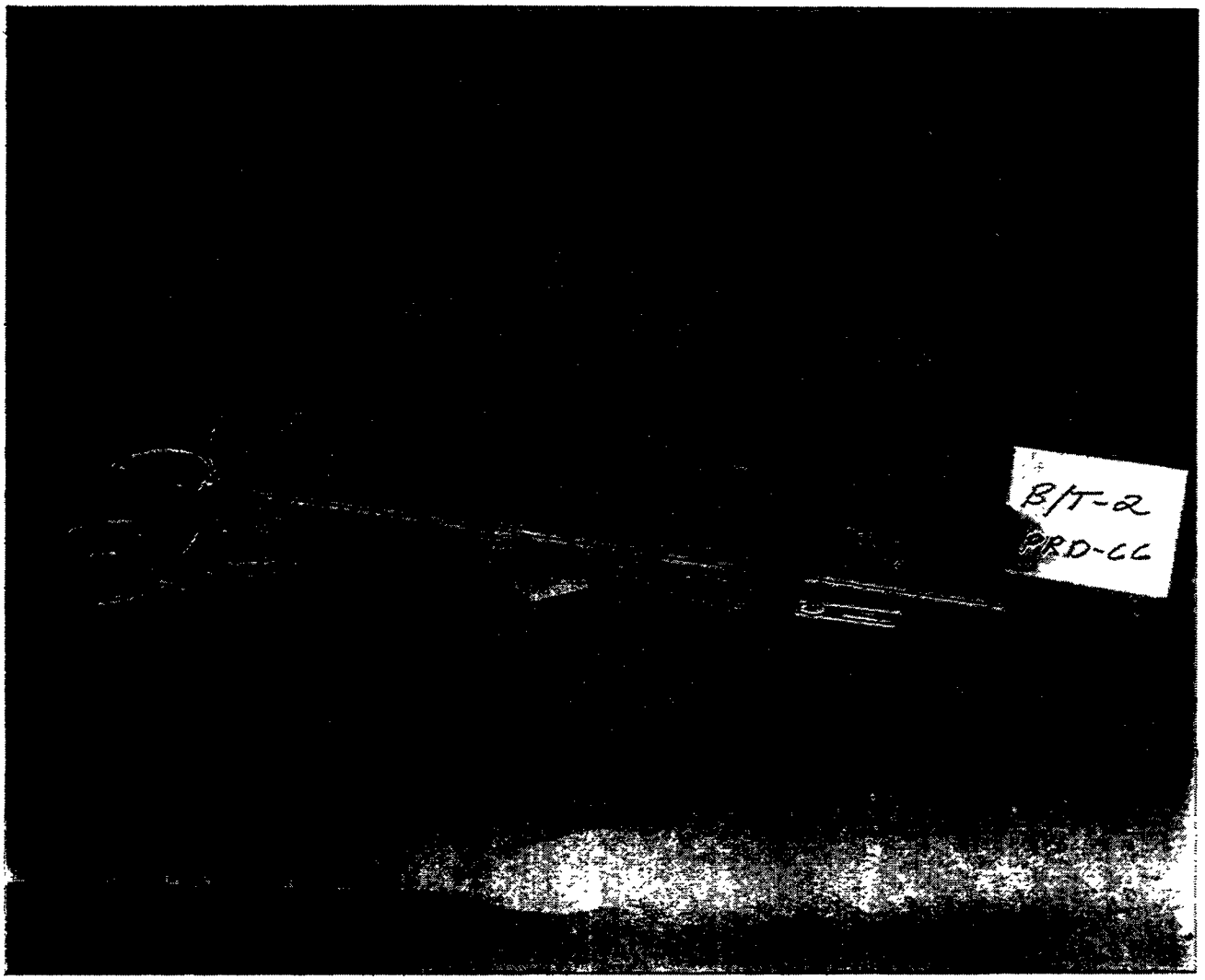

Figure 3a – Red Ash Stain Remaining Along The DuPont PRd-66 Filter Elements After 1110 Hours Of PFBC Operation In The W-APF At AEP In Test Segment #5

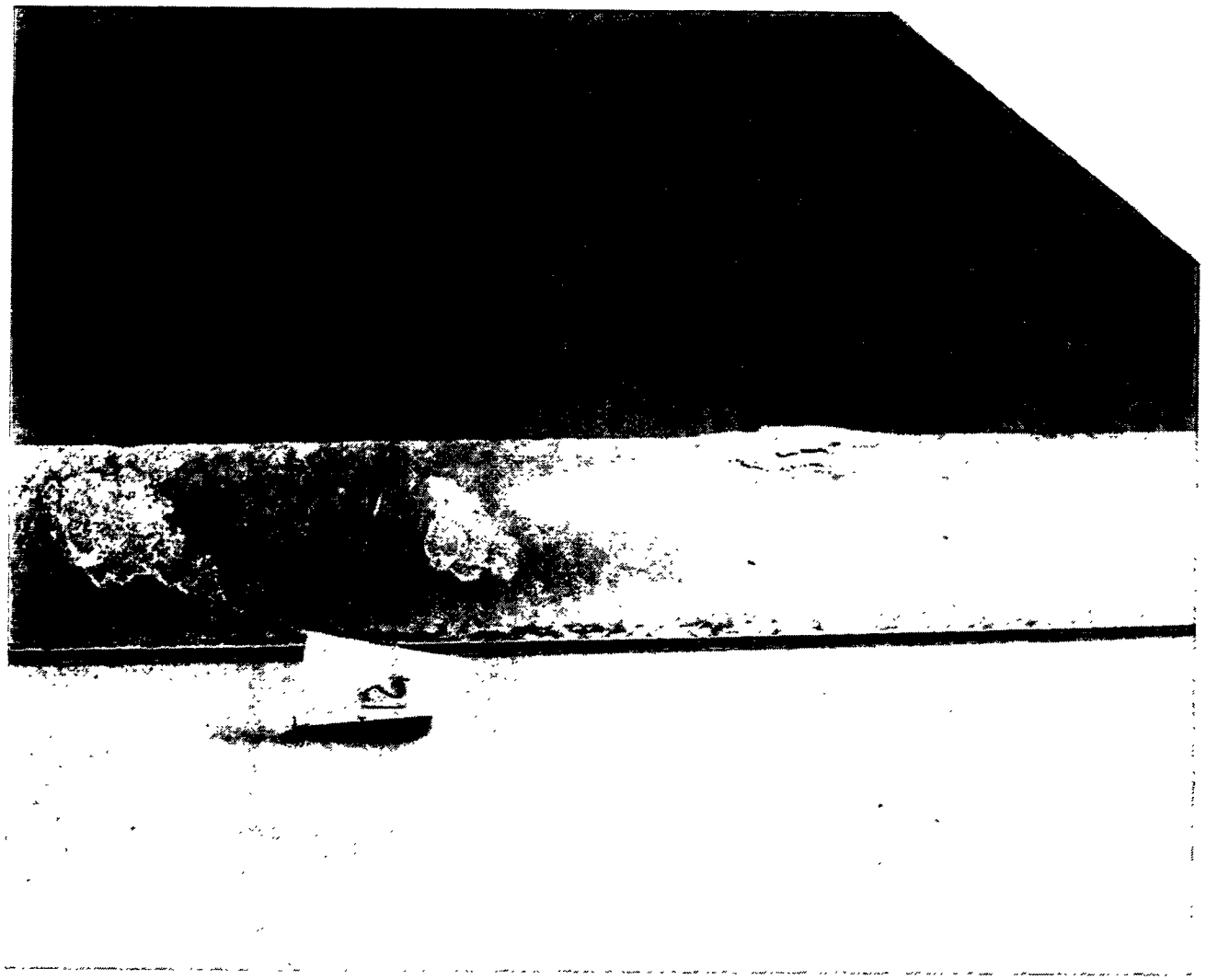

Figure 3b -- Red Ash Stain Remaining ALong The DuPont PRd-66 Filter Elements After 1110 Hours Of PFBC Operation In The W-APF At AEP In Test Segment #5

B/T-11

- Three-quarter length body fracture.
- Three-quarter fractured filters along both sides of the B/T-11 candle.
- Large divot formed beneath the gasket sleeve.
- The red stain resulted along one-half of the filter body. The red stain terminated at ~180° from the plenum tangent point.
- Massive set of divots formed down the length of the filter body. Two parallel lines of divots formed off center from the plenum tangent line. These were ~90° from the plenum tangent point. One divot track was within the red stain region; the other red track formed within the white area of the filter body.
- Divot formation ended at ~1 foot above fractured location.

B/T-10

- Three-quarter length body fracture.
- Flange fracture filter element to one side of the B/T-10 filter element; Three-quarter body fractured filter to the opposite side of the B/T-10 filter element.
- Red stain below the gasket sleeve. Red stain formed almost directly down the length of the filter body down the length of the plenum tangent line. The stain wrapped around nearly 180° to the back of the filter element.
- Large divot formed to the left of the plenum tangent point. No other divots evident.

B/T-8

- Intact candle filter.
- Flange fractured filter elements on both sides of B/T-8.
- Divots formed under the gasket.
- Red stain area resulted along both sides of the candle filter. A white area of the filter body was evident down the length of the element along the plenum tangent location.
- The as-manufactured filter body was evident along the back of the filter where ash was present.
- Fractured at the base of the hemispherical flange/body. Insert still intact; Regular filament winding pattern evident at ~1/4 inch below the insert.

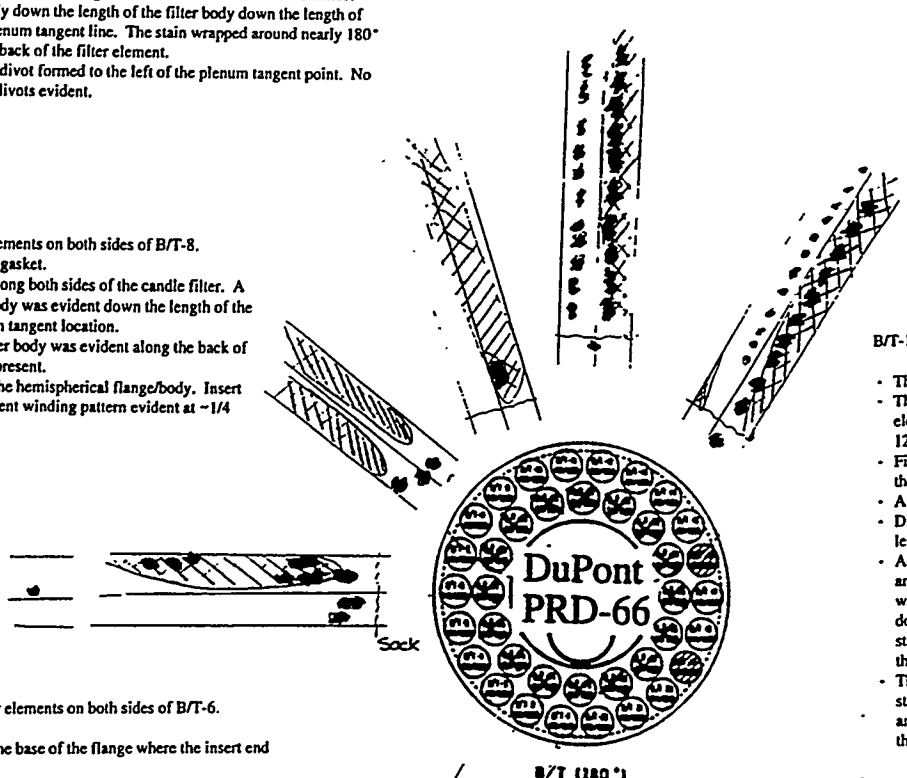

B/T-12

- Three-quarter length body fracture.
- Three-quarter fracture filter on one side of the B/T-12 filter element; flange fractured filter on the opposite side of the B/T-12 filter element.
- First divot to the left of the plenum tangent point, underneath the gasket sleeve.
- A gap of ~6 inches resulted before next divot was encountered.
- Divots ran along a line directly below the first divot, down the length of the body to the fractured location.
- A second set of divots formed along the white as-manufactured are of the filter body. These divots again formed a line which was off-center to the plenum tangent line, which continued down the length of the filter element. This formation of divots started at ~12-14 inches below the flange, and continued down the filter body to the fractured surface.
- The red stain was evident along one-half of the filter body. The stain was clearly evident to the left of the plenum tangent point, and wrapped around the filter element, ending at ~180° from the plenum tangent point.

B/T-6

- Intact filter body.
- Flange fractured filter elements on both sides of B/T-6.
- Ash filed ID bore.
- Filter was broken at the base of the flange where the insert end along the flange ID.
- Numerous divots were evident within the first 8 inches below the gasket sleeve.
- No divots were located directly along the plenum tangent point.
- Red stain resulted to the left of the tangent point along the candle filter body, extending 180° to the back of the filter element.
- The red stain ends almost where the divots begin along the mid-section of the filter element.
- Mid-body divots were 180° from plenum tangent point.
- Near the bottom of the candle, a large divot formed to the right of the plenum tangent point.
- Residual ash was left on the filter element for DuPont's evaluation. There may be more divots present along the body which are not located and/or described above.

B/T (180°)

B/T-2

- Mid-body fractured filter.
- Failed DuPont PRD-66 candle filters which fractured at the base of flange were located along both sides of the B/T-2 fractured PRD-66 filter element.
- Red stain below the gasket sleeve.
- Small divot directly tangent to plenum, below gasket.
- Red stain to right of plenum tangent point (i.e., as viewed facing the array). Red stain continued down the length of the filter to the fractured location.
- To the left of the plenum tangent point, the body retained its as-manufactured white color.
- A few small divots located at 180° from the plenum tangent point near the gasket sleeve.

Figure 4 — Location Of The Red Ash Stain And Divot Formations Along The Remaining Intact And Failed DuPont PRD-66 Candle Filters

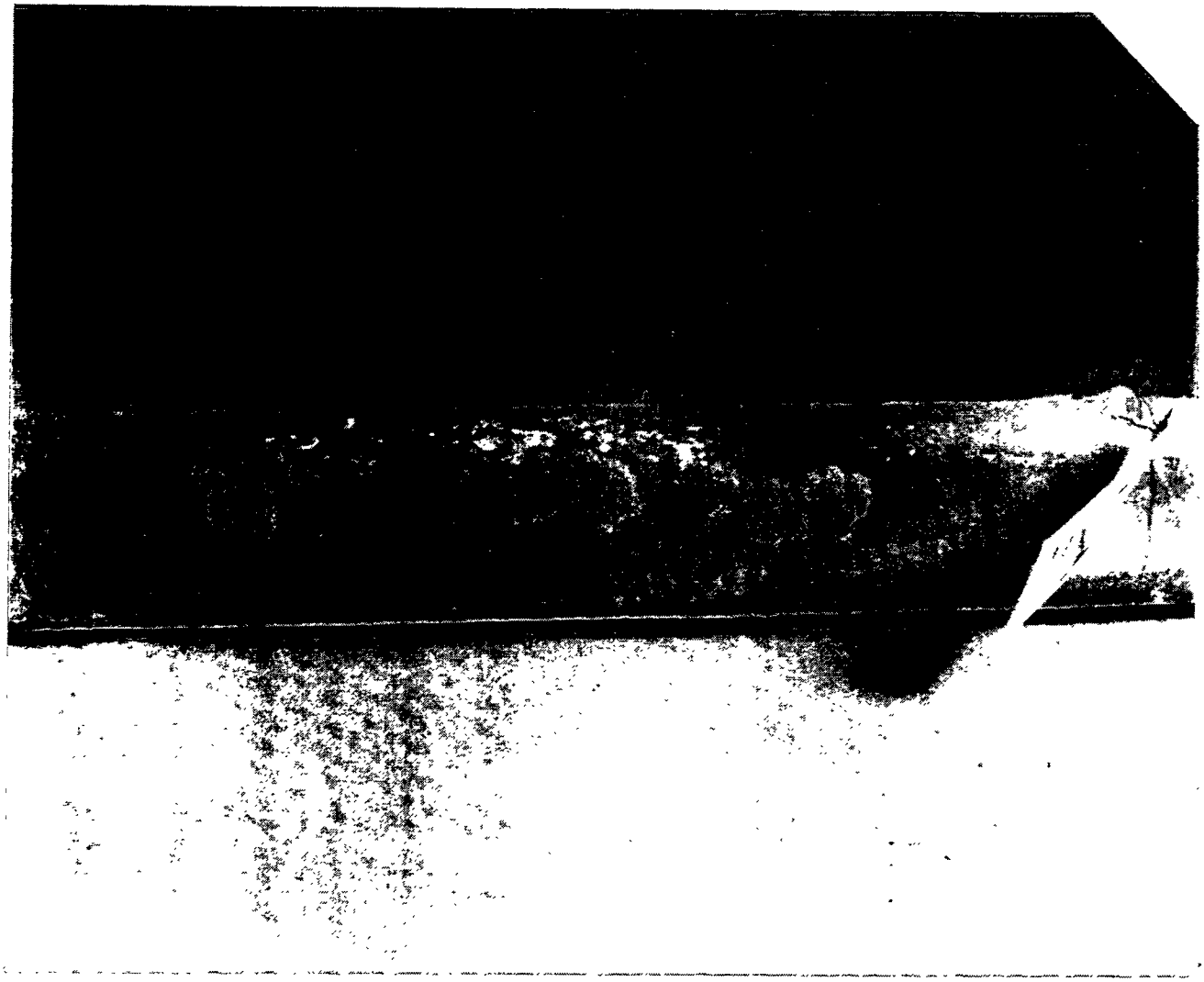

Figure 5a – Divot Formations Along The Length Of The DuPont PRD-66 Filter Body

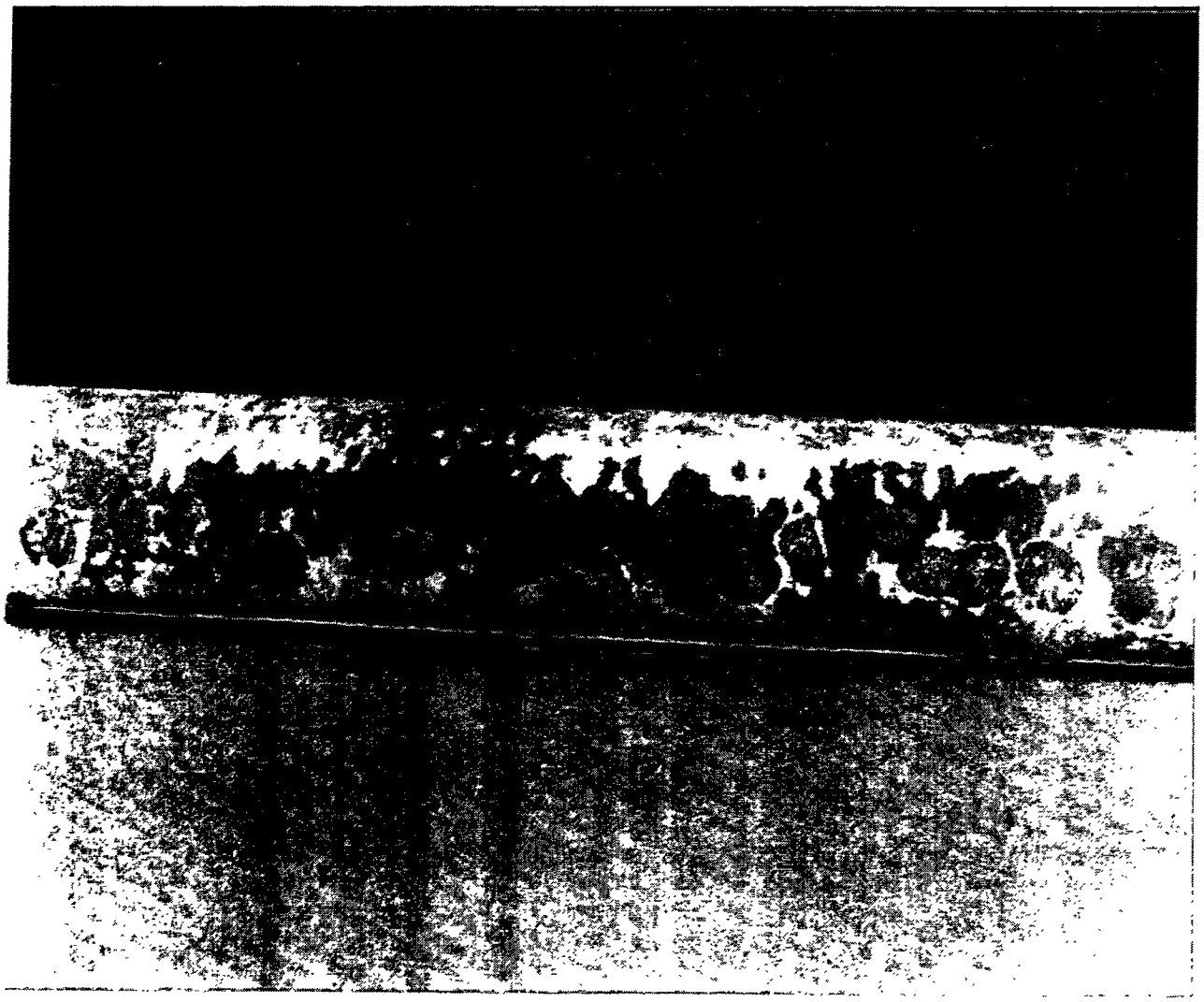

Figure 5b – Divot Formations Along The Length Of The DuPont PRD-66 Filter Body

Figure 6a – Divot Formations Along The Fractured Surfaces Of The Failed DuPont PRD-66 Filter Elements In Test Segment #5

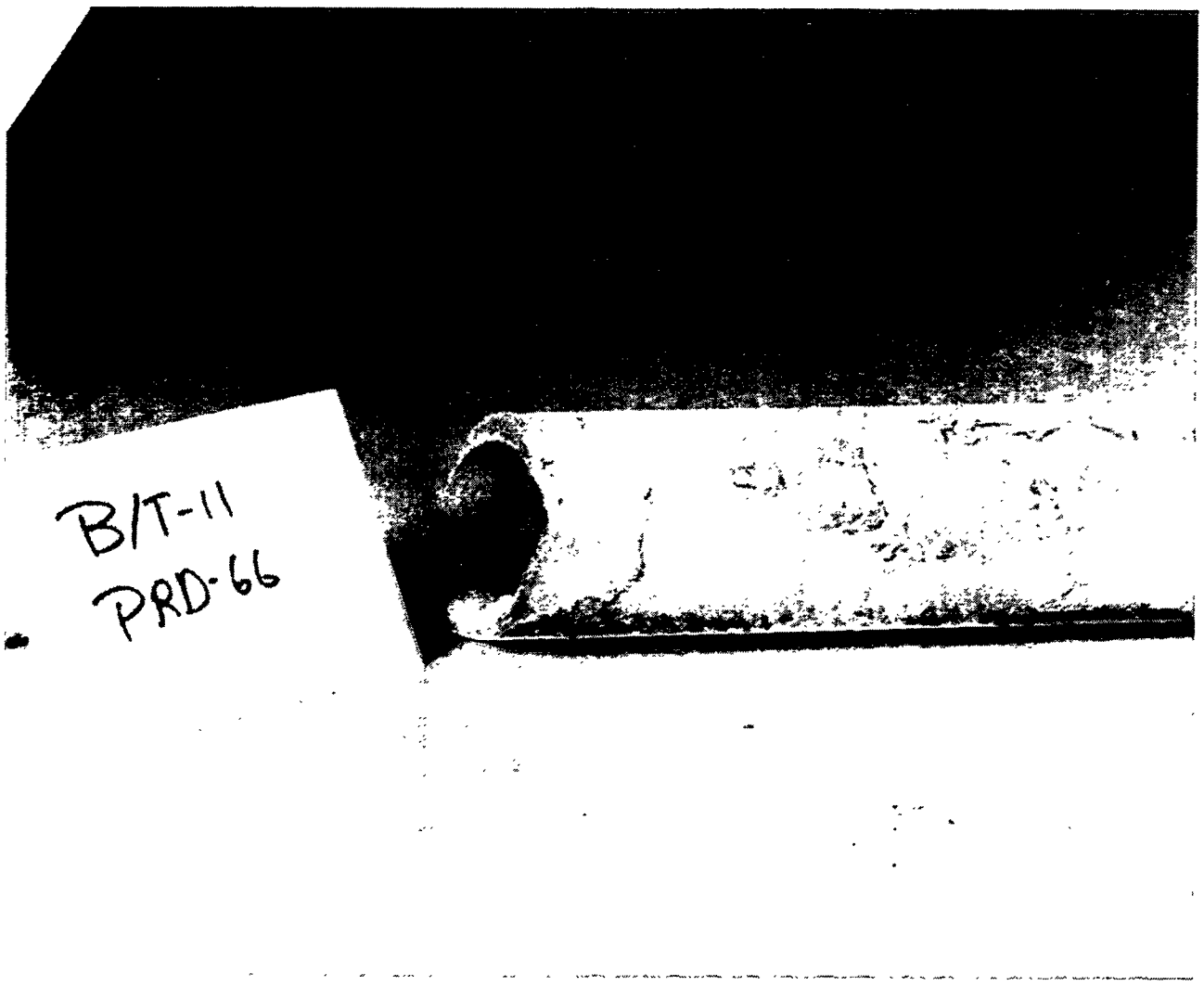

Figure 6b — Divot Formations Along The Fractured Surfaces Of The Failed DuPont PRD-66 Filter Elements In Test Segment #5

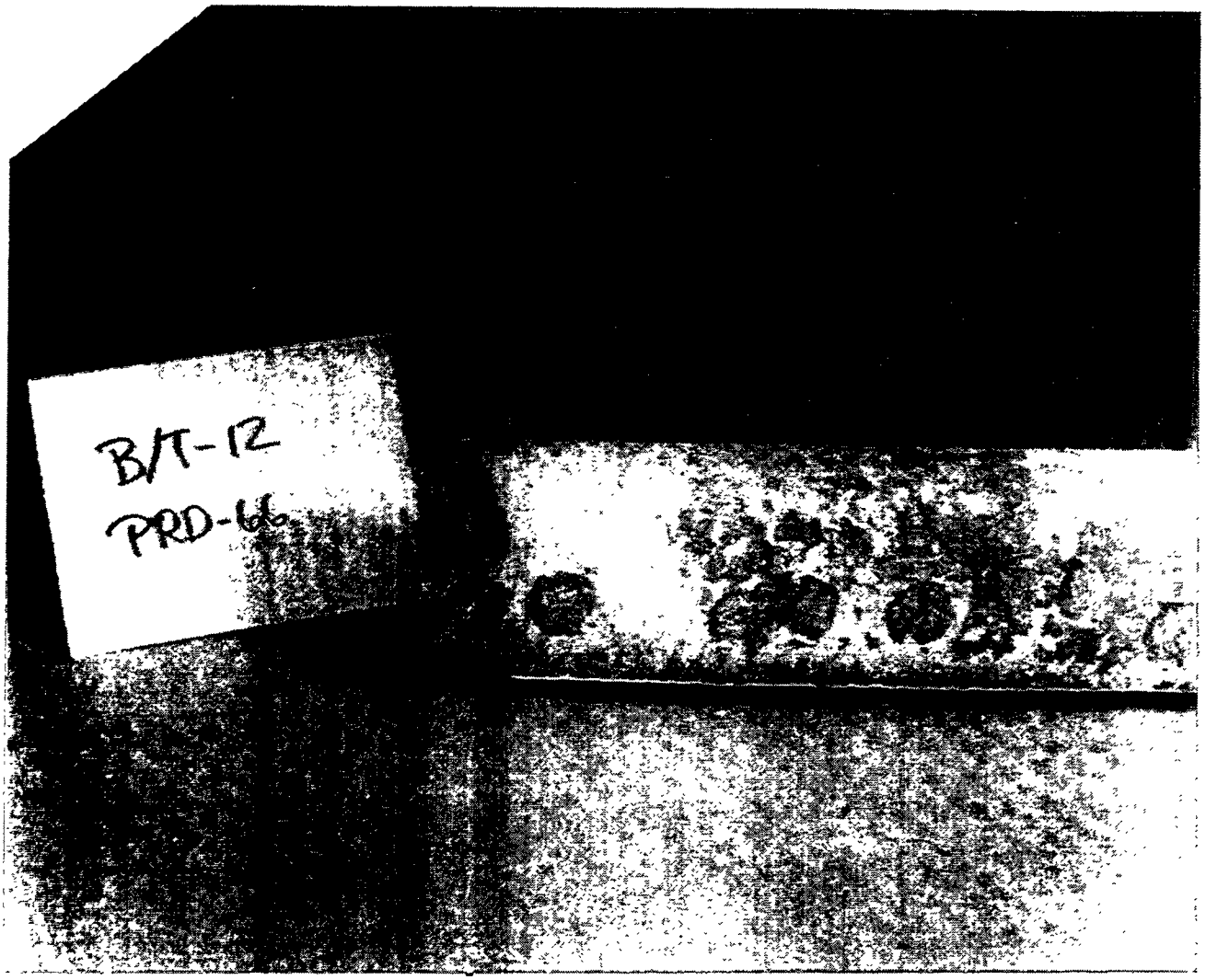

Figure 6c – Divot Formations Along The Fractured Surfaces Of The Failed DuPont PRD-66 Filter Elements In Test Segment #5

The thickness of the ash deposit along the DuPont PRD-66 candle filter varied ranged from areas of the filter element that were completely clean, to areas which contained 1-2 mm of ash (i.e., 0.25 mm (0.01 inch) at the top of the filter; 0.76 mm (0.03 inch) at the mid-section of the filter; and 1.27 mm (0.05 inch) at the bottom of the filter). Raised hardened flakes of ash were frequently observed along the filter body adjacent to the divot areas.

Ash fines were present within the two remaining filter elements, filling the ID bore to depths of 120 mm (D-252, B/T-6), and 350 mm (D-237, B/T-8). Although ash filled the ID bore of the two remaining intact DuPont PRD-66 filter elements, failure of the body did not occur during the 10 plant startup and shutdown cycles which occurred during conduct of Test Segment #5. Failure had been observed along the end caps of a Coors alumina/mullite and Schumacher Dia Schumalith F40 candle filter which had similarly been filled with ash. One interesting observation which was made was that the two remaining full length DuPont PRD-66 filter elements were positioned below the plenum pulse pipe inlet.

A reddish stain was detected along the top array dust sheds, directly below each candle filter element. The stain appeared as a stripe formation, ~100 mm (4 inches) wide. An initial observation appeared to indicate that the top array had a significantly more pronounced series of the red stripes, but when more critically evaluated, the red stripes were also present along the middle array shed. A fresh layer of dust covered the middle array sheds, possibly as a result of the ash sampling efforts which were performed immediately after the W-APF lift on May 11, 1995.

Due to the nature of the stripe formation, condensation was suggested by DuPont personnel during their visit to AEP on May 15, 1995. When attempts were made to remove the reddish strain material, Westinghouse noticed that the material was present as only a very thin layer (i.e., < 1 mm thick) along the B/T dust shed. Scanning electron microscopy/energy dispersive x-ray (SEM/EDAX) analyses of the reddish stain material that was removed from both the top and middle sheds were conducted at Westinghouse.

As shown in Figure 7, the size of the top dust shed fines ranged between several microns to ~100 μm. The agglomerate shown in Photo 2, Figure 7a, was identified by EDAX to contain 6.64% Si, 4.82% Al, 4.61% S, 4.60% Mg, 3.41% Ca, 2.06% Fe, 0.64% K, 0.25% Ti, and 72.98% O (i.e., atomic percent basis; absence of carbon in the reported qualitative compositions). Similarly the ~100 μm agglomerate shown in Photo 3, Figure 7b, was identified to contain 7.16% Mg, 6.02% Si, 5.03% Al, 4.45% Ca, 4.20% S, 1.43% Fe, 0.20% K, 0.20% Ti, and 71.31% O, while the <5 μm particle shown in Photo 4, Figure 7b, was identified to contain 9.00% Mg, 5.32% S, 4.27% Ca, 3.51% Si, 1.77% Al, 1.54% Fe, 0.44% K, 0.06% Ti, and 74.07% O. At an alternate location, the fines were identified to contain 12.23% Ca, 10.26% Mg, 7.05% Si, 6.68% S, 0.88% Al, 0.28% Fe, 0.07% Ti, and 62.49% O.

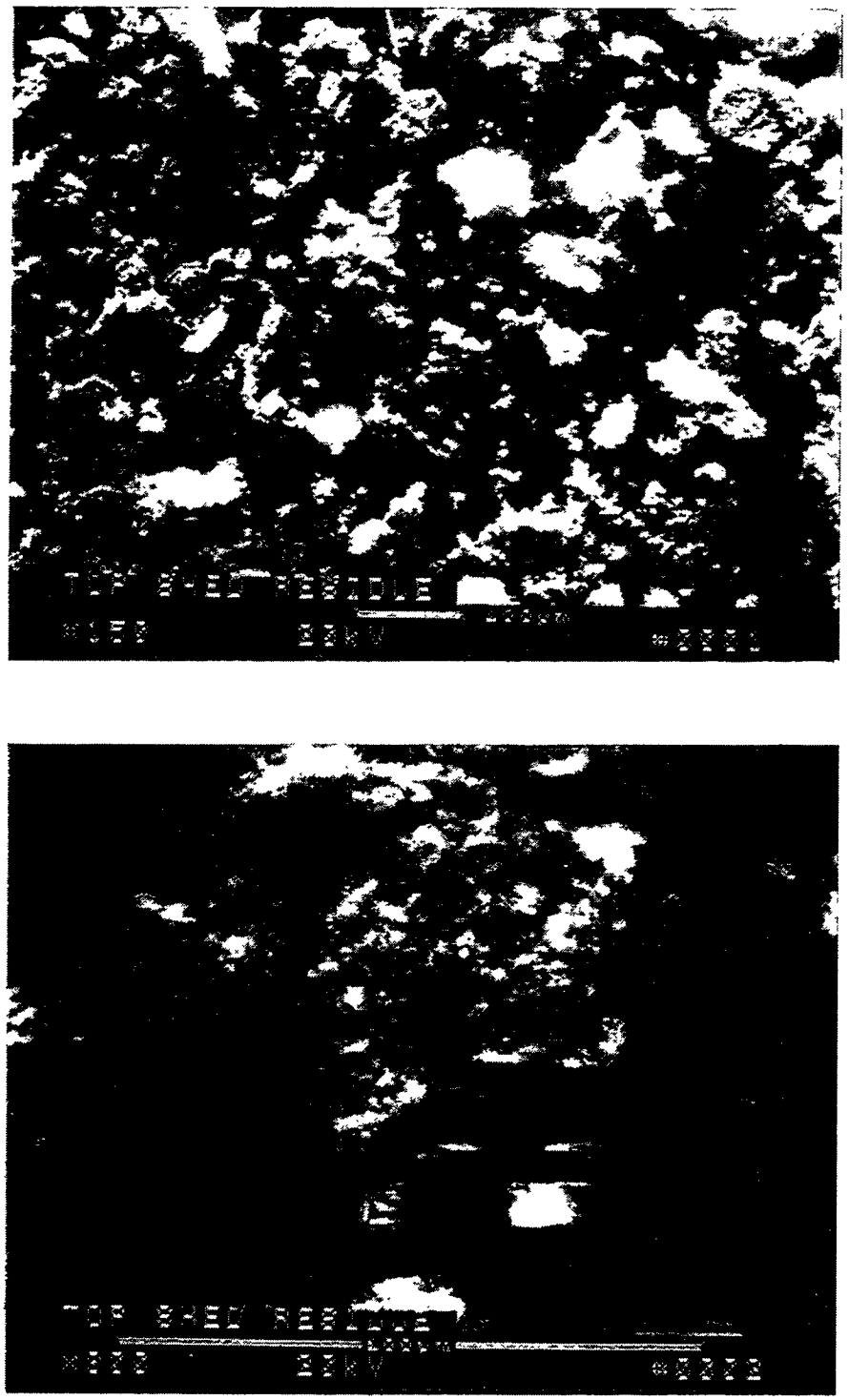

Figure 7a – Scanning Electron Micrographs Of The Red Stain Or Dust Shed Residue (B/T Array)

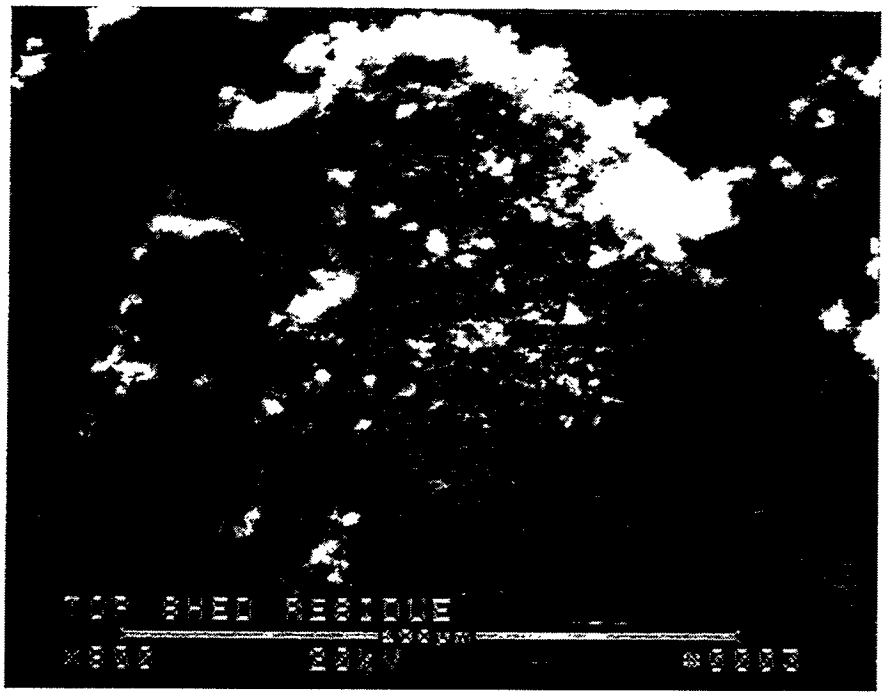

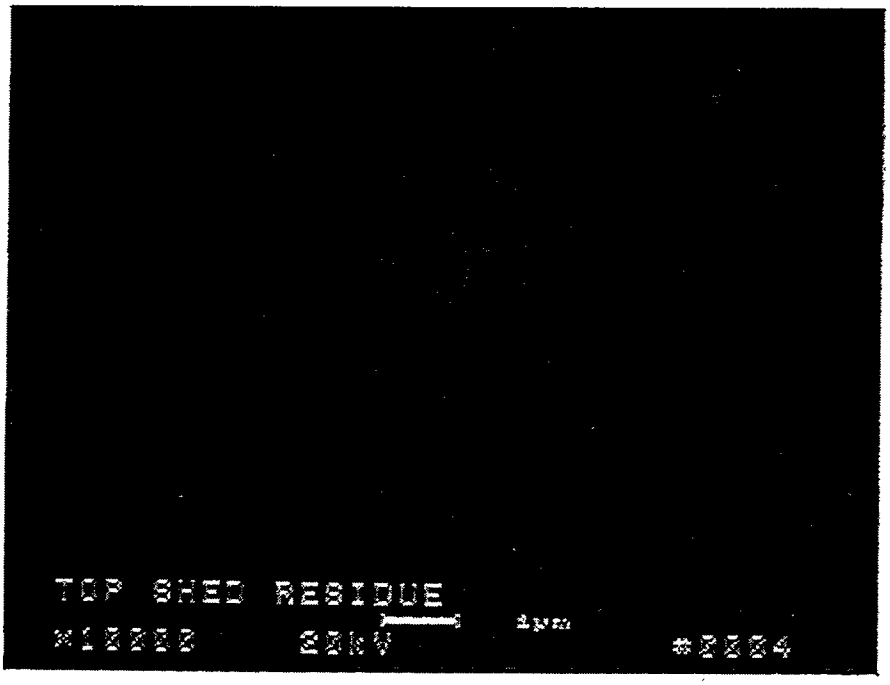

Figure 7b – Scanning Electron Micrographs Of The Red Stain Or Dust Shed Residue (B/T Array)

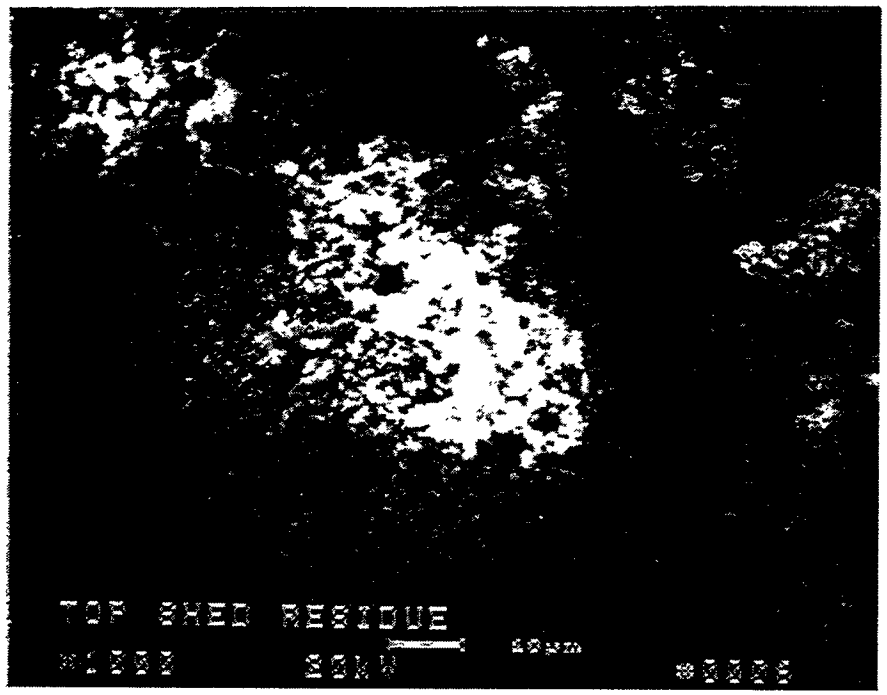

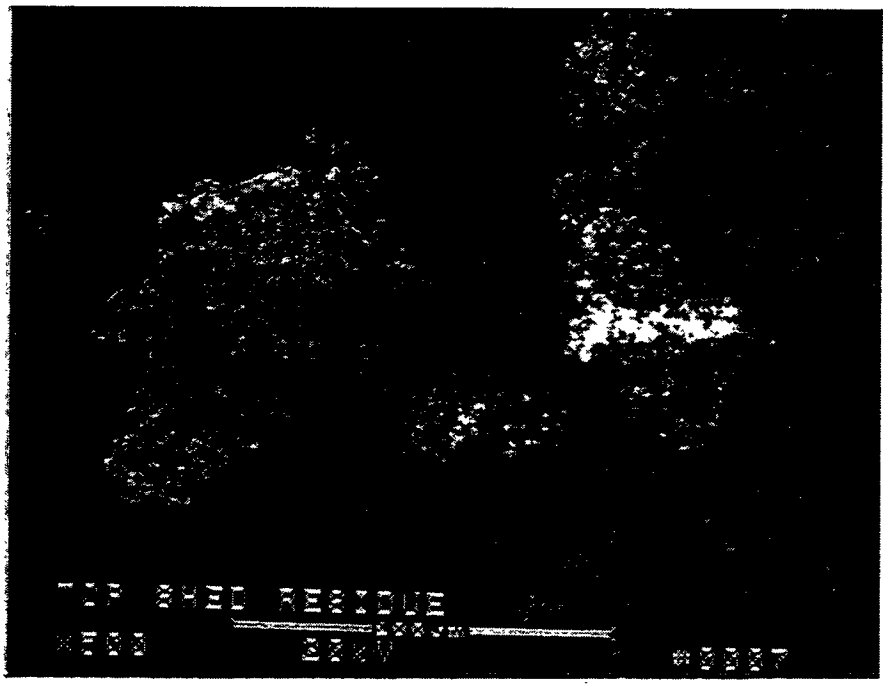

Figure 7c – Scanning Electron Micrographs Of The Red Stain Or Dust Shed Residue (B/T Array)

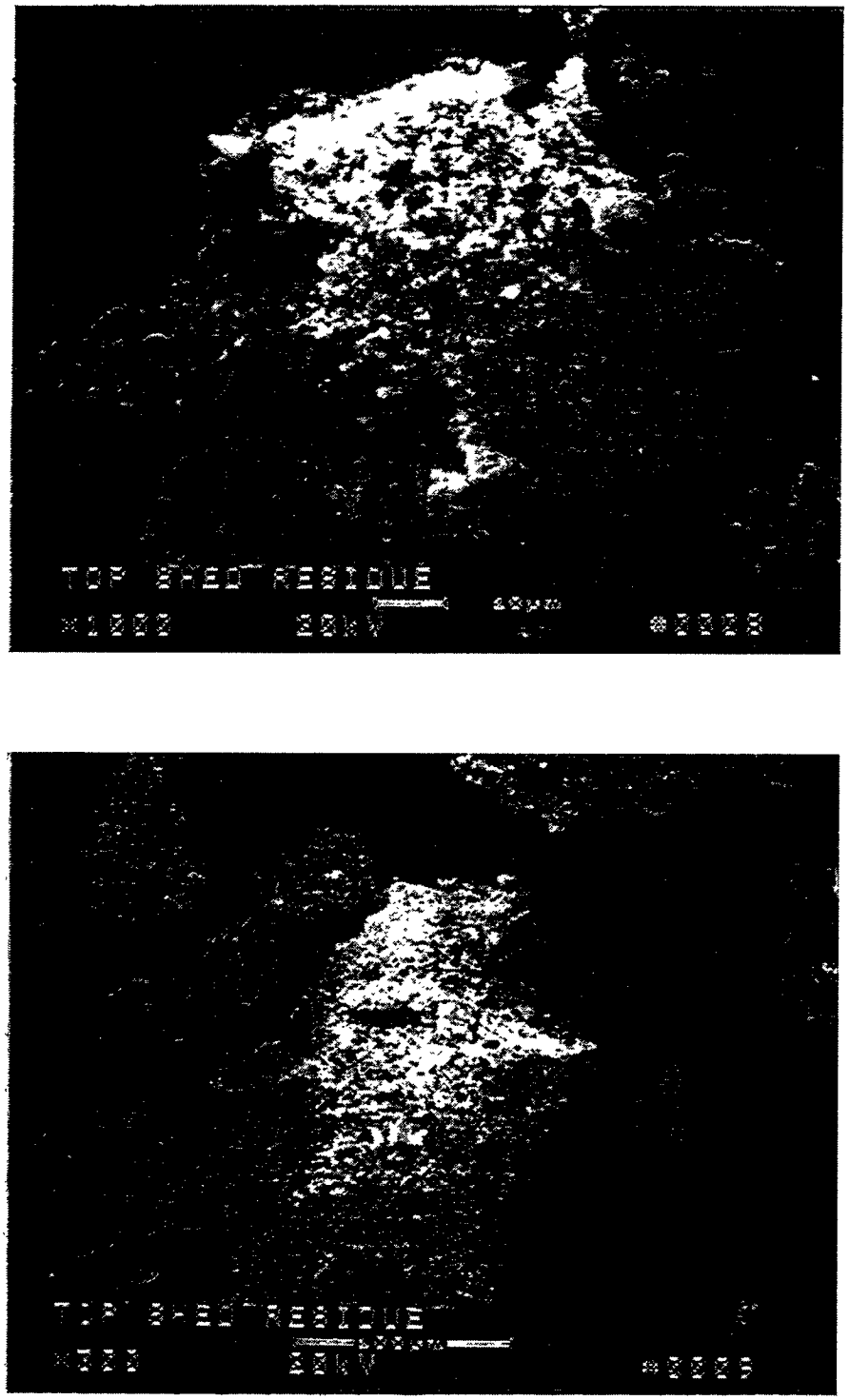

Figure 7d – Scanning Electron Micrographs Of The Red Stain Or Dust Shed Residue (B/T Array)

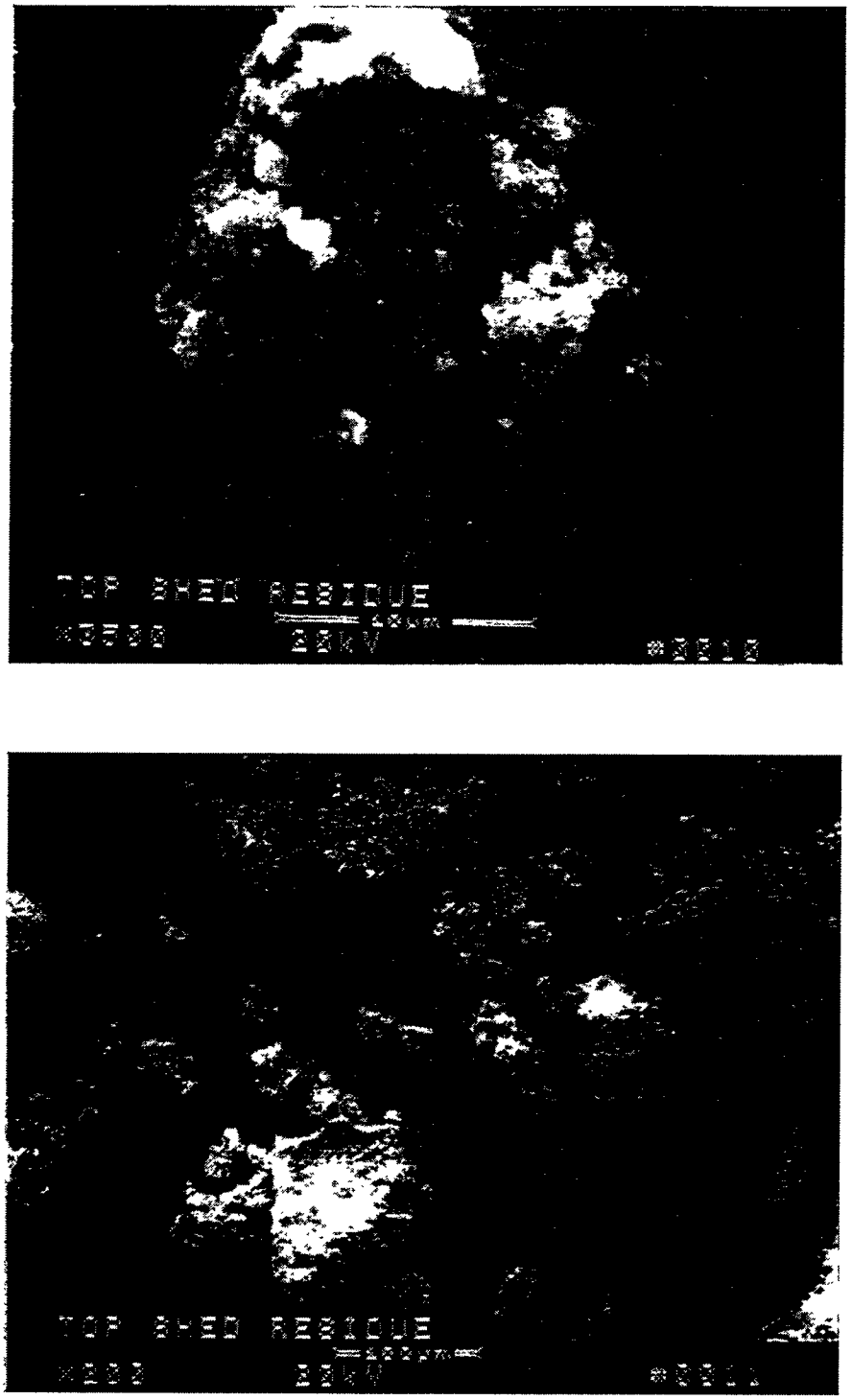

Figure 7e – Scanning Electron Micrographs Of The Red Stain Or Dust Shed Residue (B/T Array)

Additional top dust shed deposit samples were characterized. These were prepared via application of a gold coating along the surface of the fines in order to provide better resolution of the morphology of the agglomerated ash fines. The red stain typically consisted of agglomerates of densely packed sorbent, ash, or iron-enriched (i.e., ~20-30 μm particle shown in Photo 10, Figure 7e) fines.

Along the B/M dust shed, a somewhat thicker deposit of the red stripe material was present. SEM/EDAX analyses of the B/M array deposit indicated that both discrete particles, as well as agglomerates were present. The 1 mm agglomerate shown in Photo 1, Figure 8a, was identified by EDAX to contain 6.00% Ca, 5.67% S, 5.41% Si, 5.03% Al, 5.02% Mg, 1.79% Fe, 0.33% Ti, 0.25% K, and 70.50% O. Alternately the ~10 μm tightly packed or possibly sintered fines shown in Photo 2, Figure 8a, were identified to consist of 8.27% Si, 5.84% Ca, 5.83% S, 4.98% Mg, 2.78% Al, 2.05% Fe, 0.38% K, 0.08% Ti, and 69.80% O.

Additional SEMs of the material which had been removed from the B/M dust shed are shown in Figure 8b. Numerous submicron and ~10 μm fines which were present in the dust shed material, formed a relatively porous or open ash/sorbent structure. In addition, discrete, irregularly shaped fines were also present in the middle dust shed material (Figures 8c and 8d).

As opposed to acid or moisture condensation dripping from the candles, particularly along the top array as suggested by DuPont personnel, Westinghouse considered the fact that during dust cake removal, particularly during pulse cleaning, fines were released from the candle filter, which then fell and impacted the sheds — primarily directly below each filter element. The fines naturally tracked in an ~100 mm band below each candle, with minimal impact along the shed, in between adjacent candle filters. The reason why the stripe formation had not been observed in previous test segments at Tidd was most likely due to the extensive ash bridges which formed between the filter elements, as well as along the dust shed and plenum pipes, masking any evidence of ash impact along the dust sheds.

Difficulty was encountered when the remaining full length filters were removed from the filter holders. During disassembly of D-252 in B/T-6, fracture occurred below the flange, similar to where failure of the filters occurred during field operation.

Consideration was given to the possibility that D-252 in B/T-6 had been held in position by the ash cake which was lodged in between the gasketed filter and the sample holder. Prior to disassembly of D-237 in B/T-8, the candle was observed to be tightly held in position, and was most probably intact. During disassembly, the candle was removed from the holder as an intact filter element.

During disassembly from the filter holders, the top gaskets which were positioned above the flange of the DuPont PRD-66 filter elements were observed to have remained in their original position (i.e., no slippage along the top gasket), and were virtually clean. This implied that

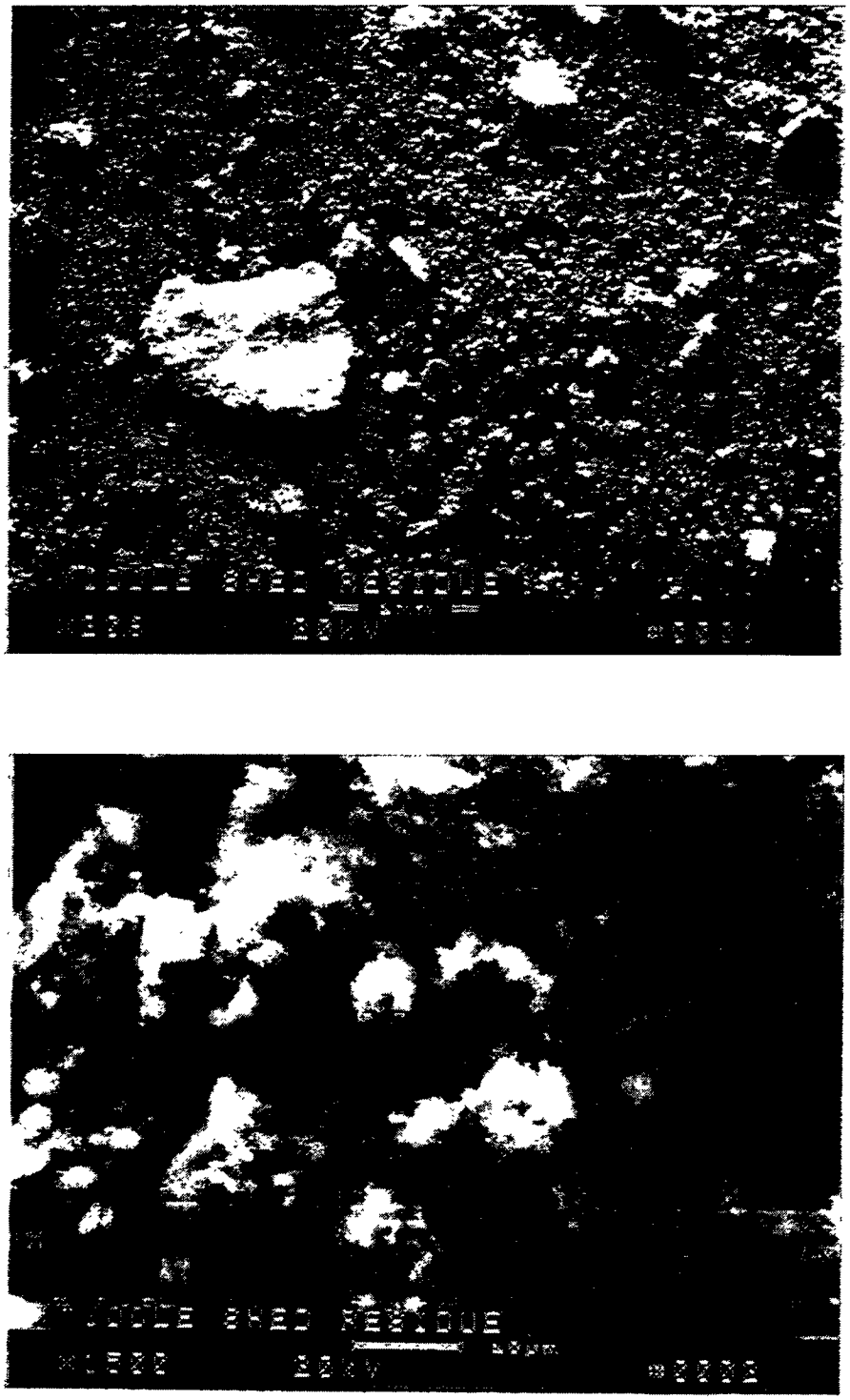

Figure 8a — Scanning Electron Micrographs Of The Red Stain Or Dust Shed Residue (B/M Array)

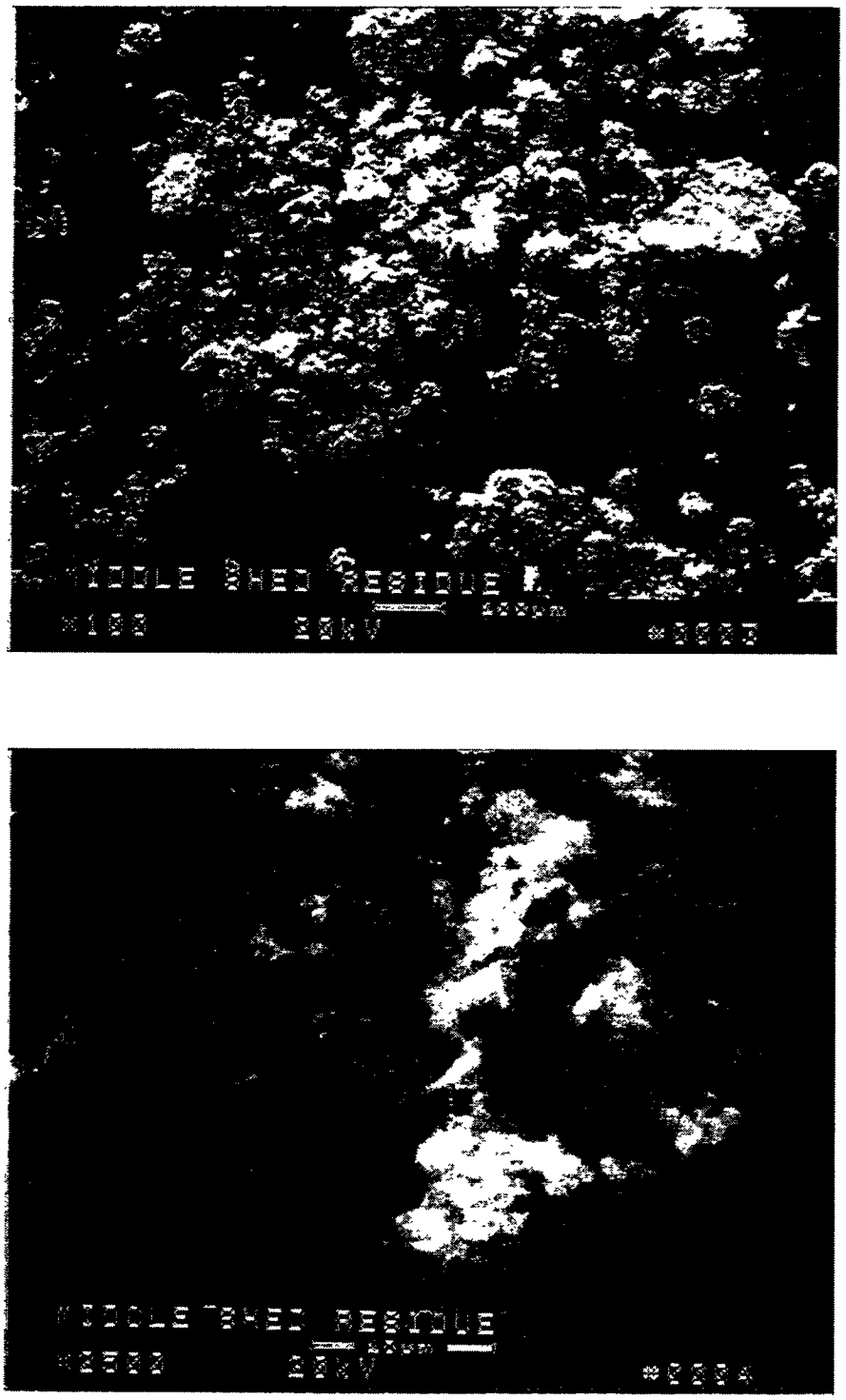

Figure 8b – Scanning Electron Micrographs Of The Red Stain Or Dust Shed Residue (B/M Array)

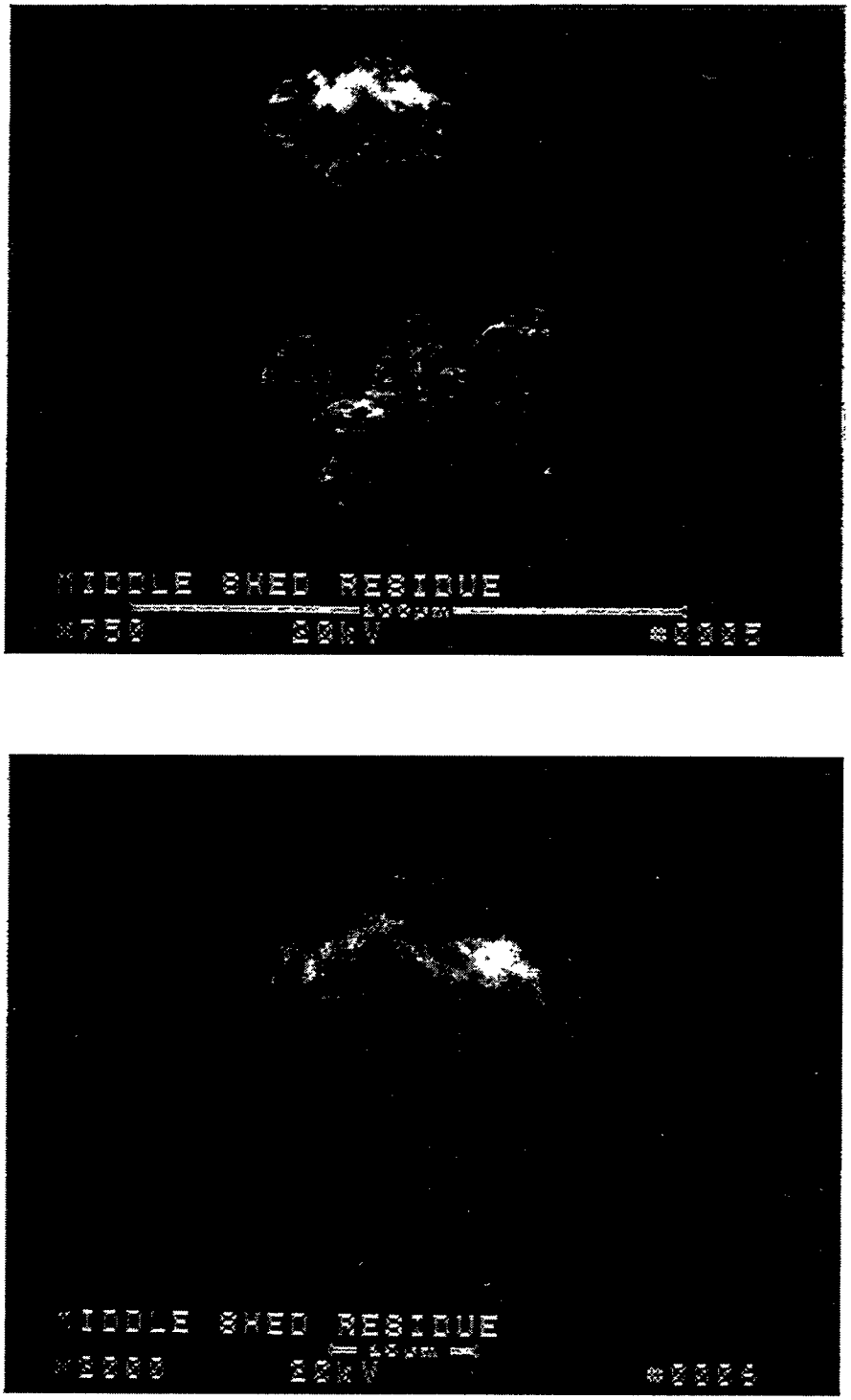

Figure 8c – Scanning Electron Micrographs Of The Red Stain Or Dust Shed Residue (B/M Array)

Figure 8d – Scanning Electron Micrographs Of The Red Stain Or Dust Shed Residue (B/M Array)

adequate and complete dust sealing had been achieved during testing in Test Segment #5 at Tidd. In order to confirm that the proper hardware had been used during assembly of the DuPont PRD-66 filter array, all bottom holder mounts and top rings were inspected. All hardware was confirmed to have been the specially designed components for use with the PRD-66 filter elements, and therefore failure of the DuPont PRD-66 filter array was dismissed on the basis of possible inadequate hardware use.

PRD-66 FAILURE MECHANISMS

In contrast to Test Segment #4 which was conducted between July and October 1994, when three DuPont PRD-66 were installed in the B/M array and were successfully operated for 1705 hours at AEP (Table 1), twenty out of the twenty-two PRD-66 filter elements failed in Test Segment #5 (i.e., January through March 1995). From a review of the operating data, failure of the PRD-66 filter elements appeared to have occurred after ~232 hours of operation, since sections of the PRD-66 matrix were identified in the ash hopper discharge. Testing continued, and after ~775 hours of operation at AEP, additional sections of the PRD-66 filter matrix were evident in the ash hopper discharge.

The DuPont PRD-66 filter elements suffered three distinct failure modes during operation in the W-APF at AEP during Test Segment #5. These included:

- Failure at the flange
- Mid-body fracture
- Divoting.

With respect to failure at the flange, a brittle fracture appeared to have resulted. As observed during removal of the failed section, the flange was tightly held in the filter holder, and frequently cracked during removal from the holder mount. Additional strength may be required in this area of the candle, in order for the PRD-66 candle filter to survive the tight clamping and constrained features observed when the elements are subjected to a PFBC environment which carries tenaciously adhering ash to the mount and sealing surface.

When the three PRD-66 elements were placed in the B/M array in Test Segment #4, the tenaciously adhering ash was not present, and permitted much easier removal of the elements from the holder mounts. Although the adhering ash made it extremely difficult to remove the filter flange segments, the question which still remains is whether ash "pinning" or binding was responsible for failure at the flange.

Since ash bridging was not evident within the W-APF system in Test Segment #5, a cantilever force applied at the bottom of the element, was not considered to be responsible for failure at the base of the PRD-66 filter element's flange. What may have contributed to filter failure was either production of a weakened area below the flange during manufacturing of the

TABLE 1
WESTINGHOUSE PFBC HOT GAS FILTER TESTING AT AEP

PFBC Test Segment	1 10/92 - 12/92	2 7/93 - 9/93	3 1/94 - 4/94	4 7/94 - 10/94	5 1/95 - 3/95
Operating Time, Hrs	464	1295	1279	1705	1110
Operating Temperature, °C	730 - 790	620 - 790	650 - 780	660 - 760	760 - 845
Filter Elements	384	384	384	288	288
Schumacher F40	384	384	384	258	5
Schumacher FT20	—	—	—	8	—
Pall Vitropore 442T	—	—	—	8	153
Coors Alumina/Mullite	—	—	—	8	98
3M CVI-SiC Composite	—	—	—	3	10
DuPont PRD-66	—	—	—	3	22

filter elements, or delivery of a substantially higher intensity and more frequently delivered pulse cycle to the top candle filter arrays. The rather "flexible" nature of the PRD-66 filter matrix may have been adequate to flex the candle to the point of fracture below the flange area. Discussions have been initiated with DuPont in an effort to possibly strengthen the candle's flange area in order to possibly alleviate this issue.

The pitting or divoting issue may have resulted from abrasion of the intact and/or fractured PRD-66 filters from either pulse cleaning gas released from adjacent failed filter elements, or from gas/particle flow paths which resulted along the top array. The rationale behind this scenario is that the positions of the divots were located along the length of the filter element, running nearly parallel down the length of the filter body. The location of the divots are "off-center" from the section of the body that was tangent to the plenum. An alternate "divot" scenario was offered by DuPont personnel who considered the possibility of condensation and collection of material below the membrane which subsequently caused a "pot-hole" phenomena to occur during plant shutdown. The argument which appears to negate this scenario is that the position of the divots is "off-center" down the length of the body, and appears to be a non-random phenomena along the length of the candle body.

One final scenario for divot formation shall be considered. That is the frequent delaminations between layers that were evident when the DuPont PRD-66 filter wall was cross-sectioned. The location of the delamination closely resembled divot depths that resulted during process operation. The unique straight line alignment may represent a "drying" line as the element was positioned or handled during manufacturing. Further confirmation with DuPont personnel is required to discuss what may perhaps be proprietary manufacturing procedures.

Typically the normal failure of the PRD-66 filter matrix is expected to result in a "step" or "staircase" profile. Examination of the fractured candle filter segments (i.e., one-half to three-quarters below the flange) appeared to indicate that opposed to the "step" or "staircase" profile, a shear plane resulted near the fractured surface. This implied that the wall had thinned in the area of a divot, which ultimately weakened and resulted in failure. Failure along the weakened area of the filter body may also have been enhanced if ash were present within the ID bore of the PRD-66 filter element. Once again, the formation of the divots, as considered by Westinghouse, were presumed to have resulted from contact of the filter elements with fines entrained in the pulse cleaning gases which were emitted from adjacent failed filter elements, and/or the gas/particle flow paths which resulted in the top array(s). This returns to the original question as to why the filters initially failed below the flange area.

COMMENT

Hydrogen sulfate was perceived to be detected at a low concentration near the filter array. This odor was more pronounced when DuPont personnel visited AEP on May 15, 1995, than at alternate times. Westinghouse considered the fact that the metal cutting which utilized arc gouging

APPENDIX G

CHARACTERIZATION OF THE OXIDE-BASED FILAMENT WOUND DuPONT PRD-66 FILTER MATRIX

M. A. Alvin
July 10, 1995

INTRODUCTION

Three DuPont PRD-66 filament wound candle filters were installed in the Westinghouse Advanced Particulate Filter (W-APF) system in Test Segment #4. These filters successfully were operated for 1705 hours without failure. An additional twenty-two DuPont PRD-66 filter elements were installed in the W-APF for use in Test Segment #5. After completing 1110 hours of pressurized fluidized-bed combustion (PFBC) operation in Test Segment #5, two PRD-66 filters remained intact, four suffered either mid-body or three-quarter body length failure, and sixteen elements fractured at the base of the flange. In this report, we will focus on

- Identifying the construction, composition, and morphology of the as-manufactured DuPont PRD-66 filter element.
- The response of the matrix to the PFBC conditions in Test Segment #5.
- A preliminary understanding of the divot formations which resulted along the outer wall of the PRD-66 filter in Test Segment #5.
- The response of the matrix to the PFBC conditions in Test Segment #4.

AS-MANUFACTURED FILTER MATRIX

The oxide-based, filament wound, DuPont PRD-66 matrix consists of a layered cordierite, mullite, cristobalite, and corundum microstructure. An amorphous phase is also present in the as-manufactured PRD-66 filter matrix. Due to the differences in the thermal coefficient of expansion for mullite, cordierite, and corundum which are present in the PRD-66 matrix, a microcracked structure is formed after high firing.

The "diamond" pattern weave of the polycrystalline refractory oxide-based fibers forms the ~7 mm structural support layer of the DuPont PRD-66 filter matrix. A thin membrane layer is wrapped along the outer surface of the support matrix, producing a light weight, bulk filter element.

The scanning electron micrographs (SEM) shown in Figure 1a illustrates the morphology of the DuPont filament wound PRD-66 filter membrane. The membrane is shown at higher magnification in Figure 1b. Area 1, Photo 43, Figure 1b, which is shown at higher magnification in Photo 44, Figure 1c, was identified by energy dispersive x-ray analysis (EDAX) to contain 38.42% Si, 30.38% O, 16.86% Al, and 14.34% Mg (i.e., atomic percent basis). Similarly, Area 2, Photo 43, Figure 1b, is shown at higher magnification in Photo 45, Figure 1c, and was identified by EDAX to contain 52.75% Al, 41.41% O, 4.92% Si, and 0.92% Mg (i.e., primarily an alumina-

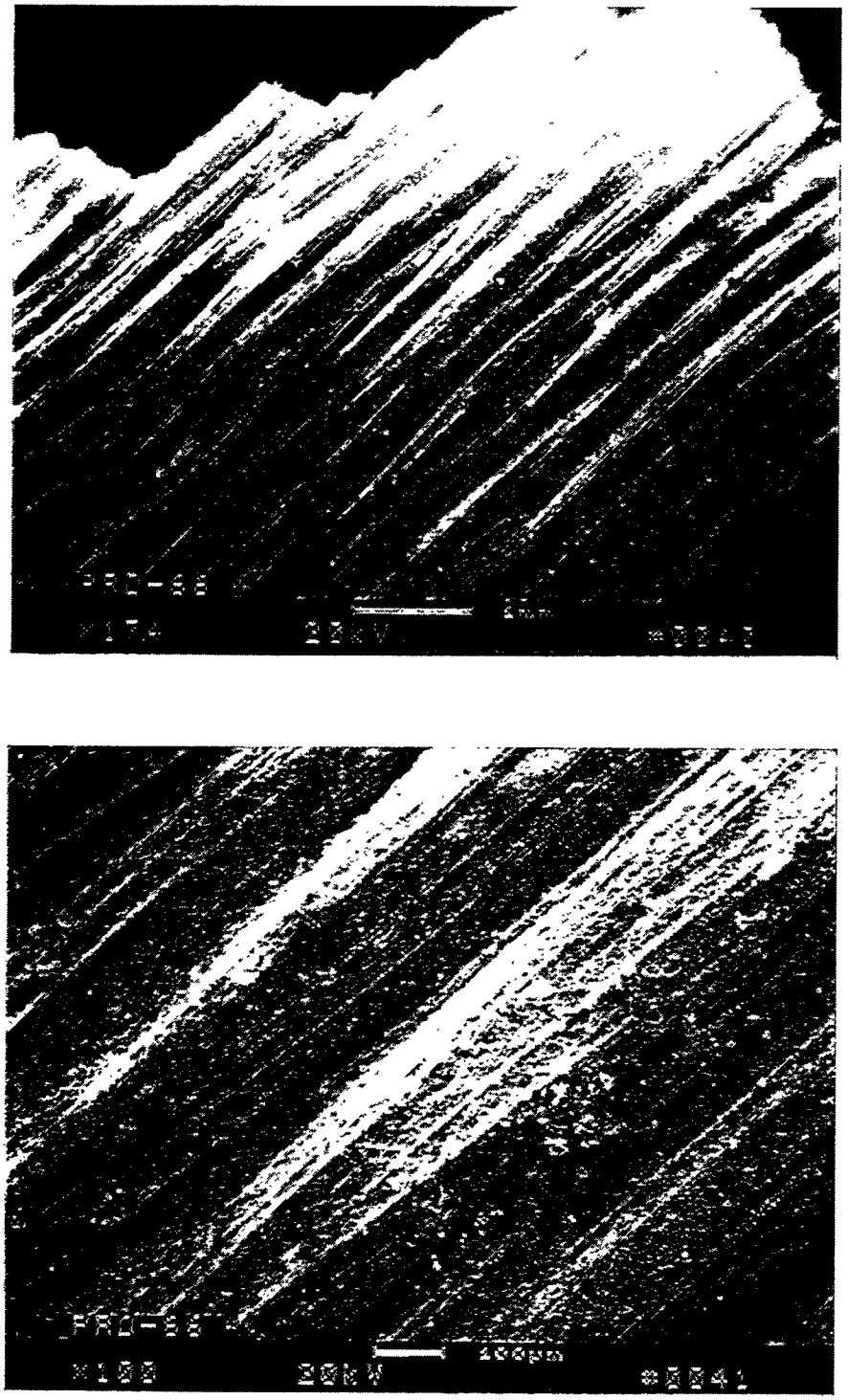

Figure 1a — Outer Membrane Surface Of The As-Manufactured DuPont PRD-66 Filter Element

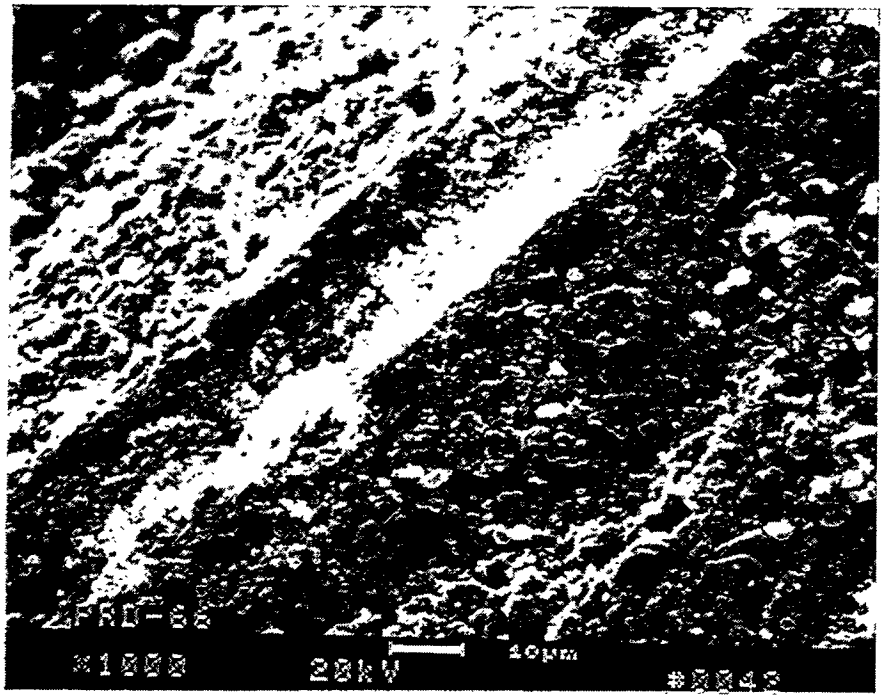

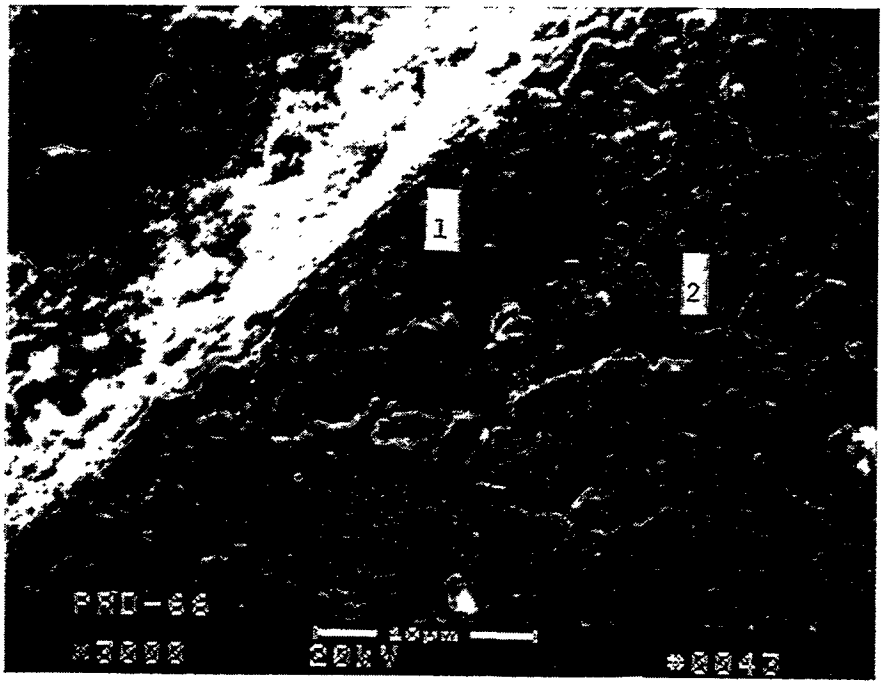

Figure 1b – Higher Magnification Micrographs Of The Outer Surface Membrane Of The DuPont PRD-66 Filter Element

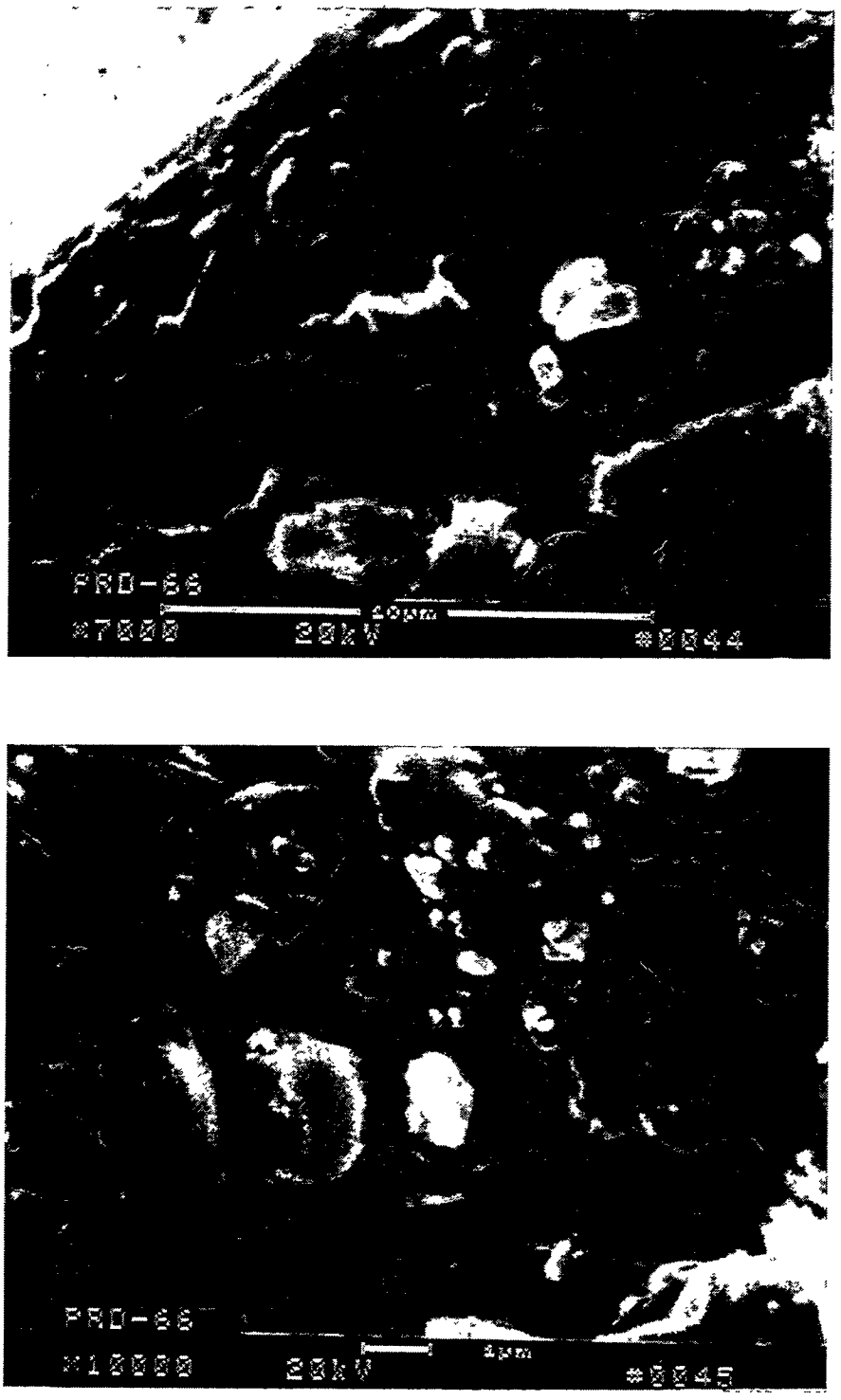

Figure 1c – Polycrystalline Nature Of The Outer Surface Of The DuPont PRD-66 Filter Membrane

Figure 1d – Fractured DuPont PRD-66 Filter Matrix Showing The Numerous Fibers In The Membrane Layer

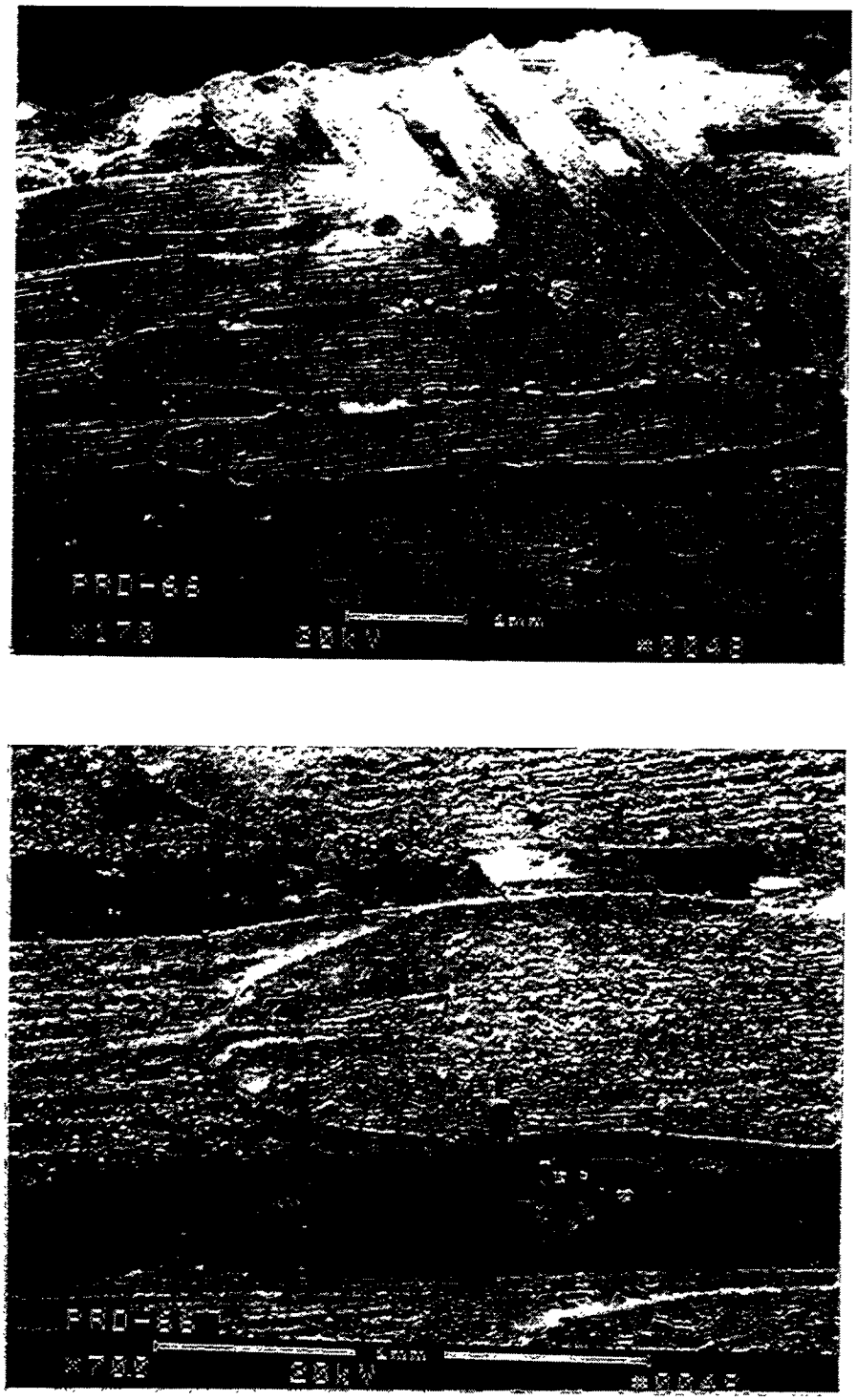

Figure 1e – Filament Wound Matrix Of The DuPont PRD-66 Filter Element

Figure 1f – Alumina-Enriched Mud Crack Areas Along The Filament Wound Matrix Of The DuPont PRD-66 Filter Element

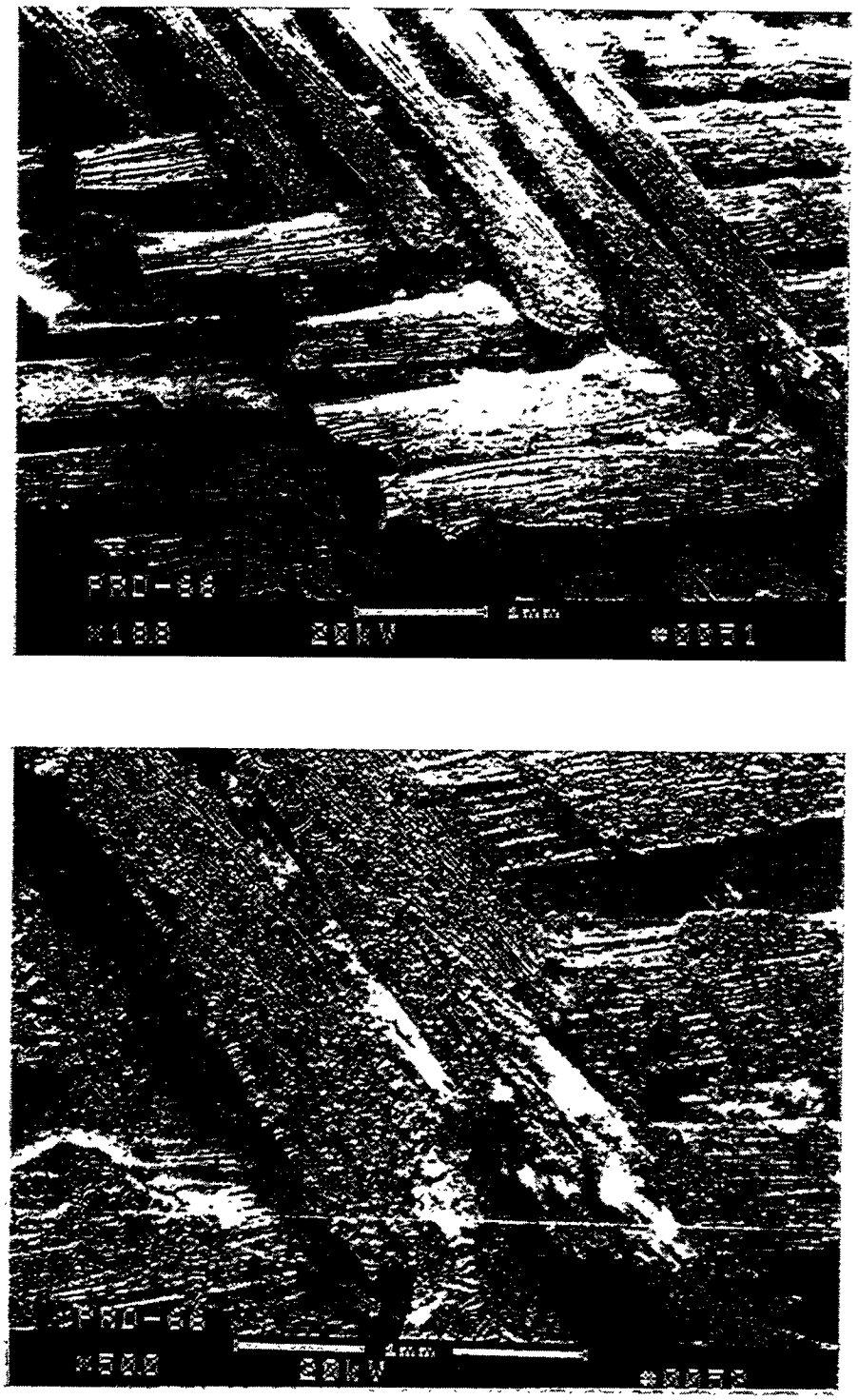

Figure 1g – Alternate Location Along The ID Surface Of The Filament Wound DuPont PRD-66 Filter Matrix

enriched matrix, containing cordierite, and possibly cristobalite and/or mullite). When fresh fractured, the fiber bundles in the filament wound membrane layer become apparent (Figure 1d).

The filament yarns or fiber bundles which are used to manufacture the ~7 mm DuPont PRD-66 filter wall are shown in Figure 1e. Mud crack formations that are enriched with alumina (i.e., 65.15% Al, 27.89% O, 5.44% Si, and 1.53% Mg) are evident throughout the filament wound structure (Figure 1f). The alumina-enriched areas resulted from accumulation of the alumina slurry which coats and bonds the fibers together during high firing. Figure 1g provides additional micrographs of the filament wound matrix at an alternate location along the ID surface of the filter element. Each filament yarn or bundle consists of numerous fibers.

The cross-sectioned filament yarns in the ~7 mm DuPont PRD-66 filter matrix are shown in Figure 2. Typically the filament yarn diameter is 0.5 mm. The relative open porosity within the matrix is formed by the intersection of the filament bundles.

The fractured bundle shown in Area 1, Photo 5, Figure 2a, is shown at higher magnification in Photo 6, Figure 2a; in Photo 7, Figure 2b; and in Photo 14, Figure 2c. Frequently voids or holes appear to form along the center of the fibers in the as-manufactured filament yarn. A mottled texture is evident along the outer surface of the individual fibers in the filament wound bundle (Photo 16, Figure 2d; Photo 17, Figure 2e). The void formations at the center of the fibers are clearly shown in Figure 2f.

Returning to Area 2, Photo 5, Figure 2a, the outer surface of the filament is shown at higher magnification in Figures 2g and 2h. A multifaceted surface forms along the outer periphery of the filament yarn. Each faceted plane consists of numerous mullite and/or corundum or cristobalite grains (Area 1, Photo 24, Figure 2i: 45.43% O, 33.79% Al, and 20.78% Si; Photo 25, Figure 2i: 57.15% Al, 34.43% O, and 8.42% Si). Figure 2j provides additional micrographs which illustrate the morphology of the fractured filament surface. The alumina-enriched area shown in Photo 27, Figure 2j (Area 1: 49.89% Al, 39.74% O, and 10.37% Si) is expected to have resulted from the alumina slurry fillet which formed at the junction of the fractured filament and a previously adjoining filament yarn.

Figures 2k and 2l provide additional micrographs along the fractured filament wound filter wall. The alumina-enriched mud cracks, particularly in the vicinity of adjoining filaments are readily evident in Photo 29, Figure 2k, and in Photo 30, Figure 2l.

An additional fractured filament in the DuPont PRD-66 filter matrix is shown in Figures 2m and 2n. The composition at the center of the fiber shown in Area 1, Photo 33, Figure 2n, was identified by EDAX to contain 48.80% Si, 20.08% O, 18.12% Al, and 12.99% Mg.

The morphology of the filament bundle at ~3.5 mm from the OD surface of the PRD-66 filter matrix is similar to that previously described. As shown in Figure 2o, numerous fibers form the filament yarn or bundle. Each filament is ~10 μm in diameter, and is generally "sintered" or bonded to an adjacent fiber in the filament yarn. The composition of the rather amorphous matrix shown in Area 1, Photo 36, Figure 2p, and in Photo 37, Figure 2p, as identified by EDAX follows: 48.13% Al, 42.00% O, 8.22% Si, and 1.65% Mg. The point of contact between adjacent fibers

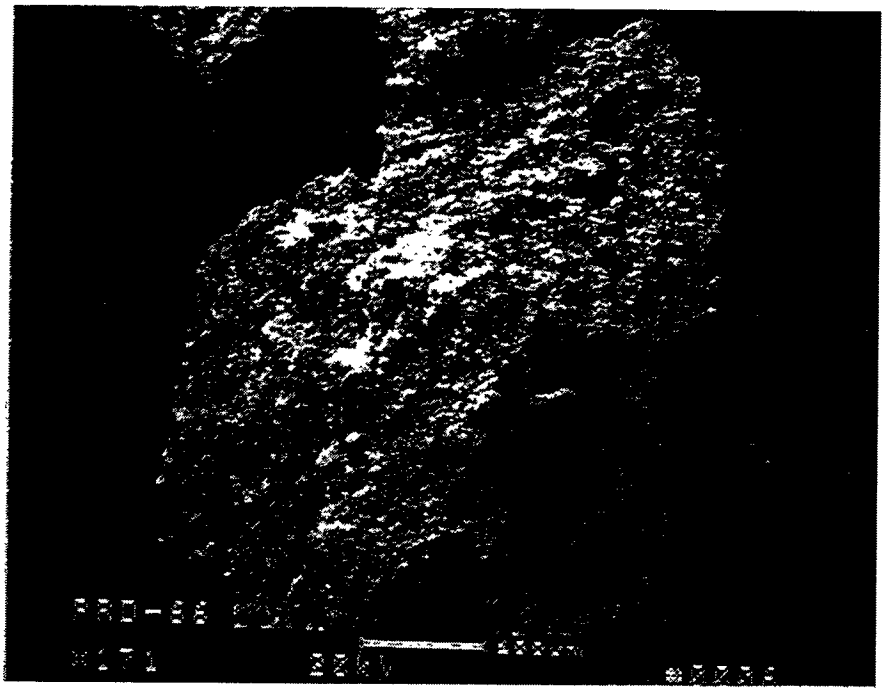

Figure 2a – Fractured Cross-Section Of The DuPont PRD-66 Filament Wound Matrix

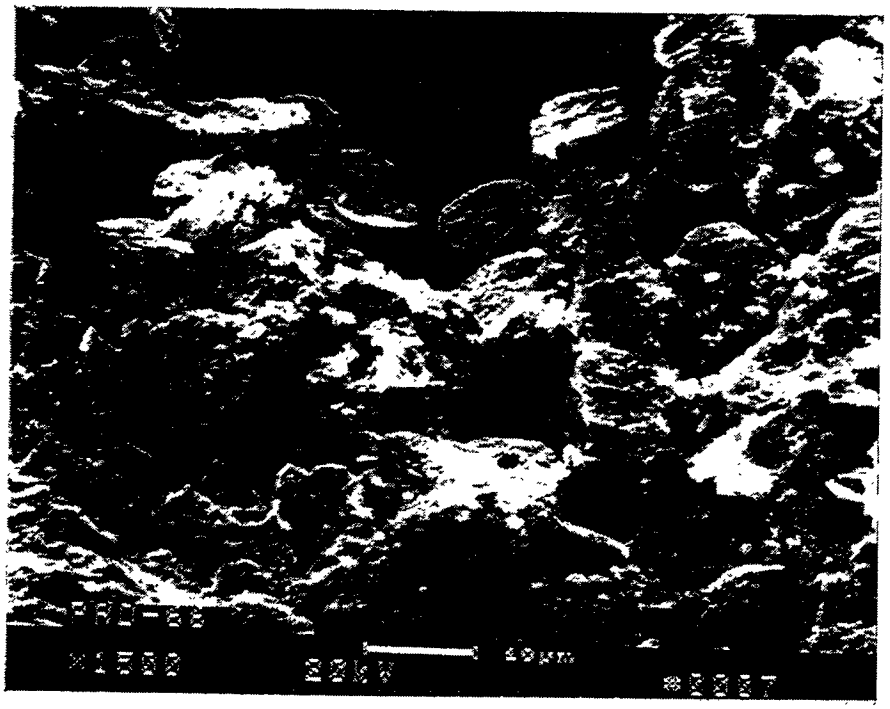

Figure 2b — Cordierite-Enriched Fibers In The DuPont PRD-66 Filament Wound Filter Matrix

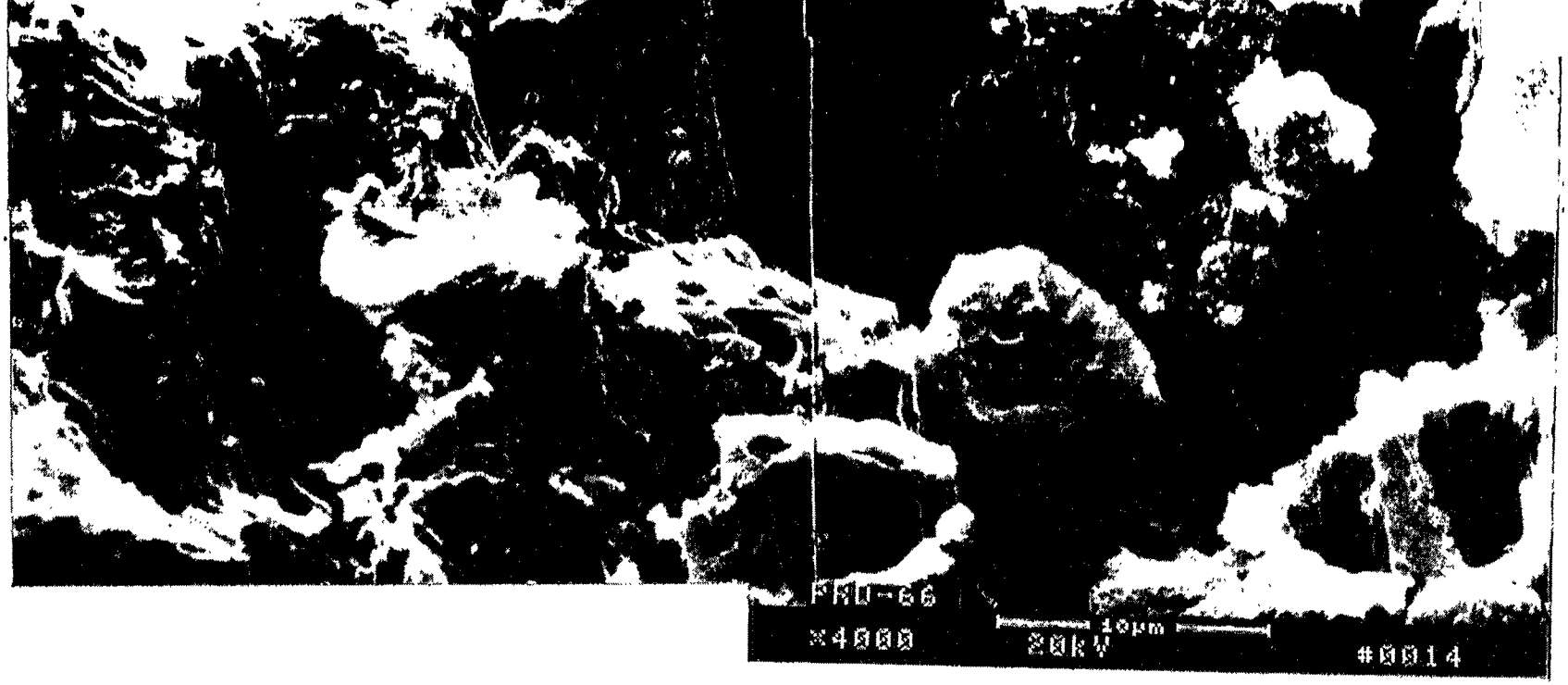

Figure 2c – High Magnification Montage Illustrating The Morphology Of The Fibers In The Filament Wound DuPont PRD-66 Filter Matrix

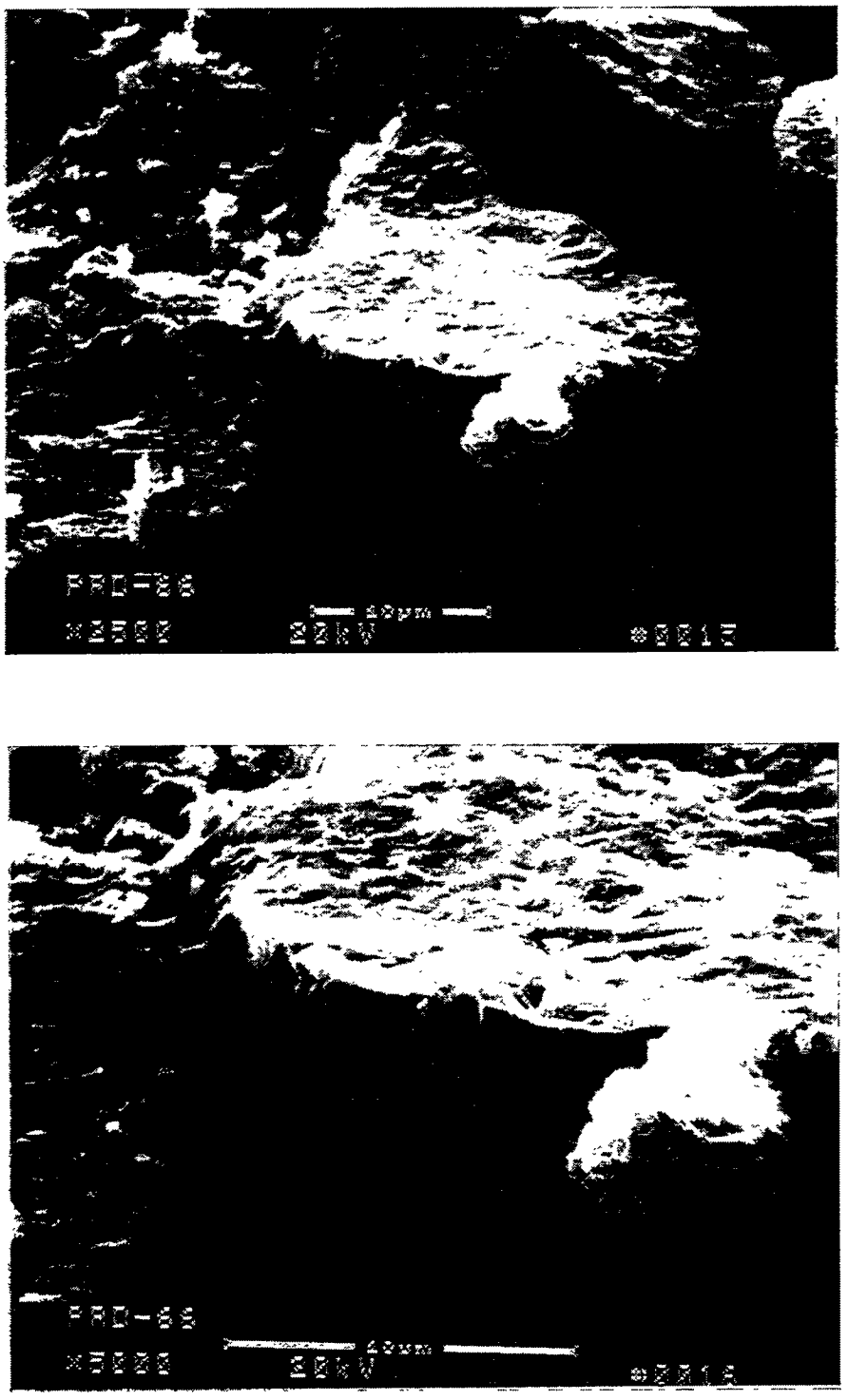

Figure 2d – Morphology Of The Fractured Fibers In The Filament Wound DuPont PRD-66 Filter Matrix. The Mottled Texture Of The Filament Surface Is Readily Evident.

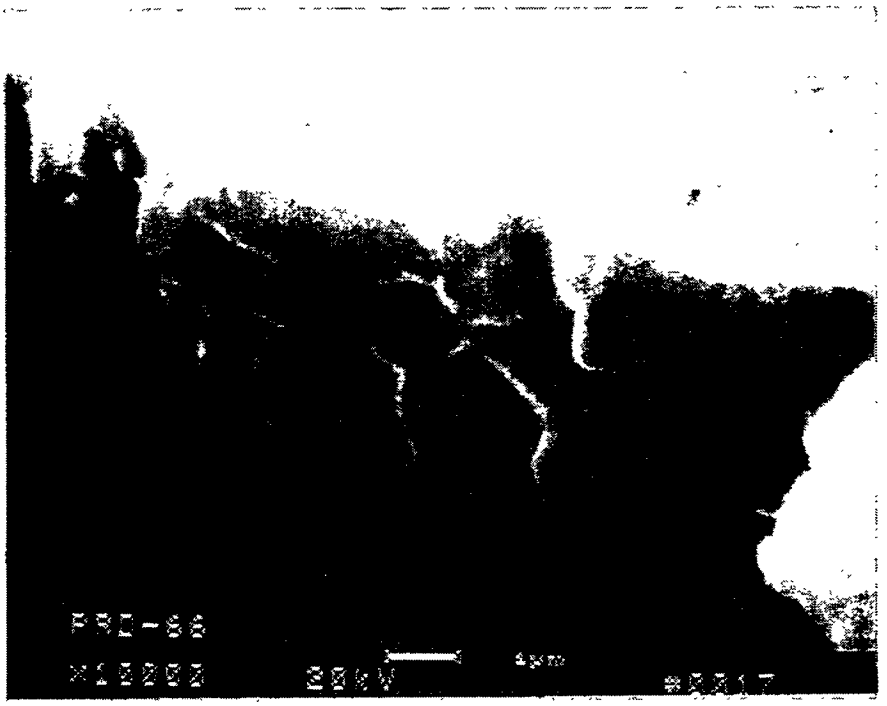

Figure 2e – Higher Magnification Micrograph Illustrating The Mottled Surface Of The Fibers In The Filament Wound DuPont PRD-66 Filter Matrix

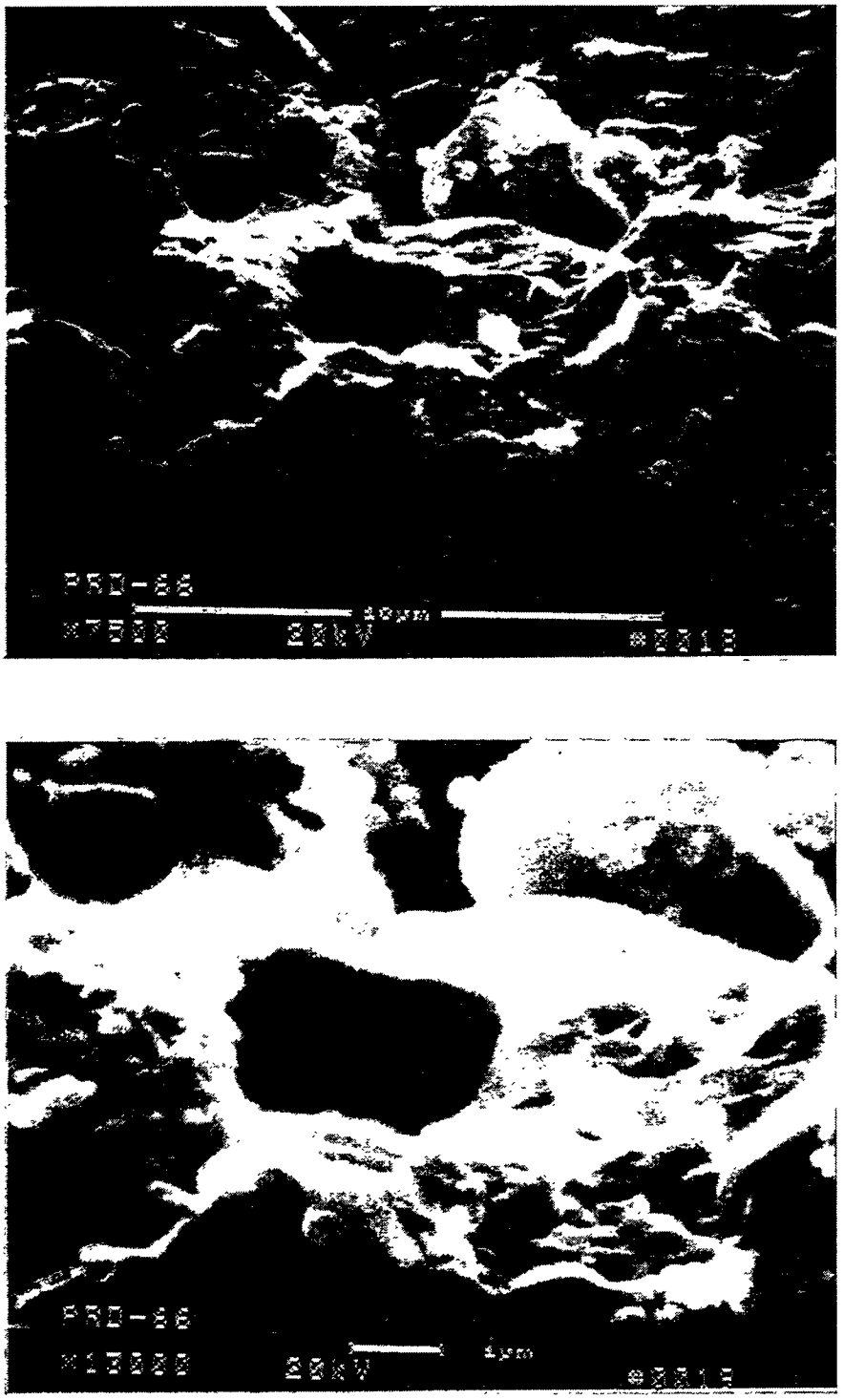

Figure 2f — Hole Formations In The Center Of The Fibers In The Filament Wound DuPont PRD-66 Filter Matrix

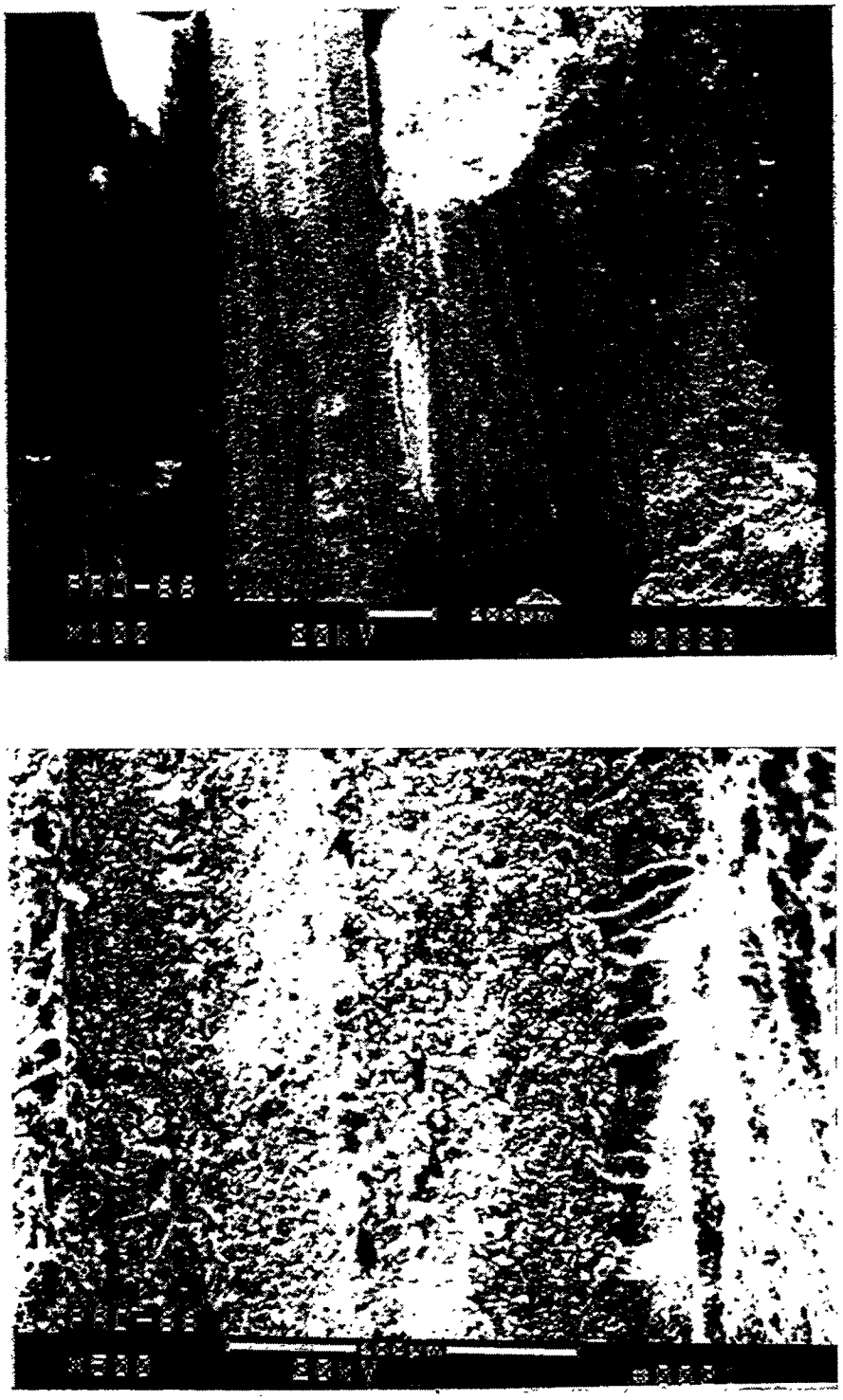

Figure 2g – Morphology Of The Outer Surface Of The Filament Fiber Bundles In The DuPont PRD-66 Filter Matrix

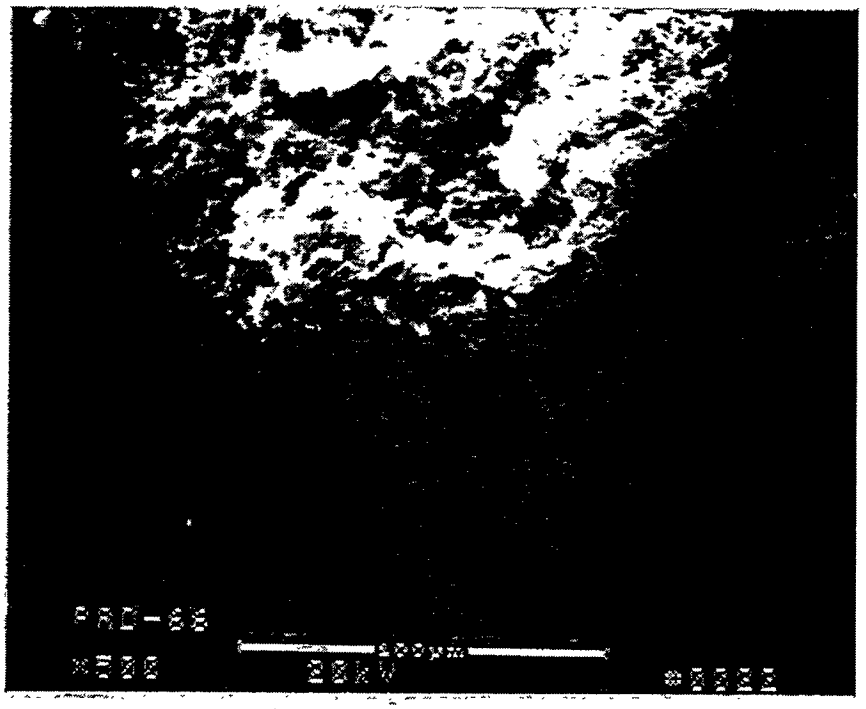

Figure 2h – Multi-Faceted Surface Of the Polycrystalline DuPont PRD-66 Filament Wound Filter Matrix

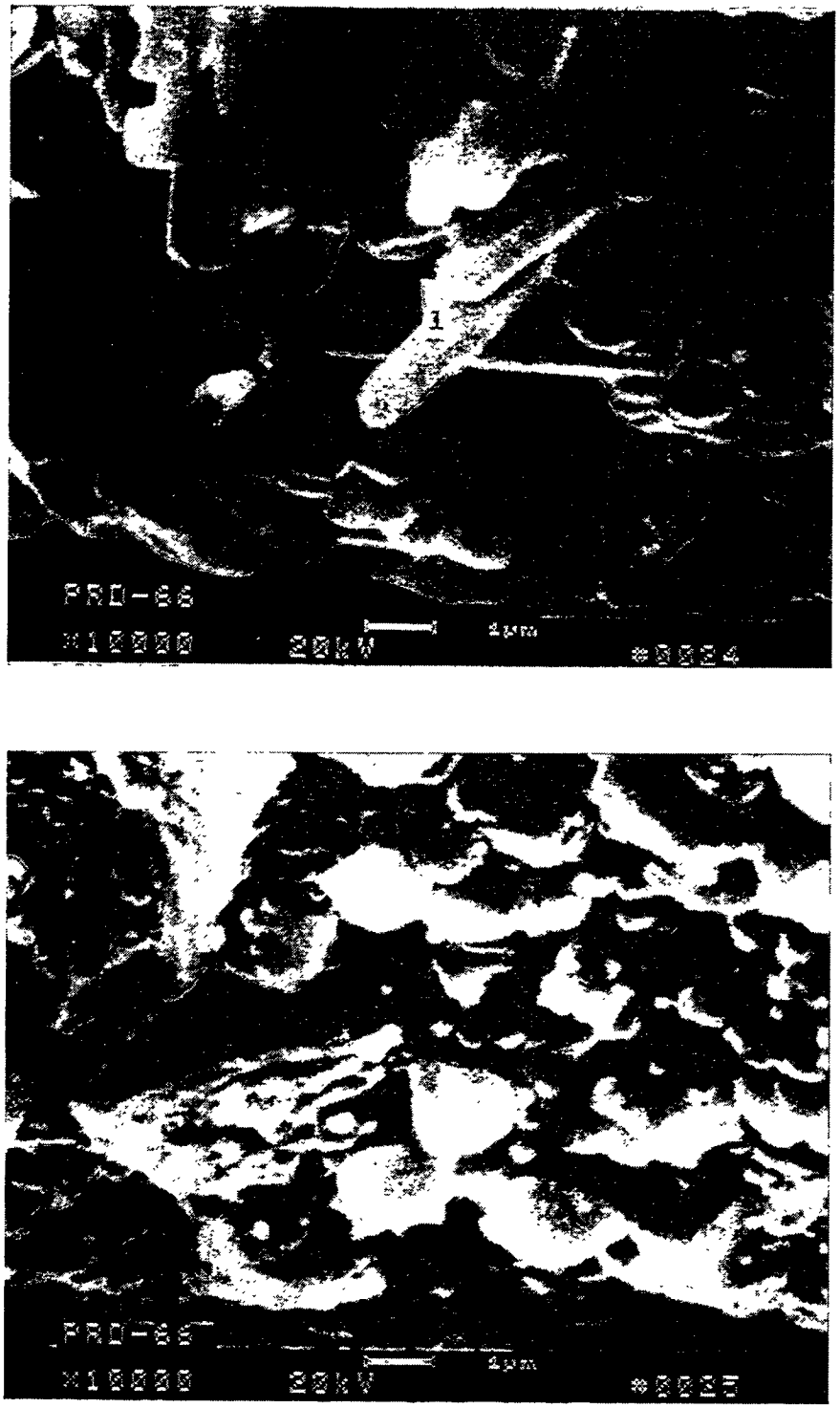

Figure 2i — Mullite And Alumina Formations Along The Outer Surface Of The DuPont PRD-66 Filament Wound Filter Matrix

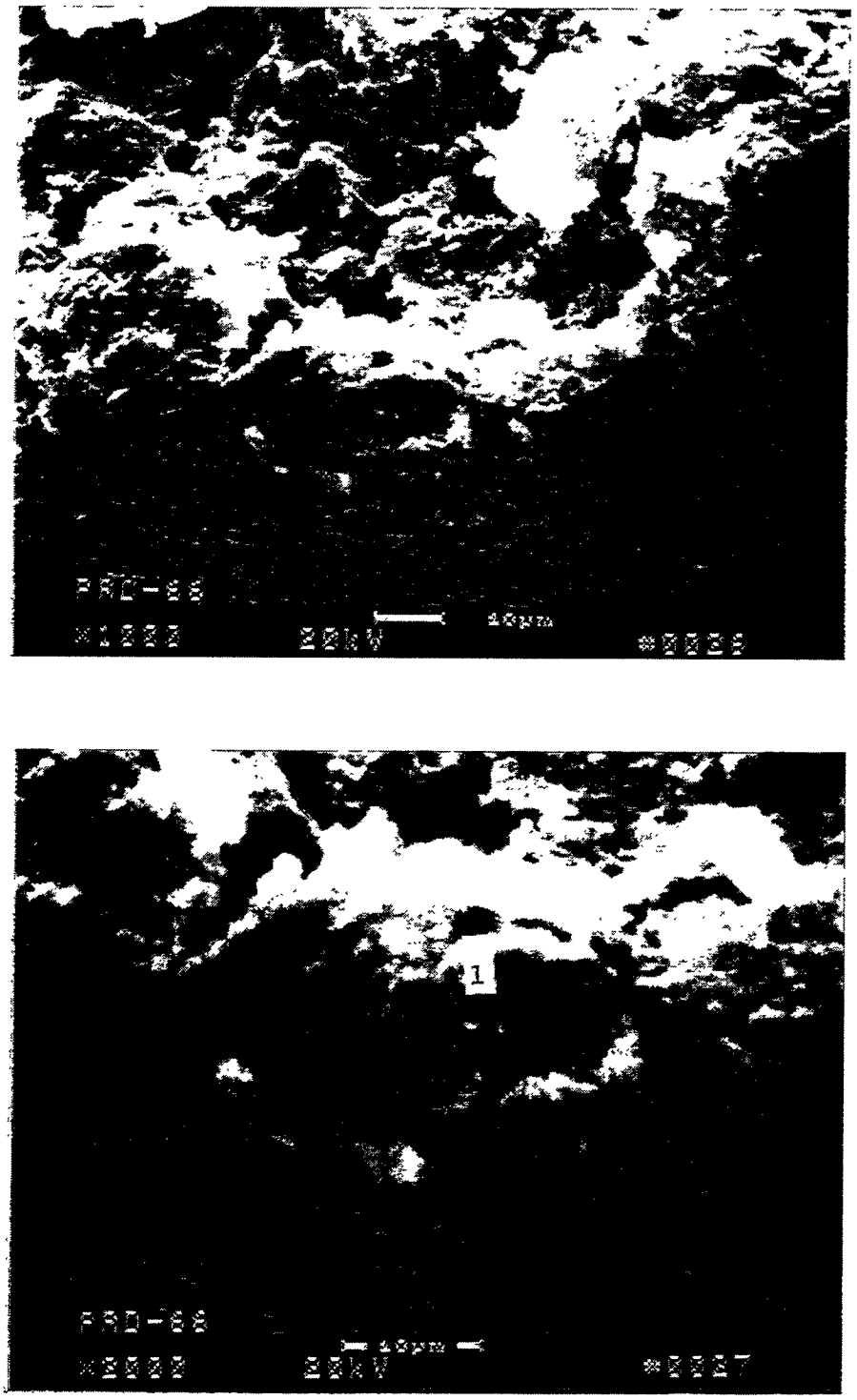

Figure 2j — Fractured DuPont PRD-66 Filament In The As-Manufactured Filter Matrix

Figure 2k – Fractured Filaments In The DuPont PRD-66 Filter Matrix. Alumina-Enriched Mud Cracks Are Evident As Fillet Areas Between Adjoining Filaments.

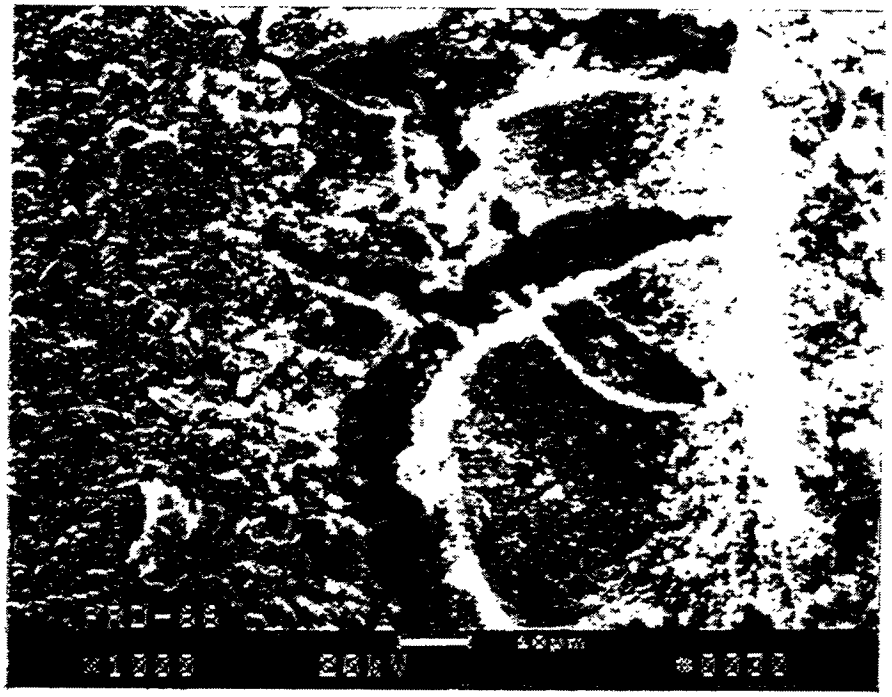

Figure 21 — Higher Magnification Micrograph Of The Alumina-Enriched Mud Crack Areas Which Form Between Adjacent Filaments

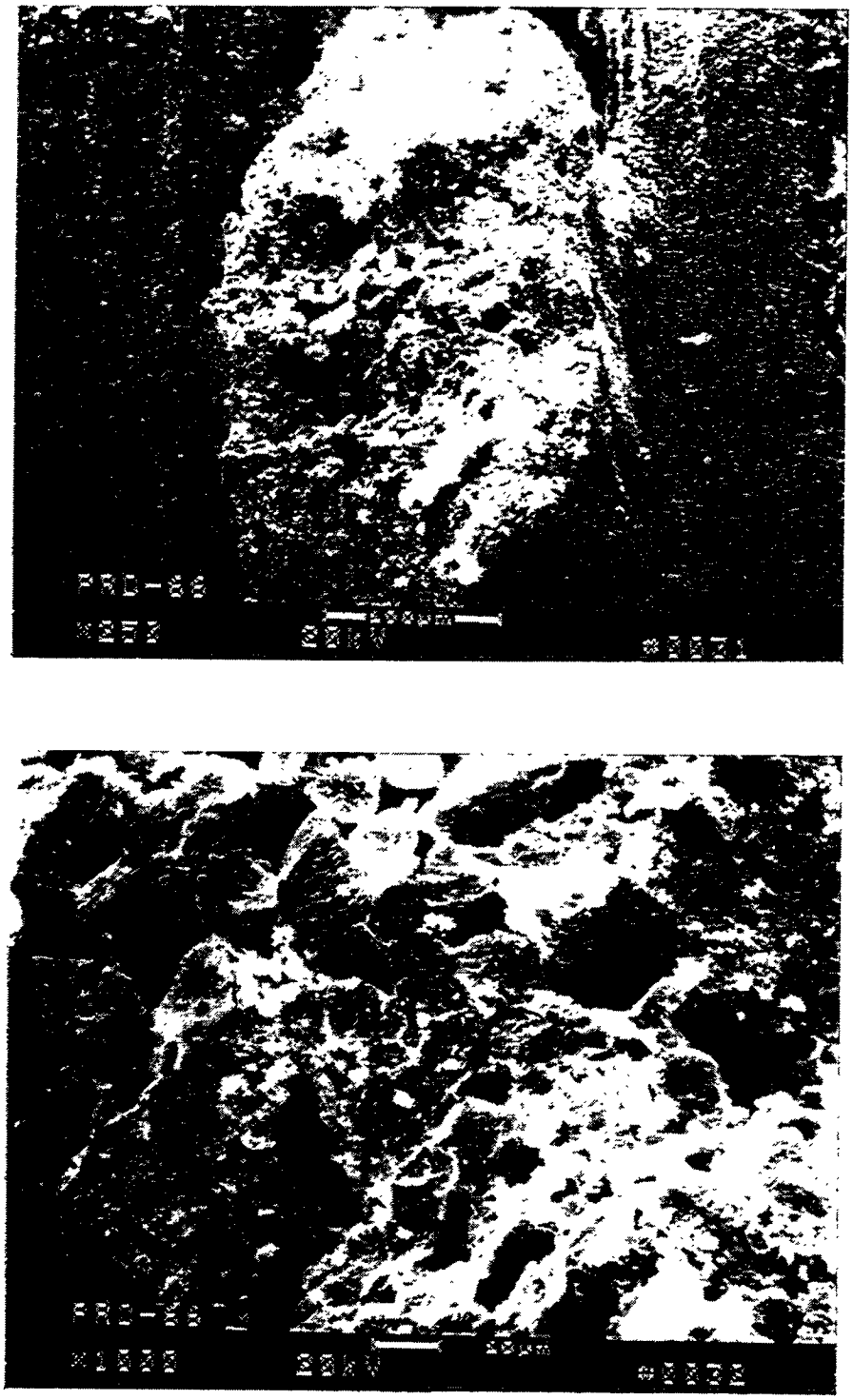

Figure 2m - Fractured Filaments In The DuPont PRD-66 Filter Matrix

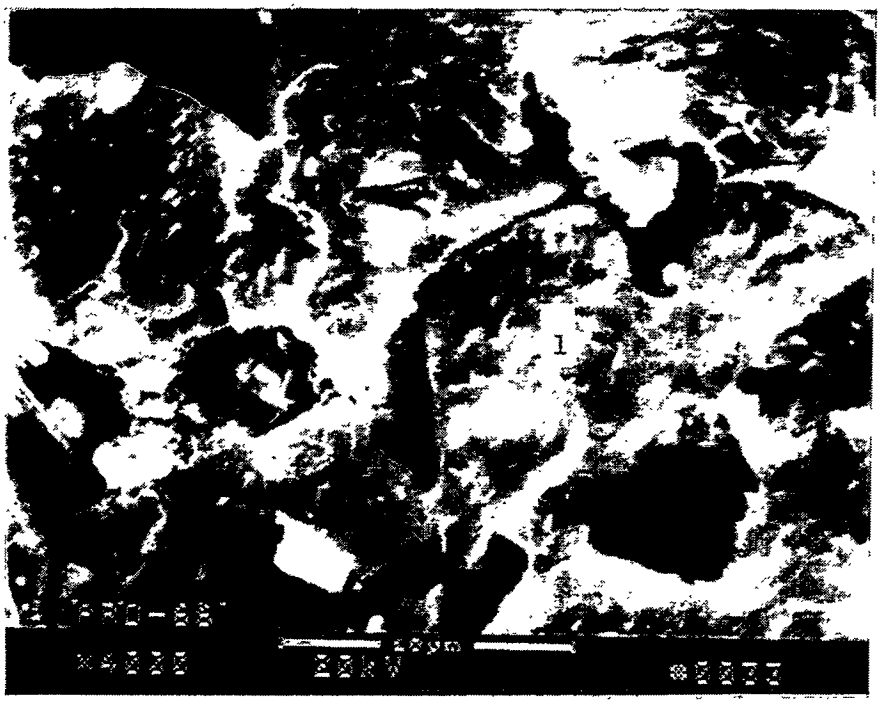

Figure 2n – Higher Magnification Micrograph Illustrating The Fractured DuPont Filament In The PRD-66 Filter Matrix

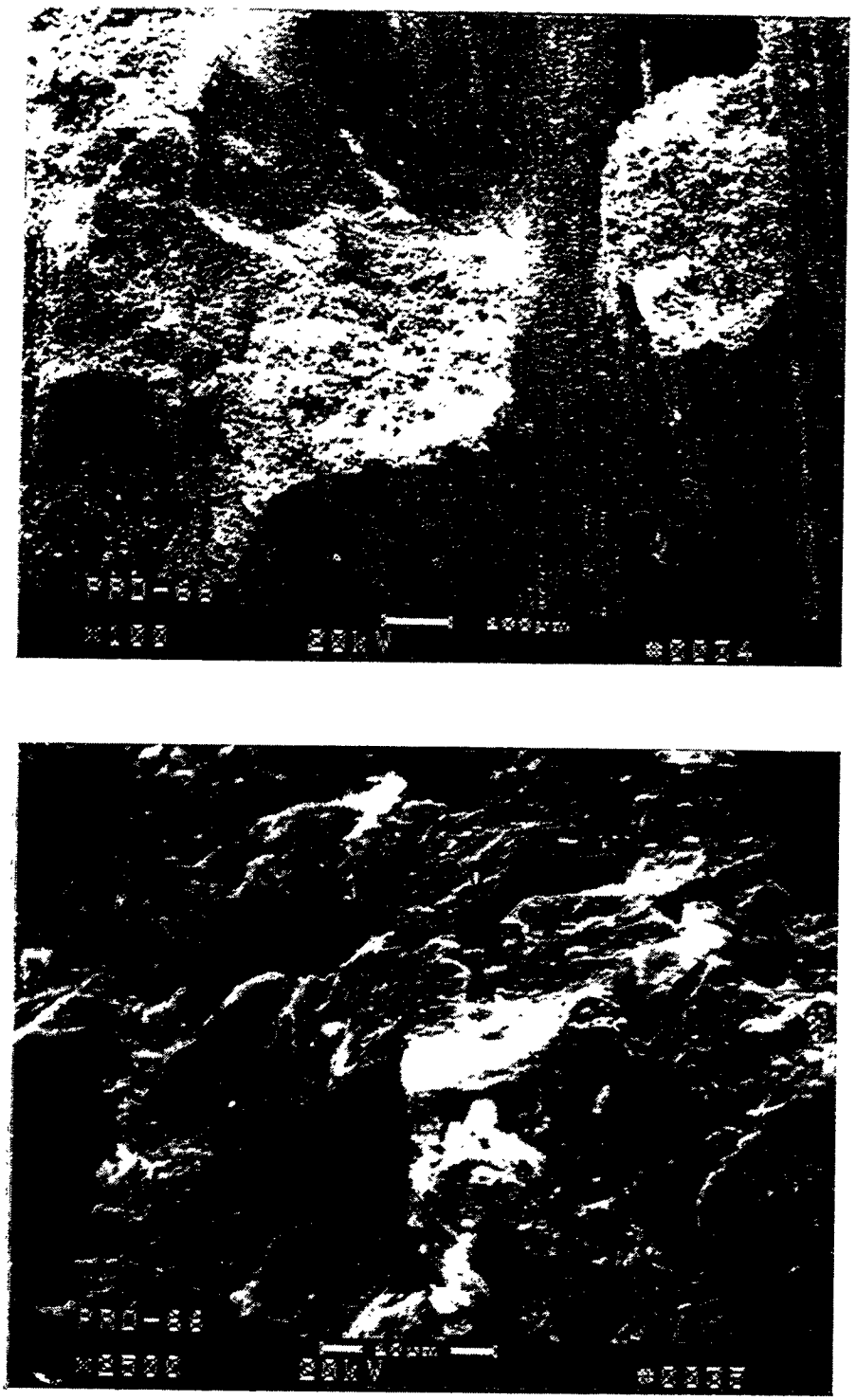

Figure 2o – Fractured Filaments At The Center Of The DuPont PRD-66 Filter Matrix

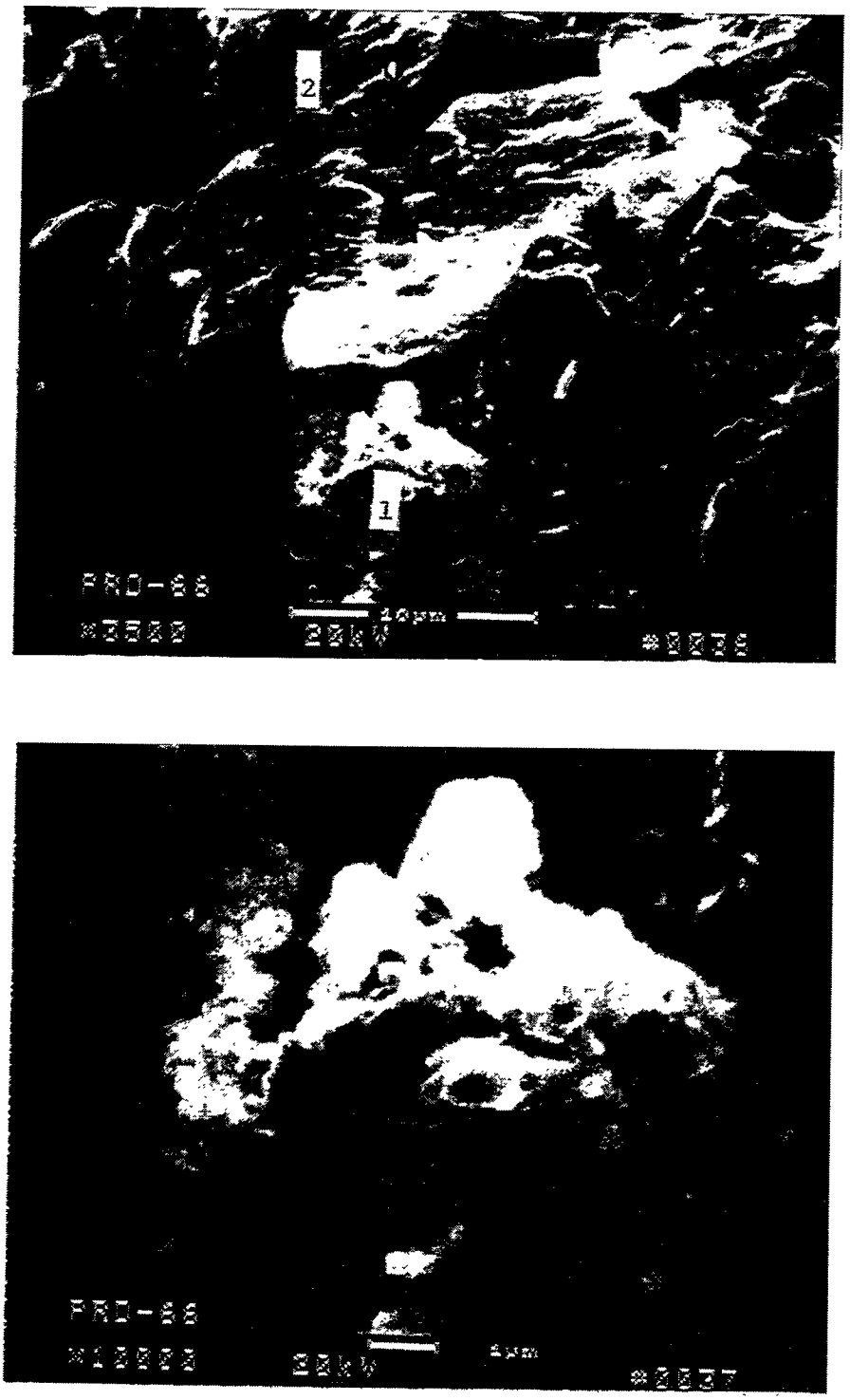

Figure 2p – Higher Magnification Micrographs Of The Fractured Filaments Near The Center Of The DuPont PRD-66 Filter Matrix

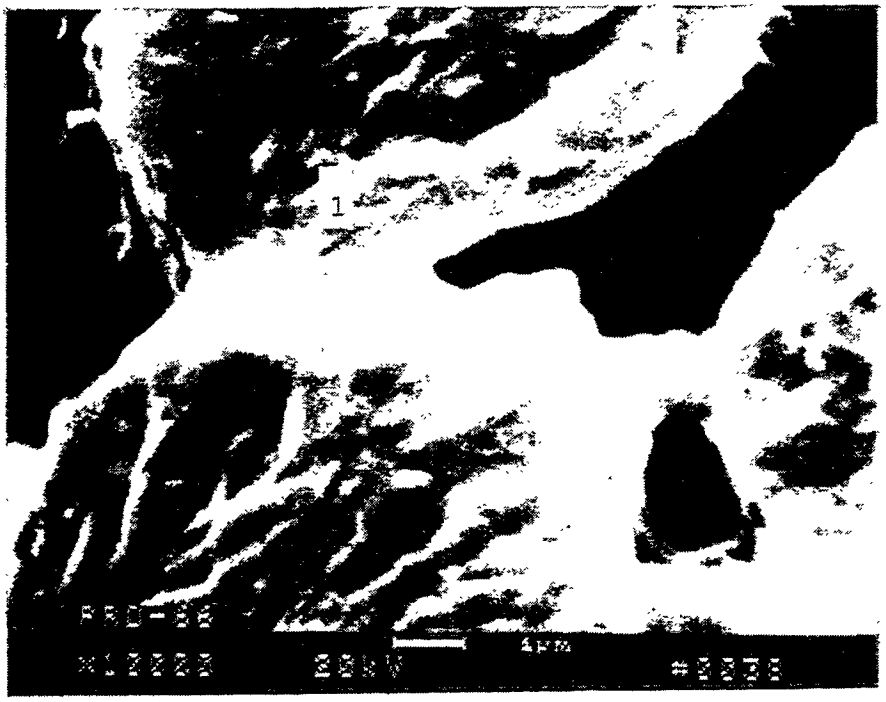

Figure 2q – "Sintered" Bond Between Adjoining Cordierite Fibers In The DuPont PRD-66 Filament Wound Oxide-Based Filter Matrix

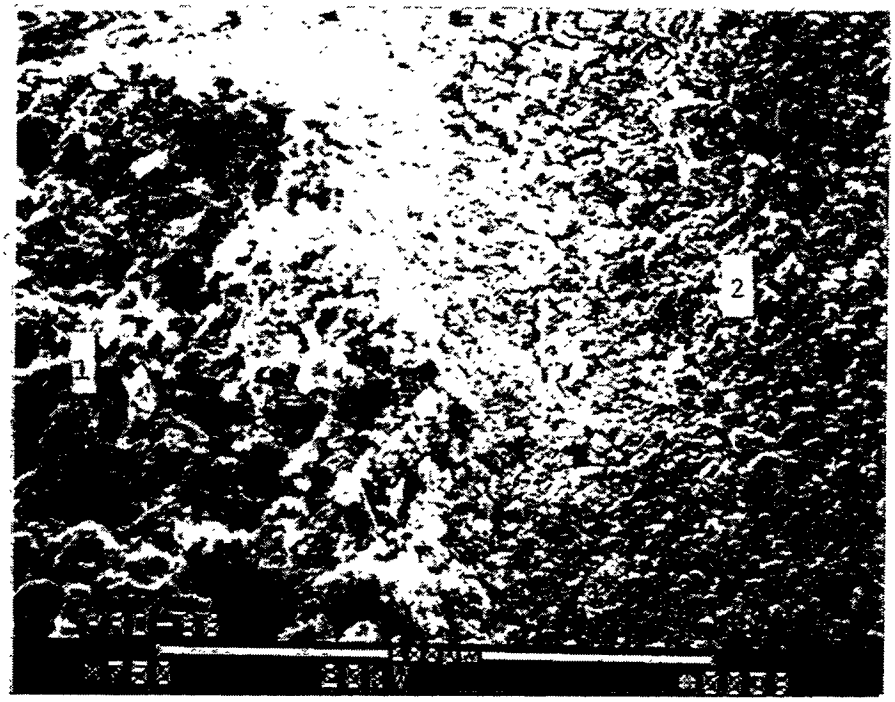

Figure 2r — Polycrystalline Outer Surface Of The DuPont PRD-66 Filament In The As-Manufacture Filter Matrix

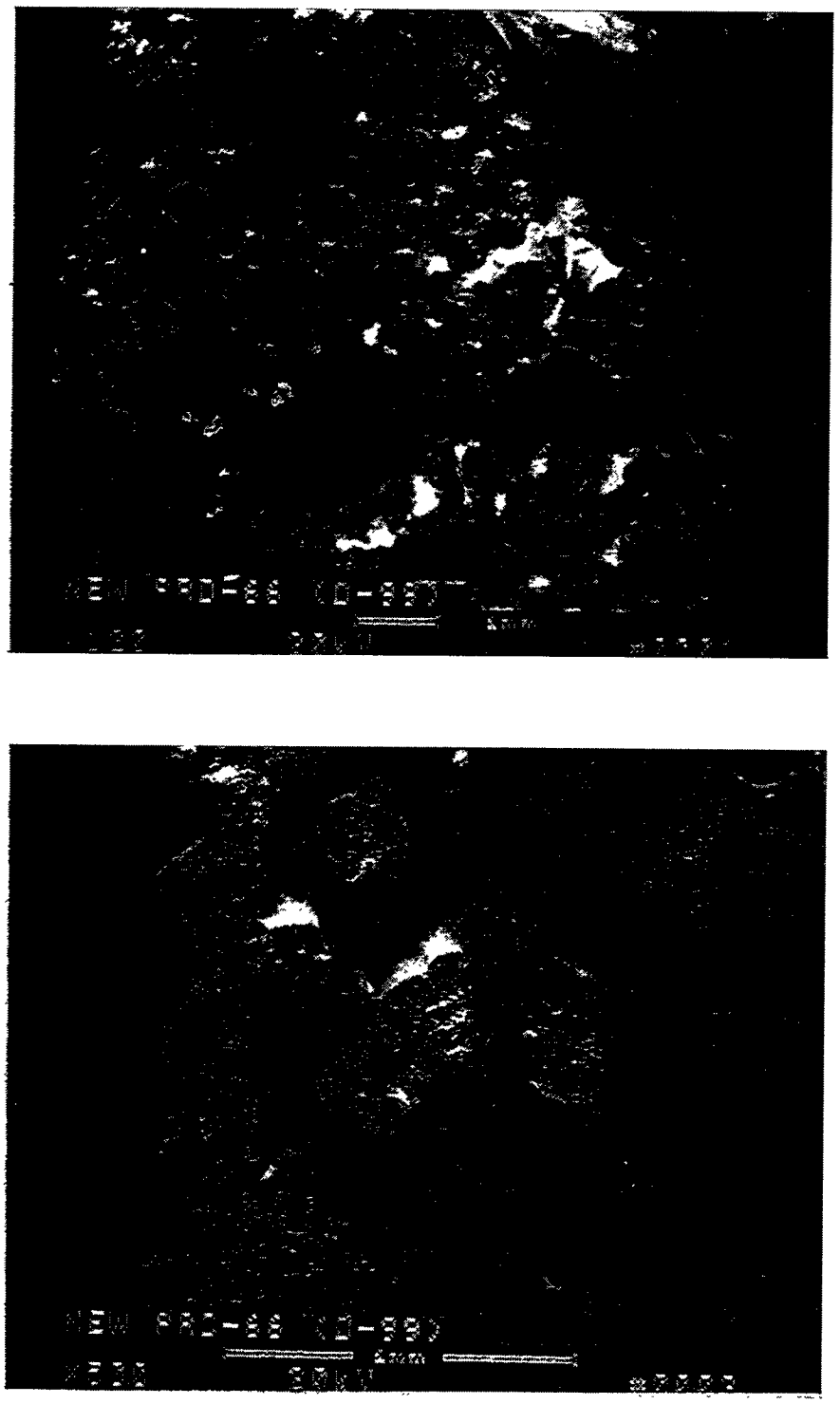

Figure 2s – Cross-Sectioned As-Manufactured DuPont PRD-66 Filter Element

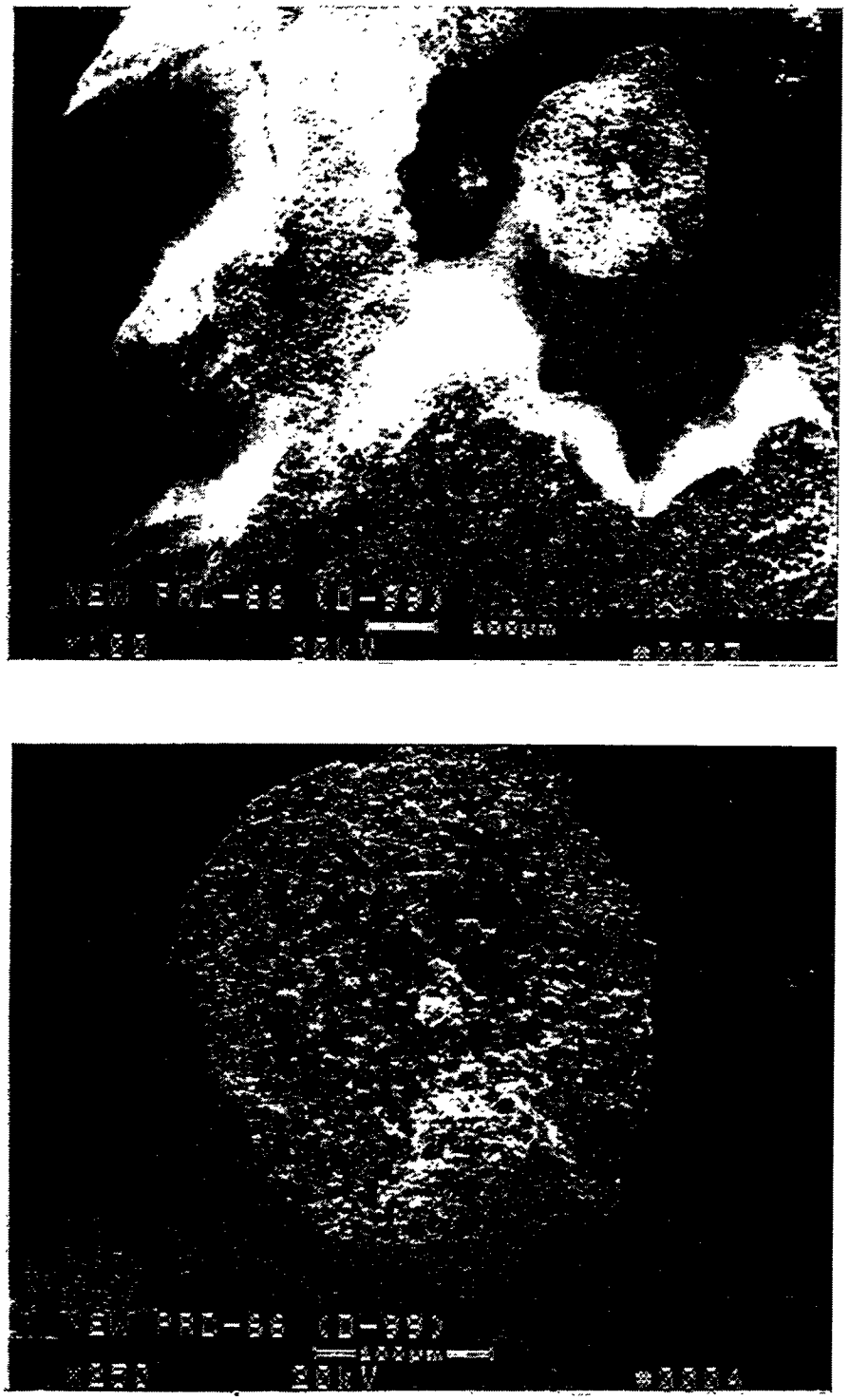

Figure 2t — Filament Bundles In The As-Manufactured DuPont PRD-66 Filter Element

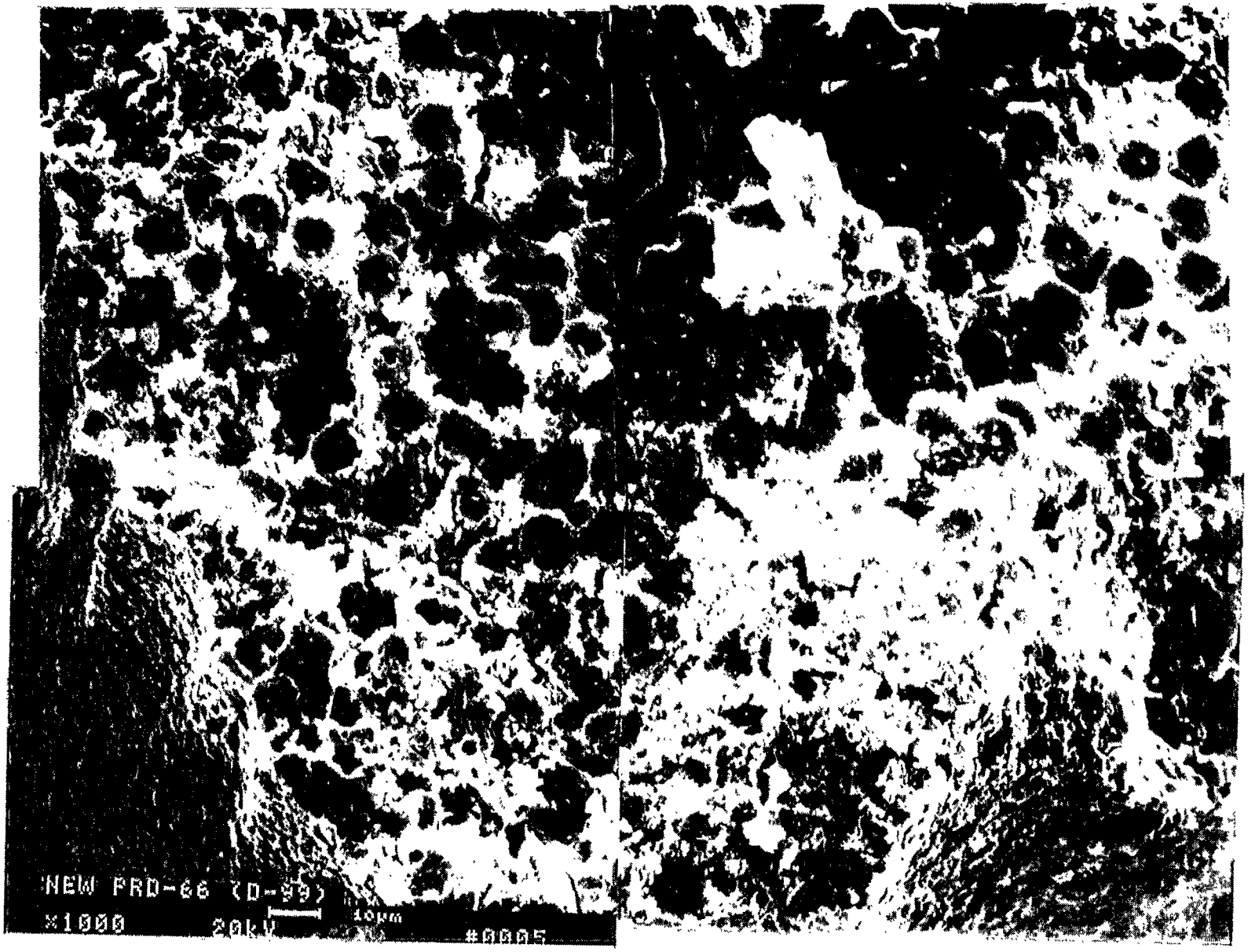

Figure 2u – Higher Magnification Micrograph Illustrating The Morphology Of The Fibers In The Filament Bundle Near The Outer Surface Of The As-Manufactured DuPont PRD-66 Filter Matrix

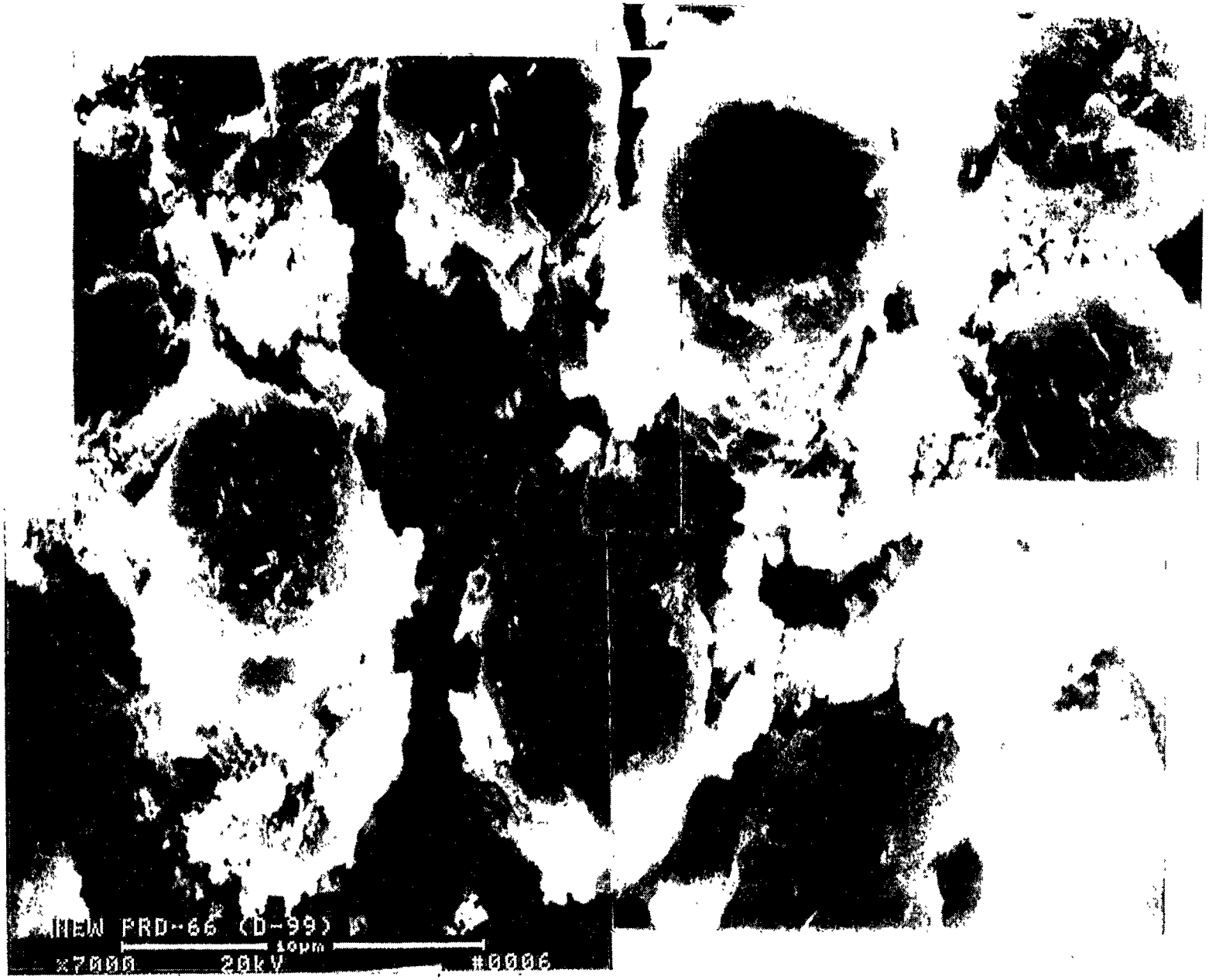

Figure 2v - Higher Magnification Micrograph Illustrating The Fibers And Polycrystalline Matrix Within The Filament Bundle

Figure 2w –Morphology Of The Fibers In The Filament Bundle Of The As-Manufactured DuPont PRD-66 Filter Matrix

Figure 2x – Higher Magnification Micrograph Illustrating The Morphology Of The Fibers Within The Filament Bundle. Frequently Voids Are Evident At The Center Of The Cordierite-Enriched Fibers.

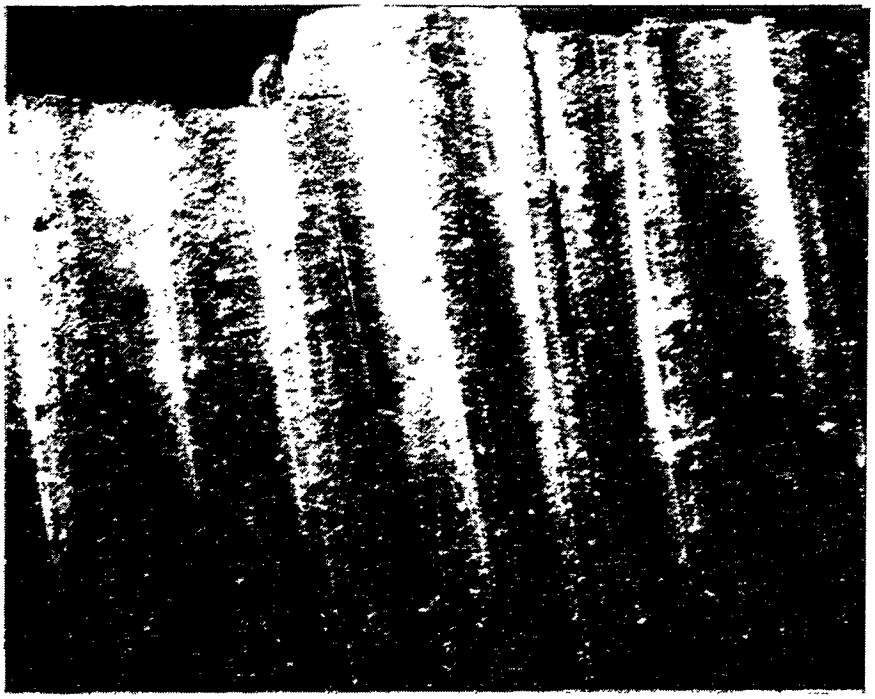

Figure 2y – Morphology Of The Membrane Surface Of The As-Manufacture DuPont PRD-66 Filter Matrix

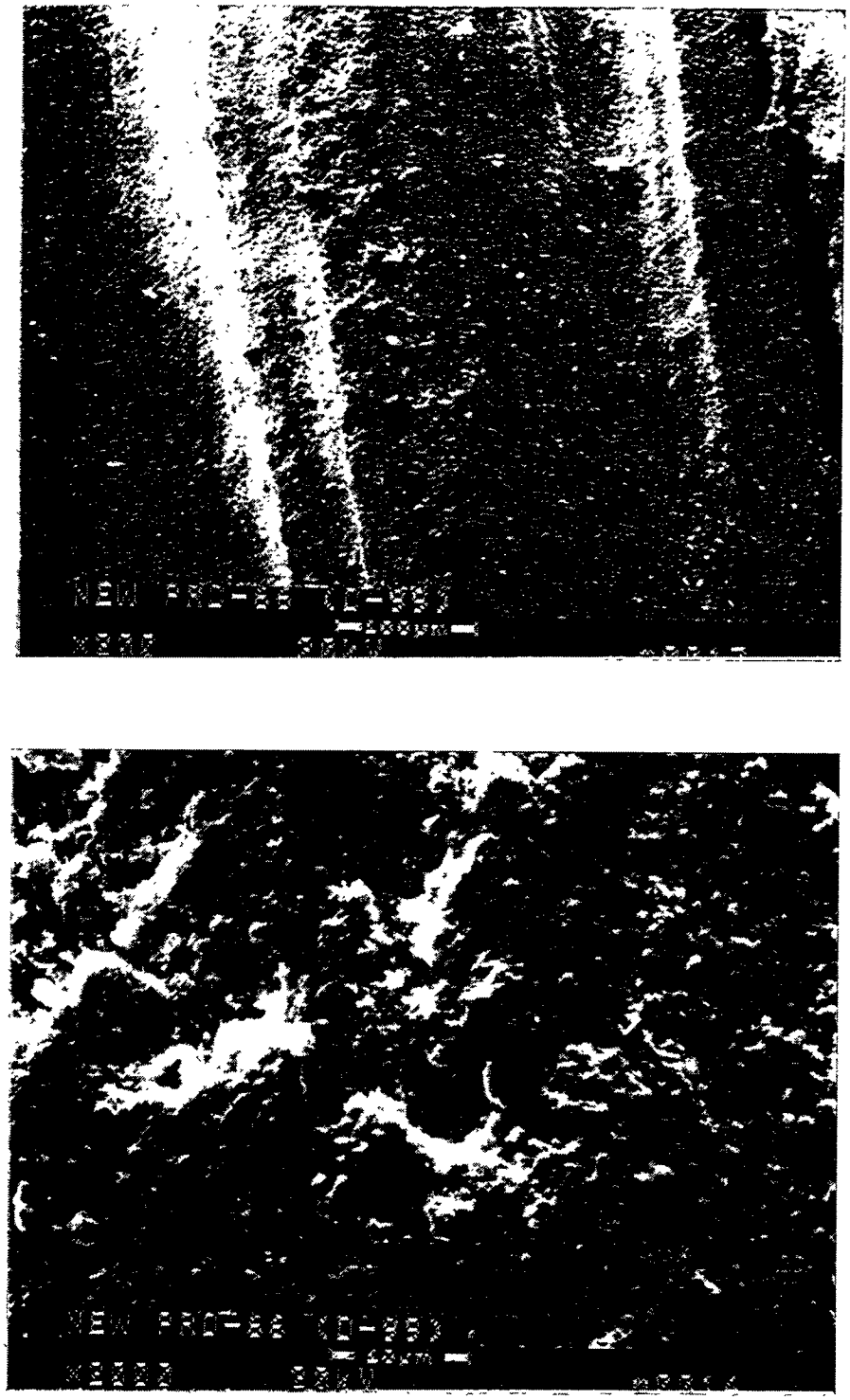

Figure 2z – Higher Magnification Micrographs illustrating The Morphology Of The Outer Membrane Surface Of The As-Manufactured DuPont PRD-66 Filter Element

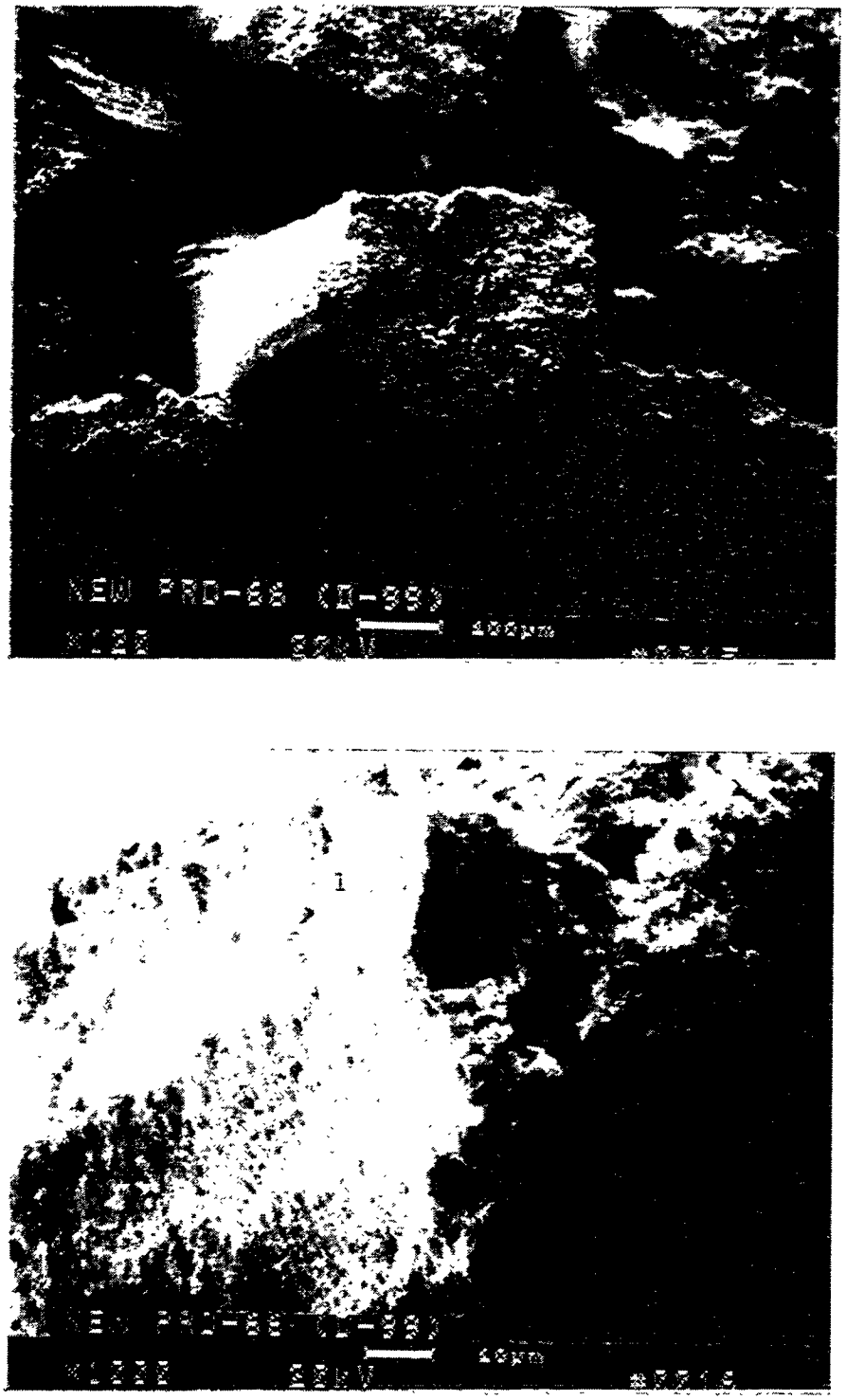

Figure 2aa — Filament Bundles Near The Outer Membrane Surface Of The DuPont PRD-66 Filter Element

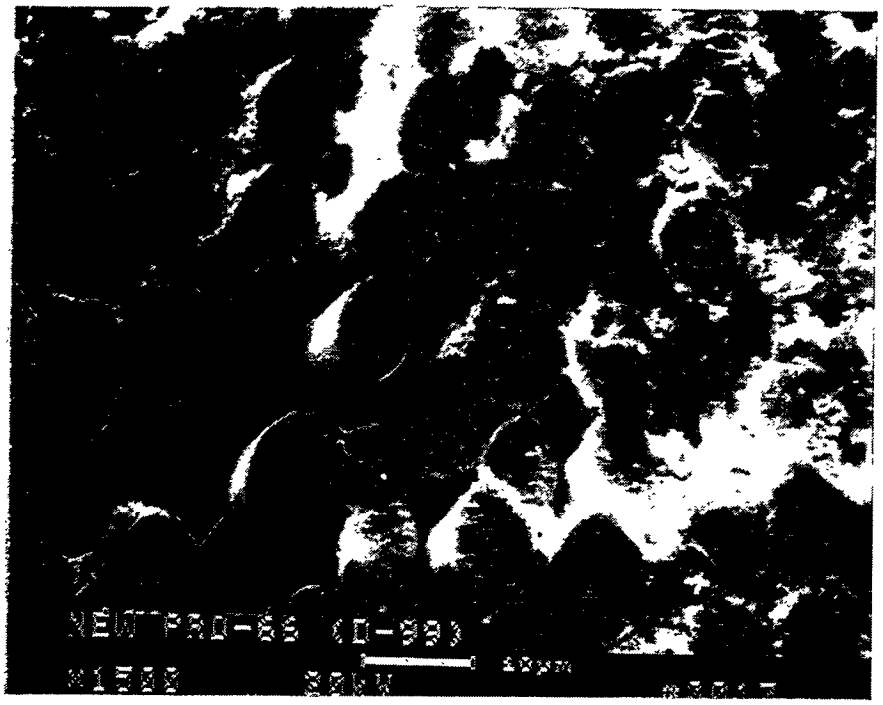

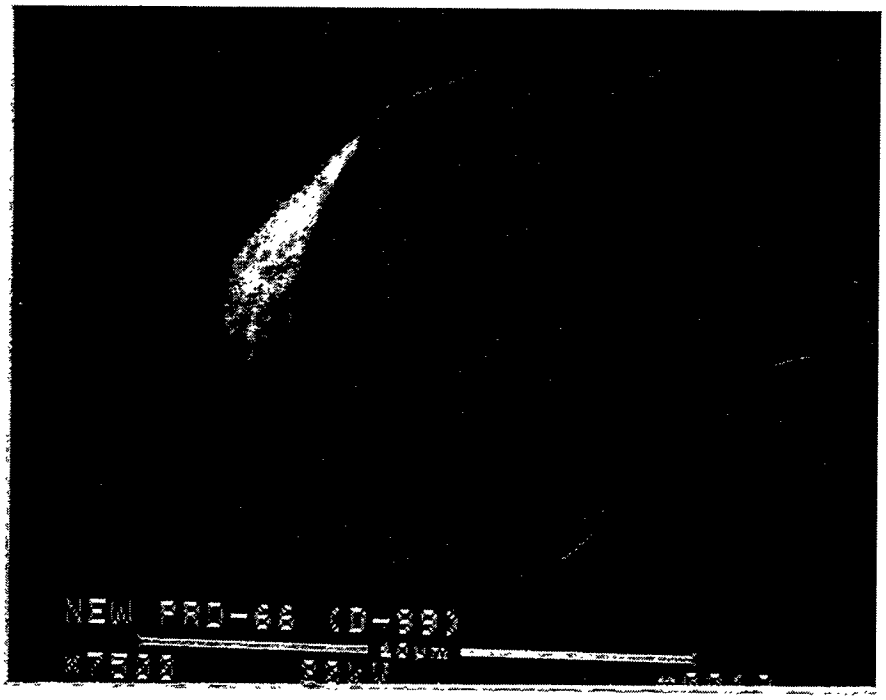

Figure 2bb – Fibers Within A Filament Bundle (Outer Membrane Surface)

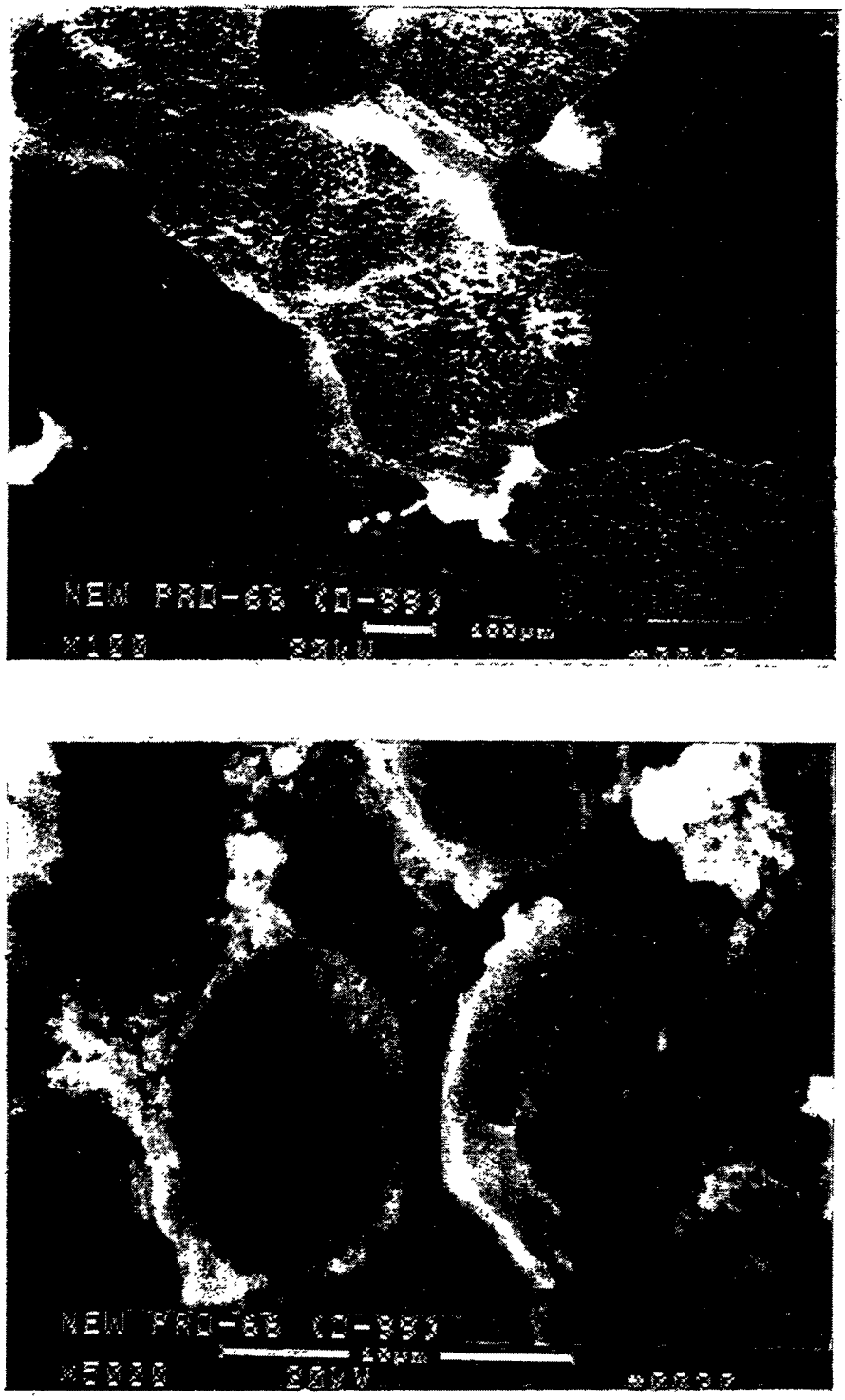

Figure 2cc – Filament Bundles Near The Outer Membrane Surface Of The As-Manufactured DuPont PRD-66 Filter Element

shown in Area 2, Photo 36, Figure 2p, is shown at higher magnification in Area 1, Photo 38, Figure 2q. The composition of the matrix in this area was identified to include 35.50% Si, 31.67% O, 22.10% Al, and 10.72% Mg.

An additional micrograph in this series is shown in Figure 2r which illustrates the fractured filament fiber bundles in Area 1, as well as the outer surface of the filament yarn in Area . The polycrystalline nature of the outer surface of the filament is readily evident.

A second as-manufactured filter element was characterized in terms of its morphology and elemental composition. This section was removed from a filter element that was identified as D-99, and was coated with gold prior to conducting the SEM/EDAX analyses.

As shown in Figure 2s, the filament wound bundles or yarns are tightly packed along the cross-sectioned filter surface. Each ~0.5 mm bundle is encapsulated by an outer polycrystalline layer or wall. The filament bundle contains numerous ~10 μm fibers (Figure 2t). Individual fibers along the periphery of the filament bundle appear to be surrounded by an additional fine grained matrix (Figure 2u) which may assist in bonding the fibers to each other. In many areas, point contact between individual fibers results without the additional polycrystalline matrix being present (Figure 2v). Frequently voids are evident at the center of individual fibers (Figure 2w and 2x).

The outer membrane of the as-manufactured filter section is shown in Figure 2y. The minor overlapping (i.e., criss-cross) wrap configuration is evident along the outer membrane. The crack formations which run the length of the fiber bundles or yarns along the membrane most likely resulted during sample preparation. Figure 2z provides higher magnification micrographs detailing the morphology of the membrane surface. EDAX analyses of the rather mottled membrane surface shown in Photo 14, Figure 2z identified the presence of 49.80% Al, 44.85% O, and 5.35% Si. A cross-section of the filament yarns in the membrane is shown in Figure 2aa. EDAX analyses of the polycrystalline outer layer of the filament bundle identified the presence of 63.26% O, 33.42% Al, and 3.32% Si (Photo 16; Figure 2aa). Individual discrete and/or polycrystalline encapsulated fibers are present within the filament bundle (Figure 2bb). Where discrete fibers are present, bonding and/or "fusing" of adjacent fibers occurred. The composition of the fiber shown in Photo 18, Figure 2bb, was identified by EDAX to contain 52.93% Si, 27.06% O, 13.88% Al, and 5.59% Mg.

An additional filament bundle is shown in Figure 2cc. As previously discussed, the outer surface of the filament bundle consists of an encapsulating polycrystalline layer which most likely resulted during high firing with the alumina slurry that was applied during processing. Infiltration of the slurry appeared to result along the outer periphery of the filament bundle, and perhaps deposited particles within the bundle (i.e., between fibers). Incomplete infiltration at the center of the filament may have resulted in discrete fiber areas that are devoid of the "polycrystalline" deposit. The composition of the fiber shown in Photo 20, Figure 2cc, was identified by EDAX to contain 50.15% Si, 30.06% O, 14.42% Al, and 5.36% Mg.

PFBC-EXPOSED DuPONT PRD-66 FILTER MATRIX (TEST SEGMENT #5)

After 1110 hours of PFBC operation at the American Electric Power (AEP) Demonstration Plant in Brilliant, Ohio, a "red stain" was evident along localized areas of the DuPont PRD-66 filter matrix (Test Segment #5). A section of the "red stain" material was initially

removed from one of the intact filter elements, and was coated with carbon in preparation for SEM/EDAX analyses.

As shown in Figure 3a, the filament yarns which form the membrane are still readily evident along the OD membrane surface. In comparison to Figure 1a, discrete fibers in the filament yarn are not as apparent after 1110 hours of PFBC test operation. Based on the EDAX analyses of the area shown in Photo 2, Figure 3a, fines were identified to be retained along the outer surface of the PRD-66 filter membrane (6.50% Si, 6.23% Mg, 6.06% Ca, 5.13% Al, 5.11% S, 1.78% Fe, 0.33% K, and 68.86% O). The morphology of the submicron fines is shown in Figure 3b. The massive deposit of submicron fines is seen to be densely packed along the OD membrane in the area where the "red stain" was evident.

When the 1110 hour PFBC filter material was cross-sectioned, the "red stain" was evident along the OD membrane surface, and did not visually appear to penetrate into the filter wall. Deposition of fines was, however, readily apparent throughout the filter wall (Figure 3c). Within the first layers of the filament yarns directly below the OD membrane, an extensive accumulation of fines was evident along the fractured fiber bundle surface. At high magnification the individual fibers are seen to have relatively mottled surfaces (Figures 3d and 3e). The deep holes and pits observed along the 1110 hour PFBC-exposed cordierite fiber surface (i.e., 15.11% Si, 8.29% Al, 6.31% Mg, and 70.28% O) were not as apparent in the as-manufactured filter matrix.

Numerous micron and submicron particles were present directly below the OD membrane. These are shown in Figures 3f, 3g, and 3h. EDAX analyses of the material shown in Photo 13, Figure 3g, indicated the presence of 18.90% Al, 5.05% Si, 1.68% Ca, 2.98% Mg, 0.64% Fe, 0.35% S, and 70.40% O. The elemental analyses may reflect the presence of mullite, corundum, and cristobalite in the outer layer which coated the cordierite fibers in the membrane or filament yarns, as well as PFBC ash/sorbent fines (i.e., detection of iron, calcium, and sulfur). EDAX analyses of the area shown in Photo 14, Figure 3h identified the presence of 18.74% Al, 8.41% Si, 2.09% Mg, 0.95% Ca, 0.81% S, 0.70% Fe, and 68.29% O. Again the elemental composition most likely reflected the presence of the PRD-66 filter matrix, as well as the presence of entrapped ash/sorbent fines.

A second section of the DuPont PRD-66 filter matrix was removed from the "red stained" area of the intact filter element. This section was coated with gold in order to provide high resolution micrographs, showing the morphology of the filter matrix. The OD membrane and several filament yarn sublayers are shown in Figure 4a. As shown in Figure 4b, fines are present within and along the cross-sectioned matrix, directly beneath the OD membrane.

The fiber strand shown in Photo 3, Figure 4b, is shown at higher magnification in Photo 4, Figure 4c. The fiber strand shown in Area 1, Photo 4, Figure 4c, was identified by EDAX to contain 59.10% O, 17.90% Si, 13.71% Al, and 9.29% Mg (i.e., cordierite). The composition of Area 2 was comparable to Area 1 (i.e., 67.50% O, 13.78% Si, 10.16% Al, 8.32% Mg, and 0.24%). Ash/sorbent fines were present in Area 3 (i.e., 68.68% O, 10.67% Si, 8.26% Al, 7.60% Mg, 2.58% Ca, 1.39% Fe, 0.58% K, and 0.24% Ti).[d] The mottled fiber surface shown in Area 4 was identified by EDAX to contain 64.44% O, 15.28% Si, 11.84% Al, and 8.43% Mg (i.e., cordierite-containing matrix). The composition of the smooth fiber surface was also identified to

[d] Since gold was used to coat the sample, any sulfur that was present at low concentrations within the fines was most likely masked during sample preparation.

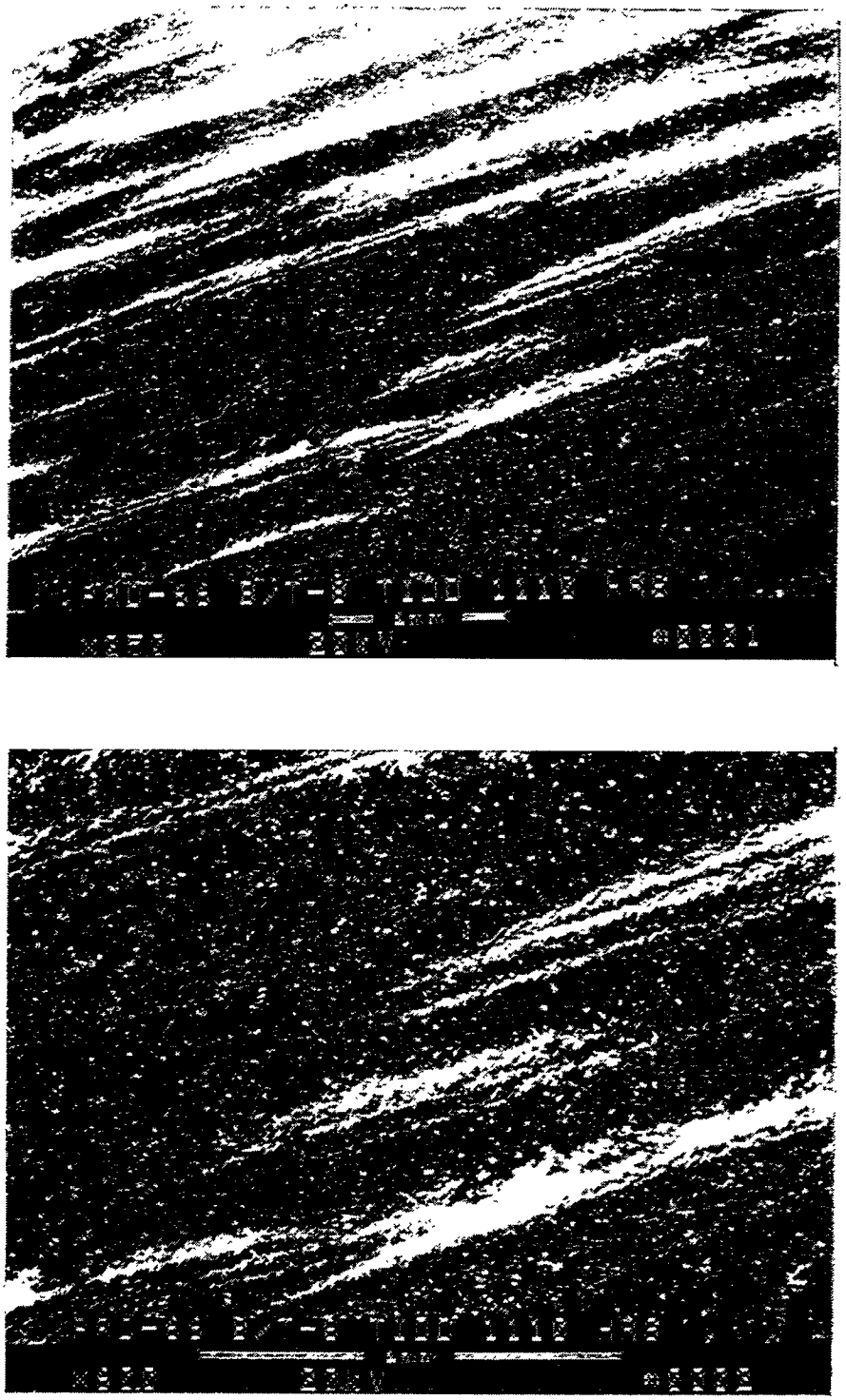

Figure 3a – DuPont PRD-66 Outer Membrane Surface After 1110 Hour Of PFBC Operation In THe W-APF At AEP

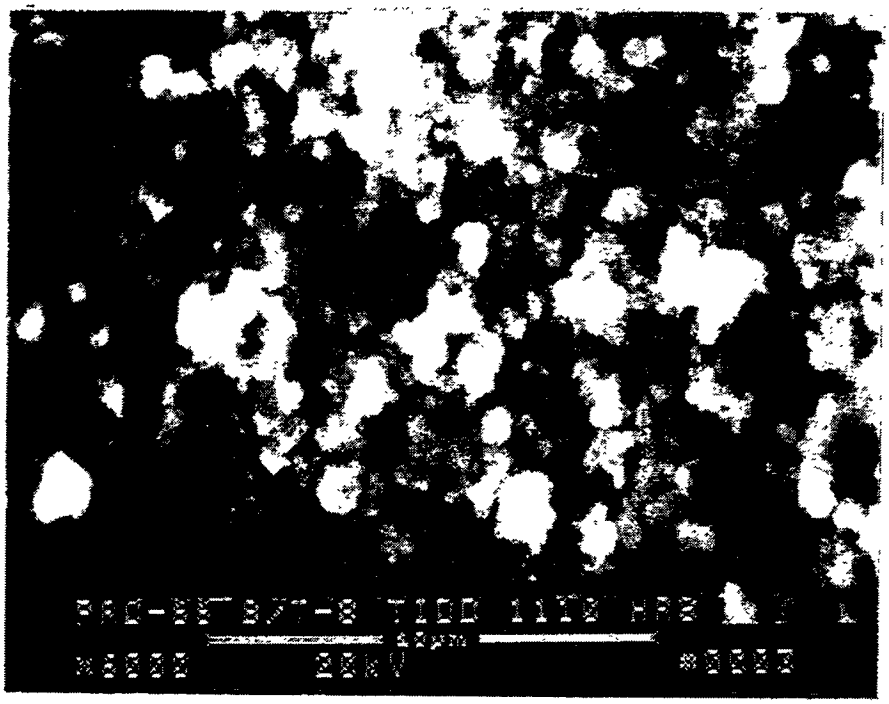

Figure 3b – Deposited Fines Along The Membrane Surface Of The 1110 Hour PFBC Exposed DuPont PRD-66 Filter Matrix

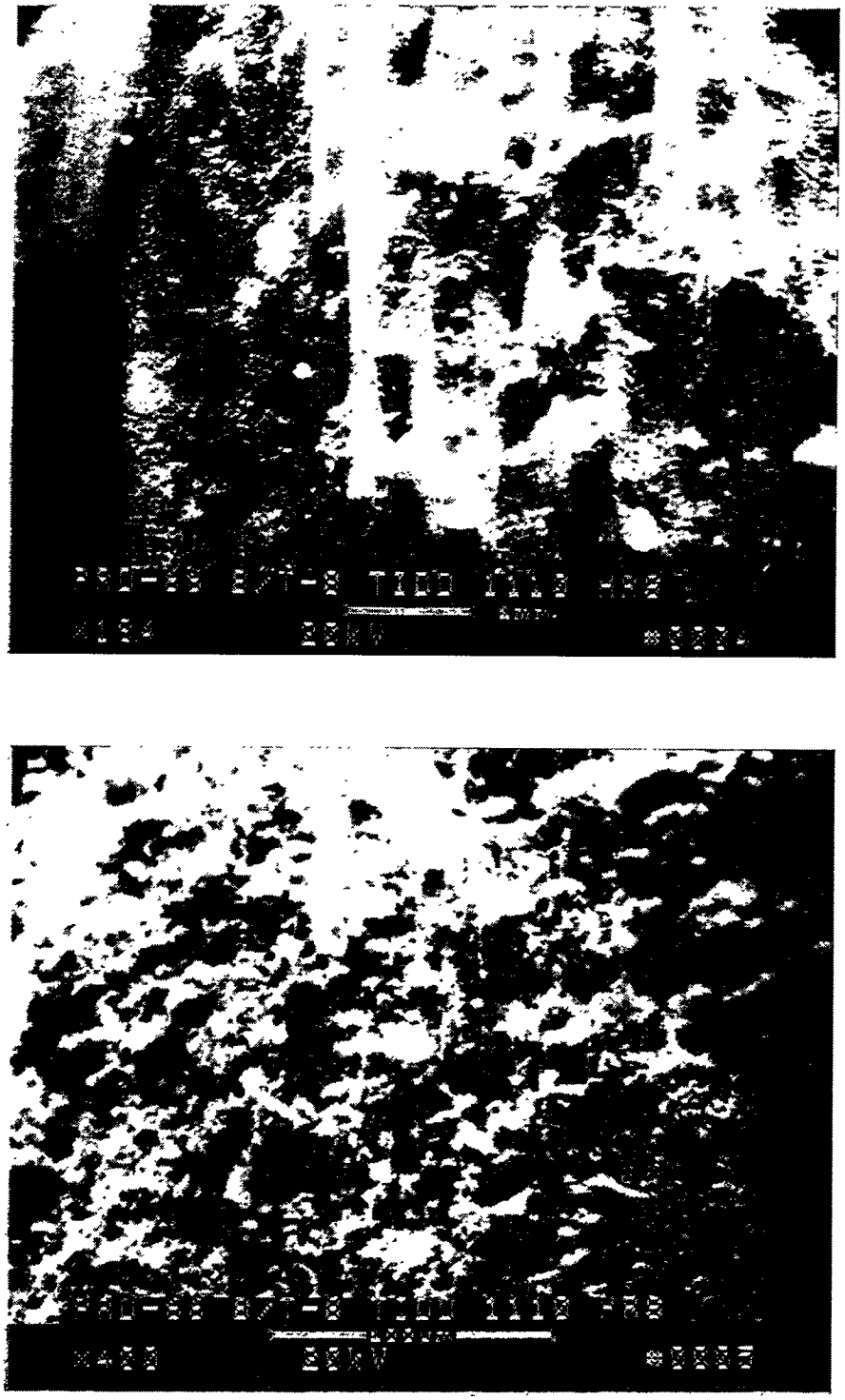

Figure 3c – Cross-Sectioned DuPont PRD-66 Filter Matrix Near The "Red Stain" Area That Formed Along The Outer Membrane Surface Of The 1110 Hour PFBC Exposed Candle Filter

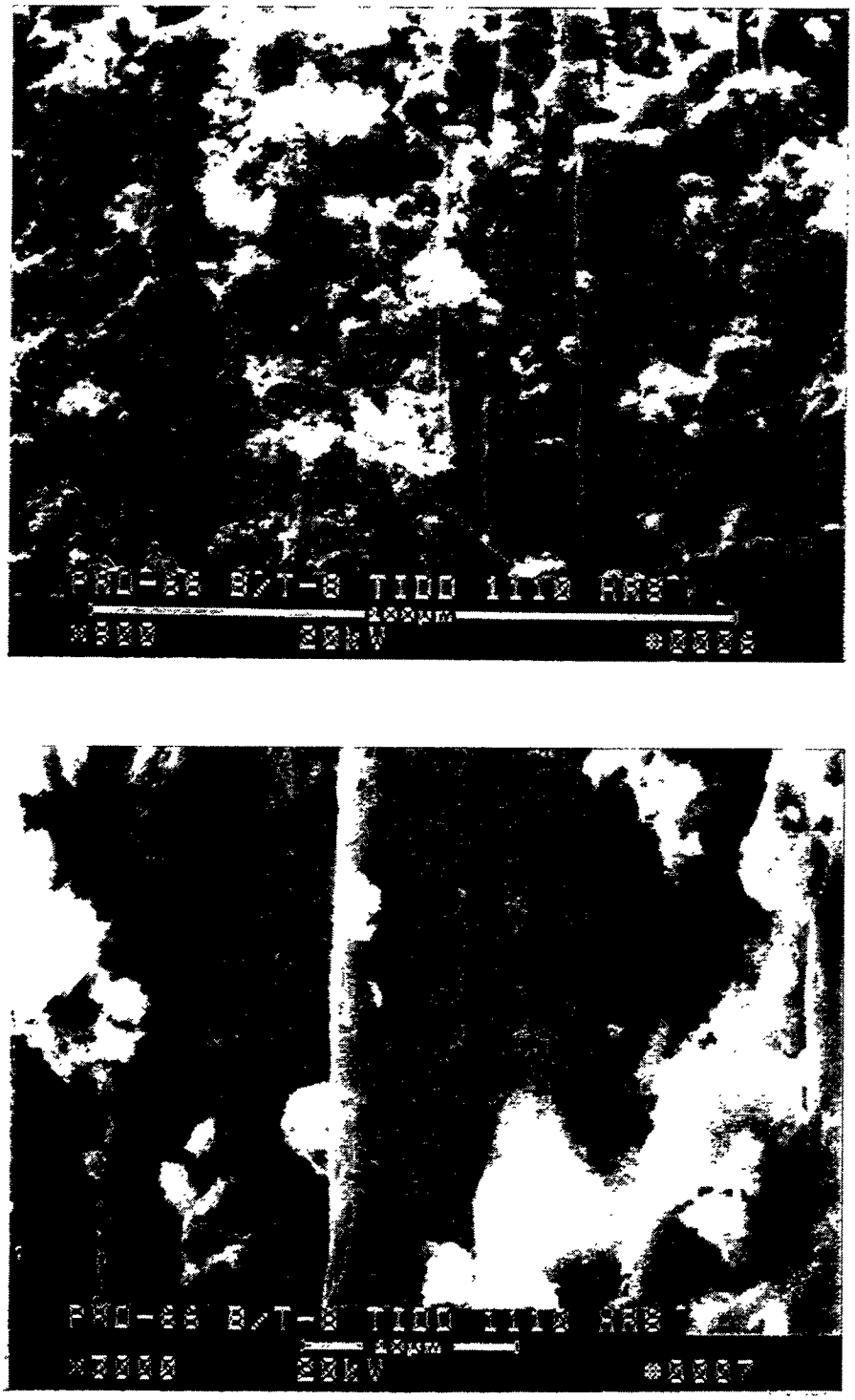

Figure 3d – Morphology Of The Cordierite Fibers In The Filament Yarns Of The 1110 Hour PFBC Exposed Filter Matrix

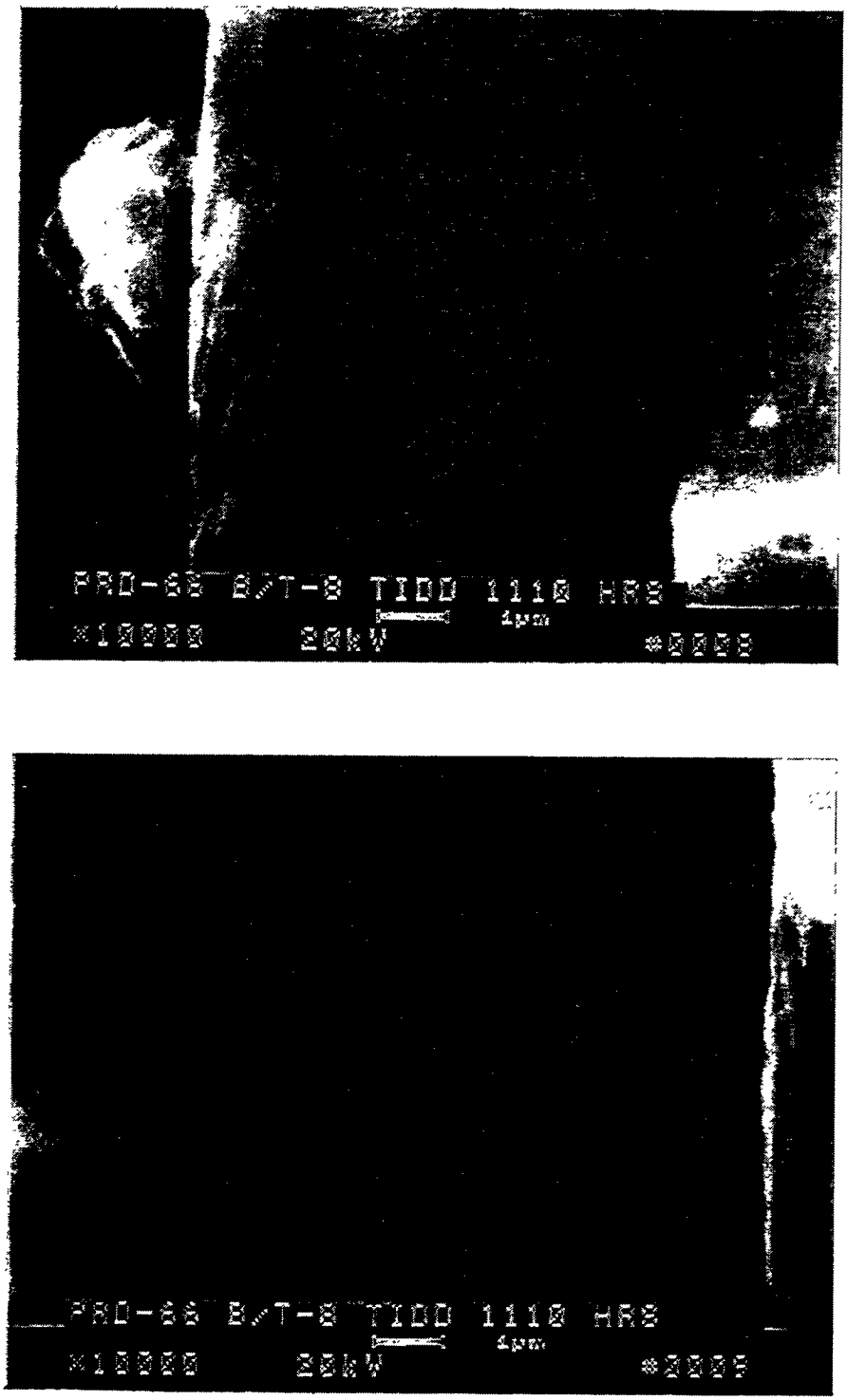

Figure 3e — Extensive Mottling And Pitting Along The Cordierite Fiber Outer Surface In The 1110 Hour PFBC Exposed DuPont PRD-66 Filament Yarn Bundles

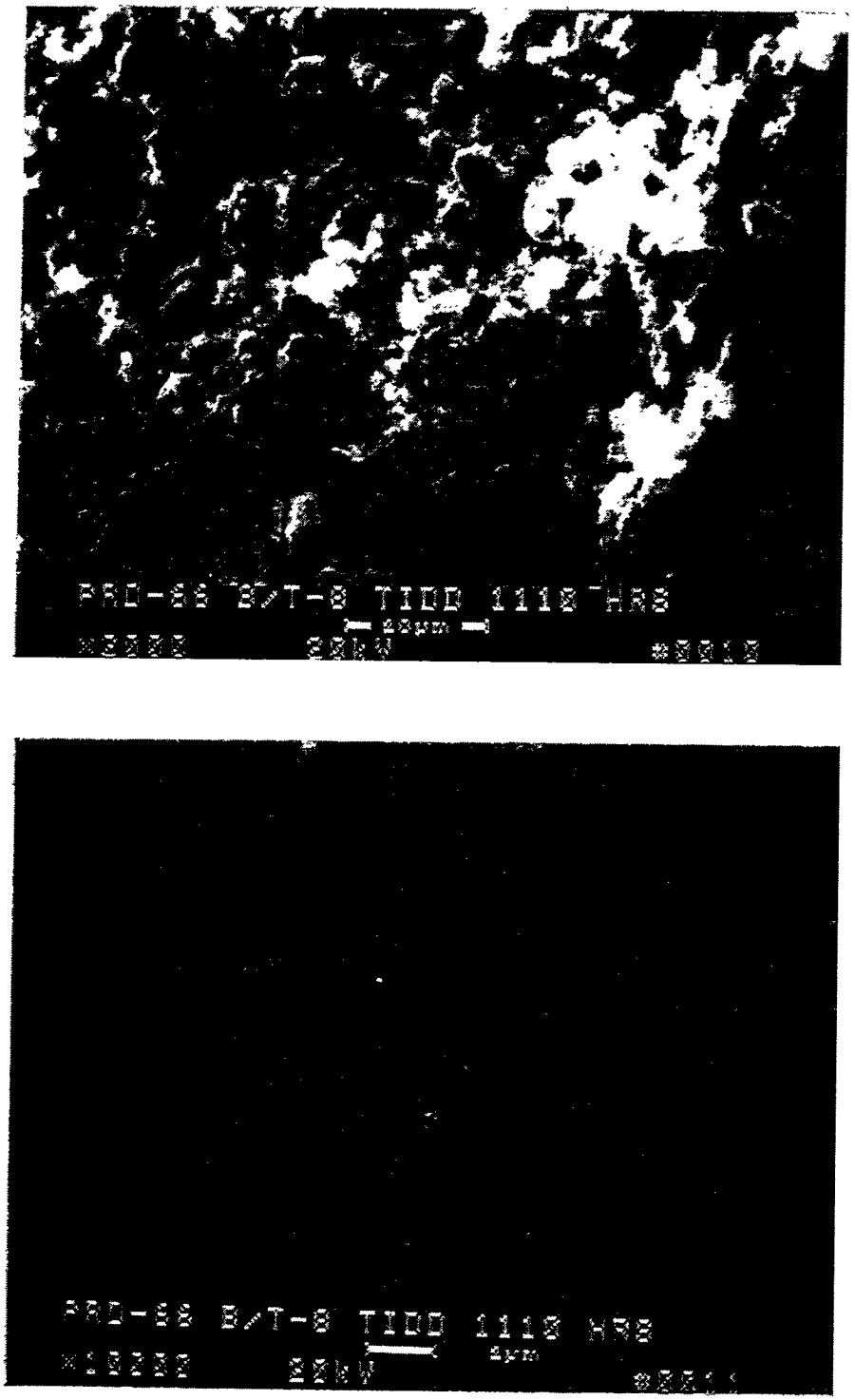

Figure 3f — Numerous Micron And Submicron Fines Present Below The OD Membrane In The 1110 Hour PFBC Exposed DuPont PRD-66 Candle Filter

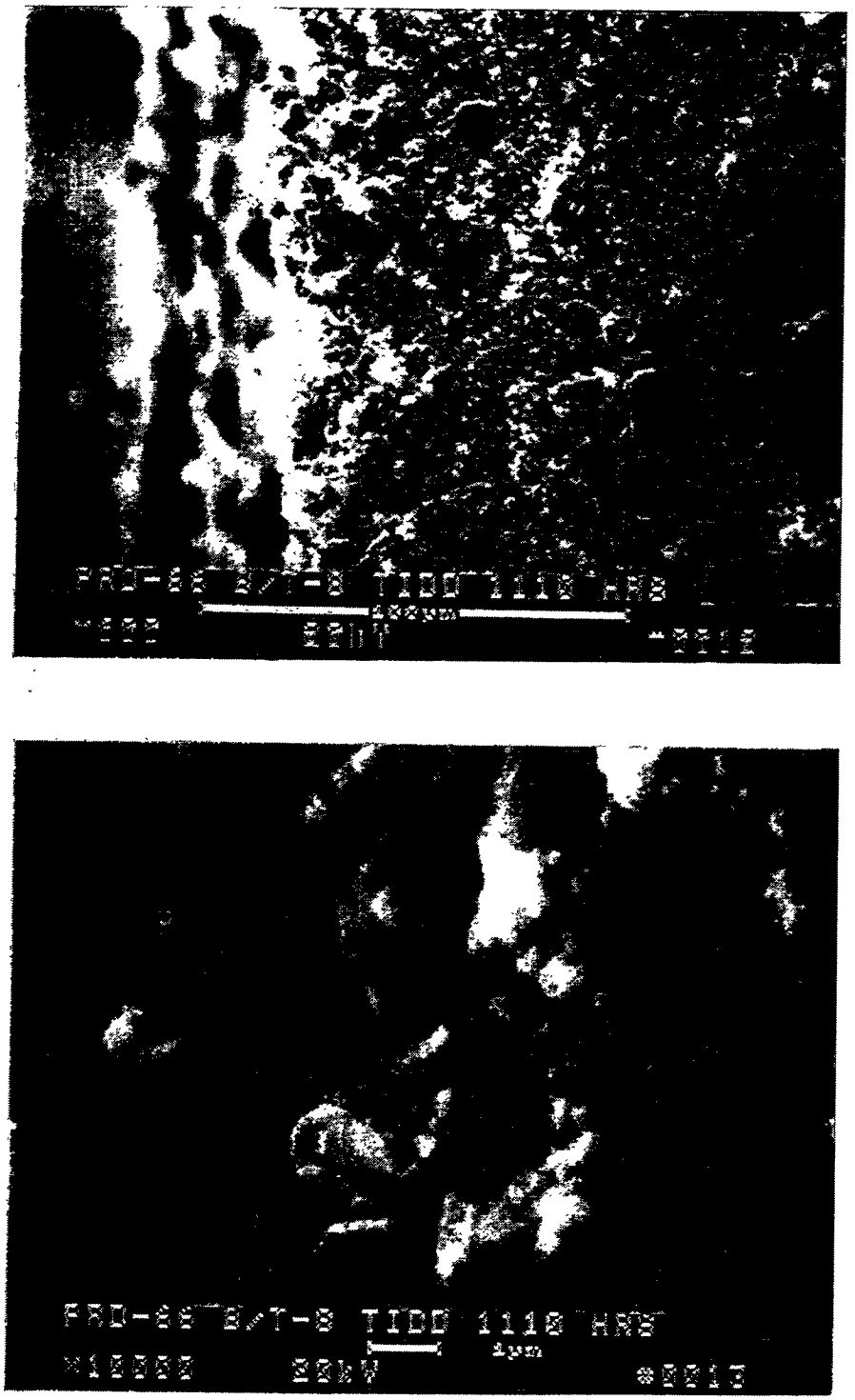

Figure 3g – Numerous Micron And Submicron Fines Present Below The OD Membrane In The 1110 Hour PFBC Exposed DuPont PRD-66 Candle Filter

Figure 3h – Higher Magnification Micrograph Of The Ash/Sorbent And Possibly PRD-66 Matrix Particles

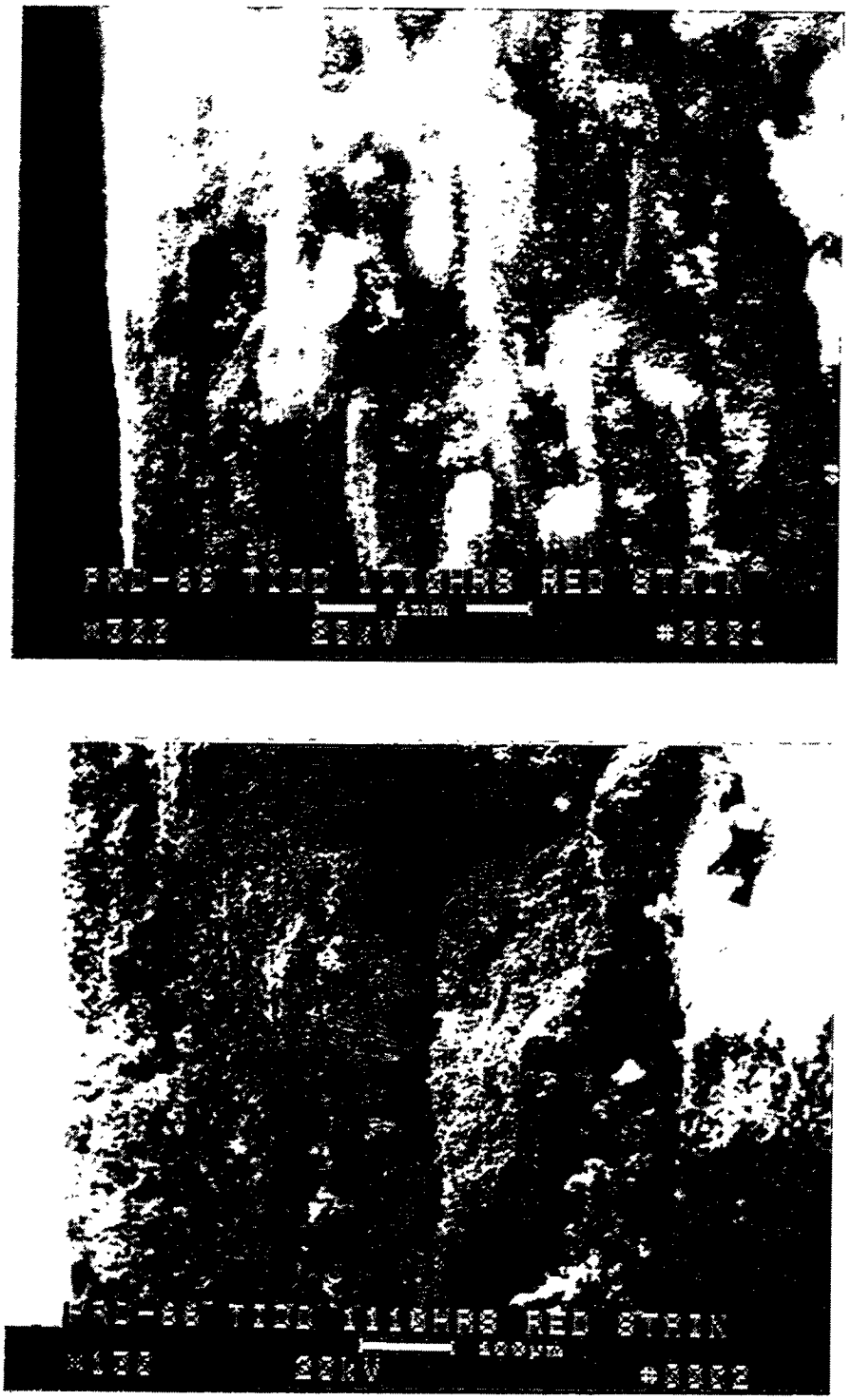

Figure 4a — Cross-Sectioned DuPont PRD-66 Filter Matrix

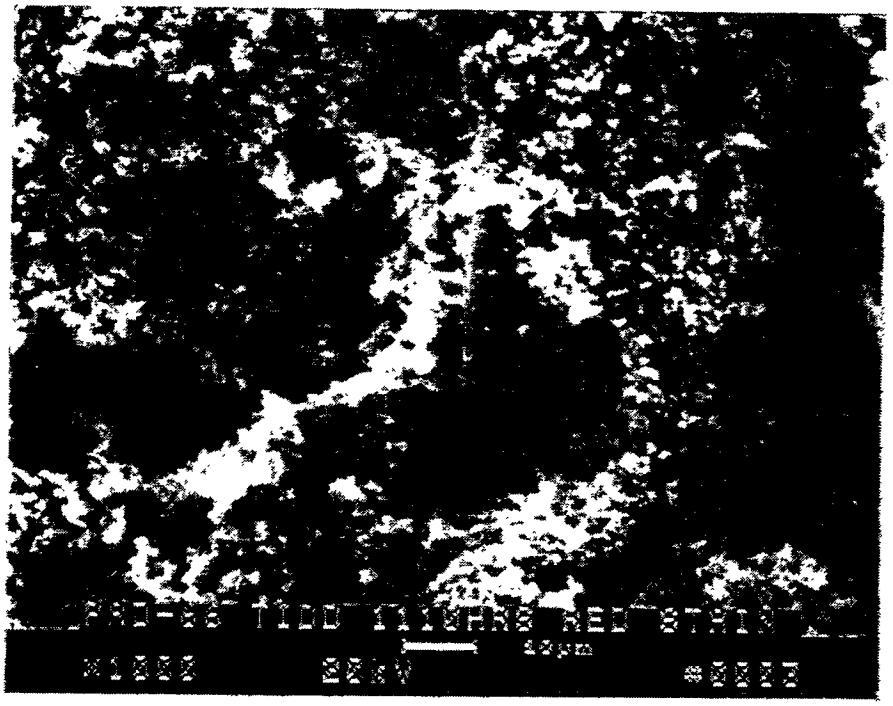

Figure 4b – Micrograph Illustrating The Presence Of Fines Along/Within The Cross-Sectioned 1110 Hour PFBC-Exposed DuPont pRD-66 Filter Matrix

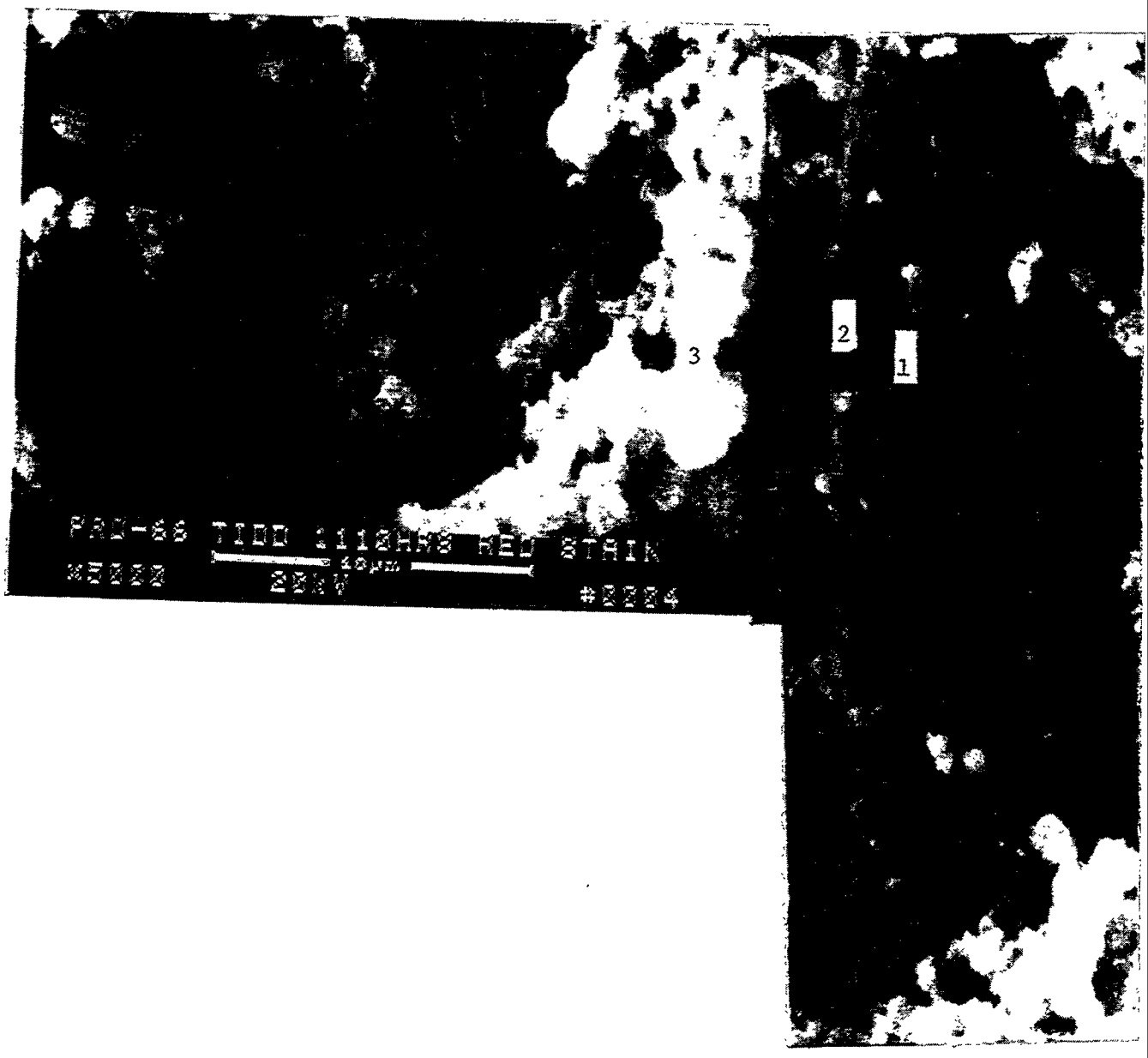

Figure 4c — Higher Magnification Montage Illustrating Tl
Mottled Cordierite Filament Yarn Bundle

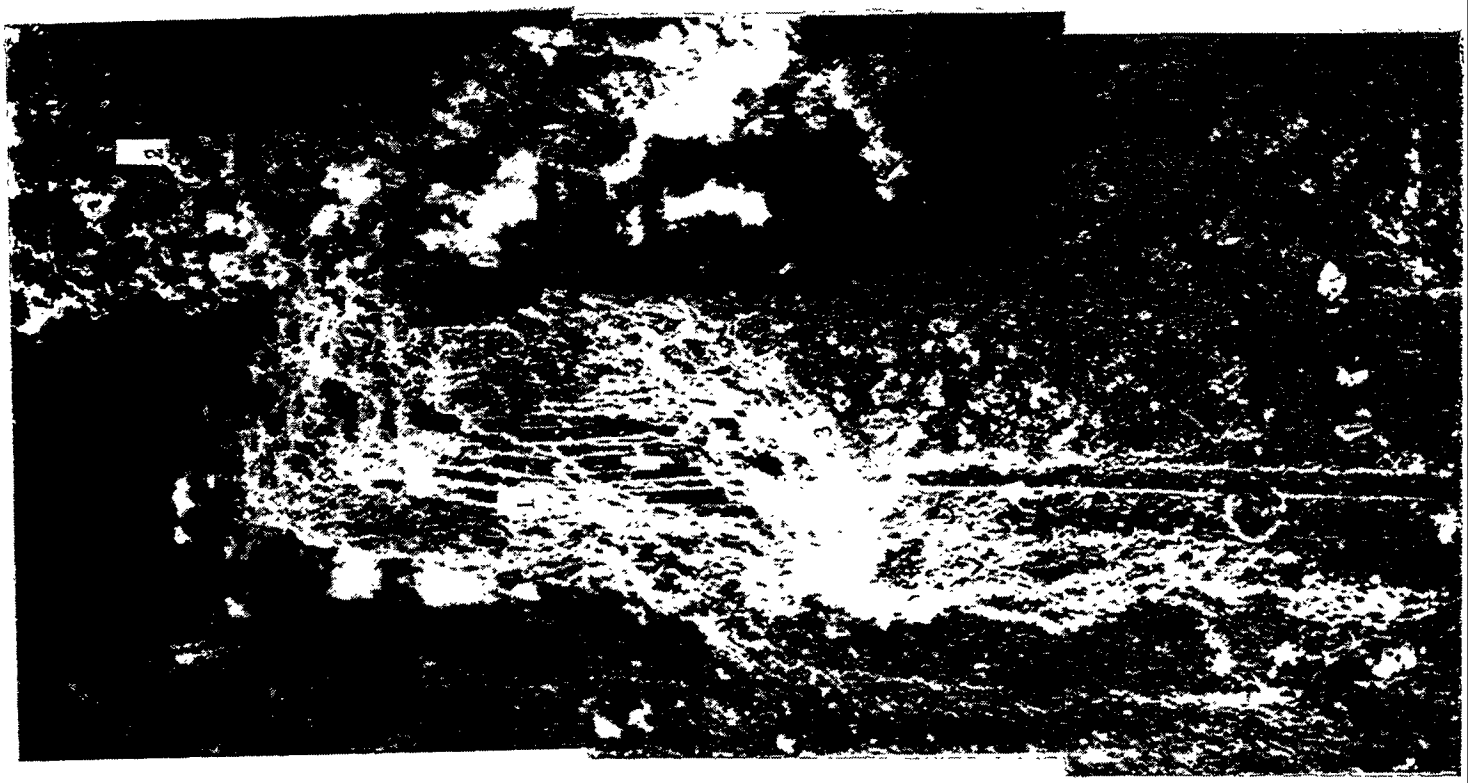

Figure 4e – Morphology Of The Cordierite Fibers In The Filament Yarn Of The 1110 Hour PFBC Exposed DuPont PRD-66 Filter Matrix

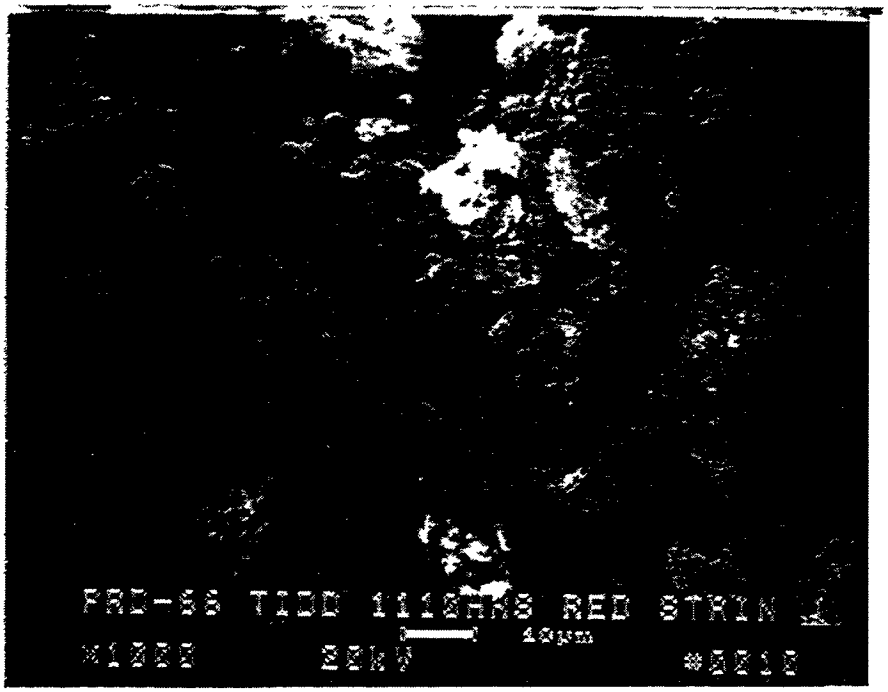

Figure 4f – Ash/Sorbent And Matrix Fines Present Between Adjacent Filament Yarn Bundles

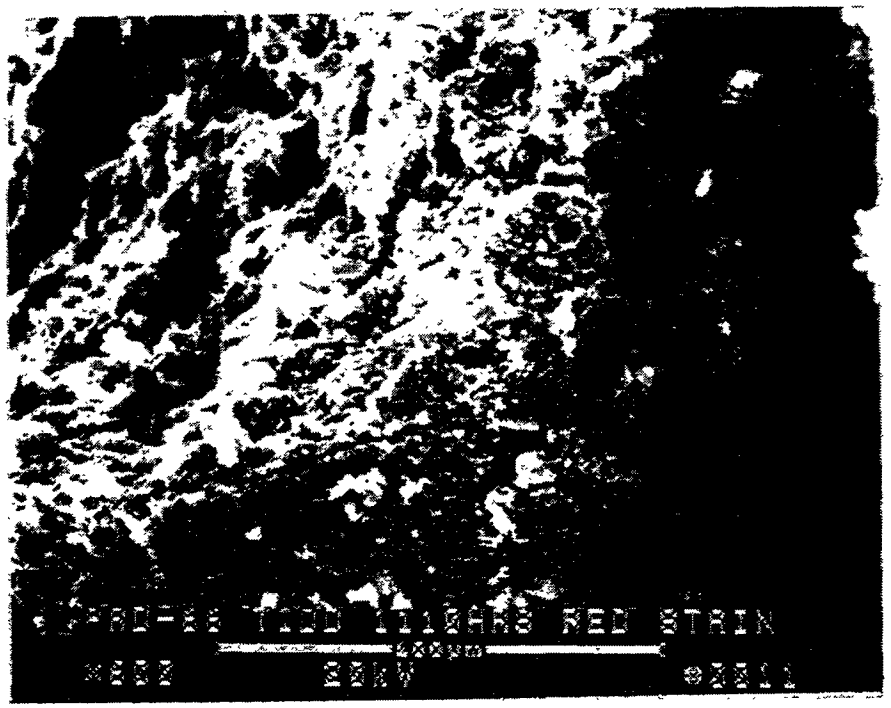

Figure 4g – Cross-Sectioned Filament Bundle In The DuPont PRD-66 Filter Matrix

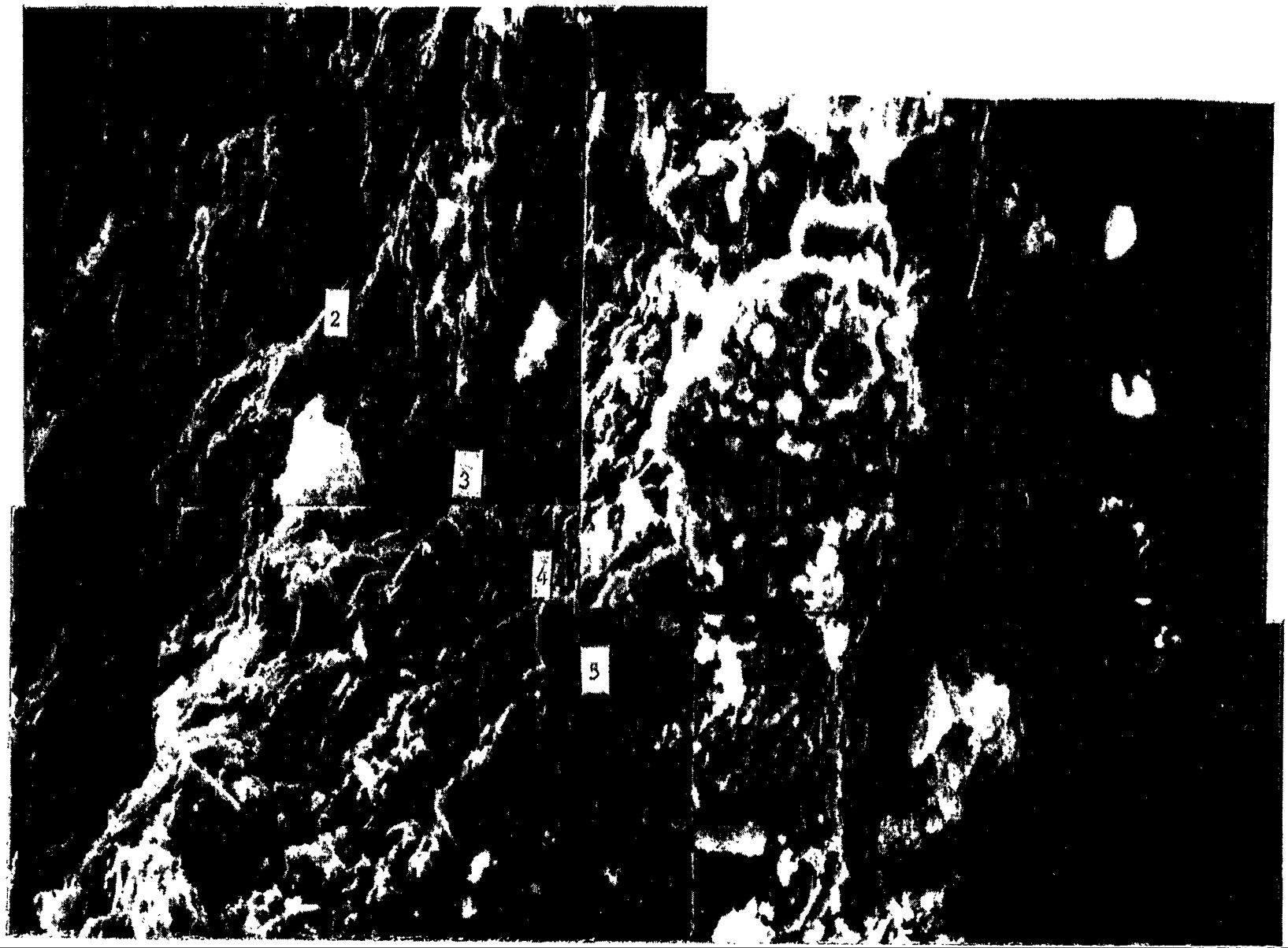
2
3
4
5

303

Figure 4h – Higher Magnification Montage Illustrating The Morphology Of The Cross-Sectioned Filament Bundle In The DuPont PRD-66 Filter Matrix

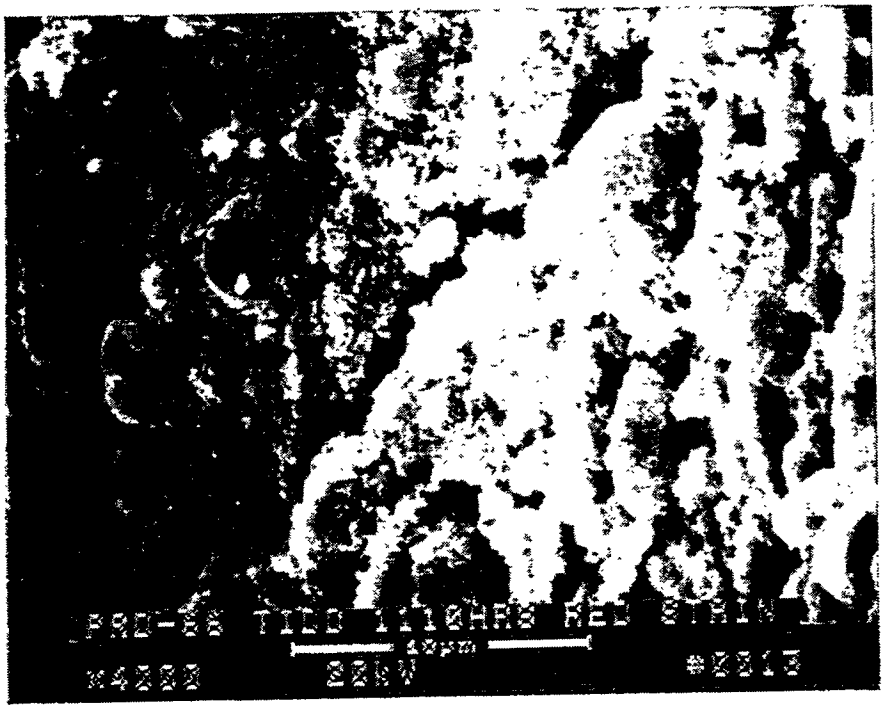

Figure 4i — Morphology Of The Matrix At The Fillet Junction Between Two Adjoining Filament Bundles In The 1110 Hour PFBC Exposed DuPont PRD-66 Filter Matrix

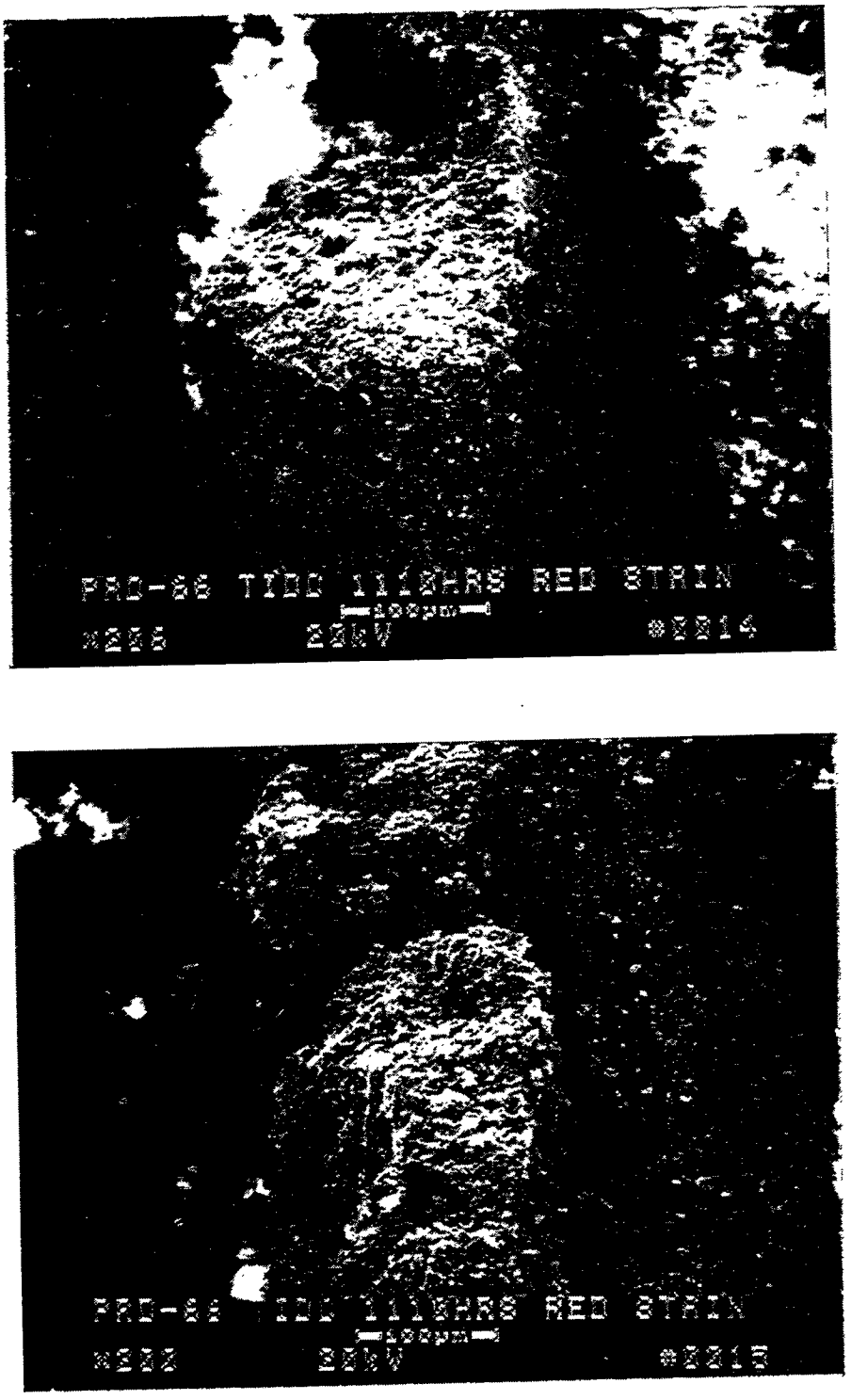

Figure 4j — Blunted, Alumina-Enriched Filament Yarn In The 1110 Hour PFBC Exposed DuPont PRD-66 Filter Matrix

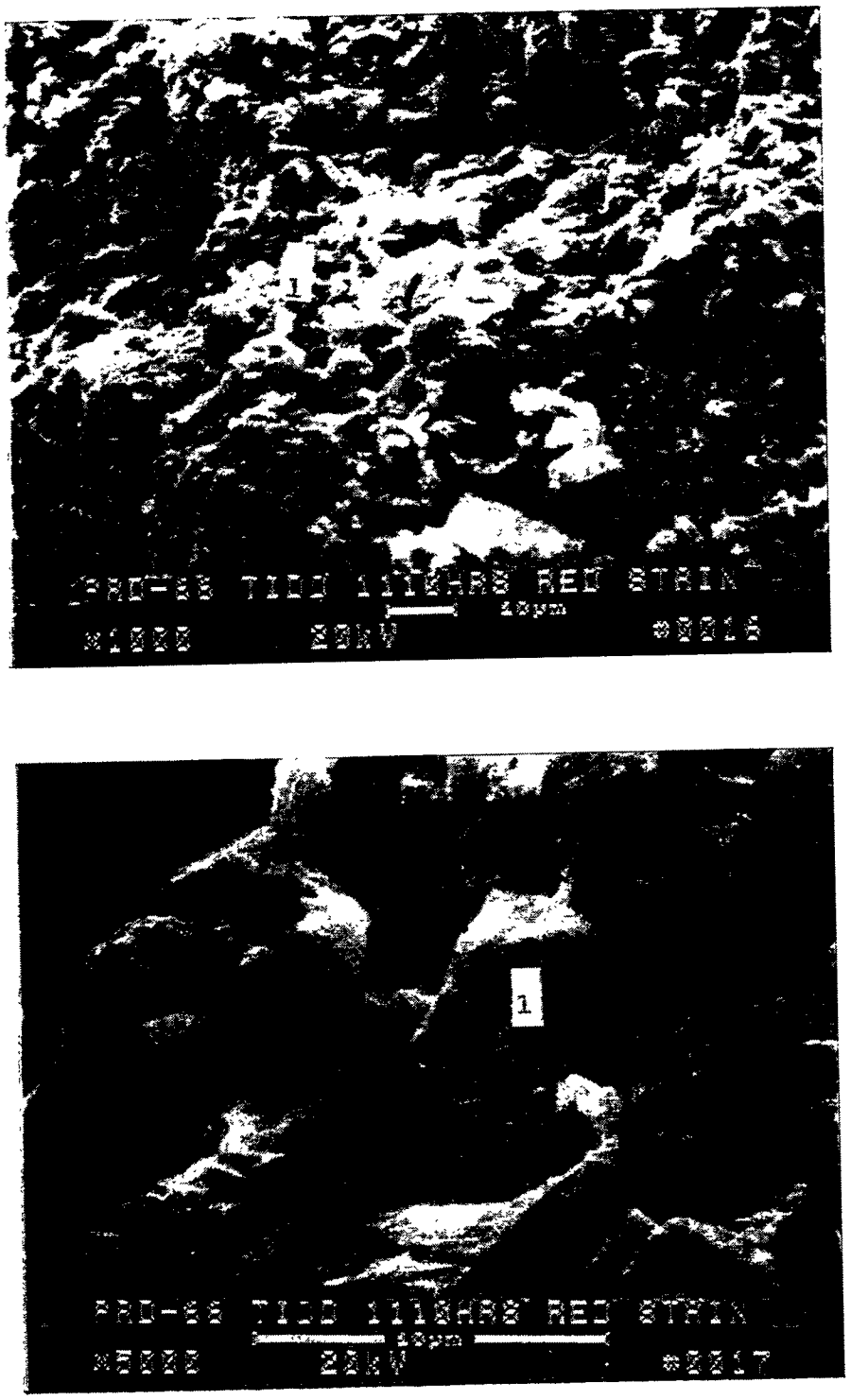

Figure 4k – Cross-Sectioned Filament Bundle At An Alternate Location Within The 1110 Hour PFBC Exposed DuPont PRD-66 Filter Matrix

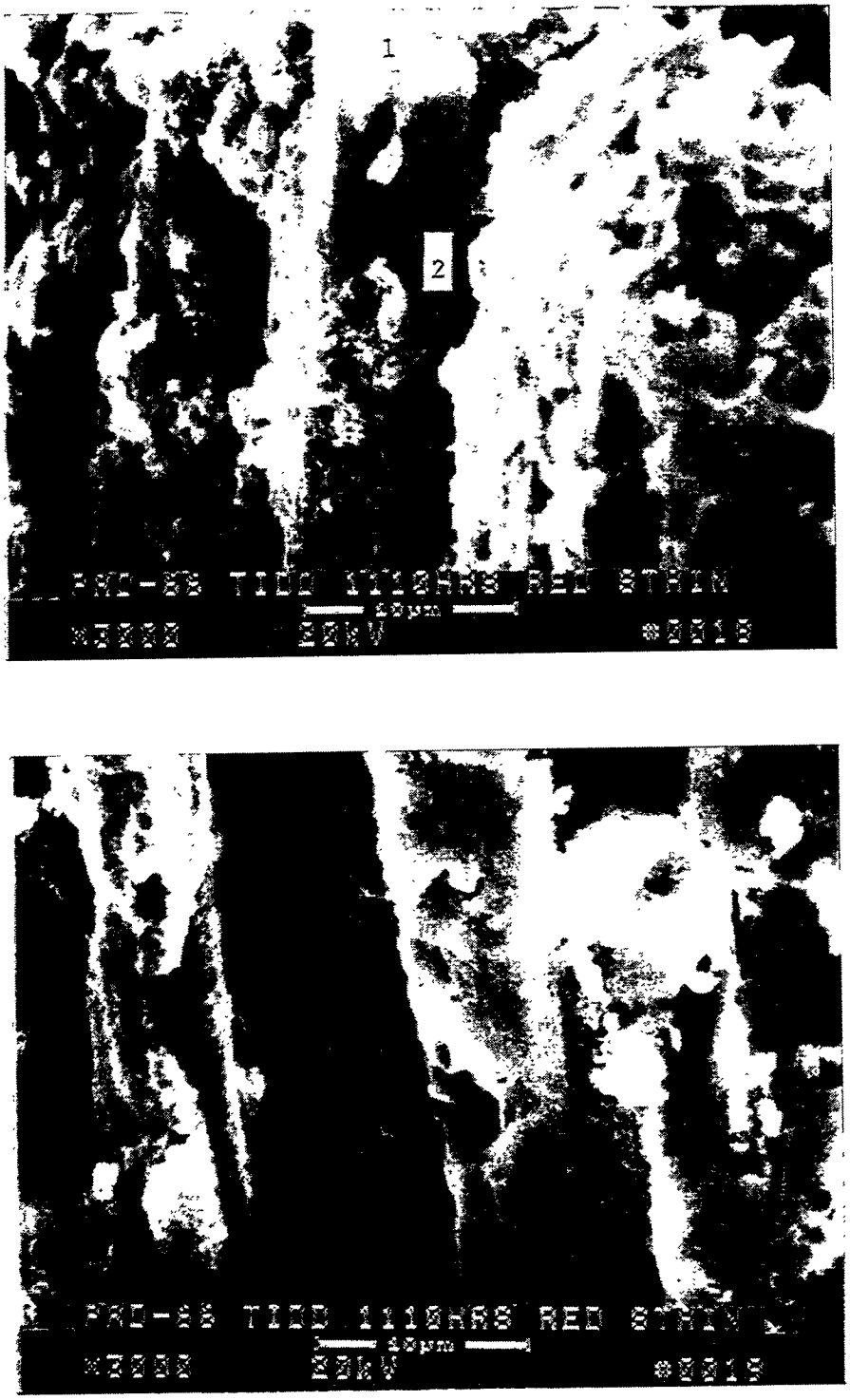

Figure 41 — Pit And Hole Formations Along The Cordierite-Enriched Fibers In The 1110 Hour PFBC Exposed DuPont PRD-66 Filter Matrix

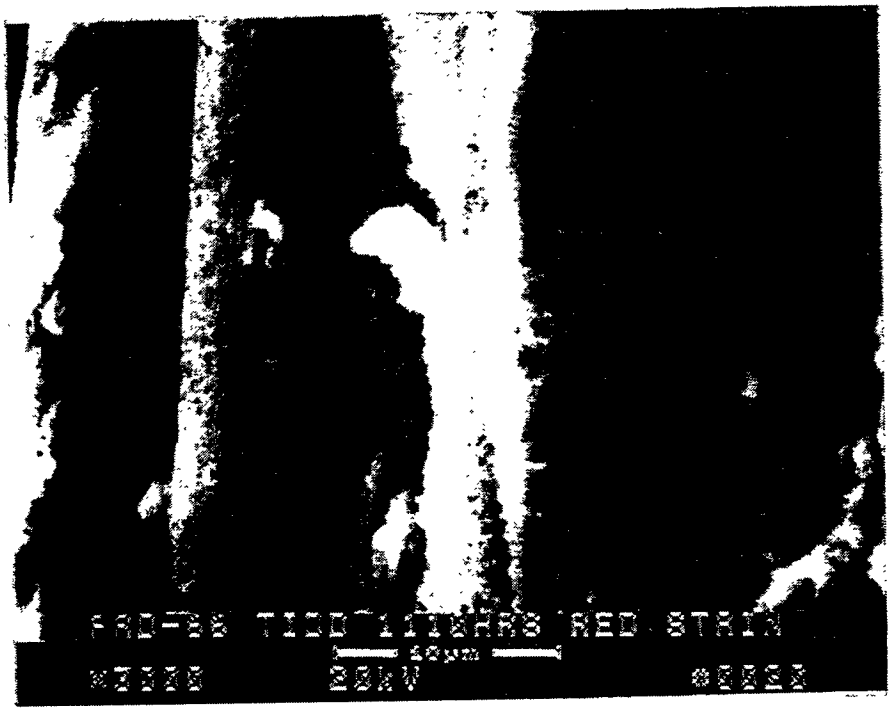

Figure 4m - Additional Micrograph Illustrating The Pit And Hole Formations Along The Filament Fibers In The DuPont PRD-66 Filter Matrix

Figure 4n – Additional Micrograph Montage Illustrating The Pit And Hole Formations Along The Filament Fibers In The DuPont PRD-66 Filter Matrix

consist of cordierite (i.e., 54.51% O, 20.54% Si, 15.79% Al, 9.16% Mg; Area 5). The fines shown in Area 6 included the presence of 60.56% O, 15.45% Si, 14.98% Al, 5.28% Mg, 2.71% Ca, 0.53% Fe, and 0.48% K.

An additional filament yarn or fiber bundle that was located below the OD membrane surface is shown in Figure 4d. The cordierite fibers are seen to be encapsulated in a mullite/alumina matrix. Mud cracks frequently form where two filament yarns overlap. Area 1, Photo 6, Figure 4d identifies the individual fibers that are present within the filament yarn. These are shown at higher magnification in Figure 4e. Holes and pits are evident along the cordierite-enriched fibers (i.e., 62.83% O, 18.97% Si, 10.68% Al, and 7.52% Mg).

The fines shown in Area 2, Photo 6, Figure 4f, are shown at higher magnification in Photo 10, Figure 4f. Although gold was used to prepare the sample. a strong sulfur concentration was evident in the EDAX analyses. The fines consisted of ash/sorbent material, and perhaps particles of the PRD-66 filter matrix (i.e., 66.71% O, 11.40% Si, 8.48% Al, 6.41% Mg, 3.32% Ca, 2.03% Fe, 0.90% S, and 0.75% K).

Figure 4g shows the mullite and alumina outer layer which encapsulates the cordierite fibers in the DuPont PRD-66 filament yarn. This entire area is shown at higher magnification in the montage presented in Photo 12, Figure 4h. Area 1 is located along the outer surface of the filament yarn. The polycrystalline area is composed of principally alumina (i.e., 50.50% Al, 46.20% O, and 3.30% Si). Area 2 which is along the outer periphery of the fiber bundle, but below the encapsulated layer, consists of 64.26% O, 15.87% Si, 12.99% Al, and 6.88% Mg (i.e., cordierite-containing fiber). Area 3 which is located between the cordierite fiber bundles and the encapsulating layer consists of 49.62% O, 24.79% Si, 19.09% Al, and 6.51% Mg (i.e., mixture of cordierite, mullite, perhaps corundum and/or cristobalite). Moving towards the outer surface of the encapsulated area (i.e., Area 4), a corundum-containing phase becomes predominant (i.e., 0.37% O, 33.42% Al, and 6.20% Si). A magnesium-enriched aluminosilicate phase formed along the outer periphery of the fiber bundle (Area 5; 67.46% O, 17.03% Si, 9.36% Al, and 6.15% Mg).

At the fillet junction where two adjacent filament yarns meet, an alumina-enriched matrix resulted (i.e., Figure 4i: 66.64% O, and 33.36% Al). The blunted filament yarn shown in Photo 14, Figure 4j, is coated with alumina.

Moving several fiber bundles into the matrix (i.e., Photo 15, Figure 4j; and Figure 4k), the cordierite fibers are evident below the polycrystalline mullite/alumina, and possibly cristobalite-containing encapsulating layer. Higher magnification of the ~7 μm cordierite fibers is shown Photo 17, Figure 4k. Frequently holes are evident at the center of the cordierite fibers (i.e., Area 1, Photo 17, Figure 4k: 54.91% O, 26.00% Si, 13.18% Al, and 5.91% Mg).

Hole and pits are frequently seen along the surface of adjacent fibers (Figure 4l). The fiber matrix principally consists of a cordierite-containing phase (Area 1, Photo 18, Figure 4l: 59.83% O, 20.73% Si, 12.62% Al, and 6.82% Mg), while the particles seen to be attached to the fiber (Area 2, Photo 18, Figure 4l) were identified to consist of 63.52% O, 25.72% Al, 8.64% Si, and 2.12% Mg.

The mottled and pitted outer surface of the cordierite fibers were observed throughout the entire ~7 mm DuPont PRD-66 filter matrix which had been exposed to PFBC conditions in the W-APF in Test Segment #5.

DIVOT FORMATIONS

The DuPont PRD-66 candle filter D-247 which had been located in position B/T-2 experienced failure during operation in the W-APF at AEP in Test Segment #5. The mid-body fractured candle filter also sustained divot formations along both the "red ash stained" and "non-red ash stained" areas of the filter body (Figure 5a). Similarly divoting resulted at Westinghouse during high temperature, high pressure accelerated pulse testing during which time limited ash was fed to the filter array containing DuPont PRD-66 and alternate candle filter elements. The formation of divots therefore appears to be independent of the accumulation of ash along the surface of the DuPont PRD-66 filter body at AEP. The formation of divots most likely results from a mechanical stress imposed on the filter body during field or bench-scale process operation.

In order to support this conclusion, a section of the B/T-2 filter element was removed near the divoted area, cross-sectioned, and carbon coated for characterization via SEM/EDAX analyses. The series of micrographs presented in Figure 5 illustrates the ash formation along the outer membrane surface; the surface of the DuPont PRD-66 filter matrix at various divoted layers (i.e., filament wound layers); and the fractured filament fiber bundles along the cross-sectioned filter wall.

Figure 5b illustrates the outer membrane layer and divot area which permitted the fractured support layer filaments to be directly contacted with the ash/sorbent fines. Area 1 shown in Photo 1, Figure 5b, is shown in the higher magnification montage provided in Figure 5c. Ash fines are readily evident along the entire surface, covering both the OD membrane filament matrix, as well as the fractured support filament layers.

The fractured filament shown in Area 1, Photo 2, Figure 5c is shown at higher magnification in Figure 5d. The raised ridge of the filament may have been stripped of its outer encapsulating layer, revealing fibers, but however due to the accumulation of fines along the surface, neither the fibers nor filament polycrystalline layer can be identified with complete certainty. The morphology of the fines is shown in Photo 4, Figure 5d, as well as in Figure 5e. EDAX analyses of the fines shown in Photo 8, Figure 5e, indicated the presence of 73.61% O, 13.47% Al, 4.62% S, 3.21% Si, 2.60% Ca, 1.71% Mg, 0.56% Fe, and 0.23% Ti. The presence of sulfur, calcium, and magnesium within the fines indicates the presence of the sorbent matrix within the ash deposit (i.e., iron, titanium, as well as silicon). The high aluminum content may have resulted from the underlying filament polycrystalline encapsulating layer. The fines which remained in this area were primarily submicron agglomerates which may have deposited and sintered together while remaining along the surface of the filter element.

The cross ridged region shown in Area 2, Photo 2, Figure 5c, is expected to contain the outer encapsulating layer of the filament bundle. This is considered since the two cross filaments which were originally positioned above the sub-layer filament in Area 2, had been removed. The Area 2 filament bundle is shown at higher magnification in Figure 5f. Once again, numerous submicron fines or agglomerates are evident in this area. The fines frequently appear as a coalesced layer, with limited porosity. EDAX analysis of the fines shown in Photo 8, Figure 5f, identified the presence of 75.66% O, 9.23% S, 5.84% Ca, 4.80% Mg, 2.10% Si, 1.85% Al, and

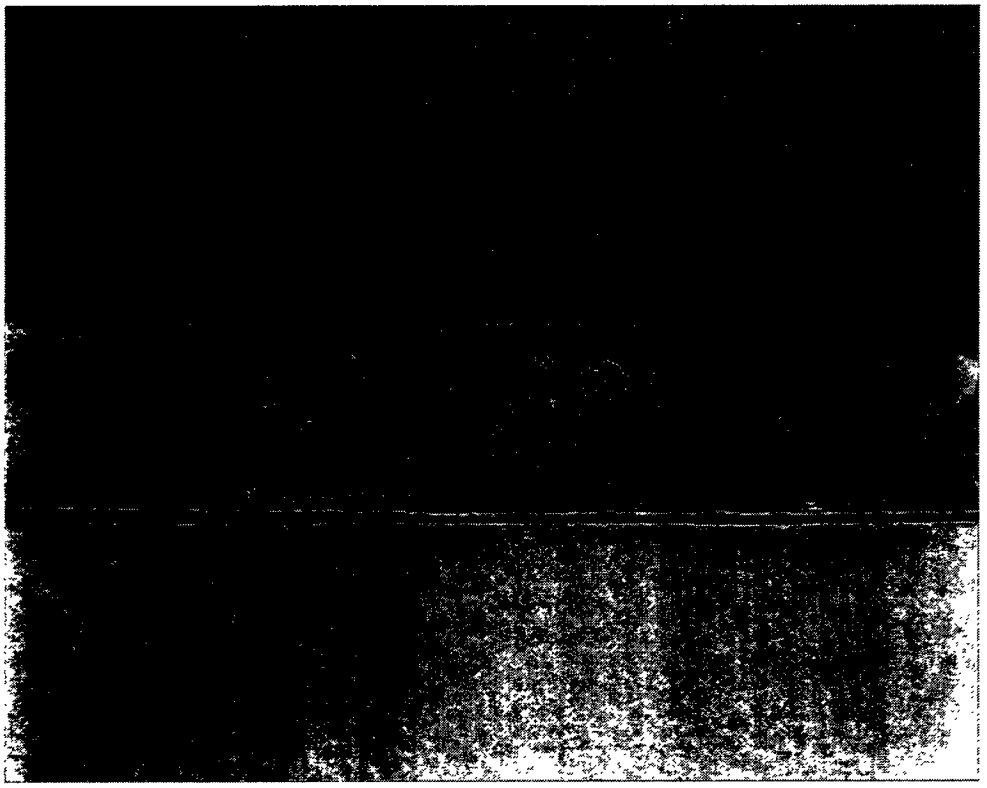

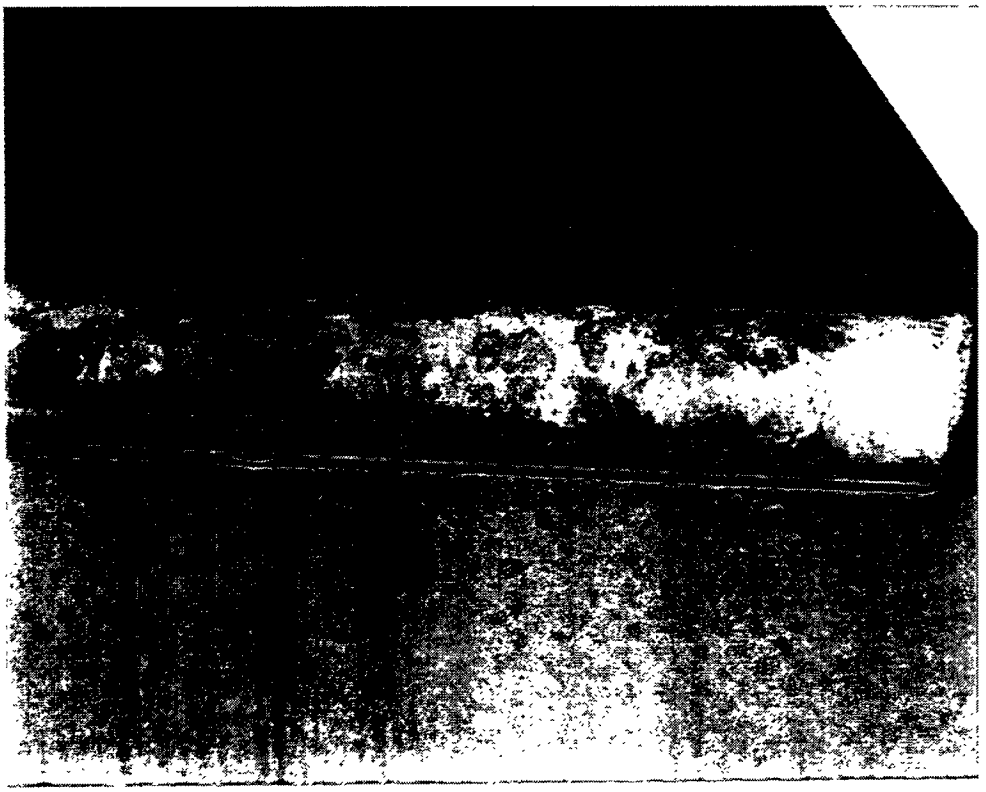

Figure 5a – Divot Formations Along The "Red Ash Stained" And "Non Red Ash Stained" Areas Of The DuPont PRD-66 Filter Element After 1110 Hours Of PFBC Operation In Location B/T-2 In The W-APF

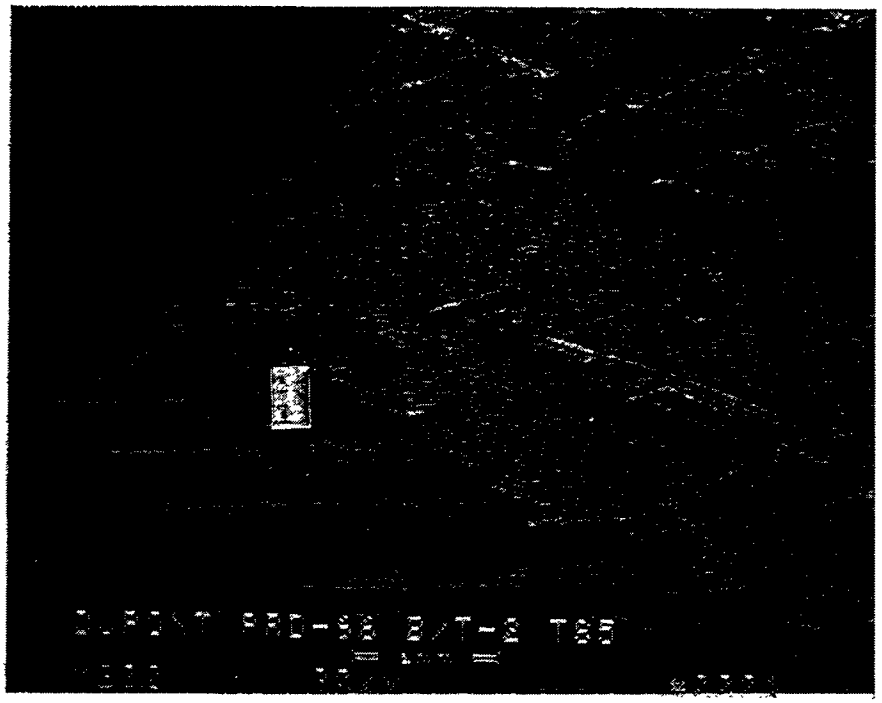

Figure 5b – Membrane Section, "Red Stained" Area, And Divot Formation Of The DuPont PRD-66 Filter Element Which Had Been Exposed For 1110 Hours At AEP

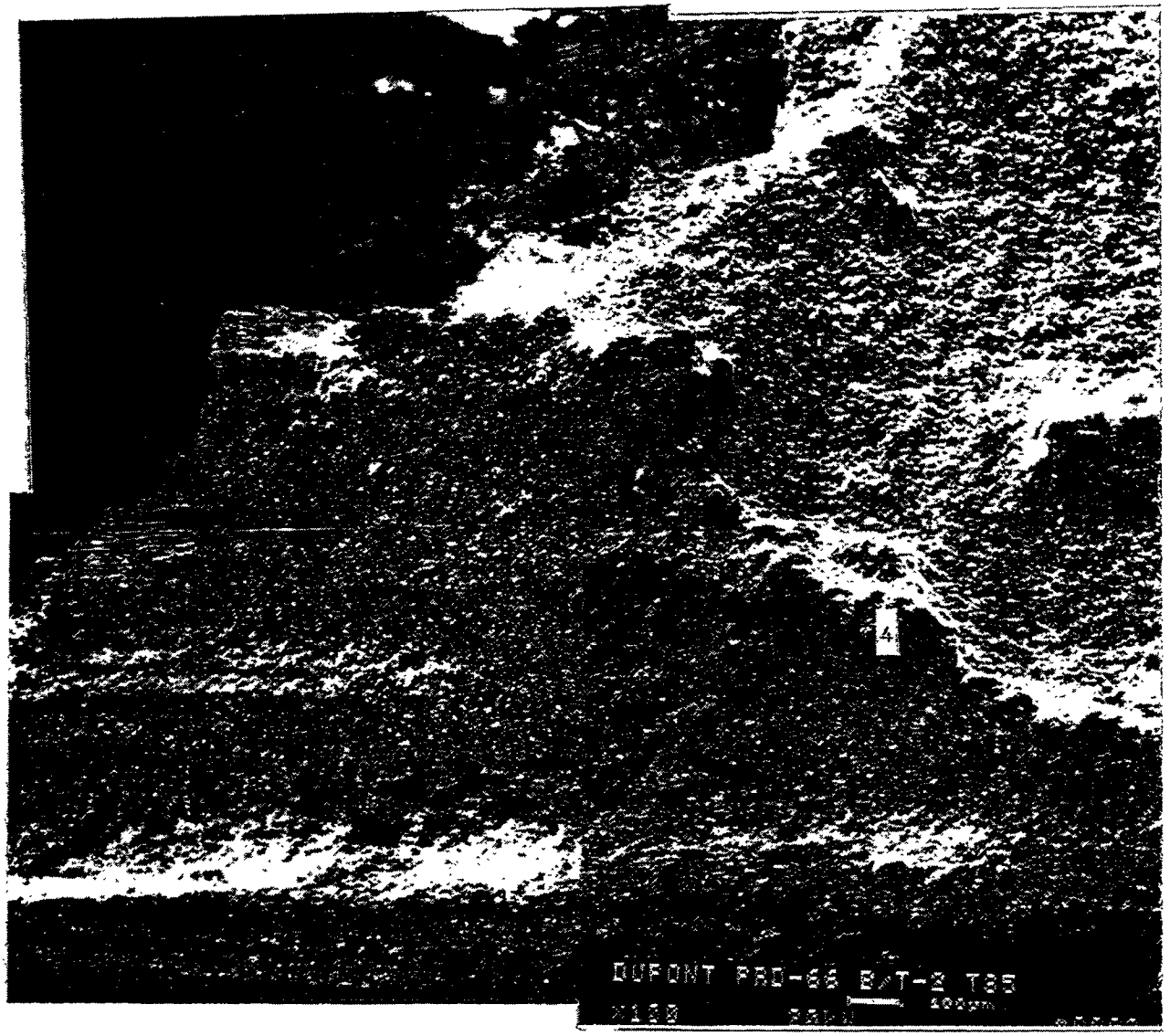

Figure 5c – Higher Magnification Micrograph Montage (
Filter Matrix

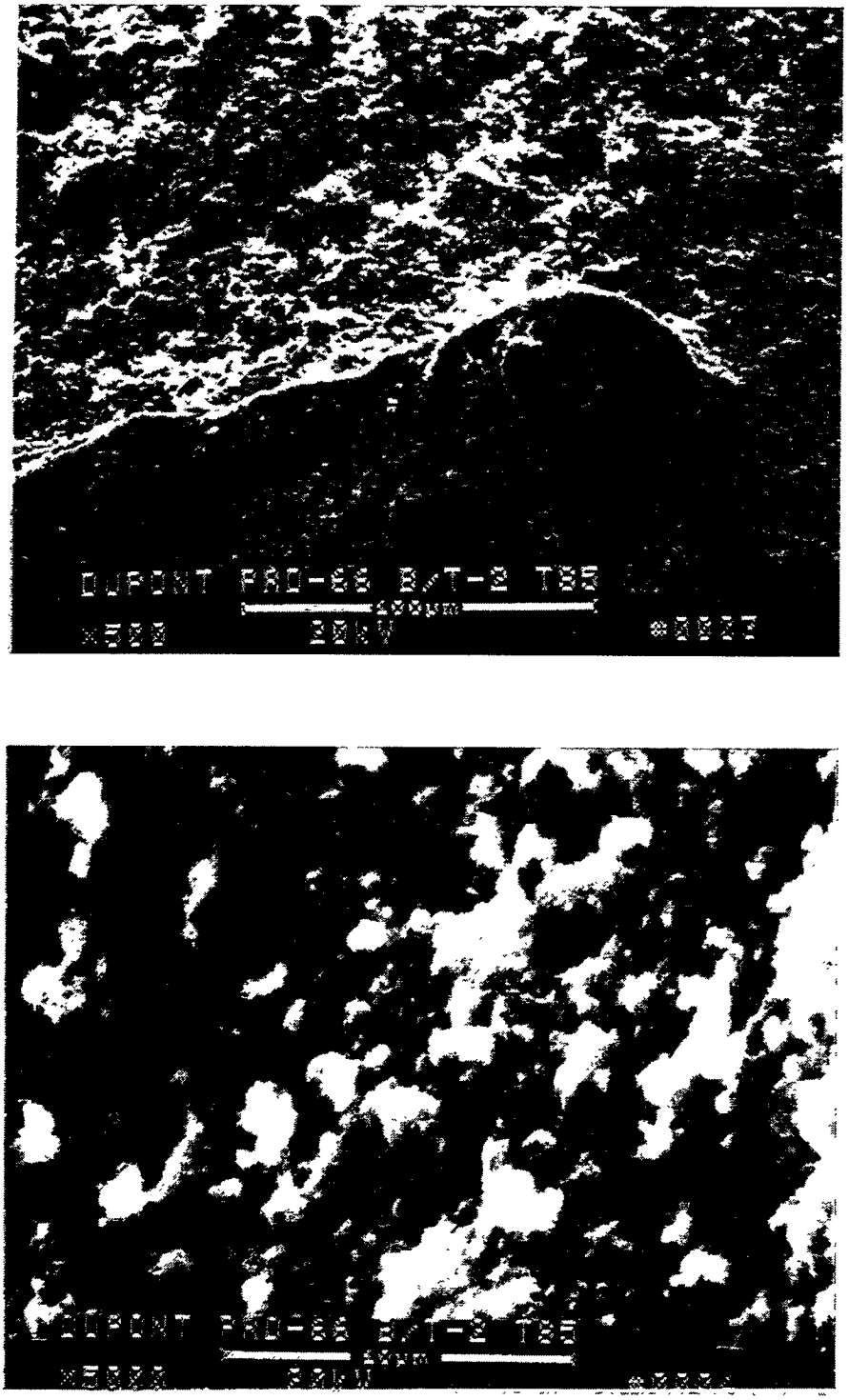

Figure 5d – Ash/Sorbent Fines Deposited Along The Fracture Filament Bundles Below The Membrane Surface Of The DuPont PRD-66 Filter Matrix

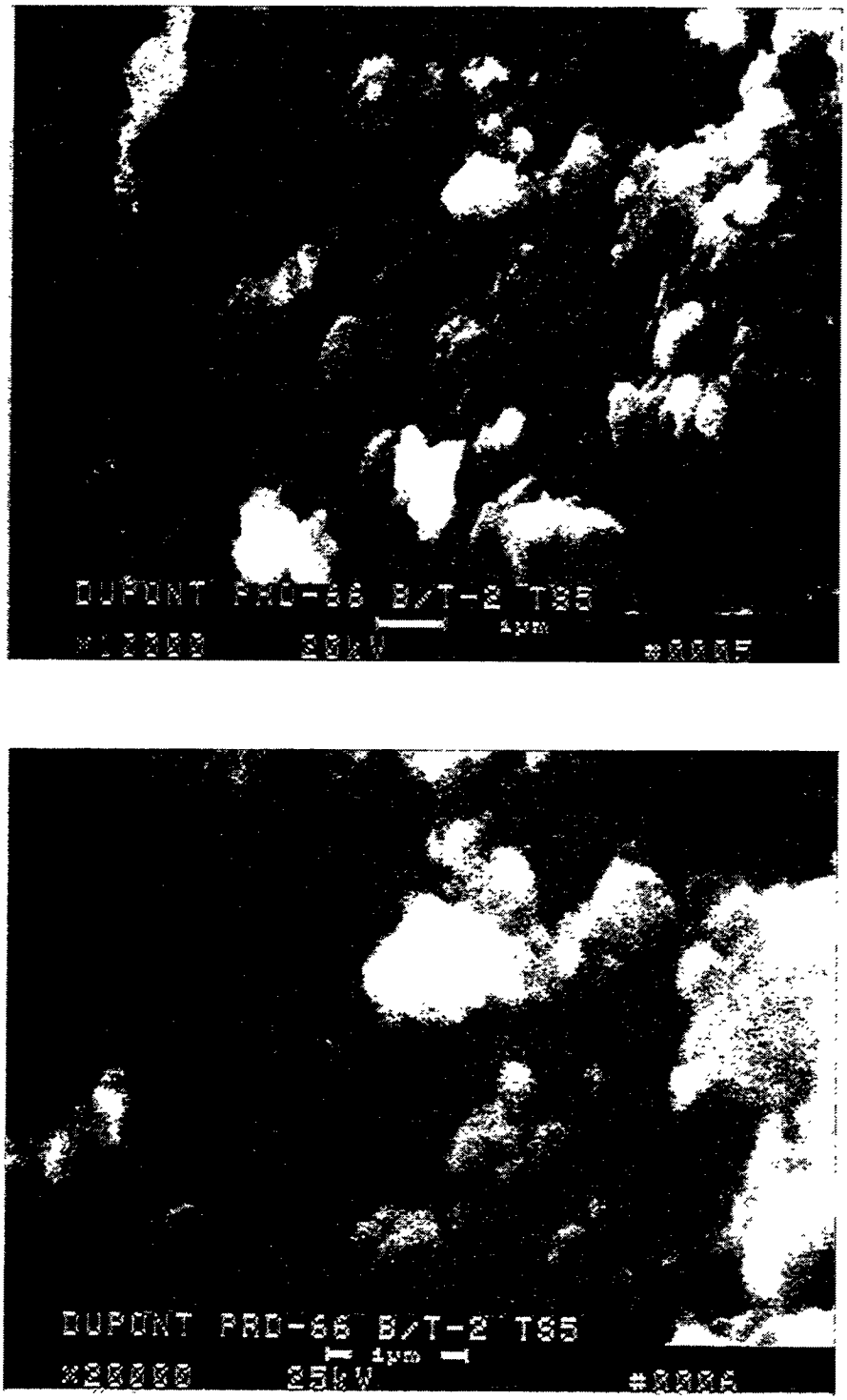

Figure 5e – Higher Magnification Micrographs Of The Ash/Sorbent Fines

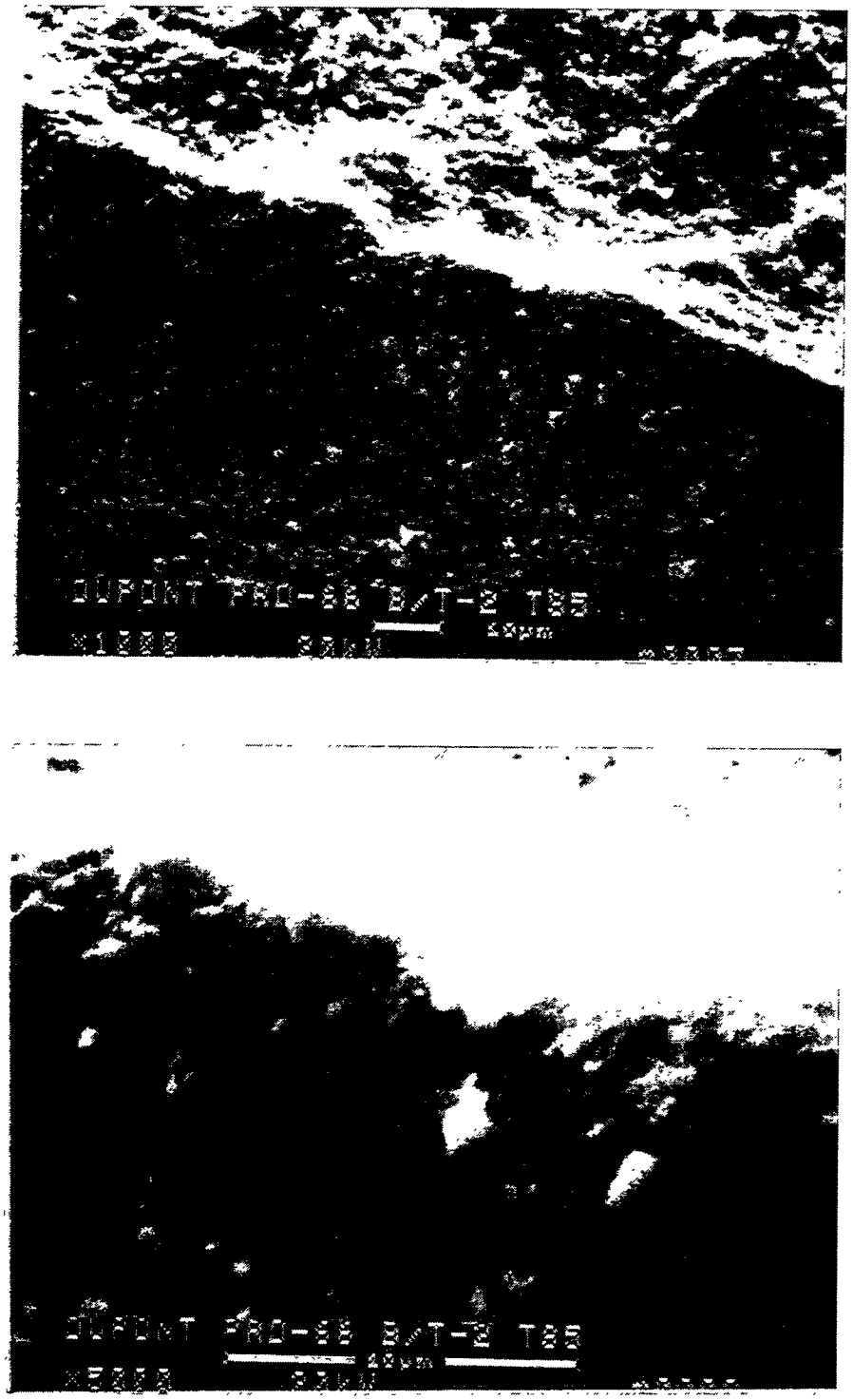

Figure 5f – Ash/Sorbent Deposited Along The Filament Bundles Below The Membrane Surface Of The DuPont PRD-66 Filter Matrix

Figure 5g – Higher Magnification Micrograph Of The Deposited Ash/Sorbent Fines

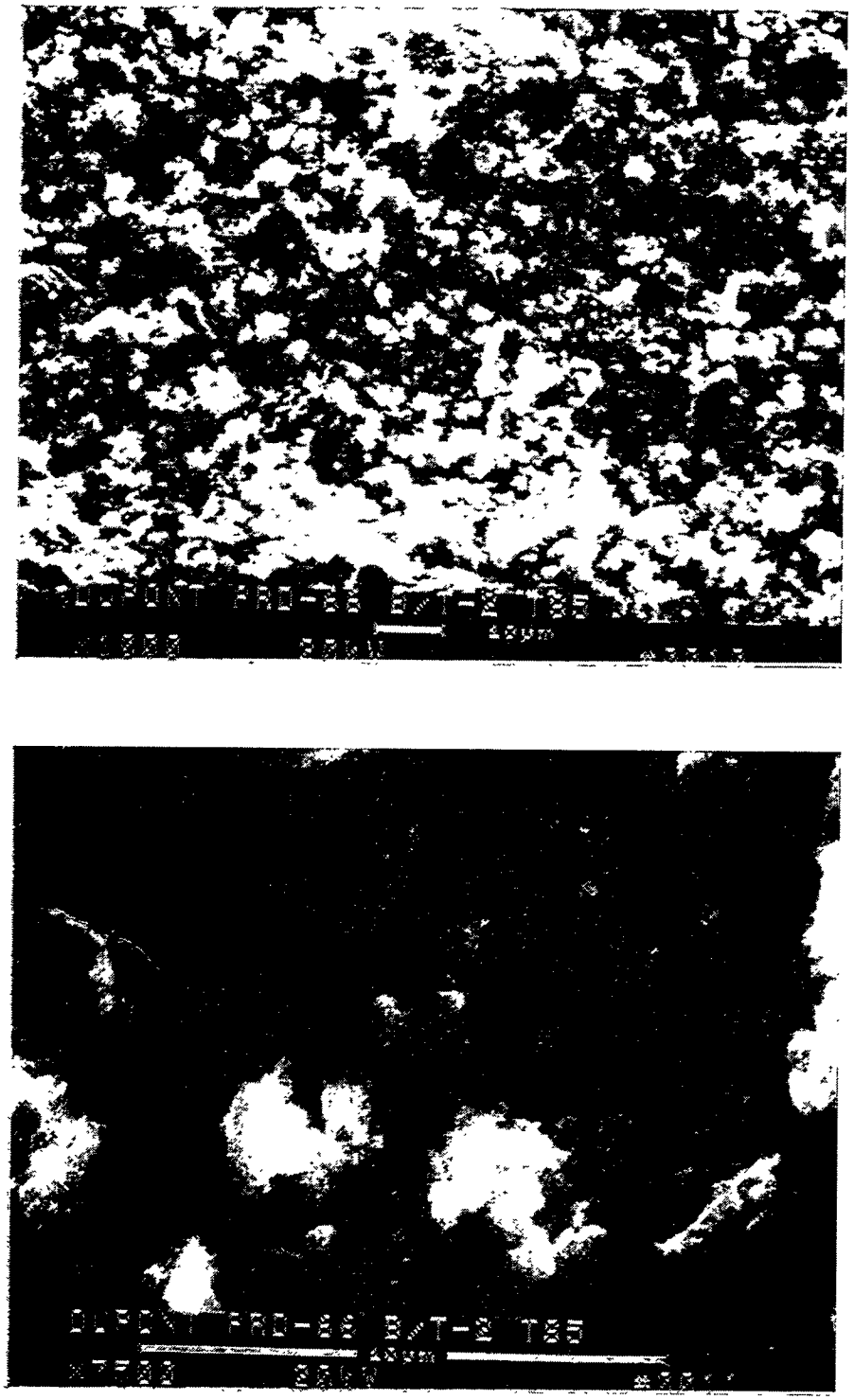

Figure 5h – Ash/Sorbent Deposited Fines Within The Pore Cavity Of The DuPont PRD-66 Filter Matrix

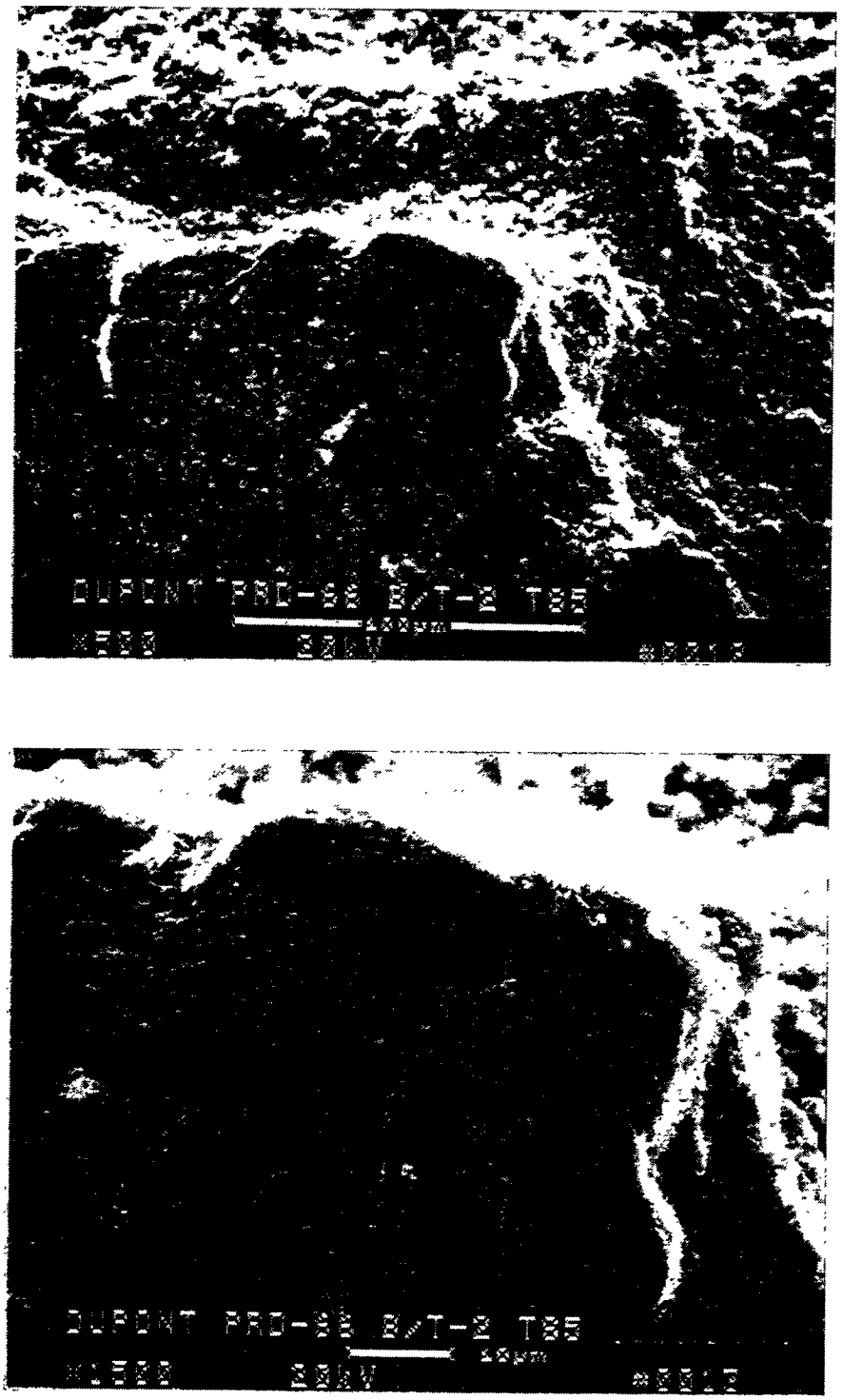

Figure 5i — Ash/Sorbent Deposit Along The Membrane Fracture Edge Of The Divot Formation

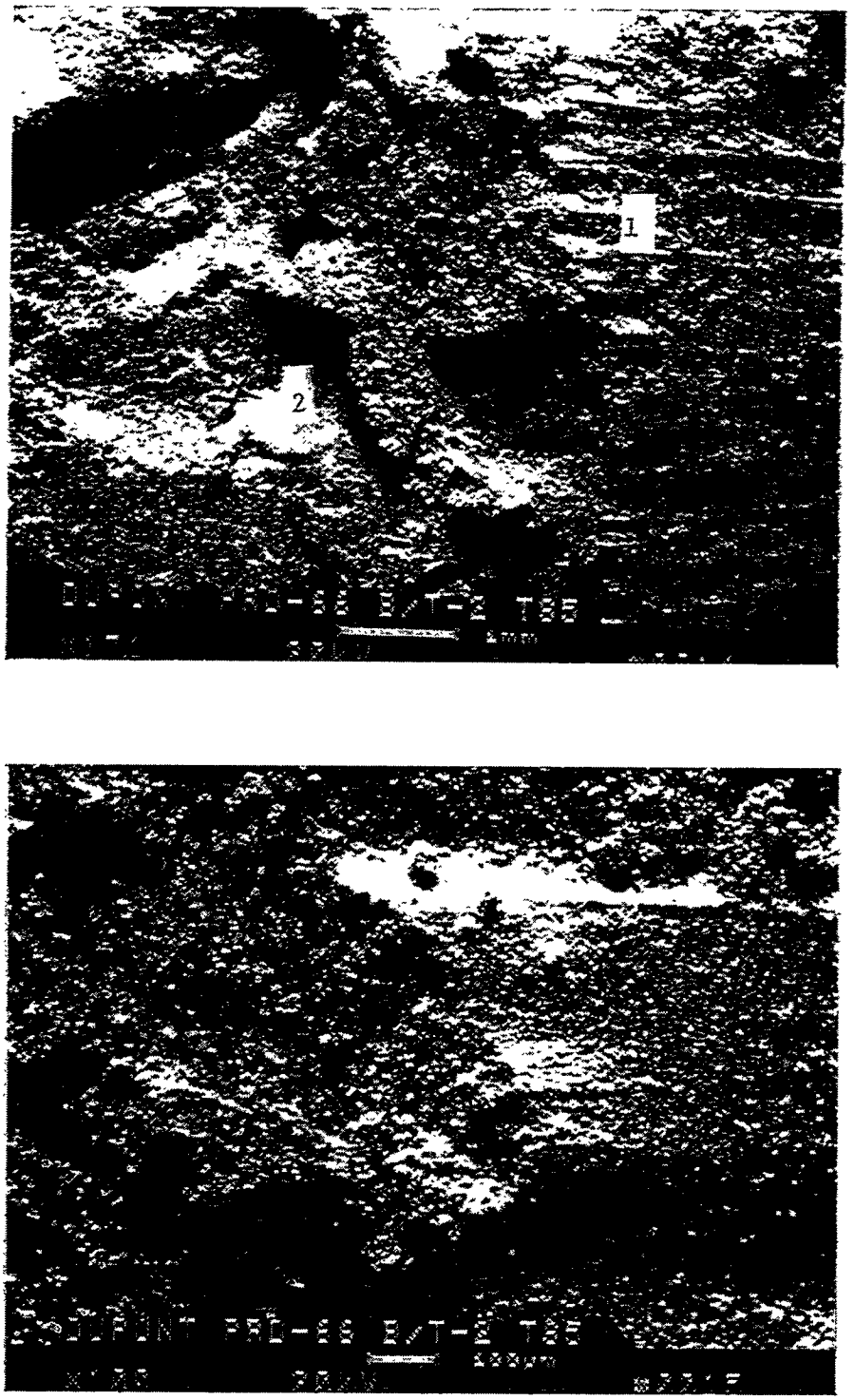

Figure 5j — Alternate Location Of The Divot Which Formed Along The Outer Surface Of The DuPont PRD-66 Filter Matrix

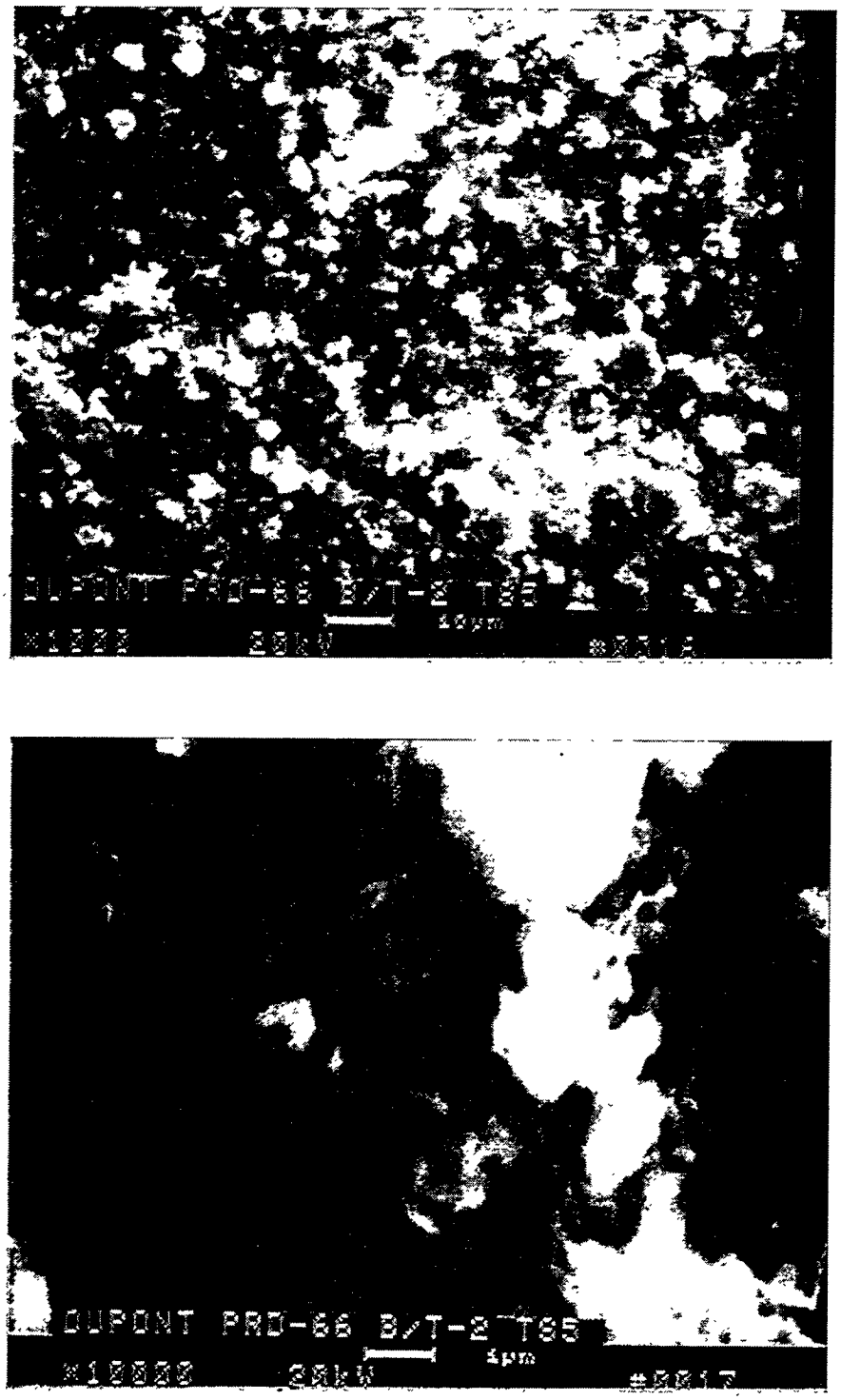

Figure 5k – Higher Magnification Micrographs Of The Fines Deposited Along The Membrane Surface

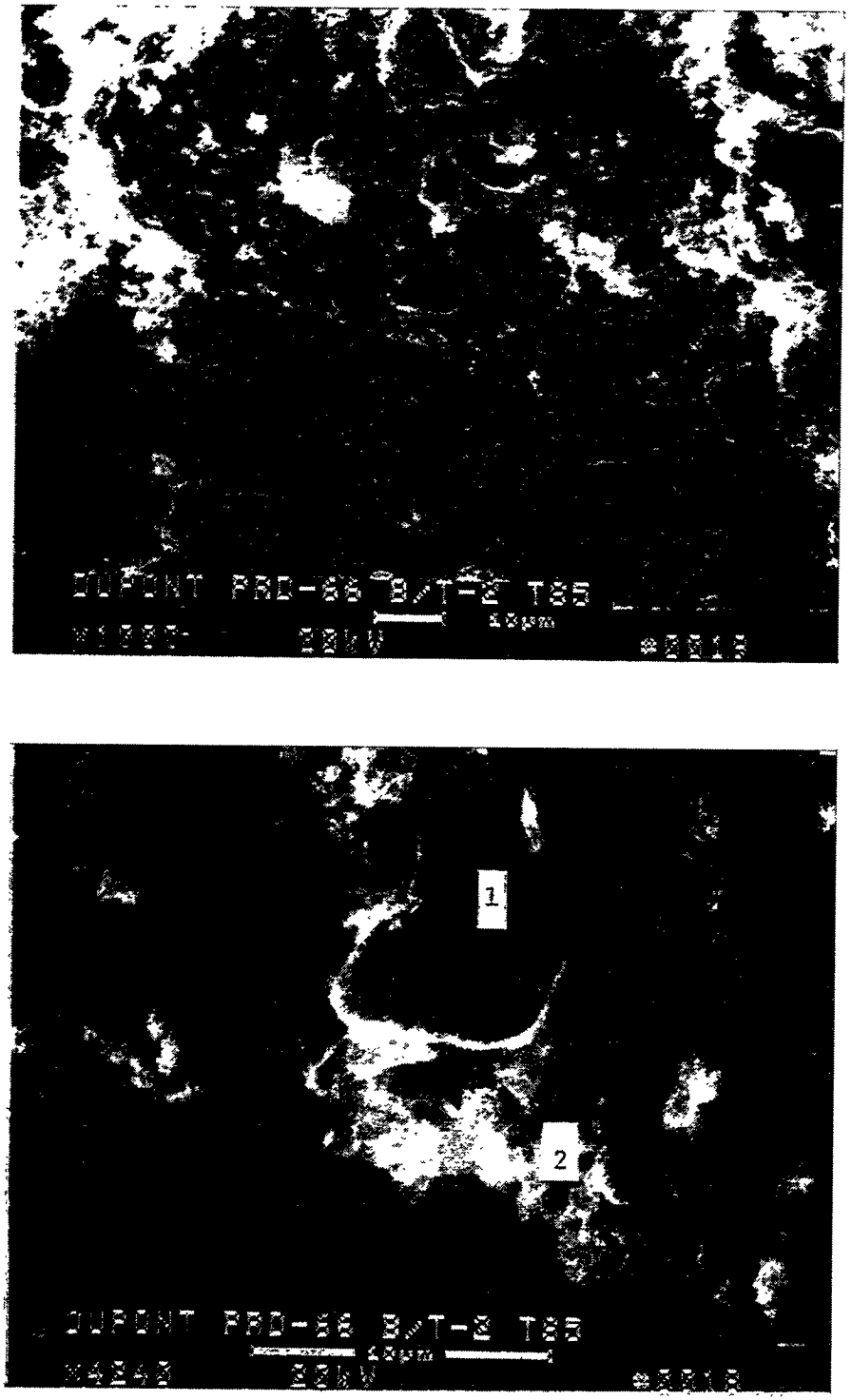

Figure 51 — Morphology Of The Fines Which Remained Along The Fractured Surface Of The Membrane Layer

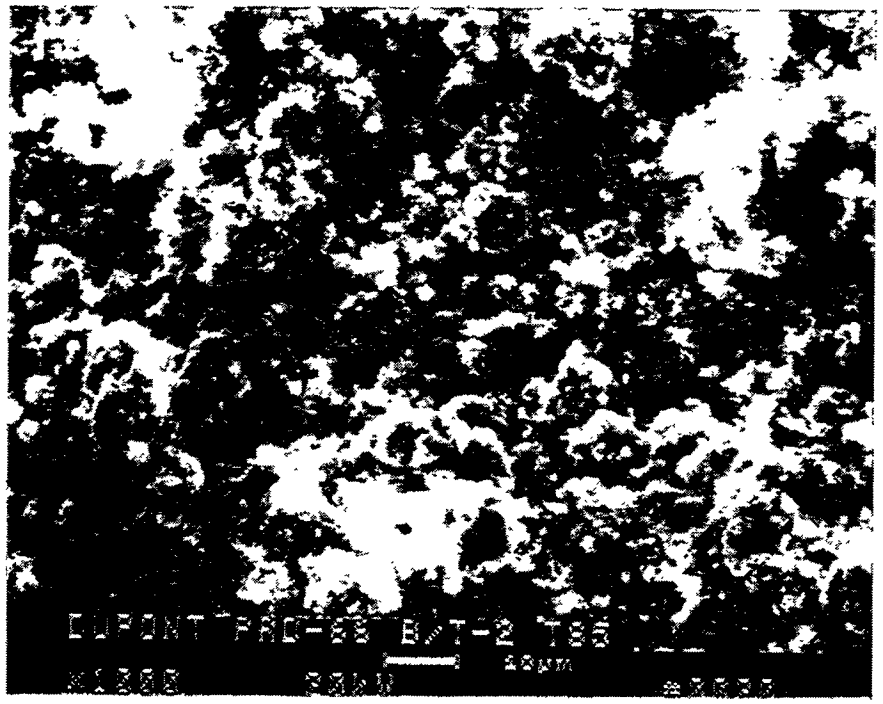

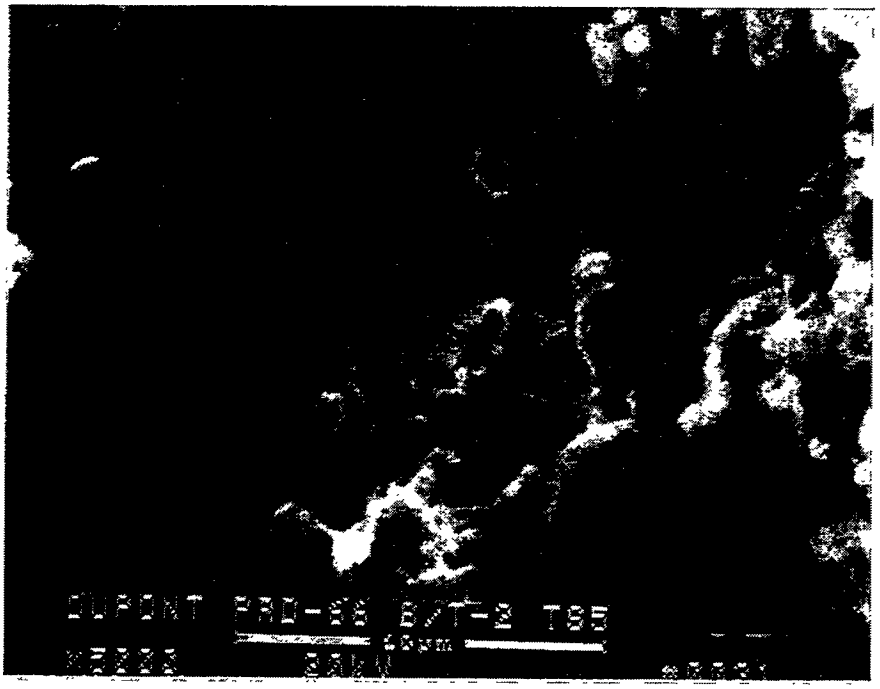

Figure 5m –Morphology Of The Ash/Sorbent Fines That Were Located At The Edge Of The Divot Formation Near The Fractured Membrane

Figure 5n – Higher Magnification Micrograph Of The Ash/Sorbent Deposited Fines

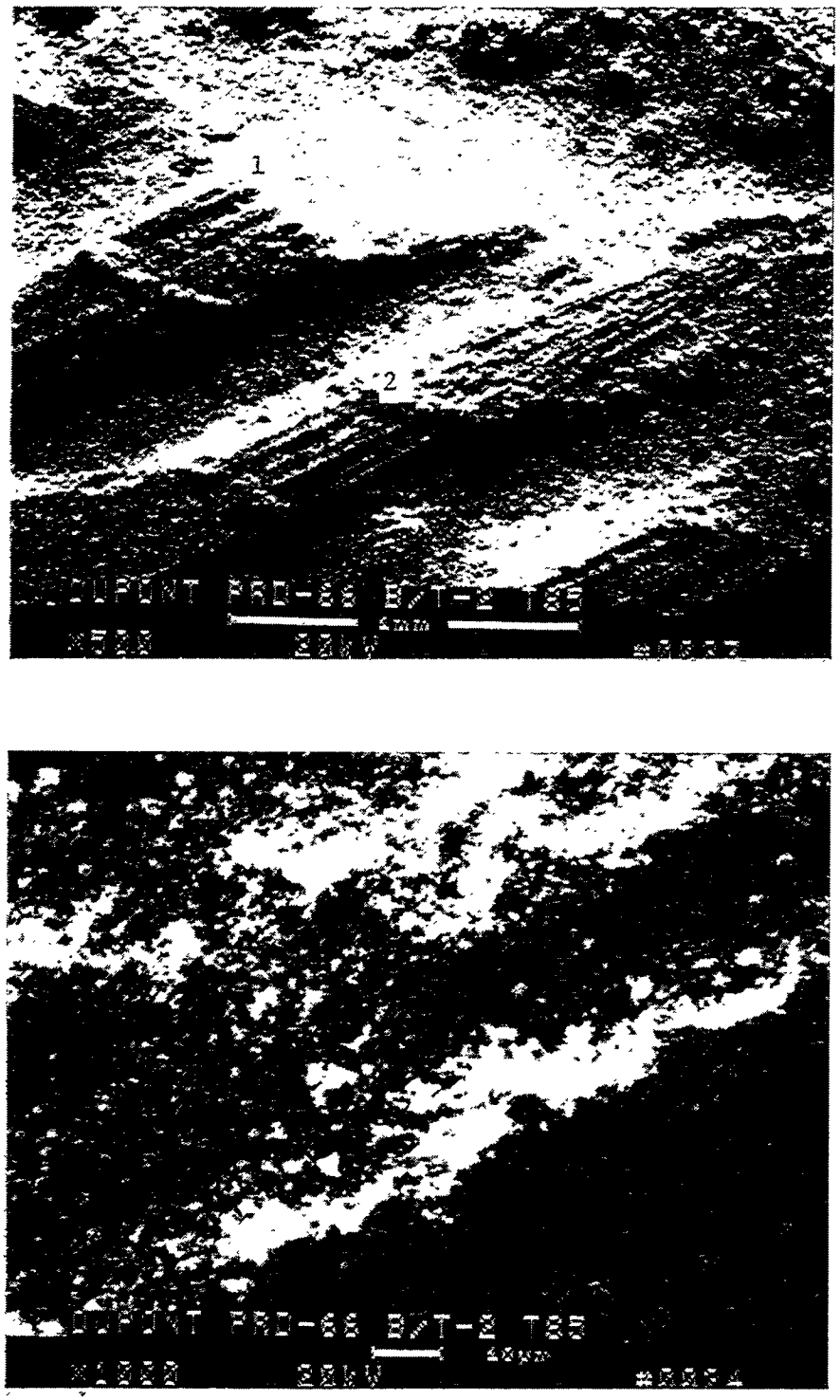

Figure 5o – Sub-Layer Filament Bundles In The Coarse Support Matrix Of The Divoted DuPont PRD-66 Filter Matrix

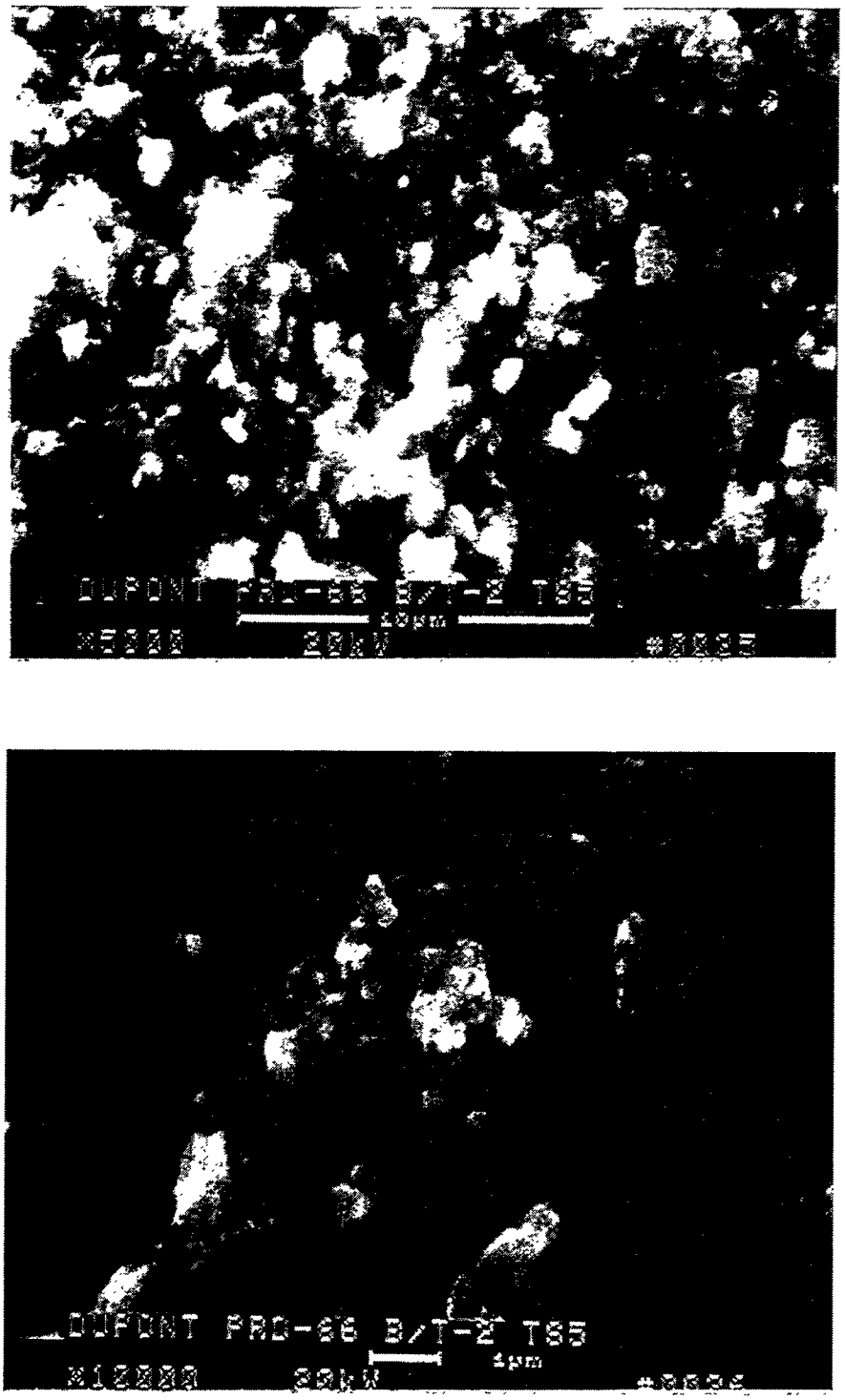

Figure 5p – Morphology Of The Ash Fines That Deposited Along The Filament Bundles In The Divot Area Of The 1110 Hours PFBC-Exposed DuPont pRD-66 Filter Matrix

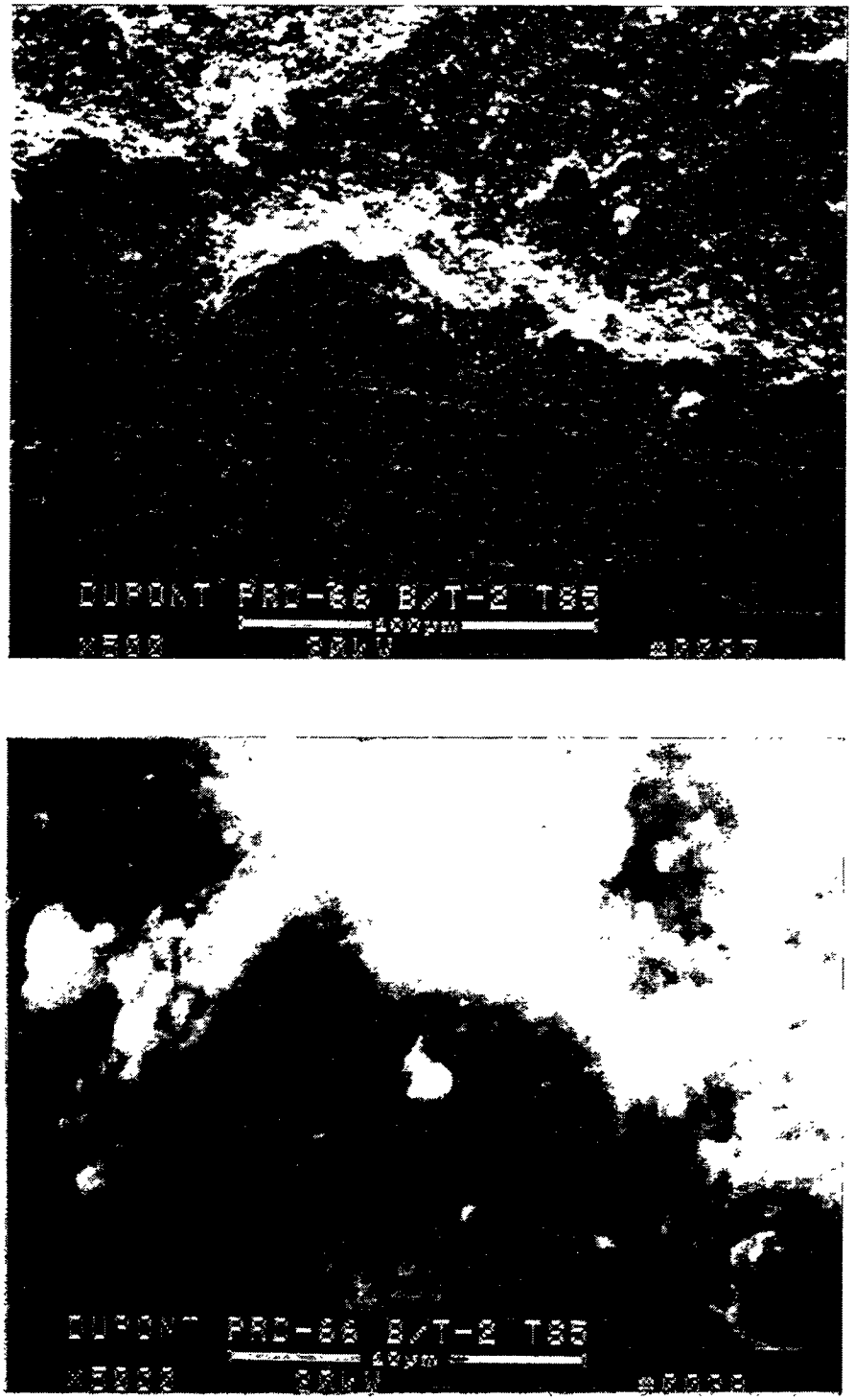

Figure 5q – Ash/Sorbent Fines Which Deposited Along The Filament Bundles In The Coarse Support Of The Divoted DuPont PRD-66 Filter Matrix

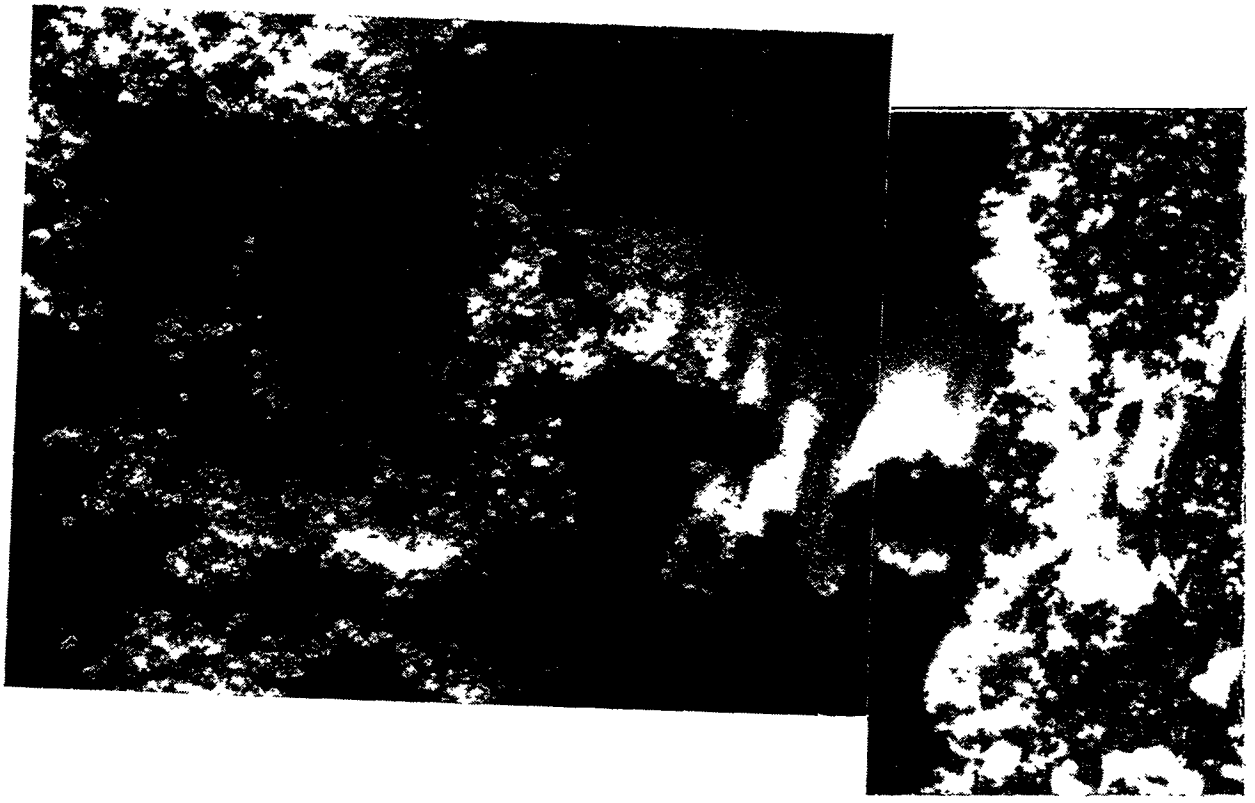

Figure 5r – Fresh Fractured Cross-Section Of The Mer
The Divoted DuPont PRD-66 Filter Matrix

Figure 5s — Morphology Of The Cross-Sectioned Filament Bundles In The Membrane Of The Divoted DuPont PRD-66 Filter Matrix

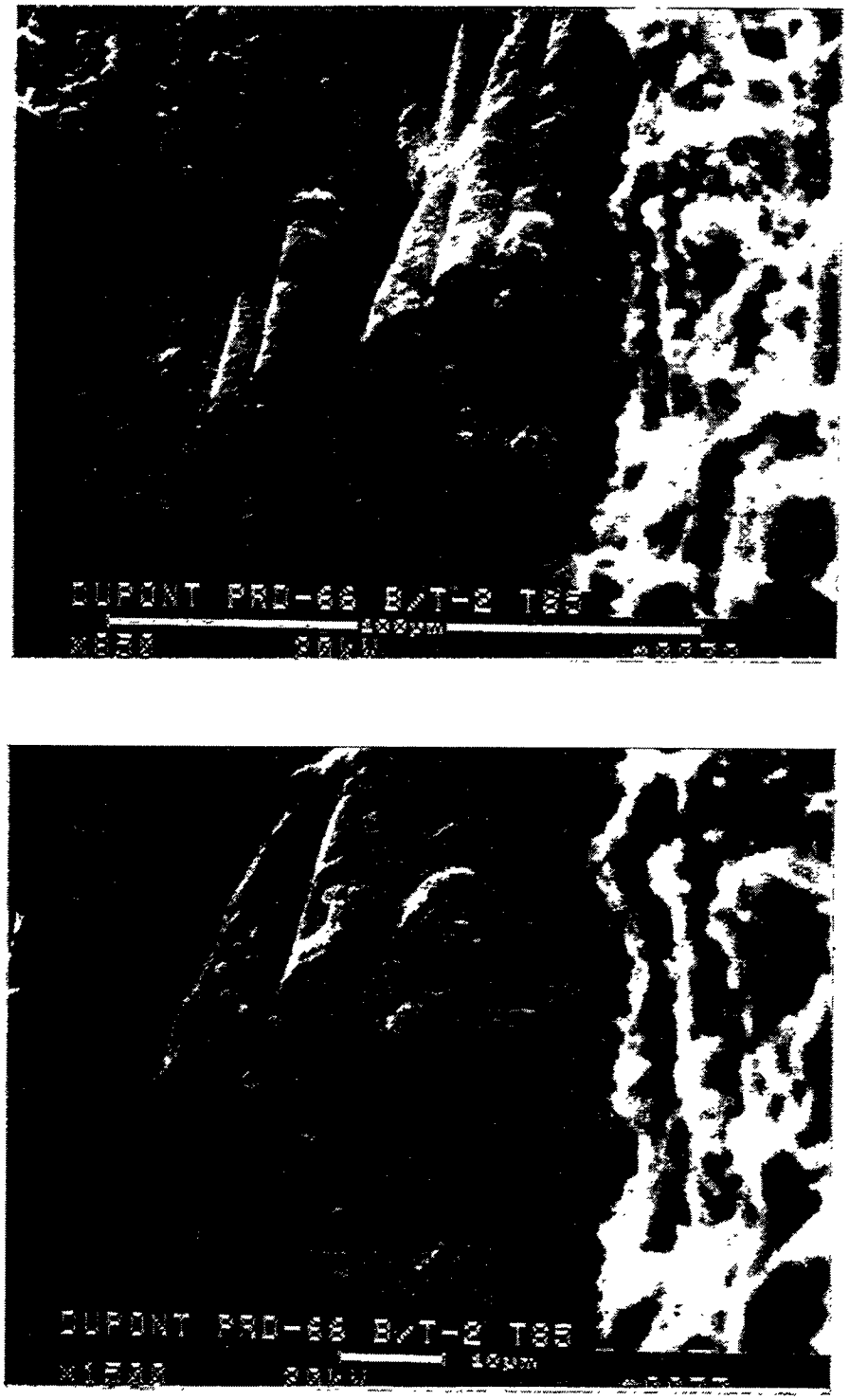

Figure 5t – Fused Or Sintered Fibers In The Filament Bundles Of The Divoted DuPont PRD-66 Filter Membrane

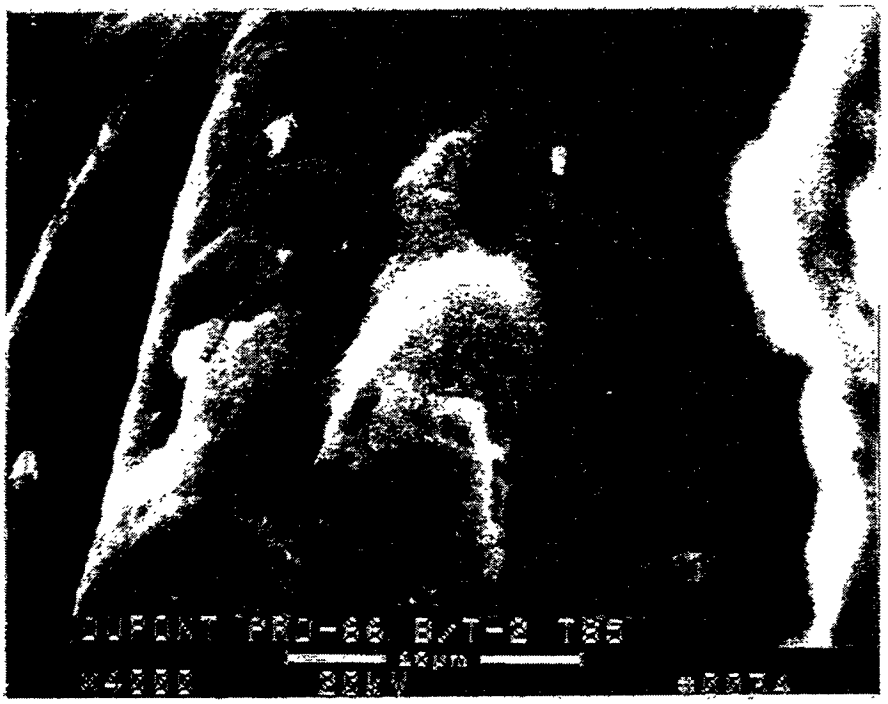

Figure 5u – Higher Magnification Micrograph Of The Fiber Surface In The Filament Bundles In The Divoted DuPont PRD-66 Filter Membrane

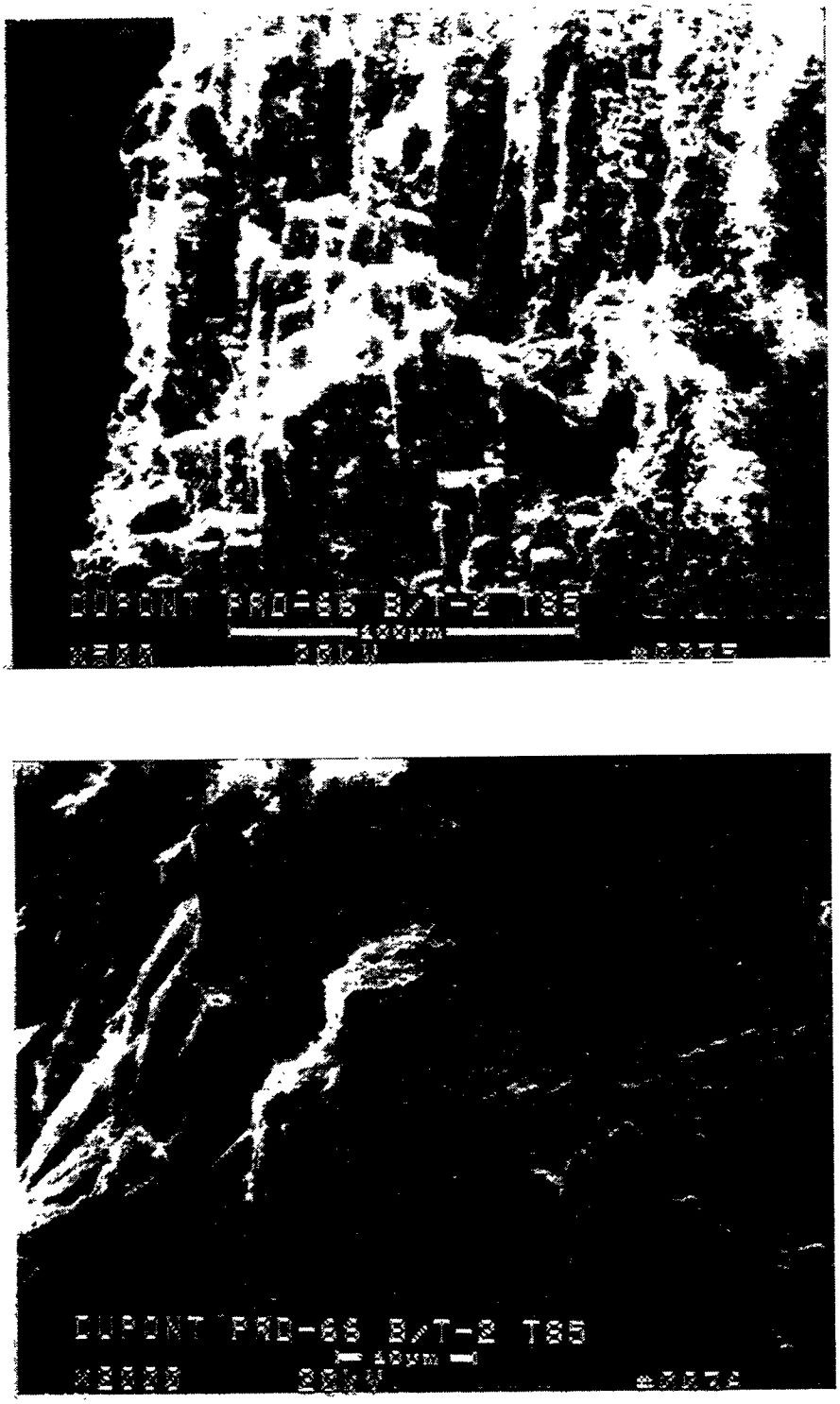

Figure 5v – Fibers In The Filament Bundles At An Alternate Location Of The Membrane In The Divoted DuPont PRD-66 Filter Matrix

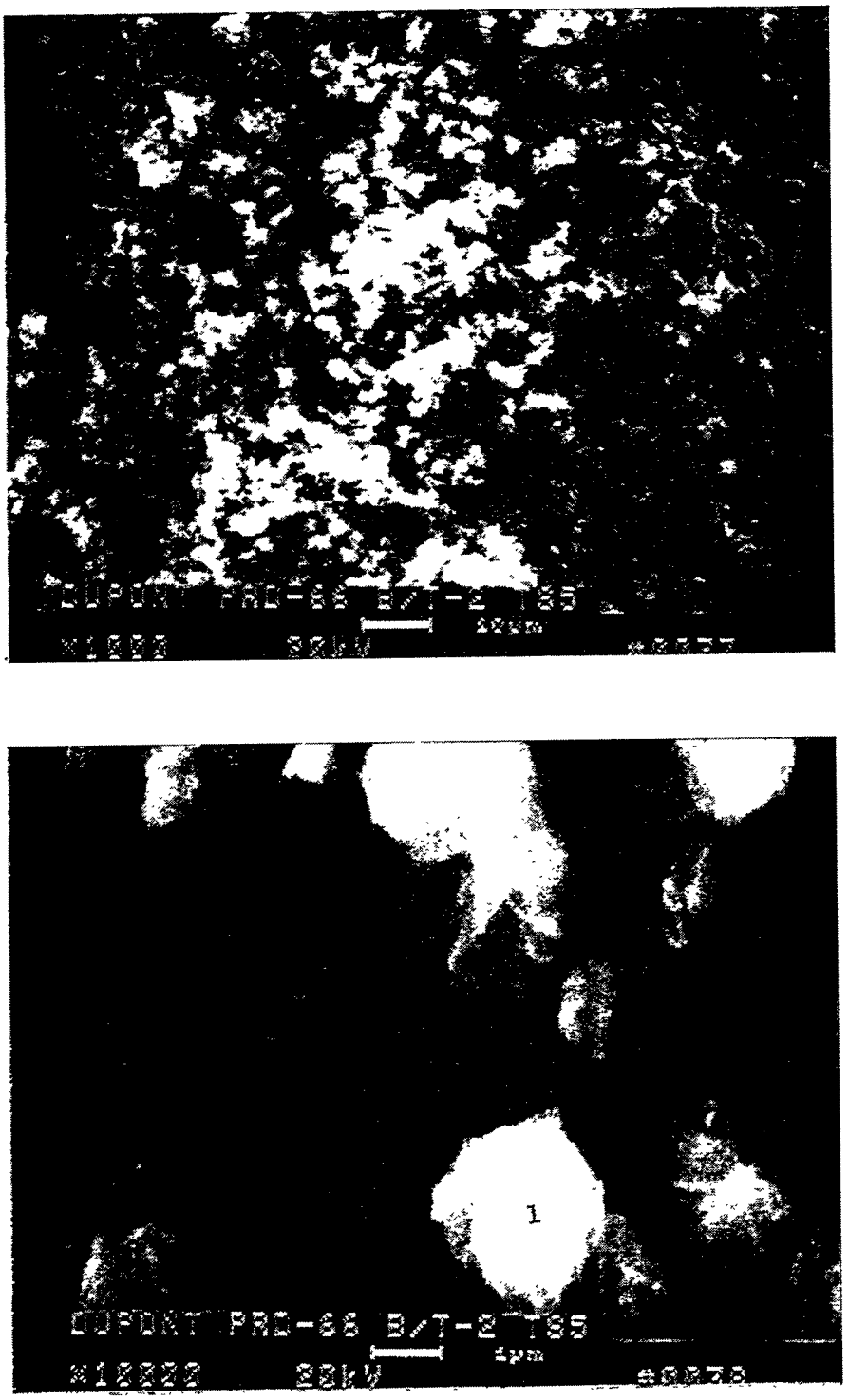

Figure 5w –Morphology Of The Fines Collected Along The Membrane Surface Of The Divoted DuPont PRD-66 Filter Matrix

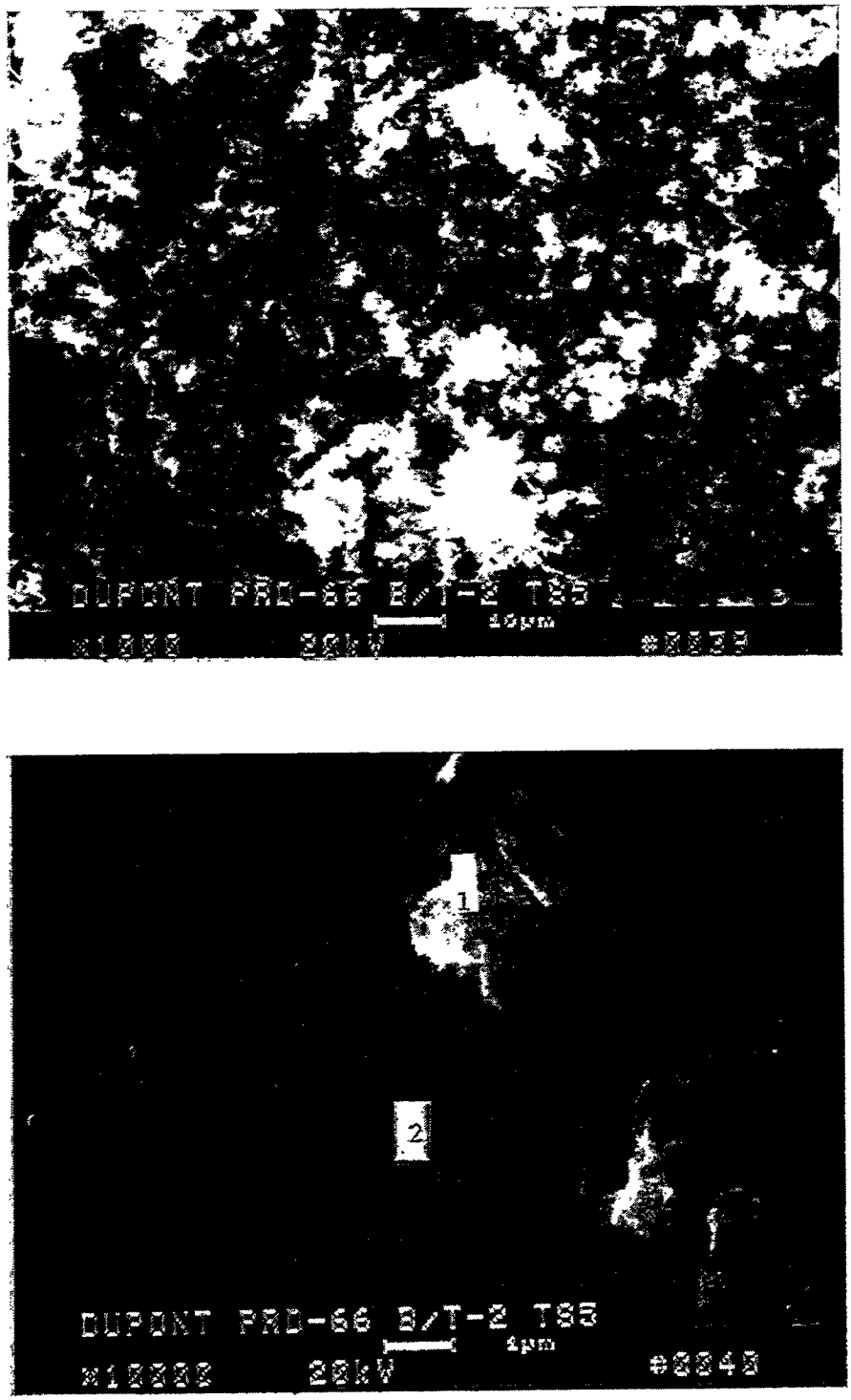

Figure 5x – Morphology Of The Fines Deposited Along The Sub-Layer Filament Bundles In The Divoted DuPont PRD-66 Filter Matrix

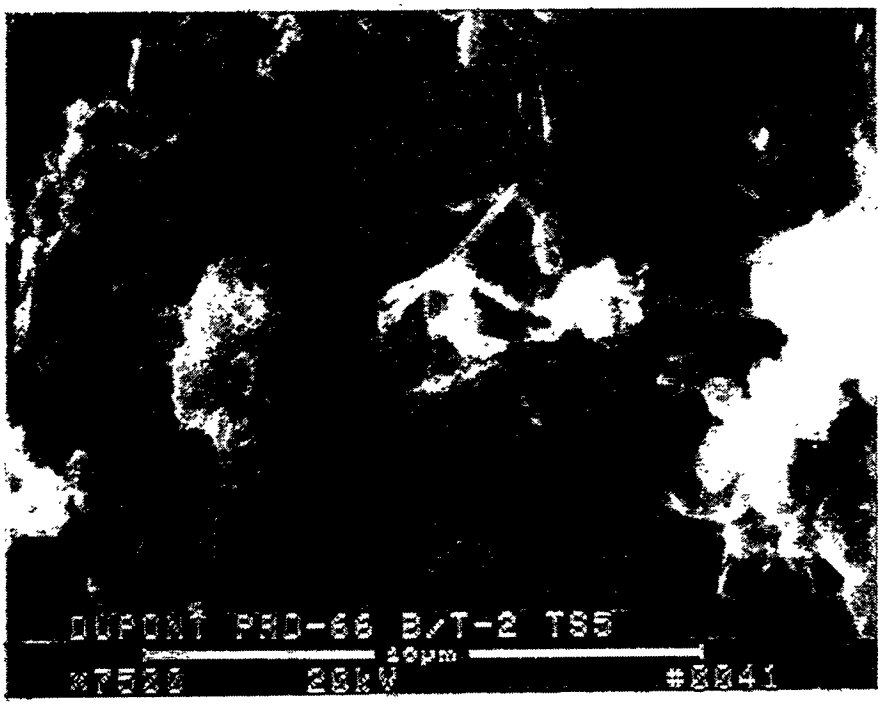

Figure 5y – Morphology Of The Fines In The Deposited Ash/Sorbent Matrix

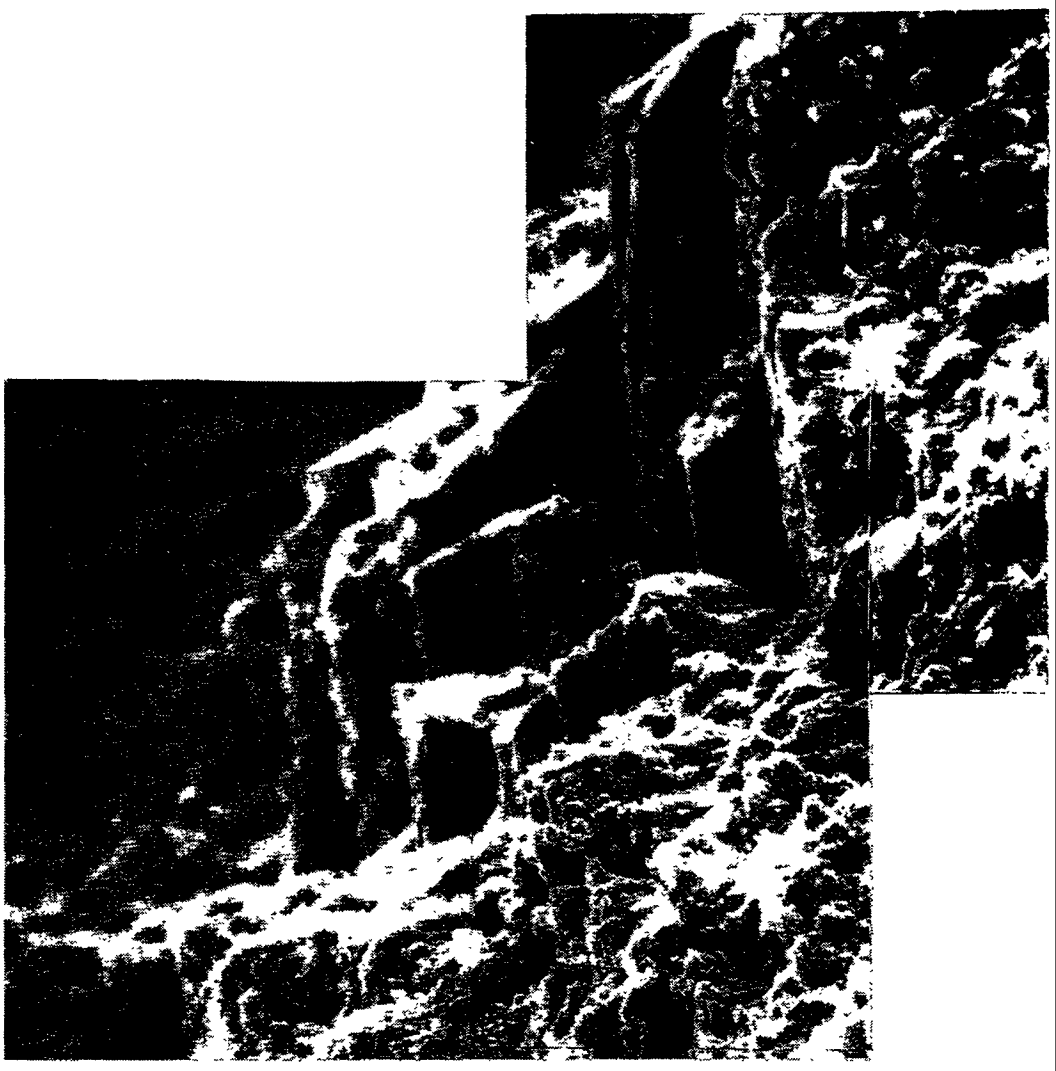

Figure 5z — Fresh Fractured Cross-Sec
Coarse Support Wall In Tl
Matrix

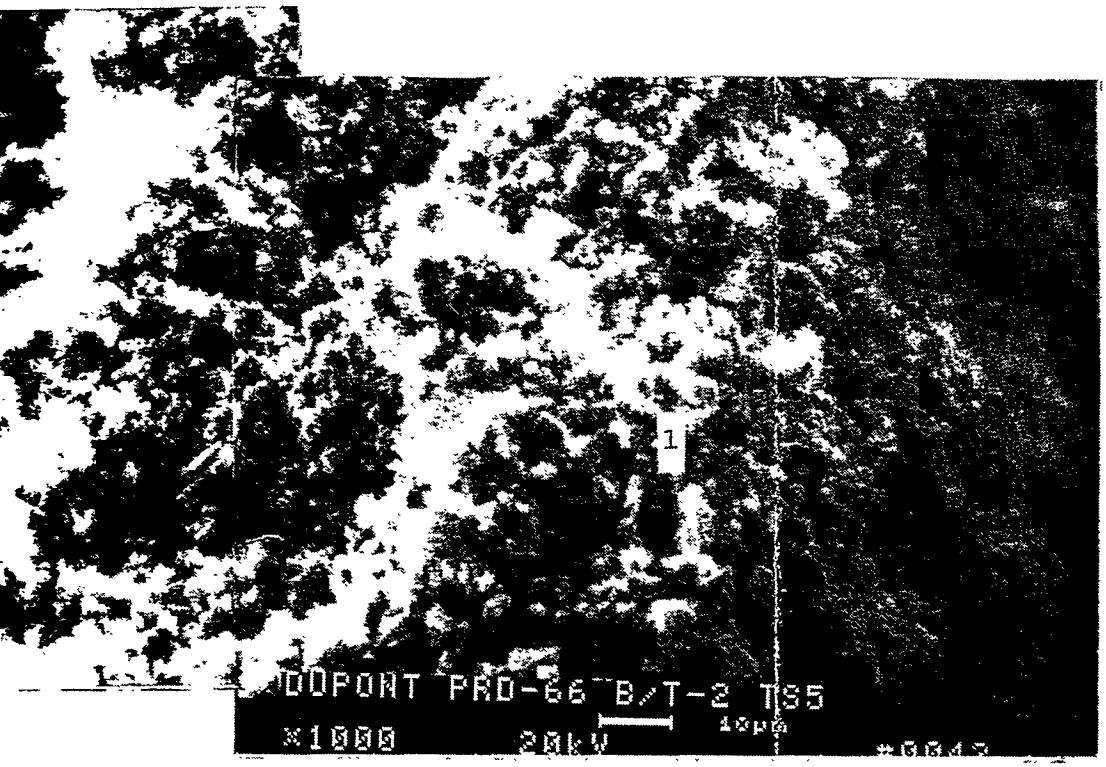

n Of The Filament Bundles In The Sub-Layer
Divoted Area Of The DuPont PRD-66 Filter

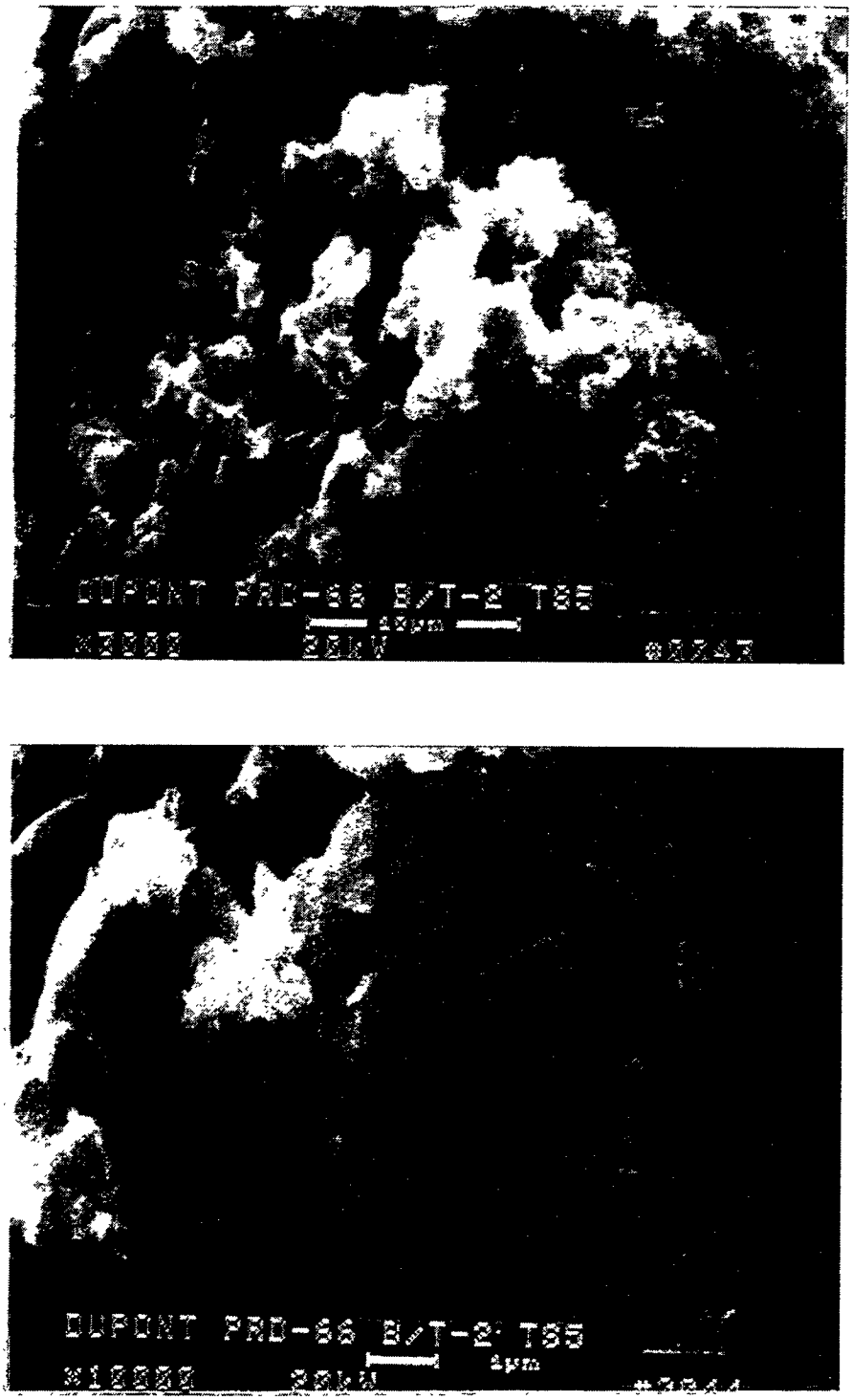

Figure 5aa – Morphology Of The Ash/Sorbent Fines That Collected Along The Filament Bundles In The Divoted Area Of The DuPont PRD-66 Filter Matrix

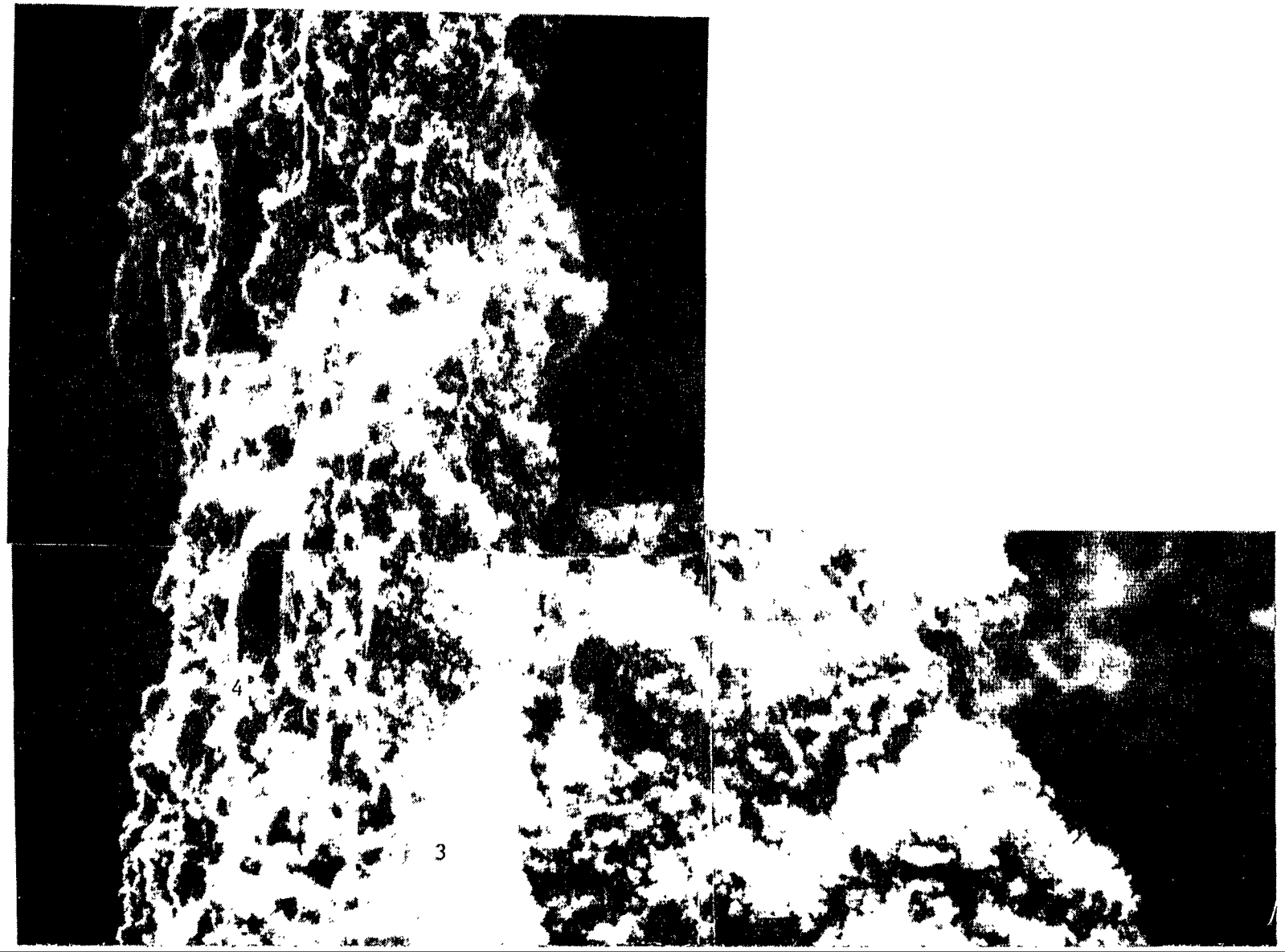
4
3

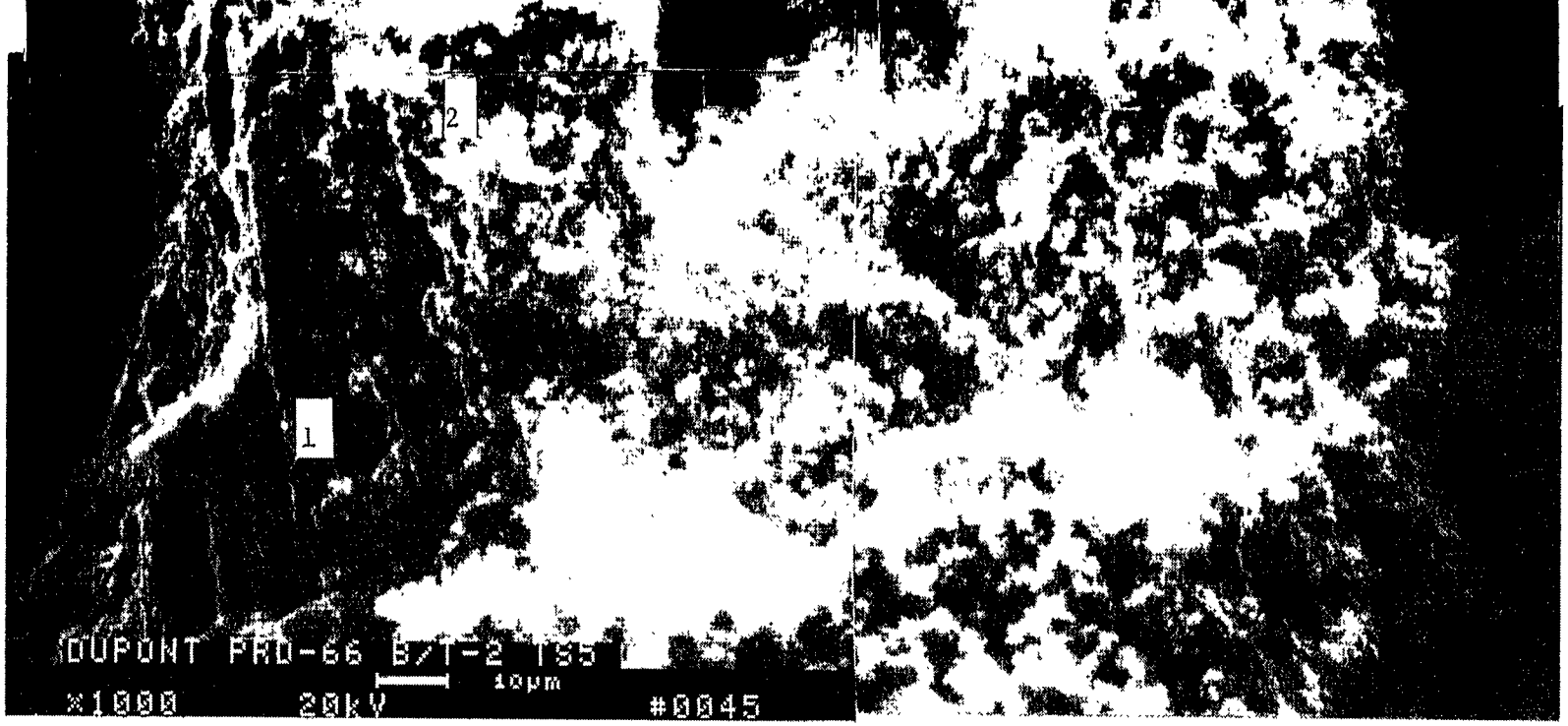

Figure 5bb – Fresh Fractured Cross-Section Of The Filament Bundles At An Alternate Location In The Sub-Layer Coarse Support Wall In The Divoted Area Of The DuPont PRD-66 Filter Matrix

0.52% Fe. Fines present at an alternate location are shown in Photo 9, Figure 5g. EDAX analysis of this material indicated the presence of 75.91% O, 7.08% S, 5.31% Mg, 4.04% Ca, 3.61% Si, 2.81% Al, 0.78% Fe, 0.33% K, and 0.14% Ti.

The dense deposit of fines shown in Area 3, Photo 2, Figure 5c, is considered to be an accumulation of particles within the "pore-like" structure that resulted during filament winding. High magnification micrographs of the particles shown in this area are provided in Figure 5h. Again, submicron fines form agglomerates. Within the ash cake layer, porosity was retained. EDAX analysis of the fines shown in Photo 11, Figure 5h, identified the presence of 69.17% O, 7.84% Ca, 6.40% Si, 5.76% S, 4.11% Mg, 3.66% Al, 1.81% Fe, 1.09% K, and 0.17% Ti.

Higher magnification micrographs of the area shown in Area 4, Photo 2, Figure 5e, are provided in Figure 5i. A very dense deposit of fines is evident in this area. The material appeared to be highly sintered and fused. EDAX analysis of this material identified the presence of 66.03% O, 13.83% S, 10.00% Ca, 3.51% Mg, 2.70% Si, 2.22% Al, 1.11% Fe, 0.51% K, and 0.09% Ti.

Similar characterization was conducted along a second area of the PRD-66 divot area. As shown in Figure 5j, the outer membrane is present, as well as the divot or depression which removed several sub-filament layers. Area 1, Photo 14, Figure 5j, is shown at higher magnification in Photo 15, Figure 5j. When the surface of the membrane is further magnified (i.e., Figure 5k), fused and/or agglomerated submicron and micron particles are evident. "Whisker-like" formations also exist within the deposited fines. EDAX analysis of this area of fines indicated the presence of 65.00% O, 8.08% Ca, 7.38% Si, 6.51% Mg, 5.86% S, 3.71% Al, 2.17% Fe, 0.78% K, and 0.50% Ti.

Two additional micrographs are provided in Figure 5l which illustrate the morphology of the fines which accumulated along the blunt or fractured surface of the membrane filament. "Melt-like" areas are present amidst the submicron agglomerates. EDAX analysis of the "melt-like" particle shown in Area 1, Photo 18, Figure 5l, indicated the presence of 80.02% O, 7.36% S, 6.94% Mg, 2.72% Ca, 2.17% Si, 0.47% Al, 0.19% Fe, 0.09% K, and 0.04% Ti. The agglomerated fines shown in Area 2, Photo 18, Figure 5l, were identified to contain 74.50% O, 7.07% Si, 5.64% Al, 4.41% Mg, 3.26% S, 3.05% Ca, 1.71% Fe, 0.27% K, and 0.08% Ti.

The morphology of the fines shown in Area 2, Photo 14, Figure 5j, is shown at higher magnification in Figure 5m. The ash cake consisted of numerous fused and/or sintered micron and submicron fines. At higher magnification (Photo 22, Figure 5n), "whisker-like" features are evident. EDAX characterization of the fines shown in Figure 5n identified the presence of 72.37% O, 9.35% Mg, 7.03% S, 4.78% Si, 3.73% Ca, 1.62% Fe, 0.89% Al, and 0.21% K.

Moving to another area along the surface of the divot we can readily see uni-directional filament bundles (Figure 5o). The outer filament bundle surface is shown at higher magnification in Photo 24, Figure 5o, and in Figure 5p. Numerous submicron and micron fines are present along the filament bundle. EDAX analyses of the fines shown in Photo 26, Figure 5p, indicated the presence of 64.04% O, 10.98% Al, 7.20% Si, 6.80% S, 4.48% Mg, 4.30% Ca, 1.26% Fe, 0.54% K, and 0.41% Ti.

Area 2, Photo 23, Figure 50 is shown at higher magnification in Figure 5q. The raised ridge section of the material appears to consist of a denser agglomeration of fines in comparison to alternate surfaces. EDAX analyses of the fines shown in Photo 28, Figure 5q identified the presence of 69.94% O, 14.53% Al, 4.97% S, 3.32% Si, 3.30% Mg, 2.65% Ca, 0.73% Fe, 0.44% K, and 0.12% Ti. The relatively high concentration of aluminum in this area may reflect the composition of the underlying PRD-66 filter matrix.

SEM/EDAX analysis was also performed along the fresh fractured divoted DuPont PRD-66 filter matrix. The fiber shown in Area 1, Photo 29, Figure 5r, may have been part of the membrane filament bundle. As shown in Figure 5s, the fibers contain holes. EDAX analysis of the fiber identifies the presence of 71.33% O, 16.51% Si, 7.07% Al, and 5.09% Mg (i.e., cordierite-containing matrix), while the polycrystalline phase shown in Area 2 was identified to contain 73.36% O, 17.48% Al, 6.79% Si, and 2.36% Mg (i.e., perhaps the outer encapsulating filament bundle layer).

Frequently the fibers which are present within the filament bundle are fused and/or sintered to each other (Figures 5t and 5u). EDAX analysis of the fiber surface shown in Photo 34, Figure 5u, identified the presence of 70.20% O, 13.99% Si, 10.11% Al, and 5.71% Mg.

Fibers at an alternate location are shown in Figure 5v. Directly adjacent to the fibers is a dense accumulation of fines (Figure 5w). At higher magnification, the fines were seen to contain numerous submicron and micron fines or agglomerates, as well as the "whisker-like" or strand formations. The composition of the particle shown in Area 1, Photo 38, Figure 5w, was identified to contain 78.60% O, 8.76% Si, 3.30% S, 3.14% Mg, 2.71% Al, 2.53% Ca, 0.63% Fe, and 0.33% K.

Moving to the outer surface of the fractured filter divot area (i.e., Area 2, Figure 29, Figure 5r), we see that the material consists of a dense deposit of fines (Figure 5x). At higher magnification, crystalline fines are present which contain 74.67% O, 7.81% Al, 5.05% Si, 4.54% S, 4.21% Mg, 2.64% Ca, 0.77% Fe, and 0.32% K. An additional micrograph of the "strand-like" interconnective network of the "whisker-like" formations is provided in Figure 5y.

At the deepest depression of the divot, the fresh fractured matrix was seen to contain a dense deposit of fines which were in direct contact with the filament bundle (Figure 5z). The ash cake particles are shown at higher magnification in Figure 5aa. The sintered and/or fused agglomerated network of ash/sorbent particles (i.e., 73.06% O, 8.13% S, 8.05% Mg, 4.89% Ca, 4.30% Si, 0.90% Al, 0.42% Fe, and 0.26% K) also contained the "whisker-like" network.

Figure 5bb provides a micrograph montage at an alternate location along the fresh fractured divot cross-section. Area 1 identifies the location of the fibers in the filament bundle, while Areas 2 and 3 contain the ash/sorbent deposited fines. Aluminum-enriched regions are evident in isolated areas of the fractured filament bundles (Area 4, Photo 45, Figure 5bb).

PFBC-EXPOSED DuPONT PRD-66 FILTER MATRIX (TEST SEGMENT #4)

Prior to conducting Test Segment #5, three as-manufactured DuPont PRD-66 candle filters were installed and operated at AEP in Test Segment #4. All three elements remained intact during the 1705 hours of operation at AEP. Two filters were subjected to residual bulk strength characterization. A section of filter D-132 (B/M-7) which had been strength tested was utilized to

conduct the SEM/EDAX analyses. As a result of sample preparation for C-ring strength analyses, the filter had been washed, cut, and dried. This was considered to have removed the majority of the fines from along the outer surface of the element, and possibly within the wall. Similarly, crystallization of magnesium sulfate which had previously been observed to occur during drying of the element, may have resulted prior to conducting the following SEM/EDAX analyses.

Initially a section of the 1705 hour PFBC-exposed DuPont PRD-66 filter matrix was coated with carbon in order to identify the elemental composition at various locations, and to preserve the detection capability of sulfur within the material. As shown in Figure 6a, the fractured cross-section of the filament yarn contains numerous fibers. The fibers are either discrete, or are surrounded by a polycrystalline matrix. Adjacent fibers are seen to bond or to be "fused" to each other. Frequently holes are evident at the center of the filament bundle fibers.

Area scan analysis of the fibers shown in Photo 1, Figure 6a, indicated the presence of 71.64% O, 18.67% Al, 5.31% Si, 2.85% Mg, 1.27% S, and 0.26% Ca. The fibers shown in Photo 2, Figure 6a, contained 67.65% O, 18.40% Si, 8.07% Al, and 5.88% Mg.

The polycrystalline outer surface of the filament bundle is shown in Photo 3, Figure 6b. The composition of what appeared to be adhering particle at Area 1, Photo 3, Figure 6b, was identified to include 80.22% O, 9.38% S, 6.42% Ca, 2.13% Al, 1.11% Mg, and 0.74% Si (i.e., presence of calcium sulfate). Area 2, Photo 3, Figure 6b, is representative of the polycrystalline filament bundle surface. EDAX identified the presence of 75.92% O, 22.24% Al, and 1.84% Si at this location. Within the filament bundle, calcium and sulfur were detected (i.e., 79.81% O, 11.14% Si, 4.09% S, 2.47% Ca, 1.92% Al, and 0.57% Mg).

Characterization directly along the polycrystalline surface identified the presence of irregularly shaped particles (i.e., Photo 4, Figure 6b). Area scan analyses of the matrix shown in Photo 4, Figure 6b, identified the presence of 75.85% O, 12.83% Al, 4.53% Mg, 4.24% S, 1.62% Si, and 0.93% Ca. The "strand-like" feature shown in Area 1, Photo 4, Figure 6b, was identified by EDAX to contain 77.01% O, 8.62% S, 8.17% Mg, 3.69% Al, 2.32% Ca, and 0.18% Si (i.e., sorbent attached particle). The particle shown in Area 2, Photo 4, Figure 6b, was identified by EDAX to contain 74.48% O, 13.08% Mg, 11.15% S, 0.84% Al, 0.26% Ca, and 0.18% Si (i.e., again a magnesium sulfate-enriched location). The mottled surface features shown in Area 3, Photo 4, Figure 6b, was identified by EDAX to contain 71.84% O, 22.39% Al, 2.28% Si, 2.08% Mg, 1.40% S, and 0.01% Ca. This area may be more representative of the polycrystalline outer layer that encapsulated the filament bundles.

An additional area of the polycrystalline surface is shown in Figure 6c. The "melt-like" matrix consisted of 72.69% O, 13.06% Al, 6.51% S, 3.95% Mg, 3.07% Ca, and 0.73% Si.

In order to provide higher resolution micrographs of the 1705 hour PFBC-exposed filter matrix, a second section of material was removed from the C-rings, and was gold coated. As shown in Figure 6d numerous filament bundles were present within the filter wall, The filament bundles contain numerous fibers that were encapsulated within a polycrystalline matrix. The cross-sectioned filament bundle is shown at higher magnification in Figure 6c. The polycrystalline matrix is evident at the periphery of the filament bundle shown in Photo 9, Figure 6e. It appears to be separated from the underlying filament bundle in several locations. Discrete fibers are evident within the cross-sectioned filament bundle. Areas are also present between fibers which include

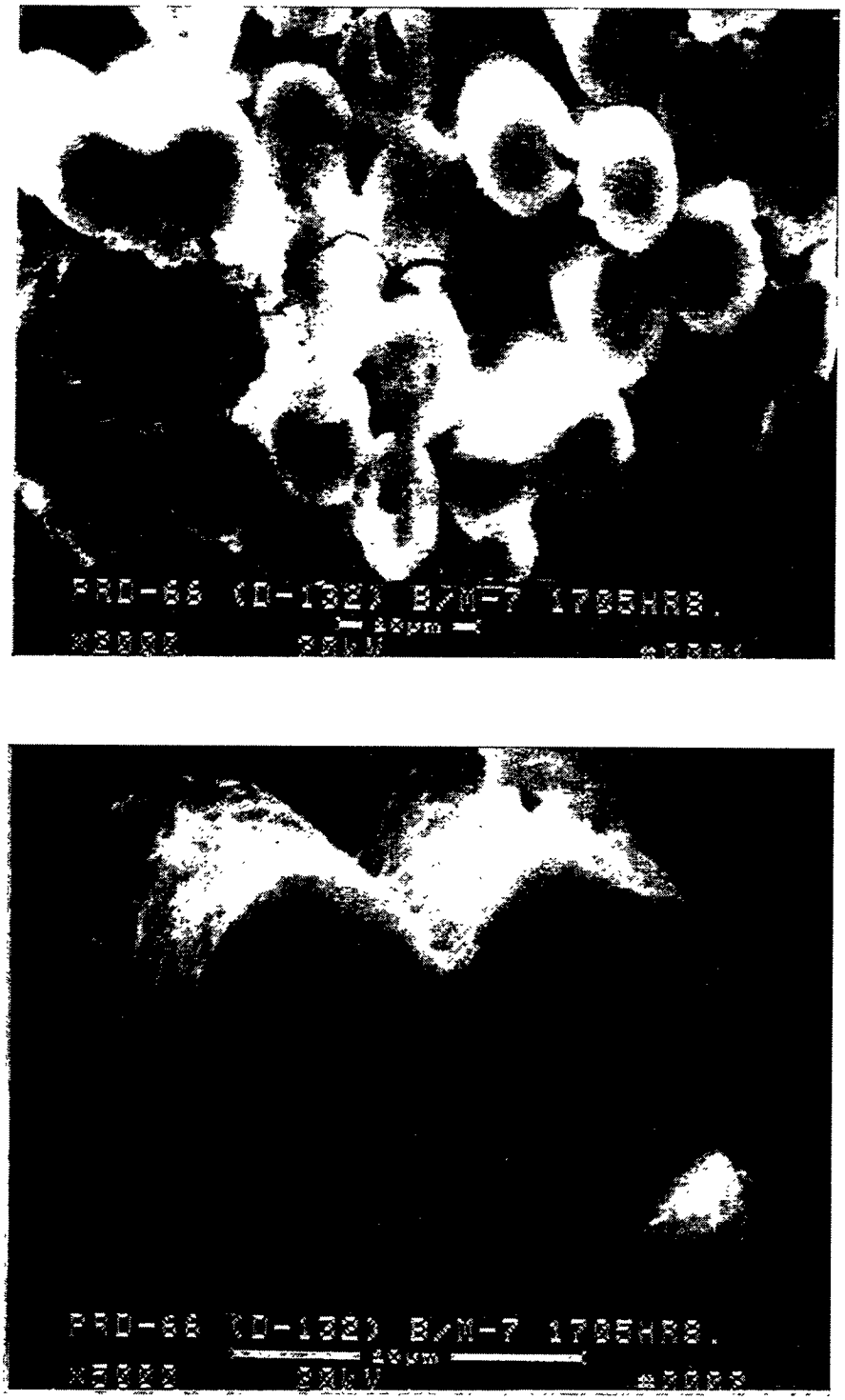

Figure 6a – Cross-Sectioned DuPont PRD-66 Filter Matrix Which Had Been Exposed To PFBC Operating Conditions For 1705 Hours At AEP (Carbon Coated)

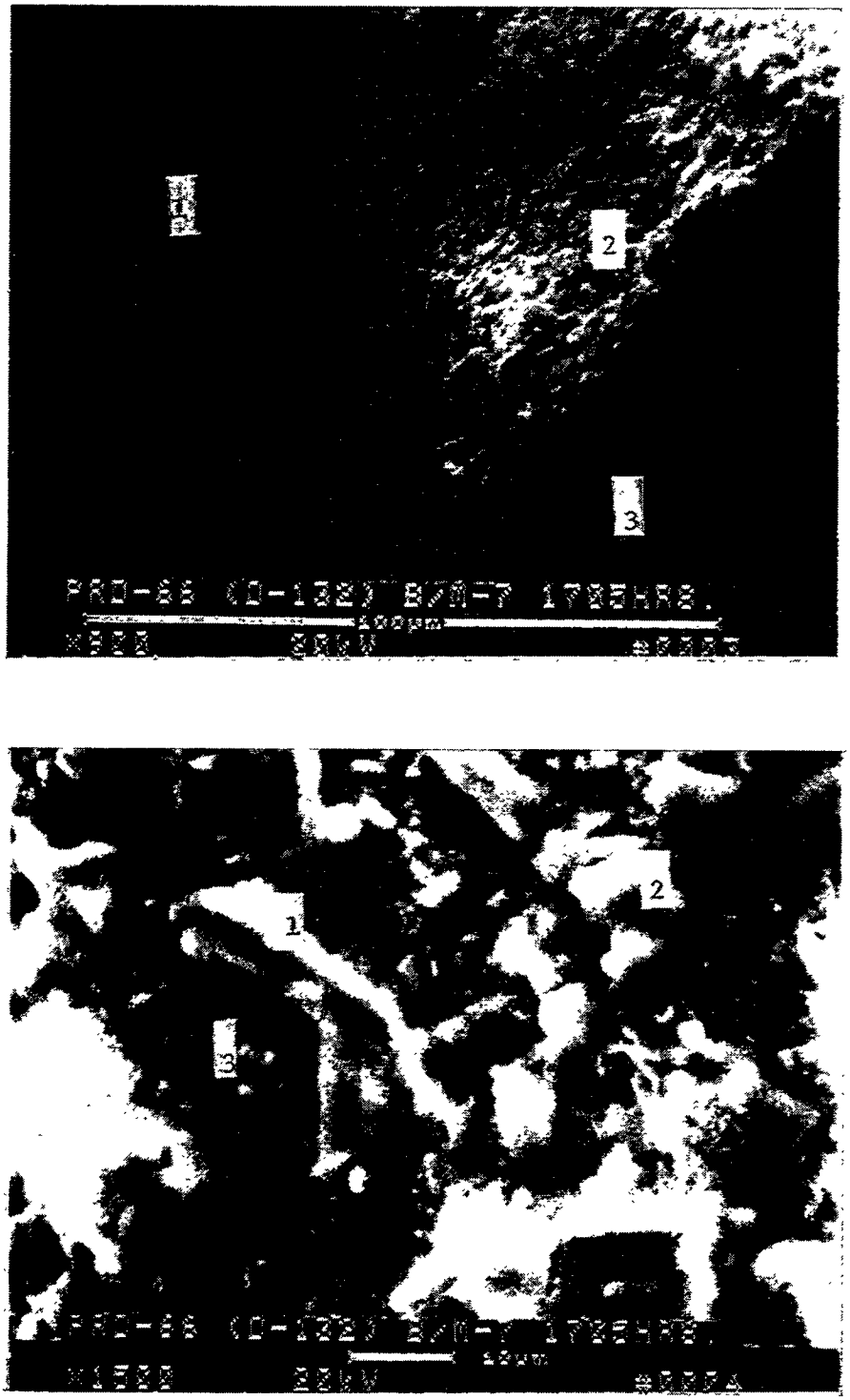

Figure 6b – Deposition Which Resulted Along The Outer Surface Of The Polycrystalline Layer That Encapsulated The DuPont PRD-66 Filament Bundle After 1705 Hours Of PFBC Operation At AEP

Figure 6c – Higher Magnification Micrograph Of The Magnesium-Sulfur-Calcium-Enriched Phase Which Remained Along The Outer Surface Of The Filament Bundle Polycrystalline Phase After 1705 Hours Of Operation At AEP (Wet Cut For Strength Testing; Carbon Coated)

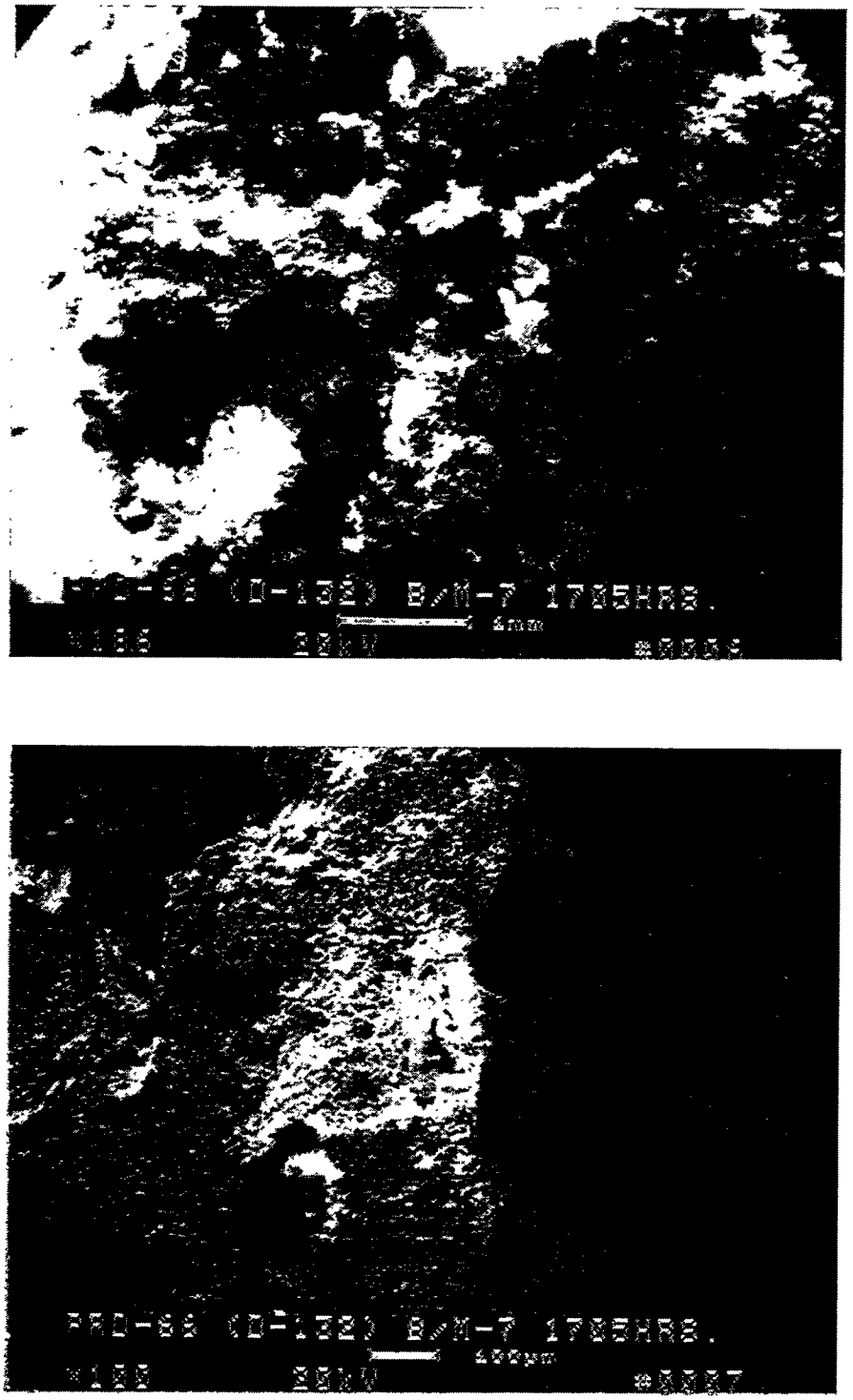

Figure 6d – Cross-Sectioned DuPont PRD-66 Filter Matrix After 1705 Hours Of Operation At AEP (Gold Coated)

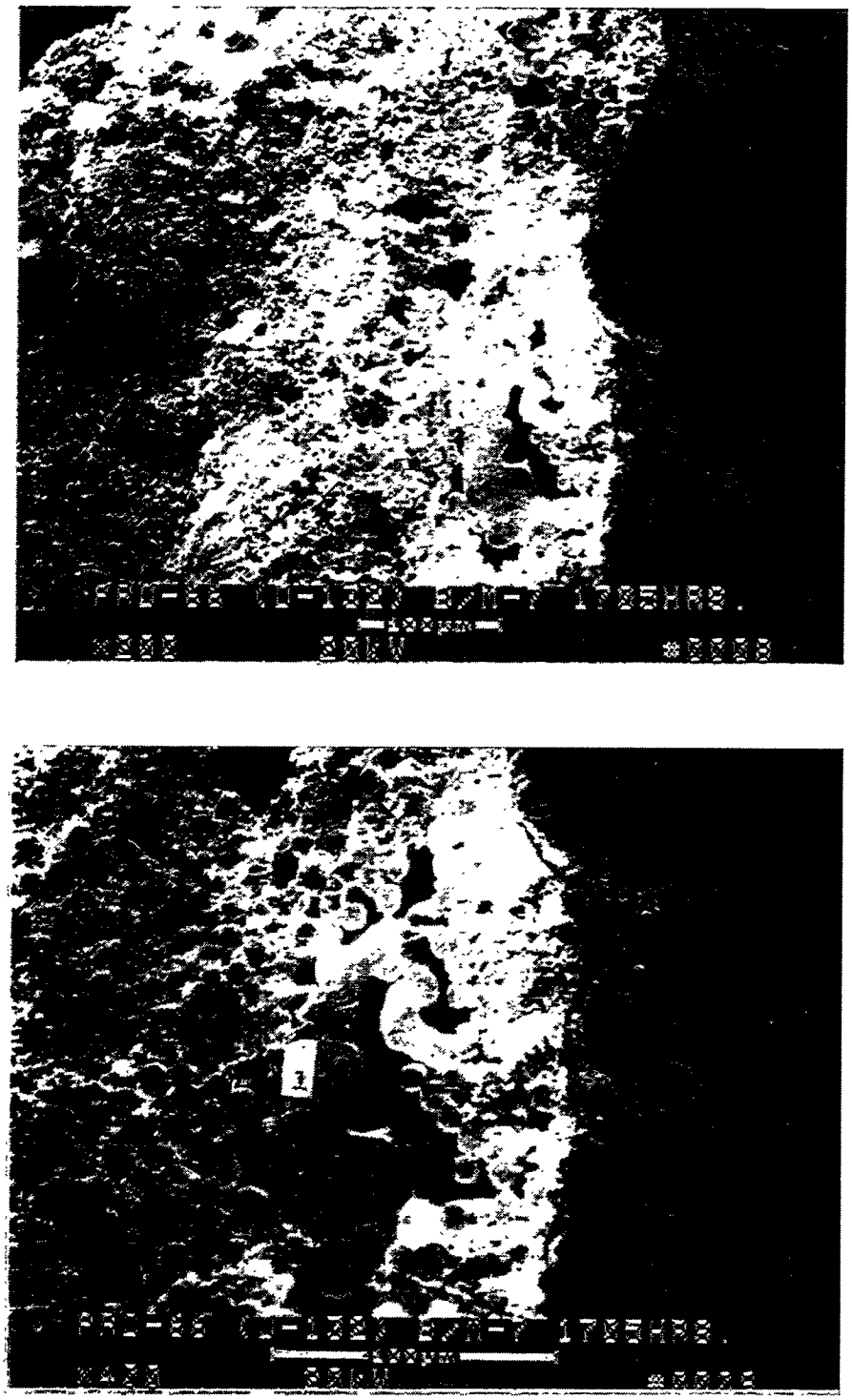

Figure 6e – Higher Magnification Micrographs Illustrating The Polycrystalline Layer That Encapsulated The Filament Bundles In The 1705 Hour PFBC-Exposed Filter Matrix

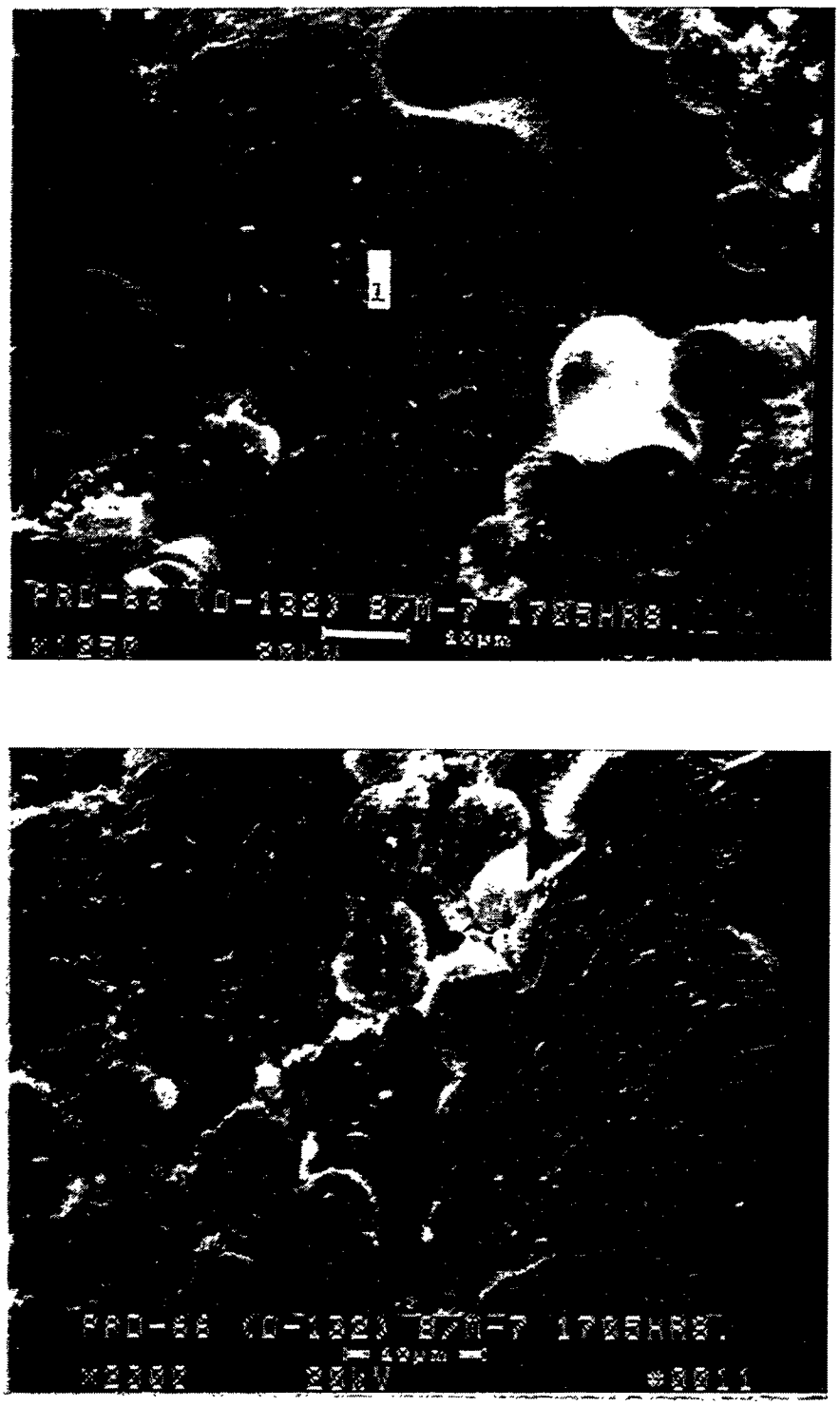

Figure 6f – Fibers In The Filament Bundle Of The 1705 Hour PFBC-Exposed DuPont PRD-66 Filter Matrix

Figure 6g – Fibers In The Filament Bundle Of The 1705 Hour PFBC-Exposed DuPont PRD-66 Filter Matrix

Figure 6h – Higher Magnification Micrograph Montage Of The Fibe
Polycrystalline Layer In The 1705 Hour PFBC-Exposed
Filter Matrix

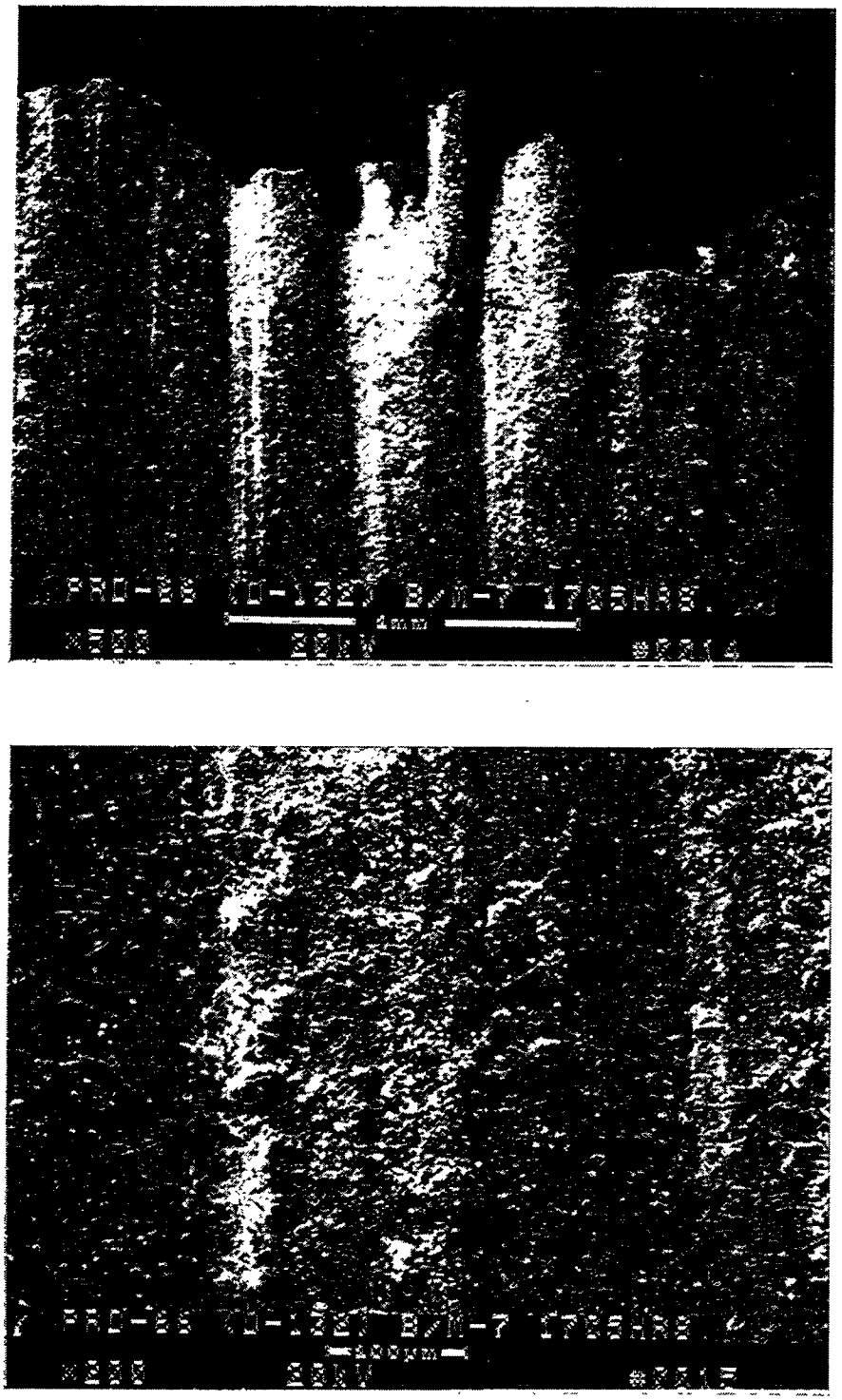

Figure 6i — Outer Membrane Surface Of The 1705 Hour PFBC-Exposed DuPont PRD-66 Filter Matrix

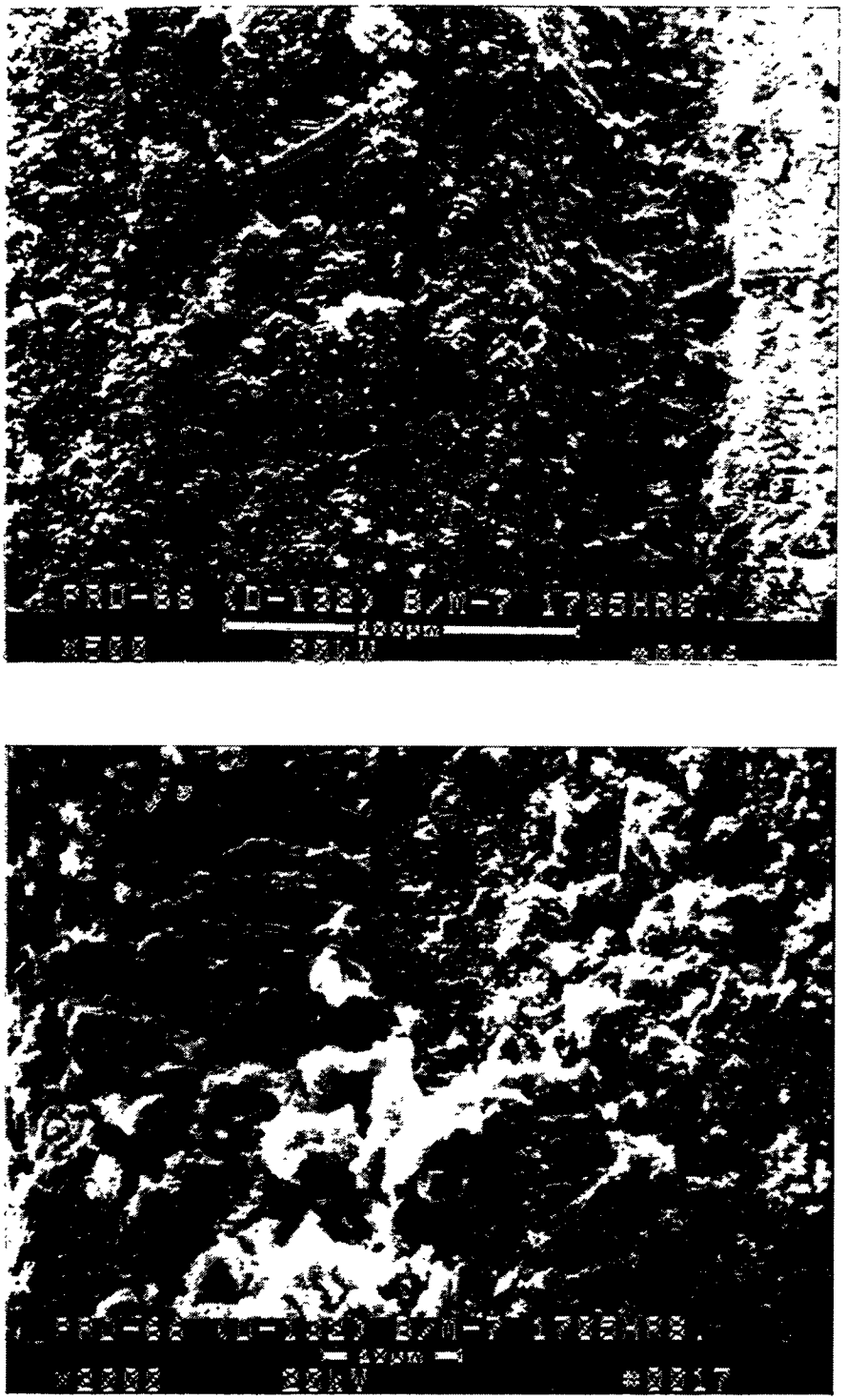

Figure 6j — Higher Magnification Micrographs Of The Surface Morphology Of The Outer Membrane Surface Of The 1705 Hour PFBC-Exposed DuPont PRD-66 Filter Matrix

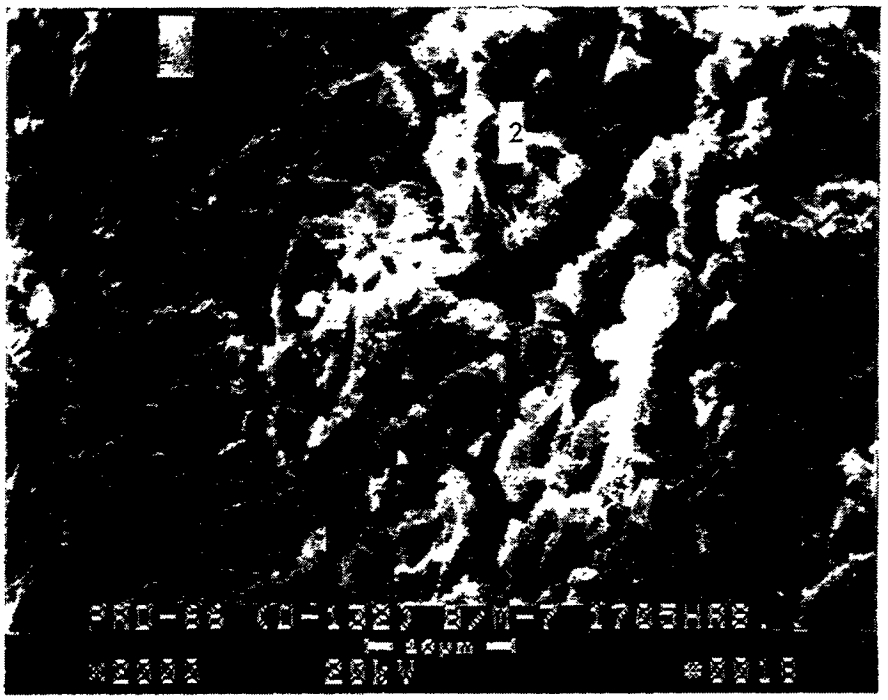

Figure 6k – Magnesium-Sulfur-Calcium-Enriched Phase That Resulted Along The Outer Membrane Surface Of The 1705 Hour PFBC-Exposed DuPont PRD-66 Filter Matrix

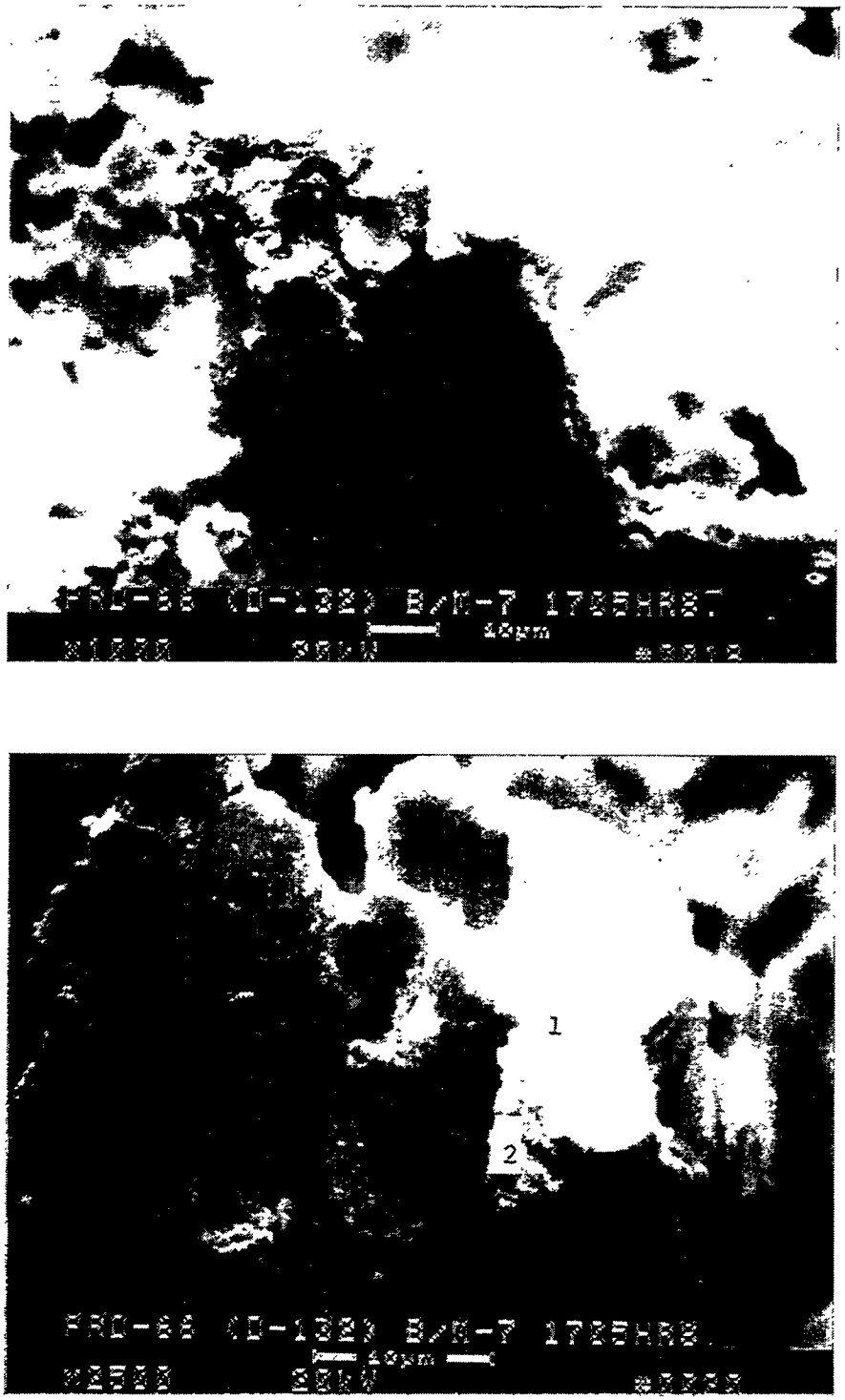

Figure 61 – Fibers In The Membrane Filament Bundles Of The 1705 Hour PFBC-Exposed DuPont PRD-66 Filter Matrix

polycrystalline phases. What is uniquely evident in Photo 9, Figure 6e, is the extensive agglomeration of the fibers in Area 1. We cannot state with certainty that the matrix originally contained the agglomerated formation, or whether process operating conditions induced "melting" of adjacent fibers (i.e., absence of the polycrystalline phase). EDAX analysis of the fiber shown in Area 1, Photo 10, Figure 6f, identified the presence of 41.81% O, 38.77% Si, 11.63% Al, and 7.79% Mg.

Photo 11, Figure 6f, illustrates the morphology of the large agglomerate at an alternate location within the filament bundle. Similarly, the fibers at an alternate location within the filament bundle are shown in Photo 12, Figure 6g. EDAX analysis of the fiber in Area 1 identified the presence of 44.37% Si, 35.06% O, 13.55% Al, and 7.02% Mg, while the polycrystalline matrix between fibers in Area 2 consisted of 51.16% O, 30.33% Al, 14.48% Si, and 4.03% Mg.

A micrograph montage is presented in Figure 6h which illustrates the morphology of the cross-sectioned filament bundle. The external layer that encapsulated the filament bundle appears to have separated from the underlying matrix. An ~10 μm polycrystalline layer encapsulated the filament bundle in this area. Below the polycrystalline layer, ~7-10 μm fibers are present. Near the periphery of the cross-sectioned filament bundle, the fibers are seen to frequently be surrounded via a polycrystalline matrix. Voids are sometimes evident at the center of the filament bundle fibers.

The morphology of the outer membrane surface is shown in Figure 6i. Although gold had been used to coat the sample, sulfur was readily detected along this area of the matrix (i.e., Area scan analysis of Photo 15, Figure 6i: magnesium, sulfur, aluminum, silicon, and oxygen). At higher magnification (i.e., Figure 6j), a very mottled surface texture was evident. The morphology of the membrane surface is shown at an alternate location in Figure 6k. In both Areas 1 and 2, Photo 18, Figure 6k, magnesium, sulfur, and oxygen were present (i.e., significantly higher than aluminum and/or silicon).

Figure 6l provides two micrographs illustrating the morphology of the fibers along the cross-sectioned membrane surface. Infiltration of the polycrystalline matrix into the fibers is evident. The composition of the fiber identified in Area 1, Photo 20, Figure 6l, consisted of aluminum, magnesium, oxygen, and silicon, while the polycrystalline phase shown in Area 2, Photo 20, Figure 6l, was identified to contain a substantially greater concentration of silicon, magnesium, and oxygen, as well as aluminum in comparison to Area 1.

CONCLUSIONS

- The formation of divots appeared to be independent of the accumulation of ash along the surface of the DuPont PRD-66 filter body. This comment is based on the fact that divots formed both along the "red ash stained" areas, as well as along the surface of the filter body where ash was not present. Similarly divoting resulted at Westinghouse during high temperature, high pressure accelerated pulse testing during which time limited ash was fed to the filter array containing DuPont PRD-66 and alternate candle filter elements. The formation of divots most likely results from a mechanical stress imposed on the filter body during field or bench-scale process operation.

- The fibers that were present in the DuPont PRD-66 filter matrix frequently appeared to be sintered together, particularly after exposure in the PFBC environment. A mottled surface morphology, as well as pits and/or holes were also observed to form along the cordierite-containing fibers after PFBC process operation.
- Submicron and micron ash particulates deposited along the surface of the DuPont PRD-66 filter matrix after operation in the W-APF in Test Segment #5. The fines generally were enriched with $CaSO_4$ and/or a Mg-Ca-S-O or Mg-Ca-Si-S-O phase. After exposure to process operating conditions, it was typically very difficult utilizing SEM/EDAX analytical techniques to distinguish between the location of the ash/sorbent deposit and the slurry/filament encapsulating matrix which contained corundum, cristobalite, and mullite (typical non-whisker mullite not evident).